JOURNAL OF BIOLOGICAL REGULATORS & HOMEOSTATIC AGENTS
Volume 30, No. 2, April - June, 2016

CONTENTS

EDITORIAL

THE DIFFERENTIATION OF MAMMALIAN OVARIAN GRANULOSA CELLS – LIVING IN THE SHADOW OF CELLULAR DEVELOPMENTAL CAPACITY

A. CHACHULA[1], W. KRANC[2], J. BUDNA[1], A. BRYJA[2], S. CIESIÓLKA[1], K. WOJTANOWICZ-MARKIEWICZ1[3], H. PIOTROWSKA[4], D. BUKOWSKA[3], M. KRAJECKI[2], P. ANTOSIK[3], KP. BRÜSSOW[3], M. BRUSKA[2], M. NOWICKI[1], M. ZABEL[1,5] and B. KEMPISTY[1,2]

[1]Department of Histology and Embryology, Poznan University of Medical Sciences, Poznan, Poland; [2]Department of Anatomy, Poznan University of Medical Sciences, Poznan, Poland; [3]Institute of Veterinary Sciences, Poznan University of Life Sciences, Poznan, Poland; [4]Department of Toxicology, Poznan University of Medical Sciences, Poznan, Poland; [5]Department of Histology and Embryology, Wroclaw Medical University, Wroclaw, Poland

Received October 19, 2015 – Accepted May 18, 2016

The first two authors contributed equally to this work

The mammalian cumulus-oocyte complex (COCs) promotes oocyte growth and development during long stages of folliculogenesis and oogenesis. Before ovulation, the follicle is formed by a variety of fully differentiated cell populations; cumulus cells (CCs) that tightly surround the female gamete, granulosa cells (GCs) and theca cells (TCs) which build the internal and external mass of the follicular wall. It is well documented that CCs surrounding the oocyte are necessary for resumption of meiosis and full maturation of the gamete. However, the role of the granulosa cells in acquisition of MII stage and/or full fertilization ability is not yet entirely known. In this article, we present an overview of mammalian oocytes and their relationship to the surrounding cumulus and granulosa cells. We also describe the processes of GCs differentiation and developmental capacity. Finally, we describe several markers of mammalian GCs, which could be used for positive identification of isolated cells. The developmental capacity of oocytes and surrounding somatic cells – a "fingerprint" of folliculogenesis and oogenesis

Oogenesis is a process of differentiation of the ovum that leads to formation of a fully mature and fertilizable oocyte in which the oocyte arises from primordial germ cells (PGCs). Previous reports have shown that mouse PGCs are visible in the extra-embryonic mesoderm at 7.5 days of embryonic development. On the other hand, nests of PGCs are visible in the fetal human and sheep ovaries by day 154 and 75, respectively, after fertilization (1). Furthermore, PGCs move into the genital ridge, where proliferation and sex determination begins. Subsequently, PGCs start to proliferate, divide mitotically with incomplete cytokinesis and finally develop germ cell cysts (2), after which mitosis stops and germ cells undergo meiotic division, resulting in primary oocytes. During meiosis, primary oocytes reach the dictyate state and

Key words: ovarian follicular cells, granulosa cells, cumulus-oocyte complex, epithelialization

Mailing address:
Bartosz Kempisty PhD,
Department of Histology and Embryology,
Department of Anatomy, Poznań University of Medical Sciences,
6 Święcickiego St., 60-781 Poznań, Poland
Tel./Fax: +48 61 8546419 / +48 61 8546455,
e-mail: etok@op.pl

0393-974X (2016)

remain arrested until the surge of luteinizing hormone (LH), which stimulates final oocyte maturation. During the meiotic arrest stage, germ cell cysts start to form follicles while oocytes become encircled by pre-granulosa cells before ultimately becoming primary follicles (3). After the formation of the primary follicle, folliculogenesis is initiated. Folliculogenesis is defined as maturation of ovarian follicles which contain immature oocyte surrounded by clusters of somatic cells. It is a separate process connected with ovum maturation, but it is tightly connected with oogenesis and supports all oogenetic sub-processes. Folliculogenesis describes the entire cycle made by ovarian follicle, from small primordial follicles to completely differentiated preovulatory follicles. These two processes are closely related and ultimately result in a mature egg from an undifferentiated oocyte.

In the ovary, the majority of oocytes are small, immature, and never grow. At the beginning of each menstrual cycle, small groups of oocytes begin to grow and mature, but only one of them is selected for further maturation, whereas the rest are eliminated by atresia. The maturation of mammalian oocytes from primordial to antral stage is a constant process induced by LH surge, which commences a series of events, i.e.: resumption of meiosis, expansion of cumulus cells (CCs) and finally ovulation. Gonadotropin secretion, particularly follicle stimulating hormone (FSH), is crucial for the developmental capacity of the oocyte and its surrounding somatic cells.

It has been reported that gonadotropins act indirectly on the oocytes via neighboring somatic cells, which are stimulated to synthesize factors crucial for oocyte growth and maturation (4). Prior to recruitment of follicles, granulosa cells (GCs) from early-antral follicles, which form one to two layers, start to express follicular stimulating hormone receptors (FSHR). In this stage, FSH induces proliferation of GCs forming antral follicles, subsequently prevents follicular atresia, stimulates expression of LH receptors (LHR) and induces steroid hormone expression, including cytochrome P450 cholesterol side-chain cleavage (P450scc) (5). During follicle development, oocytes stay detained at prophase I of meiosis. Even during meiotic arrest, the oocyte still grows and accumulates maternal mRNA and proteins in cytoplasm, which are necessary for gaining developmental capacity (6). The cytoplasm and nucleus of an oocyte must be mature to ensure its competence for maintaining embryonic development post-fertilization. In addition to mRNA accumulation, cytoplasmic maturation also includes cellular changes i.e.: elevated lipid collection, settlement of cortical granules, glutathione aggregation, gaining of competence for sperm head penetration, chromatin decondensation and embryogenesis. On the other hand, nuclear maturation in the oocyte is connected with its ability to dissolve the germinal vesicle, chromosome condensation, first polar body discharge, and its consequent arrest at metaphase II.

The oocyte which lies inside the primordial follicle has a diameter of approximately 30 μm, and when the follicular antrum is formed, it reaches diameter of 120 μm. When the oocyte is fully grown, it is able to resume meiosis (3). There are two ways to induce meiosis resumption: *in vivo* LH surge, or oocyte removal from the cumulus mass *in vitro*. Follicle size plays a crucial role *in vivo* because it is positively associated with developmental potential. As the follicle is growing, oocytes have a higher probability for fertilization, cleavage, blastocyst formation, and implantation (3). Throughout the early antral follicular stage, the oocyte gains the ability to resume meiosis, while developmental competence is acquired during final growth stage of the antral follicle in the mouse (7), pig (8) and cow (9). Developmental capacity is defined as the oocyte's ability for maturation as well as to be fertilized and to ensure a suitable environment for subsequent embryo and fetal development (10).

The origin, morphological, and biochemical aspects of granulosa cell differentiation in vivo

Granulosa cells (GCs) play an important role during follicular proliferation, differentiation, luteinization, ovulation and atresia. During folliculogenesis GCs develop gap junctions and connect to each other and to oocytes, undergoing serious morphological and physiological changes (11). The oocyte influences GC proliferation and differentiation, while GCs stimulate oocyte maturation. This bidirectional interaction provides essential nutrients for the oocyte and ensures accumulation of secreted metabolites during oocyte

development (12).

Undifferentiated oocytes in primordial follicles are surrounded by pregranulosa cells that form a single layer. Oocytes secrete factors that stimulate growth and differentiation of GCs and regulate development of immature follicles. Over time, squamous GCs transform into a cuboidal shape and then begin to proliferate, forming primary follicles which express follistatin. During the primary follicle stage, GCs form a single layer, enveloping the immature oocyte inside. In the final phase of primary follicle stage, oocytes secrete growth/differentiation factor-9 (GDF-9) and bone morphogenetic protein 6 (BMP-6), which are necessary for proper GC proliferation, follicle maturation and ovary function. Furthermore, in addition to oocyte-derived factors, estrogen signals are necessary for proper follicular development. In GCs, estrogen signaling is mediated by estrogen receptor 2 (ESR2). It has been shown that deletion of gene coding ESR2 leads to female subfertility, reduced litters, weakened follicular development and decreased ovulation rate (13). It has been reported recently, that estrogen is essential for acquisition and maintenance of cumulus cell competence to expand in cattle (14) and mouse (15). Estrogen is also one of the crucial factors required for expression of normal levels of Has2 transcript *in vitro* (15).

GDF-9 expression increases following *in vitro* maturation, therefore it is believed that GDF-9 expression could be correlated with maturation and follicular size (16). In secondary follicle formation, GCs intensively proliferate and differentiate, finally forming two to three layers of cuboidal cells. Throughout the secondary phase, FSH stimulates expression of proliferating nuclear antigen (PCNA), steroidogenic acute regulatory protein (StAR), promotes steroid synthesis and induces LHR expression (17). FSH binds to related G-protein-coupled receptors and stimulates membrane-associated adenylyl cyclase, and consequently, the concentration of intracellular cAMP is increased. Subsequently, cAMP-dependent protein kinase A (PKA) is activated, leading to altered expression and/or phosphorylation of intracellular proteins that control GC proliferation and differentiation. Reports show that GDF-9 suppresses FSH-induced cAMP synthesis and estrogen/progesterone production. Moreover, GDF-9 promotes proliferation of GCs and decreases their differentiation rate (18). FSH induces also p38 mitogen-activated protein kinase (MAPK) and extracellular signal regulated kinases 1/2 (ERK1/2) phosphorylation through the actions of PKA (17). ERK1/2 has been reported to mediate increased PCNA expression and steroid synthesis. FSH is also responsible for the up-regulation of liver receptor homolog-1 (LRH-1), which stimulates cytochrome P450 aromatase (P450arom) activity in the testis and ovary (17) (Fig. 1).

Under stimulation of oocytes, GCs in pre-antral follicles express stem cell factor (SCF) whose receptors are expressed in oocytes and thecal-interstitial cells. SCF up-regulates expression of steroidogenic factor 1 (SF-1), StAR, and P450arom while decreasing expression of FSHR in GCs (19). In the tertiary follicles, the multi-layered GCs and a freshly formed fluid-filled cavity are easily observed under microscope. Following the tertiary stage, GCs that are present in follicles differentiate into two new cell types – mural granulosa cells (mGCs) and CCs that surround oocyte. It has been reported that for the sustaining of competence to undergo cumulus expansion, combination of estrogen and oocyte-derived GDF-9 and BMP-15 is required (15). Moreover, in a pre-ovulatory follicle, four different layers are formed i.e.: membrane granulosa, periantral, cumulus oophorus, and corona radiata. At the end of preovulatory stage, an LH surge results in major changes in GC gene expression, causing meiosis resumption and cumulus expansion. Gonadotropin–dependent expression of a number of key CC genes, i.e.: *Has2*, *Ptgs2* (also known as Cox2), *Tnfaip6* and *Ptx3* is required for synthesis and stabilization of extracellular matrix by cumulus cells, proper cumulus expansion and for subsequent ovulation. The MAPK pathway may be involved in this process as it has been reported that inhibition of MAPK activation stops resumption of meiosis stimulated by LH and leads to upregulation of *Has2* and *Ptgs2* expression (20). Normal expression of these two genes among others is required for proper cumulus expansion. GDF-9 is also involved in the regulation of cumulus expansion and promotes formation of cumulus-oocyte complexes

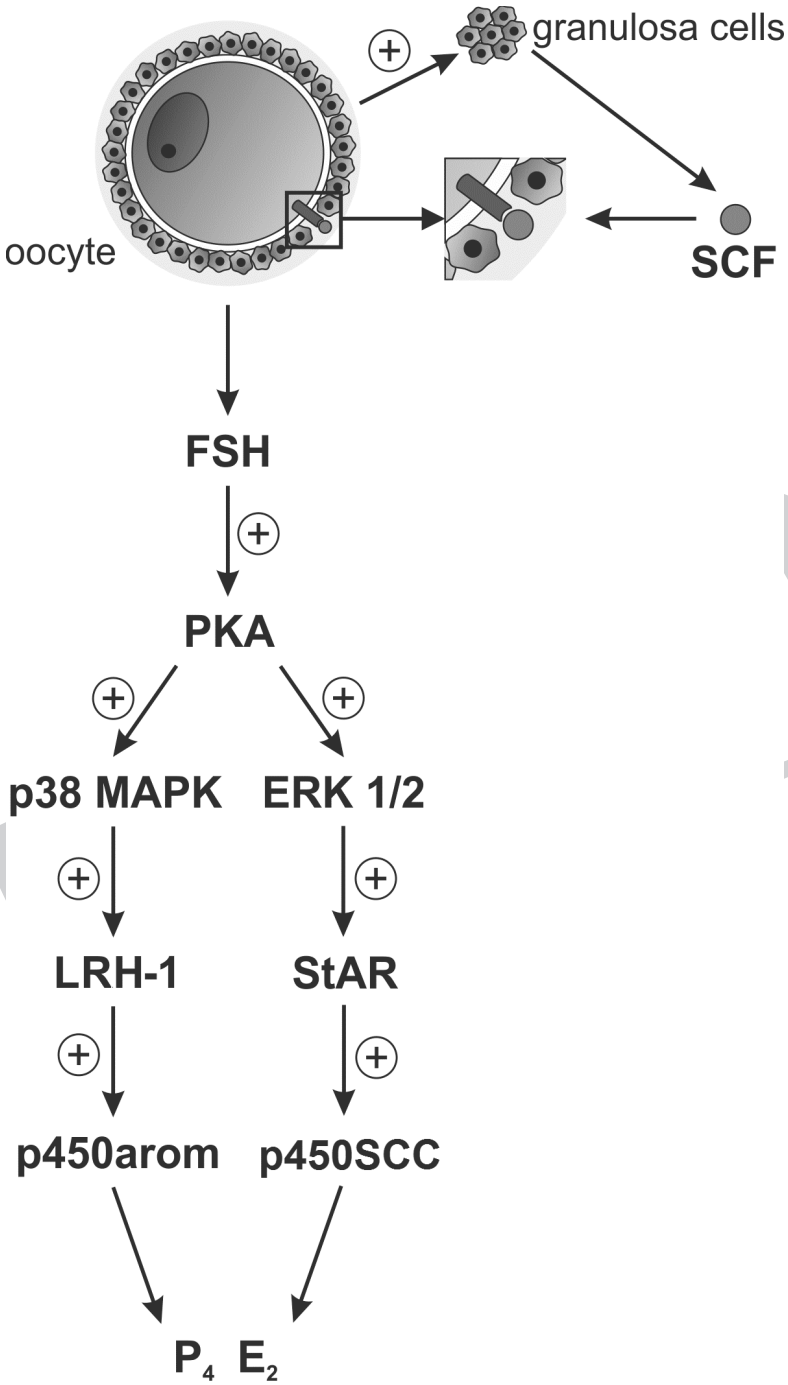

Fig. 1. *Oocyte (OC) secretes factors stimulating granulosa cells, which subsequently produce stem cell factor (SCF). SCF binds to its cognate receptor on OC membrane and increase expression of follicle stimulating hormone (FSH). FSH promotes phosphorylation of p38 mitogen-activated protein kinase (p38 MAPK) and extracellular-signal-regulated kinases 1 and 2 (ERK1/2) through protein kinase A (PKA) pathway. P38 MAPK elevates expression of liver receptor homolog-1 (LRH-1), which induces p450 aromatase (p450arom) expression in ovaries and testis. Paralelly FSH activates steroidogenic acute regulatory protein (StAR) through ERK1/2 pathway. StAR transports cholesterol from outer to inner mitochondrial membrane, where it is further processed by cholesterol side-chain cleavage enzyme (p450scc) into steroids precursors. P450arom is an enzyme responsible for aromatization of androgens into estrogens.*

(COCs). After ovulation, the rest of the follicular cells differentiates into luteal cells (LCs), which are divided into two types: large LCs formed from GCs and small LCs formed from theca cells (TCs).

The identification of GC markers – from gene expression to protein distribution

According to the relevant literature, there are several markers used to identify GCs i.e.: anti Müllerian hormone (AMH) (21), follicle regulatory protein (FRP), inhibin, melanoma cell adhesion molecule (MCAM) (22), cytochrome P450 aromatase (CYP19A1), follicle stimulating hormone receptor (FSHR), and recently discovered, mitochondria-localized glutamic acid-rich protein (MGARP), glycine dehydrogenase (GLDC), carbohydrate (N-acetylgalactosamine 4-0) sulfotransferase 8 (CHST8) and glutathione peroxidase 3 (GPX3) (23). AMH is a homodimeric disulfide-linked glycoprotein and a member of the transforming growth factor-β (TGF- β) family. AMH is also referred to as Müllerian inhibiting substance (MIS) and is involved in regression of Müllerian ducts in the male fetus during male genital tract organogenesis. AMH is expressed in Sertoli cells from the time of testicular differentiation throughout fetal life until puberty, and its secretion is tightly regulated, ensuring high expression only in males at the time when Müllerian ducts are most sensitive. In postnatal life, MIS induces mesenchymal cell differentiation into Leydig cells and stimulates androgen production (24). AMH is also expressed in female GCs from birth up to menopause stage, thus it is used as a GC marker.

Proteins that control and regulate follicle development could also be used as reliable markers. Among them, FRP seems to be reliable candidate as it is a protein secreted by GCs that affects the responsiveness of other follicles to gonadotropin stimulation, thereby inhibiting estrogen production. The influence of FRP on other cells during folliculogenesis has been widely described. Follicular fluid fractions containing FRP delay follicular maturation, and lead to extension of follicular phase and anovulation or luteal-phase dysfunction. Moreover, FRP inhibits FSH-inducible aromatase activity in porcine GCs from medium- and small-sized follicles but has no effect on estrogen secretion from large follicles. It has been reported that FRP also inhibits microsomal aromatase under *in vitro* conditions as well as 3β-hydroxysteroid dehydrogenase activity (25). FRP also alters the production and secretion of progesterone in porcine GCs. Low doses of FRP stimulate progesterone secretion, but higher doses are shown to be inhibitory.

Proteins of the TGF- β superfamily are widely expressed in oocytes and follicles as well as GCs. Inhibin, a member of the TGF- β superfamily, is a glycoprotein consisting of two subunits: an α-subunit linked by a disulfide bridge to one of two β-subunits, βA- or βB-subunit which form the inhibin A or inhibin B isoform, respectively. Inhibin is an ovarian hormone whose main endocrine function is inhibition of FSH release from the pituitary gland. It has been reported that the inhibin A isoform is most likely responsible for this repression and after an LH surge, stimulates androgen production by the TCs (26). Expression of inhibin subunit mRNA has shown that α-, βA- and βB- subunits are expressed in GC follicles, ranging from pre-antral to pre-ovulatory follicles (27). Throughout folliculogenesis, two inhibin isoforms are differentially expressed i.e.: inhibin B, which is highly expressed during early follicular phase, and inhibin A, which is upregulated during the late follicular stage when the pre-ovulatory estradiol surge occurs. Inhibin A expression varies in follicles of different size i.e.: elevated expression of inhibin A has been found in large follicles while inhibin B expression is similar in all follicles (28).

One study claimed that proteins involved in carcinogenesis could be also involved in the follicle maturation process (22). Melanoma cell adhesion molecule (MCAM) is a membrane-bound glycoprotein, and a member of the immunoglobulin superfamily. These molecules are also known as CD146, MUC18, A32 antigen, and S-Endo-1. They are composed of five Ig domains, a transmembrane domain and a cytoplasmic region. These proteins are expressed mainly by cells that make up blood vessels i.e.: smooth muscles, vascular endothelial cells, and pericytes. MCAM regulates the invasiveness of extravillous trophoblasts, thus CD146 could possibly play an important role in implantation and placentation (29). Yoshioka et al., using immunohistochemical

analysis, showed that CD146 is expressed on the human *corpus luteum* and luteinizing GCs and was not detectable in the GCs of pre-ovulatory follicles. Thus, MCAM is a cell surface marker of luteinizing GCs and the luteinization process.

Specific receptors on cell membranes could be also used as credible GC markers. FSHR is a transmembrane receptor that interacts with follicle stimulating hormone (FSH). Activation of FSHR is necessary for the hormonal activity of FSH (30), and this receptor is expressed in both ovary and testis. FSHR induces signal transduction through the activation of adenylyl cyclase by G proteins. FSH acts differently in males and females, i.e.: in females, FSH exerts its ovarian effects by inducing follicle development and regulating estrogen secretion (31).

In males, it is responsible for supporting gametogenesis by stimulation of Sertoli cells, and is responsible for seminiferous tubule integrity (32).

Estrogen synthesis genes are also targets that can be used as markers of GCs, i.e.: cytochrome P450 aromatase - an enzyme with monooxygenase activity. P450arom is a product of the CYP19 gene family and a member of cytochrome P450 superfamily (33). Aromatase is localized in the endoplasmic reticulum where it is responsible for the final steps of estrogen synthesis.

In 2015, Hatzirodos et al. discovered new potential GC markers i.e.: MGARP, GLDC, CHST8 and GPX3 (23). These genes showed relatively high expression in GCs, but their functions in the ovary are not yet characterized. There is only vestigial information regarding ovarian functions of MGARP and GLDC. It is known that GLDC sulfates N-acetylgalactosamine on LH (34), a necessary action for sex hormone synthesis. MGARP plays a role in steroidogenesis through maintenance of mitochondrial abundance and morphology; however, its potential ovarian function has only been determined by analysis of sequence similarity.

ACKNOWLEDGEMENTS

Publication of this article was made possible by grant number 2014/13/D/NZ9/04798 “SONATA” from the Polish National Centre of Science.

REFERENCES

1. Gosden RG, Bownes M. Cellular and molecular aspects of oocyte development. In: Grudzinskas JG, Yovich JL, editors. Gametes - The Oocyte. Cambridge: Cambridge Reviews in Human Reproduction; 1995. p. 23-53.
2. Pepling ME. From primordial germ cell to primordial follicle: mammalian female germ cell development. Genesis 2006; 44:622-32.
3. Eppig JJ. Regulation of mammalian oocyte maturation. In: Adashi EY, Leung PCK, editors. The Ovary. New York: Raven; 1993. p. 185-207.
4. Gilchrist RB, Ritter LJ, Armstrong DT. Oocyte-somatic cell interactions during follicle development in mammals. Anim Reprod Sci 2004; 82-83:431-46.
5. Sasson R, Rimon E, Dantes A, et al. Gonadotrophin-induced gene regulation in human granulosa cells obtained from IVF patients. Modulation of steroidogenic genes, cytoskeletal genes and genes coding for apoptotic signalling and protein kinases. Mol Hum Reprod 2004; 10:299-311.
6. Adriaens I, Cortvrindt R, Smitz J. Differential FSH exposure in preantral follicle culture has marked effects on folliculogenesis and oocyte developmental competence. Hum Reprod 2004; 19:398-408.
7. Pesty A, Broca O, Poirot C, Lefevre B. The role of PLC beta 1 in the control of oocyte meiosis during folliculogenesis. Reprod Sci 2008; 15:661-72.
8. Wu D, Cheung QC, Wen L, Li J. A growth-maturation system that enhances the meiotic and developmental competence of porcine oocytes isolated from small follicles. Biol Reprod 2006; 75:547-54.
9. Lodde V, Modina S, Maddox-Hyttel P, Franciosi F, Lauria A, Luciano AM. Oocyte morphology and transcriptional silencing in relation to chromatin remodeling during the final phases of bovine oocyte growth. Mol Reprod Dev 2008; 75:915-24.
10. Preis KA, Seidel GE, Jr., Gardner DK. Reduced oxygen concentration improves the developmental competence of mouse oocytes following in vitro maturation. Mol Reprod Dev 2007; 74:893-903.
11. Mora JM, Fenwick MA, Castle L, et al. Characterization and significance of adhesion and junction-related proteins in mouse ovarian follicles. Biol Reprod 2012; 86:153, 1-14.

12. Su YQ, Sugiura K, Eppig JJ. Mouse oocyte control of granulosa cell development and function: paracrine regulation of cumulus cell metabolism. Semin Reprod Med 2009; 27:32-42.
13. Krege JH, Hodgin JB, Couse JF, et al. Generation and reproductive phenotypes of mice lacking estrogen receptor beta. Proc Natl Acad Sci U S A 1998; 95:15677-82.
14. Rovani MT, Gasperin BG, Ilha GF, et al. Expression and molecular consequences of inhibition of estrogen receptors in granulosa cells of bovine follicles. J Ovarian Res 2014; 7:96.
15. Sugiura K, Su YQ, Li Q, Wigglesworth K, Matzuk MM, Eppig JJ. Estrogen promotes the development of mouse cumulus cells in coordination with oocyte-derived GDF9 and BMP15. Mol Endocrinol 2010; 24:2303-14.
16. Jackowska M, Kempisty B, Wozna M, et al. Differential expression of GDF9, TGFB1, TGFB2 and TGFB3 in porcine oocytes isolated from follicles of different size before and after culture in vitro. Acta Vet Hung 2013; 61:99-115.
17. Yu FQ, Han CS, Yang W, Jin X, Hu ZY, Liu YX. Role of ERK1/2 in FSH induced PCNA expression and steroidogenesis in granulosa cells. Front Biosci 2005; 10:896-904.
18. Vitt UA, Hayashi M, Klein C, Hsueh AJ. Growth differentiation factor-9 stimulates proliferation but suppresses the follicle-stimulating hormone-induced differentiation of cultured granulosa cells from small antral and preovulatory rat follicles. Biol Reprod 2000; 62:370-77.
19. Jin X, Han CS, Zhang XS, et al. Stem cell factor modulates the expression of steroidogenesis related proteins and FSHR during ovarian follicular development. Front Biosci 2005; 10:1573-80.
20. Su YQ, Denegre JM, Wigglesworth K, Pendola FL, O'Brien MJ, Eppig JJ. Oocyte-dependent activation of mitogen-activated protein kinase (ERK1/2) in cumulus cells is required for the maturation of the mouse oocyte-cumulus cell complex. Dev Biol 2003; 263:126-38.
21. Rey R, Sabourin JC, Venara M, et al. Anti-Mullerian hormone is a specific marker of sertoli- and granulosa-cell origin in gonadal tumors. Hum Pathol 2000; 31:1202-8.
22. Yoshioka S, Fujiwara H, Higuchi T, Yamada S, Maeda M, Fujii S. Melanoma cell adhesion molecule (MCAM/CD146) is expressed on human luteinizing granulosa cells: enhancement of its expression by hCG, interleukin-1 and tumour necrosis factor-alpha. Mol Hum Reprod 2003; 9:311-19.
23. Hatzirodos N, Hummitzsch K, Irving-Rodgers HF, Rodgers RJ. Transcriptome comparisons identify new cell markers for theca interna and granulosa cells from small and large antral ovarian follicles. PLoS One 2015; 10:e0119800.
24. Racine C, Rey R, Forest MG, et al. Receptors for anti-mullerian hormone on Leydig cells are responsible for its effects on steroidogenesis and cell differentiation. Proc Natl Acad Sci U S A 1998; 95:594-99.
25. Chicz RM, Nakamura RM, Goebelsmann U, et al. Follicle regulatory protein noncompetitively inhibits microsomal 3 beta-hydroxysteroid dehydrogenase activity. J Steroid Biochem 1985; 23:663-68.
26. Hillier SG, Yong EL, Illingworth PJ, Baird DT, Schwall RH, Mason AJ. Effect of recombinant inhibin on androgen synthesis in cultured human thecal cells. Mol Cell Endocrinol 1991; 75:R1-6.
27. Jaatinen TA, Penttila TL, Kaipia A, Ekfors T, Parvinen M, Toppari J. Expression of inhibin alpha, beta A and beta B messenger ribonucleic acids in the normal human ovary and in polycystic ovarian syndrome. J Endocrinol 1994; 143:127-37.
28. Kempisty B, Jackowska M, Wozna M, et al. Expression and cellular distribution of INHA and INHB before and after in vitro cultivation of porcine oocytes isolated from follicles of different size. J Biomed Biotechnol 2012; 2012:742829.
29. Shih I, Wang T, Wu T, Kurman RJ, Gearhart JD. Expression of Mel-CAM in implantation site intermediate trophoblastic cell line, IST-1, limits its migration on uterine smooth muscle cells. J Cell Sci 1998; 11(Pt 17):2655-64.
30. Kempisty B, Ziolkowska A, Ciesiolka S, et al. Association between the expression of LHR, FSHR and CYP19 genes, cellular distribution of encoded proteins and proliferation of porcine granulosa cells in real-time. J Biol Regul Homeost Agents 2014; 28:419-31.
31. Simoni M, Gromoll J, Nieschlag E. The follicle-stimulating hormone receptor: biochemistry, molecular bi-

ology, physiology, and pathophysiology. Endocr Rev 1997; 18:739-73.

32. Asatiani K, Gromoll J, Eckardstein SV, Zitzmann M, Nieschlag E, Simoni M. Distribution and function of FSH receptor genetic variants in normal men. Andrologia 2002; 34:172-76.
33. Nelson DR, Kamataki T, Waxman DJ, et al. The P450 superfamily: update on new sequences, gene mapping, accession numbers, early trivial names of enzymes, and nomenclature. DNA Cell Biol 1993; 12:1-51.
34. Xia G, Evers MR, Kang HG, Schachner M, Baenziger JU. Molecular cloning and expression of the pituitary glycoprotein hormone N-acetylgalactosamine-4-O-sulfotransferase . J Biol Chem 2000; 275:38402-9.

EDITORIAL

MICROFLUIDIC VERSUS MOLECULAR ASSAYS - DIFFERENT APPROACHES IN ASSESSING OOCYTE DEVELOPMENTAL COMPETENCE

W. KRANC[1], A. CHACHULA[2], J. BUDNA[1], K. WOJTANOWICZ-MARKIEWICZ[2,3], A. BRYJA[1], S. CIESIÓLKA[2], H. PIOTROWSKA[4], M. JESETA[5], P. ANTOSIK[3], D. BUKOWSKA[3], K.P. BRÜSSOW[3], M. BRUSKA[1], M. NOWICKI[2], M. ZABEL[2,6] and B. KEMPISTY[1,2]

[1]Department of Anatomy, Poznań University of Medical Science, Poznań, Poland; [2]Department of Histology and Embryology, Poznań University of Medical Science, Poznań, Poland; [3]Institute of Veterinary, Poznań University of Life Science, Poznań, Poland; [4]Department of Toxicology, Poznań University of Medical Sciences, Poznań, Poland; [5]Center of Assisted Reproduction, Department of Obstetrics and Gynecology, University Hospital Brno, Czech Republic; [6]Department of Histology and Embryology, Wroclaw Medical University, Wroclaw, Poland

Received November 11, 2015 – Accepted June 8, 2016

The first two authors equally contribute to the work

In recent years, molecular techniques have brought about new solutions that focus on the developmental capacity of female oocytes and reproductive performance in the mammalian species. The developmental potency is the ability of oocytes to reach the MII stage following the long stages of folliculo- and oogenesis. The main proteins involved in this process belong to the connexin (Cx) family, which are responsible for the formation of gap junction (GJC) connections between the female gamete and surrounding somatic cells. The Cx are involved in bi-directional transport of small molecules and are therefore responsible for correct oocyte-somatic cell nutrition, proliferation, and differentiation. However, the application of certain molecular techniques often leads to destabilization or destruction of the materials of interest, such as cells or whole tissues. Therefore, the applications of microfluidic methods, which are non-invasive and quantitative, give new opportunities to further this area of biomedical research. Microfluidic research is based on real-time experiments that allow for control and/or observation of the results during each step. The purpose of this review is to present both positive and negative aspects of molecular-microfluidic methods while describing the role of connexins in oocyte developmental capacity.

Microfluidics are constructed using the nano- and microtechnology production of miniaturized devices consisting of micro-channels and chambers that allow for real-time fluid flow. Technology based on microfluidics is often rooted in the assessment of physical properties of analyzed fluid and/or cells. Therefore, this technology is often applied in the pharmaceutical and chemical industries in order to assess physical and biological properties of fluids and/or cells, as well as for controlled drug delivery

Key words: oocyte, connexins, microfluidic analyses, developmental capacity

Mailing address:
Dr Bartosz Kempisty, Department of Anatomy
Department of Histology and Embryology,
Poznań University of Medical Science,
6 Święcickiego St., 60-781 Poznań, Poland
Tel.: +48 61 8546455 -Fax: +48 61 8546440
e-mail: bkempisty@ump.edu.pl

0393-974X (2016)

DISCLOSURE: ALL AUTHORS REPORT NO CONFLICTS OF INTEREST RELEVANT TO THIS ARTICLE.

and drug discovery. Based on their construction, microfluidic chips are characterized by their small size (ergonomics), minimal power consumption, and their ability to be controlled by one operator. The rapid development of microfluidic technology has led to the replacement of whole laboratory devices with one single chip that is able to carry out several chemical, biochemical, and/or biological reactions at the same time. Microfluidic chips are also utilized in biochemical catalysis as well as in real-time, controlled reactions where fluids flow permanently though the chip. Therefore, this provides several reactions on a nano-and/or micro scale. However, this "new age technology" that is a feature of "miniaturized world" has been recently used as a target in reproductive biology. In the recent past, several studies have presented the possible application of this technology in assessment of the developmental capacity of male and female gametes (1). Additionally, microfluidics has been used as a major instrument used to discern these biological processes in several species of mammals and other animal models e.g. *Xenopus laevis*.

Typically, reproductive biology research is based on the light microscopic observation of gamete morphology, one of the few non-invasive methods. When analysis is based on protein expression and/or protein distribution within the cell, fluorescence or confocal microscopy require destruction of the cell with no possibility of further use. Moreover, molecular biology assays analyzing RNA or protein expression using mammalian oocytes and/or spermatozoa also destroy the investigated pool of cells. Although molecular genetic methods are most informative, both parametric and quantitative, there is no possibility for these cells to be used further in applications such as *in vitro* cultivation (IVC), fertilization (IVF), or embryo production (IVP). Therefore, the use of microfluidic technology, which is parametric, quantitative, and non-invasive, now has increased significance for reproductive biologists.

The developmental competence of mammalian oocytes is determined by several factors: the oocyte's ability to mature *in vitro* (IVM) by reaching the MII stage; its ability to successfully undergo monospermic fertilization; the formation of zygotes (maternal zygote-transition, MZT); the activation of the embryonic genome (EGA); and its ability to achieve the periimplantation stage of growth and development (2). Therefore, the application of microfluidics in the assessment of these stages of oocyte/embryo development and further use of these cells in assays is of great significance. As shown in our previous studies, the microfluidic chip use for developmental capacity assessment in porcine and bovine oocytes/embryos is non-invasive, suggesting that recently used biological material may be successfully used for additional molecular assays (3). The connection of microfluidics and molecular assays is therefore more informative compared to the use of these technologies separately.

Application of microfluidic technology in developmental competence assessment

Recently, it has been shown that microfluidic technology may be applied in reproductive research (4, 5) Several studies are related to oocyte developmental capacity and/or embryonic survival during *in vitro* procedures. Other studies identify spermatozoa potential and cell functionality during fertilization. Although microfluidics is, in most cases, associated with analysis of a single cell, it may also be used in the examination of processes such as real-time oocyte maturation, *in vitro* oocyte fertilization, and *in vitro* embryonic development.

The "point of control" is one feature that characterizes microfluidic assays, being related to real-time monitoring of processes which take place in one chip. It has been shown that these chips may be used in a controlled substance influx and/or efflux during real-time processing on the chip. Therefore, microfluidics can be widely applied in molecular endocrinology research, so that an analysis of controlled hormone flow and cell parameter responses is possible. The monitored substance flow is used in microfluidic *in vitro* research to closely mimic the *in vivo* condition.

In addition to microfluidics based on real-time controlled substance delivery, there are other possibilities that can use this technology in the study of reproductive biology, including microspectroscopic

assays. This method is based on single oocyte/embryo absorbance analysis, where the chip consists of influx/efflux channels, a measurement chamber, and two microfibers. In these assays, the physical properties of single cell are correlated with several biological features such as oocyte/embryo morphology, follicle size, and the developmental capacity of oocytes. In addition, there was investigated developmental capacity of porcine oocytes from two types of ovarian follicles: medium and large by using microspectroscopic assays (3). They found that class I oocytes collected from large follicles displayed an increased probability of successful fertilization compared to class II oocytes. Following assay completion, the differential normalized intensity (DNI) was analyzed in the spectrum of investigated porcine oocytes. It was observed that absorbance intensity at 560 nm was associated with the class of oocytes and morphological classified gametes. The authors concluded that the shift in maximum transition was correlated with follicular quality of the recovered porcine oocytes, and this parametric and objective microfluidic based measurement may be an alternative method to standard morphological classification procedures.

In another study, the association between the four-grade morphological classification scheme for cattle oocytes and the spectral Lab-on-chip methodology was investigated (6). They analyzed porcine oocytes isolated from three different class of follicles: small, medium and large. Results showed that DNI for class I bovine oocytes was significantly increased when compared to class II, III and IV. The absorbance peak of intensity was 581 nm, 584 nm, 585 nm, and 587 nm for class I, II, III, and IV, respectively. In the case of the porcine oocyte assay, the local minimum and maximum was investigated. In all size groups, 10 oocytes were analyzed. Significant differences in optical spectra were found, with shifts of the minimum and maximum among oocytes. Moreover, the absorbance intensity point at 620 nm was highly correlated with the quality of analyzed oocyte as well as with the position of local maximum.

Similarly, Walczak et al. analyzed bovine oocytes which were divided into a four-graded morphological criteria according to cumulus cells oophorus (7). They assayed DNI in relation to local minima and maxima for oocytes in each group. They concluded that a positive association existed between the physical properties of oocytes and their biological feature-morphological characterization. It was suggested that Lab-on-Chip assessment of oocyte quality may be used following mammalian *in vitro* fertilization as an objective selection of gametes which have been characterized with proper morphology.

Molecular markers of mammalian oocytes and cumulus cell developmental competence

The developmental competence of mammalian oocytes, also known as developmental potential, is recognized as the ability of female gametes to reach maturation (MII stage) as well as successful monospermic fertilization. Proper oocyte development during folliculo-and oogenesis further determines normal zygote formation, the ability of the embryo to reach the blastocyst stage, and implantation and birth of healthy offspring. These unique steps in oocyte differentiation to implantation are regulated by several intrinsic (specific for gamete genomics) and extrinsic factors, including the transduction of maternal-endometrial signals that influence implantation site recognition (8). The global gene expression profile programs the proper functioning of these specific processes, such as nuclear and cytoplasmic maturation. They also regulate the maternal effect on embryonic growth, maternal-zygote transition (MZT), and embryonic genome activation (EGA), all of which occur during species-specific stages of embryonic development.

The ability of the oocyte to reach developmental competence is associated with several morphological, molecular, and cellular changes that occur inside the cells, further influencing gamete differentiation and development (9). Published data has shown there are several molecular markers of oocyte developmental competence determination. The most important included connexins (the most important of which are Cx37, Cx43 and Cx45) that form gap junction connections between surrounding cumulus cells and oocytes (10). Cumulus cells are responsible for transferring small molecules into

oocytes as well as the gene encoding proteins that influence correct monospermic fertilization, such as the zona pellucida glycoproteins (ZP) and integrins (11, 12).

Role of connexins in mammalian oocyte developmental competence assessment

The role of gap junctions in follicular cell proliferation and differentiation has been well established using various mammalian models. However, little is known about the influence of connexin expression and regulation during oocyte developmental competence acquisition. Expression of Cx31 and Cx43 varies in various stages of oocyte development as well as in follicles of different sizes (13). The expression of Cx31 did not vary between follicle types and/or phases of follicular waves. However, Cx43 mRNA was significantly higher in oocytes collected from medium and small follicles at the growth/stagnation phase compared to those isolated at the dominance/regression stage. This important finding suggests that Cx43 mRNA expression may be used as a marker of developmental competence in oocytes and embryos since higher Cx43 gene expression was observed in embryos produced from oocytes of increased developmental competence.

The role of cumulus cells (CC) in the acquisition of oocyte developmental and/or maturational competence is well known (14); In recent years, the effect of adenosine 3', 5'-monophosphate (cAMP) on the cross-talk between CC and oocytes in relation to developmental competence acquisition was described.. It has been shown that cAMP regulates the protein structure formation of GJ and influences the ability of COCs to reach full maturational competition. These results confirm previously presented data that suggest Cx43 may a useful marker in determining COC developmental competence (15). It is well known that more bovine embryos develop to the blastocyst stage *in vivo* than *in vitro*, a phenomena associated with decreased developmental competence of *in vitro* oocytes (16). The proper course of maturation is required for achieving the MII stage after long stages of nuclear and cytoplasmic maturation. Although many bovine oocytes undergo spontaneous nuclear maturation, little is known regarding the factors that regulate cytoplasmic maturation. A research was conducted on the effect of exogenous stimulation with FSH and/or LH on CC expansion, fertilization outcome, and the embryo development ratio in bovines (17). Looking at RQ-PCR data from FSH receptor (FSHr), LH receptor (LHr) and Cx43 in CC, they observed a significant increase in CC expansion after supplementation with porcine FSH in serum-free media. It has been suggested that expression of FSHr, LHr, and Cx43 may be used as a predictor of bovine CC expansion and/or maturation ability. Furthermore, the FSHr and Cx43 mRNA may be recognized as a markers of oocyte developmental competence.

It has been reported that serum and bovine serum albumin (BSA) have influence on Cx31 and Cx43 expression (18). The addition of serum into culture tended to increase the mRNA level encoding Cx31, although these results were not statistically significant. Contrarily, the expression of Cx43 was lower in the embryos cultured in the presence of serum. It may be suggested that the post-fertilization modification of culture media (presence or absence of serum) may influence the developmental competition of growing embryos as well as determine whether embryos will achieve the blastocyst stage. Moreover, these results demonstrated that serum significantly changed the expression of cell-cell cross talk genes (Cx31 and Cx43), which may stimulate or inhibit the growth and development of oocytes, which influences the competition of developing embryos. During long stages of oocyte development that occur during folliculo-and oogenesis, maternally-derived transcripts are stored as a specific maternal template which can be used post-fertilization during embryo growth. The stability of these transcripts is regulated by the existence of regulatory elements of the poly(A) tail at the 3' end of mRNA. In addition, it has been shown that different polyadenylation status of genes is important for developmental competition of mammalian oocytes and may significantly influence the potential of embryos to grow and develop. In addition, Brevini et al. investigated the polyadenylation status of several transcripts i.e.: Cx32 and Cx43 (19). In their experiments,

they analyzed oocytes at the germinal vesicle (GV) stage, at the end of IVM, at the end of IVF, and at the time of the first embryo cleavage division. The polyadenylation of Cx43 was characterized by a gradual reduction status whereas, in the case of Cx32, it was a gradual elongation. These results indicated that the polyadenylation status of investigated transcripts was correlated with the quality of bovine oocytes/embryos, and it was also shown that different polyadenylation patterns may contribute to increased oocyte/embryo developmental competence.

CONCLUSIONS

Studies have shown that molecular assays used in developmental competence assessment bring results precisely and quickly. However, these molecular methods are invasive and often lead to destruction of the analyzed tissue or cell. Although molecular analysis e.g. gene expression assays, give us precise, quantitative results, experiments must be repeated which does not always give similar final results. On the other hand, microfluidics opens a new era of biomedical research, which can be observed in real-time with "step-by-step" observation of experiments. More importantly, it does so without destruction or destabilization of the cultivated environment. Therefore, microfluidics brings forth new possibilities for its application in biomedicine. However, attention must still be paid to the fact that the best way to solve some experimental problems is through the application of both microfluidic and molecular assays.

ACKNOWLEDGEMENTS

This study was made possible by grant number 2014/13/D/NZ9/04798 "SONATA" from the Polish National Centre of Science.

REFERENCES

1. Kempisty B, Walczak R, Antosik P, et al. Microfluidic method of pig oocyte quality assessment in relation to different follicular size based on lab-on-chip technology. Biomed Res Int 2014; 2014:467063.
2. Trounson A, Anderiesz C, Jones G. Maturation of human oocytes in vitro and their developmental competence. Reproduction 2001; 121:51-75.
3. Śniadek P, Walczak R, Dziuban J, Jackowska M, Antosik P, Jaśkowski JM, Kempisty B. Lab-on-a-chip for quality classification of pig oocytes. Opt Appl 2011; 41:417-22.
4. Smith GD, Swain JE, Bormann CL. Microfluidics for gametes, embryos, and embryonic stem cells. Semin Reprod Med 2011; 29:5-14.
5. Knowlton SM, Sadasivam M, Tasoglu S. Microfluidics for sperm research. Trends Biotechnol 2015; 33:221-29.
6. Szczepańska P, Walczak R, Dziuban J, et al. Ocena jakościowa komórek rozrodczych zwierząt hodowlanych z wykorzystaniem mikrocytometru typu lab-chip. Elektronika 2010; 51:93-96.
7. Walczak R, Szczepańska P, Dziuban J, et al. Lab-on a-chip for developmental competence assessment of bovine oocytes. Elektronika 2010; 51:30-33.
8. Hennet ML, Combelles CM. The antral follicle: a microenvironment for oocyte differentiation. Int J Dev Biol 2012; 56:819-31.
9. Kidder GM, Vanderhyden BC. Bidirectional communication between oocytes and follicle cells: ensuring oocyte developmental competence. Can J Physiol Pharmacol 2010; 88:399-413.
10. Antosik P, Kempisty B, Jackowska M, et al. Assessment of transcript and protein levels contributing to cell cycle control and gap junction connections in morphologically variable groups of porcine cumulus-oocyte complexes. Vet Med (Praha) 2010; 55:512-21.
11. Jackowska M, Kempisty B, Antosik P, et al. The morphology of porcine oocytes is associated with zona pellucida glycoprotein transcript contents. Reprod Biol 2009; 9:79-85.
12. Kempisty B, Antosik P, Bukowska D, Jackowska M, Lianeri M, Jaskowski JM, Jagodzinski PP. Assessment of zona pellucida glycoprotein and integrin transcript contents in porcine oocytes. Reprod Biol 2009; 9:71-78.
13. Nemcova L, Machatkova M, Hanzalova K, Horakova J, Kanka J. Gene expression in bovine embryos derived from oocytes with different developmental competence collected at the defined follicular developmental stage. Theriogenology 2006; 65:1254-64.

14. Bunel A, Nivet AL, Blondin P, Vigneault C, Richard FJ, Sirard MA. Cumulus cell gene expression associated with pre-ovulatory acquisition of developmental competence in bovine oocytes. Reprod Fertil Dev 2014; 26:855-65.
15. Modina S, Luciano AM, Vassena R, Baraldi-Scesi L, Lauria A, Gandolfi F. Oocyte developmental competence after in vitro maturation depends on the persistence of cumulus-oocyte comunications which are linked to the intracellular concentration of cAMP. Ital J Anat Embryol 2001; 106:241-48.
16. Rizos D, Ward F, Duffy P, Boland MP, Lonergan P. Consequences of bovine oocyte maturation, fertilization or early embryo development in vitro versus in vivo: implications for blastocyst yield and blastocyst quality. Mol Reprod Dev 2002; 61:234-48.
17. Calder MD, Caveney AN, Smith LC, Watson AJ. Responsiveness of bovine cumulus-oocyte-complexes (COC) to porcine and recombinant human FSH, and the effect of COC quality on gonadotropin receptor and Cx43 marker gene mRNAs during maturation in vitro. Reprod Biol Endocrinol 2003; 1:14.
18. Rizos D, Gutierrez-Adan A, Perez-Garnelo S, De La Fuente J, Boland MP, Lonergan P. Bovine embryo culture in the presence or absence of serum: implications for blastocyst development, cryotolerance, and messenger RNA expression. Biol Reprod 2003; 68:236-43.
19. Brevini TA, Lonergan P, Cillo F, Francisci C, Favetta LA, Fair T, Gandolfi F. Evolution of mRNA polyadenylation between oocyte maturation and first embryonic cleavage in cattle and its relation with developmental competence. Mol Reprod Dev 2002; 63:510-17.

EDITORIAL

EXTRACORPOREAL SHOCK WAVES: PERSPECTIVES IN MALIGNANT TUMOR TREATMENT

R. FRAIRIA[1], L. BERTA[2] and M.G. CATALANO[1]

[1]Department of Medical Sciences University of Turin, Turin, Italy; [2]Med & Sport 2000 Srl, Turin, Italy

Received December 9, 2015 – Accepted June 9, 2016

Progress in basic research led to the design of new generations of anticancer drugs with some notable achievements. Over the years, more and more powerful drugs have been developed with the purpose of increasing the rate of response to therapy. As molecular power of chemotherapeutic agents increased, unfortunately also toxicity and undesired side-effects increased. The search for new therapeutic strategies to be used in the management of cancer is one of the more promising strategies to reduce chemotherapy toxicity. Extracorporeal Shock Waves (ESW), widely used for the treatment of urolithiasis, have been reported to cause modifications of cell growth both *in vitro* and *in vivo*. They exert an agonist cytotoxic effect with several chemotherapeutic agents, such as cisplatin, doxorubicin, bleomycin, paclitaxel. Moreover, as it has been reported that their main mechanism of action is an increase in cell membrane permeability, ESW are also used to deliver oligonucleotides and other small particles to cells. Recently, it was found that certain dye compounds, in particular porphyrins, can achieve a cytopathogenic effect when the disease site is subjected to ultrasound irradiation. This technique is referred to as sonodynamic therapy. Based on the new knowledge regarding the interaction between ultrasound with bulk liquid, several studies have shown a synergic effect of ESW and porphyrins *in vitro*, thus opening a new perspective in sonodynamic therapy, able to overcome some drawbacks encountered during conventional anticancer drug treatment. Finally, current advances in bioengineering encouraged the application of nano-scale technologies to medicine. Nanobubbles, composed of an external shell and a gas core, can deliver chemotropic drugs and porfirins, to target tumour tissues in response to physical triggers, and ESW features make them an ideal alternative to ultrasound in combination with drug-loaded nanobubbles in delivery strategies.

The mainstream of non-invasive therapies for treating solid tumors is chemotherapy**.** Taking into account that a crucial prerequisite for any cancer therapy is that the benefits of killing cancer cells outweigh deleterious side effects, it is admitted that any chemotherapy scheme is limited by both sub-optimal specificity for cancer cells and the probability to induce suppression of the host anti-cancer immunity. Over the years, more and more powerful drugs have been developed to increase the rate of response to therapy. As molecular power of chemotherapeutic agents increased, unfortunately also toxicity and undesired side-effects increased. Therefore, the search for new therapeutic programs to be used in the management of cancer, such as innovative methods to deliver drugs to cancer cells, immunotherapy and gene therapy, in addition to the development of new pharmaceutical molecules, is one of the more promising strategies to reduce chemotherapy toxicity.

Key words: extracorporeal shock waves, ESW, tumor treatment, oncology, sonodynamic therapy

Mailing address:
Roberto Frairia, M.D.
Department of Medical Sciences
University of Turin, Via Genova 3,
10126 Torino, Italy
Tel.: +39 0116705391 - Fax: +39 0116705366
e-mail: roberto.frairia@unito.it

0393-974X (2016)

DISCLOSURE: ALL AUTHORS REPORT NO CONFLICTS OF INTEREST RELEVANT TO THIS ARTICLE.

Extracorporeal shock waves

Extracorporeal Shock Waves (ESW) are high-energy acoustic waves produced by a generator through the conversion of electrical energy to mechanical energy. They propagate in water medium and are characterized by a definite shape with an initial positive, very rapid part of high amplitude, followed, after a few microseconds, by a sudden phase of mild negative pressure, before returning to the basic values. There are three main techniques through which ESW are generated. These are the electrohydraulic, electromagnetic, and piezoelectric principles, each of which represents a different technique of generating the shock wave (1, 2).

There are two basic effects of ESW: the primary effect is the direct generation of mechanical forces that result in the maximal pulse energy concentrated at the point where treatment is to be provided; and the secondary effect is the indirect generation of mechanical forces by cavitation which may cause damage to the tissues (1-3).

Shockwaves have been used in medicine for many years, particularly in extracorporeal lithotripsy (ESWL), which uses focused shockwaves to treat non-invasively patients with stone diseases (mostly, urinary stones) (1, 2). The excellent results achieved by ESWL stimulated research on the application of focused shockwaves in other branches of medicine. Recent progress in antitumor target therapy and delivery systems triggered by physical forces reinforces the use of ESW as a new tool to be used in anticancer delivery strategies. The present review highlights the different anticancer strategies using ESW: the cytocidal effect of ESW alone or in combination with chemotherapy drugs; sonodynamic therapy; ESW-aided gene transfer; nanotechnologies (Table I).

Cytocidal effect of ESW alone or in combination with chemotherapy drugs

Cell membranes, which have a thickness of a few molecular layers, are subjected to extremely high pressure gradients at the transit of ESW. For this reason, in the late 80s - early 90s, some authors considered exposing a spatially limited region of the body to a potentially destructive form of mechanical

Table I. *Different anticancer strategies using combination therapy with ESW.*

Anticancer Strategies	Drugs	Models	References
Cytocidal effect of ESW	-	*In vitro* *In vivo*	4, 6, 7, 13 10, 11
ESW and chemotherapic drugs	mitomycin C; cisplatin; methotrexate; adriamycin; paclitaxel; daunorubicin; bleomycin; 5-fluouracil	*In vitro* *In vivo*	8, 9, 15, 22 16, 17
Sonodynamic Therapy	5'-aminolevulinic acid (ALA)	*In vitro* *In vivo*	23, 24 27-29
Gene Transfer	DNA plasmids; interleukin-12	*In vitro* *In vivo*	43, 44 39, 44
Nanoparticles	doxorubicin; meso-tetrakis (4-sulfonatophenyl) porphyrin (TPPS)	*In vitro* *In vivo*	32 35, 36

energy. They hypothesized to take advantage of the cytotoxic/cytocidal effect of ESW, until then exclusively used for the treatment of urolithiasis, which could be regarded as an important additional support in cancer treatment. Appropriate *in vitro* and *in vivo* studies showed that ESW could cause only temporary growth delay. Nevertheless, considerable morphological changes at the cellular level were observed, including effects on plasma membrane, mitochondria, cytoplasm and nucleus (4-6). These damaging effects could sensitize tumor cells to most cytotoxic agents. Further studies (7-8) suggested that cell membrane permeabilization is the most prominent alteration induced by essentially sublethal doses of High Energy Extracorporeal Shock Waves (HESW). In respect to the potential side effects of ESW treatments, permeabilizing ESW energies were observed to induce cell mortality in a dose-dependent manner (9). Thus, concurrent treatment regimens with ESW and hydrophilic drugs looked promising, since ESW can locally render tissue more susceptible to the drug with the prospect of reduced systemic toxicity. ESW were reported to cause modifications of cell growth both *in vitro* and *in vivo* (5, 10). Zhou and Guo (11) observed, in nude rats, that high energy ESW treatment was able to delay tumor growth and reduce tumor size, without evidence of metastasis.

A substantial difficulty in comparing the results obtained by different Authors is due to the large heterogeneity of mechanical, biological and analytical variables in each experimental procedure. *In vitro* studies have shown that ESW treatment elicits immediate reduction of cell viability and ability to form colonies (5). Different sensitivities to ESW of different cell lines have been described by Brummer et al. (12). Moreover, the impact of ESW on cell survival varies not only with the cell type, but also between cell lines of the same type (13); it was hypothesized that cells in G_2-M phase cell cycle can be more easily damaged by ESW as compared to cells in G_0.

With regard to the mechanism by which ESW cause cellular damage, numerous hypotheses have been proposed. Based on the fact that cells did not show any damage when immobilized in agar, Brummer et al. (14) suggested that the collision between cells could play a role in changing their viability; it was subsequently proven that viability was not influenced by varying cell concentration (13). A possible role was also suggested of free radicals that are generated by Shock Waves in inducing cellular damage. Currently, the best hypothesis on the mechanism of cell damage elicited by shock waves is that of cavitation and the generation of jet streams in the extracellular milieu. The cells that survive after ESW exposure are still able to form tumors when inoculated into animal models, but these tumors are smaller than in controls (ESW-untreated) since a significant percentage (40 to 60%) of surviving cells that were inoculated showed sublethal-induced damage (5).

Numerous studies have shown that the combined treatment of tumor cells in suspension with some anticancer agents and ESW elicits a significant enhancement of drug cytotoxic effect (15, 16). It was noted that Shock Waves, when applied to cells *in vitro*, determine (even at low energy) a transient increase in cell membrane permeability by opening pores, allowing higher concentrations of drug to enter the cells (17, 18). This effect is similar to that obtained through the technique of electroporation, as direct access to the cytoplasm was also gained by high voltage electric pulses. Electroporation was shown to enhance the action of bleomycin and has been clinically applied to subcutaneous tumor nodules (19). It has to be pointed out that a major problem of electrochemotherapy is that the electrodes have to be in close local contact over the whole tumor surface. This prohibits its use in internal organs. ESW can, in contrast, be directly administered to internal organs such as the liver or the gut, and no surgical intervention is necessary.

Cells of human estrogen-dependent breast cancer (MCF-7) were sensitive to combined treatment with ESW and paclitaxel, an antimicrotubule agent, active against a variety of solid tumors (9). The suppression of cell proliferation induced by shock waves has been related to an apoptotic mechanism (16). Apoptosis, i.e. programmed cell death, is a cellular self-destruction mechanism which plays a key role in the surveillance against tumors (20). Induction of apoptosis occurs in response to a variety of stress

signals (21) which may include shock waves (16).

Recent studies have shown the cytotoxic action enhanced by shock waves in combination with some anticancer drugs *in vitro*: cell lines of human osteosarcoma (22), human colorectal adenocarcinoma (23) and human anaplastic thyroid cancer (24) were subjected to combined treatment (ESW and anticancer drugs). Combined exposure to anticancer drugs and shock waves resulted in a significant enhancement of cytotoxicity and induction of apoptosis in cancer cells.

Sonodynamic/photodynamic properties of ESW

In the work by Catalano et al. (24) an innovative "sonodynamic/photodynamic" technique was adopted, based on the ability of ESW to activate and render cytotoxic a photosensitizing substance: the natural porphyrin precursor 5-aminolevulinic acid (ALA), which is accumulated selectively by neoplastic cells.

In normal cells, protoporphyrin IX (PPIX), a substance with excellent photosensitizing properties, does not accumulate to a great extent because it is quickly transformed to heme by the action of ferrochelatase. In cancer cells, however, PPIX accumulates due to a defective heme biosynthesis, as a consequence of abnormal levels of some enzymes involved in this pathway. Increased activity of porphobilinogen deaminase and/or decreased activity of ferrochelatase have been reported for a number of tumors. Exogenous application of ALA can lead to a pronounced accumulation of PPIX in tumor tissue, and subsequent irradiation with the light of wave lengths (corresponding to the PPIX absorption bands) can lead to specific destruction of tumor cells. Photodynamic therapy (PDT) has developed as an important new clinical cancer treatment modality in the past 25 years, but the low penetration depth of light through the skin and tissues has limited PDT to the treatment of superficial, endoscopically reachable tumors. The main assumption regarding "sonodynamic" therapy is that it generates ultrasound energy which produces sonoluminescence to excite the protoporphyrin derivative by energy transfer. HESW induce acoustic cavitation, which results in a concentration of energy sufficient to generate a sonoluminescence emission able to cause electronic excitation of porphyrins and initiate a photochemical process, resulting in the formation of cytotoxic singlet oxygen (25). The mechanisms underlying this effect were explained on the basis of a double basic effect elicited by HESW treatment: the direct generation of mechanical forces (non-inertial cavitation) and the indirect generation of mechanical forces by cavitation (inertial cavitation). Non-inertial cavitation bubbles oscillate and cause streaming of the surrounding liquid and mechanical stress. Inertial cavitation is an extremely violent process of bubble activity that may generate highly reactive hydroxyl radicals. The subsequent energy transfer to oxygen can generate the highly reactive singlet molecular oxygen (25). This combination between inertial and non-inertial cavitation, generated by a piezoelectric shockwave device, was confirmed by Canaparo et al. (23), who observed that combined ALA-high energy ESW treatment produced significant inhibition of HT-29 (human colorectal carcinoma) cell growth. Non-inertial as well as inertial cavitation was seen to induce apoptosis as well as to inhibit cell growth by increasing the G_0/G_1 population through the intracellular activation of protoporphyrin IX.

Sonodynamic therapy (SDT) is an analogous approach to PDT based on the synergistic effect of ultrasound and chemical compound referred to as "sonosensitizer", but the attractive feature of this modality for cancer treatment emerges from the ability to focus the ultrasound energy on malignancy sites placed deeply in tissues. The ESW source can be placed on direct contact with the body and the maximum energy flow given to the inner part of the tumor can be precisely controlled. Nonetheless, at transition sites between tissues with different acoustic impedance values, there may be focal mechanical destruction, probably through the induction of cavitation and shearing stress caused by the reflected waves (26). This technique has proven to be effective *in vivo*, by inducing necrosis and apoptosis of breast cancer and colon cancer implanted in laboratory animals (27, 28).

More recently, the anticancer effect of SDT using ESW-activated protoporphyrin IX cytoxicyty on a syngeneic rat breast cancer model was confirmed

by magnetic resonance imaging (MRI). The SDT-treated group showed a significant decrease in MRI tumor size measurements 72 hours after treatment with the PPIX precursor ALA and ESW (29).

Nano-scale technology and ESW

The current advances in material science and bioengineering encouraged the application of nano-scale technologies to medicine; nanocarriers (or nano-encapsulation systems) have been introduced as promising vehicles in drug delivery. In such systems, drugs and bio-active agents are wrapped in or adsorbed on the surface of nanoparticles in order to achieve safe and effective drug delivery and gene therapy (30). When compared to traditional delivery systems, nanocarriers used in chemotherapy have higher therapeutic efficiency at low dosage and can accumulate preferentially in the desired locations due to the defective vascular architecture of most solid tumors. This enables the nanocarriers circulating in the blood to be entrapped inside the leaky vessels of the tumor, thus slowly releasing their contents. In recent years, a wide range of nanoparticles (NPs) have been employed as drug-delivery carriers for cancer therapy. NPs can carry loaded drugs to the tumor site through the blood stream taking advantage of the enhanced permeability and retention effect, due to the defective vascular architecture of the tumor tissue (31). Currently, growing attention in the field of nanomedicine is being given to micro- and nanobubbles (NBs). NBs, composed of an external shell and a gas core, can deliver diverse molecules, such as DNA and drugs, to target tissues in response to physical triggers, such as ultrasound. Based on their features, ESW may be considered an ideal alternative to ultrasound in combination with drug-loaded NBs in delivery strategies. We recently demonstrated that combining new doxorubicin-loaded glycol chitosan NBs and ESW enhanced doxorubicin anti-tumor activity in anaplastic thyroid cancer cell lines, by increasing intracellular drug release (32).

Moreover, nanoparticles may enhance the sonodynamic therapy response by playing different roles: if properly engineered, the sonosensitizer agent loaded onto NPs can pass more readily across the cell membrane, reaching its critical intracellular target. It has been demonstrated that sonosensitizers loaded onto NPs are more readily taken up by cells in respect to the free drug (41). Moreover, NPs are able not only to function as a sonosensitizer per se, but also as energy transducers (33). The synthetic water-soluble TPPS [meso-tetrakis (4-sulfonatophenyl) porphyrin] has been widely investigated as a photosensitizer because of its high tumor tissue affinity and retention rate, as well as a remarkable quantum yield of singlet oxygen formation in solution (34).

Quite recently, an innovative sonosensitizing system using ESW and a new formulation of nanoparticles [poly-methyl methacrylate core-shell nanoparticles (NPs)] loaded with TPPS was described (35). The sonodynamic treatment with nanoparticles loaded with porphyrin derivative (TPPS-NPs) and ESW was investigated with regard to the cytotoxic effect on the human neuroblastoma cell line, SH-SY5Y. Single cell treatments, such as exposure to ESW alone or TPPS alone, had no effect on SH-SY5Y cell proliferation. Indeed, the combined treatment with TPPS-NPs and ESW showed a statistically significant decrease in SH-SY5Y cell proliferation. This new sonosensitizing system significantly decreased cancer cell growth after ESW exposure, even in a three-dimensional model of neuroblastoma, suggesting its potential further application in sonodynamic anticancer therapy (35, 36).

Cancer gene therapy and ESW-aided gene transfer

Cancer gene therapy has made important progress. One established immunotherapy approach involves enhancement of the immune response against cancer through the augmentation of natural cytokines. These proteins can either be repeatedly injected or produced by plasmid DNA transfer and protein expression in cells of the tumor or host animal. Immunogenic therapy using pIL-12 has shown promise in some immunogenic mouse tumor models (37). However, systemic application is problematic, since effective doses of IL-12 are toxic to the animal. The search for new delivery methods therefore remains of great interest, particularly for established tumors. Physical methods for membrane permeation, along with their ability to promote cell transfection, may overcome

the barriers of gene transfer using non-viral vectors. These methods include electroporation, direct injection, biolistic particle delivery, laser irradiation, magnetic nanoparticles and acoustic cavitation. Because of their adaptability to *in vivo* purposes (easy to use, minimal effects on normal physiology), electroporation and acoustic cavitation seem to be the most promising techniques for gene therapy application. In particular, the utility of acoustic cavitation for cell permeation and transfection has been illustrated in different cell types, both *in vitro* and *in vivo* (38, 39).

In the last decade, some studies showed that shock waves can support transfection, i.e. the transfer of therapeutic genes to targets by temporarily increasing cell membrane permeability: DNA - or fragments, such as plasmids - can enter the cell (18, 37, 38, 40). The combination of shock waves and DNA cationization for cell transfection was explored on an *in vitro* model of suspended cells and green fluorescent protein (GFP) reporter-containing plasmid DNA (41). In terms of percentages of transfected cells, the efficiencies found were comparable to those reported by other acoustic cavitation-based approaches (42).

ESW-aided gene transfer has been associated with many advantages in cancer gene therapy: i) localization of DNA transfer to the tumor; ii) cavitation-induced cell killing resulting in tumor ablation, and, iii) the avoidance of antigenic responses associated with virus-based DNA delivery methods (43, 44). Recently, a synergistic approach was described using ultrasound and nanoparticles to deliver plasmid DNA to cancer cells, achieving really high transfection efficiency and enhancing the antitumor effect (45). With regard to shock waves, the use of the latter has lately been confirmed to permeabilize human cells and promote transfection with both cationic lipid-assembled and naked DNA (41).

Advantages, limitations and concluding remarks

The studies described above suggest that shock waves are a promising anticancer strategy for *in vivo* application since tissues located at different depths in the body can be readily targeted by extracorporeal treatment, with minimal histopathological damage. The ESW generator can be easily placed in contact with a water-based gel on the skin and ESW can be focused at the tumor site, thus potentially permitting to target tumor lesions. Finally, unlike ultrasound, ESW do have not heating effects. This could be an advantage for *in vivo* application since temperature elevation is difficult to control spatially and temporally, especially in large tumors with heterogeneous vascularization. Unfortunately, the biggest limitation in the use of ESW in cancer therapy is that, given the huge amount of pre-clinical data, solid clinical trials are missing. In fact, to date, only one "old" case report combined ESW and chemotherapy to treat metastasis of prostate cancer in the iliac muscle (46), and, very recently, long-term effectiveness of ESW was demonstrated for the treatment of lymphedema in patients with breast cancer (47).

Nevertheless, based on their multifaceted properties, the use of ESW in oncology looks promising. In fact: i) ESW act as an "ultrasound-susceptibility modifying agent" since they may induce cell permeabilization, thus allowing better delivery of chemotherapeutic drugs into cytosol; ii) shock waves enhance both the cytotoxic activities of photosensitizers and the apoptotic signal transduction pathway - they can act as a further tool in "sonodynamic/photodynamic" therapy; iii) gene transfer can be induced by ESW treatment *in vivo*, particularly with enhanced acoustic cavitation, which supports the concept that "Gene and ESW therapy might be advantageously merged"; iv) other treatment schedules are worth exploring to evaluate the potential utility of ESW in cancer therapy, especially in combination with other modalities.

REFERENCES

1. Wang CJ. An overview of shock wave therapy in musculoskeletal disorders. Chang Gung Med J 2003; 26:220-32.
2. Coleman AJ, Saunders JE. A review of the physical properties and biological effects of the high amplitude acoustic fields used in extracorporeal lithotripsy, Ultrasonics 1993; 31:75-89.
3. Delius M, Draenert K, Draenert Y, et al. Effects of

extracorporeal shock waves on bone: A review of shock wave experiments and the mechanism of shock wave action. In Siebert W, Buch M (eds). Extracorporeal shock waves in Orthopaedics. Springer Verlag Berlin 1997; 91-107.
4. Russo P, Mies C, Huryk R, Heston WDW, Fair WR. Histopathologic and ultrastructural correlates of tumor growth suppression by high energy shock waves. J Urol 1987; 137:338-41.
5. Randazzo RF, Chaussy GC, Fuchs GJ, Bhuta SM, Lovrekovich H, De Kernion JB. The in vitro and in vivo effects of extracorporeal shock waves on malignant cells. Urol Res 1988; 16:419-26.
6. Bräuner T, Brümmer F, Hülsĕr DF. Histopathology of shock wave treated tumor cell suspensions and multicell tumor spheroids. Ultrasound Med Biol 1989; 1:451-60.
7. Wörle K, Steinbach P, Hofstadter F. The combined effects of high-energy shock waves and cytostatic drugs or cytokines on human bladder cancer cells. Br J Cancer 1994; 69:58-65.
8. Rahman M. *In vitro* effects of high energy shock wave alone and combined with anticancer drugs on human bladder cancer cells. Urol Int 1994; 53:12-17.
9. Frairia R, Catalano MG, Fortunati N, Fazzari A, Raineri M, Berta L. High energy shock waves (HESW) enhance paclitaxel cytotoxicity in MCF-7 cells. Breast Cancer Res Treat 2003; 81:11-19.
10. Huber PE, Debus J. Tumor cytotoxicity in vivo and radical formation in vitro depend on the shock wave-induced cavitation dose. Radiat Res 2001; 156:301-9.
11. Zhou L, Guo Y. In vivo effect of high energy shock waves on growth and metastasis of the heterografted tumors of nude mice. Chin Med J (Engl). 1996; 109:157-61.
12. Brümmer F, Suhr D, Hülser DF. Sensitivity of normal and malignant cells to shock waves. J Stone Dis 1992; 4:243-48.
13. van Dongen JW, van Steenbrugge GJ, Romijn JC, Schröder FH. The cytocidal effect of high energy shock waves on human prostatic tumor cell lines. Eur J Cancer Clin Oncol 1989; 25:1173-79.
14. Brummer F, Brenner J, Bräuner T, Hülser DF. Effect of shock waves on suspended and immobilized L1210 cells. Ultrasound Med Biol 1989; 15:229-39.
15. Gambihler S, Delius M. In vitro effects of lithotripter shock waves and cytotoxic drugs. Br J Cancer 1992; 66:69-73.
16. Kato M, Ioritani N, Suzuki T, Kambe M, Inaba Y, Watanabe R, Sasano H, Orikasa S. Mechanism of anti-tumor effect of combination of bleomycin and shock waves. Jpn J Cancer Res 2000; 91:1065-72.
17. Delius M, Adams G. Shock wave permeabilization with ribosome inactivating proteins: a new approach to tumor therapy. Cancer Res 1999; 59:5227-32.
18. Kodama T, Doukas AG, Hamblin MR. Shock wave-mediated molecular delivery into cells. Biochim Biophys Acta 2002; 1542:186-94.
19. Dev SB, Hofmann GA. Electrochemotherapy: a novel method of cancer treatment. Cancer Treat Rev 1994; 20:105-15.
20. Steller H. Mechanism and genes of cellular suicide. Science 1995; 267:1445-49.
21. Ashush H, Rozenszajn LA, Blass M, Barda-Saad M, Azimov D, Radnay J, Zipori D, Rosenschein U. Apoptosis induction of human myeloid leukaemia cells by ultrasound exposure. Cancer Res 2000; 60:1014-20.
22. Palmero A, Berger M, Venturi C, et al. High energy shock waves enhance the cytotoxic effect of doxorubicin and methotrexate to human osteosarcoma cell lines. Oncol Rep 2006; 15:267-73.
23. Canaparo R, Serpe L, Catalano MG, Bosco O, Zara GP, Berta L, Frairia R. High energy shock waves (HESW) for sonodynamic therapy: effects on HT-29 human colon cancer cells. Anticancer Res 2006; 26:3337-42.
24. Catalano MG, Costantino L, Fortunati N, Bosco O, Pugliese M, Boccuzzi G, Berta L, Frairia R. High energy shock waves activate 5'-aminolevulinic Acid and increase permeability to Paclitaxel: antitumor effects of a new combined treatment on anaplastic thyroid cancer cells. Thyroid 2007; 17:91-99.
25. Rosenthal I, Sostaric JZ, Riesz P. Sonodynamic therapy-a review of the synergistic effects of drugs and ultrasound. Ultrason Sonochem 2004; 11:349-63.
26. Kato K, Fujimura M, Nakagawa A, Saito A, Ohki T, Takayama K, Tominaga T. Pressure-dependent effect of shock waves on rat brain: induction of neuronal apoptosis mediated by a caspase-dependent pathway. J Neurosurg 2007; 106:667-76.
27. Serpe L, Canaparo R, Berta L, Bargoni A, Zara

GP, Frairia R. High energy shock waves and 5-aminolevulinic for sonodynamic therapy: effects in a syngeneic model of colon cancer. Technol Cancer Res Treat 2011; 10:85-93.
28. Canaparo R, Serpe L, Zara GP, Chiarle R, Berta L, Frairia R. High energy shock waves (HESW) increase paclitaxel efficacy in a syngeneic model of breast cancer. Technol Cancer Res Treat 2008; 7:117-24.
29. Foglietta F, Canaparo R, Francovich A, Arena F, Civera S, Cravotto G, Frairia R, Serpe L. Sonodynamic treatment as an innovative bimodal anticancer approach: shock wave mediated tumor growth inhibition in a syngeneic breast cancer model. Discov Med 2015; 110:197-205.
30. Ahmed SE, Martins AM, Husseini GA The use of ultrasound to release chemotherapeutic drugs from micelles and liposomes. J Drug Target 2015; 23:16-42.
31. Maeda H. Tumor-selective delivery of macromolecular drugs via the EPR effect: background and future prospects. Bioconjug Chem 2010; 21:797-802.
32. Marano F, Argenziano M, Frairia R, et al. Doxorubicin-loaded nanobubbles combined with extracorporeal shock waves: basis for a new drug delivery tool in anaplastic thyroid cancer. Thyroid 2016; 26:705-16.
33. Serpe L, Foglietta F, Canaparo R. Nanosonotechnology: the next challenge in cancer sonodynamic therapy. Nanotechnol Rev 2012; 1:173-82.
34. Binder S, Kolarova H, Tomankova K, Bajgar R, Daskova A, Mosinger J. Phototoxic effect of TPPS4 and MgTPPS4 on DNA fragmentation of HeLa cells. Toxicol In Vitro 2011; 25:1169-72.
35. Canaparo R, Varchi G, Ballestri M, et al. Polymeric nanoparticles enhance the sonodynamic activity of meso-tetrakis (4-sulfonatophenyl) porphyrin in an in vitro neuroblastoma model. Int J Nanomedicine 2013; 8:4247-63
36. Varchi G, Foglietta F, Canaparo R, et al. Engineered porphyrin loaded core-shell nanoparticles for selective sonodynamic anticancer treatment. Nanomedicine (Lond) 2015; 10:3483-94.
37. Arca MJ, Krauss JC, Stome SE, Cameron MJ, Chang AE. Diverse manifestations of tumorigenicity and immunogenicity displayed by the poorly immunogenic B16-BL6 melanoma transduced with cytokine genes. Cancer Immunol Immunother 1996; 42:327-45.
38. Tschoep K, Hartmann G, Jox R, et al. Shock waves: a novel method for cytoplasmic delivery of antisense nucleotides. J Mol Med 2001; 79:306-23.
39. Miller DL, Song J. Lithotripter shock waves with cavitation nucleation agents produce tumor growth reduction and gene transfer in vivo. Ultrasound Med Biol 2002; 28:1343-48.
40. Juffermans LJ, Meijering BD, Henning RH, Deelman LE. Ultrasound and microbubble-targeted delivery of small interfering RNA into primary endothelial cells is more effective than delivery of plasmid DNA. Ultrasound Med Biol 2014; 40:532-40.
41. Millán-Chiu B, Camacho G, Varela-Echavarría A, Tamariz E, Fernández F, López-Marín LM, Loske AM. Shock waves and DNA-cationic lipid assemblies: a synergistic approach to express exogenous genes in human cells. Ultrasound Med Biol 2014; 40:1599-608.
42. Bekeredjian R, Bohris C, Hansen A, Katus HA, Kuecherer HF, Hardt SE. Impact of microbubbles on shock wave-mediated DNA uptake in cells in vitro. Ultrasound Med Biol 2007; 33:743-50.
43. Song,J, Tata D, Li L, Bao S, Miller DL. Combined shock-wave and immunogen therapy of mouse melanoma and renal carcinoma tumors. Ultrasound Med Biol 2002; 28:957-64.
44. Berger M, Frairia R, Piacibello W, Sanavio F, Palmero A, Venturi C, Pignochino Y, Berta L, Madon E, Aglietta M, Fagioli F. Feasibility of cord blood stem cell manipulation with high-energy shock waves: an in vitro and in vivo study. Exp Hematol 2005; 33:1371-87.
45. Zhou QL, Chen ZY, Wang YX, Yang F, Lin Y, Liao YY. Ultrasound-Mediated Local Drug and Gene Delivery Using Nanocarriers. Biomed Res Int 2014; Published online 2014 August 17. 2014:963891
46. Hoshi S, Orikasa S, Suzuki K, Saitoh T, Takahashi T, Yoshikawa K, Kuwahara M, Nose M. High-energy underwater shock wave treatment for internal iliac muscle metastasis of prostatic cancer: a first clinical trial. Jpn J Cancer Res 1995; 86:424-28.
47. Cebicci MA, Sutbeyaz ST, Goksu SS, Hocaoglu S, Oguz A, Atilabey A. Extracorporeal Shock wave therapy for breast cancer-related lymphedema: a pilot study. Arch Phys Med Rehabil 2016; (Epub ahead of print)

EDITORIAL

ENOX2 (or tNOX): A NEW AND OLD MOLECULE WITH CANCER ACTIVITY INVOLVED IN TUMOR PREVENTION AND THERAPY

G. RONCONI[1], G. LESSIANI[2], E. SPINAS[3], S.K. KRITAS[4], Al. CARAFFA[5], A. SAGGINI[6], P. ANTINOLFI[7], J. PIZZICANNELLA[8], E. TONIATO[9] and P. CONTI[10]

[1]UOS Clinica dei Pazienti del Territorio, Policlinico Gemelli, Roma, Italy; [2]Center of Intensive Rehabilitation, "S. Agnese", Pineto (TE), Italy; [3]Department of Surgery and Odontostomatological Sciences, University of Cagliari, Italy; [4]Department of Microbiology and Infectious Diseases, School of Veterinary Medicine, Aristotle University of Thessaloniki, Macedonia, Greece; [5]Pharmacology,University of Perugia, Perugia, Italy; [6]Department of Dermatology, University of Rome Tor Vergata, Rome, Italy; [7]Orthopedics Department, University Hospital, Perugia, Italy; [8]University of Chieti, Chieti, Italy; [9]Department of Medical, Oral and Biological Sciences, University of Chieti, Chieti, Italy; [10]Immunology Division, Postgraduate Medical School, University of Chieti-Pescara, Chieti, Italy

Received April 28, 2016 - Accepted July 15, 2016

Cancer includes a number of related diseases due to abnormal cell proliferation that spreads to nearby tissues. Many compounds (physical, chemical and biological) have been used to try to halt this abnormal proliferation, but the therapeutic results are poor, due also to the side effects. It has been reported that ecto-nicotinamide adenine dinucleotide oxidase di-sulfide-thiol exchanger 2 (ENOX2), also known as tumor-associated nicotinamide adenine dinucleotide oxidase (tNOX), was found to be located on the cancer cell surface, essential for cancer cell growth. Capsaicin and other anti-oxidants are capable of inhibiting tNOX, causing apoptosis of cells, exerting anti-tumor activity. It is interesting that some authors reported that ENOX2 is present in the serum of cancer patients several years before the clinical symptoms of the tumor. However, this result has to be confirmed. In this article we discuss ENOX2 and its inhibition as a hope of improving cancer therapy.

Cancer arises from uncontrolled cell proliferation and is one of the major health problems worldwide. The growth and development of abnormal cells provoke morbidity and mortality in people with cancer, which is often incurable. Malignant tumor cells proliferate, invade the host tissues and metastasize (1-2).

Pathological phenomena, such as immune suppression, chronic inflammation angiogenesis, remodeling of the extra-cellular matrix (ECM) and hypoxia, promote tumor growth and its propagation (3). The spreading of cancer damages local tissues, initiating an anti-tumor immune response (4-5). The immune cells (lymphocytes, macrophages, granulocytes and mast cells) release important and effective compounds against the tumor cells (Fig. 1). However, mast cells recruited by tumor-derived chemoattractants, such as MCP-1, RANTES and SCF, can selectively secrete molecules beneficial to the tumor; on the other hand they produce cytokines (IL-1,TNF, IL-4, IL-6) detrimental to the tumor (6).

Key words:ENOX2, cancer, tumor, tumor immunology, mast cells

Mailing address:
Dr Pio Conti,
Affiliated Professor, Molecular Immunopharmacology and Drug Discovery Laboratory, Tufts University, Boston, MA 02111, USA;
Professor of Immunology, Post Graduate School of Medicine,
University of Chieti-Pescara, Viale Unità d'Italia, 73, 66100 Chieti, Italy
e-mail: pconti@unich.it

0393-974X (2016)

To date, in the medical literature a high number of articles have shown that thousands of compounds possess antitumor activity, including capsaicin. Studies on capsaicin resulted cytotoxic in several cancer cells by suppressing STAT activation, degradation of Fas-associated factor 1, inducing the generation of reactive oxygen species (ROS), up-regulation of p53, p21 and BAX (which is predominantly localized in the cytosol and is a pro-apoptotic regulatory cell compound playing an important role in cellular homeostasis and pathological cell death) (7-8). The antiproliferative and chemotherapeutic agents may lead to apoptosis.

Theoharides et al. previously reported that anti-oxidants, such as capsaicin, a component of chili peppers, inhibit trigeminal nerve stimulation dura mast cells (9), release sensory neuropeptide, is effective in relief and prevention of migraine headaches, improves digestion, helps to prevent heart disease, and lowers blood cholesterol and blood pressure levels. It is also a therapeutic agent, since in several studies it has been shown to possess anti-growth activity against various cancer cell lines (10). These findings may have implications for the pathophysiology and possible therapy of inflammatory disorders, autoimmunity and cancer. However, the role of capsaicin in cancer research remains controversial and therefore to be clarified (11).

Ecto-Nicotinamide Adenine Dinucleotide Oxidase Di-sulfide-Thiol Exchanger 2 (ENOX2), also known as Tumor-Associated Nicotinamide Adenine Dinucleotide Oxidase (tNOX), was found to be located in cell surface (12). tNOX/ENOX2 derived from a family of growth-related NADH (or hydroquinone) oxidases was purified from pooled cancer patient sera about 20 years ago; it can be inhibited by capsaicin, phenoxodiol and the major green tea catechin (−)-epigallocatechin-3-gallate (EGCg) which exert an anticancer cell growth activity (12).

As it was found that capsaicin, an anti-oxidant compound, is capable of blocking the tNOX, it is likely that other anti-oxidants exert anti-tumor activity by working on the inhibition of tNOX (13) which is

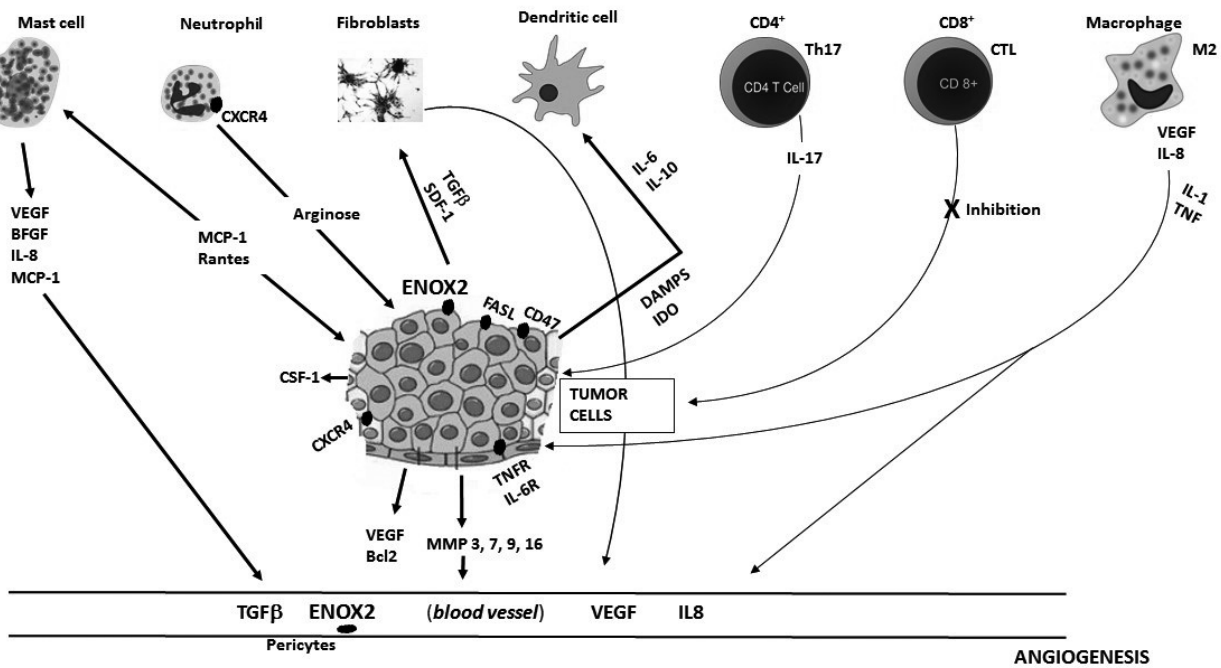

Fig. 1. *Partial schematic representation of the relationship between the immune system and tumor microenvironment. Bcl2: B cell lymphoma 2; CSF1: colony stimulating factor-1; CXCR: chemokine CXC receptor; DAMPS: damage-associated molecular patterns; ENOX 2: ecto-nicotinamide adenine dinucleotide oxidase di-sulfide-thiol exchanger 2; IDO: indoleamine 2,3 dioxygenase; IL: interleukin; MCP: monocytechemotactic protein; MMP: matrix metalloproteinases; RANTES: regulated on activation, normal T cell expressed and secreted; SDF-1 stromal cell-derived factor-1; TGFβ: transforming growth factorβ; VEGF: vascular endothelial growth factor; VEGF: vascular endothelial growth factor*

essential for cancer cell growth; while the inhibitory action exerted by the phenoxodiol on ENOX2 occurs by altering cytosolic NADH levels, leading to cytotoxic cells.

Research suggests that ENOX2 may have a role in tumor cells and not in normal adult cells, while it can also be present in embryonic cells (14). ENOX, a growth-related protein of the external cell surface, is present in both non-cancer and cancer cells but is translated only in cancer cells. The ENOX proteins function as oxidase and are present on the plasma membrane of cancer cells as an ectoenzyme, found in sera of human cancer patients and therefore circulating in plasma and identified in various cancer cell lines (15). ENOX2 is inhibited by some anti-cancer compounds including quinine and, as previously described, can be altered by capsaicin (16).

The ENOx proteins have protein disulfide-thiol interchange and hydroquinone (NADH) oxidase activities designated as ENOx tumor-associated NADH oxidase and have been identified in cancer cells. Moreover, ENOX2 expression was found to be very important for an early diagnosis of cancer development, but it also has a role in cellular growth, aging and neurodegenerative diseases (17).

ENOX2 is a specific protein cancer cell surface associated with protein disulfide-thiol and NADH oxidase activity. ENOX2 is later silenced in mature cells but reappears in cancer cells. Moreover, ENOX is a novel cancer-specific and growth-related cell-surface protein originally designed to understand the anti-tumor activity phenomenon of polyphenols, and in particular of green tea (18).

ENOX2 can also cause apoptosis in cancer cell lines by some inhibitors which enhance the levels of cytosolic NADH (15, 19). The ENOx proteins oxidize NADPH and serve for the transport of electrons in the plasma membrane. Unlike ENOx 1, mRNA ENOx 2 is produced by both tumor and non-tumor cells but not translated (15).

Patients suffering from cancer diseases present a high amount of ENOX2, both at the protein and mRNA levels. Several authors have investigated the developmental expression of tumor-associated ENOX2 and its inhibitors (20).

It is not clear why increased NADH levels resulting from ENOX2 inhibition result in decreased prosurvival sphingosine-1-phosphate and increased proapoptotic ceramide, both of which may be important in the initiation of the ENOX2 inhibitor-induced apoptotic cascade. This shows that an increase in NADH levels due to ENOX2 leads to an inhibition of sphingosine-1-phosphate and to an increase of ceramide, both involved in apoptosis (21). Therefore, ENOX2 can be included in the list of apoptosis-inducing agents targeting cancer cells.

It has been reported that capsaicin induces significant cytotoxicity on some target cell lines with an increase in oxidative stress, PARP cleavage, and apoptosis (22). This effect was associated with down-regulation of tumor-associated NADH oxidase (tNOX) mRNA and protein. Infected cells can also lead to the generation of ENOX2 (23), which can be associated to cellular distress.

ENOX2 is ubiquitous in all cancer cells and is associated with malignant cells, and for this is defined a marker of malignancy. Thus, the inhibition of Enox may be an anti-cancer target for inhibitors of quinonons, as for example the poliphenols. In fact, we previously reported that polyphenols and vitamins (24) have an anti-inflammatory and anti-cancer activity.

Recently, an interesting article reported that ENOX2 may be present in the serum of patients 4-10 years before clinical symptoms of the tumor develop (15). This very early diagnosis would allow for action against early tumor mass, as it has been seen that early detection leads to a reduction in mortality and a potential improvement of cancer patient outcomes. As also mentioned by the authors, these studies need to be confirmed on a larger scale and by other authors, given the importance of the results that could represent a big step towards the fight against tumor diseases. Moreover, we do not know whether ENOX2 is the only element involved in the development of malignant tumors or other unknown factors contribute to this phenomenon.

REFERENCES

1. Woo SR, Corrales L, Gajewski TF. Innate immune recognition of cancer. Annu Rev Immunol 2015; 33:445-74.

2. Olender J, Nowakowska-Zajdel E, Kruszniewska-Rajs C, et al. Epigenetic silencing of endothelin-3 in colorectal cancer. Int J Immunopathol Pharmacol 2016; 29(2):333-40.
3. Mellor AL, Munn DH. Immunology at the maternal-fetal interface: lessons for T cell tolerance and suppression. Annu Rev Immunol 2000; 18:367-91. Review.
4. Taniguchi M, Harada M, Kojo S, Nakayama T, Wakao H. The regulatory role of Valpha14 NKT cells in innate and acquired immune response. Annu Rev Immunol 2003; 21:483-513.
5. Chen SL, Cai SR, Zhang XH, et al. Expression of CD4+CD25+ regulatory T cells and Foxp3 in peripheral blood of patients with gastric carcinoma. J Biol Regul Homeost Agents 2016; 30(1):197-204.
6. Theoharides TC, Conti P. Mast cells: the Jekyll and Hyde of tumor growth. Trends Immunol 2004; 25(5):235-41. Review.
7. Jiang Z, Gorenstein NM, Morré DM, Morré DJ. Molecular cloning and characterization of a candidate human growth-related and time-keeping constitutive cell surface hydroquinone (NADH) oxidase. Biochemistry 2008; 47(52):14028-38.
8. Huang Jian-An. New insights into the anti-PD-L1 and anti-PD-1 reagents in cancer therapy. Eur J Inflamm 2016; 14:61-65; doi:10.1177/1721727X15626423.
9. Dimitriadou V, Buzzi MG, Moskowitz MA, Theoharides TC. Trigeminal sensory fiber stimulation induces morphological changes reflecting secretion in rat dura mater mast cells. Neuroscience 1991; 44(1):97-112.
10. Evangelista S. Novel therapeutics in the field of capsaicin and pain. Expert Rev Clin Pharmacol 2015; 8(4):373-75.
11. Liu NC, Hsieh PF, Hsieh MK, Zeng ZM, Cheng HL, Liao JW, Chueh PJ. Capsaicin-mediated tNOX (ENOX2) up-regulation enhances cell proliferation and migration in vitro and in vivo. J Agric Food Chem 2012; 60(10):2758-65.
12. Morr´e DJ, Morr´e DM. Cell surface NADH oxidases (ECTO-NOX proteins) with roles in cancer, cellular time-keeping, growth, aging and neurodegenerative diseases. Free Radical Res 2003; 37:795-808.
13. Lin MH, Lee YH, Cheng HL, Chen HY, Jhuang FH, Chueh PJ. capsaicin inhibits multiple bladder cancer cell phenotypes by inhibiting tumor-associated NADH Oxidase (tNOX) and Sirtuin1 (SIRT1). Molecules 2016; 21(7).
14. Cheng HL, Lee YH, Yuan TM, Chen SW, Chueh PJ. Update on a tumor-associated NADH oxidase in gastric cancer cell growth. World J Gastroenterol 2016; 22(10):2900-5.
15. Su YC, Lin YH, Zeng ZM, Shao KN, Chueh PJ. Chemotherapeutic agents enhance cell migration and epithelial-to-mesenchymal transition through transient up-regulation of tNOX (ENOX2) protein. Biochim Biophys Acta 2012; 1820(11):1744-52.
16. Wang HM, Chueh PJ, Chang SP, Yang CL, Shao KN. Effect of Ccapsaicin on tNOX (ENOX2) protein expression in stomach cancer cells. Biofactors 2008; 34(3):209-17.
17. Morré DJ, Hostetler B, Taggart DJ, Morré DM, Musk AW, Robinson BW, Creaney J. ENOX2-based early detection (ONCOblot) of asbestos-induced malignant mesothelioma 4-10 years in advance of clinical symptoms. Clin Proteomics 2016; 13:2.
18. Yagiz K, Snyder PW, Morré DJ, Morré DM. Cell size increased in tissues from transgenic mice overexpressing a cell surface growth-related and cancer-specific hydroquinone oxidase, tNOX, with protein disulfide-thiol interchange activity. J Cell Biochem 2008; 105(6):1437-42.
19. Sun MM, Li JF, Guo LL, et al. TGF-β1 suppression of microRNA-450b-5p expression: a novel mechanism for blocking myogenic differentiation of rhabdomyosarcoma. Oncogene 2014; 33(16):2075-86.
20. Cho N, Morré DJ. Early developmental expression of a normally tumor-associated and drug-inhibited cell surface-located NADH oxidase (ENOX2) in non-cancer cells. Cancer Immunol Immunother 2009; 58(4):547-52.
21. Wu LY, De Luca T, Watanabe T, Morré DM, Morré DJ. Metabolite modulation of HeLa cell response to ENOX2 inhibitors EGCG and phenoxodiol. Biochim Biophys Acta 2011; 1810(8):784-9.
22. Wang HM, Chuang SM, Su YC, Li YH, Chueh PJ. Down-regulation of tumor-associated NADH oxidase, tNOX (ENOX2), enhances capsaicin-induced inhibition of gastric cancer cell growth. Cell Biochem Biophys 2011; 61(2):355-66.
23. Tang X, Kane VD, Morré DM, Morré DJ. hnRNP

F directs formation of an exon 4 minus variant of tumor-associated NADH oxidase (ENOX2). Mol Cell Biochem 2011; 357(1-2):55-63.

24. Caraffa AL, Varvara G, Spinas E, et al. Is vitamin E an anti-allergic compound? J Biol Regul Homeost Agents 2016; 30(1):11-5. Review.

THE EFFECTS OF *P. GINGIVALIS* AND *E. COLI* LPS ON THE EXPRESSION OF PRO-INFLAMMATORY MEDIATORS IN HUMAN MAST CELLS AND THEIR RELEVANCE TO PERIODONTAL DISEASE

I. PALASKA[1], E. GAGARI[2] and T.C. THEOHARIDES[1,2,3]

[1]Molecular Immunopharmacology and Drug Discovery Laboratory, Department of Integrative Physiology and Pathobiology, Tufts University School of Medicine, Boston, MA, USA; [2]Oral Medicine Clinics, A. Syggros Hospital of Dermatologic and Venereal Diseases, Department of Dermatology, School of Medicine, University of Athens, Greece; [3]Department of Internal Medicine, Tufts University School of Medicine, MA, USA

Received March 29, 2016 – Accepted June 6, 2016

Mast cells (MCs) are tissue-resident immune cells that participate in a variety of allergic and inflammatory conditions, including periodontal disease, through the release of cytokines, chemokines and proteolytic enzymes. *Porhyromonas gingivalis* (*P. g*) is widely recognized as a major pathogen in the development and progression of periodontitis. Here we compared the differential effects of lipopolysaccharides (LPS) from *P. g* and *E. coli* on the expression and production of tumor necrosis factor (TNF), vascular endothelial growth factor (VEGF) and monocyte chemoattractant protein (MCP-1) by human MCs. Human LAD2 MCs were stimulated with LPS from either *P. g* or *E. coli* (1-1000 ng/ml). MCs were also stimulated with SP (2 μM) serving as the positive control or media alone as the negative control. After 24 h, the cells and supernatant fluids were collected and analyzed for β-Hexosaminidase (β-hex) spectrophotometrically, TNF, VEGF and MCP-1 release by ELISA and real-time polymerase chain reaction (PCR) for mediator gene expression, respectively. To assess the functional role of toll-like receptors (TRL) in mediator release, MCs were pre-incubated with either anti-TLR2 or anti-TLR4 (2 μg/ml) polyclonal antibody for 1 h before stimulation with LPS. When MCs were stimulated with SP (2 μM), there was a statistically significant β-hex release as well as release of TNF, VEGF and MCP-1. Stimulation of MCs with either type of LPS did not induce degranulation based on the lack of β-hex release. However, both types of LPS stimulated expression and release of TNF, VEGF and MCP-1. Although, *P. g* LPS induced significant release of TNF, VEGF and MCP-1, the effect was not concentration-dependent. There was no statistically significant difference between the effects of *P. g* and *E. coli* LPS. *P. g* LPS stimulated TNF through TLR-2 while *E. coli* utilized TRL-4 instead. In contrast, VEGF release by *P. g* LPS required both TRL-2 and TRL-4 while *E. coli* LPS required TLR-4. Release of MCP-1 was independent of TLR-2 or TLR-4. *P. g* LPS activates human MCs to generate and release TNF, VEGF and MCP-1 through different TLRs than *E. coli* LPS. MCs may, therefore, be involved in the inflammatory processes responsible for periodontal disease.

Key words: mast cells, periodontal inflammation, P. gingivalis LPS, cytokines, toll like receptors

Mailing address:
T.C. Theoharides, Ph.D., M.D.
Department of Integrative Physiology and Pathobiology,
Tufts University School of Medicine,
136 Harrison Avenue, Suite J304, Boston, MA 02111, USA
Tel.: +1 617 6366866 - Fax: +1 617 6362456
e-mail: theoharis.theoharides@tufts.edu

0393-974X (2016)

Periodontitis is among the most common human diseases affecting 5–15% of people worldwide (1). It is a chronic multifactorial inflammatory disease caused by microorganisms and characterized by progressive destruction of the tooth supporting apparatus, leading to tooth loss (2). Almost 47% of adults aged 30 years or over in the US have periodontitis (3).

Periodontal breakdown is a result of the complex interplay between the pathogenic bacteria forming the biofilm and the host's immune responses (4). During the establishment of periodontal disease, Gram-negative microorganisms increase up to 80%, colonize the gingival sulcus and form subgingival plaque, leading to the formation of periodontal pockets. The cell wall components and various toxic products of periodontal pathogens can trigger the host response and induce destruction of periodontal tissues. Recent studies have focused on the role of the immune system in the evolution of periodontal disease (5). Although a dysbiotic biofilm structure initiates the disease, periodontal tissue destruction occurs as a result of a dysregulated immune response to the microbial insult. This cross-talk between the microbiome insult and the immune response involves chemokines, cytokines and metalloproteinases (MMPs) secreted locally by host cells. Elevated cytokine levels, however, are not limited to the infected gingiva, but can be found to be increased in the circulation as well TNF, vascular endothelial growth factor, (VEGF) and monocyte chemoattractant protein-1 (MCP-1) are increased in gingival biopsy samples and gingival crevicular fluid (GCF) of periodontally affected patients, often with decreased concentrations after treatment.

During the past decade, the importance of MCs in the defense mechanism against bacterial infections has been increasingly recognized (6). MCs are bone-marrow derived, granule-containing, immune cells that are found in all connective tissues and mucosa, as well as in the peripheral and central nervous systems (7), (8). MCs are increased in periodontal inflammation and can generate many biologically active substances (9-11). Mediators derived from MCs are either stored in secretory granules and released by degranulation such as β-hex, histamine, TNF, tryptase or can be newly generated such as TNF, VEGF and MCP-1 (12).

Lipopolysacharide (LPS) is a cell-wall component of Gram negative bacteria and is a potent inducer of immune responses by stimulating various cell types including MCs which express the majority of TLR (13). LPS from most Gram-negative bacteria is recognized by TLR-4. One of the few exceptions is LPS from *P. g* that activates both TLR-2 and TLR-4 receptors (14), (15). Little is known about the effect of *P. g* on MCs and the few published *in vitro* studies used rat MCs. For Instance, it was reported that *P. g* LPS activated rat MCs to release cysteine leukotrienes (cysLTs) (16).

Here, we examined the differential effects of *P. g* and *E. coli* LPS on human MC degranulation and release of TNF, VEGF, and MCP-1.

MATERIALS AND METHODS

Reagents

Recombinant human stem cell factor (rhSCF) was kindly donated by Orphan Biovitrum AB (Stockholm, Sweden). Substance P (SP) was purchased from Sigma-Aldrich (St. Louis, MO, USA), was diluted in Milli-Q water, and a stock solution (10 mM) was prepared. Commercially available preparation of *P. g* LPS (Invivogen, San Diego, CA, USA) and *E. coli* 0111:B4 LPS (Sigma-Aldrich) was used. Bacterial LPS was purified by the supplier so as to be free from contaminating lipoproteins. ELISA kits for TNF, VEGF and MCP-1 were obtained from R&D Systems (Minneapolis, Minn, USA). Purified polyclonal antibodies to human TRL-4 and TRL-2 (100μg Mab-hTLR4, Mab-hTLR2) were obtained from Invivogen (San Diego, CA, USA). TNF, VEGF and MCP-1 Taqman probes and Taqman Master Mix were purchased from Applied Biosystems (Foster City, CA, USA).

Culture of human mast cells

The LAD2 MCs (kindly supplied by Dr. Kirshenbaum, National Institutes of Health, Bethesda, Maryland, USA) derived from a human MC leukemia patient (17), were cultured in StemPro-34 medium (Invitrogen, Carlsbad, CA, USA) supplemented with 100 U/mL of penicillin–streptomycin and 100 ng/mL of rhSCF (Swedish Orphan Biovitrum AB, Stockholm, Sweden). Cells were

maintained at 37°C in a humidified incubator at 5% CO_2. All cells were used during their logarithmic growth period. SP and LPS were dissolved in sterile distilled water.

Degranulation assay

Beta-hexosaminidase (β-hex) release was assayed using a fluorometric assay as an index of MC degranulation. LAD2 cells (0.5 × 105) were stimulated with LPS or SP for 30 min. SP (2 μmol/L) was used as the positive control and medium alone as the negative control. Supernatant fluids were collected and cell pellets were lysed with 1% Triton X-100. Supernatant fluids and cell lysates were incubated in the reaction buffer (p-nitrophenyl-N-acetyl-β-D-glucosaminide from Sigma) for 1.5 h and then 0.2 mol/L glycine was added to stop the reaction. Absorbance was measured at 405 nm. Results are expressed as the percentage of β-hex released over the total amount present in LAD2 cells.

Cell viability

Cell viability was assayed by means of trypan blue exclusion at the highest LPS concentration (1 μg/ml). More than 98% of MCs were viable after 24 h of incubation with either LPS.

Release assays for TNF, VEGF, MCP-1

LAD2 cells (1 × 105) were stimulated for 24 h to measure *de novo*–synthesized cytokine/chemokine release. The cells were stimulated with different concentrations of LPS (1-1000 ng/ml) but only the maximum and minimum are shown as there was no dose-response relationship. The cells were also stimulated for 24 h with SP (2 μM) as the positive control or media alone as the negative control. The supernatant fluids were collected by centrifugation (5 min, 150 x g) stored at –20° and assayed for TNF, VEGF and MCP-1 using enzyme-linked immunosorbent assay (ELISA) kits according to the protocol suggested by the manufacturer (R&D Systems).

RNA isolation and quantitative real-time PCR

LAD2 cells were stimulated with either SP (2 μM) or *P. g* LPS and *E. coli* LPS (1 μg/mL) for 6 h. Total mRNA was extracted with an RNeasy Mini kit (Qiagen, Valencia, CA, USA) according to the manufacturer's instructions. Relative mRNA abundance was determined from standard curves run with each experiment. An iScript cDNA synthesis kit (Bio-Rad Laboratories, Hercules, CA, USA) was used for reverse transcription of each sample. Quantitative real-time PCR was performed with TaqMan gene expression assays (Applied Biosystems, Foster City, CA, USA) for TNF (Hs99999043_m1), MCP-1 (Hs00234140_m1) and VEGF (Hs00900055_m1). Samples were run at 45 cycles by using a real-time PCR system (7300, Applied Biosystems, Foster City, CA, USA). The mRNA gene expression were normalized to human GAPDH endogenous control (4310884E, Applied Biosystems).

Blocking tests using anti-TLR antibodies

To assess the functional role of TLR-2 or TLR-4 in mediator release, MCs were incubated with either anti-TLR2 or anti-TLR4 polyclonal antibody (2 μg/ml) for 1 h before stimulation with *P. g* or *E. coli* LPS (1 μg/ml). Supernatants fluids were collected and assayed for mediators by Elisa after 24 h. The positive controls were MCs incubated with LPS, but without anti-TLRs, whereas the negative controls were MCs without both LPS and anti-TLRs.

Statistical analysis

All experiments were performed in triplicate and repeated at least 3 times (n=3). Results are presented as means ± SDs. Data between different treatment groups were analyzed by using the unpaired 2-tailed Student's *t*-test (GraphPad Prism 6). Mean values of the parameters were tested by means of the least significant difference test at significance level $p < 0.05$.

RESULTS

Effects of LPS on mast cell degranulation

SP (2 μM for 30 min) triggered statistically significant ($p<0.001$) release of β-hex in comparison with the control. Neither bacterial LPS stimulated degranulation of MCs (Fig. 1).

Effects of LPS on TNF release

The effect of *P. g* and *E. coli* LPS on the release of TNF from MCs is shown in Fig. 2 (a, b). SP (2 μM), used as positive control, stimulated 4000±965 pg/ml/10^6 cells TNF release compared to controls (150.3±6.7 pg/ml/10^6 cells), ($p<0.001$). When MCs

were stimulated either with 1 ng/ml or 1 μg/ml of *P. g* LPS, the levels of TNF was statistically significantly increased (410.0±48.69 pg/ml/10^6 and 380.7±26.9 pg/ml/10^6 cells, respectively) compared to controls ($p<0.001$). There was no statistically significant difference between the two concentrations used ($p>0.05$). When MCs were stimulated with the same concentrations of *E. coli* LPS, the levels of TNF were also significantly increased (337.4±45.87 pg/ml/10^6 and 336.4±22.43 pg/ml/10^6 cells respectively) compared to controls ($p<0.001$). There was again, no statistically significant difference between the two different concentrations used ($p>0.05$). The maximum concentration of TNF induced by *P. g* was similar to that induced by *E. coli* ($p>0.05$).

Effects of LPS on VEGF release

The effect of P. *g* and *E. coli* LPS on the release of VEGF from MCs is shown in Fig. 3 (a, b). SP (2 μM) stimulated 5917±117 pg/ml/10^6 cells VEGF release compared to controls (2032±52.96 pg/ml/10^6 cells), ($p<0.001$). When MCs were stimulated with either 1 ng/ml (3691±154.0 pg/ml/10^6) or 1 μg/ml (4199±86.17 pg/ml/10^6) of *P. g* LPS, the levels of VEGF were statistically significantly increased compared to the controls ($p<0.001$). When MCs were stimulated with the same concentrations of *E. coli* LPS, the levels of VEGF were also significantly increased ($p<0.001$). At concentration of 1 ng/ml, the release was 3525±173.1 pg/ml/10^6 and at 1μg/ml the release was 3947±181.9 pg/ml/10^6 cells. There was also no statistical significant difference between the effects of *P. g* and *E. coli* LPS ($p>0.05$).

Effects of LPS on MCP-1 release

The effect of *P. g* and *E. coli* LPS on the release of MCP-1 from MCs is shown in Fig. 4 (a, b)**.** SP (2 μM) stimulated 7281±423.4 pg/ml/10^6 cells MCP-1 release compared to controls (2899±82.12 pg/ml/10^6 cells), ($p<0.001$). When MCs were stimulated with either 1 ng/ml (4886±554.6 pg/ml/10^6) or 1 μg/ml (5343±337.4 pg/ml/10^6) *of P. g* LPS, the levels of MCP-1 was statistically significantly increased compared to the controls ($p<0.001$). There was no statistically significant difference between the two concentrations used ($p>0.05$). When MCs were stimulated with the same concentrations of *E. coli* LPS, the levels of MCP-1 were also significantly increased ($p<0.001$). At 1 ng/ml, the release was 4320±254.2 pg/ml/10^6 cells and at 1 μg/ml the release was 4985±478 pg/ml/10^6 cells. There was no statistically significant difference between the two different concentrations used ($p>0.05$).

Effects of LPS on TNF, VEGF and MCP-1 gene expression

The effect of *P. g* LPS and *E. coli* LPS on gene expression of TNF, VEGF and MCP-1 in MCs is shown in Fig. 5. SP (2 μM) induced a potent increase in the gene expression of all these molecules

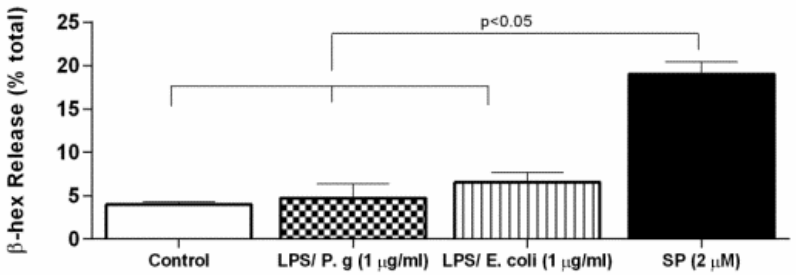

Fig. 1. *Beta-Hexosaminidase release. Supernatant fluids and cell pellets were collected 30 min after stimulation with LPS and SP. *Statistically significant differences between the control and the LPS groups ($p<0.05$, unpaired t-test). (n=3, mean ± SD).*

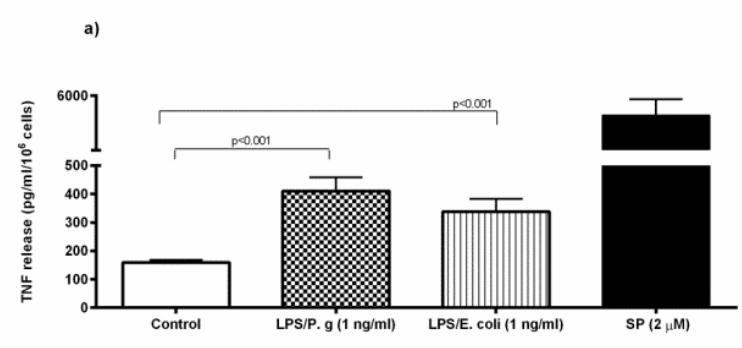

Figure 2

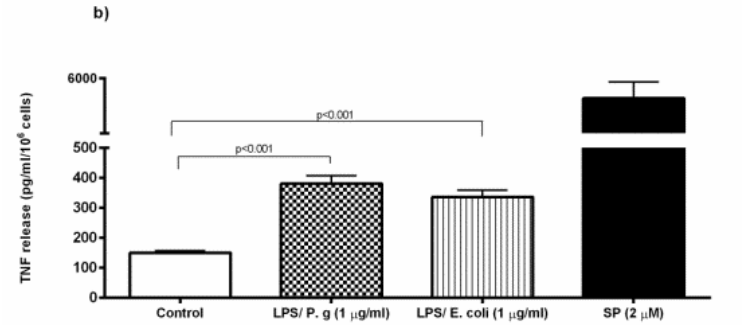

Fig. 2. *TNF release from mast cells. Supernatant fluids were collected 24 hours after stimulation with 1 ng/ml (**a**) and 1 μg/ml (**b**) of LPS and assayed by ELISA. *(p<0.05 unpaired t-test). (n=3, mean ± SD).*

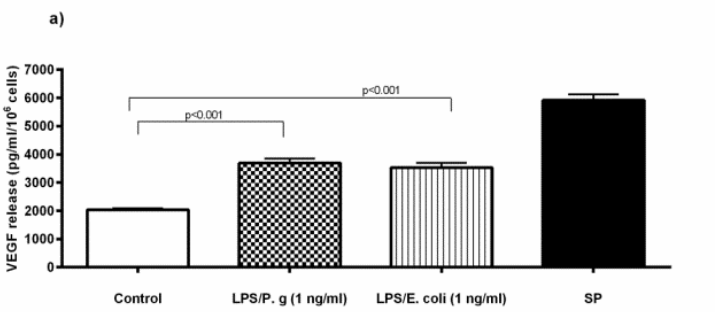

Figure 3

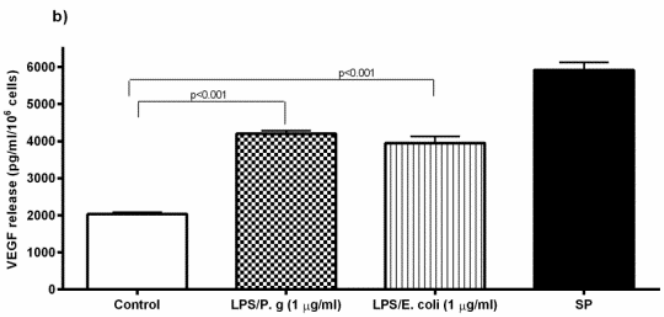

Fig. 3. *VEGF release from mast cells. Supernatant fluids were collected 24 hours after stimulation with 1 ng/ml (**a**) and 1 μg/ml (**b**) of LPS and assayed by ELISA. *(p<0.05 unpaired t-test). (n=3, mean ± SD).*

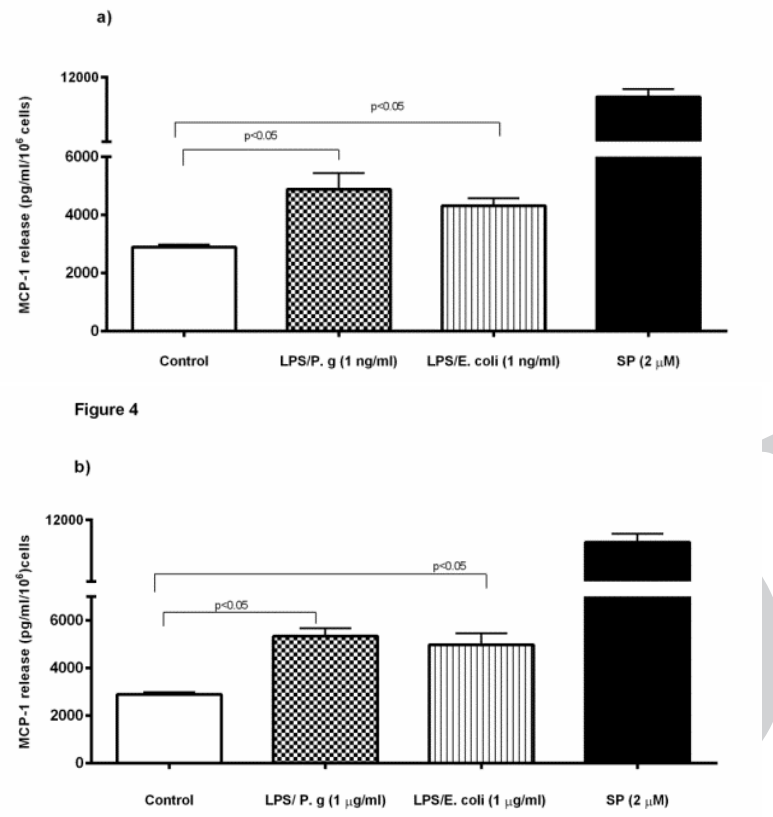

Fig. 4. *MCP-1 release from mast cells. Supernatant fluids were collected 24 hours after stimulation 1 ng/ml (**a**) and 1 μg/ml (**b**) of LPS and assayed by ELISA. *(p<0.05 unpaired t-test). (n=3, mean ± SD).*

(p<0.001). LPS from both *P. g* and *E. coli* triggered a small, but statistically significant increase of TNF and VEGF mRNA levels in MCs compared to controls (p<0.05). In contrast, MCP-1 mRNA levels were statistically significantly increased only after stimulation with *P. g* LPS (P<0.05) and not with *E. coli* LPS compared to controls.

Involvement of TLR2 and TRL4

Both anti-TRL-2 and anti-TRL-4 antibodies significantly reduced VEGF release after stimulation with either *P. g* or *E. coli* LPS (Fig. 6 a, b). However, only the anti-TRL-2, but not the anti-TLR-4 antibody, significantly reduced TNF release from MCs stimulated with *P. g* LPS (Fig. 6 c). In contrast, MCs cells pre-incubated with anti-TRL-4 only, significantly reduced (p<0.001) the levels of TNF after stimulation with *E. coli* LPS (p<0.001), (Fig. 6 d). Pre-incubation with either anti-TR-L2 or anti-TLR-4 antibodies had no statistically significant (p>0.05) effect on MCP-1 release from MCs stimulated with either LPS (Fig. 6 e, f).

DISCUSSION

In this study we showed that stimulation of MCs with either type of LPS did not induce degranulation. This finding is in accordance with other studies that reported that most pathogens do not trigger MC degranulation, but instead induce *de novo* synthesis and release of cytokines (18). We also showed that both sources of LPS induce the release of TNF, VEFG and MCP-1, but without an apparent dose response relationship between the 1 and 1000 ng/ml. Lower amounts had no effect (results not shown). The lack of a dose-response relationship implies an "off and on" response. Gene expression of these mediators was not increased at 6 hours, but there was

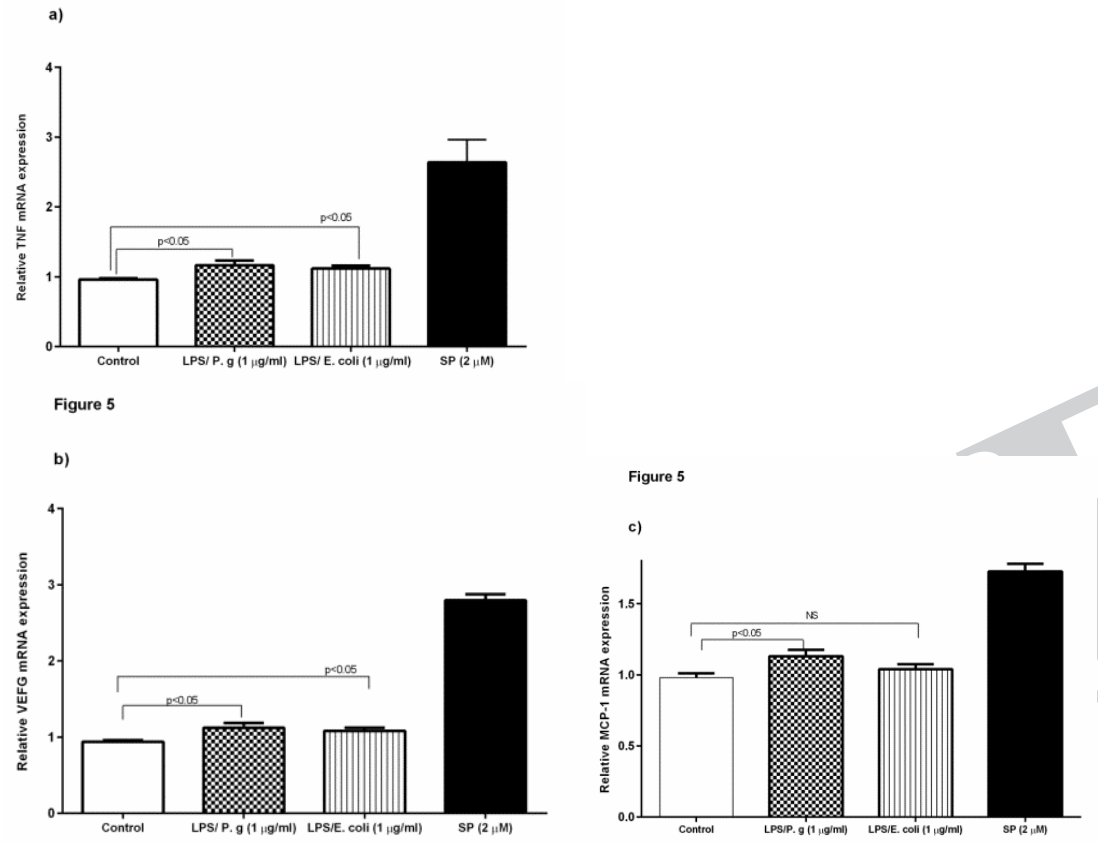

Fig. 5. *mRNA expression levels of (a) TNF (b) VEGF and (c) MCP-1 after 6 hours stimulation with LPS (1 μg/ml) and SP (2 μmol/L) by qRT-PCR (p<0.05 unpaired t-test). (n=3, mean ± SD).*

significant protein release at 24 hours. We should have measured mRNA expression also at 24 hours after stimulation to coincide with the time at which mediator release was measured.

In our study we used SP as a positive control for all experiments. SP is a neuropeptide that is involved in neurogenic inflammation and is an important neurmodulator. Recently, the nervous system has been identified as a critical regulator of inflammation in periodontal diseases (19). Several studies have shown the presence of SP in human gingival tissues and in gingival crevicular fluid of periodontally affected patients (20). Our findings are in agreement with previous studies where it was reported that SP could induce gene expression and secretion of VEGF from human LAD2 MCs and human umbilical cord blood-derived cultured MCs (hCBMCs). SP could also stimulate TNF and MCP-1 chemokine transcription and translation protein in LAD2 cells *in vitro* (21-23). SP also increases the expression of receptors for corticotropin-releasing hormone (CRH) on MCs thus further amplifying the effect of stress on inflammation.

Some studies have suggested that *P. g* LPS has an ability to stimulate cytokine production comparable to that of *E. coli*, whereas others reported a much lower potency of *P. g* LPS in various cells (24). In the present study, we did not observe any difference. This is possibly related to the *P. g* strain used, the LPS extraction method, the selection of the times for detecting cytokine levels and the target cells used. For instance different strains of the same bacterium or different extraction methods resulted in differences on LPS-induced IL-6 release from gingival fibroblasts (25).

In addition, we showed that MC pretreatment with either anti-TLR-2 or anti-TLR-4 significantly reduced VEGF release in response to both bacterial

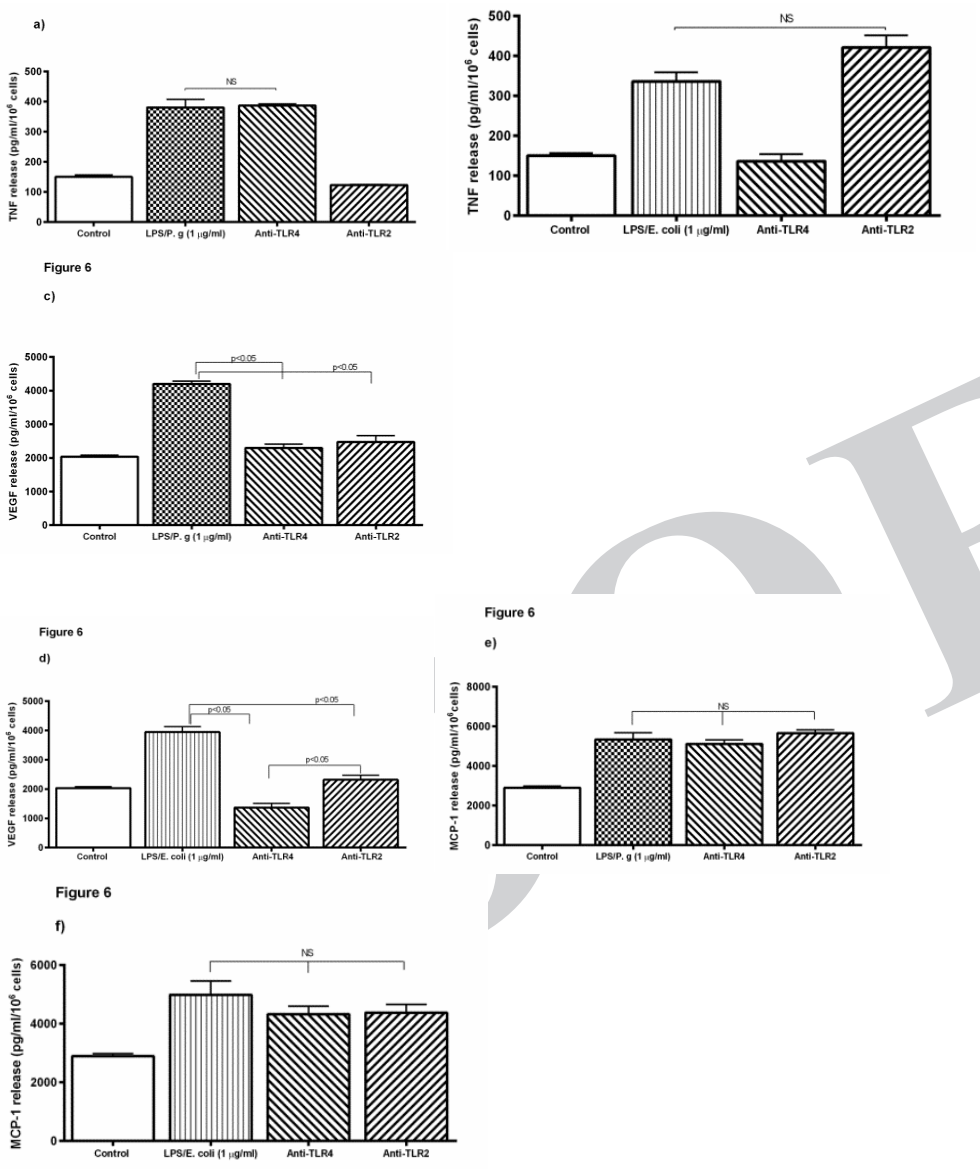

Fig. 6. *The effect of anti-TLR antibodies on release of VEGF (**a**, **b**), TNF (**c**, **d**) and MCP-1 (**e**, **f**) from LPS-stimulated mast cells. Cells were pretreated for one hour with anti-TLR2 and anti-TLR4 antibodies (2 μg/ml). Supernatant fluids were collected 24 hours after 1μg/ml LPS stimulation and assayed by Elisa *(p<0.05 unpaired t-test). (n=3, mean ± SD).*

antigens. MCP-1 release, on the other hand, was not affected by the pretreatment of MCs with anti-TLR-2 or anti-TLR-4. This may imply that MCP-1 release is controlled by TLR-9 or a different pathway in MCs. Recently it was shown that MCP-1 release was stimulated through TLR-9 in macrophages (26). Emerging trends emphasize the significance of TLR-9 in host immune responses and especially in periodontitis as it was shown that TLR-9-mediated inflammation triggered alveolar bone loss in experimental periodontitis (27). TNF release was significantly reduced after pretreatment with anti-TLR-2 in response to *P. g* LPS whereas the pretreatment with anti-TLR-4 had no effect on TNF release. On the contrary, pretreatment with anti-TLR-4 led to significant reduction of TNF in response to *E. coli* LPS. Our data showed that *P. g* LPS activates the inflammatory process mainly

through TLR-2, findings that are in agreement with previous studies showed that *P. g*-induced cytokine (mainly TNF) production was predominantly driven by the TLR-2 pathway in macrophages and endothelial cells (28, 29).

Isolated components of *P. g* can activate TLR-2 and TLR-4 on a variety of cell types especially those involved in the innate immune system, such as neutrophils macrophages and gingival fibroblasts. Human MCs express different TLR such as TLR-5, -7, -9 including TLR-2 and TRL-4. Although ligand recognition shows specificity for each receptor, the downstream signaling pathways activated by TLRs have some redundancy, generating the potential for signaling cross talk. Intriguingly, cross talk between TLR2 and TLR4 has been reported in previous studies (30).

MCs are ubiquitous in the human body and are critical for allergic reactions but also in innate and acquired immunity. MCs can secrete numerous vasoactive molecules, chemokines, cytokines, and proteases. Increasing evidence implicates MCs in inflammatory diseases, especially those exacerbated by stress such as periodontal inflammation (31).

TNF, VEGF and MCP-1 exhibit a wide variety of biologic effects related to the destruction of periodontal tissues (32). Elevated levels of these mediators are important risk factors for periodontal disease progression. High levels of these mediators have already been detected in periodontal tissues, gingival crevicular fluid and saliva of periodontally affected patients compared to healthy controls or periodontally treated patients, as well as in the serum of patients presenting with periodontal disease (33).

In conclusion, TNF, VEGF and MCP-1 release from MCs in response to *P. g* could have a major role in the pathogenesis and progression of periodontal disease. Inhibition of MC activation could provide new therapeutic targets to control the inflammatory response in periodontal tissues.

ACKNOWLEDGEMENTS

We thank Dr. A Kirshenbaum (National Institutes of Health, Bethesda, Maryland, USA) for LAD2 cells and the Orphan Biovitrum AB (Stockholm, Sweden) for SCF. This work was funded in part by NIH grant awarded to TCT.

DISCLOSURE: TCT is the inventor of US patent No. 8,268,365 and US patent No. 2011-0027397 A1. The other Authors declare no conflict of interest.

REFERENCES

1. Richards D. Review finds that severe periodontitis affects 11% of the world population. Evid Based Dent 2014; 15:70-71.
2. Bartold PM, Van Dyke TE. Periodontitis: a host-mediated disruption of microbial homeostasis. Unlearning learned concepts. Periodontol 2000 2013; 62:203-17.
3. Papapanou PN. The prevalence of periodontitis in the US: forget what you were told. J Dent Res 2012; 91:907-8.
4. Benakanakere M, Kinane DF. Innate cellular responses to the periodontal biofilm. Front Oral Biol 2012; 15:41-55.
5. Cekici A, Kantarci A, Hasturk H, Van Dyke TE. Inflammatory and immune pathways in the pathogenesis of periodontal disease. 2014; 64:57-80.
6. Abraham SN, St John AL. Mast cell-orchestrated immunity to pathogens. Nat Rev Immunol 2010; 10:440-52.
7. Tete S, Tripodi D, Rosati M, et al. Role of mast cells in innate and adaptive immunity. J Biol Regul Homeost Agents 2012; 26:193-201.
8. Sismanopoulos N, Delivanis DA, Alysandratos KD, Angelidou A, Therianou A, Kalogeromitros D, Theoharides TC. Mast cells in allergic and inflammatory diseases. Curr Pharm Des 2012; 18:2261-77.
9. Steinsvoll S, Helgeland K, Schenck K. Mast cells--a role in periodontal diseases? J Clin Periodontol 2004; 3:413-19.
10. Huang S, Lu F, Chen Y, Huang B, Liu M. Mast cell degranulation in human periodontitis. J Periodontol 2013; 84:248-55.
11. Sheethal HS, Uma K, Rao K, Priya NS, Umadevi HS, Smitha T. A quantitative analysis of mast cells in inflammatory periapical and gingival lesions. J Contemp Dent Pract 2014; 15:300-305.
12. Theoharides TC, Valent P, Akin C. Mast cells,

mastocytosis, and related disorders. N Engl J Med 2015; 19:1885-86.
13. Sandig H, Bulfone-Paus S. TLR signaling in mast cells: common and unique features. Front Immunol 2012; 3:185.
14. Kocgozlu L, Elkaim R, Tenenbaum H, Werner S. Variable cell responses to P. gingivalis lipopolysaccharide. J Dent Res 2009; 88:741-45.
15. Coats SR, Reife RA, Bainbridge BW, Pham TT, Darveau RP. Porphyromonas gingivalis lipopolysaccharide antagonizes Escherichia coli lipopolysaccharide at toll-like receptor 4 in human endothelial cells. Infect Immun 2003; 71:6799-807.
16. Babolewska E, Witczak P, Pietrzak A, Brzezinska-Blaszczyk E. Different potency of bacterial antigens TLR2 and TLR4 ligands in stimulating mature mast cells to cysteinyl leukotriene synthesis. Microbiol Immunol 2012; 56:183-90.
17. Kirshenbaum AS, Akin C, Wu Y, Rottem M, Goff JP, Beaven MA, Rao VK, Metcalfe DD. Characterization of novel stem cell factor responsive human mast cell lines LAD 1 and 2 established from a patient with mast cell sarcoma/leukemia; activation following aggregation of FcepsilonRI or FcgammaRI. Leuk Res 2003; 27:677-82.
18. Leal-Berumen I, Conlon P, Marshall JS. IL-6 production by rat peritoneal mast cells is not necessarily preceded by histamine release and can be induced by bacterial lipopolysaccharide. J Immunol 1994; 152:5468-76.
19. Cekici A, Kantarci A, Hasturk H, Van Dyke TE. Inflammatory and immune pathways in the pathogenesis of periodontal disease. Periodontol 2000 2014; 64:57-80.
20. Lundy FT, Mullally BH, Burden DJ, Lamey PJ, Shaw C, Linden GJ. Changes in substance P and neurokinin A in gingival crevicular fluid in response to periodontal treatment J Clin Periodontol 2000; 27:526-30.
21. Castellani ML, Galzio RJ, Felaco P, et al. VEGF, substance P and stress, new aspects: a revisited study. J Biol Regul Homeost Agents 2010; 24:229-37.
22. Theoharides TC, Zhang B, Kempuraj D, et al. IL-33 augments substance P-induced VEGF secretion from human mast cells and is increased in psoriatic skin. Proc Natl Acad Sci U S A 2010; 107:4448-53.
23. Shapira L, Frolov I, Halabi A, Ben-Nathan D. Experimental stress suppresses recruitment of macrophages but enhanced their P. gingivalis LPS-stimulated secretion of nitric oxide. J Periodontol 2000; 71:476-81.
24. Andrukhov O, Ertlschweiger S, Moritz A, Bantleon HP, Rausch-Fan X. Different effects of P. gingivalis LPS and E. coli LPS on the expression of interleukin-6 in human gingival fibroblasts Acta Odontol Scand 2014; 72:337-45.
25. Lee JG, Lee SH, Park DW, et al. Toll-like receptor 9-stimulated monocyte chemoattractant protein-1 is mediated via JNK-cytosolic phospholipase A2-ROS signaling. Cell Signal 2008; 1:105-11.
26. Kim PD, Xia-Juan X, Crump KE, Abe T, Hajishengallis G, Sahingur SE. Toll-like receptor 9-mediated inflammation triggers alveolar bone loss in experimental murine Periodontitis. Infect Immun 2015; 7:2992-3002.
27. Wang PL, Ohura K. Porphyromonas gingivalis lipopolysaccharide signaling in gingival fibroblasts-CD14 and Toll-like receptors. Crit Rev Oral Biol Med 2002; 13:132-42.
28. Hajishengallis G, Tapping RI, Harokopakis E, et al. Differential interactions of fimbriae and lipopolysaccharide from Porphyromonas gingivalis with the Toll-like receptor 2-centred pattern recognition apparatus. Cell Microbiol 2006; 8:1557-70.
29. Maekawa T, Krauss JL, Abe T, et al. Porphyromonas gingivalis manipulates complement and TLR signaling to uncouple bacterial clearance from inflammation and promote dysbiosis. Cell Host Microbe 2014 6:768-78.
30. Lee KS, Scanga CA, Bachelder EM, Chen Q, Snapper CM. TLR2 synergizes with both TLR4 and TLR9 for induction of the MyD88-dependent splenic cytokine and chemokine response to Streptococcus pneumoniae. Cell Immunol 2007; 2:103-10
31. Papathanasiou E, Palaska I, Theoharides TC. Stress hormones regulate periodontal inflammation. J Biol Regul Homeost Agents 2013; 27:621-26.
32. Graves D. Cytokines that promote periodontal tissue destruction. J Periodontol 2008; 79:1585-91.
33. Ozer YO, Berker E, Mesci L, Eratalay K, Tepe E, Tezcan I. Analysis of TNF-alpha (-308) polymorphism and gingival crevicular fluid TNF-alpha levels in aggressive and chronic periodontitis: A preliminary report. Cytokine 2015; 72:173-77.

OBESTATIN DIRECTLY CONTROLS CHICKEN OVARIAN CELL FUNCTIONS

A.V. SIROTKIN[1,2], M. MÉSZÁROSOVÁ[1], A.H. HARRATH[3] and R. GROSSMANN[4]

[1]Department Zoology and Anthropology, Constantine the Philosopher University, Nitra, Slovakia; [2]Department Genetics and Reproduction, Research Institute of Animal Production, Lužianky, Slovakia; [3]Zoology Department, College of Science, King Saud University, Riyadh, Saudi Arabia; [4]Department Functional Genomics and Bioregulation, Friedrich Loeffler Institute, Mariensee, Neustadt, Germany

Received December 11, 2015 – Accepted June 23, 2016

The aim of the present *in-vitro* study was to examine the role of obestatin in the direct control of basic avian ovarian granulosa cell functions – proliferation, apoptosis and secretory activity. In addition, the effects of obestatin on hormone release by cultured ovarian granulosa cells and follicular fragments (containing both granulosa and theca cells) were examined. We identified the effect of obestatin addition (0.1, 10 or 100 ng/ml medium) on the accumulation of markers of proliferation (PCNA, cyclin B1, MAPK/ERK1,2) and nuclear (TdT) and cytoplasmic (bax, caspase 3) apoptosis, as well as the release of progesterone (P), testosterone (T) and estradiol (E) by cultured chicken granulosa cells. Furthermore, the action of obestatin addition (0.1, 10 or 100 ng/ml medium) on the release of P, T, E and arginine-vasotocin (AVT) by cultured fragments of chicken ovarian follicles was examined. The accumulation of proliferation and apoptosis markers was assessed by immunocytochemistry and SDS PAGE-Western immunoblotting. The release of hormones was determined by an EIA. It was observed that obestatin addition could inhibit the accumulation of proliferation markers (PCNA and cyclin B1, but not of MAPK/ERK1,2), promote the expression of nuclear (TdT) and cytoplasmic (bax, caspase 3) apoptosis markers and suppress P, T, and E release by cultured granulosa cells. In cultured ovarian follicular fragments, obestatin promoted P, T, and E, but not AVT, release. These observations represent the first demonstration that (i) obestatin can directly control avian ovarian cell proliferation, apoptosis and hormone release and (ii) the interrelationship between theca and granulosa cells can determine the characteristics of obestatin action on ovarian secretory activity.

Metabolic hormones, including obestatin, can be mediators of the effects of metabolic conditions on reproduction in mammals (1). Obestatin can decrease food intake, gastric emptying and contractile activity of the jejunum and reduce weight gain in rats (2), inhibit GH and promote ACTH release by mouse pituitary cells (3). Obestatin may affect physiological systems by affecting both the CNS and peripheral structures (2) including the ovaries. Addition of obestatin promoted the accumulation of both proliferation (PCNA, cyclin B1, MAP kinase) and apoptosis (bax, caspase 3, p53) related proteins and the release of progesterone (P) but not of testosterone (T) or estradiol (E) by cultured porcine ovarian granulosa cells (4), and it did not affect porcine oocyte maturation (5). The role of obestatin in the metabolic control of avian reproduction remains to be elucidated. In contrast to mammals, in chickens, obestatin production has not yet been identified, and obestatin did not affect food intake

Key words: obestatin, chicken, ovary, granulosa, theca, proliferation, apoptosis, steroid hormones, arginine-vasotocin

Mailing address:
Prof. Alexander V. Sirotkin,
Dept. Zoology and Anthropology,
Constantine the Philosopher University,
Tr. A. Hlinku 1, 949 74 Nitra, Slovakia
Tel: +421-903561120,
e-mail: asirotkin@ukf.sk

0393-974X (2016)

(6, 7). On the other hand, obestatin treatment did affect the expression of other metabolic hormones, including ghrelin and its receptor in the chicken hypothalamus and ovaries, and the response to food restriction (8). Furthermore, obestatin administration *in vivo* stimulated basal P and E but not T and vasotocin release by cultured chicken ovarian fragments. Moreover, obestatin promoted the suppressive effect of food restriction on these ovarian functions (9). It remains unknown whether obestatin can affect chicken ovarian cells directly or via the upstream hypothalamo-hypophyseal system. The direct action of obestatin on basic avian ovarian cell functions, including proliferation, apoptosis, and the release of hormones, has not been studied. Furthermore, ovarian follicles contain two basic functional cell layers – the granulosa and theca cells. The significance of interrelationships between the granulosa and theca cells within the ovarian follicle in the response to obestatin also remains to be established.

The aim of our study was to examine whether obestatin addition can directly affect chicken ovarian cell functions by evaluating markers of proliferation and apoptosis and the release of ovarian hormones by ovarian granulosa cells cultured with and without obestatin. Furthermore, we compared the action of obestatin on hormone release by cultured granulosa cells and fragments of whole ovarian follicles (containing both granulosa and theca cells). For the assessment of proliferation, the markers and regulators of the cell cycle, PCNA [a marker of S-phase of mitosis, (10)], cyclin B1 [a marker of the G2 phase, (11, 12)] and MAPK/ERK1,2 [a promoter of cell proliferation (13-15)] were analyzed. For the detection of apoptosis, markers of nuclear [TdT, (16)] and cytoplasmic/mitochondrial [bax, caspase 3, (17)] apoptosis were used. To measure the secretory activity, the release of endocrine promoters of ovarian functions, including the steroid hormones P, T, and E and the peptide hormone AVT, was analyzed. These hormones are considered indexes of ovarian secretory activity, respond to hormonal stimuli and are the key regulators of both mammalian (15) and chicken (11, 13, 15, 18) ovarian functions.

MATERIALS AND METHODS

Animal experiments, tissue collection and culture

Young (approximately 7 months of age) White Leghorn hens (LSL), weighing 1.1-1.2 kg and with an egg-laying rate of more than 95%, were housed in individual cages under standard conditions at the Experimental Station of the Friedrich Loeffler Institute on a 12 h L:12 h D photoperiod (illumination 8:00-20:00). The conditions of their care, manipulations and use corresponded to the instructions of EC no.178/2002 and the related EC documents and were approved by the local ethics commission. The animals were sacrificed by decapitation, and the largest (F1-F2) follicles were isolated from the ovary. The stage of folliculogenesis was determined by recording the time of the last oviposition and by the size and the position of the next ovarian follicle.

In experiments using follicular fragments, fragments of the follicular wall (5 mm in diameter, weighing 24±8 mg) were isolated as described previously (11, 13). After washing three times in sterile culture medium (DMEM/F-12 1:1 mixture supplemented with 10% bovine fetal serum and 1% antibiotic-antimycotic solution (all from Sigma, St. Louis, USA), these fragments were cultured with or without human recombinant obestatin (Sigma, St. Louis, USA) dissolved in the culture medium immediately before the experiment at doses of 0.1 10 or 100 ng/ml of medium in 2 ml of culture medium in Falcon 24-well plates (Becton Dickinson, Lincoln Park, USA) for 2 d at 38.5°C under 5% CO_2 in humidified air. This protocol provides maximal accumulation of ovarian hormones in the culture medium and the most reliable characteristics of ovarian secretory activity (13).

In experiments with granulosa cell cultures, granulosa cells were gently scraped with a lancet from the inner surface of fresh isolated washed ovarian follicles, washed 3 times by centrifugation and resuspended in culture medium. The cells were incubated in 2 ml of medium in Falcon 24-well plates (Becton Dickinson) and Lab-Tek chamber slides (Nunc Inc., Naperville, USA) at a density of 10^6 cells/ml (determined by a hemocytometer) at 38.5°C under 5% CO_2 in humidified air. After 4 days of pre-incubation (creating 50-60% confluent cell monolayer), the medium was replaced with fresh medium with or without the treatment. The experimental groups of granulosa cells were treated with human recombinant

obestatin (Sigma, 0.1, 10 or 100 ng/ml of incubation medium). The control cells were incubated without treatment, and the medium was also incubated without ovarian fragments or granulosa cells (assay blank).

After 2 days in culture, the medium was gently aspirated by syringe and frozen at -24°C until an EIA and RIA were performed. The cell monolayer was lysed in sample buffer (2.5 ml of 4x stacking gel buffer: 3.0 g Tris-base, 50 ml deionized water, pH 6.8 plus 4.0 ml 10% SDS, 2.0 ml glycerol, 2.0 mg bromophenol blue, and deionized water to 10 ml) and subjected to 3 cycles of freezing (-18°C) and thawing and 10 min of centrifugation at 600xg in Eppendorf tubes to achieve cell lysis prior to electrophoresis and Western blotting.

After culturing, the medium from the chamber slides was removed, and the wells were washed in ice-cold PBS (pH 7.5), fixed for 1 h at room temperature (25°C) in 4% paraformaldehyde, dehydrated in alcohols (70%, 80%, and 96%; 10 min each) and stored in 96% alcohol at -4°C for immunocytochemical and TUNEL analyses.

After culture but before lysis and fixation, the cell concentration and viability were determined by Trypan blue staining and counting on a hemocytometer. No statistically significant differences in these indices were observed between the groups (1.2-1.4 x 10^6 cells and 70-80%, respectively).

Immunocytochemical analysis

The intracellular proliferation- and apoptosis-associated markers were detected in granulosa cells plated on chamber-slides using immunocytochemistry. The ImmunoCruz Staining System and primary mouse monoclonal antibodies against PCNA, MAPK/ERK1, 2, and bax (which cross-react with corresponding mouse, rat, human and chicken antigens; all from Santa Cruz Biotechnology, Inc., Santa Cruz, USA; dilution 1:100) were used as directed by the manufacturer. For the visualization of the primary antibody, the corresponding secondary antibody from the ImmunoCruz Staining System or secondary polyclonal rabbit IgG labeled with horseradish peroxidase (Santa Cruz; dilution 1:1000 or Sevac, Prague, Czech Republic; dilution 1:2000) and the DAB reagent (Roche Diagnostics Corporation, IN, USA, 10%) were used. These cells were mounted in glycerol mounting medium (DAKO Corp., Carpinteria, CA, USA). In some experiments, these intracellular substances were visualized using secondary polyclonal goat antibodies against mouse IgGs labeled with the fluorescent marker FITC (Santa Cruz or DAKO; dilution 1:1000) and mounted in Vectashield with DAPI (Vector Laboratories, Inc. Burlingame, CA, USA). The presence of peptides was determined by light and fluorescent microscopy (LEICA). Cells in which the primary antibody was omitted that were treated with the secondary antibody were used as negative controls.

TUNEL assay

For the analysis of apoptosis, the chamber-slides were subjected to a TUNEL [TdT-mediated dUTP nick end labeling (16)] assay using an In Situ Cell Death Detection Kit and FITC (Boehringer Mannheim, GmbH, Mannheim, Germany) according to the manufacturer's instructions. Fixed and permeabilized cells incubated without TdT but with secondary HRP-conjugated antibody and FITC were used as negative controls. Permeabilized cells incubated with bovine pancreatic DNAse I (Boehringer Mannheim GmbH; 0.01 mg/ml; 10 min at room temperature) before TdT treatment to induce DNA fragmentation were used as positive controls. The general cell morphology and percentage of TUNEL-positive cells in each culture were determined by visual evaluation of the cultures, and the determination of the TUNEL-positive and TUNEL-negative cell numbers was performed with fluorescent microscopy.

Protein gel electrophoresis and Western immunoblotting

These experiments were performed as previously described (19). Frozen lysates of granulosa cells plated on the bottom of wells were thawed at room temperature, boiled at 95°C for 3 min, centrifuged at 600 x g and subjected to SDS-PAGE polyacrylamide gel electrophoresis. Equal amounts of lysate (10 µl) were loaded onto a polyacrylamide stacking gel (3.0 g Tris-base, 50 ml ddH_2O, pH 6.8) followed by a 10% polyacrylamide running gel (36.3 g Tris-base, 200 ml ddH_2O, pH 8.8) and run at a constant voltage of 200 V. Following electrophoresis, the samples were transferred to a nitrocellulose membrane parablot NCP (Macherey–Nagel, Düren, Germany) for 1 h at 100 V using a mini trans-blot system (Bio-Rad Labs, Richmond, CA, USA). Proteins on the membrane were visualized with 0.1% Ponceau Red dye in 5% acetic acid (Sigma, St. Louis, Mo,

USA). Non-specific binding of antiserum was prevented by incubation of the membranes in 5% BSA (Amersham International plc, Little Chalfont, Bucks, UK) in TTBS (20 nM Tris-base, 137 nM NaCl, and 0.1% Tween-20) overnight at 4°C. The membranes were washed for 15 min each in TTBS (pH 7.5). The endogenous peroxidase in the samples was quenched by incubation in 3% H_2O_2 for 15 min. The membranes were probed for 1 h with mouse monoclonal antibodies against cyclin B1, MAPK/ERK1,2, caspase 3 and GAPDH (loading control) (Santa Cruz Biotechnology Inc., dilution 1:250). Thereafter, the membranes were washed for 15 min each in TTBS, then incubated with secondary polyclonal goat antibodies against mouse IgGs, and labeled with horseradish peroxidase (Sevac; dilution 1:1000). The antibody was then rinsed with TTBS, and the immunoreactive bands were visualized using the detection reagents of the Upstate Visualizer™ Western Blot system (Temecula, CA, USA) and exposed on ECL Hyper-film (Amersham International plc, Little Chalfont, Bucks, UK). The molecular weights of fractions were evaluated using a molecular weight calibration kit (18, 24, 45 and 67 kDa; ICN Biomedicals Inc, Irvine, CA, USA). Granulosa cell lysate without hormone treatment was used as a negative control. The protein amounts were corrected for differences in GAPDH levels.

Immunoassay

The concentrations of progesterone (P), testosterone (T), estradiol (E) and arginine-vasotocin (AVT) were determined in 25 µl aliquots of incubation medium by an EIA (P, T, and E) and an RIA (AVT), which were previously validated for use in culture medium.

The P concentrations were measured as described previously (20). Rabbit antiserum against P was obtained from the Research Institute for Animal Production "Schoonoord", Netherlands. The cross-reactivity with E_2, dihydrotestosterone, T and 17 beta hydroxyprogesterone was ≤0.1%. The sensitivity of the EIA was 12.5 pg/ml. The inter- and intraassay coefficients of variation did not exceed 3.3% and 3.0%, respectively.

T was assayed according to the method used by Münster (21) using antisera against steroids (produced at the Institute of Animal Science, Neustadt, Germany). The sensitivity of the assay was 10 pg/ml. The cross-reactivity of the T antiserum to dihydrotestosterone was ≤96%, the cross-reactivity to androstenedione was ≤3%, the cross-reactivity to P_4 and E_2 was ≤0.01%, the cross-reactivity to cortisol was ≤0.02% and the cross-reactivity to corticosterone was≤0.001%. The inter- and intraassay coefficients of variation were 12.3% and 6.8%, respectively.

The E concentrations were evaluated according to the method used by Münster (21) using antisera against steroids (produced at the Institute of Animal Science, Neustadt, Germany), and the assay sensitivity was 5 pg/ml. The cross-reactivity of the E_2 antiserum to estrone was < 2%, the cross-reactivity to estriol was≤ 0.3%, the cross-reactivity to T was ≤ 0.004% and the cross-reactivity to P_4 and cortisol was≤0.0001%. The inter- and intraassay coefficients of variation did not exceed 16.6% and 11.7%, respectively. The AVT concentration was determined using an RIA according to the method used by Gray and Simon (22). The anti-AVT antiserum was kindly provided by Dr. D.A. Gray (Max-Plank Institute for Physiological and Clinical Research, Bad Nauheim, Germany), and the cross-reactivity with mesotocin and angiotensin II was≤1.0%. The sensitivity of the RIA was 0.3 pg/ml. The inter- and intraassay coefficients of variation did not exceed 8.8% and 7.2%, respectively.

Statistics

Each experimental group was represented by six culture wells or four chamber-slide wells. The proportions of cells containing specific immunoreactivity were calculated from an inspection of at least 1,000 cells per chamber. Assays of the hormone levels in the incubation media were performed in duplicate. The data shown represent the means of values obtained in three separate experiments performed on separate days using separate pools of ovaries, each obtained from 8 animals. The samples intended for EIA or immunocytochemistry were processed separately, while the samples intended for SDS PAGE-Western immunoblotting (6 samples x 3 experiments = 18 samples per group) were pooled before processing. The values of blank controls (serum supplemented medium incubated without cells) were subtracted from the specific values determined by the EIA/RIA in cell-conditioned medium to exclude any non-specific background (less than 15% of total values). The rates of substance secretion by cultured ovarian fragments and granulosa cells were calculated per mg tissue/day or

per 10^6 cells/day, respectively. The program Sigma Stat / Sigma Plot 11.0 (Systat Software, GmbH, Erkhart, Germany) was used to examine the normal distribution of data. Significant differences between the experiments were evaluated using one-way ANOVA. Data from the experimental and control groups were compared by a Wilcoxon-Mann-Whitney multiple range test using Sigma Stat / Sigma Plot 11.0 statistical software (Systat Software, GmbH). Differences from control that produced a value of $P < 0.05$ were considered statistically significant.

RESULTS

Isolated ovarian fragments and granulosa cells could survive in culture, accumulate intracellular substances and secrete hormones. Granulosa cells could attach to the bottom of culture wells and produce a confluent monolayer (Fig. 1). Immunocytochemistry in combination with light and fluorescent microscopy, SDS PAGE-Western immunoblotting and TUNEL revealed the presence of proliferation-related (PCNA, MAPK/ERK1,2, cyclinB1) and apoptosis-associated (bax, TdT, caspase 3, Figs. 1, 2, 3) proteins within the chicken ovarian cells, while EIAs/RIA demonstrated the release of P_4, T, E_2 and AVT by these cells into the culture medium (Figs. 4, 5).

These parameters were influenced by the addition of obestatin. Immunocytochemistry and TUNEL showed that obestatin addition reduced the percentage of cultured granulosa cells containing PCNA (when added at a dose of 1 and 10 ng/ml, but not at doses of 100 ng/ml, at this dose obestatin promoted PCNA accumulation, Fig. 2A), TdT (at doses of 1 and 10 ng/ml, but not at 100 ng/ml, Fig. 2C) and bax (at all doses, Fig. 2D). No influence of obestatin treatment on the accumulation of MAPK/ERK1,2 was found (Fig. 2B).

SDS PAGE-Western immunoblotting showed a visible obestatin-induced disappearance or reduction in the accumulation of cyclin B1 (when obestatin was added at a dose of 1 or 10 ng/ml) and an increase in the accumulation of caspase 3 in cultured granulosa cells. No visible changes in MAPK/ERK1,2 accumulation were observed (Fig. 2).

EIAs showed that obestatin addition reduced the release of P (at all doses, Fig. 3A) T (at all doses, Fig. 3B) and E (at doses of 10 and 100 ng/ml, while at a dose of 1 ng/ml some increase in hormone release occurred, Fig. 3C). On the other hand, the addition of obestatin to ovarian fragments increased the release of P_4, (at a dose of 10 ng/ml, but not at other doses,

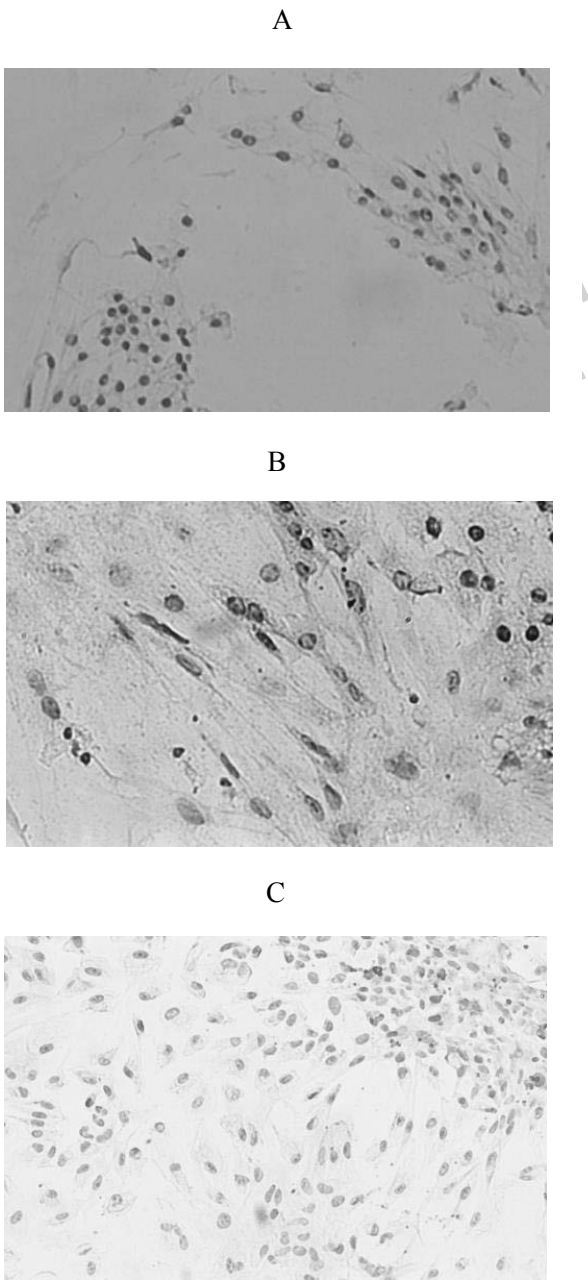

Fig. 1. *The presence of PCNA (**A**, x 400, immunocytochemistry and light microscopy), bax (**B**, x 800, immunocytochemistry and light microscopy) and TdT (**C**, x 400, TINEL) in cultured chicken ovarian granulosa cells.*

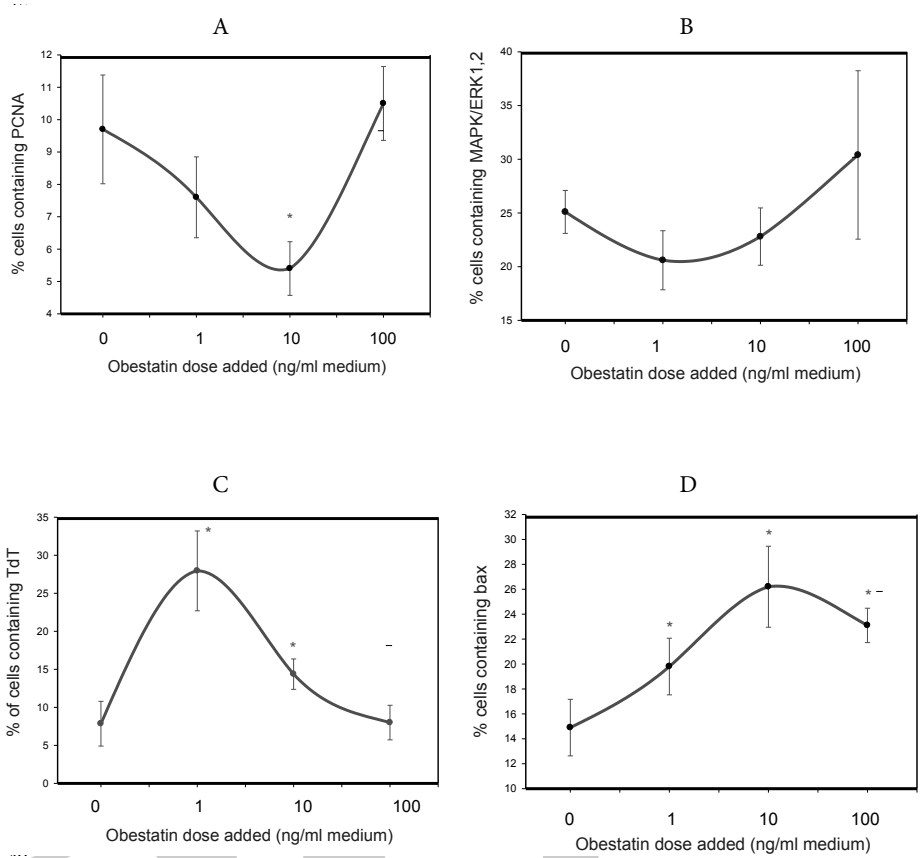

Fig. 2. *Effect of obestatin addition on the accumulation of PCNA (**A**), MAPK/ERK1,2 (**B**), TdT (**C**) and bax (**D**) in cultured chicken granulosa cells. The data were obtained from immunocytochemistry. The values indicate the mean +- S.E.M. * indicates significant (P < 0.05) differences between obestatin (0.1, 10 or 100 ng/ml)-treated and control (0 ng/ml) cells.*

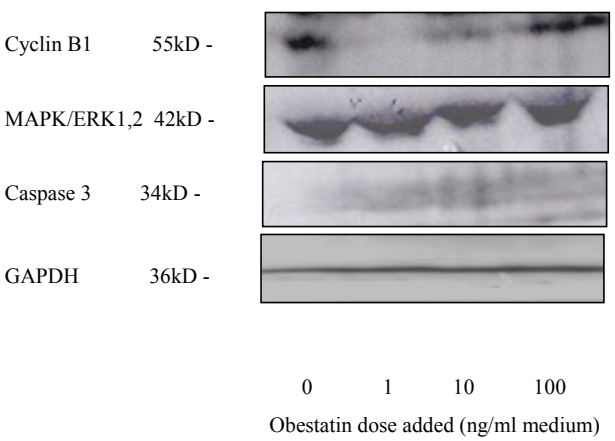

Fig. 3. *Effect of obestatin (0.1, 10 or 100 ng/ml medium) on the accumulation of cyclin B1, MAPK/ERK1,2, caspase 3 and GAPDH (housekeeping protein, loading control) in cultured chicken granulosa cells. The data were obtained from SDS PAGE-Western immunoblotting . The molecular weights of fractions are indicated on the left. The data regarding the densitometry of the fractions are not shown.*

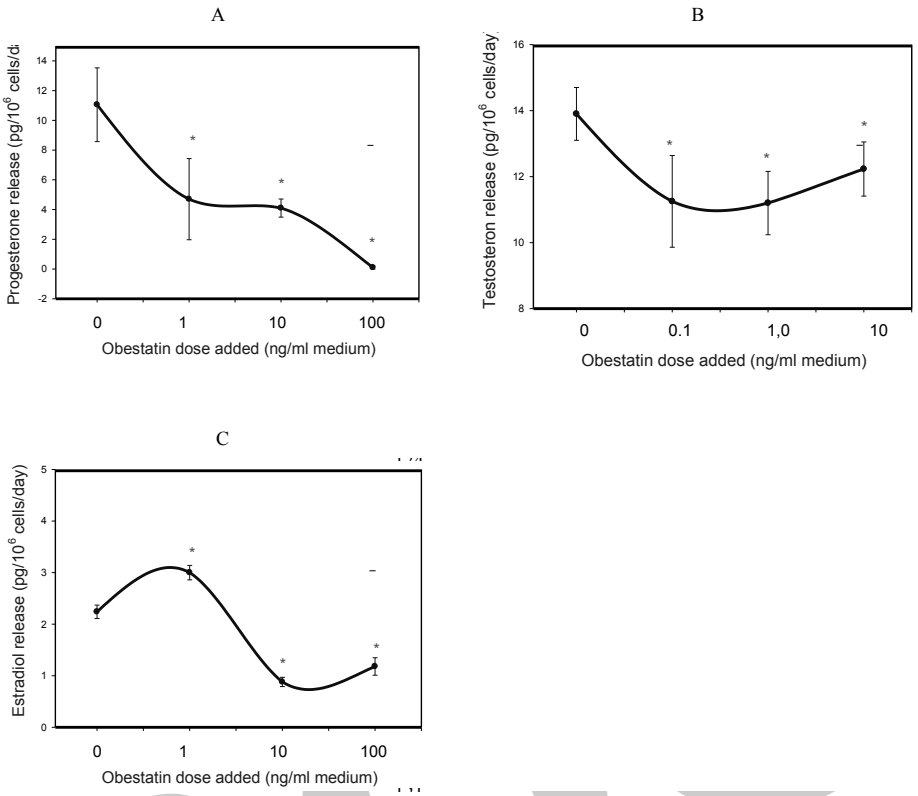

Fig. 4. *Effect of obestatin addition on the release of progesterone (**A**), testosterone (**B**) and estradiol (**C**) by cultured chicken granulosa cells. The data were obtained from EIA. The legends are identical to those of Fig. 1.*

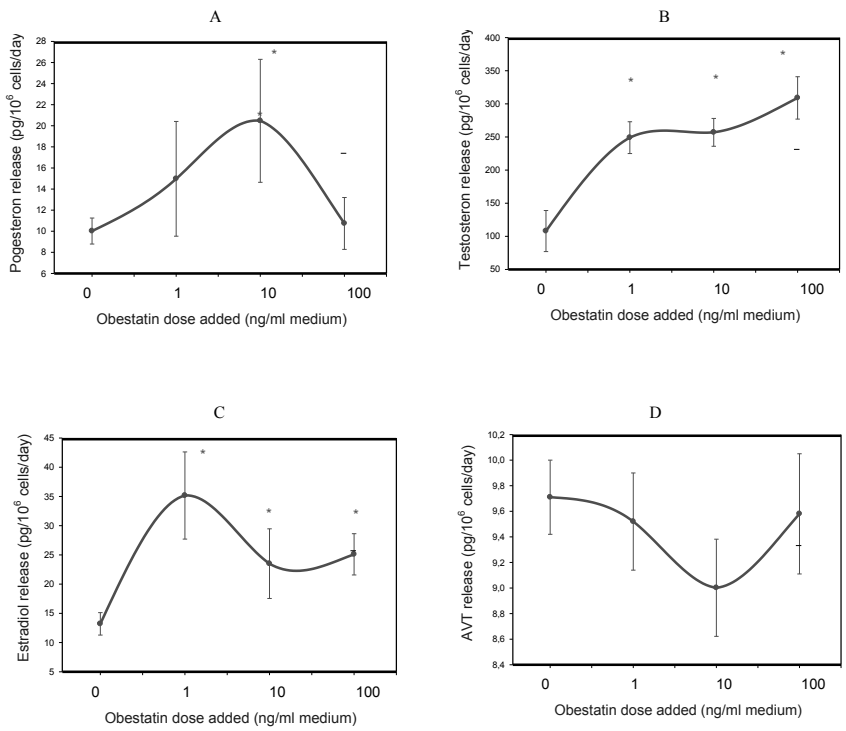

Fig. 5. *Effect of obestatin addition on the release of progesterone (**A**), testosterone (**B**), estradiol (**C**) and arginine-vasotocin (**D**) by cultured chicken ovarian fragments. The data were obtained from EIA. The legends are identical to those of Fig. 1.*

Fig. 4A), T (at all doses, Fig. 4B) and E_2 (at all doses, Fig. 4C). No significant influence of obestatin addition was found on AVT release (Fig. 4C).

DISCUSSION

The presence of proliferation-related substances within cultured ovarian granulosa cells and the ability of these cells and ovarian fragments to release hormones and respond to obestatin addition suggest that these substances were viable and useful as models for the direct influence of obestatin on ovarian functions.

The ability of obestatin addition to decrease the accumulation of proliferation markers (PCNA and cyclin B1 but not MAPK/ERK1,2), increase the accumulation of markers of nuclear (TdT) and cytoplasmic (bax, caspase 3) apoptosis and alter the release of steroid hormones by cultured ovarian cells observed in our experiments represents the first demonstration of direct action of obestatin on avian ovarian cell proliferation, apoptosis and hormone release. Previously, such a direct effect was demonstrated only on porcine cultured ovarian granulosa cells (4), whilst in this species obestatin increased both proliferation and apoptosis of granulosa cells. Therefore, obestatin can affect avian reproduction not only via known hypothalamic regulators (6-8, 15), but also through direct effects on ovarian cells. The differences in observed obestatin action on chicken (suppression of proliferation and promotion of apoptosis and all steroid hormones release) and porcine (promotion of both proliferation and apoptosis and of P, but not of T and E output) granulosa cells demonstrate substantial species-specific differences in direct obestatin effect on ovarian cells.

A reduction in the accumulation of proliferation markers and the promotion of apoptosis-related substances suggest a potential direct anti-gonadotropic effect of obestatin on chicken ovarian granulosa cells. This anti-gonadotropic effect could be due to the ability of obestatin to reduce the levels of steroid hormones that are involved in the maintenance of both chicken and mammalian ovarian functions (15, 18). This hypothesis may be confirmed by our present observations of obestatin action on ovarian steroidogenesis. Furthermore, this hypothesis is in line with our previous (9) observations of the ability of obestatin injections to alter ovarian steroid hormone release, although these injections did not affect the ovulation rate.

The available data concerning the action of obestatin on chicken ovarian hormones suggest different sites of obestatin action in this process and/or the importance of interrelationships between these sites in the control of avian ovarian secretory activity. In our previous experiments (9), obestatin injections (potentially targeting both CNS and the ovarian tissues) promoted P and E and suppressed T and AVT release. In our present experiments, obestatin addition to ovarian follicular fragments (containing both theca cells and granulosa, but not hypothalamic cells) promoted the release of P, T and E but did not affect AVT output. Finally, in the culture containing only ovarian granulosa cells, obestatin inhibited the release of all steroid hormones. A comparison of these observations suggests different patterns of action of obestatin on ovarian hormone release via the CNS, theca and granulosa compartments of the ovarian follicles. Furthermore, the opposite action of obestatin on the granulosa and granulosa+theca suggests the importance of both morphological and functional interrelationships between the granulosa and theca layers of the ovarian follicle in response to obestatin. Different actions of obestatin on theca and granulosa cells might be suggested, although validation of this hypothesis requires further experiments with culture and co-culture of theca and granulosa cells.

Understanding the sites and the role of obestatin in the control of reproductive processes requires further study. Nevertheless, the present observations represent the first demonstration that (1) obestatin can directly control avian ovarian cell proliferation, apoptosis and hormone release and (2) the interrelationship between the CNS, theca and granulosa cells can determine the characteristics of obestatin action on ovarian secretory activity.

ACKNOWLEDGEMENTS

The authors express their deep gratitude to G. Neuhaus for skillful technical help in arranging the experiments and AVT RIA, I. Stelter for EIA of steroid hormones, K. Tothova and Z. Kuklova for assistance in statistical processing of the data, as well as to Dr. D.A. Gray (Max-Plank Institute for

Physiological and Clinical Research, Bad Nauheim, Germany) for the kind gift of antiserum against AVT. This work was financially supported by the German and Slovak Ministries of Agriculture. Furthermore, the authors extend their appreciation to the International Scientific Partnership Program ISPP at King Saud University for funding this research work through ISPP# 0013)

REFERENCES

1. Roa J, Tena-Sempere M. Connecting metabolism and reproduction: roles of central energy sensors and key molecular mediators. Mol Cell Endocrinol 2014; 397:4-14.
2. Zhang JV, Ren PG, Avsian-Kretchmer O, Luo CW, Rauch R, Klein C, Hsueh AJ. Obestatin, a peptide encoded by the ghrelin gene, opposes ghrelin's effects on food intake. Science 2005; 310:996-9.
3. Luque RM, Córdoba-Chacón J, Ibáñez-Costa A, et al. Obestatin plays an opposite role in the regulation of pituitary somatotrope and corticotrope function in female primates and male/female mice. Endocrinology 2014; 155:1407-17.
4. Mészárosová M, Sirotkin AV, Grossmann R, Darlak K, Valenzuela F. The effect of obestatin on porcine ovarian granulosa cells. Anim Reprod Sci 2008; 108:196-207.
5. Sirotkin AV, Bezáková A, Laurinčík J, Matejovičová B. Involvement of the metabolic hormones leptin, ghrelin, obestatin, IGF-I and of MAP kinase in control of porcine oocyte maturation. Animal 2011; 5:94-9.
6. Song Z, Verhulst PJ, Ansari Z, Thijs T, Depoortere I, Everaert N, Decuypere E, Buyse J. Peripheral „chicken" obestatin administration does not affect feed intake and gut muscle contractility of meat-type and layer-type chicks (Gallus gallus domesticus). Regul Pept 2012; 177:60-7.
7. Song Z, Everaert N, Wang Y, Decuypere E, Buyse J. The endocrine control of energy homeostasis in chickens. Gen Comp Endocrinol 2013; 190:112-7.
8. Sirotkin AV, Pavlova S, Tena-Sempere M, Grossmann R, Jiménez MR, Rodriguez JM, Valenzuela F. Food restriction, ghrelin, its antagonist and obestatin control expression of ghrelin and its receptor in chicken hypothalamus and ovary. Comp Biochem Physiol A Mol Integr Physiol 2013; 164:141-53.
9. Sirotkin AV, Grossmann R. Interrelationship between feeding level and the metabolic hormones leptin, ghrelin and obestatin in control of chicken egg laying and release of ovarian hormones. Comp Biochem Physiol A Mol Integr Physiol 2015; 184C:1-5.
10. Ulrich HD, Takahashi T. Readers of PCNA modifications. Chromosoma 2013; 122:259-74.
11. Sirotkin AV, Grossmann R. The role of protein kinase A and cyclin-dependent (CDC2) kinase in the control of basal and IGF-II-induced proliferation and secretory activity of chicken ovarian cells. Anim Reprod Sci 2006; 92:169-81.
12. Wolgemuth DJ. Function of cyclins in regulating the mitotic and meiotic cell cycles in male germ cells. Cell Cycle 2008; 7:3509-13.
13. Sirotkin AV, Grossmann R. Role of tyrosine kinase- and MAP kinase-dependent intracellular mechanisms in control of ovarian functions in the Domestic fowl *(Gallus domesticus)* and in mediating effects of IGF-II. J Reprod Dev 2003; 49:99-106.
14. Lei YY, Wang WJ, Mei JH, Wang CL. Mitogen-activated protein kinase signal transduction in solid tumors. Asian Pac J Cancer Prev 2014; 15:8539-48.
15. Sirotkin AV. Regulators of Ovarian Functions. Nova Science Publishers, Inc., New York, USA. 2014; p.194.
16. Loo DT. In situ detection of apoptosis by the TUNEL assay: an overview of techniques. Methods Mol Biol 2011; 682:3-13.
17. Gillies LA, Kuwana T. Apoptosis regulation at the mitochondrial outer membrane. J Cell Biochem 2014; 115:632-40.
18. Rangel PL, Gutierrez CG. Reproduction in hens: is testosterone necessary for the ovulatory process? Gen Comp Endocrinol 2014; 203:250-61.
19. Sirotkin AV, Meszarosová M. Comparison of effects of leptin and ghrelin on porcine ovarian granulosa cells. Domest Anim Endocrinol 2010; 39:1-9.
20. Prakash BS, Meyer HH, Schallenberger E, van de Wiel DF. Development of a sensitive enzymeimmunoassay (EIA) for progesterone determination in unextracted bovine plasma using the second antibody technique. J. Steroid Biochem 1987; 28:623-7.
21. Münster E. Entwicklung von enzymimmunologischen Messverfahren auf Mikrotitrationsplatten zur

Bestimmung von Testosteron und Progesteron im Blutplasma. Thesis. Institut for Animal Production and Breeding of the University of Hohemheim. 1989; p.154.

22. Gray DA, Simon E. Mammalian and avian antidiuretic hormone: studies related to posible species variation in osmoregulatory systems. J Comp Physiol 1983; 151:241-6.

EVALUATION OF CD4$^+$ CD25$^+$ FoxP3$^+$ REGULATORY T CELLS DURING TREATMENT OF PATIENTS WITH BRUCELLOSIS

M.R. HASANJANI ROUSHAN[1], M. BAYANI[1], S. SOLEIMANI AMIRI[1], M. MOHAMMADNIA-AFROUZI[2], H.R. NOURI[2] and S. EBRAHIMPOUR[1]

[1]Infectious Diseases and Tropical Medicine Research Center, Babol University of Medical Sciences, Babol, Iran; [2]Cellular and Molecular Biology Research Center, Babol University of Medical Sciences, Babol, Iran

Received April 8, 2016 – Accepted May 4, 2016

Cell-mediated immunity (CMI) plays a critical role in the control of brucellosis. Regulatory T cells (Tregs) have a functional character in modulating the balance between host immune response and tolerance, which can eventually lead to chronic infection or relapse. The aim of this study was to assess the alteration of Tregs in cases of brucellosis before and after treatment. Thirty cases of acute brucellosis with the mean age of 41.03±15.15 years (case group) and 30 healthy persons with the mean age of 40.63± 13.95 years (control group) were selected and assessed. Peripheral blood mononuclear cells (PBMCs) were isolated from peripheral blood of all individuals. We analyzed the alteration of Treg cell count using flow cytometry for CD4, CD25, and FoxP3 markers. The level of CD4$^+$ CD25$^+$ FoxP3$^+$ Treg cells was increased in active patients compared with controls (2.5±0.99% vs 1.6± 0.84%, p= 0.0004), but it had declined in the treated cases (1.83±0.73%, p=0.02). The level of Tregs was elevated in three relapsed cases. The frequency of Tregs and Treg/Teff (effector T cell) ratio was correlated with inverse serum agglutination test (SAT) and, 2-mercaptoethanol (2-ME) titers as markers of treatment in brucellosis. Based on our findings, we suggest that regulatory cells, such as CD4+ CD25+ FoxP3+ Treg cells, may contribute to the development of infection processes involving immune responses in brucellosis, and evaluation of regulatory T-cell levels may be a potential diagnostic strategy for the treatment outcome in chronic and relapsed cases of brucellosis.

Brucellosis is a common zoonotic infection and remains a great challenge for human beings worldwide, especially in the Middle East, Arabian peninsula, Indian subcontinent, central and south America (1, 2). Brucellosis is a multi-organ infectious disease that may present with a wide spectrum of clinical manifestations, including involvement of the central nervous system (CNS), musculoskeletal, hepatic and cardiovascular systems (3). Because of these issues, treatment is associated with seriousness of difficulties. Host protection against pathogen depends on cell-mediated immunity, particularly T cells and activated antigen-presenting cells (APCs) (4). In recent years, CD4$^+$ CD25$^+$ FoxP3$^+$ circulating regulatory T cells (Tregs) have become an important focus of studies. As a subset of T cells, Tregs constitute up to 5% of peripheral CD4$^+$ T cells in peripheral blood of healthy humans (5). Active suppression of immune responses is the preliminary role of Tregs in the host that may lead to a chronic form

Key words: brucellosis, CMI, treg cells, treatment regimen

Mailing address:
Dr Soheil Ebrahimpour,
Infectious Diseases and Tropical Medicine Research Center,
Babol University of Medical Sciences,
Babol, Iran
Tel.: +989111149309 - Fax: +981132207918
e-mail: drsoheil1503@yahoo.com.

0393-974X (2016)

of many bacterial or viral infections. In other words, elevated levels of regulatory cells and increased suppressive capacity are associated with chronic disease. It was shown that Tregs were able to restrict the effectiveness of helper T cells and contribute to progression of *B.abortus* infection (6). In addition, *Schistosoma haematobium* infection is associated with increased level of Tregs, which is a strategy for survival in the host. However, the percentage of Tregs is decreased after treatment with Praziquantel (7). Other findings indicated that in the absence of Tregs, a dysregulated response to *Staphylococcus aureus* enterotoxin B could lead to T cell activation, especially in colitis (8). Generally, many researchers have shown that Tregs were increased in infections, which can be significantly associated with the inhibition of immune response to infectious agents (7, 9-11). In brief, cell-mediated immunity involves the activation of bactericidal mechanisms as in the case in brucellosis. Given that different populations have various immune responses, the response to treatment is thus related to multiple immune factors such as some T-cell subsets (Tregs).

Despite comprehensive research, there is still much that remains unclear about the association between regulatory cells and infections during therapy. Therefore, the purpose of this study was to determine these regulatory cells and their levels in patients with brucellosis as a substantial re-emerging infectious disease alongside treatment regimen.

MATERIALS AND METHODS

Participants

From July 2014 to February 2016, 60 persons (30 cases of brucellosis and 30 healthy individuals) with the mean age of 40.83±14.44 years were assessed at the department of Infectious Diseases of Babol Medical University in Babol, northern Iran.

Thirty brucellosis patients (25 males and 5 females) with the mean age of 41.03±15.15 years (range 2 to 80 years) who had been recently diagnosed and had not received any type of treatment were selected as case group (AB), and 30 healthy age- and gender-matched volunteers with the mean age of 40.63±13.95 years were selected as control group (HC). Additionally, brucellosis patients who received medication or treated cases formed the follow-up group (FB). Brucellosis in patients before and after treatment was diagnosed when they had a positive blood culture (blood inoculated in Castaneda biphasic medium and incubated for six weeks at 37°C as identification test for Brucella species), standard agglutination test (SAT) titer ≥1:320, 2-mercaptoethanol (2-ME) titer ≥1:80 with typical clinical signs and symptoms of human brucellosis (fever, sweating, fatigue, arthralgia, muscle and back pain). For all cases, Coombs Wright test was also carried out. Blood culture and serological tests were performed on healthy individuals and all had negative results. Cases of pregnancy, meningitis, endocarditis and spondylitis were excluded from the study.

All patients received gentamicin 5 mg/kg/day for 1week plus doxycycline 100 mg/bid for 45 days. After treatment all subjects were followed-up for one year to detect relapsed cases. Relapse was defined when the clinical picture reappeared and reduced titers of SAT, and 2 ME titers increased again after completion of therapy. This research protocol was approved by the ethics committee of Babol University of Medical Sciences. All the participants signed written informed consent form.

Sampling and isolation of PBMCs

Blood samples were collected in ethylene diamine tetra-acetic acid (EDTA) containing tubes. Two blood samples (15 ml) were obtained from all cases before and after termination of treatment, one for blood culture and serological tests and another for the isolation of peripheral blood mononuclear cells and flow cytometry for assessment of Tregs. In short, PBMCs were isolated from about 5 ml fresh whole blood samples using Ficoll-Paque density gradient centrifugation (Biowest, Nuaille, France) at 400 g for 35 min at room temperature.

Flow cytometry

As a substantial tool for research on the complexity of immune system, multi-parameter flow cytometry was used to distinguish Tregs and determine the expression of cell markers. PBMCs were washed twice and re-suspended in phosphate buffer saline (PBS) with 0.1% bovine serum albumin *(*BSA) as staining buffer. In Brief, about 1×10^6 mononuclear cells were stained with PerCP-Cy5.5-conjugated mAb against CD4 (Clone RPA-T4;BD Biosciences, San Jose, CA, USA) and Fluorescein

isothiocyanate (FITC)-conjugated mAb against CD25 (Clone MEM-181; Exbio, Praha, Czech Republic) for 30 min at 4°C in the dark. Intracellular staining for Foxp3 was carried out as follows: the cells were fixed and permeabilized with FoxP3 staining buffer (Exbio) according to the manufacturer's instructions. The cells were then stained with PE-conjugated mAb against FoxP3 (Clone 3G3; Exbio, Praha, Czech Republic). Moreover, compensation control was run or the negative control was fluorochrome-matched mAbs with proper isotypes to recognize the background fluorescence. Overall, the samples were analyzed with Partec CyFlow Space flow cytometer (Partec GmbH, Münster, Germany), and the findings were analyzed using FlowMax (Partec) and FlowJo software (Tree Star, Ashland, Ore, USA). A minimum of 1×10^5 events at lymphocyte gate were analyzed. Mean fluorescence intensity (MFI) of $FoxP3^+$ cells gated on $CD4^+$ $CD25^+$ Tregs was analyzed.

Statistical analysis

All data were tabulated in Microsoft Excel spreadsheets with an exclusive identification code for each Participant. Those collected were analyzed by GraphPad Prism statistical software 6.0 (GraphPad Software, Inc., San Diego, CA, USA). The variables were presented as mean± standard deviation (SD) and were compared between independent groups by student's *t*-test (unpaired, two-tailed) and between the two dependent groups (before and after treatment) by paired *t*-test. Pearson's correlation coefficient was used for the correlation analysis. Differences with a *p*-value of < 0.05 were considered to be statistically significant.

RESULTS

Demographic characteristics and laboratory test results

Demographic data of brucellosis patients and healthy controls are shown in Table I. Eighteen (37%) patients were residents of rural areas and others were from urban areas. Two (6.7%) patients had SAT titer ≥ 1:640, 10 (33.3%) SAT titer ≥1:320 and 13 (43.3%) with SAT titers ≥1:160. Moreover, 13 (43.3%) patients had 2ME titer ≥1:160 and 10 (33.3%) 2ME titer ≥1:80. Most patients had a high titer in Coomb's test (at least 1:320), 13 (43.3%) patients had Coomb's test titers ≥ 1:640, and 11 (36.6%) had Coomb's test titers ≥ 1:320. Peripheral white blood cell counts >11,000/ ml were found in 13 (46.6%) cases and ESR >30 mm/h in 10 (33.3%) cases.

Frequency of $CD4^+$ T cell subpopulations

Typical data on $CD4^+$Tcell subpopulations in a healthy control, a patient and a treated case (follow-up) are shown in Fig. 1. Furthermore, the frequencies of $CD4^+$Tcell subpopulations from the three groups are shown as mean ± SD in Fig. 2. We found no significant difference between patients (AB, FB) and controls in the percentage of $CD4^+$ Tcells. To identify the level of $CD4^+CD25^+$ cells, this subpopulation was divided into two groups in accordance with $CD25^+$expression level ($CD4^+$ $CD25^{high}$ cells and $CD4^+$ $CD25^{low}$ cells). Our findings showed significant difference in the percentage of $CD4^+$ $CD25^{high}$ cells in AB and controls as well as between AB and FB groups (P= 0.03 and P=0.04, respectively). To assess the frequency of $CD4^+$ $CD25^+$ Treg cells and $CD4^+$ $CD25^+$ T-effector cells, the $CD4^+CD25^+$ subpopulation was apportioned to two groups based on the expression of FoxP3. Our results showed significant increase in the percentage of $CD4^+$ $CD25^+$ $FoxP3^+$ Treg cells in the AB group and controls (P= 0.0004). Antibiotic treatment resulted in a significant reduction in the percentage of $CD4^+$ $CD25^+$ $FoxP3^+$ Treg cells in FB compared to AB group (P= 0.02). Surprisingly, the level of Treg cells was elevated in three relapse cases. However, we found that the percentage of $CD4^+$ $CD25^+$ $FoxP3^-$ Teff cells (effector cells) was not significantly different between the groups. Additionally, these findings showed significant difference in the percentage of Treg/Teff ratio between AB and control groups (P= 0.02), but not between FB and AB groups.

Correlating the frequency of Treg cells with serological aspects of brucellosis

Subsequently, the correlation of brucellosis serological tests with the frequency of Treg cells was determined in the AB and FB groups. As shown in Fig. 3, in the AB group we observed a significant positive correlation between the percentage of $CD4^+CD25^+$ $FoxP3^+$ Treg cells and inverse titers of

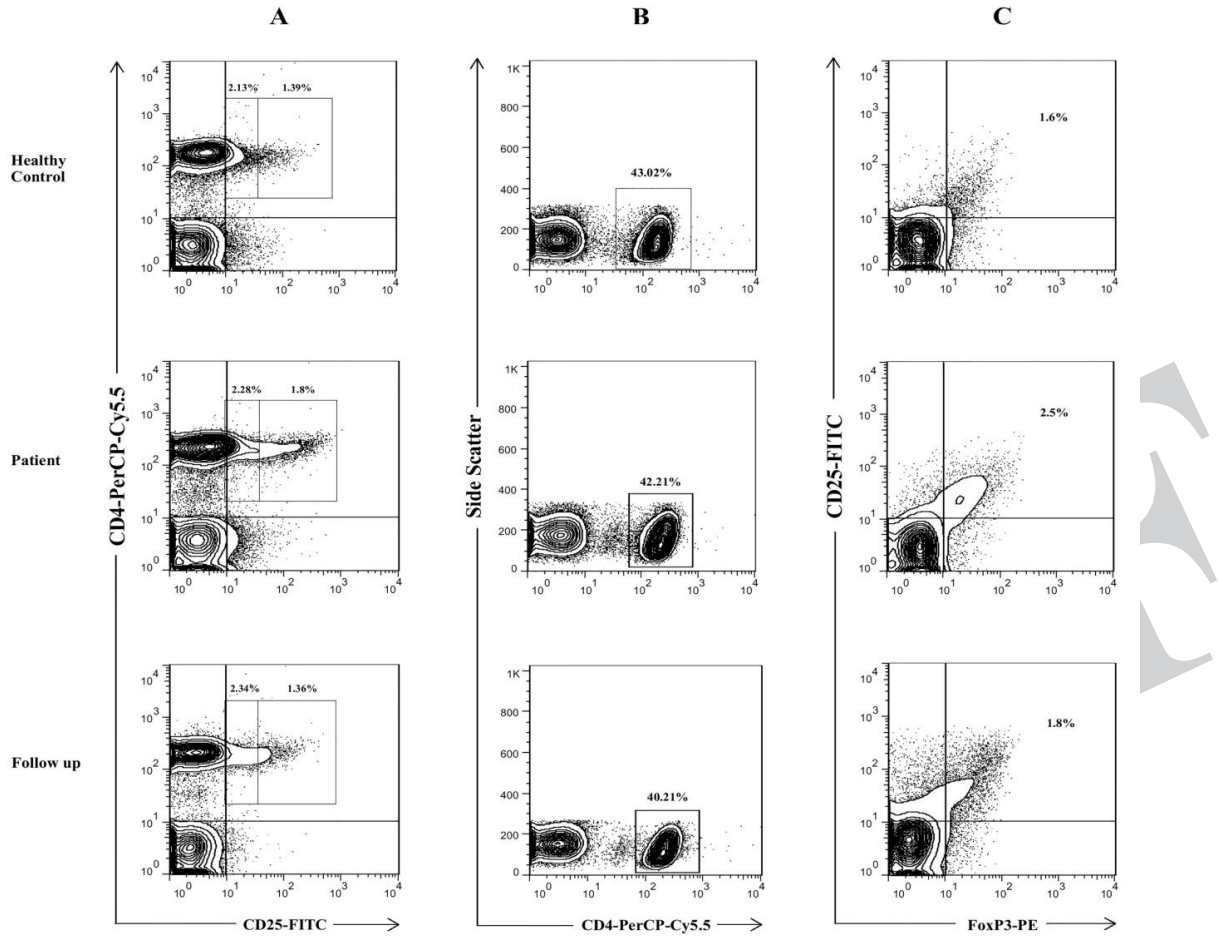

Fig. 1. *Flowcytometry analysis of Treg cell populations in agent control, patients and treated cases (follow-up). Initially, PBMC were isolated by Ficoll density gradient centrifugation and were stained for cell surface markers CD4, CD25 and intracellular protein FOXP3. Then, the cells were gated on lymphocytes via their forward and side scatter properties.* ***A)*** *The gates show percentage of* $CD4^+CD25^+$ *in gated lymphocytes.* ***B)*** *The gates administrate the percentage of* $CD4^+$ *in gated lymphocytes.* ***C)*** *The gates present percentage of* $CD25^+FOXP3^+$ *in* $CD4^+$ *gated lymphocytes.*

SAT and 2-ME (r =0.4, P= 0.027, and r= 0.45, P= 0.012, respectively). Additionally, in the FB group, a significant positive correlation was observed between the percentage of $CD4^+CD25^+$ $FoxP3^+$ Treg cells and inverse titers of SAT and 2-ME (r =0.47, P=0.009, and r= 0.35, P= 0.051, respectively). A similar case occurred in relation to Treg/Teff ratio in the AB and FB, as in the AB group, a statistically significant positive correlation was found between Treg/Teff ratio and inverse titers of SAT and 2-ME (r =0.556, P=0.001, and r= 0.447, P= 0.013, respectively). In addition, a significant positive correlation was shown between Treg/Teff ratio and decreased inverse titers of SAT and 2-ME in the FB group (r =0.39, P=0.029, and r= 0.38,P= 0.037, respectively).

DISCUSSION

Cell-mediated immunity is the critical immune response to Brucella infection, and involves $CD4^+$ and $CD8^+$ T-lymphocytes. Antigens of bacteria impel the production of Th1 cytokines. Therefore, Th1 immune response is necessary for the clearance of infection. However, many studies have shown that during brucellosis, Th1 response is never able to entirely clear the infection (12, 13). Treg cells constitute a permanent lineage of dedicated

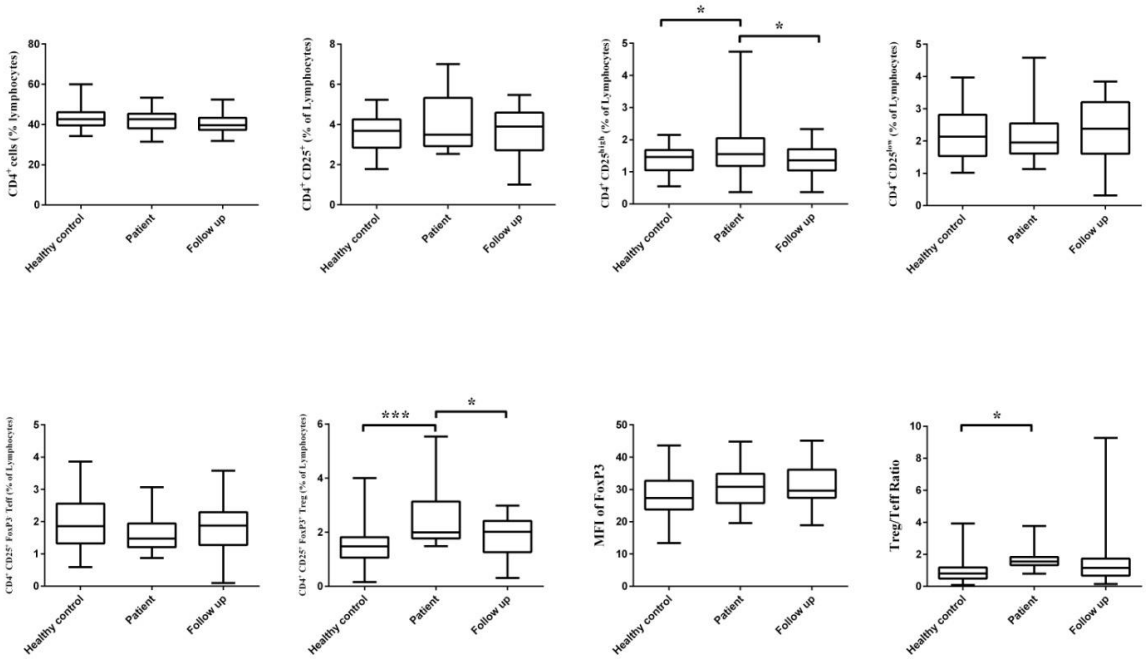

Fig. 2. *Frequency of CD4⁺ subpopulations in healthy controls, patients and treated cases (follow-up). Values are shown as mean ±SD.* p-value of < 0.05 was considered to be significant.*
** P<0.05, **P<0.01,***P<0.001.*

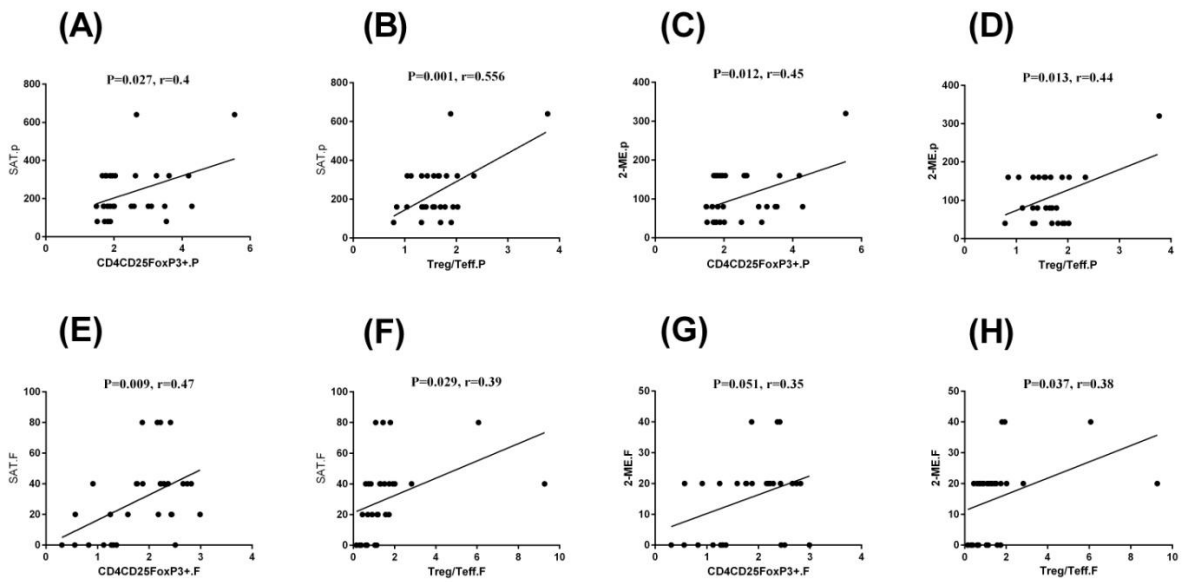

Fig. 3. *Correlation between brucellosis serological tests with the frequency of Treg cells and Treg/Teff ratio. There is positive correlation between SAT with Tregs (**A**) and Treg/Teff (**B**) in patients. Positive correlation is shown between 2-ME with Tregs (**C**) and Treg/Teff (**D**) in patients. There is positive correlation between SAT with Tregs (**E**) and Treg/Teff (**F**) in follow-up. Positive correlation is shown between 2-ME, Tregs (**G**) and Treg/Teff (**H**) in follow-up. P; patient, F; treated cases (follow-up).*

regulator cells crucial for suppression of immune response and preservation of immune tolerance (14). Some studies have revealed the correlation between Treg cells and disease progress from healthy condition to acute and chronic phases of infection, which may cause disruption of immunity in patients. For example, regulatory T cells were elevated in patients with active pulmonary tuberculosis and are capable of impeding the proliferation of $CD4^+$ T cells in these cases (15). In *Leishmania major* infection, elimination of Treg cells is associated with an elevated number of effector T cells and reduced involvement of pathogen (16). In this study, we assessed the association between regulatory T cells and Brucella infection during therapy with gentamicin plus doxycycline as a standard treatment regimen. So far, in the endemic regions, SAT and 2-ME tests have been used for the diagnosis of brucellosis, treatment results or follow-up of treated cases (17). Therefore, we investigated the correlation between SAT and 2-ME test results with percentage of Treg cells. We found a reduction in SAT and 2-ME titers after completion of treatment, and the therapy was therefore successful. Moreover, the percentage of $CD4^+$ $CD25^+$ $FoxP3^+$ Treg cells and $CD4^+$ $CD25^{high}$ cells (as a type of regulatory cells) were declined while the percentage of $CD4^+CD25^+$ $FoxP3^+$ Treg cells and $CD4^+CD25^{high}$ cells in active patients were increased. Therefore, gentamicin plus doxycycline treatment can decrease Treg cells in brucellosis. As is evident, in this study we evaluated the frequency of Treg cells in brucellosis after antibiotic therapy for the first time. Compatible with our data, some other studies reported that in the synovial fluid of patients with antibiotic-responsive Lyme arthritis who received doxycycline, the percentage of $FoxP3^+$ Treg cells was significantly lower than in synovial fluid of patients with antibiotic-refractory arthritis (18). Similar to the findings of our research, other reports using gene expression analysis of human blood T cells showed that several genes associated with differentiation of Treg cells were down-regulated in T cells stimulated in the vicinity of some beta-lactam antibiotics such as cefuroxime (19). On the contrary, Kulte et al. reported that Treg levels in HIV-infected patients were increased even after 5 years of receiving highly active anti-retroviral therapy (HAART). Higher Treg levels in HIV-infected cases may be due to enhanced thymic production of naive Treg cells (20).

In agreement with the results of previous studies, our current research revealed the increased percentage of $CD4^+$ $CD25^+$ cells in a treated group versus control and followed-up groups, suggesting that Th cells are activated in the treated group (21). In agreement with the results of our study, other researchers showed that the percentage of peripheral $CD4^+$ $CD25^+$ $FoxP3^+$ Treg cells was increased in a treated group, in other words, activation of the immune system triggered the stimulation of Treg cells (22). Contrary to our data, Saadoun et al. showed that Treg cells were reduced in patients with vasculitis (autoimmune condition) resulting from hepatitis C virus (HCV), in which case IL-2 led to Treg recovery and improvement

Table I. *Demographical data of the patients and the control group*

Characteristic	Brucellosis Patients	controls
Number	30	30
Sex (Male/Female)	25/ 5	25/ 5
Age, year, Mean ± SD	41.03±15.15	40.63±13.95
Residency(Rural/ Urban)	18/ 12	17/ 13

of clinical aspects (23). Interaction between the microorganism and immune system can induce the reduction of Treg cells in vasculitis.

Treg/Teff ratio was increased in patients versus healthy controls at the beginning of the study, although this ratio was not significantly decreased after treatment, suggesting that Treg cells can be produced via stimulation of T cells by Brucella antigens during infection. Gentamicin plus doxycycline could potentially result in reduced Treg induction, but may not be capable of increasing T-effector cells sufficiently. The limitation of this research was consideration of only one treatment regimen in the treatment of uncomplicated brucellosis, and further detailed investigation of alteration in the function of $CD4^+$ $CD25^+$ $FoxP3^+$ Treg cells and their cytokine secretion, such as IL-10, TGF-β and IL-35, with several therapies are recommended. Treatment failure and relapse are the major problems in the treatment of brucellosis. Interestingly, consideration of the frequency of $CD4^+CD25^+$ $FoxP3^+$ Treg cells during relapse may be useful to understand the mechanisms for development and diagnosis of relapse when routine serological tests are not reliable. Moreover, in this study, localized involvement cases, such as spondylitis, endocarditis and meningitis, were excluded; therefore, investigations of regulatory T-cell levels in these conditions are recommended.

In conclusion, we found documents on the involvement of Treg cells in the pathogenesis of brucellosis. During the active phase of brucellosis, Treg cells can be found in high numbers in the peripheral blood. Our findings indicated positive correlation between improvement of patients› condition or treated cases with the frequency of $CD4^+$ $CD25^+$ $FoxP3^+$ Treg cells. These results suggest that the level of Treg cells most likely established a potential diagnostic and therapeutic strategy for the diagnosis of relapsed or chronic cases of brucellosis.

ACKNOWLEDGEMENTS

The authors acknowledge the cooperation of the entire personnel of the Department of Infectious Diseases, Babol Medical University and the staff of the Babol Razi Medical Laboratory.

This project was fully sponsored by the Infectious Diseases Research Center, Babol University of Medical Sciences, Babol, Iran (Project number= 9237518)

REFERENCES

1. Hasanjani Roushan MR, Ebrahimpour S. Human brucellosis: An overview. Caspian J Intern Med 2015; 6:46-47.
2. Asiimwe BB, Kansiime C, Rwego IB. Risk factors for human brucellosis in agro-pastoralist communities of south western Uganda: a case–control study. BMC Res Notes 2015; 8:405.
3. Young EJ, Hasanjani Roushan MR, Shafae S, Genta RM, Taylor SL. Liver histology of acute brucellosis caused by Brucella melitensis. Human Pathol 2014; 45:2023-228.
4. Skendros P, Boura P. Immunity to brucellosis. Revue scientifique et technique (International Office of Epizootics) 2013; 32:137-47.
5. Velavan T, Ojurongbe O. Regulatory T cells and parasites. J Biomed Biotechnol 2011; 2011:8.
6. Pasquali P, Thornton AM, Vendetti S, et al. CD4+CD25+ T regulatory cells limit effector T cells and favor the progression of brucellosis in BALB/c mice. Microbes Infect 2010; 12:3-10.
7. Schmiedel Y, Mombo-Ngoma G, Labuda LA, et al. CD4+ CD25 hi FOXP3+ regulatory T cells and cytokine responses in human schistosomiasis before and after treatment with praziquantel. PLoS Negl Trop Dis 2015; 9:e0003995.
8. Heriazon A, Zhou P, Borojevic R, et al. Regulatory T cells modulate staphylococcal enterotoxin B-induced effector T-cell activation and acceleration of colitis. Infect Immun 2009; 77:707-13.
9. Feng H, Yin J, Han YP, et al. Regulatory T cells and IL-17(+) T helper cells enhanced in patients with chronic hepatitis B virus infection. Int J Clin Exp Med 2015; 8:8674-85.
10. Gonzalez SM, Zapata W, Rugeles MT. Role of regulatory T cells and inhibitory molecules in the development of immune exhaustion during human immunodeficiency virus type 1 infection. Viral Immunol

2016; 29:2-10.
11. González FB, Calmon-Hamaty F, Nô Seara Cordeiro S, et al. Trypanosoma cruzi Experimental Infection Impacts on the Thymic Regulatory T Cell Compartment. PLoS Negl Trop Dis 2016; 10:e0004285.
12. Skendros P, Pappas G, Boura P. Cell-mediated immunity in human brucellosis. Microbes Infect 2011; 13:134-42.
13. Vitry M-A, Mambres DH, De Trez C et al. Humoral immunity and CD4+ Th1 cells are both necessary for a fully protective immune response upon secondary infection with Brucella melitensis. J Immunol 2014; 192:3740-52.
14. Bilate AM, Lafaille JJ. Induced CD4+ Foxp3+ regulatory T cells in immune tolerance. Annual rev immunol 2012; 30:733-58.
15. Pang H, Yu Q, Guo B et al. Frequency of regulatory T-Cells in the peripheral blood of patients with pulmonary tuberculosis from Shanxi Province, China. PLoS ONE 2013; 8:e65496.
16. Johanns TM, Ertelt JM, Rowe JH, Way SS. Regulatory T cell suppressive potency dictates the balance between bacterial proliferation and clearance during persistent Salmonella infection. PLoS Pathog 2010; 6:e1001043.
17. Roushan MRH, Amiri MJS, Laly A, Mostafazadeh A, Bijani A. Follow-up standard agglutination and 2-mercaptoethanol tests in 175 clinically cured cases of human brucellosis. Int J Infect Dis 2010; 14(3):e250-e253.
18. Shen S, Shin JJ, Strle K, et al. Treg cell numbers and function in patients with antibiotic-refractory or antibiotic-responsive lyme arthritis. Arthritis Rheum 2010; 62:2127-37.
19. Mor F, Cohen IR. Beta-lactam antibiotics modulate T-cell functions and gene expression via covalent binding to cellular albumin. Proc Natl Acad Sci USA 2013; 110:2981-86.
20. Kolte L, Gaardbo J, Skogstrand K, Ryder L, Ersbøll AK, Nielsen S. Increased levels of regulatory T cells (Tregs) in human immunodeficiency virus-infected patients after 5 years of highly active anti-retroviral therapy may be due to increased thymic production of naive Tregs. Clin Experiment Immunol 2009; 155:44-52.
21. Skendros P, Boura P, Chrisagis D, Raptopoulou-Gigi M. Diminished percentage of CD4+ T-lymphocytes expressing interleukine-2 receptor alpha in chronic brucellosis. J Infect 2007; 54:192-97.
22. Bahador A, Hadjati J, Hassannejad N, et al. Frequencies of CD4+ T regulatory cells and their CD25 high and FoxP3 high subsets augment in peripheral blood of patients with acute and chronic brucellosis. Osong Public Health and Research Perspectives 2014; 5:161-68.
23. Saadoun D, Rosenzwajg M, Joly F et al. Regulatory T-cell responses to low-dose interleukin-2 in HCV-induced vasculitis. N Engl J Med 2011; 365:2067-77.

ZNF185 INHIBITS GROWTH AND INVASION OF LUNG ADENOCARCINOMA CELLS THROUGH INHIBITION OF THE AKT/GSK3B PATHWAY

J. WANG, H-H. HUANG and F-B. LIU

Department of Thoracic Surgery, The First People's Hospital Affiliated to Shanghai Jiaotong University, Shanghai, China

Received February 17, 2015 – Accepted June 27, 2016

The first two authors contributed equally to this work

Zinc finger (ZNF) proteins, a diverse family of proteins, have multiple biological functions in cancer. Increased expression of ZNF185 has been involved in the regulation of tumor growth and metastasis. However, the function and underlying mechanisms of ZNF185 in the tumorigenesis of lung adenocarcinoma (LAC) remain unclear. The protein expression of ZNF185 was examined in human LAC tissues by immunohistochemical assay. After lentiviral vector-mediated ZNF185 overexpression was infected into the LAC cell lines (A549 and LETPα-2), cell growth and invasive potential were respectively evaluated by MTT and Transwell assays. We found that the protein expression of ZNF185 was significantly downregulated in LAC tissues compared with the adjacent non-cancerous tissues (ANCT) (37.10% vs 58.06%, P=0.015), and was negatively correlated with the lymph node metastasis of the LAC patients (P=0.005). Furthermore, overexpression of ZNF185 reduced cell proliferation and invasion in LAC cells, followed by the downregulation of p-AKT, p-GSK3β, VEGF and MMP-9 expression. Taken together, our findings indicate that the decreased expression of ZNF185 is linked to the tumor metastasis in human LAC patients, and ZNF185 overexpression inhibits the growth and invasion of LAC cells through inhibition of the AKT/GSK3β signaling, suggesting that ZNF185 may represent a potential therapeutic target for the treatment of LAC.

Lung cancer is the most common cause of cancer-related death with the highest incidences and the worse prognosis. (1). Although many strategies, including surgical resection, chemo- or radiotherapy, have been applied to treat lung cancer, the recurrence rate of lung adenocarcinoma (LAC) is still high and survival rate appears low compared with the other types of lung cancer (2). Multiple gene abnormalities such as *KRAS*, *p53*, and *EGFR* have been involved in the tumorigenesis of LAC. Therefore, identification of tumor biomarkers related to LAC progression is crucial to our understanding of cancer metastasis (3).

Zinc finger (ZNF) proteins are a massive and diverse family of proteins that exert various biological functions in cancer. The subfamily of ZNF proteins is an important mediator during developmental processes, of which the conserved ZNF503 promotes mammary epithelial cell proliferation and enhances cell invasion (4). Krüppel-like ZNF217 is proved to be a candidate oncogene associated with poor prognosis and metastases and promotes invasion and epithelial-mesenchymal transition (EMT) in breast cancer (5). ZNF322A encoding a classical Cys2His2 zinc finger transcription factor as a potential

Key words: ZNF185, growth, invasion, lung adenocarcinoma

Mailing address:
Dr Fa-Bing Liu,
Department of Thoracic Surgery, The First People's Hospital Affiliated to Shanghai Jiaotong University,
No. 650, New Songjiang Road, Shanghai 201620, China
Tel.: +86 21 37798556 - Fax: +86 21 37798556
e-mail: liufabing12@163.com

0393-974X (2016)

oncogene deregulates alpha-adducin, cyclin D1 and p53, leading to lung tumorigenesis and poor prognosis (6). Silencing of ZNF746 reduces the invasion and EMT in non-small cell lung cancer (NSCLC) cells, suggesting that ZNF746 may be an important therapeutic target in lung tumorigenesis (7).

Lin-l 1, Isl-1 and Mec-3 (LIM) domain proteins participate in many biological processes, including cancer. As one of the LIM domain proteins, ZNF185 is involved in oncogenesis. For instance, the mRNA expression of ZNF185 was significantly downregulated in tumor tissues compared with the matched normal tissues in multiple malignancies including craniocervical squamous cell carcinoma (8), non-small-cell lung cancer (9) and prostate cancer (10) due to transcriptional silencing by methylation. Moreover, ZNF185 suppresses proliferation and anchorage-independent growth of prostate cancer cells and may function as a tumor-suppressor protein by associating with the actin-cytoskeleton in prostate cancer (11). In contrast, expression of ZNF185 has a positive relationship with liver-metastasis as a potential prognostic biomarker in colorectal cancer (12). But, the detailed properties and functions of ZNF185 in LAC need to be further explored. In the present study, we found that decreased expression of ZNF185 was correlated with tumor invasion in LAC patients and overexpression of ZNF185 inhibited cell growth and invasion in LAC cells.

MATERIALS AND METHODS

Materials

LAC cell lines (A549, NCI-H520, NCI-H1703, H460 and LETPα-2) used for our experiments were obtained from the Institute of Biochemistry and Cell Biology (Shanghai, China). Lentivirus-mediated ZNF185, negative control vector, and virion-packaging elements were purchased from Genechem (Shanghai, China). Human LAC tissues and the corresponding ANCT were collected from Department of Thoracic Surgery, The First People's Hospital Affiliated to Shanghai Jiaotong University. The tissue microarray of LAC was made by Shanghai Outdo Biotech CO. LTD (Shanghai, China). All the antibodies were purchased from Cell Signaling Technologies (Boston, USA). ZNF185 primer was synthesized by ABI (Framingham, USA).

Drugs and reagents

Dulbecco's Modified Eagle medium (DMEM) and fetal bovine serum (FBS) were purchased from Thermo Fisher Scientific Inc. (Waltham, MA); TRIzol Reagent and Lipofectamine 2000 were obtained from Invitrogen (Carlsbad, CA, USA); M-MLV Reverse Transcriptase was purchased from Promega (Madison, WI), USA; SYBR Green Master Mix was obtained from Takara (Otsu, Japan); and the ECL Plus Kit was obtained from GE Healthcare (Piscataway, NJ, USA).

Clinical samples and data

Tissue microarray was prepared for IHC test. Human LAC tissues and the corresponding ANCT were obtained from biopsy in a total of 62 consecutive LAC cases admitted to our hospital from January 2010 to December 2015. The study was approved by the Medical Ethics Committee of Shanghai Jiaotong University and written informed consent was obtained from the patients or their parents before sample collection. Two pathologists respectively checked all of the cases.

Immunohistochemical staining

Tissue microarray sections were processed for IHC analysis of ZNF185 protein as follows. For anti-ZNF185 IHC, unmasking was performed with 10 mM sodium citrate buffer, pH 6.0, at 90°C for 30 min. Sections were incubated in 0.03% hydrogen peroxide for 10 min at room temperature, to remove endogenous peroxidase activity, and then in blocking serum for 30 min at room temperature. Anti-ZNF185 antibody was used at a dilution of 1:200. The antibody was incubated overnight at 4°C. Sections were then washed three times for 5 min in PBS. Non-specific staining was blocked with 0.5% casein and 5% normal serum for 30 min at room temperature. Normal serum or PBS was used to replace anti-ZNF185 antibody in negative controls.

Quantification of protein expression

The expression of ZNF185 was semiquantitatively assessed as the total immunostaining scores, calculated as the product of a proportion score and an intensity score. The proportion score reflected the fraction of positive staining cells (0, none; 1, ≤10%; 2, 10% to ≥25%; 3, >25% to 50%; 4, >50%), and the intensity score represented the staining intensity (0, no staining; 1, weak; 2, intermediate;

3, strong). Finally, a total expression score (the product of the two scores) was given ranging from 0 to 12. Based on the analysis, ZNF185 expression was categorized into negative (score 0, -), weak (score 1-3, +), intermediate (score 4-6, ++), and strong (score 7-12, +++). ZNF185 expression was categorized into negative and positive expression.

Cell culture and infection

LAC cell lines were cultured in DMEM medium supplemented with 10% heat-inactivated FBS, 100U/ml of penicillin, and 100 μg/ml of streptomycin. Cells in this medium were placed in a humidified atmosphere containing 5% CO_2 at 37°C. Cells were subcultured at a 1:5 dilution in medium, and replated at 5×10^4 cells/well in 24-well plates containing serum-free growth medium with polybrene (5 mg/ml). When cells reached 50% confluence, they were infected with experimental virus or control virus, and cultured at 37°C and 5% CO2 for 4 h. The ZNF185-infected clone and the negative control vector-infected cells were named as ZNF185 group and NC group.

Quantitative Real-time PCR

To quantitatively determine the mRNA expression level of ZNF185 in LAC cells, Real-time PCR was performed. Total RNA was extracted for each clone using TRIzol according to the manufacturer's protocol. Reverse transcription was carried out using M-MLV and cDNA amplification was performed using the SYBR Green Master Mix kit according to the manufacturer's guidelines. Three separate experiments were performed for each clone.

Western blot assay

LAC cell lines were harvested and extracted using lysis buffer (Tris-HCl, SDS, mercaptoethanol, and glycerol). Cell extracts were boiled for 5 min in loading buffer, and then an equal amount of cell extracts was separated on 15% SDS-PAGE gels. Separated protein bands were transferred onto polyvinylidene fluoride (PVDF) membranes, which were subsequently blocked in 5% skim milk powder. Primary antibodies were diluted according to the manufacturer's instructions and incubated overnight at 4°C. Subsequently, horseradish peroxidase-linked secondary antibodies were added at a dilution of 1:1000 and incubated at room temperature for 2 h. The membranes were washed 3 times with PBS, and the immunoreactive bands were visualized using the ECL Plus Kit according to the manufacturer's instructions. The relative protein levels in different cell lines were normalized to the concentration of GAPDH. Three separate experiments were performed for each clone.

Cell proliferation assay

Cell proliferation was analyzed using the MTT assay. Briefly, cells were incubated in 96-well-plates at a density of 1×10^5 cells per well with DMEM medium supplemented with 10% FBS. Cells were treated with 20 μl of MTT dye at 0, 24 h, 48 h, and 72 h, and subsequently incubated with 150 μl of DMSO for 5 min. The color reaction was measured at 570 nm using an Enzyme Immunoassay Analyzer (Bio-Rad, Hercules, CA, USA).

Transwell invasion assay

Transwell filters were coated with Matrigel (3.9 μg/μl; 60–80 μl) on the upper surface of a polycarbonate membrane (diameter, 6.5 mm; pore size, 8 μm). After incubating at 37°C for 30 min, the Matrigel solidified and served as the extracellular matrix for analysis of tumor cell invasion. Harvested cells (1×10^5) in 100 μl of serum-free DMEM were added into the upper compartment of the chamber. A total of 200 μl of conditioned medium derived from NIH3T3 cells was used as a source of chemoattractant, which was placed in the bottom compartment of the chamber. After 24 h of incubation at 37°C with 5% CO_2, the medium was removed from the upper chamber. The non-invaded cells on the upper side of the chamber were scraped off with a cotton swab. Cells that had migrated from the Matrigel into the pores of the inserted filter were fixed with 100% methanol, stained with hematoxylin, then mounted and dried at 80°C for 30 min. The number of cells invading through the Matrigel was counted in 3 randomly selected visual fields from the central and peripheral portion of the filter by using an inverted microscope (200× magnification). Each assay was repeated 3 times.

Statistical analysis

All data are from at least three individual experiments. SPSS 20.0 was used for the statistical analysis. Kruskal-Wallis H test and *Chi*-squared test were used to analyse the data in all groups. One-way analysis of variance (ANOVA) was used to analyze the differences. The LSD method of multiple comparisons was used when the probability for ANOVA was statistically significant. Statistical significance was set at $P < 0.05$.

RESULTS

Expression of ZNF185 in LAC tissues and cells

The protein expression level of ZNF185 was detected by IHC in LAC tissues and by Western blotting in LAC cell lines (A549, NCI-H520, NCI-H1703, H460 and LETPα-2). As shown in Fig. 1A, the positive expression level of ZNF185 was markedly decreased in LAC tissues compared with that in ANCT (37.10% *vs* 58.06%; *P*=0.015) (Table I), and it had the lower expression level in human LAC cell lines (A549 and H460) compared with the other ones (Fig. 1B).

Correlation of ZNF185 expression with clinicopathologic characteristics in LAC patients

The association between ZNF185 expression and clinicopathologic factors was analyzed. As indicated in Table II, decreased expression of ZNF185 was correlated with the lymph node metastases in LAC patients (*P*=0.005). However, no significant correlation was found between ZNF185 expression and other factors including age, sex of the patients, and pathological stage, TNM stage and tumour size of the LAC (*P*>0.05, respectively).

Effect of ZNF185 overexpression on the expression of AKT/GSK3β signaling

After lentivirus-mediated ZNF185 overexpression was infected into LAC cell lines (A549 and H460) for 24 h, the expression levels of ZNF185 and AKT/GSK3β signaling were detected by Real-time PCR (Fig. 2A) and Western blot assays (Fig. 2B), indicated that ZNF185 overexpression significantly downregulated the protein expression levels of p-AKT and p-GSK3β, but had no effect on the AKT and GSK3β expression compared with the NC group.

Effect of ZNF185 overexpression on cell proliferation

To confirm the effect of ZNF185 overexpression on cell proliferative activity, we examined the OD

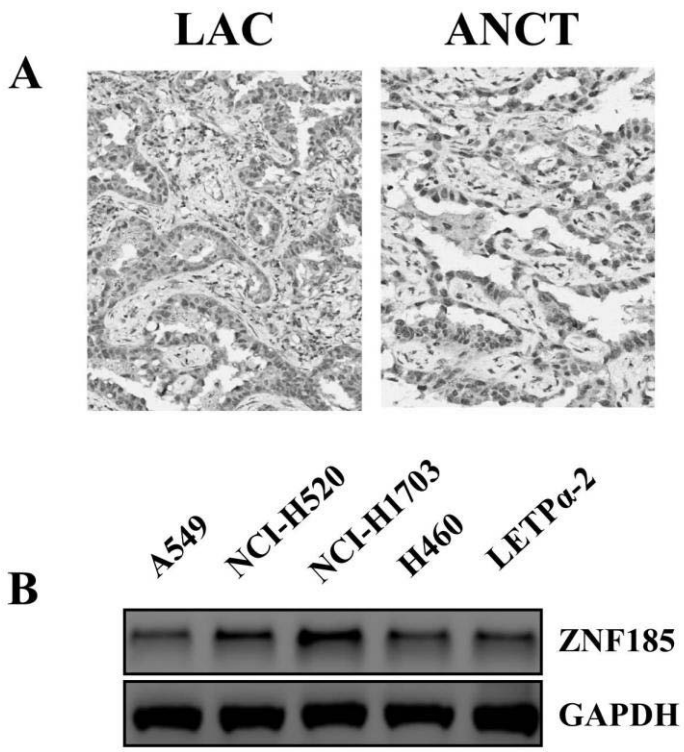

Fig. 1. *The expression levels of ZNF185 in LAC tissues (× 200) and cell lines. **A**) The protein expression level of ZNF185 was detected by using IHC staining. Positive protein expression of ZNF185 was found decreased in LAC tissues compared with the ANCT. **B**) Western blotting was used to examine the protein expression levels of ZNF185 in LAC cell lines (A549, NCI-H520, NCI-H1703, H460 and LETPα-2).*

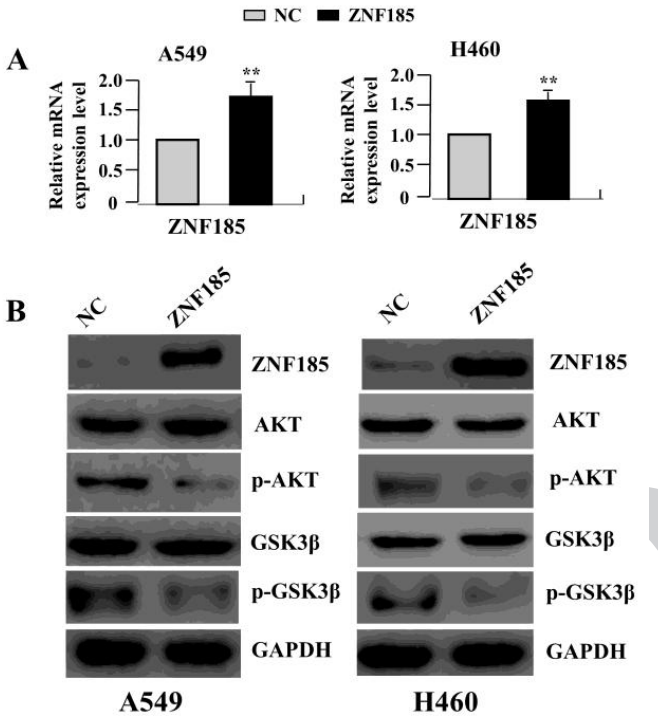

Fig. 2. *The effect of ZNF185 overexpression on the AKT/GSK3β signaling.* ***A)*** *After lentivirus-mediated ZNF185 overexpression was infected into LAC cell lines (A549 and H460) for 24 h, the mRNA expression of ZNF185 detected by Real-time PCR was significantly increased in ZNF185 group compared with the NC group (each **P < 0.01).* ***B)*** *The protein expression of p-AKT and p-GSK3β examined by Western blot assay was decreased in the ZNF185 group compared with the NC group.*

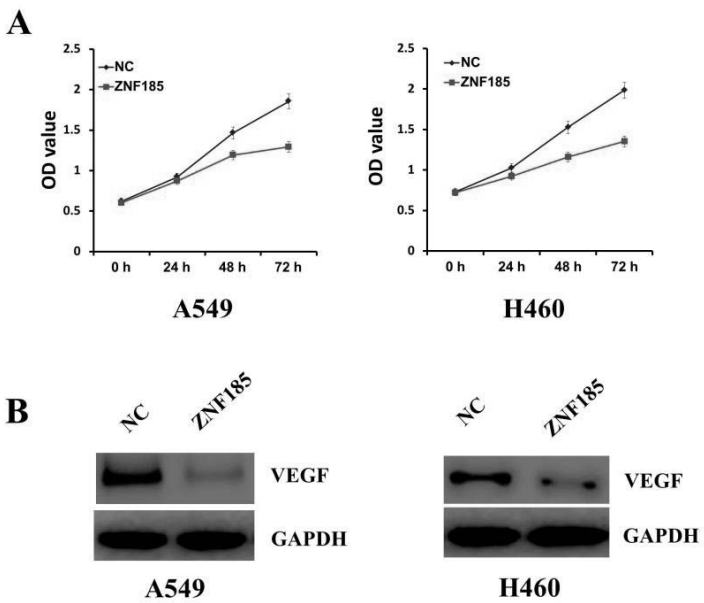

Fig. 3. *The effect of ZNF185 overexpression on cell proliferation.* ***A)*** *Cell proliferative activity was examined by MTT. ZNF185 overexpression significantly reduced the proliferative activities of LAC cells in a time-dependent manner compared with the NC group.* ***B)*** *The protein expression of VEGF was detected by Real-time PCR, indicating a significant decrease in the ZNF185 group compared with the NC group.*

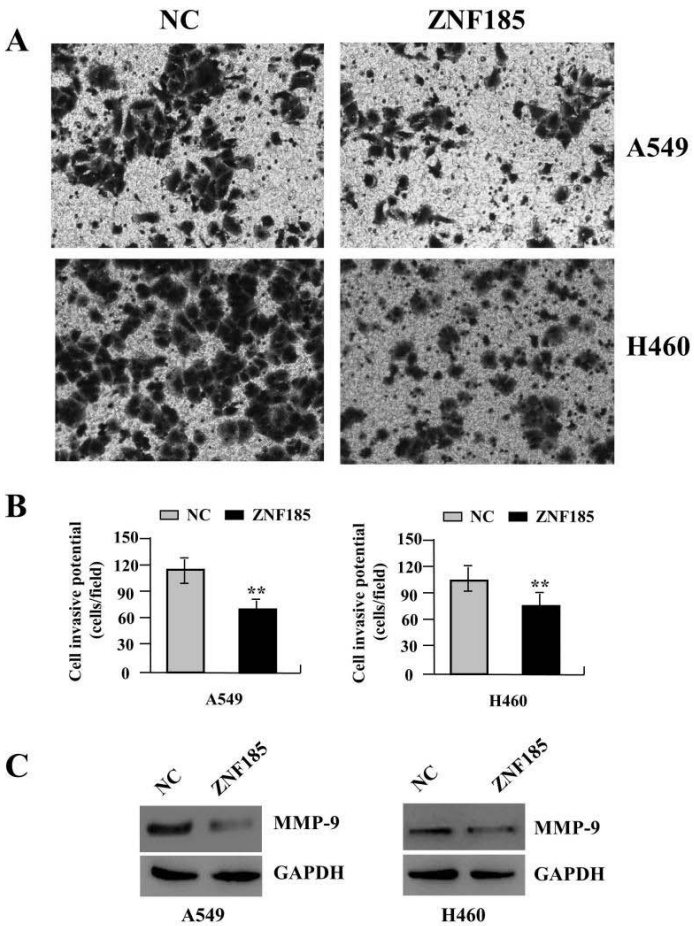

Fig. 4. *The effect of ZNF185 overexpression on cell invasion.* ***A)*** *The invasive potential was determined by Transwell assay.* ***B)*** *The invasive potential of LAC cells was decreased in the ZNF185 group compared with the NC group (**P < 0.01).* ***C)*** *The protein expression of MMP-9 examined by Western blot assay was significantly downregulated in the ZNF185 group compared with the NC group.*

Table I. *The protein expression of ZNF185 in human LAC tissues.*

Target	Group	N	Cases (n)				Positive rate (%)	χ^2	*P*
			-	+	++	+++			
ZNF185	GC	62	39	12	7	4	37.10		
	ANTT	62	26	16	11	9	58.06	5.872	0.015

LAC : lung adenocarcinoma ; ANCT: adjacent non-cancerous tissue

Table II. *The correlation of ZNF185 expression with clinicopathologic characteristics in LAC patients.*

Variables	Cases (n)	ZNF185		*P*
		-	+	
Total	62	39	23	
Age (years)				
≥60	37	25	12	
<60	25	14	11	0.359
Sex				
Male	33	24	9	
Female	29	15	14	0.090
Tumor size (cm)				
≥5	39	23	16	
<5	23	16	7	0.408
Pathological stage				
Ⅰ+Ⅱ	53	34	19	
Ⅲ+Ⅳ	9	5	4	0.624
TNM stage				
T0+T1	57	36	21	
T2+T3	5	3	2	0.889
Lymph node metastasis				
Negative	26	11	15	
Positive	36	28	8	0.005

values of the LAC cells by MTT assay. We found that ZNF185 overexpression reduced the proliferative activities in LAC cell lines (A549 and H460) in a time-dependent manner compared with the NC group (Fig. 3A). The protein expression level of VEGF, detected by Western blot assay (Fig. 3B), was found remarkably downregulated in ZNF185 group compared with the NC group.

Effect of ZNF185 overexpression on cell invasion

To decide the effect of ZNF185 overexpression on cell invasion, a Transwell assay was carried out. The invasive potential of the LAC cells in Transwell assay was determined by the ability of cells to invade a matrix barrier containing laminin and type IV collagen. Representative micrographs of Transwell filters were shown in Fig. 4A. We found that the invasive potential of LAC cells was obviously lowered in the ZNF185 group compared with the NC group (***P*<0.01) (Fig. 4B). The protein expression level of MMP-9, examined by Western blot assay (Fig. 4C), was found significantly downregulated in ZNF185 group compared with the NC group.

DISCUSSION

LIM-domain protein AJUBA inhibits malignant mesothelioma cell proliferation through regulation of the Hippo signaling pathway (13). ZNF185 belongs to the LIM domain protein family containing two zinc-finger motifs in the C-terminus, mainly located on chromosome Xq28 in the kidney, prostate, pancreas, blood, placenta and lung (14). ZNF185 is transcriptionally silenced in prostate

cancer and is inversely associated with the tumor progression (10). To clarify the possible biological functions of ZNF185 in LAC, we examined the expression of ZNF185 in LAC tissues and cell lines at the protein level, indicating that ZNF185 was significantly downregulated in LAC tissues and cell lines (A549 and H460). More importantly, decreased expression of ZNF185 was correlated with the lymph node metastasis in LAC patients, suggesting that decreased ZNF185 expression might promote the tumorigenesis of LAC.

ZNF185, a novel actin-cytoskeleton-associated LIM domain-containing protein, is localized to F-actin structures, and overexpression of ZNF185 suppresses cell proliferation and anchorage-independent growth in prostate cancer cells, suggesting that ZNF185 may function as a tumor-suppressor associated with the actin-cytoskeleton (11). To further clarify the biological functions of ZNF185 in LAC, we estimated the effects of ZN185 overexpression on LAC cell proliferation and invasive potential by MTT and Transwell assays. Consequently, the overexpression of ZNF185 inhibited cell proliferation and invasion in A549 and H460 cell lines, indicating that ZNF185 might act a tumor suppressive role in LAC.

AKT pathway plays an important role in the tumorigenesis of various types of human cancer. It has been found that AKT/GSK3β signaling is activated and promotes cell growth in human small cell lung carcinoma (SCLC) (15). Inhibition of the AKT/GSK3β signaling suppresses the cell proliferation and induces cell apoptosis in A549 lung cancer cells (16). Intriguingly, PKC412 decreases the ZNF198-fibroblast growth factor receptor 1 fusion tyrosine kinase and participates in the treatment of stem cell myeloproliferative disorder (17). However, the molecular regulatory mechanisms of ZNF185 in LAC remain poorly understood. In the present study, we used Western blotting, demonstrating that overexpression of ZNF185 downregulated the protein expression of p-AKT and p-GSK3β, but exerted no effect on AKT and p-GSK3β expression. These findings suggested that ZNF185 might inhibit the tumorigenesis of LAC through inactivation of the AKT/GSK3β signaling.

AKT/VEGF/MMP-9 pathway has been investigated and upregulated in advanced NSCLC and VEGF overexpression promotes the expression of MMPs correlated with the infiltration and metastasis of lung cancer (18). In addition, inhibition of the VEGF and MMP-9 expression through the AKT/GSK3β signaling pathway inhibits cancer cell invasion and metastasis (19). Furthermore, we found that ZNF185 decreased the protein expression of VEGF and MMP-9, and the inactivation of AKT/GSK3β signaling might mediate the antitumor effect of ZNF185 in LAC cells, suggesting that ZNF185 might inhibit proliferation and invasion of LAC cells through inhibition of the AKT/GSK3β/VEGF/MMP-9 pathway.

In conclusion, our findings indicate that the decreased expression of ZNF185 is correlated with the tumor metastasis in human LAC patients, and ZNF185 overexpression inhibits the growth and invasion of LAC cells through inhibition of the AKT/GSK3β signaling, suggesting that ZNF185 may represent a potential therapeutic target for the treatment of LAC.

REFERENCES

1. Siegel R, Ma J, Zou Z, Jemal A. Cancer statistics, 2014. CA Cancer J Clin 2014; 64(1):9-29.
2. Ishikawa M, Sonobe M, Imamura N, Sowa T, Shikuma K, Date H. Expression of the GLI family genes is associated with tumor progression in advanced lung adenocarcinoma. World J Surg Oncol 2014; 12:253.
3. Murata Y, Minami Y, Iwakawa R, et al. ECT2 amplification and overexpression as a new prognostic biomarker for early-stage lung adenocarcinoma. Cancer Sci 2014; 105(4):490-97.
4. Shahi P, Slorach EM, Wang CY, Chou J, Lu A, Ruderisch A, Werb Z. The transcriptional repressor ZNF503/Zeppo2 promotes mammary epithelial cell proliferation and enhances cell invasion. J Biol Chem 2015; 290(6):3803-13.
5. Vendrell JA, Thollet A, Nguyen NT, et al. ZNF217 is a marker of poor prognosis in breast cancer that drives epithelial-mesenchymal transition and invasion. Cancer Res 2012; 72(14):3593-606.
6. Jen J, Lin LL, Chen HT, et al. Oncoprotein ZNF322A

transcriptionally deregulates alpha-adducin, cyclin D1 and p53 to promote tumor growth and metastasis in lung cancer. Oncogene 2015 Aug 17. doi: 10.1038/onc.2015.296. [Epub ahead of print]

7. Kim B, Sohn EJ, Jung JH, Shin EA, You OH, Im J, Kim SH. Inhibition of ZNF746 suppresses invasion and epithelial to mesenchymal transition in H460 non-small cell lung cancer cells. Oncol Rep 2014; 31(1):73-78.
8. Gonzalez HE, Gujrati M, Frederick M, et al. Identification of 9 genes differentially expressed in head and neck squamous cell carcinoma. Arch Otolaryngol Head Neck Surg 2003; 129(7):754-59.
9. Medina PP, Carretero J, Ballestar E, Angulo B, Lopez-Rios F, Esteller M, Sanchez-Cespedes M. Transcriptional targets of the chromatin-remodelling factor SMARCA4/BRG1 in lung cancer cells. Hum Mol Genet 2005; 14(7):973-82.
10. Vanaja DK, Cheville JC, Iturria SJ, Young CY. Transcriptional silencing of zinc finger protein 185 identified by expression profiling is associated with prostate cancer progression. Cancer Res 2003; 63(14):3877-82.
11. Zhang JS, Gong A, Young CY. ZNF185, an actin-cytoskeleton-associated growth inhibitory LIM protein in prostate cancer. Oncogene 2007; 26(1):111-22.
12. Furukawa D, Chijiwa T, Matsuyama M, et al. Zinc finger protein 185 is a liver metastasis-associated factor in colon cancer patients. Mol Clin Oncol 2014; 2(5):709-13.
13. Tanaka I, Osada H, Fujii M, et al. LIM-domain protein AJUBA suppresses malignant mesothelioma cell proliferation via Hippo signaling cascade. Oncogene 2015; 34(1):73-83.
14. Zheng Q, Zhao Y. The diverse biofunctions of LIM domain proteins: determined by subcellular localization and protein-protein interaction. Biol Cell 2007; 99:489-502.
15. Arcaro A, Khanzada UK, Vanhaesebroeck B, Tetley TD, Waterfield MD, Seckl MJ. Two distinct phosphoinositide 3-kinases mediate polypeptide growth factor-stimulated PKB activation. EMBO J 2002; 21(19):5097-108.
16. Liao K, Li J, Wang Z. Dihydroartemisinin inhibits cell proliferation via AKT/GSK3β/cyclinD1 pathway and induces apoptosis in A549 lung cancer cells. Int J Clin Exp Pathol 2014; 7(12):8684-91.
17. Chen J, Deangelo DJ, Kutok JL, et al. PKC412 inhibits the zinc finger 198-fibroblast growth factor receptor 1 fusion tyrosine kinase and is active in treatment of stem cell myeloproliferative disorder. Proc Natl Acad Sci U S A 2004; 101(40):14479-84.
18. Hu J, Chen C, Su Y, DU J, Qian X, Jin Y. Vascular endothelial growth factor promotes the expression of cyclooxygenase 2 and matrix metalloproteinases in Lewis lung carcinoma cells. Exp Ther Med 2012; 4(6):1045-50.
19. Tang L, Yue B Cheng Y, et al. Inhibition of invasion and metastasis by DMBT, a novel trehalose derivative, through Akt/GSK-3β/β-catenin pathway in B16BL6 cells. Chem Biol Interact 2014; 222C:7-17.

EPITHELIALIZATION AND STROMALIZATION OF PORCINE FOLLICULAR GRANULOSA CELLS DURING REAL-TIME PROLIFERATION - A PRIMARY CELL CULTURE APPROACH

S. CIESIÓŁKA[1], A. BRYJA[2], J. BUDNA[1], W. KRANC[2], A. CHACHUŁA[1], D. BUKOWSKA[3], H. PIOTROWSKA[4], L. POROWSKI[2], P. ANTOSIK[3], M. BRUSKA[2], KP. BRÜSSOW[3], M. NOWICKI[1], M. ZABEL[1,5] and B. KEMPISTY[1,2]

[1]Department of Histology and Embryology, Poznan University of Medical Sciences, Poznan, Poland; [2]Department of Anatomy, Poznan University of Medical Sciences, Poznan, Poland; [3]Institute of Veterinary Sciences, Poznan University of Life Sciences, Poznan, Poland; [4]Department of Toxicology, Poznan University of Medical Sciences, Poznan, Poland; [5]Department of Histology and Embryology, Wroclaw Medical University, Wroclaw, Poland

Received December 18, 2015 – Accepted May 4, 2016

The process of oocyte growth and development takes place during long stages of folliculogenesis and oogenesis. This is accompanied by biochemical and morphological changes, occurring from the preantral to antral stages during ovarian follicle differentiation. It is well known that the process of follicle growth is associated with morphological modifications of theca (TCs) and granulosa cells (GCs). However, the relationship between proliferation and/or differentiation of porcine GCs during long-term *in vitro* culture requires further investigation. Moreover, the expression of cytokeratins and vimentin in porcine GCs, in relation to real-time cell proliferation, has yet to be explored. Utilizing confocal microscopy, we analyzed cytokeratin 18 (CK18), cytokeratin 8 + 18 + 19 (panCK), and vimentin (Vim) expression, as well as their protein distribution, within GCs isolated from slaughtered ovarian follicles. The cells were cultured for 168 h with protein expression and cell proliferation index analyzed at 24-h intervals. We found the highest expression of CK18, panCK, and Vim occurred at 120 h of *in vitro* culture (IVC) as compared with other experimental time intervals. All of the investigated proteins displayed cytoplasmic distribution. Analysis of real-time cell proliferation revealed an increased cell index after the first 24 h of IVC. Additionally, during each period between 24-168 h of IVC, a significant difference in the proliferation profile, expressed as the cell index, was also observed. We concluded that higher expression of vimentin at 120 h of *in vitro* proliferation might explain the culmination of the stromalization process associated with growth and domination of stromal cells in GC culture. Cytokeratin expression within GC cytoplasm confirms the presence of epithelial cells as well as epithelial-related GC development during IVC. Moreover, expression of both cytokeratins and vimentin during short-term culture suggests that the process of GC proliferation is also highly associated with porcine ovarian follicular granulosa cell differentiation *in vitro*.

Key words: pig, granulosa cells, cytokeratin, vimentin, real-time proliferation

Mailing address:
Bartosz Kempisty PhD,
Department of Histology and Embryology,
Department of Anatomy, Poznań University of Medical Sciences,
6 Święcickiego St., 60-781 Poznań, Poland
Tel./Fax: +48 61 8546418/8546440
e-mail: bkempisty@ump.edu.pl

0393-974X (2016)

The mammalian female gamete undergoes growth and development during long stages of folliculo- and oogenesis. At these stages, oocytes accumulate a large amount of RNA and proteins, which are necessary for embryo growth and development during the periimplantation period (1, 2). During folliculogenesis, the ovarian follicles are formed from the preantral to antral stage. This period is associated with the proliferation and differentiation of theca cells (TCs), granulosa cells (GCs), and the cumulus oophorus that directly surrounds the oocyte during its growth in the follicle (3). Normal embryo growth is determined by the developmental capacity of oocytes, which is defined as the ability of female gamete to reach maturation (nuclear and cytoplasmic) and successful monospermic fertilization. There are several external and internal factors that determined the proper maturation of oocytes (4- 6) however, the most important is the cross talk between an oocyte and its surrounding somatic cells. The oocyte with surrounding somatic cumulus cells forms the cumulus-oocyte complex (COCs) (7, 8).

The process of antral follicle formation during folliculogenesis is significantly associated with the growth, proliferation, and differentiation of ovarian granulosa cells. In most somatic cells, the process of proliferation leads to cell senescence. However, the process of granulosa cell and/or pre-granulosa cell proliferation in the preantral stage is related to the differentiation of these cells into luteal cells. The luteinization of granulosa cells is associated with oestrus cycle stage and a positive pregnancy outcome, both of which are regulated by the secretion of specific hormones such as LH, FSH, hCG, and progesterone (9, 10).

The potency of mammalian GCs is described as the ability of these cells to be cultured in a primary culture model soon after their recovery from preantral and/or antral follicles. The stability of the GCs in primary culture is sustained by addition of hormones and growth factors, which are the components of fetal bovine serum (FBS) (11). Therefore, the process of GC proliferation in primary culture is associated with their differentiation into luteal cells.

Moreover, GC proliferation during ovarian folliculogenesis can be accompanied by epithelialization and/or stromalization of porcine GCs. The aim of this study was to examine both differentiation processes (epithelialization and/or stromalization) and determine which one of them plays a crucial role in a short-time primary culture of porcine GCs.

The process of cell proliferation, as well as cell cycle regulation, is associated with formation of intermediate filaments, formed by cytokeratins, which build the intracytoplasmic cytoskeleton. Since cytokeratins are acceptable markers of epithelial tissues and cells, we investigated the expression and distribution of cytokeratin 18 (CK18) and pan cytokeratin (panCK) in porcine GCs during short-term, primary culture. Moreover, the vimentin expression, used as the stromal cell indicator, was investigated during real-time, primary cultivation of porcine GCs.

MATERIALS AND METHODS

Animals

A total of 24 puberal crossbred Landrace gilts bred on a local commercial farm with mean age 155 days (range 140–170 days) and mean weight 100 kg (95-120 kg) were used in this study. All of the animals were housed under identical conditions and fed the same forage (depending on age and reproductive status). All experiments were approved by the local Ethics Committee of the Poznan University of Life Sciences, Poland (permission no. 32/2012).

Collection of porcine ovaries and in vitro culture of granulosa cells

The ovaries (n=48) and reproductive tracts were recovered at slaughter and transported to the laboratory at 38ºC in 0.9% NaCl within 30 min post-extraction. To provide optimum conditions for GC culture *in vitro*, the ovaries of each animal were placed in PBS supplemented with fetal bovine serum (FBS; Sigma-Aldrich Co., St. Louis, MO, USA). Thereafter, single preovulatory large follicles with diameters estimated at the levels more than 5 mm (n=130) were opened into a sterile Petri dish by puncturing with a 5-ml syringe and 20-G needle, and the COCs and follicular fluid (FF) were recovered. The follicular fluid was then used to isolate GCs, whereas the

COCs were discarded.

Medium consisted of Dulbecco's Modified Eagle's Medium (DMEM/F12, Sigma-Aldrich, USA), 2% fetal calf serum (FCS) (PAA, Linz, Austria), 10 mg/ml ascorbic acid (Sigma-Aldrich, USA), 0.05 μM dexamethasone (Sigma-Aldrich, USA), 200 mM L-glutamine (Invitrogen, USA), 10 mg/ml gentamycin (Invitrogen, USA), 10,000 units/ml penicillin and 10,000 μg/ml streptomycin (Invitrogen, USA). Cells were cultivated at 38.5°C under aerobic conditions (5% CO_2). We used $3x10^6$ cells per dish for culture and $5x10^3$ cells per one E-Plate in RTCA system.

In vitro GCs culture using a real-time cellular analyzer (RTCA)

GCs recovered from follicular fluid (after puncturing of single follicles) were transferred into an E-Plate 16 of a real-time cell analyzer (RTCA, Roche-Applied Science, GmbH, Penzberg, Germany), which consisted of an RTCA Analyzer, an RTCA DP Station and RTCA Software. The GCs were then cultured in 200 μl of standard culture medium that consisted of DMEM (Sigma-Aldrich, USA), as mentioned above, for 0-168 h at 38.5°C under 5% CO_2 in air. The cultivation medium was replaced every 44 h. Additionally, after each step of cell culture, the cell index (CI) and the normalized cell index were used to evaluate the relative and quantitative changes in electrical cell impedance. The cell status was determined using RTCA software. Once the cells were attached (lag phase, first 24 h of culture) the electrical impedance was measured. Since the cells start with the log phase (logarithmic increase of proliferation, next 24-48 h of culture), after several cell divisions, the electrical impedance was increased. The cell index and the normalized cell index were measured from the electrical impedance of proliferative cells.

Confocal microscopic observations of protein distribution

During 168 h of *in-vitro* culture, at 24-h intervals GCs were collected and fixed using an acetone-methanol (1:1, v/v) solution for 10 min at -20ºC and washed three times in PBS/PVP (0.2%). To block non-specific binding, the samples were incubated in 3% BSA in PBS with 0.1% Tween-20 for 30 min at room temperature (RT). GCs were incubated for 1 h at RT with either a mouse monoclonal anti-vimentin antibody [VI-10] (Abcam), mouse monoclonal anti-cytokeratin 8 + 18 + 19 antibody [2A4] (Abcam), or a mouse monoclonal anti-cytokeratin 18 antibody (Dako Denmark A/S). The antibodies were diluted 1:500 in PBS containing 1.5% BSA and 0.1% Tween-20. After several washes with PBS containing 0.1% Tween-20, the samples incubated with primary antibodies were treated with MFP488-labeled goat anti-mouse IgG (H+L) (MoBiTec GmbH, Germany) diluted 1:500 in PBS with 0.1% Tween-20 for 1 h at RT. After washing in PBS with 0.1% Tween-20, the GCs were stained and mounted with Fluoroshield with DAPI - histology mounting medium (Sigma Aldrich, Saint Louis, USA) and examined by an LSN 510 confocal system with an Olympus Fluoview 10i microscope. All confocal microscopic images were analyzed using Imaris 7.2 (BitPlane, Zurich, Switzerland) software. The protein expression pattern was estimated as the fluorescence intensity measured by Imaris 7.2 program.

Statistical analysis

A one-way ANOVA followed by Tukey's post-hoc test was used to compare the results of the real-time quantification of the proliferation index. The experiments were carried out in a minimum three replicates. The results quantifying the cell proliferation index were obtained using an RTCA system. The differences were considered to be significant at $*P<0.05$, $**P<0.01$ and $***P<0.001$ for the qualitative and quantitative analyses of protein expression. The software program GraphPad Prism version 4.0 (GraphPad Software, San Diego, CA, USA) was used for statistical calculations.

RESULTS

Following confocal microscopic observation of protein distribution and semi-quantitative analysis of protein expression, we analyzed CK18, panCK, and Vim as markers of porcine follicular granulosa cell epithelialization and stromalization. CK18 was analyzed through 168 h of *in vitro* real time cultivation at 24 h intervals. We observed increased expression of CK18 after 120 h of IVC as compared to 24 h, 48 h, 72 h, 96 h, and 168 h ($P < 0.05$, $P < 0.05$, $P < 0.01$, $P < 0.05$, and $P < 0.05$, respectively). We did not find differences in CK18 expression between 120 and 144 h of IVC (Fig.1). Similarly, panCK expression was higher compared to 48 h, 72 h, 96 h, and 168 h ($P < 0.05$, $P < 0.001$,

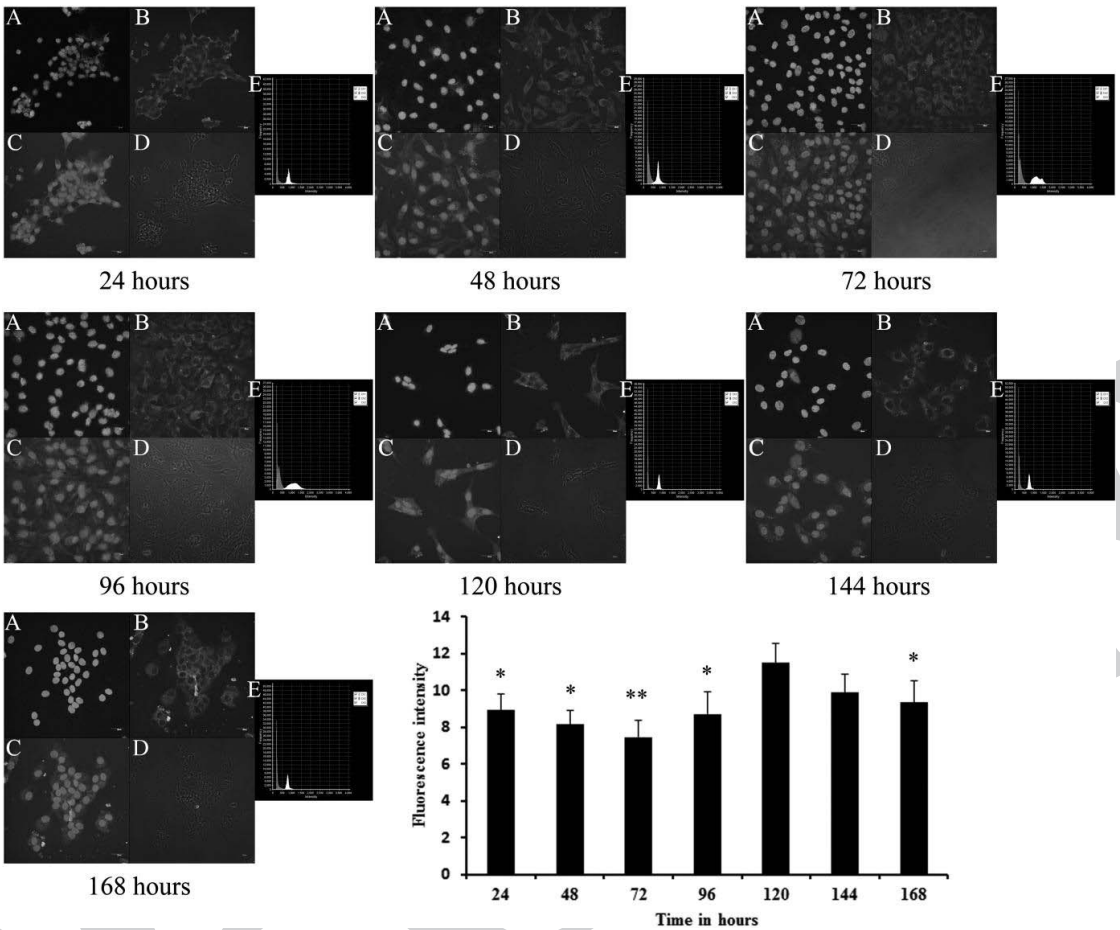

Fig. 1. *Confocal microscopic observation of CK18 protein levels and cellular distribution in porcine GCs at 24 h, 48 h, 72 h, 96 h, 120 h, 144 h, and 168 h of IVC. The GCs that were collected after 24 h, 48 h, 72 h, 96 h, 120 h, 144 h, and 168 h of IVC were stained with 0.1 µg/ml 4,6-diamino-2-phenylindole in mineral oil following staining for porcine CK18 (mouse monoclonal anti-cytokeratin 18 antibody). Secondary antibodies were labeled with FITC (fluorescence isothiocyanate), which emits a green fluorescent signal after excitation at 488 nm. The fluorescence intensity was measured using Imaris software. The differences were considered to be significant at P<0.05, P<0.01, and P<0.001. The scale bars represent 40 µm.*

$P < 0.001$ and $P < 0.05$, respectively). We did not observe differences in expression of panCK between 24 h and 144 h of IVC (Fig. 2). When comparing expression between CK18, panCK, and vimentin, the latter showed the greatest increase. Similar to other investigated proteins, expression of vimentin was increased after 120 h of IVC as compared to 24 h, 48 h, 72 h, 96 h, and 168 h ($P < 0.001$, $P < 0.01$, $P < 0.01$, $P < 0.01$, and $P < 0.05$, respectively). All analyzed proteins were distributed in cell cytoplasm, and nuclear localization was observed after each step of IVC (Fig. 3).

Cell proliferation progression was assayed after using the RTCA system for parametric and quantitative analysis of cell index. When the total proliferation period from 0-168 h was analyzed, (Fig. 4A) no differences in the cell index were observed: however, when compared with the first step of proliferation (0–24 h), (Fig. 4B) we found decreased proliferation in five of the twelve investigated groups ($P < 0.001$ for all groups, respectively). Similarly, after analysis of 24–48 h, 48–72 h, and 72-96 h (Fig. 4C, 4D, 4E) we also observed various proliferation intensities, which are expressed as the cell index value

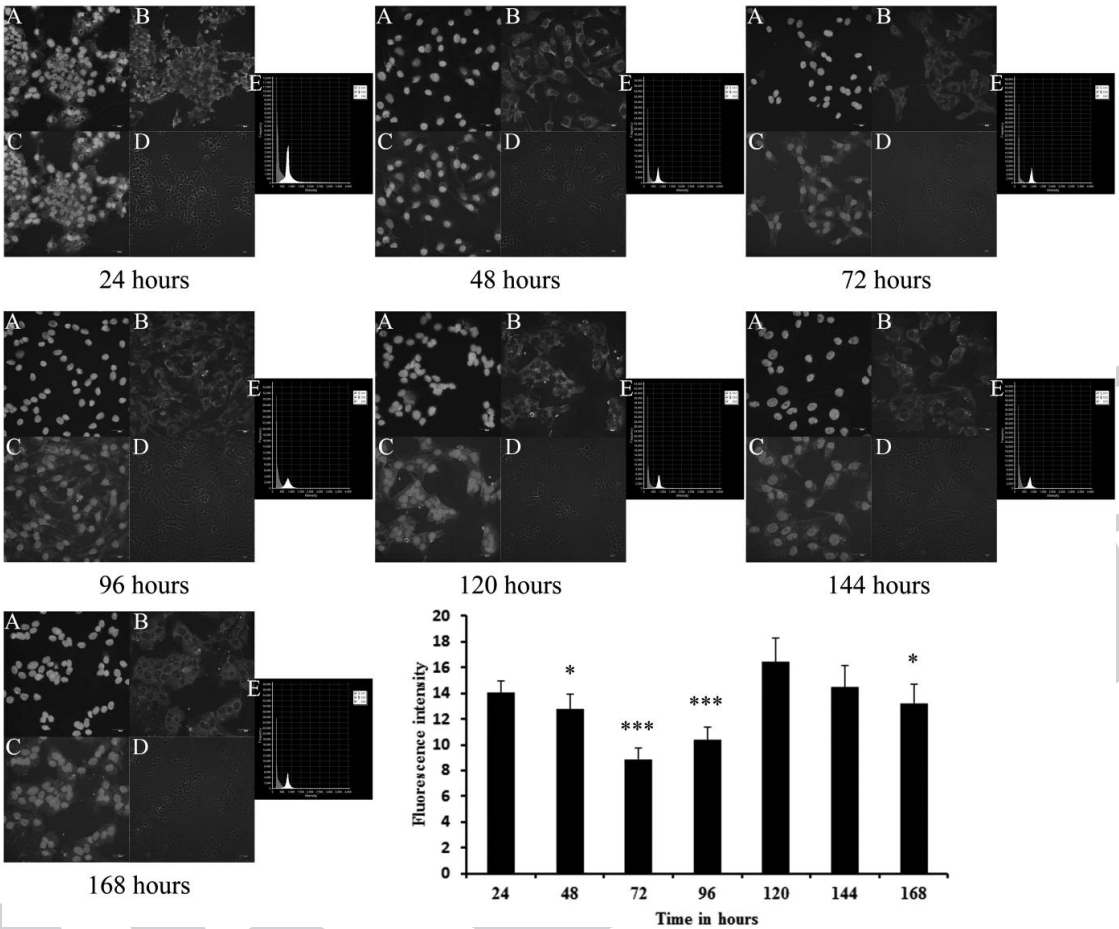

Fig. 2. *Confocal microscopic observation of panCK protein levels and cellular distribution in porcine GCs at 24h, 48 h, 72 h, 96 h, 120 h, 144 h, and 168 h of IVC. The GCs that were collected after 24 h, 48 h, 72 h, 96 h, 120 h, 144 h, and 168 h of IVC were stained with 0.1 µg/ml 4,6-diamino-2-phenylindole in mineral oil following staining for porcine panCK (mouse monoclonal anti-cytokeratin 8 + 18 + 19 antibody). Secondary antibodies were labeled with FITC (fluorescence isothiocyanate), which emits a green fluorescent signal after excitation at 488 nm. The fluorescence intensity was measured using Imaris software. The differences were considered to be significant at P<0.05, P<0.01, and P<0.001. The scale bars represent 40 µm.*

($P < 0.01$ and $P < 0.001$ for each group, respectively). After media replacement at 96 h of IVC, the cell proliferation stability was determined (Fig. 4F). At this stage, difference at level $P < 0.01$, was detected. Between 120 and 144 h of proliferation, a decreased proliferation index was observed (Fig. 4G). The last stage of proliferation, 144-168 h, was characterized by differences in cell index in nine of the twelve investigated groups (Fig.4H).

Viability control accessed by RTCA was useful also for monitoring GCs cultured for 168 h for confocal microscope observation. RTCA result was informative as both pools of cells were recovered from the same gilt. Furthermore, we observed increase in GC colonies each day of IVC. Cells under the microscope presented intact nucleus, no apoptotic bodies nor necrotic swelling. Cell membrane remained uninterrupted.

DISCUSSION

It is well recognized that maintenance of the mammalian oocyte full maturation stage (MII) is associated with proper growth of ovarian follicle,

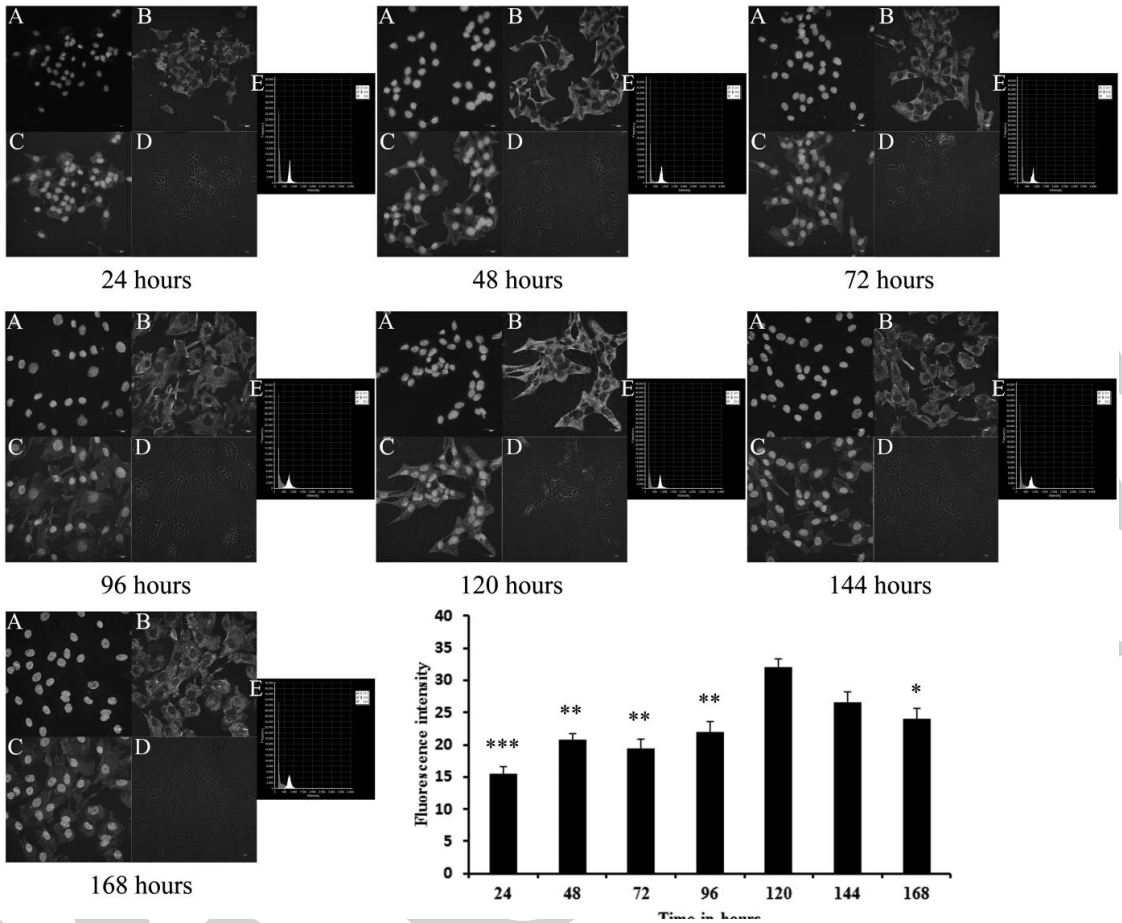

Fig. 3. *Confocal microscopic observation of vimentin protein levels and cellular distribution in porcine GCs at 24 h, 48 h, 72 h, 96 h, 120 h, 144 h, and 168 h of IVC. The GCs that were collected after 24 h, 48 h, 72 h, 96 h, 120 h, 144 h, and 168h of IVC were stained with 0.1 µg/ml 4,6-diamino-2-phenylindole in mineral oil following staining for porcine vimentin (mouse monoclonal anti-vimentin antibody). Secondary antibodies were labeled with FITC (fluorescence isothiocyanate), which emits a green fluorescent signal after excitation at 488 nm. The differences were considered to be significant at $P<0.05$, $P<0.01$, and $P<0.001$, The scale bars represent 40 µm.*

which forms the strict environment for the developed female gamete. Moreover, oocyte maturation is accompanied by proliferation and differentiation of surrounding cumulus-granulosa cells. Both of these processes are regulated by specific hormones, which are involved in both positive and negative feedback pathways. It was recently suggested that, during short-term in vitro primary cultivation (0-168 hours), the porcine GCs may differentiate into luteal cells; however, long-term cultivation (3-4 weeks) of these cells may lead to their differentiation into ovarian-granulosa-derived stem cells (12). Additionally, it has been shown that a subpopulation of GCs display stemness characteristics and transdifferentiation potential in the growing follicles (13). In this study, we investigated the real-time proliferation of porcine GCs in association with expression of luminal epithelial and stromal cell markers as well as their possible differentiation during the in vitro cultivation period. The expression of cytokeratins and vimentin may lead to new information concerning GC epithelial and/or stromal specificity and plasticity in an in vitro primary culture model.

Anderson et al. showed, using in situ DNA 3'- end-

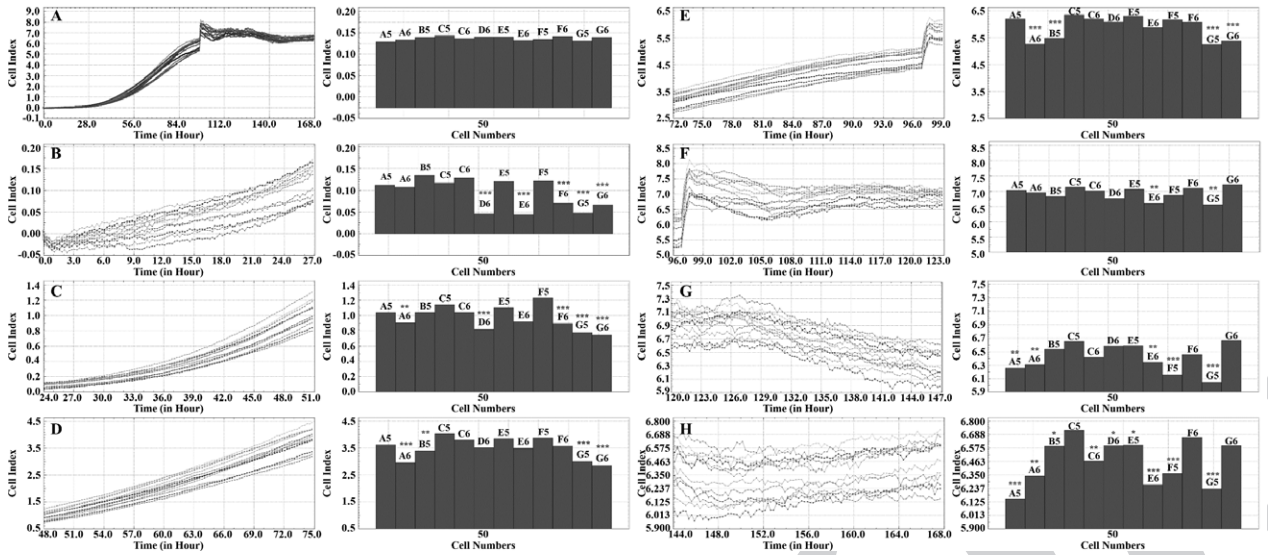

Fig. 4. *Normalized proliferation index of porcine GCs cultivated for 168 hours. Porcine granulosa cells were recovered from follicles of pubertal gilts and treated with collagenase for 10 min at 38.5°C. The cells were immediately transferred into an E-Plate 16 of a real-time cell analyzer. The experiment consisted of six replicates involving the cultivation of the same population of collected cells. At each step of the experiment, the proliferation index was assessed for real-time in vitro cultivation for the time periods of 0-168 h (**A**), 0-24 h (**B**), 24-48 h (**C**), 48-72 h (**D**), 72-96 h (**E**), 96-120 h (**F**), 120-144 h (**G**), 144-168 h (**H**). The differences were considered to be significant at the level of $^{*}P<0.05$, $^{**}P<0.01$, and $^{***}P<0.001$. At first 0-24 h the cells are in lag phase. After 24-48 h, the cells proliferation index is increased, and the cells are in log phase.*

labeling with non-radioactive digoxigenindidesoxy-UTP (dig-ddUTP) (14), that antral follicle apoptosis was induced in cumulus-granulosa cells and other GCs that form the antrum. Moreover, they observed that during formation of cystic follicles, apoptosis systematically progresses from cumulus cells surrounding oocytes into mural GCs. The GCs express significant levels of vimentin, while mural GCs display keratin expression. These results also indicate that mural GCs precede transformation into a specific follicular epithelium accompanied with apoptotic progression. It was recently presented that, during early stages of folliculogenesis and oogenesis, the cell population that forms the ovarian tissues undergoes significant changes, such as differentiation and transdifferentiation (15). After using cell type-specific protein markers, such as transforming growth factor beta 1 and beta 2 (TGb1, TGFb2), they described the process of ovarian somatic cell differentiation into GCs and theca cells (TCs). The results from these experiments suggested that differentiation of somatic cells into GCs belongs to the first steps of mammalian ovarian morphogenesis. The results of the above-mentioned experiments suggest that the cytodifferentiation process of GCs that takes place during ovarian folliculogenesis is accompanied by epithelialization and stromalization of GCs. This hypothesis was first approved by Czernobilsky et al. who investigated the intermediate filament (IF) system in various ovarian cells of human, pig and rat. Using electron microscopy and immunolocalization, they observed differential distribution of cytokeratins and vimentin within stromal and/or epithelial layers of ovarian tissues. They observed a strong vimentin signal in ovarian stromal and luteinized stromal nodules. Moreover, in pig and rat ovaries, cytokeratins were not stained in GCs although they displayed significant vimentin expression. Interestingly, vimentin expression was frequently detected in cultured epithelial cells but not commonly found in ovarian epithelial tissues. These results indicated the highly differentiated

distribution of both cytokeratins and vimentin among human, pig and rat ovarian tissues, supporting the hypothesis that the expression of these proteins is regulated in a species-dependent manner (16).

Although the presence of cytokeratins and vimentin was previously well-recognized in ovarian tissues of several mammalian species, the expression and distribution of these proteins isolated from GC antral follicles still require further investigation. Moreover, the expression of cytokeratins and vimentin in porcine GCs during short-term, real-time primary cultivation has yet to be described. Therefore, this study aimed to analyze the distribution of both of these proteins, which examines the epithelialization and stromalization process within the porcine GCs, isolated from follicles, during primary culture. Recently, the process of cell and tissues stromalization was intensively investigated in several types of cancers with special relation to tumor growth, differentiation, and metastasis (17- 19). In addition, it was observed by Micke et al. that stromalization belongs to the process that encompasses the mobilization of fibroblasts (20). Moreover, several studies on breast, pancreatic, prostatic, and ovarian cancer indicated that treatment of normal fibroblasts with tumor cells leads to phenotypic changes such as higher expression of activation markers as well as differentiation of these cells into cancer associated fibroblasts (CAFs) (21, 22). Moreover, it was shown that stromalization is also accompanied by TGFb-induced expression of PDGF. It has been shown that following paladin treatment, this leads to differentiation of normal dermal fibroblasts into myofibroblasts, which display several morphological, phenotypic, and proteomic differences (20, 23). Vimentin is a well-recognized marker of stromal cells especially during the growth and differentiation of tumor cells (24). The authors investigated the effect of host aging on mammary tumor growth and found that caveolin (Cav)-1-deficient tumor was characterized by increase stromal content of vimentin positive myofibroblasts. They showed that vimentin predicted not only the stromal character and/or oxidative stress but was also associated with activation of phospho-S6 kinase, a marker associated with aging. Our research indicated that vimentin expression is highly associated with real-time progress of GC proliferation. In this context, proliferation is always recognized as cellular aging that may lead to cellular differentiation and/or apoptosis. Our recent study showed that porcine GCs express the LHR gene and protein, which proves that cells undergo differentiation into luteal cells during real-time primary cultivation (25). However the current experiments indicate increased expression of vimentin at 120 h of IVC, which may be a sign of cellular stromalization since the cytokeratin 18 (CK18) and cytokeratin 8 + 18 + 19 (panCK), markers of cellular epithelialization, were much lower. Moreover, it may be suggested that stromalization of GCs during primary IVC are significantly associated with luteinization of these cells in vitro.

It was recently shown by Paladini et al. that keratins are involved in keratinocyte preparation and reorganization during wound epithelialization (26). Additionally, it was observed in other studies that epithelialization and/or re-epithelialization is highly associated with the organization keratin, which has been investigated using wound remodeling after skin injury. Our experiments also indicated increased expression of CK18 and panCK at 120 h, suggesting the same time of GC epithelialization and stromalization during primary IVC. Several recent studies indicated the role of keratins in re-epithelialization of keratinocytes during cell specific migration and proliferation initiated at 16-24 h following skin injury in humans (27- 29), mice (30, 31), rabbits (32), dogs (33), and pigs (34). Moreover, it was observed by Bereiter-Hahn and Clark that cellular mitotic activity is significantly associated with the re-epithelialization process of epidermal wounds, which is also correlated with recruitment and migration of keratinocytes in the injury (35, 36). These observations are partially confirmed by our results, as an increased proliferation index was associated with higher expression of cytokeratins. This suggests that epithelialization of GCs is accompanied by cellular proliferation during primary culture in vitro.

Our results suggest that stromalization and epithelialization of porcine follicular GCs may occur

during short-term primary culture. Since vimentin was more highly expressed than CK18 and panCK, the significant dominance of stromal cells in the culture was also determined.

ACKNOWLEDGEMENTS

Publication of this article was made possible by grant number 2014/13/D/NZ9/04798 "SONATA" from the Polish National Centre of Science.

REFERENCES

1. Miyano T, Manabe N. Oocyte growth and acquisition of meiotic competence. Soc Reprod Fertil Suppl 2007; 63:531-38.
2. Prather RS, Ross JW, Isom SC, Green JA. Transcriptional, post-transcriptional and epigenetic control of porcine oocyte maturation and embryogenesis. Soc Reprod Fertil Suppl 2009; 66:165-76.
3. Shi K, He F, Yuan X, Zhao Y, Deng X, Hu X, Li N. Genome-scale gene expression characteristics define the follicular initiation and developmental rules during folliculogenesis. Mamm Genome 2013; 24(7-8):266-75.
4. Yuan HJ, Han X, He N, et al. Glucocorticoids impair oocyte developmental potential by triggering apoptosis of ovarian cells via activating the Fas system. Sci Rep 2016; 6:24036.
5. Sun QY, Nagai T. Molecular mechanisms underlying pig oocyte maturation and fertilization. J Reprod Dev 2003; 49(5):347-59.
6. Kimura N, Hoshino Y, Totsukawa K, Sato E. Cellular and molecular events during oocyte maturation in mammals: molecules of cumulus-oocyte complex matrix and signalling pathways regulating meiotic progression. Soc Reprod Fertil Suppl 2007; 63:327-42.
7. Sato E, Yokoo M. Morphological and biochemical dynamics of porcine cumulus-oocyte complexes: role of cumulus expansion in oocyte maturation. Ital J Anat Embryol 2005; 110(2 Suppl 1):205-17.
8. Blaha M, Nemcova L, Kepkova KV, Vodicka P, Prochazka R. Gene expression analysis of pig cumulus-oocyte complexes stimulated in vitro with follicle stimulating hormone or epidermal growth factor-like peptides. Reprod Biol Endocrinol 2015; 13:113.
9. Murphy BD. Models of luteinization. Biol Reprod 2000; 63:2-11.
10. Duffy DM, Stouffer RL. Luteinizing hormone acts directly at granulosa cells to stimulate periovulatory processes: modulation of luteinizing hormone effects by prostaglandins. Endocrine 2003; 22:249-56.
11. Horisberger MA. A method for prolonged survival of primary cell lines. In Vitro Cell Dev Biol Anim 2006; 42:143-48.
12. Kossowska-Tomaszczuk K, De Geyter C. Cells with stem cell characteristics in somatic compartments of the ovary. Biomed Res Int 2013; 2013:310859.
13. Dzafic E, Stimpfel M, Virant-Klun I. Plasticity of granulosa cells: on the crossroad of stemness and transdifferentiation potential. J Assist Reprod Genet 2013; 30:1255-61.
14. Anderson E, Lee GY. The polycystic ovarian (PCO) condition: apoptosis and epithelialization of the ovarian antral follicles are aspects of cystogenesis in the dehydroepiandrosterone (DHEA)-treated rat model. Tissue Cell 1997; 29:171-89.
15. Roy SK, Hughes J. Ontogeny of granulosa cells in the ovary: lineage-specific expression of transforming growth factor beta 2 and transforming growth factor beta 1. Biol Reprod 1994; 51:821-30.
16. Czernobilsky B, Moll R, Levy R, Franke WW. Co-expression of cytokeratin and vimentin filaments in mesothelial, granulosa and rete ovarii cells of the human ovary. Eur J Cell Biol 1985; 37:175-90.
17. Chang WK, Carmona-Fontaine C, Xavier JB. Tumour–stromal interactions generate emergent persistence in collective cancer cell migration. Interface Focus 2013; 3:20130017.
18. Gupta PB, Proia D, Cingoz O, Weremowicz J, Naber SP, Weinberg RA, Kuperwasser C. Systemic stromal effects of estrogen promote the growth of estrogen receptor – negative cancers. Cancer Res 2007; 67:2062-71.
19. Provenzano PP, Inman DR, Eliceiri KW, et al. Collagen density promotes mammary tumor initiation and progression. BMC Med 2008; 6:11.
20. Micke P, Ostman A. Tumour-stroma interaction: cancer-associated fibroblasts as novel targets in anti-cancer therapy? Lung Cancer 2004; 45:Suppl 2:163-75.
21. Pietras K, Pahler J, Bergers G, Hanahan D. Functions of paracrine PDGF signaling in the proangiogenic tumor

stroma revealed by pharmacological targeting. PLoS Med 2008; 5:e19.
22. Akashi T, Minami J, Ishige Y, Eishi Y, Takizawa T, Koike M, Yanagishita M. Basement membrane matrix modifies cytokine interactions between lung cancer cells and fibroblasts. Pathobiology 2005; 72:250-59.
23. Brentnall TA, Lai LA, Coleman J, Bronner MP, Pan S, Chen R. Arousal of cancer-associated stroma: overexpression of palladin activates fibroblasts to promote tumor invasion.. PLoS One 2012; 7:e30219.
24. Mercier I, Camacho J, Titchen K, et al. Caveolin-1 and accelerated host aging in the breast tumor microenvironment: chemoprevention with rapamycin, an mTOR inhibitor and anti-aging drug. Am J Pathol 2012; 181:278-93.
25. Kempisty B, Ziółkowska A, Ciesiółka S, et al. Association between the expression of LHR, FSHR and CYP19 genes, cellular distribution of encoded proteins and proliferation of porcine granulosa cells in real-time. J Biol Regul Homeost Agents 2014; 28(3):419-31.
26. Paladini RD, Takahashi K, Bravo NS, Coulombe PA. Onset of re-epithelialization after skin injury correlates with a reorganization of keratin filaments in wound edge keratinocytes: defining a potential role for keratin 16. J Cell Biol 1996; 132:381-97.
27. Odland G, Ross R. Human wound repair. I. Epidermal regeneration. J Cell Biol 1968; 39:135-51.
28. Ortonne JP, Loning T, Schmitt D, Thivolet J. Immunomorphological and ultrastructural aspects of keratinocyte migration in epidermal wound healing. Virchows Arch A Pathol Anat Histol 1981; 392:217-30.
29. Mansbridge JN, Knapp AM. Changes in keratinocyte maturation during wound healing. J Invest Dermatol 1987; 89:253-63.
30. Croft CB and Tarin D. Ultrastructural studies of wound healing in mouse skin. I. Epithelial behaviour. J Anat. 1970; 106: 63-77.
31. Krawczyk WS. A pattern of epidermal cell migration during wound healing. J Cell Biol 1971; 49:247-63.
32. Viziam CB, Matoltsy AG, Mescon H. Epithelialization of small wounds. J Invest Dermatol 1964; 43:499-507.
33. Winstanley EW. The epithelial reaction in the healing of excised cutaneous wounds in the dog. J Comp Pathol 1975; 85:61-75.
34. Winter GD. Formation of the scab and the rate of epithelization of superficial wounds in the skin of the young domestic pig. Nature 1962; 193:293-94.
35. Bereiter-Hahn, J. Epidermal cell migration and wound repair. In Biology of the Integument, Vol. 2: Vertebrates. Springer-Verlag. Berlin, 1987: p. 443-471.
36. Clark RAF. Mechanisms of cutaneous wound repair. In Dermatology in General Medicine. T.B. Fitzpatrick, A.Z. Eisen, K. Wolff, I.M. Freedberg, and M.D. Austen, ed. McGraw-Hill. New York, 1993: p. 473-86.

KRÜPPEL-LIKE FACTOR 2 SUPPRESSES GROWTH AND INVASION OF GASTRIC CANCER CELLS *IN VITRO* AND *IN VIVO*

QQ. MAO, JJ. CHEN, L. DONG, L. ZHONG and X. SUN

Gastroenterology Department and Endoscopy Center of Fudan University Affiliated Huashan Hospital North Hospital, Shanghai, China

Received December 23, 2015 – Accepted June 17, 2016

The first two authors contributed equally to this work

Krüppel-like factor 2 (KLF2), a novel tumor-suppressor gene, is implicated in diverse cellular processes, including cell growth, apoptosis, and invasion. However, the role and action mechanisms of KLF2 in gastric cancer (GC) need be further elucidated. The expression of KLF2 was investigated by immunohistochemical assay in human GC tissues, and lentivirus-mediated KLF2 overexpression was transfected into GC cells (AGS and HGC-27) for assessing cell proliferation and invasion, respectively indicated by MTT and Transwell assays. Subcutaneous GC tumor models were constructed for estimating tumor growth *in vivo*. As a result, the expression level of KLF2 was decreased in GC tissues compared with the para-carcinoma tissues (31.03% *vs* 53.45%, *P*=0.035), and negatively correlated with the lymph node metastasis in GC patients (*P*=0.02). Moreover, overexpression of KLF2 inhibited the cell proliferation and invasive potential and downregulated the protein expression of PCNA, Bcl-2 and MMP-9 in GC cells. The result *in vivo* showed KLF2 overexpression reduced the xenograft tumor growth. In conclusion, our findings indicate that KLF2 may function as a tumor suppressor involved in the progression of human GC.

Gastric cancer (GC) with high incidence ranks the fourth commonest cancer and the second leading cause of cancer-related mortality in all types of cancers worldwide (1, 2). The long-term survival of 40–60% GC patients is seriously affected by postoperative recurrence and tumor metastasis despite great advancement of new diagnosis and treatment strategies (3). The reason lies in the poor understanding of the exact molecular mechanisms of GC. Thus, identification of the molecular mechanism and discovery of new therapeutic targets for GC are urgently needed.

Krüppel-like factor (KLF) family of transcription factors, also known as SP1-like, is a multigene family of transcription factors with a zinc finger domain (4. 5). KLFs have been discovered as suppressors or activators of transcription in a cell type and promoter-dependent manner (6). Among KLFs, some play a role in biological activity as potential tumor suppressor genes, such as KLF11, KLF6, and KLF4, however KLF5 promotes proliferation of breast cancer cells (7-10). KLF2, which is diminished in many tumor tissues, has anti-carcinogenic activities (11, 12). The tumor suppressive function of KLF2 may be achieved by inhibiting proliferation, improving the apoptosis sensitivity and modulating

Key words: KLF2, Gastric cancer, growth, invasion

Mailing address:
Prof. Xu Sun,
Gastroenterology Dept. & Endoscopy Center, Fudan University
Affiliated Huashan Hospital, North Hospital,
LuXiang Road No. 108, Shanghai 200000, China
Tel.: +86 21 66894836 - Fax: +86 21 66894836
e-mail: sunxu4835@sina.com

0393-974X (2016)

DISCLOSURE: ALL AUTHORS REPORT NO CONFLICTS OF INTEREST RELEVANT TO THIS ARTICLE.

vessel stabilization (12-14).

It has been reported that several types of molecules and signaling pathways mediate the regulation of KLF2 in cancer cells, of which KLF2 upregulates p21 (15) and cytosolic phospholipase A2 alpha (16), and downregulates KRAS (17), peroxisome proliferator-activated receptor-gamma (18), vascular cell adhesion molecule-1 (19), E-selectin (20), WEE1 (21), vascular endothelial growth factor receptor-2 (22) and CXCR4 (23). Nevertheless, the features and functions of KLF2 in GC and the underlying molecular mechanisms are not fully understood. We hypothesized that KLF2 may function as a tumor suppressor in GC and serve as a potential therapeutic target for the treatment of GC.

MATERIALS AND METHODS

Materials

The GC cell lines (AGS and HGC-27) used in the experiments were from the Institute of Biochemistry and Cell Biology (Shanghai, China). Lentivirus-mediated KLF2 overexpression vector (GV129, Ubi-MCS-EGFP-3FLAG), negative control vector and virion-packaging elements were from Genechem (Shanghai, China). The primers of KLF2, PCNA, Bcl-2 and MMP-9 were synthesized by ABI (USA). All antibodies were from Santa Cruz Biotechnology (USA).

Drugs and reagents

Dulbecco's Modified Eagle medium (DMEM) and fetal bovine serum (FBS) were from Thermo Fisher Scientific Inc (Waltham, MA, USA); TRIzol Reagent and Lipofectamine 2000 were from Invitrogen (Carlsbad, CA, USA); M-MLV Reverse Transcriptase was from Promega (Madison, WI, USA); SYBR Green Master Mixture was from Takara (Otsu, Japan). ECL-PLUS/Kit was from GE Healthcare (Piscataway, NJ, USA). *In-situ* cell death kit was from Boehringer Mannheim (Germany).

Clinical samples and data

Human GC tissues and corresponding adjacent non-cancerous tissues (ANCT) were obtained from biopsy prior to chemotherapy in a total of 58 cases of GC admitted to our hospital from January 2007 to December 2012. The study was approved by the Medical Ethics Committee of Fudan University and written informed consent was obtained from the patients or their parents before sample collection.

Immunohistochemical staining

Anti-KLF2 antibodies were used for immunohistochemical (IHC) detection of the expression of KLF2 protein in tissue microarrays. Tissue microarray sections were processed for IHC analysis of KLF2 protein. Sections were incubated in 0.03% hydrogen peroxide for 10 min at room temperature to remove endogenous peroxidase activity, and then in blocking serum for 30 min at room temperature. Anti-KLF2 antibody was used at a dilution of 1:200. Sections were then washed three times for 5 min in PBS. Normal serum or PBS was used to replace anti-KLF2 antibody in negative control. KLF2 expression was semi-quantitatively estimated as the total IHC staining scores (24). The proportion score reflected the fraction of positive staining cells (0, none; 1, ≤10%; 2, 10% to ≥25%; 3, >25% to 50%; 4, >50%), and the intensity score represented the staining intensity (0, no staining; 1, weak; 2, intermediate; 3, strong). Finally, a total score was given ranging from 0 to 12. Based on the analysis in advance, KLF2 expression was categorized into negative (score 0, -), weak (score 1-3, +), intermediate (score 4-6, ++), and strong (score 7-12, +++). Score <4 was defined as low expression while score≥4 was considered as high expression. The scoring was independently assessed by two pathologists.

Cell culture and transfection

GC cells were cultured in DMEM medium supplemented with 10% heat-inactivated FBS, 100U/ml of penicillin and 100μg/ml of streptomycin. They were all placed in a humidified atmosphere containing 5% CO_2 at 37°C. On the day of transduction, GC cells were replated at 5×10^4 cells/well in 24-well plates containing serum-free growth medium with polybrene (5 mg/ml). Positive stable transfectants were selected and expanded for further study. The clone in which the lentivirus mediated KLF2 transfected was named as KLF2 group, the negative control vectors transfected were named as NC group, and GC cells were named as Ctrl group.

Quantitative Real-time PCR

To quantitatively determine the mRNA expression

levels, Real-time PCR was used. Total RNA of each clone was extracted with TRIzol according to the manufacturer's protocol. Reverse-transcription was carried out using M-MLV and cDNA amplification was carried out using SYBR Green Master Mix kit according to the manufacturer's instructions. The primers were as follows: **β**-actin forward primer, GGCCAACCGCGAGAAGAT, **β**-actin reverse primer, CGTCACCGGAGTCC ATCA; KLF-2 forward primer, CGCTTCGAAGCGATCACCG, KLF-2 reverse primer ACGGTGCAGTCAGTCCG; MMP-9 forward primer, CGCGCTGGGCTTAG ATCAT, MMP-9 reverse primer, GGTGCCGGATGCCATTC; Bcl-2 forward primer, TCGCCCTGTGGATGACTGAG, Bcl-2 reverse primer CAGAGTCTTCAGAGAC AGCCAGGA; PCNA forward primer, AGCGTCAGTTTAGCTTAAAG, PCNA reverse primer CGCGGTAGGATTCCAG. Data were analyzed using the comparative Ct method (25). Three separate experiments were performed for each clone.

Western blot assay

GC cells were harvested and extracted using lysis buffer (Tris-HCl, SDS, Mercaptoethanol, Glycerol). Cell extracts were boiled for 5 min in loading buffer and then equal amount of cell extracts were separated on 15% SDS-PAGE gels. Separated protein bands were transferred into polyvinylidene fluoride (PVDF) membranes and the membranes were blocked in 5% skim milk powder. The primary antibodies were diluted according to the instructions of antibodies and incubated overnight at 4°C. Then, horseradish peroxidase-linked secondary antibodies were added at a dilution ratio of 1:1000, and incubated at room temperature for 2 h. The membranes were washed with PBS for three times and the immunoreactive bands were visualized using ECL-PLUS/Kit according to the kit instruction. The relative protein level in different cell lines was normalized to β-actin concentration. Three separate experiments were performed for each clone.

MTT assay

Cell growth *in vitro* was evaluated using a 3-[4,5-dimethylthiazol-2-yl]-2,5-diphenyltetrazolium bromide (MTT; Sigma) assay. Briefly, 1 x 10^4 cells were plated in 96-well plates and grown overnight. When cells grew for 24 h and 48 h, 20 μL of MTT (5 g/L) was added into each well for 4 h. After the medium containing MTT was aspirated, the formazan crystals were dissolved in 200 ml dimethyl sulfoxide. The absorbance was recorded using a 96-well spectrophotometer at wavelength of 570 nm.

Transwell invasion assay

Transwell filters were coated with matrigel (3.9 μg/μl, 60-80 μl, KeyGEN Biotech Co., Ltd. Nanjing, China) on the upper surface of a polycarbonic membrane (diameter 6.5 mm, pore size 8 μm, KeyGEN Biotech Co., Ltd. Nanjing, China). After incubating at 37°C for 30 min, the matrigel solidified and served as the extracellular matrix for analysis of tumor cell invasion. Harvested cells (1×10^5) in 100 μl of serum free DMEM were added into the upper compartment of the chamber. The lower chamber was filled with 200 μl complete medium. After 24 h incubation at 37°C with 5% CO_2, the medium was removed from the upper chamber. The non-invaded cells on the upper side of the chamber were scraped off with a cotton swab. The cells that had migrated from the matrigel into the pores of the inserted filter were fixed with 100% methanol, stained with Hematoxylin, and mounted and dried at 80°C for 30 min. The number of cells invading through the matrigel was counted in three randomly selected visual fields from the central and peripheral portion of the filter using an inverted microscope (200×magnification). Each assay was repeated three times.

Flow-cytometric analysis

To detect cell apoptosis, GC cells were trypsinized, washed with cold PBS and resuspended in binding buffer. FITC-AnnexinV and PI (KeyGEN Biotech Co., Ltd. Nanjing, China) were added to the fixed cells for 20 min in darkness at room temperature. Then, Annexin V binding buffer was added to the mixture before the fluorescence was measured on FAC sort flow cytometer. The cell apoptosis was analyzed using Cell Quest software (Becton Dickinson, USA). Three separate experiments were performed for each clone.

In vivo tumor xenograft studies

Six-week-old female immune-deficient nude mice (BALB/c-nu) were bred at the laboratory animal facility. One mouse was injected subcutaneously with 1 x 10^7 GC cells in 50 μl of PBS pre-mixed with an equal volume of matrigel matrix (Becton Dickinson). This mouse was monitored daily, and developed a subcutaneous tumor. When the tumor size reached approximately 5 mm

in length, it was surgically removed, cut into 1~2 mm^3 pieces, and re-seeded subcutaneously and individually into the other 15 mice, which were randomly and averagely divided into Ctrl, NC and KLF2 groups the day after surgery. Injections were repeated every other day after initial treatment for 21 days. The tumor volume every three days was measured with a caliper, using the formula volume = (length x width)^2 / 2. The mice were sacrificed after the final injection and tumors were resected aseptically for weight and volume calculation.

Statistical analysis

SPSS 21.0 was used for the statistical analysis. Kruskal-Wallis H test and *Chi*-squared test were used to analyze the expression rate in all groups. One-way analysis of variance (ANOVA) was used to analyze the differences between groups. The LSD method of multiple comparisons was used when the probability for ANOVA was statistically significant. Statistical significance was set at $P < 0.05$.

RESULTS

The expression of KLF2 in human GC tissues

The expression of KLF2 protein was examined by IHC staining. As shown in Fig. 1A, we found that the positive expression of KLF2 was significantly decreased in 31.03% (19/58) of GC tissues compared with that in 53.45% (31/58) of ANCT (Table I, P=0.035).

Correlation of KLF2 protein expression with clinicopathologic characteristics in GC patients

The correlation between KLF2 expression and the clinical and histopathologic features was analyzed. As shown in Table II, no significant association was found between KLF2 expression and the factors including age and sex of the patients, or the size, tumor differentiation and TNM staging of the tumors (each P>0.05). However, KLF2 expression was negatively correlated with the lymph node metastases in GC patients (P=0.02).

Effect of KLF2 overexpression on the PI3K/AKT signaling

To verify the effect of KLF2 overexpression on the expression of PI3K/AKT signaling in GC cells, the expression levels of KLF2, p-PI3K and p-AKT were detected by Real-time PCR (Fig. 1B) and Western blot assays (Fig. 1C).

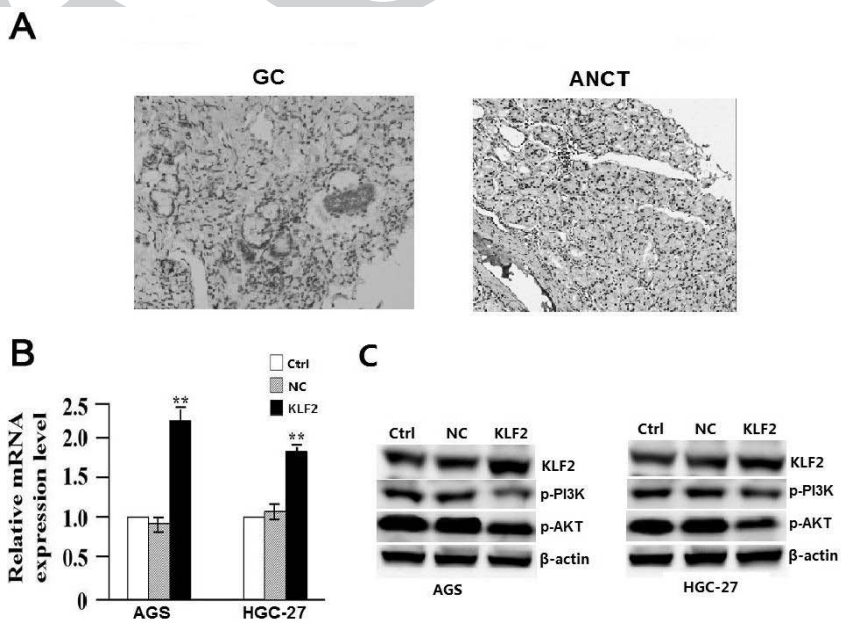

Fig. 1. *The protein expression of KLF2 in GC tissues (× 200). **A**) The positive protein expression of KLF2 was downregulated in GC tissues compared with the ANCT. **B**) After lentivirus-mediated KLF2 overexpression was infected into GC cell lines (AGS and HGC-27) for 24 h, the mRNA expression levels of KLF2 were detected by Real-time PCR (each **P < 0.01). C) The protein expression levels of p-PI3K and p-AKT were examined by Western blot assay.*

Table I. *The protein expression of KLF2 in human GC tissues.*

Marker	Group	Total	N				Positive rate (%)	χ^2	*P*
			-	+	++	+++			
KLF2	GC	58	39	9	7	3	31.03		
	ANCT	58	27	16	9	6	53.45	4.468	0.035

GC: gastric cancer; ANCT: adjacent non-cancerous tissues

Table II. *The correlation of KLF2 expression with clinicopathologic features of GC patients.*

Variables	Cases (n)	KLF2		*P* value
		-	+	
Total	58	39	19	
Number of patients				
Age (years)				
⩽55	21	14	7	
＞55	37	25	12	0.944
Sex				
Male	42	28	14	
Female	16	11	5	0.881
Tumor size (cm)				
⩽3.5	27	19	8	
＞3.5	31	20	11	0.639
Tumor differentiation				
Well+Moderately	22	12	10	
Poorly	36	27	9	0.110
TNM staging				
Ⅰ+Ⅱ	19	12	7	
Ⅲ+Ⅳ	39	27	12	0.647
Metastatic lymph node				
Negative	24	12	12	
Positive	34	27	7	0.02

Effect of KLF2 overexpression on cell proliferation and apoptosis

To evaluate the effect of KLF2 overexpression on tumor proliferation and cell apoptosis, we observed cell proliferative activities by MTT assay and cell apoptosis by Flow-cytometric analysis. We found that KLF2 overexpression significantly inhibited cell proliferative activities (Fig. 2A) and augmented cell apoptotic indexes (Fig. 2B) in GC cells compared with the Ctrl and CON groups (each $^{**}P<0.01$). In addition, we examined the expression levels of PCNA and Bcl-2 by Real-time PCR (Fig. 2C) and Western blot assays (Fig. 2D) to survey whether KLF2 overexpression regulates their expression. It was revealed that the expression levels of PCNA and Bcl-2 were markedly downregulated in the KLF2 group compared with the Ctrl and CON groups ($^{**}P<0.01$).

Effect of KLF2 overexpression on cell invasion

To confirm the effect of KLF2 overexpression on cell invasion, we investigated cell invasive potential by Transwell assay. As indicated in Fig. 3A, we found that the number of the infiltrating cells was significantly reduced in the KLF2 group (129.6±18.8; 75.3±9.5) compared with the Ctrl (247.3±23.5; 113.4±17.3) and NC groups (238.5±26.2; 98.1±12.7) in AGS and HGC-27 cells (each $^{**}P<0.01$). In addition, we detected the expression levels of MMP-9 by Real-time PCR and Western blot assays (Fig. 3B) in KLF2 infected GC cells. We found that the expression levels of MMP-9 were downregulated in KLF2 group compared with the Ctrl and CON groups ($^{**}P<0.01$).

Antitumor effect of KLF2 overexpression on GC cells in vivo

Our *in vitro* experiments confirmed that KLF2 overexpression efficiently inhibited proliferation

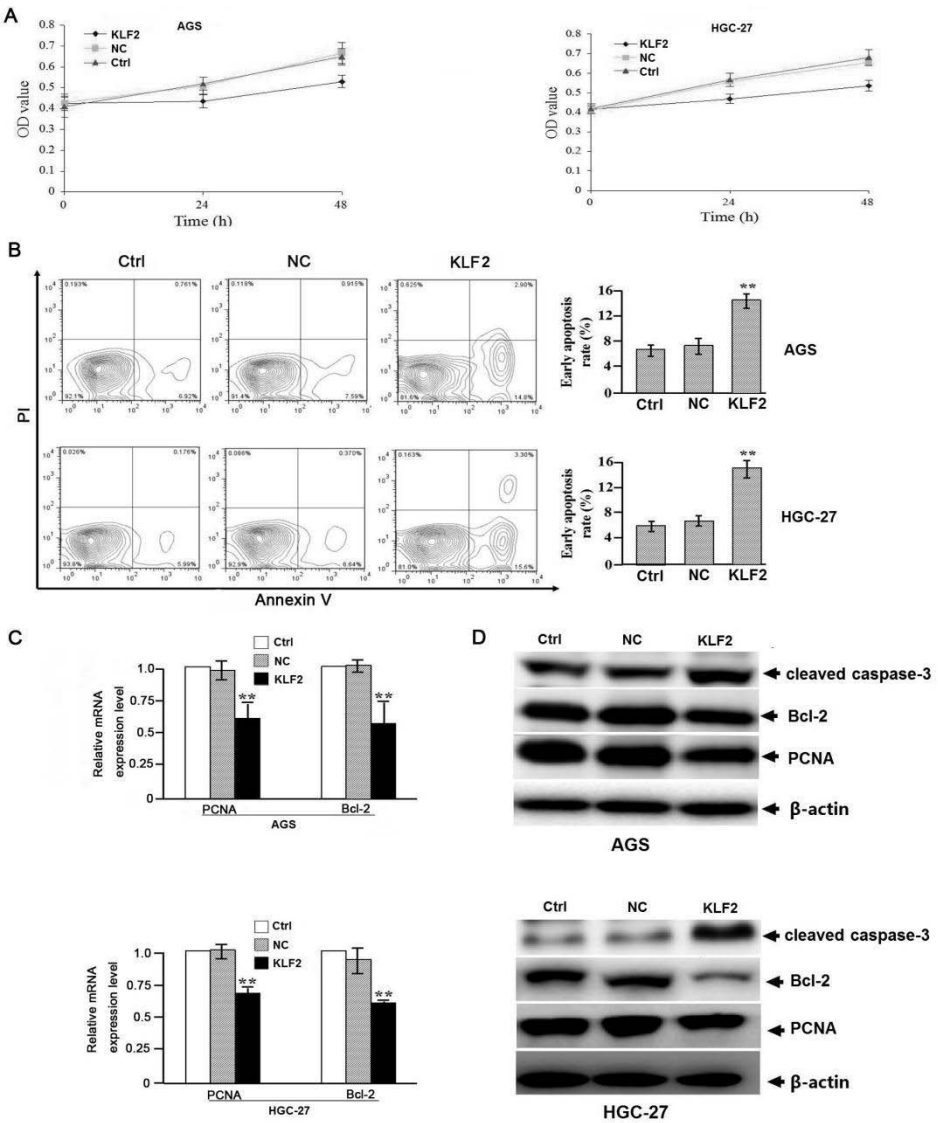

Fig. 2. *The effect of KLF2 overexpression on cell proliferation and apoptosis.* ***A)*** *MTT assay showed that KLF2 overexpression significantly inhibited the proliferative activities of GC cells.* ***B)*** *Flow-cytometric analysis indicated that KLF2 overexpression induced cell apoptosis compared with the Ctrl and NC groups (**P < 0.01).* ***C)*** *Real-time PCR and* ***(D)*** *Western blot assays indicated the decreased expression of PCNA and Bcl-2 in the KLF2 group compared with the Ctrl and NC groups (each **P<0.01).*

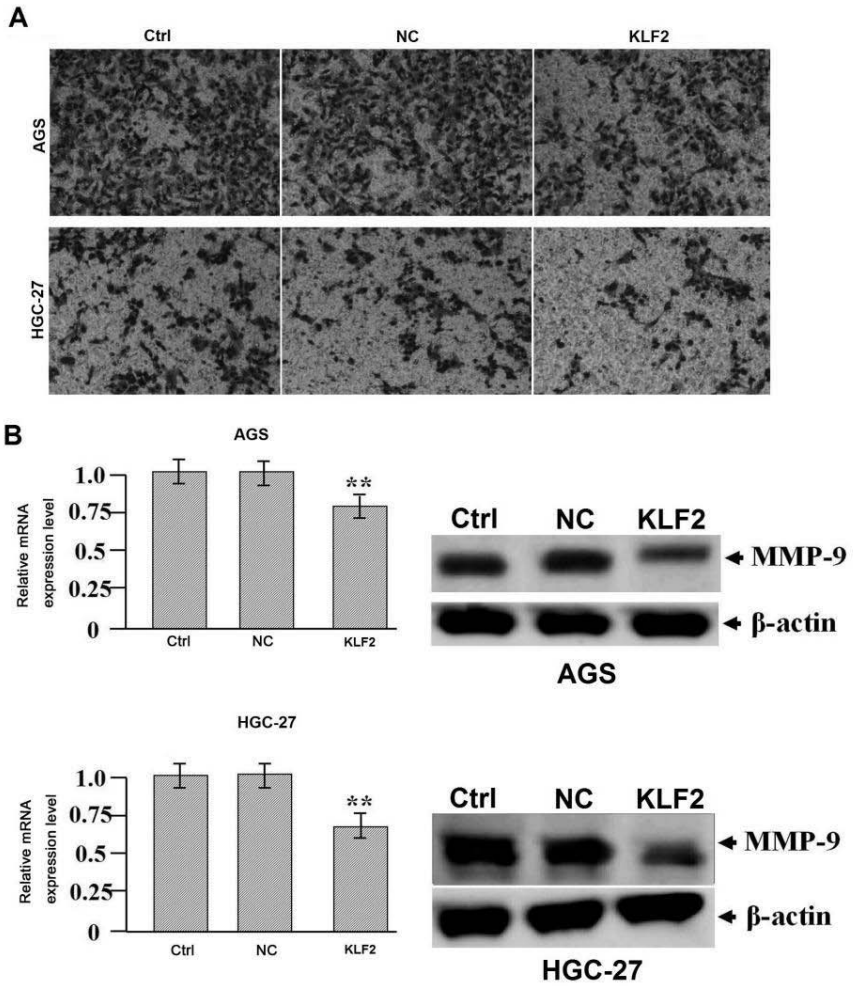

Fig. 3. *The effect of KLF2 overexpression on cell invasion.* ***A)*** *Transwell assay indicated that the invasive potential of GC cells was lowered in KLF2 group compared with the Ctrl and NC groups.* ***B)*** *Real-time PCR and Western blot assays indicated the decreased expression of MMP-9 in the KLF2 group compared with the Ctrl and NC groups (each **P<0.01).*

and invasion in GC cells. Thus, we further observed the antitumor effect of KLF2 overexpression *in vivo* by establishing the GC AGS xenograft model. Each mouse was respectively challenged by *in situ* injection of Ctrl (PBS; n=5), NC (n=5) and KLF2 (n=5). During the first three weeks of recovery, the tumors in the KLF2 group grew slower compared with the Ctrl and NC groups (Fig. 4A, B). In addition, the GC volume was smaller and the weight was lighter (Fig. 4C) compared with the Ctrl and NC groups (**P<0.01). We also found that the protein expression levels of p-PI3K, p-AKT, Bcl-2, MMP-9 and PCNA were down-regulated in the KLF2 group compared with the Ctrl and NC groups by analyzing tumor lysates with Western blotting (Fig. 4D).

DISCUSSION

KLF proteins fulfill a range of cell differentiation and proliferation functions in a wide range of organisms (26, 27). Biological activities of KLFs depends on their Cys2/His2 zinc-finger domains that preferentially bind to GC-rich target sequences (26). A large body of evidence suggests that KLF2

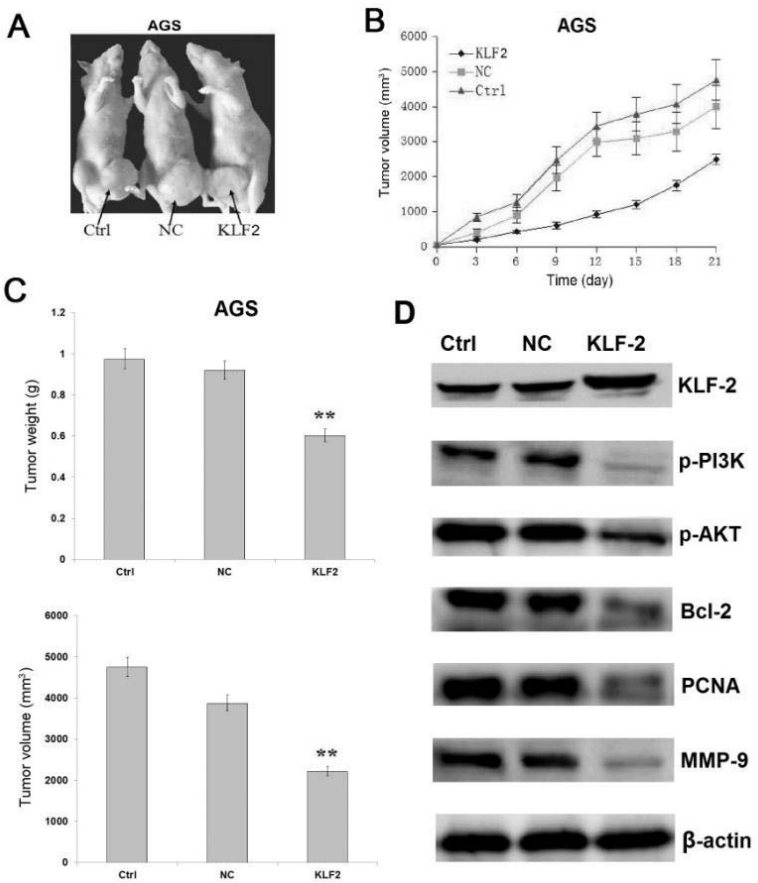

Fig. 4. *KLF2 overexpression inhibited GC cell growth in vivo.* ***A, B****) During the first three weeks recovery, the tumors in KLF2 group grew slower compared with the Ctrl and NC groups.* ***C****) The GC volume and (****D****) weight were much smaller in the KLF2 group compared with the Ctrl and NC groups (**P<0.01)*

dominantly functions as a tumor repressor for its diminished expression in malignancies and its growth inhibitory, pro-apoptotic and anti-angiogenic roles (27). In the present study, we detected the protein expression level of KLF2 in GC tissues, revealing that KLF2 was significantly downregulated in GC tissues. More importantly, decreased expression of KLF2 was correlated with the lymph node metastasis in GC patients, suggesting that loss of KLF2 expression might be involved in promoting the tumorigenesis of GC.

The PI3K/AKT pathway plays a critical role in controlling cancer cell survival and apoptosis. Mounting data have shown that AKT signaling is frequently activated in gastrointestinal tumors and closely associated with prognosis of patients with gastric cancer (28, 29). Cell proliferation is enhanced by oncogenic activation of PI3K/AKT molecules through increasing PCNA level (30). The induction of apoptosis was accompanied by the inactivation of the PI3K/AKT signaling pathway through increasing the Bcl-2 expression (31). Moreover, tumor invasion and metastasis can be achieved through activation of PI3K/AKT pathway by inducing the expression of MMP-9, carrying out an important role in tumor cell migration (32). KLF2 inhibits the tumorigenicity by inhibition of the PI3K/AKT pathway (33). Intriguingly, our results also showed that the overexpression of KLF2 reduced cell proliferation and invasion and downregulated the expression of p-PI3K, p-AKT, PCNA, Bcl-2 and MMP-9 in GC cell lines, indicating that KLF2 might function as a

tumor suppressor in GC cells.

In short, our findings indicate that the decreased expression of KLF2 is correlated with the tumor metastasis in human GC patients, and KLF2 overexpression inhibits the growth and invasion of GC cells through inhibition of the PI3K/AKT signaling, suggesting that KLF2 may represent a potential therapeutic target for the treatment of GC.

REFERENCES

1. Ferro A, Peleteiro B, Malvezzi M, et al. Worldwide trends in gastric cancer mortality (1980-2011), with predictions to 2015, and incidence by subtype. Eur J Cancer 2014; 50:1330-44.
2. Siegel R, Ma J, Zou Z, Jemal A. Cancer statistics, 2014. CA: a cancer journal for clinicians 2014; 64(1):9-29.
3. Cao Y, DePinho RA, Ernst M, Vousden K. Cancer research: past, present and future. Nature Rev Cancer 2011; 11(10):749-54.
4. Anderson KP, Kern CB, Crable SC, Lingrel JB. Isolation of a gene encoding a functional zinc finger protein homologous to erythroid Krüppel-like factor: Identification of a new multigene family. Mol Cell Biol 1995; 15:5957-65.
5. Black AR, Black JD, Azizkhan-Clifford J. Sp1 and kruppel-like factor family of transcription factors in cell growth regulation and cancer. J Cell Physiol 2001; 188:143-60.
6. Kaczynski J, Cook T, Urrutia R. Sp1- and Kruppel-like transcription factors. Genome Biol 2003; 4:206.
7. Dang DT, Chen X, Feng J, Torbenson M, Dang LH, Yang VW. Overexpression of Kruppel-like factor 4 in the human colon cancer cell line RKO leads to reduced tumorigenecity. Oncogene 2003; 22:3424-30.
8. Fernandez-Zapico ME, Mladek A, Ellenrieder V, Folch-Puy E, Miller L, Urrutia R. An mSin3A interaction domain links the transcriptional activity of KLF11 with its role in growth regulation. EMBO 2003; 22:4748-58.
9. Kremer-Tal S, Narla G, Chen Y, et al. Downregulation of KLF6 is an early event in hepatocarcinogenesis, and stimulates proliferation while reducing differentiation. J Hepatology 2007; 46:645-54.
10. Liu R, Zheng HQ, Zhou Z, Dong JT, Chen C. KLF5 promotes breast cell survival partially through fibroblast growth factor-binding protein 1-pERK- mediated dual specificity MKP-1 protein phosphorylation and stabilization. J Bio Chem 2009; 284:16791-98.
11. Duhagon MA, Hurt EM, Sotelo-Silveira JR, Zhang X, Farrar WL. Genomic profiling of tumor initiating prostatospheres. BMC genomics 2010; 11:324.
12. Wang F, Zhu Y, Huang Y, et al. Transcriptional repression of WEE1 by Kruppel-like factor 2 is involved in DNA damage-induced apoptosis. Oncogene 2005; 24:3875-85.
13. Wu J, Lingrel JB. KLF2 inhibits Jurkat T leukemia cell growth via upregulation of cyclin-dependent kinase inhibitor p21WAF1/CIP1. Oncogene 2004; 23(49):8088-96.
14. Lin Z, Natesan V, Shi H, et al. Kruppel-like factor 2 regulates endothelial barrier function. Arterioscler Thromb Vasc Biol 2010; 30:1952-59.
15. Wu J, Lingrel JB. KLF2 inhibits Jurkat T leukemia cell growth via upregulation of cyclin-dependent kinase inhibitor p21WAF1/CIP1. Oncogene 2004; 23:8088-96.
16. Wick MJ, Blaine S, Van Putten V, Saavedra M, Nemenoff RA. Lung Krüppel-like factor (LKLF) is a transcriptional activator of the cytosolic phospholipase A2 alpha promoter. Biochem J 2005; 387:239-46.
17. Fernandez-Zapico ME, Lomberk GA, Tsuji S, et al. A functional family-wide screening of SP/KLF proteins identifies a subset of suppressors of KRAS-mediated cell growth. Biochem J 2011; 435:529-37.
18. Buckley AF, Kuo CT, Leiden JM. Transcription factor LKLF is sufficient to program T cell quiescence via a c-Myc-dependent pathway. Nat Immunol 2001; 2:698-704.
19. SenBanerjee S, Lin Z, Atkins GB, et al. KLF2 is a novel transcriptional regulator of endothelial proinflammatory activation. J Exp Med 2004; 199:1305-15.
20. Banerjee SS, Feinberg MW, Watanabe M, et al. The Krüppel-like factor KLF2 inhibits peroxisome proliferator-activated receptor-gamma expression and adipogenesis. J Biol Chem 2003; 278:2581-84.
21. Wang F, Zhu Y, Huang Y, et al. Transcriptional repression of WEE1 by Krüppel-like factor 2 is involved in DNA damage-induced apoptosis. Oncogene 2005; 24:3875-85.
22. Bhattacharya R, Senbanerjee S, Lin Z, et al. Inhibition of vascular permeability factor/vascular en-

dothelial growth factor-mediated angiogenesis by the Krüppel-like factor KLF2. J Biol Chem 2005; 280:28848-51.
23. Uchida D, Onoue T, Begum NM, et al. Vesnarinone downregulates CXCR4 expression via upregulation of Krüppel-like factor 2 in oral cancer cells. Molecular Cancer 2009, 12; 8:62 doi: 10.1186/1476-4598-8-62.
24. Zhang J, Zhang R, Lu WW, et al. Clinical significance of HMGB1 expression in human gastric cancer. Int J Immunopath Ph 2014; 27(4):543-51.
25. Jin S, Zhang QY, Kang XM, Wang JX, Zhao WH. Daidzein induces MCF-7 breast cancer cell apoptosis via the mitochondrial pathway. Ann Onc 2010; 21(2):263-68.
26. Zhao C, Meng A. Sp1-like transcription factors are regulators of embryonic development in vertebrates. Dev Growth Differ 2005; 47:201-11.
27. Lomberk G, Urrutia R. The family feud: turning off Sp1 by Sp1-like KLF proteins. Biochem J 2005; 392:1-11.
28. Michl P, Downward J. Mechanisms of disease: PI3K/AKT signaling in gastrointestinal cancers. Z Gastroenterol 2005; 43:1133-39.
29. Ying J, Xu Q, Liu B, Zhang G, Chen L, Pan H. The expression of the PI3K/AKT/mTOR pathway in gastric cancer and its role in gastric cancer prognosis. Onco Targets Ther 2015; 8:2427-33.
30. Kang S, Bader AG, Vogt PK. Phosphatidylinositol 3-kinase mutations identified in human cancer are oncogenic. Proc Natl Acad Sci USA 2005; 102: 802-7.
31. Yu HY, Kim SO, Jin CY, et al. β-lapachone-induced apoptosis of human gastric carcinoma AGS cells is caspase-dependent and regulated by the PI3K/Akt pathway. Biomol Ther 2014; 22:184-92.
32. Kanaki T, Bujo H, Mori S, et al. Functional analysis of aortic endothelial cells expressing mutant PDGF receptors with respect to expression of matrix metalloproteinase-3. Biochem Biophys Res Commun 2002; 294:231-37.
33. Sako K, Fukuhara S, Minami T, et al. Angiopoietin-1 induces Kruppel-like factor 2 expression through a phosphoinositide 3-kinase/AKT-dependent activation of myocyte enhancer factor 2. J Biol Chem 2009; 284(9):5592-601.

VITAMINS D3 AND K2 MAY PARTIALLY COUNTERBALANCE THE DETRIMENTAL EFFECTS OF PENTOSIDINE IN EX VIVO HUMAN OSTEOBLASTS

R. SANGUINETI[1], F. MONACELLI[1], A. PARODI[2], A.L. FURFARO[3], R. BORGHI[1], D. PACINI[1], M.A. PRONZATO[2], P. ODETTI[1], L. MOLFETTA[4] and N. TRAVERSO[2]

[1]DIMI, University of Genova, Genoa, Italy; [2]DIMES, University of Genova, Genoa, Italy
[3]Giannina Gaslini Institute, Genoa, Italy; [4]DINOGMI, University of Genova, Genoa, Italy

Received November19, 2015 – Accepted February 23, 2016

Osteoporosis is a metabolic multifaceted disorder, characterized by insufficient bone strength. It has been recently shown that advanced glycation end products (AGEs) play a role in senile osteoporosis, through bone cell impairment and altered biomechanical properties. Pentosidine (PENT), a well-characterized AGE, is also considered a biomarker of bone fracture. Adequate responses to various hormones, such as 1,25-dihydroxyvitamin D_3, are prerequisites for optimal osteoblasts functioning. Vitamin K_2 is known to enhance in vitro and in vivo vitamin D-induced bone formation. The aim of the study was to assess the effects of Vitamins D3 and K2 and PENT on in vivo osteoblast activity, to convey a possible translational clinical message. Ex vivo human osteoblasts cultured, for 3 weeks, with vitamin D_3 and vitamin K_2 were exposed to PENT, a well-known advanced glycoxidation end product for the last 72 hours. Experiments with PENT alone were also carried out. Gene expression of specific markers of bone osteoblast maturation [alkaline phosphatase, ALP; collagen I, COL Iα1; and osteocalcin (bone-Gla-protein) BGP] was measured, together with the receptor activator of nuclear factor kappa-B ligand/osteoproteregin (RANKL/OPG) ratio to assess bone remodeling. Expression of RAGE, a well-characterized receptor of AGEs, was also assessed. PENT+vitamins slightly inhibited ALP secretion while not affecting gene expression, indicating hampered osteoblast functional activity. PENT+vitamins up-regulated collagen gene expression, while protein secretion was unchanged. Intracellular collagen levels were partially decreased, and a significant reduction in BGP gene expression and intracellular protein concentration were both reported after PENT exposure. The RANKL/OPG ratio was increased, favouring bone reabsorption. RAGE gene expression significantly decreased. These results were confirmed by a lower mineralization rate. We provided in vitro evidence that glycoxidation might interfere with the maturation of osteoblasts, leading to morphological modifications, cellular malfunctioning, and inhibition of the calcification process. However, these processes may be all partially counterbalanced by vitamins D_3 and K_2. Therefore, detrimental AGE accumulation in bone might be attenuated and/or reversed by the presence or supplementation of vitamins D_3 and K_2.

Osteoporosis, a multi-factorial progressive skeletal metabolic disease, is characterized by low mass density and structural deterioration of the bone micro-architecture, which leads to enhanced bone

Key words: AGEs, osteoporosis, osteoblasts, reabsorptive effects, Vit K2 and Vit D3 supplementation

Mailing address:
Dr Nicola Traverso,
DIMES- Section of General Pathology,
Via LB Alberti, 2 - 16132, Genova, Italy
Tel.: +39 010 353 88 35 - Fax: +39 010 353 88 36
e-mail: nicola.traverso@unige.it

0393-974X (2016)

DISCLOSURE: ALL AUTHORS REPORT NO CONFLICTS OF INTEREST RELEVANT TO THIS ARTICLE.

fragility and increased susceptibility to fractures (1). Bone homeostasis relies on a fine balance between new apposition by osteoblasts and reabsorption by osteoclasts, which drives bone remodeling. Among the wide spectrum of bone disorders, osteoporosis is one of the most important, due to increasing prevalence and associated economic costs in the Western world. Thus, understanding the mechanisms that affect the complexities of bone remodeling is essential (2).

Osteoporosis has a multifaceted pathogenesis, influenced by nutritional and hormonal factors. Recent understanding of bone remodeling suggests that inflammatory factors, such as cytokines, are mediators of inflammation and may contribute to osteoporosis (3). Moreover, scientific evidence exists that glycoxidation could be involved in the pathogenesis of bone loss, both during aging and in diabetes (4-5).

Generation of advanced glycation end-products (AGEs) is a spontaneous, inevitable process *in vivo*. AGEs increase during aging in all tissues, including bone, and contribute to structural and functional changes of bone proteins, leading to intra- or inter-molecular cross-linking (6). These alterations may explain the deleterious effects of AGEs on bone biomechanical properties (7). AGEs regulate the proliferation and differentiation of osteoblasts, and AGE-specific binding sites are present in cultured osteoblast-like cells (5). Interactions between AGEs and the receptor, RAGE, activate nuclear factor κ-B (NFκB) in osteoblasts, resulting in increased expression of inflammatory cytokines, growth factors and adhesion molecules (8). Therefore, AGE accumulation in bone has been associated with alterations in cortical and trabecular biomechanical properties and bone cell functional impairment (9). Pentosidine (PENT) is a reliable, well-characterized marker of non-enzymatic glycation in collagen (6): a significant increase was first observed in diabetes mellitus, end-stage renal failure and during the aging process (10). Other recent studies have observed PENT accumulation with advancing age (4), and it may be also considered a biomarker of bone fracture (11).

Receptor activator of nuclear factor kappa-B ligand (RANKL) plays a central role in bone remodeling. It is primarily expressed by osteoblasts and is a RANK ligand (also expressed in osteoclasts). Osteoprotegerin (OPG), a decoy receptor that binds RANKL in osteoblasts and hinders the RANKL/RANK ligand interaction, is known to prevent crosstalk between osteoblast and osteoclast precursors, inhibiting differentiation into mature osteoclasts. When activated by RANKL binding, RANK induces osteoclast differentiation, resulting in higher bone reabsorption. OPG, acting as a soluble receptor for RANK, prevents the activation of osteoclasts, protecting bone mass integrity. Therefore, the RANKL/OPG ratio is considered an index of balance between bone formation and reabsorption (12); if RANKL increases compared to OPG, bone equilibrium shifts towards reabsorption. Adequate responses to various hormones, such as 1,25-dihydroxyvitamin D_3 (calcitriol), are prerequisites for optimal osteoblast functioning (13). Osteoblast-specific nuclear vitamin D receptors (VDRs) are considered main targets for calcitriol action in bone. *In vitro*, calcitriol inhibits osteoblast cell proliferation and stimulates production of RANKL as well as several non-collagenous proteins, including osteocalcin (BGP) and alkaline phosphatase (ALP), thereby enhancing the functional activity of mature osteoblast cells (14).

The products of osteoblast activity are critical for bone matrix formation (COL Iα1), maturation and mineralization (ALP, BGP). Decreased expression of osteoblasts-specific genes is suggestive of cellular malfunctioning.

Recent studies have suggested that vitamin K_2 enhances vitamin D-induced bone formation *in vitro* and *in vivo*, stimulating osteoblast-specific gene expression (ALP, COL Iα1 and BGP) (15-17).

The aim of the present work was to assess in human osteoblasts the effects of PENT alone, or the combination of PENT plus vitamins D3 and K2 on markers of differentiation (ALP, COL Iα1, BGP), function (calcification and the RANKL/OPG ratio), RAGE expression and to compare these effects with those of PENT alone.

MATERIALS AND METHODS

Chemicals

TrypLE™ Express is an animal origin-free recombinant enzyme, which was used for dissociating primary human osteoblasts by cleaving peptide bonds on the C-terminal sides of lysine and arginine. TRIzol® is a solution of

phenol and guanidine isothiocyanate, designed to isolate separate fractions of RNA, DNA, and proteins from cells. TrypLE™ and TRIzol®, were obtained from Invitrogen Life Technologies (Carlsbad, CA, USA); specific reagents for RT-PCR were from Promega (Milan, Italy); tissue culture dishes were obtained from BD Biosciences (New Jersey, USA) and all other reagents from Sigma-Aldrich S.r.l. (Milan, Italy).

Isolation of human trabecular bone-derived cells

Trabecular bone samples intended for disposal were obtained from patients who underwent orthopedic surgery and who were free from bone-related diseases, diabetes or autoimmune pathologies. All donors provided written informed consent before surgery.

Human osteoblast (HObs) cells were isolated from trabecular bone samples. Bone chips were washed with PBS and cut into 2-mm diameter sections prior to digestion in collagenase P (1.2 mg/ml in Dulbecco's Modified Eagle Medium (DMEM), Sigma-Aldrich S.r.l., Milan, Italy) for 2 h at 37°C. The digested bone chips were seeded in 30 cm^2 tissue culture dishes with DMEM containing 10% fetal bovine serum (FBS, Sigma-Aldrich S.r.l., Milan, Italy), 2 mM L-glutamine and mixed antibiotics (basal DMEM) at 37°C in a 5% CO_2 humidified atmosphere. After several days, HObs outgrowth from bone chips was observed. Medium was changed twice weekly and bone chips were removed at the 7^{th} day to prevent contamination. HObs reached confluence within 3 weeks of culturing.

Bone nodule formation

HObs were grown until confluent, removed with TRYPLE Express and plated at 3 x 10^5 in 10 cm^2 tissue culture dishes. After achieving confluence, nodule formation was induced using basal DMEM supplemented with 0.3 mM ascorbic acid, 10 mM sodium-glycerophosphate and 0.1 μM dexamethasone (osteogenic medium). Medium was changed every 3–4 days. The experiment was performed at cell confluence.

Experimental conditions

HObs were cultured for 21 days in osteogenic medium in the presence of 10^{-9} M vitamin D_3 (18-19) and 10^{-6} M vitamin K_2 (20-21), and containing 0 or 0.25 μM PENT (CTR, 0.25 μM PENT) for the last 72 hours. Samples treated with 0.25 μM alone were also prepared.

Samples for PENT treatment were prepared as previously reported (22) and evaluated according to the modified Odetti method by HPLC (23). Morphological characteristics and proliferation rate of PENT-treated HObs were observed after 7, 14 and 21 days using an optical microscope (magnification 100X).

Cell viability

The viability and proliferation rate were evaluated in control cells and 0.25 μM PENT-treated HObs using the 3-(4,5-dimethylthiazolyl-2)-2,5-diphenyltetrazolium bromide (MTT) assay according to the manufacturer's instructions. After being cultured, MTT colorimetric assay was performed with incubation in 3-(4,5-dimethylthiazol-2-yl)-2,5-diphenyltetrazolium bromide (M5655 Sigma-Aldrich St Louis MO, USA); then, the cells were lysed with a propanol acid solution (2-Propanol plus 0.04N hydrochloridric acid, Sigma-Aldrich St Louis MO, USA) for colorimetric measurement in a spectrophotometer (570 nm with correction at 650 nm). The values were expressed in percentage of viable cells compared to the control group.

mRNA isolation and RT-PCR

RAGE, RANKL, OPG, ALP, COL Ia1, BGP, gene expressions were evaluated with total RNA extraction by the one-step phenol-guanidinium isothiocyanate method using TRIzol® reagent according to the manufacturer's recommendations. RT-PCR was performed as previously described (24) using specific primers designed based on sequences available in the data banks (Table I). RT-PCR results were normalized using the housekeeping gene GAPDH. Digital images of PCR products were analyzed using the Gel-Doc system (Bio-Rad Laboratories, Milan, Italy), and the bands were quantified with Quantity One software (Bio-Rad Laboratories Inc., Milan, Italy). Results are expressed as percent of the control.

Protein determination

Protein concentrations were determined using a modified Bradford method (Quick Start kit, Bio-Rad Laboratories Inc., Milan, Italy) (25).

Human collagen type I

Collagen Iα1 (COL Iα1) was quantified using a specific immunoassay kit (Cosmo Bio Co. Ltd, Tokyo,

Table I. *Specific designed primers based on sequences available in the data banks.*

Gene	Primer sequence (strand)	Product size (bp)	Temperature (°C)	PCR (cycles)
ALP	5'-3' ACGTGGCTAAGAATGTCATC	470	47	40
	3'-5' CTGGTAGGCGATGTCCTTA			
COL Iα1	5'-3' AAGAGGCGAGAGGGTTTCC	475	51	32
	3'-5' ATCACCAGGTTCACCTTTCG			
BGP	5'-3' GGCAGCGAGGTAGTGAAGAG	306	53	39
	3'-5' CTGGAGAGGAGCAGAACTGG			
RAGE	5'-3' GATCCCCGTCCCACCTTCTCCTGTAGC	556	68	40
	3'-5' CACGGCTCCTCCTCTTCCTCCTGGTTTTCTG			
IL-1α	5'-3' TGGCACAATCTCGGCTCACTG	385	63	42
	3'-5' TCTAGGTGAACATGCGTTATTGC			
LIF	5'-3' TGGACGTGACCTACGGCCCTG	465	63	39
	3'-5' TGCAGGTCCAGCCATCAGACC			
RANKL	5'-3' CGATGGTGGATGGCTCATGG	380	56	38
	3'-5' CCTGATCCGGATCCAGTAAGG			
OPG	5'-3' CCCTGTGTGAGGAGGCATTC	320	56	28
	3'-5' GCTGTGAAGGAACCTGATGG			
GAPDH	5'-3' GCTCATGACCACAGTC	970	60	35
	3'-5' TGTAGGCCATGAGGTC			

Japan). The limit of detection was 0.02 µg/ml. COL Iα1 was evaluated inside the cell and in the media as a secreted protein.

Alkaline phosphatase (ALP)

ALP was quantified as intracellular and extracellular (conditioned media) activity using the SensoLyte TM pNPP Alkaline Phosphatase Assay Colorimetric Kit (AnaSpec, DBA-Italia, Milan, Italy) according to the manufacturer's instructions.

Osteocalcin (BGP)

Osteocalcin concentrations were determined with a commercially available kit (Gla-type Osteocalcin EIA kit, Zymed Laboratories, Invitrogen Immunodetection, Carlsbad, CA, USA) according to the manufacturer's specifications. The limit of detection was 0.25 ng/ml. BGP was measured as intracellular and secreted proteins.

Nodule mineralization

Calcium-rich deposits and nodular patterns *in vitro* were determined by alizarin red-S (ARS) staining. Mineralized nodules were destained by cetyl-pyridinium chloride (26). ARS extracts were read at 550 nm and results are reported as optical density (OD) compared to a standard curve of an ARS solution.

Statistical analysis

The results represent the mean of at least three independent experiments performed under the same conditions. Analyses were performed using GraphPad Prism 4.0 (GraphPad Software, San Diego, CA, USA). Results are expressed as the mean ± SD. Statistical significance was evaluated by the non-parametric Mann Whitney test and ANOVA test with Dunnett's post-test respectively. P-values <0.05 were considered statistically significant.

RESULTS

Twenty-four hours after plating, no cell growth was observed in any chip sample. Round or polygonal

HObs were observed migrating from the bone chips within the 4th day of culture. Between the 7th and the 14th day, cells began migrating and proliferating more rapidly, and the cells exhibited a high proliferation rate after 3 weeks in culture.

HObs cultured for 21 days with 0.25 μM PENT did not show any cytotoxic effects: cell viability was about 90±9% compared to the controls.

Alkaline phosphatase, Collagen Iα1 and BGP gene expression was detectable in HObs in the third week of incubation with osteogenic medium enriched with vitamins D_3 and K_2, confirming differentiation toward the osteoblast phenotype.

ALP gene expression was unaffected in the presence of PENT+vitamins (+5%) (p, ns), while PENT alone reduced this expression in comparison to PENT free samples. No change in the intracellular protein activity (+3%) was observed, while PENT alone induced a drastic reduction of the activity, and a slight decrease (-13%) in secreted ALP activity was detected (p, ns), while PENT alone induced a slight increase of the activity (Fig. 1).

An 85% increase in COL Iα1 gene expression was observed in the cells treated with PENT+vitamins, ($p<0.01$), while PENT alone induced a slight reduction of expression. No changes were shown in secreted collagen. Intracellular protein was reduced by PENT treatment and the addition of the vitamins were able to attenuate this reduction(-14%) (p, ns) (Fig. 2).

Reduced BGP gene expression (-38%) was observed in the cells treated with PENT with vitamins($p<0.01$), while PENT alone did not induce any variation. A relevant decrease of intracellular protein was observed both in the treatment with PENT alone (-73%) and in treatment with PENT+vitamins (-64%)($p<0.01$). This was associated with a non-significant increase in secreted BGP (p, ns) in both groups of treated cells (Fig. 3).

During osteogenic differentiation, control cells in presence of vitamins D_3 and K_2 produced typical mineralized nodules. Incubation with PENT induced a significant inhibition (-40% *vs* controls) of bone matrix deposition ($p<0.01$), while the addition of vitamin induced a partial recovery of mineralization (Fig. 4). Morphological changes in the cells (less spindle shaped, large and branched) were observed, including pale coloration, disorganization and fewer bone nodules. RAGE RNA messenger analysis showed, after osteoblasts treatment with PENT alone, a sharp decrease of expression, which was reduced in the cells treated with PENT+vitamins, (-26% *vs* control) (p<ns) (Fig. 5).

Osteoblast treatment with PENT+vitamins induced an increase of RANKL gene expression (+250%) ($p<0.01$) and a slight decline of OPG gene expression (-12%) (p, ns). Consequently, the RANKL/OPG ratio was increased (RANKL/OPG ratio: 2.3) ($p<0.01$) (Fig. 6). On the contrary, PENT alone induced a sharp decrease of this ratio.

The main results of the present study are summarized in Table II.

DISCUSSION

Bone collagen has a relatively long half-life, which makes it susceptible to advanced glycoxidation (4, 27-29). There is evidence that the fluorescence of AGEs is higher in older bone donors than in younger patients, as well as in older osteons, compared to newly formed ones (30). AGE formation and accumulation in bone tissue is believed to contribute to the deterioration of bone quality and to the decline of bone mass. AGE-modified collagen is reported to regulate osteoblast differentiation and proliferation (7, 29). A close relationship between reduced osteoblast function, age and diabetes-related bone mass decrease has also been reported in literature (7, 31).

Moreover, a growing body of evidence has shown that the quality and molecular structure of bone is affected by glycation, both in diabetes and during aging (28, 32).

A previous study showed that pentosidine without vitamins D_3 and K_2 induced an overall reduction of COL Ia1, ALP and RAGE expression with 0.25 μM PENT, while BPG expression was apparently unaffected (27).

In the present study, human osteoblasts, obtained *ex vivo* and cultured *in vitro*, were seeded with vitamin K_2 and D_3 for three weeks and added with PENT 0.25 μM in the medium for the last 72 hours, to mimic pathophysiological clinical conditions (23).

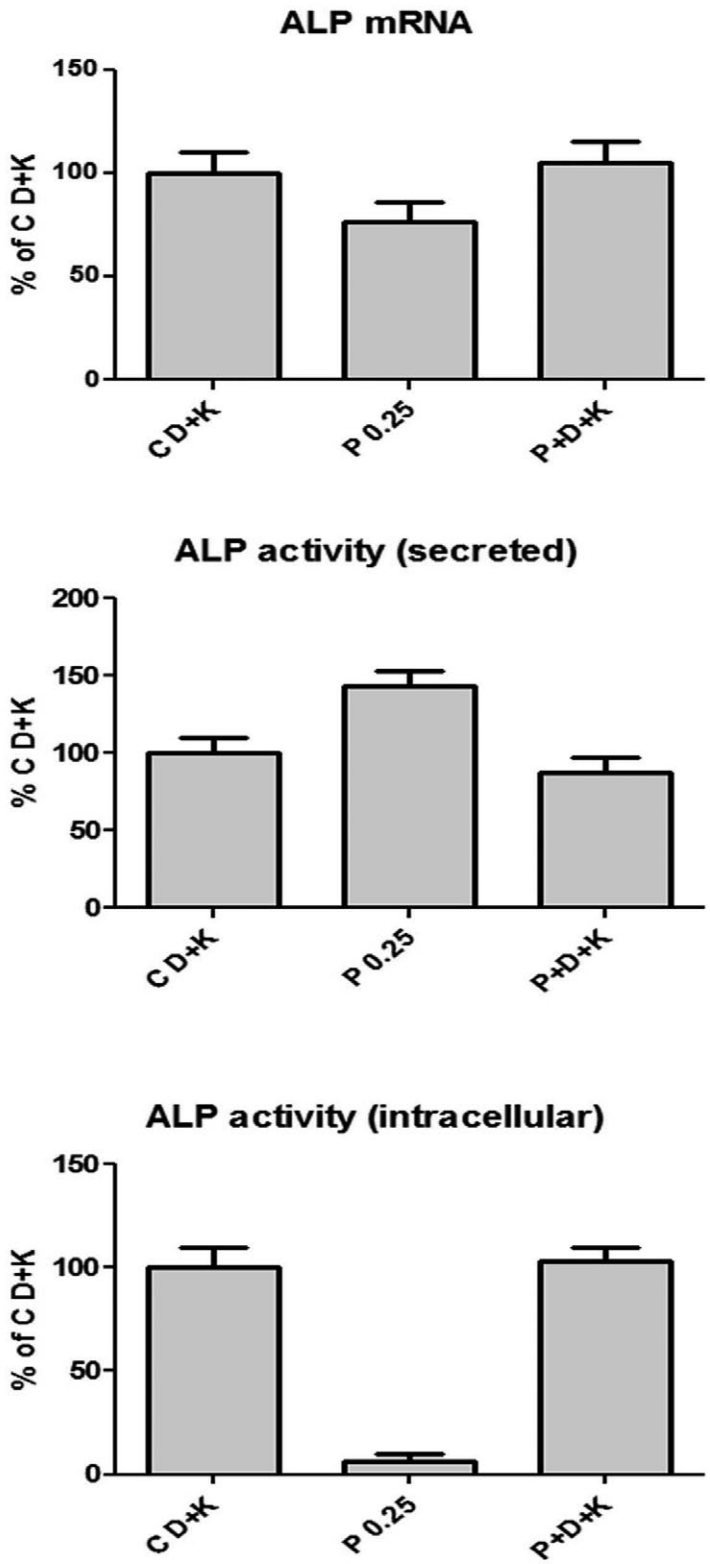

Fig. 1. *mRNA expression (upper panel), secreted activity evaluation (middle panel) and intracellular activity evaluation (lower panel) for Alkaline Phosphatase (ALP). C D+K: control cells with vitamins D3 and K2; P 0.25: cells treated with 0.25 μM Pentosidine; P+D+K: cells treated with pentosidine, and vitamins D3 and K2.*

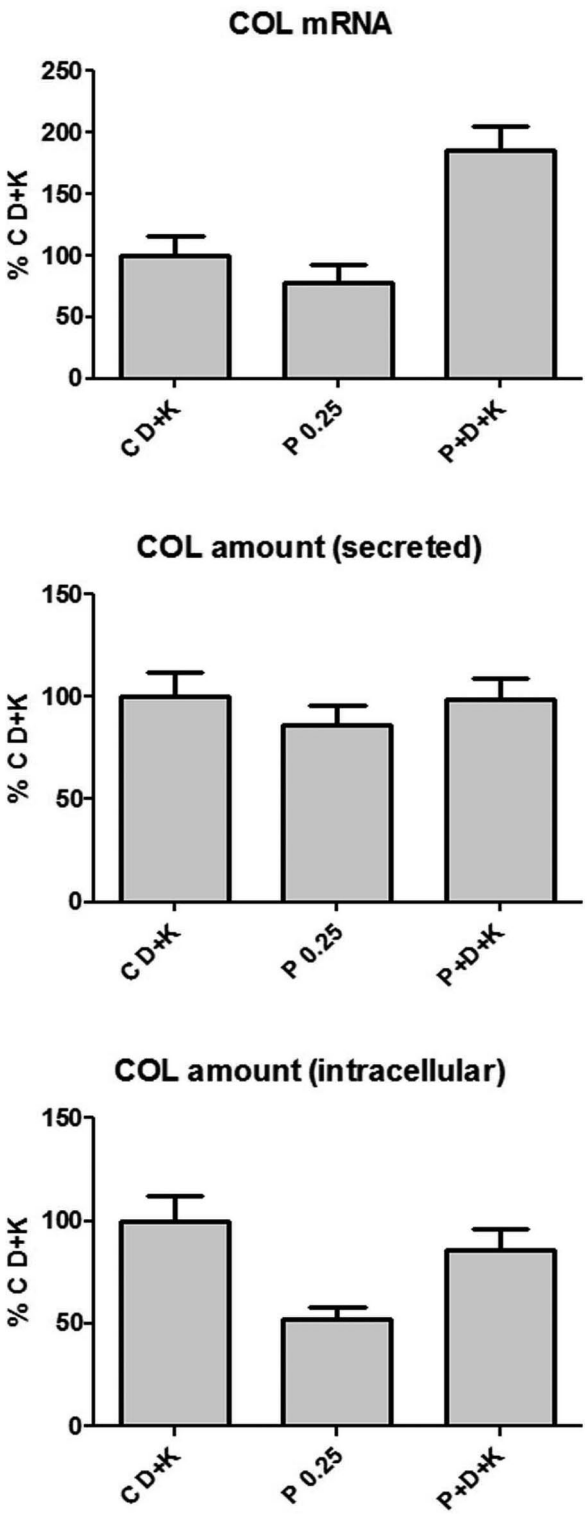

Fig. 2. *mRNA expression (upper panel) and secreted protein quantitation (middle panel) and intracellular protein quantitation (lower panel) for Collagen Ia1 (Col Ia1). C D+K: control cells with vitamins D3 and K2; P 0.25: cells treated with 0.25 μM Pentosidine; P+D+K: cells treated with pentosidine, and vitamins D3 and K2.*

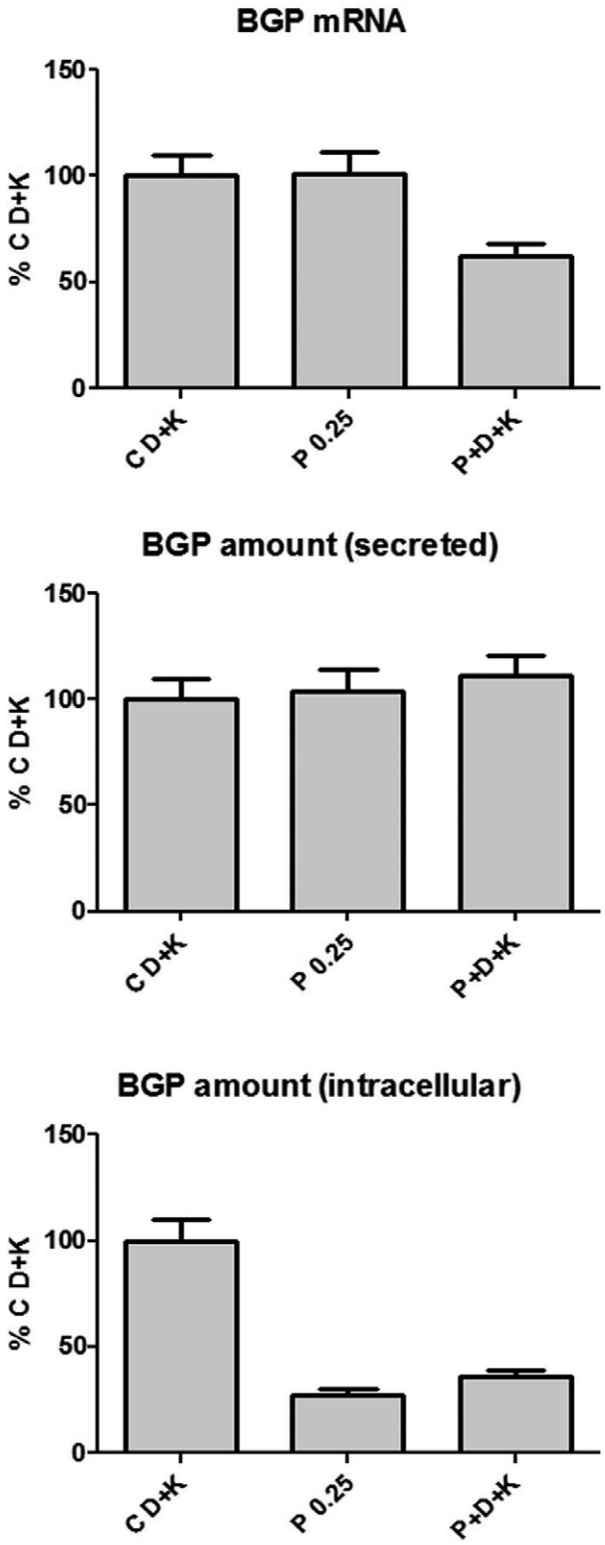

Fig. 3. *mRNA expression (upper panel), secreted protein quantitation (middle panel) and intracellular protein quantitation (lower panel) for osteocalcin (BPG). C D+K: control cells with vitamins D3 and K2; P 0.25: cells treated with 0.25 μM Pentosidine; P+D+K: cells treated with pentosidine, and vitamins D3 and K2.*

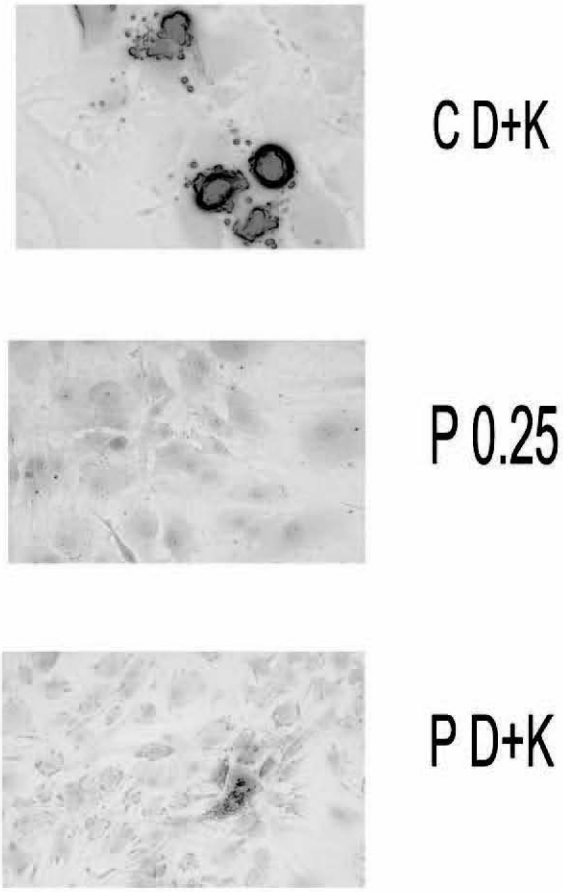

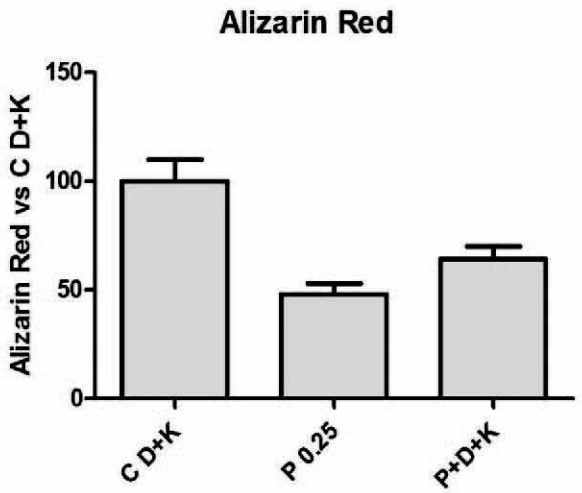

Fig. 4. *Upper three panels: Representative images of mineralization in Control with Vitamin D+K (C D+K), pentosidine alone (P 0.25) and Pentosidine with vitamin D+K (P D+K). Magnification 100x. Lower panel: Alizarin test after extraction calculated in % of the Control conditions) C D+K: control cells with vitamins D3 and K2; P 0.25: cells treated with 0.25 μM Pentosidine; P D+K: cells treated with pentosidine, and vitamins D3 and K2.*

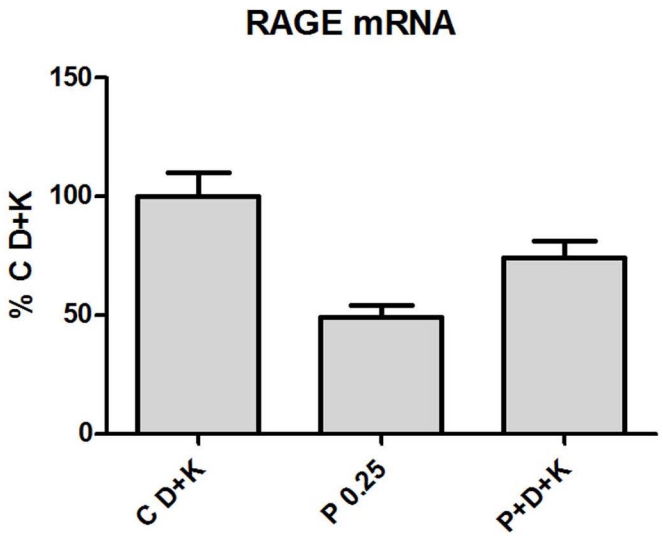

Fig. 5. *mRNA expression for Receptor of AGEs (RAGE). C D+K: control cells with vitamins D3 and K2; P 0.25: cells treated with 0.25 μM Pentosidine; P+D+K: cells treated with pentosidine, and vitamins D3 and K2.*

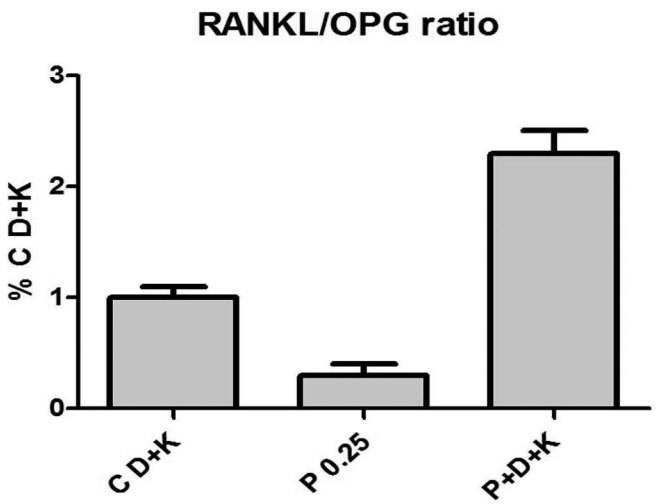

Fig. 6. *RANKL/OPG ratio. C D+K: control cells with vitamins D3 and K2; P 0.25: cells treated with 0.25 μM Pentosidine; P+D+K: cells treated with pentosidine, and vitamins D3 and K2.*

Samples treated with 0.25 μM were also evaluated.

The medium environment enriched with PENT+vitamins induced several and interesting molecular changes. Glycation induced collagen expression up-regulation, but no significant changes were observed in intracellular levels and protein secretion rate, while PENT alone induced a decreased intracellular amount of collagen. Up-regulation of specific mRNA transcription indicates a prevalent positive vitamin-mediated effect on collagen production, compared to PENT-mediated inhibition. Furthermore, several papers have reported that AGEs may hamper the normal functional activity of osteoblasts, inducing a remarkable decrease in collagen secretion (4, 13, 15-17, 27) .

The results of the PENT+vitamins treatment showed no increase of alkaline phosphatase gene expression, a non-significant decrease of protein

Table II. *Main results of osteoblast treatment with PENT and vitamins, expressed as alteration of cell functional activity in terms of gene expression, intracellular protein content and extracellular protein respectively.*

Molecule	Gene expression	Intracellular protein	Extracellular protein
ALP	+5%	+3%	-13%
COL Iα1	+85%**	-14%	0%
BGP	-38%**	-64%**	+11%
RAGE	-26%	-	-
RANKL	+250%***	-	-
OPG	-12%	-	-
Test	Rate		
Mineralized nodules	-40%	-	-

***p<0.05 PENT vs controls (CTR); ***p<0.005 PENT vs controls (CTR)*

activity in the medium, while intracellular protein activity was steady. It is important to highlight that PENT alone induced a drastic reduction of ALP activity inside the cells. Alkaline phosphatase gene is expressed during the calcification process of newly formed bone tissue and it is a reliable marker of osteoblast activation. The observed molecular pattern indicated that the presence of vitamins is able to counteract the detrimental effects of AGEs on bone, favoring osteoblast functional activity.

Osteocalcin is preferentially expressed by osteoblasts and is considered a marker of activity, influencing bone mineralization and bone quality (hardness). Although the precise role of osteocalcin in bone is still controversial (33-34), osteocalcin plasma levels are considered the most sensitive markers of bone formation. In this study, gene expression and the intracellular concentration of BGP were both reduced by the PENT+vitamins treatment, although its secreted protein concentration was unaffected. The result indicated that the milieu (PENT+ vitamins) might inhibit osteoblast activity; these data are further supported by a lack of calcified nodules in the PENT-incubated plates, whereas calcified alizarin-positive neo tissue was detected in control osteoblasts.

The modulation of AGE receptors is likely mediated by selective AGEs, which may inhibit proliferation of osteoblasts through the suppression of several intracellular signaling pathways, as suggested by Okazaki (31). A significant decrease of RAGE gene expression was previously observed with osteoblast medium enriched with PENT alone (28), even if pentosidine is a weak ligand of RAGE (35).

In the present study, in the PENT+vitamins-treated cells, RAGE gene expression decrease was instead smaller and non-significant, indicating that PENT minimally affected AGE receptor production in the presence of vitamins D3 and K2.

Moreover, the results of the treatment with PENT+vitamins showed a strong increase of RANKL and a negligible decline of OPG, with a significant increase of RANKL/OPG ratio, favoring a pro-reabsorbitive environment, which could indicate

an easier regeneration of old bone structures. PENT alone induced an increase of this ratio, which could indicate a harder but more fragile bone structure.

On the basis of our results, it may be conceived that AGEs have a dramatic bone reabsorption effect in a milieu poor of cofactors (i.e., low vitamins D_3 and K_2), a condition often observed in the elderly population. In contrast, normal concentrations or supplementation of these vitamins may, at least, partially attenuate the detrimental AGE effects on bone (e.g., hindered mineralization, reduced BPG expression, lowered RANKL/OPG ratio and overall osteoblast malfunctioning).

In vivo AGE accumulation in bone may be regarded as an inducing factor for bone reabsorption and osteoporosis. Yamaguchi has recently shown an increased risk of fractures in diabetic patients, despite an average bone mass density and concluded that bone quality, not quantity, is associated with an elevated risk of fractures (36). Thus, glycoxidation may be considered a contributing factor of poor bone quality, resulting in a higher risk of fractures. Further to this issue, urinary PENT has been proposed as a marker of fracture risk in osteoporotic patients, who have undergone therapy with bisphosphonates (37).

However, all the aforementioned data should be reconsidered on the basis of bone D3 and K2 vitamin concentrations; the presence of these vitamins may count for important biochemical changes in bone, which may also exert therapeutic effects on bone metabolic diseases, such as senile osteoporosis.

In conclusion, the evidence of the present study confirmed the detrimental role of AGEs, favoring osteoporosis (deficit of nodules formation, high RANKL/OPG ratio, decrease of BGP). Conversely, the results also address the significant role of vitamins in counteracting the unfavorable effects of AGEs on bone. As a translational clinical message, this study supports the mandatory therapy of Vit D3 and K2 supplementation to maintain vitamin D_3 and K_2 levels in elderly patients within optimal concentrations. This is of foremost importance for the elderly as the maintenance of adequate plasmatic Vit D3 and K2 levels may counterbalance AGE bone detrimental effects.

REFERENCES

1. NIH Consensus Development Panel on Osteoporosis Prevention, Diagnosis, and Therapy, March 7-29, 2000: highlights of the conference. South Med J 2001; 94(6):569-73.
2. Henriksen K, Neutzsky-Wulff AV, Bonewald LF, Karsdal MA. Local communication on and within bone controls bone remodeling. Bone 2009; 44(6):1026-33.
3. Ginaldi L, Di Benedetto MC, De Martinis M. Osteoporosis, inflammation and ageing. Immun Ageing 2005; 2:14-18.
4. Odetti P, Rossi S, Monacelli F, Poggi A, Cirnigliaro M, Federici M, Federici A. Advanced glycation end products and bone loss during aging. Ann N Y Acad Sci 2005; 1043:710-7.
5. Hein G, Weiss C, Lehmann G, Niwa T, Stein G, Franke S. Advanced glycation end product modification of bone proteins and bone remodelling: hypothesis and preliminary immunohistochemical findings. Ann Rheum Dis 2006; 65(1):101-4.
6. Sell DR, Monnier VM. Structure elucidation of a senescence cross-link from human extracellular matrix. Implication of pentoses in the aging process. J Biol Chem 1989; 264(36):21597-602.
7. Hein GE. Glycation endproducts in osteoporosis--is there a pathophysiologic importance? Clin Chim Acta 2006; 371(1-2):32-6
8. Thornalley PJ. Cell activation by glycated proteins. AGE receptors, receptor recognition factors and functional classification of AGEs. Cell Mol Biol (Noisy-le-grand) 1998; 44(7):1013-23.
9. Banse X, Devogelaer JP, Lafosse A, Sims TJ, Grynpas M, Bailey AJ. Cross-link profile of bone collagen correlates with structural organization of trabeculae. Bone 2002; 31(1):70-6.
10. Monnier VM, Sell DR, Nagaraj RH, Miyata S, Grandhee S, Odetti P, Ibrahim SA. Maillard reaction-mediated molecular damage to extracellular matrix and other tissue proteins in diabetes, aging, and uremia. Diabetes 1992; 41 Suppl 2:36-41.
11. Saito M, Fujii K, Marumo K. Degree of mineralization-related collagen crosslinking in the femoral neck cancellous bone in cases of hip fracture and controls. Calcif Tissue Int 2006; 79(3):160-8.

12. Grimaud E, Soubigou L, Couillaud S et al. Receptor activator of nuclear factor kappaB ligand (RANKL)/ osteoprotegerin (OPG) ratio is increased in severe osteolysis. Am J Pathol 2003; 163(5):2021-31.
13. Kveiborg M, Rattan SI, Clark BF, Eriksen EF, Kassem M. Treatment with 1,25-dihydroxyvitamin D3 reduces impairment of human osteoblast functions during cellular aging in culture. J Cell Physiol 2001; 186(2):298-306.
14. Anderson PH, Lam NN, Turner AG, Davey RA, Kogawa M, Atkins GJ, Morris HA. The pleiotropic effects of vitamin D in bone. J Steroid Biochem Mol Biol 2013; 136:190-94.
15. Miyake N, Hoshi K, Sano Y, Kikuchi K, Tadano K, Koshihara Y. 1,25-Dihydroxyvitamin D3 promotes vitamin K2 metabolism in human osteoblasts. Osteoporos Int 2001; 12(8):680-7.
16. Ozeki K, Aoki H, Fukui Y. The effect of adsorbed vitamin D and K to hydroxyapatite on ALP activity of MC3T3-E1 cell. J Mater Sci Mater Med 2008; 19(4):1753-57.
17. Sun L, Tamaki H, Ishimaru T, Teruya T, Ohta Y, Katsuyama N, Chinen I. Inhibition of osteoporosis due to restricted food intake by the fish oils DHA and EPA and perilla oil in the rat. Biosci Biotechnol Biochem 2004; 68(12):2613-15.
18. Torricelli P, Fini M, Giavaresi G, Giardino R. Human osteoblast cultures from osteoporotic and healthy bone: biochemical markers and cytokine expression in basal conditions and in response to 1,25(OH)2D3. Artif Cells Blood Substit Immobil Biotechnol 2002; 30(3):219-27.
19. Jevon M, Sabokbar A, Fujikawa Y, Hirayama T, Neale SD, Wass J, Athanasou NA. Gender- and age-related differences in osteoclast formation from circulating precursors. J Endocrinol 2002; 172(3):673-81.
20. Akedo Y, Hosoi T, Inoue S et al. Vitamin K2 modulates proliferation and function of osteoblastic cells in vitro. Biochem Biophys Res Commun 1992; 187(2):814-20.
21. Yamaguchi M, Weitzmann MN. Vitamin K2 stimulates osteoblastogenesis and suppresses osteoclastogenesis by suppressing NF-kappaB activation. Int J Mol Med 2011; 27(1):3-14.
22. Grandhee SK, Monnier VM. Mechanism of formation of the Maillard protein cross-link pentosidine. Glucose, fructose, and ascorbate as pentosidine precursors. J Biol Chem 1991; 266(18):11649-53.
23. Odetti P, Fogarty J, Sell DR, Monnier VM. Chromatographic quantitation of plasma and erythrocyte pentosidine in diabetic and uremic subjects. Diabetes 1992 ;41(2):153-59.
24. Bassi AM, Ledda S, De Pascale MC, Penco S, Rossi S, Odetti P, Cottalasso D. Antioxidant status in J774A.1 macrophage cell line during chronic exposure to glycated serum. Biochem Cell Biol 2005; 83(2):176-87.
25. Bradford MM. A rapid and sensitive method for the quantitation of microgram quantities of protein utilizing the principle of protein-dye binding. Anal Biochem 1976; 72:248-54.
26. Gregory CA, Gunn WG, Peister A, Prockop DJ. An Alizarin red-based assay of mineralization by adherent cells in culture: comparison with cetylpyridinium chloride extraction. Anal Biochem 2004; 329(1):77-84.
27. Sanguineti R, Storace D, Monacelli F, Federici A, Odetti P. Pentosidine effects on human osteoblasts in vitro. Ann N Y Acad Sci 2008; 1126:166-72.
28. Saito M, Marumo K. Collagen cross-links as a determinant of bone quality: a possible explanation for bone fragility in aging, osteoporosis, and diabetes mellitus. Osteoporos Int 2010; 21(2):195-214.
29. Katayama Y, Akatsu T, Yamamoto M, Kugai N, Nagata N. Role of nonenzymatic glycosylation of type I collagen in diabetic osteopenia. J Bone Miner Res 1996; 11(7):931-37.
30. Dong XN, Qin A, Xu J, Wang X. In situ accumulation of advanced glycation endproducts (AGEs) in bone matrix and its correlation with osteoclastic bone resorption. Bone 2011; 49(2):174-83.
31. Okazaki K, Yamaguchi T, Tanaka K, Notsu M, Ogawa N, Yano S, Sugimoto T. Advanced glycation end products (AGEs), but not high glucose, inhibit the osteoblastic differentiation of mouse stromal ST2 cells through the suppression of osterix expression, and inhibit cell growth and increasing cell apoptosis. Calcif Tissue Int 2012; 91(4):286-96.
32. Tang SY, Zeenath U, Vashishth D. Effects of non-enzymatic glycation on cancellous bone fragility. Bone 2007; 40(4):1144-51.
33. Neve A, Corrado A, Cantatore FP. Osteocalcin: skeletal and extra-skeletal effects. J Cell Physiol

2013; 228(6):1149-53.
34. Kavukcuoglu NB, Patterson-Buckendahl P, Mann AB. Effect of osteocalcin deficiency on the nanomechanics and chemistry of mouse bones. J Mech Behav Biomed Mater 2009; 2(4):348-54.
35. Valencia JV, Weldon SC, Quinn D, Kiers GH, DeGroot J, TeKoppele JM, Hughes TE. Advanced glycation end product ligands for the receptor for advanced glycation end products: biochemical characterization and formation kinetics. Anal Biochem 2004; 324(1):68-78.
36. Yamaguchi T. Bone fragility in type 2 diabetes mellitus. World J Orthop 2010; 1(1):3-9.
37. Shiraki M, Kuroda T, Shiraki Y, Tanaka S, Higuchi T, Saito M. Urinary pentosidine and plasma homocysteine levels at baseline predict future fractures in osteoporosis patients under bisphosphonate treatment. J Bone Miner Metab 2011; 29(1):62-70.

LETTER TO THE EDITOR

EXPOSURE TO ELECTROMAGNETIC FIELDS ABOARD HIGH-SPEED ELECTRIC MULTIPLE UNIT TRAINS

D. NIU[1], F. ZHU[1], R. QIU[1] and Q. NIU[2]

[1]Electrical Engineering School, Southwest Jiaotong University, China; [2]Department of Occupational Health, Shanxi Medical University, China

Received March 1, 2016 – Accepted May 12, 2016

High-speed electric multiple unit (EMU) trains generate high-frequency electric fields, low-frequency magnetic fields, and high-frequency wideband electromagnetic emissions when running. Potential human health concerns arise because the electromagnetic disturbances are transmitted mainly into the car body from windows, and from there to passengers and train staff. The transmission amount and amplitude distribution characteristics that dominate electromagnetic field emission need to be studied, and the exposure level of electromagnetic field emission to humans should be measured. We conducted a series of tests of the on board electromagnetic field distribution on several high-speed railway lines. While results showed that exposure was within permitted levels, the possibility of long-term health effects should be investigated.

To the Editor,

High-speed electric multiple unit (EMU) trains have been operating for many years in China and some other countries, including France, Germany and Japan. Chinese EMU trains collect 50 Hz alternating current (AC) from pantograph-catenary contact from 27.5 KV overhead traction power systems. The AC voltage between catenary and ground produces power frequency electric fields. When the EMU train is running, the catenary transfers tens to hundreds of amperes of current, which produce proportionate power frequency magnetic fields. When pantograph-catenary vibration is large enough, contact between the catenary and overhead power system may be lost, such that the voltage between them increases sharply to break down the air and cause a gaseous electric discharge (1-2), the so-called off-line electric arc. During the discharge, the pantograph and catenary form electrodes and cause high-frequency electromagnetic emission.

The large-scale operations of high-speed EMU trains and resulting electromagnetic disturbances raise questions about environmental safety, reliability, and the possibility of adverse health effects on passengers and on-board train staff. Due to the shielding effect of the EMU shell, magnetic fields are mainly transmitted to the trains' inhabitants via the windows, but the specific value and distribution features of the magnetic field are not clearly understood (3-5).

We measured the electromagnetic fields on board three main types of high-speed EMU trains operating in China. The magnetic field values were compared with those in common-speed trains and the dif-

Key words: electric multiple unit (EMU) train, electromagnetic disturbance, electromagnetic field emission, exposure level, human health

Mailing address:
Prof. Feng Zhu, PhD
Electrical Engineering School,
Southwest Jiaotong University, China
e-mail: zhufeng@swjtu.edu.cn

0393-974X (2016)

ferences assessed and evaluated relative to the Chinese and international exposure limits. The results provide a baseline on which to assess the possible adverse human health effects.

MATERIALS AND METHODS

All the measurements described below were performed according to IEC 62236-2-2008 (6).

Measurement of power-frequency electric field

The power frequency electric fields were measured with an electric field intensity meter (RJ-5, measuring range: 1 V/m-20000 V/m, frequency range: 30Hz-2000Hz (MeiCheng high-frequency electromagnetic instrument plant, Yancheng, Jiangsu, China).

Measurement of high-frequency electric field

High-frequency electric fields were measured with a three-dimensional electric field intensity meter (TES-593, measuring range: 0.3-800v/m, frequency range: 100 KHz-8 GHz (TES electrical electronic corporation, Taipei, Taiwan, China).

Measurement of low-frequency magnetic field

Low-frequency magnetic fields were measured with a three-dimensional magnetic field strength meter [TES-1393, measuring range: 0.01 μT-199.9μT, frequency range: 30 Hz-2 KHz, (TES electrical electronic corporation, Taipei, Taiwan, China)].

Measurement of high frequency electromagnetic field

High-frequency electromagnetic fields were measured with an Electro-Magnetic Interference (EMI) receiver with antennas (ESCI R&S Receiver, measuring range: +30 to -147dBm, frequency range: 9KHz-3GHz, [(Rohde & Schwarz corporation, Munich, Bavaria, Germany; HFH2-Z2 loop antenna, frequency range: 9 KHz-30 MHz; HK116 bi-conical antenna, frequency range: 30 MHz-300 MHz; HL223 log-periodical, frequency range: 300 MHz-1 GHz (Rohde & Schwarz corporation, Munich, Bavaria, Germany)], which can show frequency components of electromagnetic interferences.

Measurement of EM fields aboard EMUs

Given the differences between various high-speed railway lines and EMU train types, and to develop representative measurements, we used a test line (China Railway Science Academy test line) and operational lines (Chengdu-Chongqing and Wuhan-Guangzhou high-speed railway line), and different EMU train types (CRH2, CRH3 and CRH5). The EMC laboratory of Southwest Jiaotong University organized and implemented the measurements in February and May, 2015. The measurements included: tests of driver's cab *vs* passenger car; cars equipped with and without pantographs; tests of car windows *vs* the car center; tests of different electric arc prone sections of rail power system line (electric phase-break sections, overlapping sections); tests of different working conditions (background, full scale traction, overlapping section; at the highest attainable speed *vs* full-scale maximum braking) and tests on different vehicular equipment on EMU. The items measured included: power frequency electric field, high frequency electric field, low-frequency magnetic field and high-frequency electromagnetic field.

RESULTS

Measurement of electric field

The mean power frequency electric field intensity and high-frequency electric field intensity on board different EMU lines and car types were 0.02-0.13 KV/m, and 1.85-14.93 V/m, respectively. According to the International Commission on Non-Ionizing Radiation Protection (ICNIRP) limit (2014) (7*)*, the power electric field strength limits to controlled environment and to the general public are 10 kV/m and 5 kV/m, respectively. According to the Chinese National Standard GBZ2.2-2007 (8), the high-frequency electric field strength limit is 50 V/m. Obviously, the electric field environment on board in our measurements is within the permitted range of these standards.

Magnetic field intensity

The magnetic fields are mainly caused by the traction current and high-current vehicle devices. The magnetic fields measured in different cars under various operational conditions are shown in Table I. The magnetic field values in the car equipped with a pantograph (0.101-0.139μT) was higher than those in common cars (0.097-4.400μT),

and the highest value was 4.400 μT in full scale traction operational condition, which in common cars was 0.139 μT. The magnetic fields measured for different vehicle equipment are shown in Table II, the magnetic field values vary greatly in different equipment in the train cars.

The low-frequency magnetic field value near the window was higher in comparison to that in the center of the car, and was also related to train speed. The relationship of magnetic amplitude probability

Table I. *Magnetic fields measured in different cars and different operational conditions (Max hold mode).*

	Background	Full scale traction	Full scale brake	electric phase-break section	Overlapping section	At the highest speed
Car with pantograph	0.405 μT	4.400 μT	4.230 μT	4.311 μT	0.097 μT	2.89 μT
Common Car	0.102 μT	0.139 μT	0.127 μT	0.132μT	0.101 μT	0.118 μT

Table II. *Magnetic fields measured for different vehicle equipment.*

Car	Device	Value (μT)
1#	Brake unit	0.438±0.002
2#	Electrical cabinet	2.622±0.015
3#	Vehicle power supply	2.977±0.021
4#	High voltage alternating current. Auto train protection	1.045±0.010
5#	Air conditioning cabinet	0.242±0.022
2#	Vehicle brake	0.148±0.011
3#	Vehicle power supply	4.286±0.013
3#	Brake control unit	0.660±0.005
4#	Battery charger	0.252±0.002
4#-5#	Carriage connecting end	2.895±0.021
5#	Equipment cabin	0.808±0.008
5#-6#	Carriage connecting end	20.951±0.021
5#-6#	Carriage connecting end floor	16.646±0.011
6#	Control panel	0.118±0.013
6#	Battery charger	0.955±0.003
6#	24# cabinet	1.225±0.012
7#	One terminal electrical cabinet	0.776±0.007
8#	Switch cabinet (When the EMU is running.)	0.234±0.021
8#	Switch cabinet (When the EMU is stopping.)	0.774±0.017

Table III. *Relationship **of** magnetic amplitude probability and **train** speed.*

Train type and number	Speed	Amplitude probability distribution			
		0≤B<0.2μT	0.2μT≤B<2μT	2μT≤B<20μT	20μT≤B
EMU,G85	300 km/h	1%	91%	7%	1%
EMU,D6131	120 km/h	2%	90%	7.1%	0.9%
Common speed train,K678	90 km/h	18%	72.1%	9.7%	0.2%
Common speed train,K722	80 km/h	26%	70.91%	3%	0.09%

B: magnetic field value

and speed are shown in Table III. With incremental speed, the magnetic amplitude probability less than 0.2 μT decreases on the whole and that greater than 20 μT increases significantly. According to the ICNIRP (2014), the magnetic field strength limits to a controlled environment (occupational environment) and to the general public are 500 μT and 100 μT, respectively; thus, the measurement results are within the permitted range of the standard.

High-frequency electromagnetic emission

The typical electromagnetic emission was measured on board while the EMU trains were passing through electric arc prone sections of the rail power system line, such as overlapping section and electrical phase break section. The high-frequency electromagnetic emission field was 40-120dBμV/m (0.000,1v/m-1V/m), and the emission field was 20dB larger in the electrical phase break section than in the overlapping section when the EMU train was running. The value range is near the standard of the International Electrotechnical Commission (IEC 62236) for railway emission, but far less than the Chinese national environment health standard GB 9175-88 limits.

DISCUSSION

We found the intensity of electric fields was much lower than the limit value of the standards, therefore discussion here is focused on the magnetic fields. The on-board magnetic field values were smaller than 2 μT, and the maximum value is 37 μT. The ICNIRP 2014 sets the public exposure limit as 100 μT and the occupational exposure limit as 500 μT. The exposure limit of low-frequency magnetic field emission in the present study was within the scope of the permit issued by ICNIRP (2014) and the Chinese national environment health standard GB 8702-2014.

The possible adverse health effect induced by exposure to low-frequency magnetic field emission on the EMU driver and attendants should be taken seriously. Some medical studies reported that the magnetic field values >0.2 μT have potential adverse effects on human health, including leukemia and nervous system diseases (9-10). Swiss scientists studied a cohort of 20,141 Swiss railway employees with 464,129 person-years of follow-up between 1972 and 2002 (11) and suggested a possible link between long-term exposure to ELF-MF and Alzheimer's disease. Additionally, myeloid leukemia has been linked with exposure to low-frequency magnetic fields (11). Alfredsson and colleagues (1996) reported an increased incidence of lymphocytic leukemia in a cohort study (1976-1990) of 7,466 Swedish male train engine drivers and 2,272 conductors (12).

Since magnetic field values are much higher in high-speed EMU trains than in common trains, as indicated from our study, health of their drivers and attendants should be monitored. Additionally, since the magnetic fields are region-specific within the EMU cars, caution dictates that train attendants should avoid staying in locations with the stronger magnetic fields. The strength of present study is that

we have comprehensively measured and compared electromagnetic field emissions in different EMUs, different rail lines, different operation conditions, different locations on train, and between EMUs and common speed trains, which has not been reported till now. Meanwhile the weakness in the present study is the lack of health surveillance data of EMU attendants, which is the aim of our next study.

ACKNOWLEDGEMENTS

The present study was supported by a 863 research project "Study on electromagnetic interference and protection scheme caused by pantograph off-line arc" supported by The People's Republic of China Ministry of Science and Technology (2009AA110303).

The authors thank Prof. Peter Spencer in Oregon Health & Science University, USA, for the language improvement.

REFERENCES

1. Zhang W, Ming M, Chen L. The Effect of contact line sag and irregularities of contact surface on sliding contact current collecting. Railway Society 2000; 6:50-54.
2. Wu J, Qian Q. Pantograph and catenary system's electrical contact properties. China Railway Sciences 2008; 3:108-11.
3. Harrison DM, Roy S, Jay O. Association of cortical lesion burden on 7-T magnetic resonance imaging with cognition and disability in multiple sclerosis. JAMA Neurol 2015; 72:1004-12.
4. Kato I, Young A. Electric blanket use and risk of thyroid cancer in the women's health initiative observational cohort. Women Health 2015; 21:1-13.
5. Lewicka M, Henrykowska GA. The impact of electromagnetic radiation of different parameters on platelet oxygen metabolism - in vitro studies. Adv Clin Exp Med 2015; 24:31-35.
6. International Electrotechnical Commission Railway applications-electromagnetic compatibility. Part 2: Emission of the whole railway system to the outside world. IEC 2008; 62236-2. Edition 2.
7. International Commission on Non-Ionizing Radiation Protection. ICNIRP Guidelines for limiting exposure to electric fields induced by movement of the human body in a static magnetic field and by time varying magnetic fields below 1Hz. Health Physics 2014; 106:418-25.
8. Ministry of Health, PR China. Occupational exposure limits for hazardous agents in the workplace. Part 2: Physical agents. GBZ 2007; 2:2-2007.
9. Ahlbom A, Day N, Feychting M, et al. A pooled analysis of magnetic fields and childhood leukaemia. Br J Cancer 1983; 83:692-98.
10. Attwell D. Interaction of low frequency electric fields with the nervous system: the retina as a model system. Radiat Protect Dosim 2003; 106:341-48.
11. Röösli M, Lörtscher M, Egger M, et al. Mortality from neurodegenerative disease and exposure to extremely low-frequency magnetic fields: 31 years of observations on Swiss railway employees. Neuroepidemiology 2007; 28:197-206.
12. Alfredsson L, Hammar N, Karlehagen S. Cancer incidence among male railway engine-drivers and conductors in Sweden, 1976-90. Cancer Causes Control 1996; 7:377-81.

LETTER TO THE EDITOR

PERCUTANEOUS CORONARY INTERVENTION FOR POOR CORONARY MICROCIRCULATION REPERFUSION OF PATIENTS WITH STABLE ANGINA PECTORIS

JS. LI, XJ. ZHAO, BX. MA and Z. WANG

Department of Cardiology, Binzhou Medical University Hospital, Binzhou, China

Received February 7, 2015 – Accepted June 22, 2015

Percutaneous coronary intervention (PCI) has been extensively applied to repair the forward flow of diseased coronary artery and can achieve significant curative results. However, some patients with acute myocardial infarction (AMI) develop non-perfusion or poor perfusion of cardiac muscle tissue after PCI, which increases the incidence of cardiovascular events and the death rate. PCI can dredge narrowed or infarct-related artery (IRA) and thus induce full reperfusion of ischemic myocardium. It is found in practice that some cases of AMI still have no perfusion or poor perfusion in myocardial tissue even though coronary angiography suggests opened coronary artery after PCI, which increases the incidence of vascular events and mortality. Therefore, to explore the detailed mechanism of PCI in treating coronary microcirculation of patients with stable angina pectoris, we selected 140 patients with stable angina pectoris for PCI, observing the index of microcirculatory resistance (IMR) of descending branch and changes of myocardial injury markers and left ventricular systolic function, and made a subgroup analysis based on the correlation between clinical indexes, IMR and other variables of diabetic and non-diabetic patients, PCI-related and non-PCI-related myocardial infarction patients. The results suggest that IMR of anterior descending branch after PCI was higher compared to that before PCI, and the difference was significant (P<0.05); creatine kinase-MB (CK-MB), myohemoglobin and high sensitive troponin T were all increased after PCI, and the difference was also significant (P<0.05); brain natriuretic peptide (BNP) level became higher after PCI, with significant difference (P<0.05); left ventricular ejection fraction (LVEF) declined after PCI, and the difference before and after PCI was statistically significant (P<0.05). Moreover, subgroup analysis results of the three groups all demonstrated statistically significant differences. PCI can effectively increase microcirculatory resistance of patients with stable angina pectoris, especially those who develop both stable angina pectoris and diabetes. Patients with higher microcirculatory resistance before PCI are more likely to develop PCI-related myocardial infarction after PCI.

To the Editor,

Coronary heart disease (CHD), a commonly seen disease, ranks high among major death causes worldwide; incidence of CHD has become increasingly higher in China in recent years (1, 2). Currently, percutaneous coronary intervention (PCI) is frequently used for treating CHD, but patients with stable angina pectoris may have poor

Key words: stable angina pectoris, percutaneous coronary intervention, coronary microcirculation, index of microcirculatory resistance

Mailing address:
Dr Xijun Zhao,
No.661 Huanghe 2nd Road,
Department of Cardiology, Binzhou Medical University Hospital, Binzhou, Shandong, 256603, China
e-mail: zxjzhaoxj@163.com

0393-974X (2016)

prognosis due to changed coronary microcirculation after PCI (3). Coronary microcirculation refers to the microcirculation system composing arteriole, blood capillary, and venule which is the major resistance vessel for coronary artery and myocardial metabolism. Once the coronary microcirculation system is impacted by one or more adverse factors, coronary microcirculation disturbance occurs (4, 5). Some scholars refer to coronary microcirculation disturbance as coronary microvascular dysfunction (CMVD).

With the wide application of interventional treatment, coronary microcirculation disturbance (CMD) (6-8) is frequently seen and more importance has been attached to CMD by physicians. Current studies concerning CMD mainly focus on the influence of PCI on patients with acute myocardial infarction (AMI). However, for patients with stable angina pectoris, whether PCI can affect the coronary microcirculation of patients with stable angina pectoris (9, 10) and whether patients with different IMR after treatment will have different prognosis is still not known (11). Therefore, in this study, we carried out PCI on patients with stable angina pectoris and discussed the influence of PCI on coronary microcirculation of those patients as well as roles of serum asymmetric dimethylarginine (ADMA) and high-sensitivity C-reactive protein (hs-CRP) and possible mechanisms.

MATERIALS AND METHODS

General data

One hundred and forty patients with stable angina pectoris who received treatment in the Affiliated Hospital of Bingzhou Medical College, Shandong, China between June, 2013 and June, 2015 were selected as the study population. Among these subjects, 92 were males and 48 were females, with average age of (64.54±6.75) years and average body mass index (BMI) of (24.41±1.37). The patients were confirmed as having stable angina pectoris according to the criteria formulated by the Chinese Society of Cardiology. Of the 140 subjects, 56 had a history of smoking, 56 cases developed high blood pressure and 76 cases suffered from diabetes. Moreover, 24 cases of three vascular lesions, 68 cases of two vascular lesions and 48 cases of one vascular lesion were proved with coronary arteriography. Inclusion criteria (12, 13) were: (i) coronary arteriography suggesting vascular lesion in proximal part or middle part of anterior descending branch; lumen stenosis in the narrowest site larger than 70%; thrombolysis in myocardialinfarction (TIMI) flow in grade III; lumen stenosis of other blood vessels larger than 70%; (ii) symptoms remaining even after optimal medical treatment; (iii) without acute myocardial infarction (AMI), history of coronary artery bypass grafting and PCI, fatal arrhythmia or high blood pressure (systolic pressure>160 mmHg and/or diastolic pressure>105 mmHg) and with normal liver and hepatic function; with no contraindication to aspirin or clopidogrel; (iv) without disease or condition that could induce changes of inflammatory markers, such as malignant tumor, inflammatory disease, autoimmune disease; without thyroid disease, estrogen-replacement therapy and fever (body temperature>37.5°C), surgical operation (within 3 months prior to being admitted into hospital), trauma or infectious disease, thromboembolic disease, valvular heart disease, cardiomyopathy, heart transplantation, congestive heart-failure (level III~IV cardiac function) and left ventricular dysfunction [left ventricular ejection fraction (LVEF<40%)]. This study was approved by the ethics committee of Binzhou Medical University Hospital and all the patients signed informed consent to participate in the study.

Method

Before PCI (14, 15), coronary arteriography was carried out through the radial artery approach using the Seldinger method; one or two stents [length: (26.29±3.22) mm; diameter: (3.12±0.15) mm] were inserted. After PCI, patients were intravenously dripped with 800~1000 μ/h heparin sodium (12500 μ/mI, Jiangsu Wanbang Biomedical Co., Ltd., China) for 22 h and subcutaneously injected with 7500 μ heparin sodium, 12 h/time, for three days.

Observation index

Five mL venous blood was collected from each patient before PCI and one hour after surgery. Brain natriuretic peptide (BNP) and creatine kinase-MB (CK-MB), myohemoglobin and high sensitive troponin T levels were detected using Vitros 5.1 FS automatic biochemistry analyzer and Ortho-Clinical Diagnostics reagent. Echocardiography examination was performed to measure

LVEF, left ventricular end-diastolic dimension (LVEDD) and left ventricular end-systolicdimension (LVESD). Index of microcirculatory resistance was measured before and after PCI. Changes of IMAR of anterior descending branch, myocardial injury markers and left ventricular systolic function were observed before and after PCI.

Statistical analysis

The data obtained were statistically processed by SPSS 19.0. Continuous variable was expressed as mean ± standard deviation (SD) and counting variable was expressed as percentage. Normally distributed continuous variables were compared using the *t*-test. Comparison of values before and after PCI was carried out using the Student's paired *t*-test. Comparisosn between diabetic patients and non-diabetic patients, between PCI related myocardial infarction patients and non-PCI related myocardial infarction patients were performed using independent sample *t*-test. Non-normally distributed continuous variables were compared using Mann-Whitney U-test. Correlation between IMR and other variables was analyzed using Pearson's correlation analysis and multivariate linear regression analysis. Correlation levels were high if $r>0.08$ and low if $r<0.3$. Differences were considered to be statistically significant if $P<0.05$.

RESULTS

Comparison of IMR of anterior descending branch before and after PCI

IMR of patients was 26.97±5.61 after PCI, much higher than that before PCI (23.18±5.31), and the difference had statistical significance ($t=20.134$, $P<0.05$).

Comparison of myocardial injury markers before and after PCI

The levels of Creatine kinase-MB (CK-MB), myohemoglobin and high sensitive troponin T was 123.28±50.63 (ng/ml), 57.63±20.35 (U/L) and 0.052±0.032 (ng/ml) after PCI, much higher than that before PCI (44.68±11.86ng/ml, 17.02±4.16U/L and 0.007±0.001 ng/ml) and differences were all statistically significant ($P<0.05$). After PCI, 5 cases developed PCI-related myocardial infarction and 1 case had no-reflow phenomenon in coronary artery, but no patient died.

Comparison of left ventricular systolic function before and after PCI

BNP level was 67.53±24.37 (pg/ml) after PCI, much higher than that before PCI [49.43±16.52 (pg/ml)], and the difference had statistical significance ($Z=4.994$, $P<0.05$). LVEF decreased from 57.94±4.58 (%) before PCI to 56.10±3.39 (%) after PCI, and the difference was statistically significant ($t=43.678$, $P<0.05$). LVEDD and LVESD before and after treatment were observed with no remarkable differences ($P>0.05$).

Subgroup analysis: comparison of clinical data between patients with PCI related myocardial infarction patients and without PCI related myocardial infarction before and after PCI

Comparison of clinical data between patients with and without PCI-related myocardial infarction before and after PCI is shown in Table I. Results demonstrated that glycosylated hemoglobin HbA_{1c}, postoperative high sensitive troponin T, preoperative and postoperative CK-MB, postoperative myohemoglobin, postoperative BNP and preoperative and postoperative IMR levels of patients with PCI-related myocardial infarction were high than those of patients without PCI-related myocardial infarction, and the differences had statistical significance ($P<0.05$). Postoperative Fraction Flow Reserve (FFR), preoperative and postoperative coronary flow reserve (CFR) levels of patients with PCI-related myocardial infarction was lower than those of patients without PCI-related myocardial infarction, and the difference had statistical significance ($P<0.05$).

A subgroup analysis was carried out on patients with and without PCI-related myocardial infarction. It can be concluded from the above experimental results that HbA_{1c} may be a high risk factor for incidence of myocardial infarction after PCI, i.e., patients with poorly controlled diabetes and blood sugar are more likely to develop PCI-related myocardial infarction (PCIrMF); preoperative IMR of patients with PCIrMF was higher than that of patients without PCIrMF, indicating that patients with higher IMR before surgery are more likely to have PCIrMF; CFR level of patients with PCIrMF was lower than that of patients without PCIrMF, suggesting that patients with PCIrMF may

have had coronary artery microcirculation disturbance before surgery.

Subgroup analysis: comparison of clinical data of diabetic patients and non-diabetic patients before and after PCI

Comparison of clinical data of diabetic patients and non-diabetic patients before and after PCI is shown in Table II. The results suggest that HbA1c, postoperative high sensitive troponin T, myohemoglobin, CK-MB and BNP levels of diabetic patients were higher than those of non-diabetic patients, and the differences had statistical significance ($P<0.05$); IMR of diabetic patients was higher than that of non-diabetic patients and the difference was remarkable ($P<0.05$); IMR change (ΔIMR) of diabetic patients were more obvious than that of non-diabetic patients, and the difference had statistical significance ($P<0.05$); CFR, difference of CFR before and after PCI (ΔCFR) and LVEF of diabetic patients were all lower than those of non-diabetic patients, and the difference had statistical significance ($P<0.05$).

It can be found from the experimental results that diabetic patients developed severe myocardial damage after PCI compared to non-diabetic patients. IMR of diabetic patients was higher than that of non-diabetic patients both before and after PCI and the difference of IMR before and after PCI (ΔIMR) of diabetic patients was more significant. CFR of diabetic patients was lower than that of non-diabetic patients both before and after PCI, and the difference of CFR before and after PCI (ΔCFR) of diabetic patients was less obvious. Changes of IMR are induced by PCI-related coronary artery microcirculation disturbance. Imbalance increase of ΔIMR, preoperative CFR and ΔCFR all indicated that diabetic patients may have had microcirculation disturbance before surgery.

Analysis of correlation between IMR of anterior descending branch and various indexes before and after PCI as well as multi-variable linear regression analysis

Table III shows the analysis of the correlation between IMR of anterior descending branch and various indexes before and after PCI. It was found that IMR of anterior descending branch before and after PCI was in a medium positive correlation with HbAlc, postoperative CK-MB, postoperative myohemoglobin, stenosis degree of anterior descending branch and postoperative BNP level ($P<0.05$), in a medium negative correlation with preoperative and postoperative CFR and LVEF ($P<0.05$).

According to multiple regression analysis of IMR of anterior descending branch and relevant indexes, linear regression equation with regard to IMR of anterior descending branch and related indexes was: (IMR of anterior descending branch after PCI)=-21.468+2.897*(HbA_{lc})-1.321*(postoperative CFR)+0.393*(stenosis degree of anterior descending branch)+39.915*(postoperative troponin).

The above experimental results revealed that preoperative IMR was in a close relationship with postoperative myocardial damage and left ventricular systolic function, and IMR might be a predictive factor for postoperative adverse cardiac events. Balance changes of related indexes after PCI may be caused by intervention of PCI. The results suggest that coronary microcirculation was in an obvious correlation with left ventricular systolic function in short term, however, due to defects of test design, we failed to further reexamine BNP and carry out cardiac color ultrasound. Hence, whether such cardiac function injury is short-term or irreversible could not be determined.

DISCUSSION

PCI, which is effective in opening blood vessels and ensuring reperfusion of ischemic myocardium, is an effective method for treating CHD (16, 17). However, angina symptoms of some patients fail to be relieved after reperfusion treatment. Clinically, IMR is frequently used for assessing coronary artery microcirculation (18, 19). The results of this study demonstrate that IMR of anterior descending branch after PCI was much higher than that before PCI, indicating that the coronary microcirculation of patients had been damaged and that this may be correlated to coronary microembolization, though

Table I. *Comparison of clinical data between patients with PCI-related myocardial infarction and without PCI-related myocardial infarction before and after PCI.*

	Patient with PCI related myocardial infarction	Patient without PCI related myocardial infarction	t value	P value
No. of cases (n)	20(14%)	120(86%)		
Age (year)	66.40±2.97	64.23±7.41	10.518	0.000
BMI	84.13±4.68	82.13±3.63	1.488	0.146
Cholesterol (CH) (mmol/L)	6.47±0.29	6.34±0.35	0.807	0.425
Low density lipoprotein (LDL) (mmol/L)	3.63±0.28	3.63±0.28	0.817	0.420
High density lipoprotein (HDL) (mmol/L)	1.35±0.19	1.34±0.19	0.146	0.885
Triglyceride (TG) (mmol/L)	0.91±0.28	1.17±0.47	-1.203	0.238
HbA_{1c} (%)	6.76±0.75	5.92±0.64	5.280	0.000
Degree of coronary artery stenosis (%)	83.80±3.83	83.20±4.43	0.284	0.778
Preoperative troponin (ng/ml)	0.01±0.00	0.01±0.00	0.649	0.521
Postoperative troponin (ng/ml)[#]	0.12±0.04	0.03±0.01	12.475	0.001
Preoperative CK-MB (U/L)	12.21±5.55	14.12±4.21	-2.249	0.031
Postoperative CK-MB (U/L)	86.45±13.92	54.27±14.30	3.338	0.002
Preoperative myohemoglobin (ng/ml)	38.00±10.58	44.56±11.89	-1.368	0.181
Postoperative myohemoglobin (ng/ml)[#]	195.36±46.24	102.24±21.37	5.466	0.000
Preoperative FFR	0.67±0.04	0.70±0.05	-0.979	0.335
Postoperative FFR	0.98±0.00	0.99±0.01	-3.272	0.003
Preoperative BNP (pg/ml)	43.20±23.42	50.63±17.06	-0.857	0.398
Postoperative BNP (pg/ml)	96.80±32.39	62.80±21.81	3.909	0.000
Preoperative CFR	1.28±0.25	1.67±0.43	-2.854	0.019
Postoperative CFR[#]	2.14±0.16	3.28±1.18	-2.130	0.041
Preoperative LVEF (%)	56.60±6.02	58.16±4.39	-0.702	0.488
Postoperative LVEF (%)	55.60±4.88	57.36±4.61	-0.787	0.437
Preoperative IMR	29.37±2.46	22.37±4.96	3.068	0.004
Postoperative IMR	32.74±2.98	25.62±5.62	2.740	0.010

[#] variances of two groups is non-homogeneous and processed by t test; postoperative myohemoglobin: P=0.000, postoperative troponin: P=0.000, postoperative CFR: P=0.000; other variance are homogeneous, P>0.05.

Table II. *Comparison of clinical data of diabetic and non-diabetic patients before and after PCI.*

	Diabetic patients	Non-diabetic patients	t value/Z value	P value
No. of cases (n)	76(54%)	64(46%)		
HbAlc (%)	6.75±0.47	5.38±0.25	t=10.518	0.000
Stenosis degree of anterior descending branch (%)	84.13±4.68	82.13±3.63	t=1.488	0.146
Preoperative troponin (ng/ml)*	0.01±0.00	0.01±0.00	Z=-0.539	0.612
Postoperative troponin (ng/ml)*	0.06±0.05	0.04±0.04	Z=-2.060	0.039
Preoperative CK-MB (U/L)	16.26±4.54	17.88±4.00	t=-1.104	0.278
Postoperative CK-MB (U/L)*	65.95±20.88	50.31±18.57	Z=-2.453	0.014
Preoperative myohemoglobin (ng/ml)	44.89±11.22	44.56±13.36	t=0.080	0.937
Postoperative myohemoglobi (ng/ml)*	146.53±54.89	107.19±32.44	Z=-2.457	0.014
Preoperative FFR*	0.68±0.06	0.70±0.04	Z=-1.115	0.265
Postoperative FFR*	0.98±0.05	0.99±0.004	Z=-2.070	0.380
Preoperative CFR	1.44±0.39	1.82±0.39	t=-2.923	0.006
Postoperative CFR*	2.41±0.71	3.97±1.04	Z=-3.855	0.000
ΔCFR	0.97±0.48	2.14±0.76	t=-5.527	0.000
Preoperative LVEF (%)*	57.00±4.27	59.06±4.84	Z=-1.433	0.152
Postoperative LVEF (%)*	55.53±3.63	59.00±5.06	Z=-2.095	0.036
Preoperative BNP (pg/ml)*	52.11±19.02	46.56±16.52	Z=-0.931	0.352
Postoperative BNP (pg/ml)*	76.44±24.18	57.44±24.97	Z=-2.288	0.022
Preoperative IMR	26.61±3.31	19.54±4.59	t=5.281	0.000
Postoperative IMR	30.34±3.56	22.25±4.99	t=5.590	0.000
ΔIMR	3.74±1.59	2.70±1.04	t=2.226	0.033

* *non-normal continuous variable and comparison between groups is performed with Mann-Whitney test;*
ΔIMR=postoperative IMR - preoperative IMR;
ΔCFR=postoperative CFR - preoperative CFR.

Table III. *Correlation between IMR of anterior descending branch and related indexes before and after PCI.*

	IMR of anterior descending branch before PCI		IMR of anterior descending branch after PCI	
	Correlation coefficient	P value	Correlation coefficient	P value
Age	-0.041	0.815	0.593	0.738
BMI	0.110	0.528	0.930	0.596
CH	0.357	0.350	0.285	0.960
LDL	0.277	0.107	0.246	0.155
HDL	0.08	0.996	0.005	0.977
TG	-0.204	0.240	-0.154	0.376
HbA1c	0.723	0.000	0.732	0.000
SUA	-0.005	0.979	-0.123	0.480
Scr	0.281	0.102	0.293	0.880
Preoperative CK-MB	-0.273	0.113	-0.298	0.082
Postoperative CK-MB	0.502	0.002	0.515	0.002
Preoperative high sensitive troponin	0.123	0.481	0.169	0.331
Preoperative myohemoglobin	-0.163	0.350	-0.172	0.323
Postoperative myohemoglobin	0.446	0.007	0.431	0.010
Preoperative FFR	-0.305	0.740	-0.324	0.058
Preoperative IMR			0.972	0.000
Postoperative IMR	0.972	0.000		
Preoperative CFR	-0.550	0.001	-0.504	0.002
Postoperative CFR	-0.717	0.000	-0.725	0.000
Degree of stenosis	0.461	0.005	0.544	0.001
Preoperative LVEF	-0.501	0.002	-0.539	0.001
Postoperative LVEF	-0.478	0.040	-0.514	0.002
Preoperative BNP	0.050	0.777	0.057	0.746
Postoperative BNP	0.521	0.001	0.480	0.004

SUA: serum uric acid; Scr: serum creatinine.

no slow flow and reflow occurred.

To date, great importance has been attached to PCI-related myocardial damage. It has been found that the incidence of myocardial infarction ranges from 5% to 30% after PCI, and myocardial infarction usually occurs at the site close to treated blood vessels or at the distal end of the blood vessels treated (20). Therefore, dynamic changes of cardiac damage markers should be timely observed after PCI in order to help to understand whether myocardial infarction has occurred. The results of the current study showed that LVEF of patients decreased after PCI, but BNP level increased; myohemoglobin, CK-MB, and high sensitive troponin T levels all had significant increases after PCI, suggesting that patients with stable angina have myocardial damage after PCI and risk of acute cardiac insufficiency exists even though cardiac function is improved after surgery.

Diabetes is a high risk factor for coronary heart disease. A long-term follow-up in a recent research (21) suggests that in diabetes patients over 65 years of age who had undergone PCI, diabetes was found to be an independent predictive factor for death and myocardial infarction. But the specific reason is still unknown. Among diabetes patients, those with normal coronary microcirculation usually have a higher long-term survival rate compared to those with disordered coronary microcirculation. This study also found that patients with diabetes had more serious cardiac damage compared to non-diabetes patients, which is consistent with the above research results.

Most of the research results are consistent with the expectation; however, some are inconsistent. One study (9) suggested that the difference of IMR before and after PCI had no statistical significance, however, this study had the opposite finding which may be because of the small sample size. Therefore, further studies with larger sample cohorts remain to be carried out in the future.

REFERENCES

1. Camm AJ, Manolis A, Ambrosio G, et al. Unresolved issues in the management of chronic stable angina. Int J Cardiol 2015; 201:200-207.
2. Zhao K, Li YJ, Gao QY. Role of red blood cell distribution width in predicting contrast induced nephropathy in patients with stable angina pectoris undergoing percutaneous coronary intervention. Int J Cardiol 2015; 197:276-78.
3. Alonso JJ, Muñiz J, Gómez-Doblas JJ, et al. Prevalence of stable angina in Spain. results of the OFRECE study. Rev Espa Cardiol (Eng Ed) 2015; 68(8):691-99.
4. Toutouzas K, Anousakis-Vlachochristou N, Patsa C, et al. Late differences in outcomes of patients with stable angina and an isolated lesion in the proximal left anterior descending artery treated with new-generation drug-eluting stents. Int J Cardiol 2015; 183:27-32.
5. Mavrakanas TA, Chatzizisis YS. Bivalirudin in stable angina and acute coronary syndromes. Pharmacol Ther 2015; 152:1-10.
6. Li Y, Yang DY, Lu LH, et al. Thermodilutional confirmation of coronary microvascular dysfunction in patients with recurrent angina after successful percutaneous coronary intervention. Can J Cardiol 2015; 31(8):989997.
7. Gil KE, Pawlak A, Frontczak-Baniewicz M, Gil RJ, Nasierowska-Guttmejer A. The proposed new classification of coronary microcirculation as the predictor of the heart failure progression in idiopathic dilated cardiomyopathy. Cardiovasc Pathol 2015; 24(6):351-58.
8. Fiarresga A, Selas M, Oliveira E, et al. Invasive assessment of the coronary microcirculation using the index of microcirculatory resistance: Description and validation of an animal mode. Rev Port Cardiol (Eng Ed) 2014; 33(4):207-12.
9. Layland J, Judkins C, Palmer S, Whitbourn R, Wilson-O'Brien A, MacIsaac A, Wilson A. The resting status of the coronary microcirculation is a predictor of microcirculatory function following elective PCI for stable angina. Int J Cardiol 2013; 169(2):121-25.
10. Chen CL, Zheng H, Xuan Y, Amat A, Chen L, Yu J, Wang J. The cardioprotective effect of hypoxic and ischemic preconditioning in dogs with myocardial ischemia-reperfusion injury using a double-bypass model. Life Sci 2015; 141(15):25
11. Zhao JL, Yang YJ, you SJ, Cui CJ, Gao RL.

Carvedilol preserves endothelial junctions and reduces myocardial no-reflow after acute myocardial infarction and reperfusion. Int J Cardiol 2007; 115(3):334-41.
12. Zhao K, Li YJ, Gao QY. Role of red blood cell distribution width in predicting contrast induced nephropathy in patients with stable angina pectorisundergoing percutaneous coronary intervention. Int J Cardiol 2015; 197:276-78.
13. Liu CP, Lin MS, Chiu YW, Lee JK, Hsu CN, Hung CS, Kao HL. Additive benefit of glycoprotein IIb/IIIa inhibition and adjunctive thrombus aspiration during primary coronary intervention: Results of the Initial Thrombosuction and Tirofiban Infusion (ITTI) trial. Int J Cardiol 2012; 156(2):174-79.
14. Wu N, Zhang XW, Jia PY, Jia DL. Hypercholesterolemia aggravates myocardial ischemia reperfusion injury via activating endoplasmic reticulum stress-mediated apoptosis. Exp Mol Pathol 2015; 99(3):449-54.
15. Arnold SV, McGuire DK, Spertus JA, et al. Glucose-lowering medications and angina burden in patients with stable coronary disease: results from the type 2 diabetes evaluation of ranolazine in subjects with chronic stable angina (terisa) trial. Am Heart J 2015; 170(4):753-59.e2.
16. Zhou XY, Chen MX, Wang SY, Yu LL, Jiang H. MG53 protein: A promising novel therapeutic target for myocardial ischemia reperfusion injury. Int J Cardiol 2015; 199:424-25.
17. Gu Y, Bai YP, Wu J, Hu LQ, Gao B. Establishment and characterization of an experimental model of coronary thrombotic microembolism in rats. Am J Pathol 2010; 177(3):1122-30.
18. Ji J, Yang JA, He X, Ling WP, Chen XL. Cardiac-targeting transfection of tissue-type plasminogen activator gene to prevent the graft thrombosis and vascular anastomotic restenosis after coronary bypass. Thromb Res 2014; 134(2):440-48.
19. Ge GH, Zhang Q, Ma JW, Qiao ZY, Huang JH, Cheng WB, Wang HW. Protective effect of Salvia miltiorrhiza aqueous extract on myocardium oxidative injury in ischemic-reperfusion rats. Gene 2014; 546(1):97-103.
20. Li J, Zhang HR, Zhang CH. Role of inflammation in the regulation of coronary blood flow in ischemia and reperfusion: Mechanisms and therapeutic implications. J Mol Cell Cardiol 2012; 52(4):865-72.
21. Hillegass WB, Patel MR, Klein LW, et al. Long-term outcomes of older diabetic patients after percutaneous coronary stenting in the United States: a report from the National Cardiovascular Data Registry, 2004 to 2008. J Am Coll Cardiol 2012; 60(22):2280-2289.

LETTER TO THE EDITOR

ANALYSIS OF HIGH RISK FACTORS FOR ENDOSCOPIC RETROGRADE CHOLANGIOPANCREATOGRAPHY BILIARY METALLIC STENTING AFTER MALIGNANT DUODENAL STRICTURE SEMS IMPLANTATION

JF. YAO[1], L. ZHANG[2] and H. WU[2]

[1]Department of Ultrasonography, Zhengzhou Central Hospital, Zhengzhou City, Henan Province, China;
[2]Department of Gastroenterology, Zhengzhou Central Hospital, Zhengzhou City, Henan Province, China

Received September 24, 2015 – Accepted May 4, 2016

The first two authors contributed equally to this work

The aim of this study was to explore the success rates and high risk factors for endoscopic retrograde cholangiopancreatography (ERCP) biliary metallic stenting after self-expandable metallic stent (SEMS) implantation in patients with malignant duodenal stricture. A retrospective cohort study was conducted. Forty-two unresectable patients with malignant duodenal stricture who received endoscopic SEMS implantation between February 2012 and February, 2015 in the Department of Digestive Diseases of Xijing Hospital were enrolled in the study. These patients underwent subsequent ERCP biliary metallic stenting due to malignant biliary stricture. The clinical and iconography materials of these patients were retrospectively analyzed. ERCP biliary metallic stenting was successfully carried out on 71.4% of patients with previous malignant duodenal stricture SEMS implantation. In type 1 duodenal strictures 88% success rate of ERCP guided biliary decompression was obtained *vs* 18.2% success rate in Type 2 duodenal strictures. In both type 1 and 2 duodenal strictures of a length greater than 3.5 cm, ERCP was 44.4% successful *vs* 89% successful for strictures less than 3.5cm. Multiple regression analysis revealed that duodenal stricture length ≥3.5 cm (OR, 9.85; 95% CI, 1.21-79.88) and 80 or 90 mm duodenal stent (OR, 17.03; 95% CI,1.99-145.81) were independent risk factors for the failure of ERCP (biliary drainage or biliary decompression) in the patients with previous SEMS implantation. Moreover, duodenal stents of 60 mm had a higher success rate of 88%, *vs* 18.2% in 80-90 mm stents. Nevertheless, the success rates of type III strictures were 100%, including synchronous and asynchronous implantation of SEMS implantation and ERCP biliary metallic stenting. For unresectable malignant duodenal stricture patients with SEMS implantation, subsequent ERCP biliary metallic stenting was safe and effective. The length of malignant duodenal stricture, longer duodenal stents and type II duodenal stricture were high risk factors for the failure of ERCP biliary metallic stenting.

To the Editor,

For unresectable patients with malignant duodenal stricture, endoscopic duodenal self-expandable metallic stent (SEMS) implantation can effectively solve gastroduodenal output duct obstruction, improve enteral nutrition status and enhance the median survival time (1). However, lesser postoperative adverse events also exist, such as

Key words: malignant duodenal stricture, self-expanding metallic stent, ERCP, malignant biliary stricture

Mailing address:
Dr Li Zhang,
Department of Gastroenterology,
Zhengzhou Central Hospital,
No.195, Tongbai Road, Zhengzhou City, 450007, PR China
e-mail: zmzhangli166@126.com

0393-974X (2016)

stent translocation, invasion and obstruction of stent lumen by tumor growth towards both ends of stents. Likewise, for unresectable patients with malignant biliary stricture, endoscopic SEMS implantation can effectively solve biliary obstruction, with few postoperative problems and speedy recovery (3).

For the patients suffering malignant duodenal stricture with malignant biliary stricture, the difficulty of subsequent endoscopic retrograde cholangiopancreatography (ERCP) biliary metallic stenting increases after SEMS implantation. Through a retrospective case analysis, this study explored the success rates of ERCP biliary metallic stenting, postoperative complications and risk factors for operation failures under exceptional circumstances.

MATERIALS AND METHODS

Subjects

The ethics committee of our hospital approved the study and all the subjects signed an informed consent. The patients with malignant duodenal stricture type I or type II who received endoscopic SEMS implantation between February 2012 and February 2015 at Xijing Hospital of Digestive Disease and who needed subsequent ERCP biliary metallic stenting due to metallic biliary stenting (MBS) were enrolled. Classification criteria of malignant duodenal strictures were: Type I - duodenal bulb juxta pyloric stricture, no lesion towards duodenal papilla; Type II - duodenum descending papilla horizontal portion, duodenal papilla invasion from stricture lesion; and Type III - duodenal segment proximal to ligament of Trietz without involvement of papilla.

The inclusion criteria were as follows: i. malignant duodenal stricture diagnosed by endoscopic evaluation with pathologic tissue consistent with malignancy; barium meal or CT diagnosed malignant duodenal stricture type I, type II or type III; no surgeon-assessed surgical removal indication or surgical treatment refusal from the patient's family; ii. malignant biliary stricture after metallic stenting because of malignant duodenal stricture through contrast-enhanced CT, MRT diagnosis and patient's medical history, and bilirubin two times higher than the upper limit; ERCP biliary metallic stenting were requested by the patient's family; patients with malignant duodenal stricture who accepted endoscopic SEMS implantation and needed ERCP biliary metallic stenting subsequently due to MBS. The exclusion criteria: endoscopic operation contraindication.

Malignant duodenal stricture SEMS implantation

Stents were loaded into a papillary muscle knife with a guide wire through a gastroscope or transnasal gastroscope, entered into the duodenum traversing the duodenal stricture as distally as possible. During the process, contrast agent was injected so that the situation of the distant end of stricture segments and stricture length could be seen. Fluoroscopy was used to ensure the stent traversed the entire malignant stricture. Balloon catheters were used to expand stricture segments. After the endoscope was removed, the stent releaser reached the stricture position and released the stent under X-ray observation. Radiographic imaging confirmed stent placement. The stent juxta stomach position was ascertained again by endoscopy. Briefly, the pyloric orifice of type I and type III should be 0.5~1 cm and the juxta stricture opening of type III 0.5~1 cm. The obstruction was graded according to stomach outflow obstruction scoring system (SOOSS) within one week or month after surgery.

Maligant biliary stricture ERCP biliary metallic stenting

ERCP was completed by a senior endoscopist. Prior to biliary stenting, X-ray and endoscopic evaluation was used to ensure appropriate stent expansion and assess for migration. For the stents invaded by tumor, balloon cleaning or columnar balloon expansion were carried out. Lastly, ERCP biliary metallic stenting was made through duodenoscope. The results of the operation were examined by X-ray (4).

Post-operative endpoints

When Total bilirubin (TBil) decreased >30% within one week after surgery, the operation was considered as being successful (5). Postoperative pancreatitis, hemorrhage, perforation and other

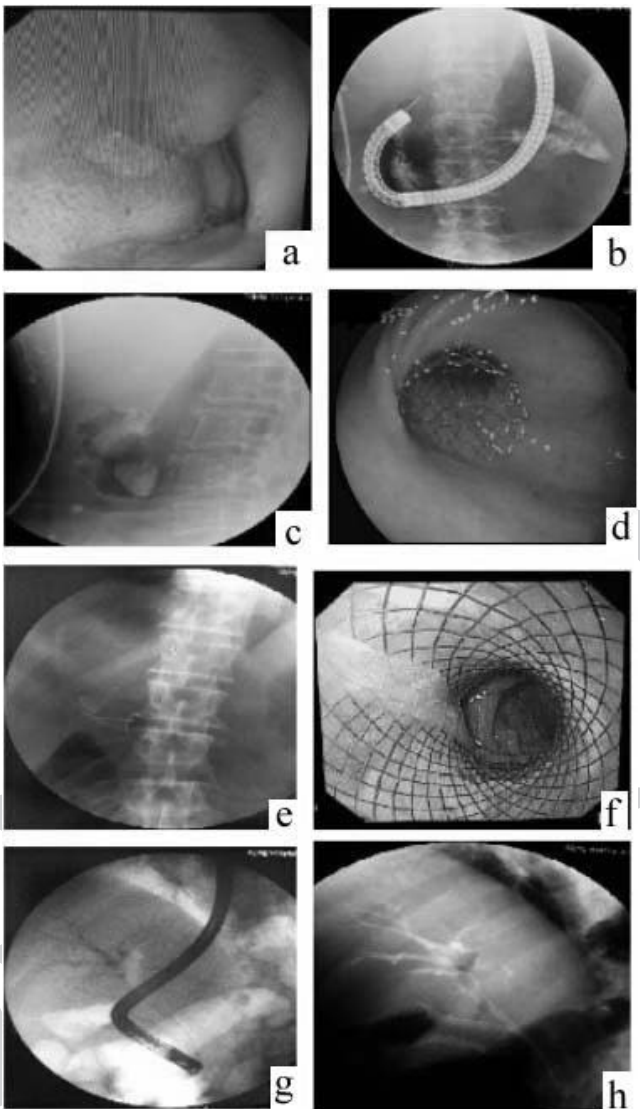

Fig. 1. ***a)*** *Endoscopic enteric cavity stenosed opening.* ***b)*** *Endoscopic duodenal papillary muscles knife radiography with guide wire showing stenotic segments.* ***c)*** *X-ray guided part expansion of intestinal stents.* ***d)*** *Microscopic overall intestinal expansion.* ***e)*** *X-ray showed overall-expanded stents after one month's implantation.* ***f)*** *Endoscope passing through overall-expanded intestinal stents under microscope.* ***g)*** *Biliary ducts stent implantation after duodenoscope passed through duodenum;* ***h)*** *X-ray showed double stents of biliary stent and duodenal stent after successful biliary stent implantation.*

complications were monitored. The results of the operation were evaluated according to the degree of postoperative abdominal pain and whether there were any of the above-mentioned complications.

Statistical analysis

Statistical analysis was made of the patients' general information. Student's *t*-test was used to analyse measurement data; *Chi*-squared test or Fisher's exact test was adopted when enumeration data were analyzed. Independent risk factors affecting the success rate of the ERCP surgery were calculated using Logistic regression analysis. Multi-factor model was applied when the variable $P < 0.1$ in single-factor analysis. SPSS19.0 software was adopted. There was statistical significance when bilateral $P < 0.05$.

RESULTS

Forty-two patients (30 male, 71.4%, and 12 female) with an average age of 64.5±5.4 years

Table I. *Baseline information of the patients.*

Category	Results(n=42)
Age (years)	64.5±5.4
Male [n（%）]	30（71.4%）
Type of tumor[n（%）]	
Gastric cancer	20
Duodenal cancer	9
Pancreatic cancer	10
Ampullary carcinoma	3
Stricture length, cm	3.4±0.8
Type [n（%）]	
Type I (Gastric cancer, Duodenal cancer)	25
Type Ⅱ (Pancreatic and Ampullary carcinoma)	11
Type Ⅲ (Pancreatic cancer, Duodenal cancer)	6
Stent length [n（%）]	
60mm	30
80mm	7
90mm	5
Stent translocation [n（%）]	
Peroral translocation	2
Anal translocation	2
Implantation time [n（%）]	
Within one month	12
Within one-two months	16
Within two-three months	11
>three months	3

were enrolled in this study. Twenty-five cases of duodenal stricture type I (59.5%), 20 cases of gastric cancer and 5 cases of duodenal cancer were included (24 cases with 60 mm stents and 1 duodenal cancer case with 90 mm stent). Eleven cases of type II (26.2%), 8 cases of pancreatic cancer and 4 cases of ampullary carcinoma were included (1 case with ampullary carcinoma with 60 mm stent, 6 cases with 80 mm stents, 4 cases 90 mm stents). The average length of duodenal stricture was 3.4±0.8 cm, the detailed implanted times are shown in Table I. Peroral translocation of the 80 mm stents took place in 2 cases of pancreatic cancer within one month; anal translocation for the 60 mm stents took place in 2 cases of gastric cancer within one month (Table I). Six cases of type III (14.3%), 4 cases of duodenal cancer and 2 cases of pancreatic cancer were included. Four cases of biliary stent implantation with concurrent intestinal stent implantation (double guide wire retention was made during operation; intestinal stents were placed after biliary stents); 2 asynchronous cases. The total success rate of ERCP biliary metallic stenting after SEMS implantation in patients with malignant duodenal stricture was 71.4% (30/42). Type 3 had the highest success rate of 100%, followed by Type I (88%) and type II (18.2%) (regression analysis was not incorporated due to no failure cases because ERCP biliary metal stenting was unaffected since type III intestinal stents were not near the duodenal papilla). There was no statistical significance with regard to age, sex and implantation time between the successful group and failure group. Type II (including pancreatic and ampullary carcinoma cases) with stricture length ≥ 3.5 cm and 80 or 90 mm stents were in the majority in the ERCP failure group (n=12 cases). Duodenal stricture length ≥ 3.5 cm (OR, 9.85; 95% CI, 1.21~79.88) and 80 or 90 mm intestinal stents (OR, 17.03; 95% CI, 1.99~145.81) were the independent risk factors for the failure of ERCP biliary metallic stenting after SEMS implantation. 91% of patients with malignant duodenal stricture type II were implanted with 80- or 90-mm stents. Therefore, the overlapping of malignant duodenal stricture type II and 80- or 90-mm duodenal stents was also an independent risk factor.

No surgery–related gastrointestinal bleeding, perforation, post-ERCP pancreatitis or other complications or deaths resulted in any of the cases in this study. Among the patients with failed ERCP biliary metallic stenting (n = 12 cases), 11 cases underwent obstructive jaundice removal through percutaneous transhepatic choledochus drainage (PTCD) guided by B-ultrasound; one case did not undergo further treatment.

DISCUSSION

Approximately 60% of patients with malignant duodenal stricture need biliary metallic stenting to remove malignant biliary obstruction after duodenal SEMS implantation (6). The ERCP endoscope is a side viewing endoscopy. With a lower success rate, ERCP biliary metallic stenting is difficult in patients with previous duodenal SEMS implantation. This study explored the success rates and risk factors for the failure of ERCP biliary metal stenting after duodenal SEMS implantation. Duodenal tumor length ≥ 3.5 cm and the preoperative implanted 80- or 90-mm duodenal stents (type II stricture) were considered as the factors possibly increasing the risk of the failure of ERCP.

Different degrees of the implanted duodenal stents had a certain influence on ERCP surgery. Biliary stent placement for type III stricture had 100% success rate since the 0.5~1 cm distance between intestinal stent peroral and stricture opening kept the former away from duodenal papilla so that the papilla was uncovered and ERCP biliary metallic stenting operation was unaffected. Duodenal stents (with length of 80 mm) resulted as having only 33% success rate, but this rate can be increased if the stents are far from the duodenal papilla. The rate for duodenal bare metal stent (BMS) translocation was 1.5%~14% while for the metal coated stents it was 26%~56% (7). Before ERCP, the intestinal SEMS situation should be fully understood, calculating whether the main papilla opening is covered by intestinal stent mesh. ERCP is not difficult under normal conditions. For the cases with covered papilla, because of stent translocation or mecism, the success rate could be increased by stent mesh expansion through balloon and metal wire incision through APC or Allis clamp (7). However, cases of postoperative intestinal perforation have been reported because of the the unsound long-term effect of balloon dilatation due to stent technology (memory function) development. For example, for patients with longer stricture segments and a planned implantation of > 60 mm intestinal stents, concurrent implantation or special type intestinal stents could be an option (8).

In conclusion, from the results of our retrospective study, subsequent ERCP biliary metallic stenting can be considered as safe and effective for patients with duodenal SEMS implantation. The risk for ERCP failure was increased when the duodenal stricture length ≥ 3.5 cm and 80 or 90 mm duodenal stents were implanted preoperatively.

REFERENCES

1. Jury G, Amieva L, Bouzas G, et al. Gastric outlet obstruction in malignant stricture: self expanding metal stents. Acta Gastroenterol Latinoam 2012; 42(4):273-77.
2. Siddiqui AA, Mehendiratta V, Loren D, Hong SK, Kowalski T. Fully covered self-expandable metal stents are effective and safe to treat distal malignant biliary strictures, irrespective of surgical resectability status. J Clin Gastroenterol 2011; 45(9):824-27.
3. Zhou WZ, Yang ZQ, Liu S, Zhou CG, Xia JG, Zhao LB, Shi HB. A newly designed stent for management of malignant distal duodenal stricture. Cardiovasc Intervent Radiol 2015; 38(1):177-81.
4. Pan YM, Wang TT, Gao DJ, Wu J, Hu B. Simultaneous stenting in bile duct and duodenum under endoscope for treatment of malignant biliary and duodenal obstruction. Acad J Second Mil Med Univ 2013; 34(3):261-65.
5. Kim K-R, Shin JH, Youn Han G-M, et al. Percutananeous self-expandble metallic stent implantation for cancer recurrence at the hepatico jejunostomy site. J Vasc Interv Radiol 2008; 19(10):1454-59.
6. Dormann A, Meisner S, Verin N, Wenk Lang A. Self-expanding metal stents for gastroduodenal malignancies: systematic review of their clinical effectiveness. Endoscopy 2004; 36(6):543-50.
7. Waidmann O, Trojan J, Friedrich-Rust M, et al. SEMS *vs* cSEMS in duodenal and small bowel obstruction: high risk of migration in the covered stent group. World J Gastroenterol 2013; 19(37):6199-206.
8. Moon JH, Choi HJ, Ko BM, et al. Combined endoscopic stent-in-stent implantation for malignant biliary and duodenal obstruction by using a new duodenal metal stent (with videos). Gastrointest Endosc 2009; 70(4):772-77.
9. Kim KO, Kim TN, Lee HC. Effectiveness of combined biliary and duodenal stenting in patients

with malignant biliary and duodenal obstruction. Scand J Gastroenterol 2012; 47(8-9):962-67.
10. Cheng DX, Li XP, Ye GL. Failure cause and treatment for malignant gastroduodenal stricture stent implantation. Chinese J Digest Endosc 2009; 26(3):158-59.

LETTER TO THE EDITOR

DYNAMICS OF MONOCYTE SURFACE RECEPTORS AFTER BURNS: A PILOT STUDY

J. YU, X. GAO, X. CHEN, X. JIN, N. ZHANG, Y. XUE, X. ZHOU, K. SHI, Z. JIN and W-W. WU

Burns and Plastic Reconstruction Unit, the First Hospital of Jilin University, Changchun, China

Received January 19, 2016 – Accepted April 21, 2016

Previous studies suggested that monocytes may play a vital role in infection and sepsis following burn injury. The aim of this study was to determine whether burn injury had any effect on the levels of expression of monocyte cell-surface receptors at different phases post burn injury. Ten adult burn victims with burns of > 25% of the total body surface area were included in this study. Blood samples were collected on the first, third and seventh day post burn injury. The peripheral blood mononuclear cells were extracted, with or without lipopolysaccharide stimulation. The monocyte phenotypes of CD14, CD16, HLA-DR, CD163, TLR2 and TLR4 were characterized by flow cytometry. Six healthy volunteers were recruited as controls. The percentage of expressed CD14+ monocytes increased during the first day, and then decreased on the third and seventh day after burn injury. The percentages of CD14+ cells expressing CD16 and HLA-DR decreased on the first day, followed by an increase on the third and seventh day post burn. In comparison, the percentage of CD14+ monocytes expressing TLR2 and TLR4 was higher on the first day in burn patients than that of control participants, followed by no change on the third and seventh day post burn injury. There was no significant difference in the percentages of CD14+ expressing CD163 between the two groups. This study showed that the expression of the specific receptors on the surface of monocyte is affected by burn injury. The changes in the expression levels of these receptors may contribute to burn-induced infection susceptibility.

To the Editor,

Major burns still threaten lives, despite recent advances in both diagnosis and treatment. It is usually accompanied with a hyperactive innate immune system and inflammation (1). Multiple studies have attempted to clarify the role that various monocyte surface receptors play in burn patients, especially in those with various complications (2, 3). CD14+ monocytes can differentiate into a variety of cells, recognize other pathogen-associated molecular patterns and to bind bacterial lipopolysaccharide (LPS). Studies have shown that CD14 plays a role in the diagnosis of sepsis following burn injury (2, 4). Down-regulation of CD14 led to the deactivation of monocytes (4), which was characterized, among other things, by a reduction of HLA-DR expression. Also, CD14+CD16+ have been shown to produce an abundance of tumor necrosis factor-α (TNF-α) (5). Toll-like receptors (TLRs) play a role in the host's response to pathogens and sterile injury-associated inflammatory responses. Soluble CD163 (sCD163), which is shed into the extracellular due to a proteolytic cleavage near the cell membrane, is an early indicator of the susceptibility to sepsis after burn injury.

Key words: burn, CD14, CD16, CD163, flow cytometry monocyte, HLA-DR; TLR

Mailing address:
Dr Wei-Wei Wu,
Burns and Plastic Reconstruction Unit,
the First Hospital of Jilin University,
No. 1409 Ximinzhu Street, Changchun 130061, China.
Tel.: +86 431 81879162
e-mail: wu.wei-wei@yandex.com

0393-974X (2016)

Normally, CD163 functions as innate immune sensor for both gram-positive and -negative bacteria (6).

However, few studies have investigated a combined effect of these antigens. Therefore, this study attempted to understand the role of monocytes in burn injury by analyzing the monocyte phenotype. Immune system dysfunction increased the susceptibility to secondary infections and sepsis, leading causes of death among severely burned patients (7).

MATERIALS AND METHODS

Participants

Ten adult victims with burns of > 25% total body surface area (TBSA) were admitted to the inpatient service of the First Hospital of Jilin University (Changchun, China) from June 2011 to March 2012. Those individuals diagnosed with diseases of the immune system, or who had received chemotherapy, hormones or immuno-enhancers in the past, were excluded. Six healthy volunteers (HC) undergoing health examinations were recruited as controls.

Peripheral blood samples (10 ml) were collected in heparinized tubes for lymphocyte profiling on arrival and on the first, third and seventh day post burn (PBD). Written informed consent was signed by all subjects before sample collection and the experimental protocol was approved by the Ethics Committee of the First Hospital of Jilin University (Changchun, China).

Burn care

All patients were treated by the Parkland formula (lactated Ringer's solution 4 ml/kg/%burn for 24 hours). Vital signs (body temperature, pulse rate, respiration rate and blood pressure) and urinary output were monitored and documented every hour. Enteral nutrition was instituted on admission. Early excision and grafting for full-thickness burns were administrated within 24–48 h of admittance to the hospital. Autologous skin grafts were performed when donor skin was available. Regular dressings containing a combination of silver and sulfadiazine (Flamazine) were used and changed every day for superficial and partial thickness dermal burns.

Flow cytometry analysis

We isolated mononuclear cells from individual patient's peripheral blood (PBMCs) by density-gradient centrifugation using Ficoll-Paque Plus (Amersham Biosciences, Little Chalfont, UK). With, or without duplicates after stimulation with LPS (Sigma-Aldrich, St. Louis, USA) in the presence of Roswell Park Memorial Institute – 1640 medium [RPMI-1640, Thermo-Fisher Biochemical Product (Beijing) Co., Ltd, Beijing, China] supplemented with 10% fetal calf serum (FCS, Hyclone, USA) in 5% CO_2 was incubated at 37°C for 6 hours (14). Subsequently, the cells were harvested, washed with cold phosphate-buffered saline (PBS) and stained with Percp-Cy™5.5 mouse-anti-human CD14, FITC mouse-anti-human CD16, APC mouse-anti-human HLA-DR, PE mouse-anti-human CD163 (GolgiPlug; BD Biosciences, San Jose, USA), PE-anti-human TLR2 and PE-anti-human TLR4 (eBioscience, Inc., San Diego, USA) at 4°C in the dark for 20 min. Mouse isotype-matched controls (FITC-IgG1, PE-IgG1, Percp-Cy™ IgG2a and APC-IgG2b; BD Biosciences, San Jose, USA) were used as negative controls. The frequency of different subsets of monocytes was determined by flow cytometry using an FACSCalibur (BD Biosciences, San Jose, USA) flow cytometer. The data were analyzed using FlowJo software (version 5.7.2; TreeStar, Ashland, OR, USA).

Statistical analysis

The data were expressed as a median and range. Differences between groups were analyzed by the Mann-Whitney U non-parametric test using SPSS software (version 19.0; SPSS, Inc., Chicago, IL, USA). Spearman's rank correlation test was used to assess the relationship between variables. A two-sided P value < 0.05 was considered statistically significant.

RESULTS

Participant demographics

The ages of burn injury patients ranged from 19 to 45 years (median 32.7 years). The burn area range was 30-45% TBSA (median 34.5% TBSA). None of the patients developed sepsis and the survival rate was 100%. There was no significant difference in the distribution of age and genders between the burn injury patients and HC group (Table I).

Table I. *Patients' demographic and clinical characteristics.*

	Total number	Age (year)	TBSA (%)	Outcome
Burned patient	10 (6M / 4F)	32.7 ± 7.13	34.5 ± 5.5	All survived
Healthy control	6 (4M / 2F)	30.3 ± 7.94	N/A	N/A

M: Male; F: Female; TBSA: total body surface area; N/A: not applicable

CD14+ monocytes in the burn patients were over-expressed

The CD14+ monocyte profile from the different subpopulations was examined by flow cytometry as described in Methods. The percentage of blood CD14+ monocytes was significantly increased in burn injury patients in the early post-burn stage (1 day = PBD1) as compared to monocyte levels observed in HC subjects ($P = 0.014$, Fig. 1).

Different receptor profiles expressed on the monocytes at earlier phase of burn injury

One day after burn injury, the percentage of CD14+ monocytes expressing HLA-DR harvested from burn injury patients was significantly lower than in HC ($P = 0.002$, Fig. 2a). This indicated that the antigen presentation by CD14+ monocytes was decreased in the burn injury patients. The CD16 expression in HLA-DR+CD14+ monocytes was also significantly lower than in the HC one day after burn injury ($P = 0.04$, Fig. 2b).

The expression of both TLR2 and TLR4 on CD14+ and HLA-DR+CD14+ monocytes ($P = 0.008$, $P = 0.031$, $P = 0.043$ and $P = 0.03$, respectively, Fig. 2c-f) was higher in the burn injury patients than in the HC group. Analysis of CD163 expression levels following burn injury did not show any significant difference when compared to the HC ($P = 0.69$, data not shown).

Different receptor profiles expressed on the monocytes at later phase of burn injury

After the initial analysis of various receptors expressed on the monocytes at the early phase of burn injury, their expression levels were further analyzed at a relatively later phase (7 days = PBD7). The number of CD14+ monocytes at PBD7 decreased when compared to PBD1 ($P = 0.035$, Fig. 2g). The frequency of HLA-DR decreased at PBD3 compared to PBD1 ($P = 0.075$), followed by a significant increase by PBD7 compared to both PBD1 and PBD3 ($P = 0.025$, $P = 0.003$, respectively, Fig. 2h). As expected, the frequency of CD16 increased over time and was significantly higher at PBD7 than at PBD1 ($P = 0.037$, Fig. 2i).

DISCUSSION

Our findings provide several valuable insights on the modulation of innate immune cell response as a response to a burn injury. Burn injury caused an increase of CD14+ monocytes in the blood of the patients as early as PBD1. This confirms previous studies, which showed an increase in the expression of CD14 in other tissues after a burn (8, 9). Analysis of the receptor profile on the CD14+ monocytes showed a decrease in HLA-DR expression. Such patients had a higher mortality rate and increased the chance of developing septic complications (24, 25). As the patient's condition stabilized (by PBD7), the number of HLA-DR+CD14+ monocytes increased. These results are consistent with a published report by Venet et al. (10).

The immune system undergoes initial inhibition following a burn injury, making patients more susceptible to infections (7), suggested even in this study since the number of CD14+CD16+ monocytes decreased at PBD1 and remained low over three days and eventually increased by PBD7. This is

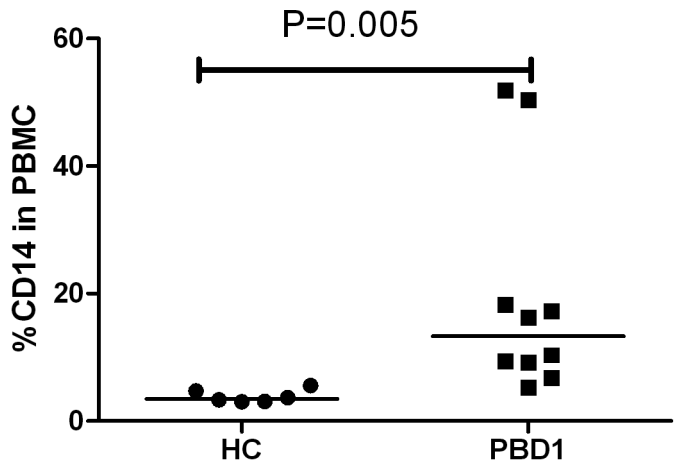

Fig. 1. *Increased number of CD14+ monocytes in PBMC from burn injury patients. Flow cytometry was used to differentiate the CD14+ monocytes from PBMCs isolated from patients and HC one day after burn injury (PBD1). Harvested cells were gated initially on PBMCs. At least 50,000 events were analyzed for each sample. The dot plot data represent the CD14+ monocyte percentages. The horizontal lines represent the median. HC: healthy controls, PBD#: post burn injury day*

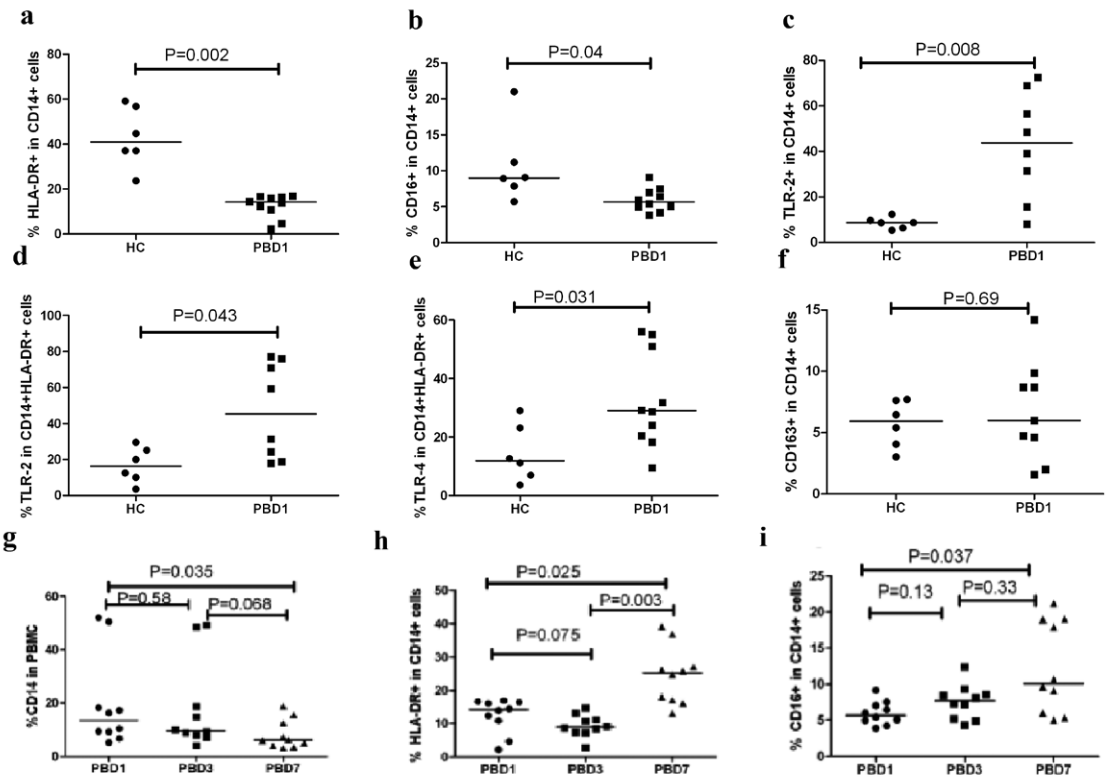

Fig. 2. *Frequency of various cell-surface receptors expressed on CD14+ monocytes.* ***a)*** *HLA-DR+CD14+ early after the burn injury.* ***b)****CD14+CD16+ early after the burn injury.* ***c)****TLR2+CD14+ early after the burn injury.* ***d)*** *TLR2+HLA-DR+CD14+ early after the burn injury.* ***e)*** *TLR4+HLA-DR+CD14+ early after the burn injury.* ***f)****CD163+CD14+ early after the burn injury.* ***g)*** *CD14+ in PMBC later after the burn injury.* ***h)*** *CD14+ in PMBC later after the burn injury.* ***i)****HLA-DR+CD14+ later after the burn injury. Harvested cells were gated initially on PBMCs and then on CD14+ monocytes. At least 50,000 events were analyzed for each sample. Summarized data show the percentage of peripheral blood CD14+ monocytes expressing a particular receptor. Data are expressed as the mean percent of individual samples from at least two separate experiments. The horizontal lines represent the median. HC: healthy controls, PBD# – post burn injury day.*

bolstered by the findings of Vindenes et al. (26), who found decreased IgG-dependent phagocytosis after burns. With regard to the HC, there were no significant changes in expression of CD14+CD163+ monocytes. This may be due to shedding of the membranous CD163 into endochylema. Both the TLR2 and TLR4 were over-expressed on the CD14+ and CD14+HLA-DR+ monocytes; responses were delayed till 3-7 days post-injury in accordance with previously published data (11). It is documented that TLR4 activation is in part mediated by enhanced activation of the p38 signaling pathway, and TLR2 may also have such a relationship (12). Our findings strongly suggest that the TLR hyper-responsiveness likely contributes to inflammatory complications after a burn (1).

In conclusion, our results show that CD14+ monocytes and different receptors, such as CD16, HLA-DR, CD163, TLR2, and TLR4, expressed on the surface of monocytes play an important role in the events following a burn injury. However, additional research is required to further our knowledge on burn injury modulation of the innate immune response, and provide better insight into the development of methods to restore normal immune function following a burn injury.

REFERENCES

1. Schwacha MG. Macrophages and post-burn immune dysfunction. Burns 2003; 29:1-14.
2. Johansson J, Sjogren F, Bodelsson M, Sjoberg F. Dynamics of leukocyte receptors after severe burns: an exploratory study. Burns 2011; 37:227-33.
3. Zhang AQ, Yue CL, Gu W, Du J, Wang HY, Jiang J. Association between CD14 promoter -159C/T polymorphism and the risk of sepsis and mortality: a systematic review and meta-analysis. PLoS One 2013; 8:e71237.
4. Docke WD, Randow F, Syrbe U, et al. Monocyte deactivation in septic patients: restoration by IFN-gamma treatment. Nat Med 1997; 3:678-81.
5. Ziegler-Heitbrock L. The CD14+ CD16+ blood monocytes: their role in infection and inflammation. J Leukoc Biol 2007; 81:584-92.
6. Moller HJ. Soluble CD163. Scand J Clin Lab Invest 2012;72:1-13.
7. Church D, Elsayed S, Reid O, Winston B, Lindsay R. Burn wound infections. Clin Microbiol Rev 2006; 19:403-34.
8. Zang QS, Maass DL, Wigginton JG, et al. Burn serum causes a CD14-dependent mitochondrial damage in primary cardiomyocytes. Am J Physiol Heart Circ Physiol 2010; 298:H1951-8.
9. Steinstraesser L, Alarcon W, Fan MH, et al. Thermal injury induces expression of CD14 in human skin. Burns 2002; 28:223-30.
10. Venet F, Tissot S, Debard AL, et al. Decreased monocyte human leukocyte antigen-DR expression after severe burn injury: Correlation with severity and secondary septic shock. Crit Care Med 2007; 35:1910-7.
11. Schwacha MG, Chaudry IH. The cellular basis of post-burn immunosuppression: macrophages and mediators. Int J Mol Med 2002; 10:239-43.
12. Chen XL, Sun L, Guo F, et al. High-mobility group box-1 induces proinflammatory cytokines production of Kupffer cells through TLRs-dependent signaling pathway after burn injury. PLoS One 2012; 7:e50668.

LETTER TO THE EDITOR

ROSUVASTATIN ALLEVIATES THE DEVELOPMENT OF MONOCROTALINE-INDUCED PULMONARY HYPERTENSION IN RATS

L. ZHANG[1], TX. ZHANG[2], N. LIU[1], JY. ZHANG[1], XY. ZHAO[1], H. ZHANG[1] and DL. SHEN[1]

[1]Department of Cardiology, The First Affiliated Hospital of Zhengzhou University, Zhengzhou City, China; [2]Biological Science, The Pennsylvania State University, Pennsylvania State, USA

Received October 12, 2015 – Accepted May 5, 2016

Statins can increase endothelial function through enhancement of the expression and activity of endothelial nitric oxide synthase (eNOS). The aim of this study is to evaluate the effect of rosuvastatin on the number of circulating endothelial progenitor cells (EPCs) and endothelial expression of eNOS in monocrotaline-induced pulmonary hypertensive rats. Sixty Sprague-Dawley (SD) rats were divided into three groups of 20: control (group A), pulmonary hypertension (PAH) + rosuvastatin group (group B), and PAH (group C). Monocrotaline (MCT; 60 mg/kg) was injected (intraperitoneally) to induce PAH. Rats in group B received rosuvastatin [10 mg/(kg. day)] for 2 weeks. Peripheral blood (5 mL) was aspirated from the femoral artery of each rat before and after 2 weeks of treatment. Mononuclear cells were isolated and subcultured to obtain EPCs. Small and moderately sized pulmonary arteries were collected 2 weeks later for histological analyses. eNOS gene expression in endothelial cells of pulmonary arteries were then determined at mRNA and protein levels. eNOS expression at mRNA and protein levels and the number of circulating EPCs were reduced significantly in groups B and C compared with group A ($P < 0.05$), and a significant difference between group B and group C ($P < 0.05$) was observed. Vascular remodeling in small and moderately sized pulmonary arteries was attenuated markedly in group B compared with group C. These results suggest that rosuvastatin can ameliorate the remodeling of pulmonary arteries in MCT-induced PAH rats by increasing the number of circulating EPCs and eNOS upregulation.

To the Editor,

Pulmonary arterial hypertension (PAH) refers to pulmonary vascular disease affecting the arterioles (1). PAH has the features of increased pulmonary arterial pressure and pulmonary resistance that are characterized by severe arteriopathy (2-3). The precise cause of PAH is not known. Recent advances in basic scientific research point to abnormalities in the function of pulmonary endothelial cells as causing or contributing to the development of PAH (4). The essence of vascular endothelial dysfunction is the imbalance between damage and repair to endothelial cells.

Endothelial progenitor cells (EPCs) are bone marrow-derived stem cells that can differentiate into mature endothelial cells (5). Studies have shown

Key words: burn, CD14, CD16, CD163, flow cytometry monocyte, HLA-DR; TLR

Mailing address:
Dr JY. Zhang,
The First Affiliated Hospital
Zhengzhou University,
No.1, Eastern Jianshe Road,
Zhengzhou City, 450052, PR China
e-mail: zhangjinying166@126.com

0393-974X (2016)

DISCLOSURE: ALL AUTHORS REPORT NO CONFLICTS OF INTEREST RELEVANT TO THIS ARTICLE.

that EPCs play an important part in replacement of a dysfunctional endothelium (6) and improvement of endothelial function. However, accumulated evidence suggests that the level of circulating EPCs is lower and the EPC function is reduced in PAH (7-9).

Intriguingly, several studies have demonstrated the potential modulatory role of statins on circulating EPCs (10) and endothelial nitric oxide synthase (eNOS) (11). Statins can mobilize EPCs in bone marrow and enhance their ability to proliferate and migrate to repair injured endothelial cells. Statins also can upregulate the expression and activation of eNOS by generating endothelium-derived relaxing factor. In the present study, circulating EPCs and the modulatory role of statins on eNOS were investigated.

MATERIALS AND METHODS

Animals and drug administration

The protocol for animal experimentation was in accordance with the rules on animal management set by the Chinese Ministry of Health (document number 55, 2001) and those of the Ethics Committee of Zhengzhou University (Zhengzhou, China).

Six-week-old male rats were used. All rats had free access to food and water. PAH was induced by intraperitoneal injection of 60mg/kg monocrotaline (MCT; Sigma–Aldrich, Saint Louis, MO, USA) dissolved in 0.5mol/L HCl solution (12).

The rats were divided randomly into three groups of 20: group A (control), intraperitoneal injection of 0.9% (physiologic) saline; group B, intraperitoneal injection of MCT + rosuvastatin; group C, intraperitoneal injection of MCT. Rats in group B received rosuvastatin (10 mg/kg/day) for 2 weeks. Five milliliters of peripheral blood was aspirated from the femoral artery of each rat before and after 2 weeks to obtain EPCs. The procedures employed to isolate and culture endothelial cells were as described previously (12). Animals were sacrificed at week-2. Lung tissues were extracted, frozen immediately, and stored at –70°C.

RNA extraction and real time-polymerase chain reaction (PCR)

Extraction of total RNA was undertaken using Trizol reagent (Invitrogen, Carlsbad, CA, USA) from endothelial cells of pulmonary arteries. The quality of RNA was analyzed by gel electrophoresis. RNA was reverse-transcribed using an AMV First Strand cDNA Synthesis kit (Roche Diagnostics, Basel, Switzerland) according to the manufacturer's instructions. Real-time PCR was carried out using ABI SYBR Green PCR Master Mix (Applied Biosystems, Foster City, CA, USA). Gene-expression assays were undertaken with an RT-PCR cycler and detection system (ABI Step One Plus; Applied Biosystems). The $2^{-\Delta\Delta CT}$ method was used to calculate mRNA expression. Expression of eNOS mRNA was normalized to β-actin as an internal control.

Western blotting

Cells were collected and lysed with protease inhibitor in 1× lysis buffer on ice for 30 min. Proteins were separated by electrophoresis on 8% sodium dodecyl sulfate-polyacrylamide gel and transferred to polyvinylidene difluoride membranes. Membranes were blocked with 5% non-fat milk and incubated with primary antibodies against eNOS (1:1000 dilution), AP-1 (1:1000), and β-actin (1 : 5000) in TBS-T at room temperature for 1 h. After washing three times with TBS-T, membranes were incubated with the secondary antibodies at room temperature for 1 h. Blots were probed and then exposed to X-ray films. Gel imaging system was employed for images. Quantitative analyses were carried out using ImageJ software, and the expression level was normalized to β-actin.

Cell culture

Peripheral blood (5 mL) was aspirated from the femoral artery of each rat prior to and 2 weeks after the study. Samples at the start of experimentation were defined as the baseline level of cultured EPCs in each rat. At the end of 2 weeks, samples were evaluated to determine levels of cultured EPCs in each group. Peripheral blood mononuclear cells (PBMNCs) were collected by density gradient centrifugation with Lymphoprep solution (Axis-Shield Diagnostics, Dundee, Scotland). PBMNCs were resuspended at $1\times10^6/cm^2$ in endothelial cell growth medium M199. PBMNCs were cultured with endothelial cell growth medium M199 supplemented with 10% fetal bovine serum, ascorbic acid, heparin sulfate, 2% penicillin/streptomycin, and 50 ng/mL human recombinant vascular endothelial growth factor (VEGF).

The cell suspension was plated onto 24-well culture plates (1 mL/well) pre-coated with fibronectin (Sigma–Aldrich) and incubated at 37°C in a humidified environment with 5% CO_2. To identify the cultured cells as EPCs after 7 days of culture, they were fixed with 4% paraformaldehyde and stained using fluorescein isothiocyanate-conjugated Ulex europaeus agglutinin (UEA-1; Sigma–Aldrich). In addition, uptake of DiI-labeled acetylated low-density lipoprotein (DiI-acLDL; Invitrogen) was monitored because cultured EPCs are known to be positive for UEA-1 and acLDL (5). Double-positive cells that adhered to fibronectin-coated dishes were counted in five randomly selected fields using an inverted fluorescent microscope.

Histopathologic analyses

All rats were sacrificed at the end of week 2 and lung samples were collected. Six micron sections were used for this protocol. Tissue sections were rinsed for 2 min in 100% ethanol and transferred to 95% ethanol for 2 min, then 70% ethanol for 2 min. Finally, tissue sections were rinsed 2 times for 2 min each in PBS. The tissue sections were treated for 10 min with PBS solution with 0.01% Triton X-100. The sections were washed 2 times for 5 min each in PBS. Endogenous peroxide activity was blocked by incubating sections in 0.3% H2O2 in PBS for 30 min. The sections were washed 2 times for 5 min each in PBS. The tissue sections were blocked for 45 min in PBS with 5% donkey serum. The tissue sections were incubated with Anti-ACTIVE Caspase-3 antibody or Anti-PARP p85 antibody for 60 min. and washed 3 times with PBS. The samples were then incubated with biotin-conjugated donkey anti-rabbit pAb for 60 min., and after washing were developed with DAB substrate kit (Vector Laboratories) for 10 min. After washing, the sections were observed under microscope.

The images were acquired and processed by using the Vector system according to the manufacturer's instructions.

Statistical analyses

Data are the mean ± standard deviation (SD). Differences were compared using one-way analysis of variance followed by the Student–Newman–Keuls *post hoc* test for significance. SPSS v17.0 (IBM, Armonk, NY, USA) was used to conduct statistical analyses. $P<0.05$ was considered significant.

RESULTS

Effect of rosuvastatin on eNOS expression at mRNA and protein levels in endothelial cells

Real-time RT-PCR was carried out to ascertain whether rosuvastatin influences eNOS expression at the mRNA level (Fig. 1A). Compared with group A, eNOS expression at the mRNA level was decreased significantly in groups B and C. The eNOS mRNA level in group C was significantly lower than that in group B (0.52±0.06 *vs* 0.66±0.05, $P < 0.05$), suggesting that rosuvastatin can increase eNOS expression at the mRNA level.

Results of Western blotting are shown in Fig. 1B. The level of eNOS protein was decreased in groups B and C. The level of eNOS protein in group C was significantly lower than that in group B (0.58±0.03 *vs* 0.43±0.04, $P < 0.05$). These data were consistent with changes in mRNA levels and suggested that rosuvastatin can increase eNOS expression at mRNA and protein levels in endothelial cells.

Effect of rosuvastatin on circulating EPCs

After 7 days of culture, cells were defined as EPCs undergoing differentiation using immunofluorescent labeling with FITC-lectin and DiI-acLDL. Most cells were shown to be positive for FITC-lectin and DiI-acLDL using confocal laser scanning microscopy .

The number of circulating EPCs was analyzed. Compared with group A, the cell number was decreased significantly in group B (38.4±5.2 *vs* 54.6±4.3, $P < 0.05$) and in group C (17.8±4.9 *vs* 54.6±4.3, $P < 0.05$), respectively. A significant difference in the number of circulating EPCs between group B and group C (38.4±5.2 *vs* 17.8±4.9; $P < 0.05$) was observed. These findings suggested that the number of circulating EPCs was decreased in PAH rats, and that rosuvastatin can increase the number of circulating EPCs.

Pathologic changes in lung tissues

Specimens of peripheral pulmonary arteries obtained from rats with PAH demonstrated a high prevalence of muscularization compared with those obtained from rats without PAH. These muscularized arteries could obstruct pulmonary

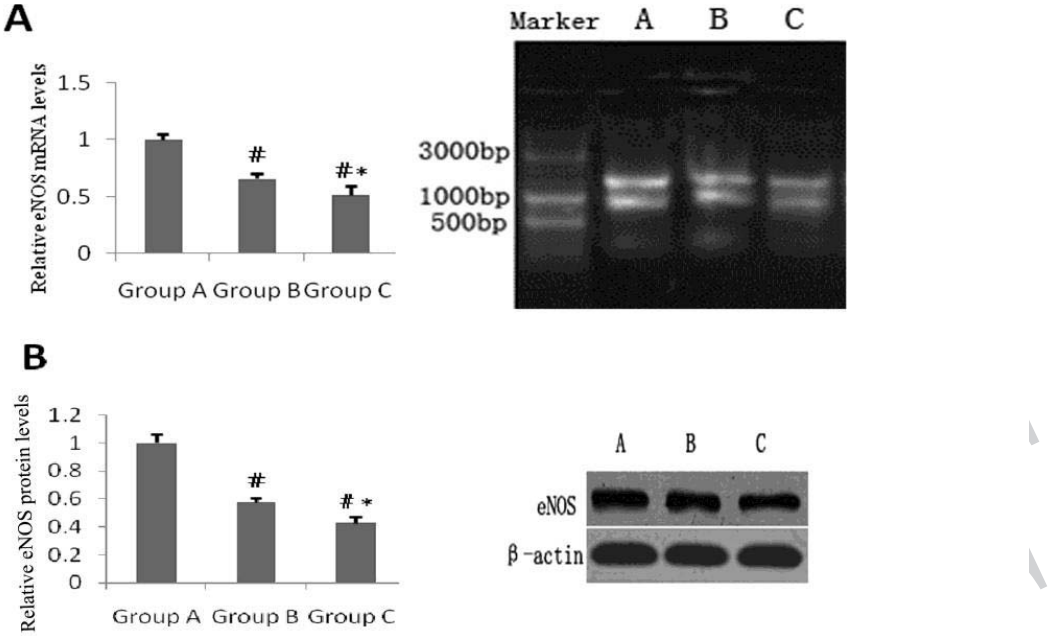

Fig. 1. *Analyses of eNOS expression. eNOS expression at mRNA and protein levels was detected by real-time RT-PCR and western blotting, respectively.* ***A)*** *Quantitative real-time RT-PCR results and representative (right panel) mRNA electrophoresis map.* ***B)*** *Quantitative (left panel) and representative (right panel) western blotting results. Three independent experiments were carried out. Data are the mean ± SD. Compared with group A, #P < 0.05. Compared with group B, *P < 0.05.*

arteries and arterioles in groups B and C. Pulmonary arterioles in group B showed a decreased tendency of muscularization according to H&E staining.

DISCUSSION

Dysfunction of endothelial cells is an early event in PAH development. eNOS is the predominant source of NO production in the pulmonary circulation. eNOS is a key regulator of pulmonary circulation tone and a key mediator of resting tone. Whether reduced production of NOS is a cause or result of PAH is not known. Here, we demonstrated that eNOS expression was decreased significantly in MCT-induced PAH rats and, simultaneously, vascular remodeling was seen in pulmonary arterioles, which has significance for the pathogenesis of PAH.

EPCs in the treatment of PAH have become a new "hot topic". Our study shows that in rats which received MCT, a significantly reduced number of circulating EPCs was observed, as well as more severe pulmonary vascular remodeling. Therefore, the normal number of EPCs may provide protective effects on the maintenance and repair of the endothelium. However, data from a previous study demonstrated that in a rat model of PAH, not only was the number and function of circulating EPCs decreased markedly, but there was also a decrease in the plasma concentration of NO that was positively correlated with the number of circulating EPCs.

The present study had limitations. We could not elucidate the signaling pathway in rosuvastatin-induced upregulation of eNOS expression. Whether MCT causes impairment of EPC function was not elucidated.

In conclusion, this study shows that rosuvastatin administration could represent a novel strategy for PAH treatment.

ACKNOWLEDGEMENTS

Thanks to Science and Technology Talents Team Construction Program of Zhengzhou City-Science and Technology Talents (131PLJRC670) and Science and Technology Research Projects of Henan Province (13A320623) for their financial support.

REFERENCES

1. Fritz JS, Blair C, Oudiz RJ, et al. Baseline and follow-up 6-min walk distance and brain natriuretic peptide predict 2-year mortality in pulmonary arterial hypertension. Chest 2013; 143:315-23.
2. Rabinovitch M. Molecular pathogenesis of pulmonary arterial hypertension. J Clin Invest 2012; 122:4306-13.
3. Chamberlain G, Fox J, Ashton B, Middleton J. Concise review: mesenchymal stem cells: their phenotype, differentiation capacity, immunological features, and potential for homing. Stem Cells 2007; 25:2739-49.
4. Budhiraja R, Tuder RM, Hassoun PM. Endothelial dysfunction in pulmonary hypertension. Circulation 2004; 109:159-65.
5. Asahara T, Murohara T, Sullivan A, et al. Isolation of putative progenitor endothelial cells for angiogenesis. Science 1997; 275(5302):964-67.
6. Hill JM, Zalos G, Halcox JP, Schenke WH, Waclawiw MA, Quyyumi AA, Finkel T. Circulating endothelial progenitor cells, vascular function, and cardiovascular risk. N Engl J Med 2003; 348(7):593-600.
7. Diller GP, van Eijl S, Okonko DO, et al. Circulating endothelial progenitor cells in patients with Eisenmenger syndrome and idiopathic pulmonary arterial hypertension. Circulation 2008; 117(23):3020-30.
8. Fadini GP, Schiavon M, Rea F, Avogaro A, Agostini C. Depletion of endothelial progenitor cells may link pulmonary fibrosis and pulmonary hypertension. Am J Respir Crit Care Med 2007; 176(7):724-25.
9. Junhui Z, Xingxiang W, Guosheng F, Yunpeng S, Furong Z, Junzhu C. Reduced number and activity of circulating endothelial progenitor cells in patients with idiopathic pulmonary arterial hypertension. Respir Med 2008; 102 (7):1073-79.
10. Vasa M, Fichtlscherer S, Adler K, Aicher A, Martin H, Zeiher AM, Dimmeler S. Increase in circulating endothelial progenitor cells by statin therapy in patients with stable coronary artery disease. Circulation 2001; 103(24):2885-90.
11. Antoniades C, Bakogiannis C, Leeson P, et al. Rapid, direct effects of statin treatment on arterial redox state and nitric oxide bioavailability in human atherosclerosis via tetrahydrobiopterin-mediated endothelial nitric oxide synthase coupling. Circulation 2011; 124(3):335-45.
12. Gomez-Arroyo JG, Farkas L, Alhussaini AA, Farkas D, Kraskauskas D, Voelkel NF, Bogaard HJ. The monocrotaline model of pulmonary hypertension in perspective. Am J Physiol Lung Cell Mol Physiol 2012; 302:L363-69.

LETTER TO THE EDITOR

HEPATIC FIBROSIS AND SUPERSONIC SHEAR IMAGING IN PATIENTS WITH DIFFERENT ETIOLOGICAL CHRONIC HEPATIC DISEASES

L.L. SUN[1,2], W. CHANG[2,3], L.Q. JIAO[1], X. CUI[1] and G. DONG[1]

[1]Department of Ultrasonography, The First Affiliated Hospital of Zhengzhou University, Zhengzhou City, Henan Province, China; [2]Department of ICU, The First Affiliated Hospital of Zhengzhou University, Zhengzhou City, Henan Province, China

Received December 17, 2015 – Accepted May 25, 2016

The first two authors contributed equally to this work

The objective of the present study was to investigate whether hepatic fibrosis difference of supersonic shear imaging (SSI) value existed in patients with different etiological chronic hepatic diseases. Retrospective analysis was used to study chronic hepatitis. All the subjects were diagnosed by shear wave elastography and percutaneous liver biopsy. The shear moduli were analyzed to check whether any difference existed between groups. For the chronic hepatitis B, autoimmune hepatitis and fatty hepatitis, the shear moduli in S0 stage were (8.50±3.1)kPa, (9.41±2.5)kPa, (8.97±3.8)kPa; the shear moduli in S1 stage were (9.54±3.0)kPa, (10.42±5.1)kPa, (9.51±4.6)kPa; the shear moduli in S2 stage were (11.77±4.8) kPa, (13.25±5.6)kPa, (11.03±6.0)kPa; the shear moduli in S3 stage were (14.96±6.1)kPa, (19.03±7.8) kPa, (15.38±7.8)kPa; the shear moduli in S4 stage were (20.36±7.5)kPa, (24.99±9.5)kPa, (19.53±5.6)kPa. Shear wave elastography could measure the different etiological chronic hepatic diseases.

To the Editor,

Hepatic fibrosis refers to the excess collagen deposition in the liver, which is divided into S0 stage, S1 stage, S2 stage, S3 stage and S4 stage based on the destruction scope, severity and effect on hepatic micro-circulation (1). Early diagnosis of hepatic fibrosis severity degree is important to guide the clinical treatment for the chronic hepatitis patients.

In recent years, the development of shear wave elastography provides new opportunity for the diagnosis of hepatic fibrosis. Supersonic shear imaging (SSI) is one of the latest elasticity imaging technologies. SSI is also called as shear wave elastography (SWE). Previous studies have proved that SSI can accurately detect liver stiffness and then evaluate hepatic fibrosis. The area under the operating characteristic curve for the subjects with diagnosed severe fibrosis is as high as 0.982 (2, 3).

In the present study, the hepatitis elasticity moduli were compared and analyzed for hepatic fibrosis and liver cirrhosis with normal disease causes, such as chronic hepatitis B, autoimmune hepatitis and fatty hepatitis, in order to realize the application of SSI measurement value in patients with chronic hepatitis due to different causes.

MATERIALS AND METHODS

Study subjects

The study included 581 cases of chronic hepatitis

Key words: Shear wave elastography, SSI, Hepatic fibrosis, autoimmune hepatitis, primary biliary cirrhosis, overlap syndrome

Mailing address:
Dr Gang Dong, Department of Ultrasonography,
The First Affiliated Hospital of Zhengzhou University,
No. 1 Eastern Jianshe Road, Zhengzhou City,Henan Province, 450052, China
Tel:. +86 0371 6691328 - Fax: +86 0371 6691328
e-mail: donggang1202@163.com

0393-974X (2016)

patients who had received percutaneous liver biopsy in The First Affiliated Hospital of Zhengzhou University between May 2011 and September 2015. Of the 582 patients, 175 were cases of chronic hepatitis B, 287 cases with autoimmune hepatitis and 119 cases with steatohepatitis. All patients signed informed consent.

Instruments and methods

All the patients were tested with the SuperSonic Imagine Aixplorer, 4C convex array probe with 1.0~6.0 MHz of probe frequency. Hepatic anterior right area was chosen for the detection of all the patients. When the SWE mode was chosen, the patients were required to hold their breath for 3~5 seconds. Stabilized images were kept. Shear moduli were employed to detect on the round detection area with 2 cm diameter in the imaging area, and kPa was set as the unit. This was repeated 5 times, and the average value was analyzed. The measured value was SSI. The higher the shear moduli, the higher the tissue hardness (3). All the patients had undergone percutaneous liver biopsy within one week after the SSI detection, according to the Viral Hepatitis Prevention Plan for chronic hepatitis pathological classification of 2001. The hepatic inflammation activities were divided into G0, G1, G2, G3 and G4 stages, and the degrees of fibrosis were divided into S0, S1, S2, S3 and S4 stage (1-3). Fasting venous blood was taken for clinical biochemical detection and routine examination (3).

Statistical analysis

The SPASS 17.0 statistical software (SPASS package) was applied to analyze the data. Measurement data that met Gaussian distribution were expressed as mean±SD. One-way ANOVA and non-parametric test were used to analyze the comparisons between groups. Kruskal-Wallis detection was used for non-parametric tests between many groups. Spearman rank correlation analysis was employed to study the correlation between two variables. Spearman test was used for comparisons between two groups. Receiver operating characteristic (ROC) curve was taken to analyze the accuracy of SSI diagnostic hepatic fibrosis. $P<0.05$ was marked for the statistically significant difference.

RESULTS

SSI measured value in different fibrosis classification stages of chronic hepatitis B, autoimmune hepatitis and fatty hepatitis

As shown in Table I, with the increase of fibrosis degree, the shear moduli gradually increased for chronic hepatitis B, autoimmune hepatitis and fatty hepatitis, P values all were less than 0.05. When all of them were at the same stage of fibrosis classification, there was no statistical significance on the SSI measured value for chronic hepatitis B, autoimmune hepatitis and fatty hepatitis, $P^*>0.05$. Shear wave elastography could measure the different etiological chronic hepatic diseases.

SSI measured value on chronic hepatic fibrosis classification

The area under the SSI predicted ROC curves of different fibrosis degree is shown in Table II. For the chronic hepatitis B, autoimmune hepatitis and fatty hepatitis, the shear moduli in S0 stage were (8.50±3.1)kPa, (9.41±2.5)kPa, (8.97±3.8)kPa; the shear moduli in S1 stage were (9.54±3.0)kPa, (10.42±5.1)kPa, (9.51±4.6)kPa; the shear moduli in S2 stage were (11.77±4.8)kPa, (13.25±5.6)kPa, (11.03±6.0)kPa; the shear moduli in S3 stage were (14.96±6.1)kPa, (19.03±7.8)kPa, (15.38±7.8)kPa; the shear moduli in S4 stage were (20.36±7.5) kPa, (24.99±9.5)kPa, (19.53±5.6)kPa. Shear wave elastography could measure the different etiological chronic hepatic diseases.

SSI predicted diagnosis cutoff value, sensitivity and specificity

As shown in Table III, the impact on the SSI measured value for patients with ascites is clear, and its sensitivity and specificity is high.

DISCUSSION

According to the statistics, the incidence of chronic hepatitis shows a rising trend in China. Its main pathogenesis is viral hepatitis (4). In recent years, the incidence of alcoholic hepatitis has shown a yearly ascendant trend (5). Hepatic fibrosis is the

Table I. *SSI mean predict value of different pathological stages in hepatitis B, autoimmune hepatitis and fat*

Fibrosis classification	Chronic hepatitis B		Autoimmune hepatitis		Fatty hepatitis		P
	case	SSI measured value (kPa)	case	SSI measured value (kPa)	case	SSI measured value (kPa)	
S0	41	8.500±3.1	19	9.405±2.5	48	8.971±3.8	<0.05
S1	59	9.544±3.0	87	10.420±5.1	53	9.515±4.6	<0.05
S2	29	11.769±4.8	109	13.255±5.6	11	11.027±6.0	<0.05
S3	25	14.960±6.1	40	19.026±7.8	4	15.375±7.8	<0.05
S4	21	20.362±7.5	35	24.989±9.5	3	19.533±5.6	<0.05

Table II. *The area under the SSI predicted ROC curves of different degrees of fibrosis of chronic hepatitis B, autoimmune hepatitis and fatty hepatitis.*

Fibrosis stage	Total	Chronic hepatitis B	Autoimmune hepatitis	Fatty hepatitis
S0	0.318 (108 cases)	0.255 (41 cases)	0.298 (19 cases)	0.414 (48 cases)
S1	0.325 (200 cases)	0.372 (59 cases)	0.261 (88 cases)	0.489 (53 cases)
S2	0.563 (147 cases)	0.548 (29 cases)	0.492 (107 cases)	0.544 (11 cases)
S3	0.716 (67 cases)	0.709 (25 cases)	0.725 (38 cases)	0.777 (4 cases)
S4	0.861 (59 cases)	0.882(21 cases)	0.865 (35 cases)	0.931 (3 cases)

Note: the SSI predicted and diagnosed fibrosis in S3 stage and S4 stage had better diagnostic value. The diagnostic value of fatty hepatitis was higher than that of chronic hepatitis B and autoimmune hepatitis.

Table III. *The cutoff value, sensitivity and specificity comparison of different pathological stages of chronic hepatitis B, autoimmune hepatitis and fatty hepatitis.*

	Cutoff value (kPa)			Sensitivity 100%			Specificity 100%		
	chronic hepatitis B	Autoimmune hepatitis	fatty hepatitis	chronic hepatitis B	Autoimmune hepatitis	fatty hepatitis	chronic hepatitis B	Autoimmune hepatitis	fatty hepatitis
S3	11	11.8	11.07	76	84.2	75	63	53.9	82
S4	13.9	15.77	13.997	85.7	85.7	100	84.4	72.8	85

Note: SSI measured value had higher sensitivity and specificity on S3 stage and S4 stage of fatty hepatitis.

common pathological process of chronic hepatitis B, fatty hepatitis, and autoimmune hepatitis. The early accurate evaluation on fibrosis degree has vital significance for clinical treatment guidance and prognosis improvement (6).

This study included several common etiological chronic hepatitis patients, and investigated the application value of SSI technology on different etiological chronic hepatitis through the comparative analysis of SSI measured value of hepatic tissue. The results show that some SSI diagnoses had high diagnostic value for chronic hepatitis hepatitis B (S2 stage, S3 stage and S4 stage), fatty hepatitis (S2 stage, S3 stage and S4 stage) and autoimmune hepatitis (S3 stage and S4 stage), which were correlated to the related literature reports (2, 3) (7, 9). It was reported that the SSI measured values increased successively for the post-hepatitis B fibrosis group, the post-hepatitis C fibrosis group and the alcoholic cirrhosis group, and statistical significance was found between each group (10). In the present study, there was no statistical difference on the SSI measured value difference for S4 stage hepatitis B, fatty hepatitis and autoimmune hepatitis, which might be related to the different research subjects. Autoimmune hepatitis patients were added in this study. The cases of fatty hepatitis were more than those of the non-alcoholic fatty hepatitis (107 cases for the non-alcoholic fatty hepatitis patients, 12 cases for alcoholic fatty hepatitis patients). This study found that there was no significant difference between the SSI mean value of the chronic hepatitis B, fatty hepatitis and autoimmune hepatitis, indicating that SSI measured value diagnosis had no significant correlation on hepatic fibrosis and etiological causes.

The impacts on the SSI measured value for patients with ascites is clear, and still have the same sensitivity and specificity. The novelty is that the study confirms the applicability and accuracy of SSI, and the noninvasive method is effective to assess liver fibrosis.

There are some limitations to the study. Firstly, the results should be confirmed by further study including a larger cohort of patients. Secondly, the sensitivity and specificity of the method should be improved.

SSI technology had noninvasive, painless, quantitative detection and repeatable advantages, and had great application values on the diagnosis of different etiological chronic hepatitis fibrosis, which requires further discussion for the diagnostic value of SSI measured value on the pathogenesis of chronic hepatitis.

In conclusion, the impacts on the SSI measured value for patients with ascites is clear, and its sensitivity and specificity is high.

REFERENCES

1. Davidson G, Barnes G, Bass D, Cohen M, Fasano A, Fontaine O, Guandalini S. Infectious diarrhea in children: Working Group Report of the First World Congress of Pediatric Gastroenterology, Hepatology, and Nutrition. J Pediatr Gastroenterol Nutr 2002; 35:S143-50.
2. Ferraioli G, Tinelli C, Dal Bello B. Accuracy of shear wave elastography for assessing liver fibrosis in chronic hepatitis C: a pilot study. Hepatol 2012; 56:2125-33.
3. Bavu E, Gennisson JL, Couade M. Noninvasive in vivo liver fibrosis evaluation using supersonic shear imaging: a clinical study on 113 hepatitis C virus patients. Ultrasound Med Biol 2011; 37:1361-73.
4. Liang X, Bi S, Yang W. Epidemiological serosurvey of hepatitis B in China - declining HBV prevalence due to hepatitis B vaccination. Vaccine 2009; 27:6550-57.
5. Marventano S, Salomone F, Godos J, Pluchinotta F, Del Rio D, Mistretta A, Grosso G. Coffee and tea consumption in relation with non-alcoholic fatty liver and metabolic syndrome: A systematic review and meta-analysis of observational studies. Clin Nutr 2016; S0261-5614(16)00103-5.
6. Kaspar MB, Sterling RK. Hyperbilirubinaemia in HIV-HCV co-infected patients on antiretroviral therapy: drug effect or liver disease severity? BMJ Open Gastroenterol 2016; 3:e000072.
7. Kim MS, Kim BI, Kwon HJ, et al. Discordance between conventional ultrasonography and ElastPQ for assessing hepatic fibrosis in chronic hepatitis B: frequency and independent factors. J Med Ultrason 2016; 43(2):201-10.

8. Piscaglia F, Salvatore V, Mulazzani L, Cantisani V, Schiavone C. Ultrasound shear wave elastography for liver disease. a critical appraisal of the many actors on the stage. Ultraschall Med 2016; 37:1-5.
9. Guibal A, Renosi G, Rode A, et al. Shear wave elastography: An accurate technique to stage liver fibrosis in chronic liver diseases. Diagn Interv Imaging 2016; 97:91-99.
10. Mohammed F, Manohar V, Jose M, Thapasum AF, Mohamed S, Shamaz BH, D'Souza N. Estimation of copper in saliva and areca nut products and its correlation with histological grades of oral submucous fibrosis. J Oral Pathol Med 2015; 44:208-13.

LETTER TO THE EDITOR

BODY COMPOSITION IN HEALTHY OLDER PERSONS: ROLE OF THE RATIO OF EXTRACELLULAR/TOTAL BODY WATER

E. MALCZYK[1], S. DZIĘGIELEWSKA-GĘSIAK[2], E. FATYGA[2], E. ZIÓŁKO[2], T. KOKOT[2] and M. MUC-WIERZGOŃ[2]

[1]Institute of Dietetics, University of Applied Sciences in Nysa, Poland; [2]School of Public Health in Bytom, Silesian Medical University, Department of Internal Medicine, Poland

Received November 17, 2015 - Accepted May 4, 2016

The aim of this study was to identify the best prognostic parameters for quickly assessing fluid volume status in the context of nutritional status and water balance in older persons and to facilitate decision-making of the general practitioner (GP). This pilot study was conducted with 142 volunteers aged 60 years or older who were Polish students of the University of the Third Age. Inclusion and exclusion criteria for the study were defined. Assessment tools included: the Mini Nutritional Assessment questionnaire (MNA®) and the anthropometric measurements. Weight and body composition analysis were determined by Bioelectrical Impedance Analysis (BIA) using the Tanita MC-780 multi frequency segmental Body Composition Analyzer. According to the MNA scale, 89.2% of the sample was well-nourished and 10.8% were at risk of malnutrition. A total of 47.1% participants had normal body mass index, 20.6% were overweight, and 32.3% were obese. The BIA showed that females had more fat mass (FM) compared to males (35.84% *vs* 23.90%), while men had more free fat mass (FFM) and total body water (TBW; 61.16% *vs* 45.22% and 53.31% *vs* 45.22% respectively). There were no statistically significant differences in FM, FFM, and TBW by age. The ratio of Extracellular to Total Body Water (ECW/TBW) was higher in women than in men (46.76% *vs* 43.66%). Of all measures, only ECW/TBW increased significantly with age and sex, especially after 65 years. We propose that ECW/TBW may be used as the first, simple, and fast indicator of water volume status in the context of nutritional status and water balance in older subjects. Systematic control of the ECW/TBW by GP or nurse may increase senior independence, resulting in longer self-maintenance at home and reduced hospital admissions.

To the Editor,

Natural aging processes lead to changes in nutritional status and in water-electrolyte balance. As people age, several changes in body composition may be observed, such as: muscle mass replaced by fat, total body water (TBW) volume decrease, free fat mass (FFM) reduction that is accompanied by an increase in fat mass (FM) (1, 2). Total body water – the sum of intra- and extra-cellular fluids (ICF and ECF) – is inherently related to FFM and FM levels. Physiologically, TBW consists of 55% ICF and 45% ECF. Fat tissue contains about 30% water, while fat-free tissues contain about 70-80% water. Reduction in free fat mass correlates with TBW depletion.

Identification of nutritional problems and water-electrolyte homeostasis can facilitate strategies whose need in elderly patients depends on their clinical status: those in good health, patients with co-

Key words: body composition, healthy older persons, nutritional status, water balance, ECW/TBC ratio

Mailing address:
Prof. Małgorzata Muc-Wierzgoń,
School of Public Health in Bytom,
Silesian Medical University, Dept. of Internal Medicine,
Żeromskiego 7 st, 41-902 Bytom 41-902, Poland
Tel./fax: +48/32 2812122
e-mail: mwierzgon@sum.edu.pl

0393-974X (2016)

DISCLOSURE: ALL AUTHORS REPORT NO CONFLICTS OF INTEREST RELEVANT TO THIS ARTICLE.

morbidities, or the frail elderly (3, 4). In the elderly, water comprises 60-65% of total body weight. A decrease in dietary water intake of only 2% may lead to dehydration and other clinical manifestations such as delirium or kidney failure (5, 6). Anthropometric measurements such as body weight, body mass index (BMI), and waist circumference are limited by operator variability and precision (6, 7). It is important to use effective, noninvasive, easy, and economic methods to evaluate clinical conditions in elderly patients. Bioelectric impedance analysis (BIA) is known to accurately measure the nutritional status and water distribution in an individual based on empirical equations (8, 9), but data of healthy older subjects are rare. Ritchie et al. (10) determined the validity of the Tanita BIA system for body composition assessment in older adults. According to the authors, this system provides a valid measure of body fat percentage for older adults, and could be a convenient and practical approach for studying large groups of patients in public health settings.

The aim of this study was to identify the best prognostic parameters for quickly assessing fluid volume status in the context of nutritional status and water balance in older persons and to facilitate decision-making of the general practitioner.

MATERIALS AND METHODS

Materials

This pilot study was conducted initially on 192 persons aged 60 years or older, who were Polish students of the University of the Third Age. Participants were asked to attend a clinic examination at which time they completed a structured questionnaire regarding detailed medical history and a risk behavior assessment.

The inclusion criteria of the study involved non-smoking subjects who did not systematically use any medication, had no special diet, did not use supplements, were non-drinkers, and who did not have an acute or chronic disease (e.g., all factors that might influence water homeostasis).

Exclusion criteria included a positive history of stroke, coronary artery disease or heart failure, liver cirrhosis, chronic renal diseases, diabetes, neoplastic disease, and inflammatory disease, dementia, patients who had received extremity amputation, and those with implanted cardiac devices, metal pins, plates, or joint prostheses. Additional exclusion criteria included use of any drugs that might influence water homeostasis, including: diuretics, angiotensin converting enzyme ACE inhibitors, laxatives, antidepressants, steroids, antipsychotics, and antibiotics.

Finally, 142 older volunteers were included in the study. The study protocol was approved by the Bioethics Committee of the Medical University of Silesia (KNW/0022/KB1/38/16), and informed consent was obtained from all subjects.

Methods

The procedures consisted of :

i. completing the MNA® questionnaire by subjects. The MNA® is a screening tool to help identify elderly persons who are malnourished or at risk of malnutrition (11). The sum of the MNA scores were used to distinguish between persons with adequate nutrition (MNA score ≥ 24), at risk of malnutrition (MNA score 17.5-23.5), and patients experiencing protein calorie malnutrition (MNA < 17);

ii. anthropometric measurements and body composition assessment**.** Body height was measured to the nearest 0.1 cm using a non-metallic and non-stretchable tape. The weight and body composition analysis were determined by electrical bioimpedance using the Tanita MC-780 multi frequency segmental Body Composition Analyzer (Tanita Corporation, Tokyo). The MC-780 uses the latest multi-frequency technology to record a comprehensive range of measurements in just 20 seconds, from segmental fat and muscle mass to basal metabolic rate, visceral fat levels, phase angle and intra/extra cellular body water (12). Research has shown that using multi-frequency provides essential data on intracellular and extracellular water.

In the study, factors that could have potentially influenced readings were standardized: supine position, a recently emptied bladder, a minimum of five minutes of rest before the test, removal of watches or major jewelry, and ambient air or skin temperature. The mean of three measurements was used as the representative value. Measurements were performed in the morning, after a minimum eight hour fast. Using this data, BMI for each senior was calculated (weight/height^2) .

Statistical analysis

Statistica version 10.0 for Windows was used for statistical analysis. The normality of value distribution was checked by the Shapiro-Wilk test. Results that had a Gaussian distribution were analyzed by a one-way analysis of variance (ANOVA) test or Student's *t*-test, and those with a non-Gaussian distribution were verified by a non-parametric Kruskal-Wallis and Mann-Whitney U test, in order to assess the differences between the studied groups. The Tukey post-hoc test was introduced. The Pearson or Spearman rank correlation test was used to evaluate the strength of the association between two variables. A level of significance of $p<0.05$ was taken as indicative of significant differences.

RESULTS

The analyzed group was composed of 66 men and 76 women aged 60-83 years. The mean age was 66.98±5.55 years for women and 68.81±6.81 years for men. Most of the participants were 60-75 years old (88.9% of the women and 81% of the men). Men were more likely to report regular exercise than women (61.9% *vs* 30.9%; p=0.0000). According

Table I. *Comparison of BMI and parameters derived from bioimpedance analysis (BIA) in analysis group.*

		Age (years)			P-value*
Variable	**Gender**	60-65 mean ± SD; median (min-max)	66-75 mean ± SD; median (min-max)	>75 mean ± SD; median (min-max)	
BMI [kg/m^2]	W	28.00±4.85; 26.80 (20.6-44.0)	28.59±4.62; 27.60 (21.7-41.6)	30.84±5.18; 30.90 (23-39.9)	0.1477
	M	28.40±4.45; 27.50 (22.8-35.6)	28.24±2.66; 28.40 (24.8-32.5)	27.00±2.16; 27.15 (24.3-29.4)	0.7842
Fat Mass [%]	W	34,60±5,63; 34,75 (20,5-44,9)	36,86±5,72; 37.50 (24.1-46.4)	36.23±6.30; 36.40 (23.4-44.5)	0.2502
	M	23.89±5.45; 23.45 (16.5-30.9)	24.13±3.16; 24.60 (18.6-28.3)	23.40±2.76; 22.95 (20.6-27.1)	0.9578
FFM [kg]	W	45.67±4.37; 45.50 (36.4-56.1)	44.74±4.51; 45.10 (35.5-56.5)	45.59±7.25; 43.50 (34.0-56.5)	0.6948
	M	63.69±5.54; 61.50 (52.4-69.6)	60.46±4.99; 57.50 (53.6-69.8)	57.68±3.13; 57.35 (54.2-61.8)	0.1500
TBW [%]	W	46.23±3.93; 46.05 (39.1-56.1)	44.43±3.99; 43.90 (37.8-53.2)	44.72±4.41; 44.70 (38.8-53.7)	0.1608
	M	53.31±3.22; 53.00 (49.8-57.8)	53.66±2.56; 53.00 (50.5-57.00)	52.53±1.75; 52.80 (50.3-54.2)	0.7914
ECW/ TBW [%]	W	**46.03±1.66^a; 46.05 (41.9-48.7)**	47.29±1.86^b; 47.50 (44.0-51.1)	47.29±2.56 b; 47.70 (42.3-51.7)	**0.0135**
	M	**42.90±0.71^a; 42.70 (42.1-44.3)**	43.62±1.39 ^{ab};44.00 (41.2-45.2)	45.28±0.91 ^{b}; 45.35 (44.1-46.3)	**0.0083**

**p was calculated by analysis of variance ANOVA (normal distribution), or Kruskal-Wallis test (for non-normal distribution); post hoc analysis - Tukey test*

to the MNA scale, 89.2% of investigated persons were well-nourished, and 10.8% were at risk for malnutrition. There were no malnourished elderly persons. Among well-nourished participants, the mean MNA score was 26.25±1.46. At-risk patients had a mean 22.05±1.57 score on the MNA scale.

Anthropometric measurements

A total of 47.1% participants had a normal BMI, 20.6% were overweight, and 32.3% were obese. Average female BMI was 28.59±4.8 [kg/m^2], while for men the average BMI was 28.07±3.28 [kg/m^2]. According to BMI, more women had a normal body composition than men (54.3% *vs* 19%; p =0.0000). Among overweight participants, there were more men than women (57.2% *vs* 11.1%; p=0.0000).

Analysis of parameters derived from BIA

Table I shows BMI and the parameters derived from BIA: FM, FFM, TBW, and ECW/TBW. Females had more FM in comparison with males (35.84% *vs* 23.9%), while men had more FFM and TBW than women (61.16% *vs* 45.22% and 53.31% *vs* 45.22%, respectively). ECW/TBW was higher in women than in men (46.76% *vs* 43.66%). There were no statistical differences between FM, FFM, and TBW by age. We observed that ECW/TBW increased with age for women from 46.03% to 47.29% (Fig. 1), and from 42.9% to 45.29% for men. In males the tendency towards decreased FFM was also observed.

DISCUSSION

Elderly persons are at the highest risk for developing malnutrition and dehydration (13). In this study, we analyzed well-nourished healthy elderly people to identify water balance indices that may stratify those at dehydration risk. Water imbalance and under-nutrition are preventable disorders and early identification of such conditions may improve people's quality of life, reduce disease burden, and improve clinical costs and outcomes (14, 15). We used several easy and cheap methods: the MNA questionnaire and the Tanita BIA system. Assessment of hydration status through weight change is relatively quick and easy, provides a crude assessment, and requires measurements taken at least two times for confirmation.

The BMI relationship with body composition components differs with age, sex, ethnicity, and body shape (7, 16). It is still not known when and how fast we tend to increase fat mass and decrease muscle mass (9, 10, 17). In our research, BMI tends to increase with age overall, and in men it further

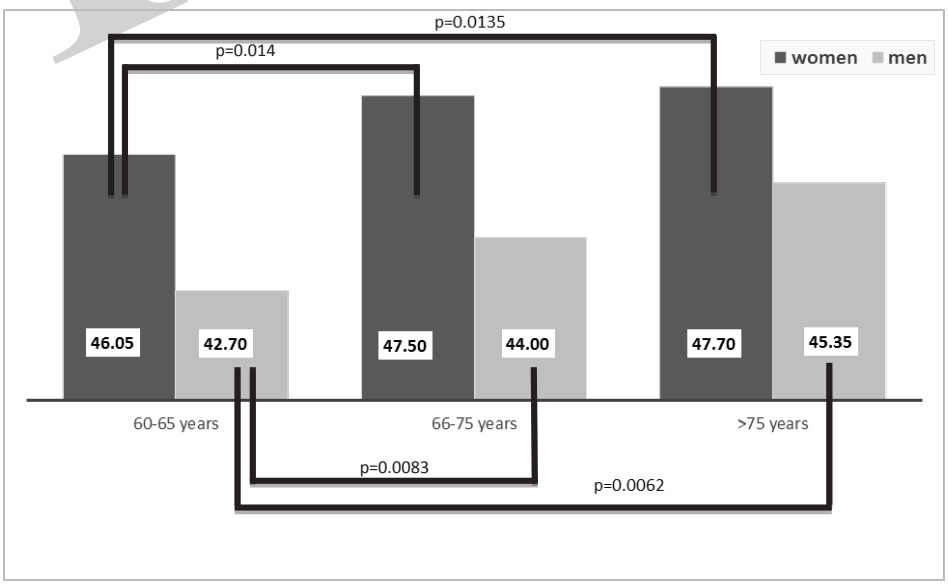

Fig. 1. *Post-hoc Tucan test for ECW/TBW [%] in women and men. Significant differences are given.*

decreases slightly over the age of 75 years. BMI alone may be an insufficient nutritional assessment method in the elderly as it may mask muscle mass loss. Progressive loss of both skeletal muscle mass and strength (sarcopenia) is an important geriatric problem that is still not well recognized in routine clinical practice (18).

The results of the body composition analysis of the healthy seniors indicate that only ECW/TBW increased significantly with age for both females (46.03% to 47.29%, p = 0.0135) and males (42.9% to 45.28%, p = 0.0083), and that this change was greater in men than in women. Lean body mass loss was higher for men and significantly decreased with age. Similar results have been shown by other studies (19, 20), which have pointed to TBW and ECW/TBW as important biomarkers for diagnosing the state of hydration and muscle strength. A valid hydration screen would enable the identification of otherwise healthy older persons who are at risk for water imbalance, and may assist in better prevention or faster treatment of dehydration.

In conclusion, we propose the measurement of ECW/TBW ratio as the first, simple, and fast indicator of water balance in older subjects. Systematic controls of this ratio by a GP or nurse may increase senior's independence, resulting in longer self-maintenance at home and reduced hospital admissions.

REFERENCES

1. Verbalis J. Disorders of body water homeostasis. Best Pract Res Clin Endocrinol Metab 2003, 17:471-503.
2. El-Sharkawy AM, Sahota O, Maughan RJ, Lobo DN. The pathophysiology of fluid and electrolyte balance in the older adult surgical patient. Clin Nutr 2014, 33:6-13.
3. Hooper L, Bunn D, Jimoh FO, Fairweather-Tait SJ. Water-loss dehydratation and aging. Mech Ageing Dev 2014; 136-137:50-58.
4. Testa G, Pavone V, Mangano S, et al. Normal nutritional components and effects of bone metabolism in prevention of osteoporosis. J Biol Regul Homeost Agents 2015; 29:729-36.
5. Faes MC, Spigt MG, Olde Rikkert MGM. Dehydration in geriatrics. Geriatr Aging 2007; 10(9):590-96.
6. Zizza CA, Ellison K, Wernette CM. Total water intakes of community-living middle-old and oldest-old adults. J Gerontol Biol Sci Med Sci 2008; 4:481-86.
7. Suliga E. Health behaviours related to the nutrition of adults and elderly people. Hygeia Public Health 2010; 45(1):44-48.
8. Lee JE, Jo IY, Lee SM, et al. Comparison of hydration and nutritional status between young and elderly hemodialysis patients through bioimpedance analysis. Clin Int Aging 2015; 10:1327-34.
9. Franco-Villoria M, Wright CM, McColl JH, et al. Assessment of adult body composition using bioelectrical impedance: comparison of researcher calculated to machine outputted values. BMJ Open 2016; 6:e008922. doi:10.1136/bmjopen-2015-008922.
10. Ritchie JD, Miller CK, Smiciklas-Wright H. Tanita foot-to-foot bioelectrical impedance analysis system validated in older adults. J Am Diet Assoc 2005; 105:1617-19.
11. Kaiser MJ, Bauer JM, Ramsch C, et al. MNA-International Group. Validation of the Mini Nutritional Assessment short-form (MNA-SF): a practical tool for identification of nutritional status. Nutr Health Aging 2009; 13:782-88.
12. Lizuka Y, Lizuka H, Mieda T, et al. Association between neck and shoulder pain, back pain, low back pain and body composition parameters among the Japanese general population. BMC Musculoskeletal Disorders 2015; 16:333-39.
13. Avantaggiato G, Bertuzzi M, Pascali V, Candotto F. Carinci. The theories of aging: reactive oxygen species and what else? J Biol Regul Homeost Agents 2015; 29(S1):156-63.
14. Zubelewicz-Szkodzińska B, Szkodziński J, Danikiewicz A, et al. Effects of simvastatin on pro-inflammatory cytokines in patients with hypercholesterolemia. Kardiol Pol 2013; 12:470-73.
15. Camina Martín MA, Silleras BD, Redondo del Río MP. Body composition analysis in older adults with dementia. Anthropometry and bioelectrical impedance analysis: a critical review. Europ J Clin Nutr 2014; 68:1228-33.
16. Gallagher D, Visser M, Sepulveda D, Pierson RN, Harris T, Heymsfield SB. How useful is body mass

index for comparison of body fatness across age, sex, and ethnic groups? Am J Epidemiol 1996; 143:228-39.
17. Müller MJ, Geisler C, Pourhassan C, Glüer CC, Bosy-Westphal A. Assessment and definition of lean body mass deficiency in the elderly. Eur J Clin Nutr2014; 68:1220-27.
18. Krzymińska-Siemaszko R, Wieczorkowska-Tobis K. Assesment of sarcopenia in elderly – a contribution of the methodology. J of Med Sciences 2012; 1:16-20.
19. Yamada M, Arai H, Nagai K, Tanaka B, et al. Development of a new fall risk assessment index for older adults. Int J Gerontol 2012;6(3):160-62.
20. Kehayias JJ, Ribeiro SM, Skahan A, Itzkowitz L, Dallal G, Rogers G, Khodeir M. Water homeostasis, frailty and cognitive function in the nursing home. J Nutr Health Aging 2012; 16(1):35-39.

LETTER TO THE EDITOR

EXPRESSIONS OF NDRG1, VEGF AND Ki-67 IN CONDYLOMA ACUMINATUM

GW. YIN, Y. GUO and B. JIN

Department of Dermatology, The First Affiliated Hospital of Zhengzhou University, Zhengzhou City, PR China

Received February 22, 2016 – Accepted June 20, 2016

The objective of this study was to explore the expressions and significance of NDRG1 (N-myc downregulated gene family 1), VEGF (vascular endothelial growth factor) and Ki-67 in lesions of Condyloma Acuminatum (CA). Immunohistochemistry was adopted to measure the expressions of NDRG1, VEGF and Ki-67 in 48 cases of CA and 18 normal skin controls. The positive rates of NDRG1, VEGF and Ki-67 were 63. 83.33% (40/48), 93.75% (45/48) and 85.42% (41/48) in the CA tissues, and 27.78% (5/18), 94.44% (17/18) and 61.11% (11/18) in the controls, respectively. The intensities of the expressions of NDRG1, VEGF and Ki-67 in CA tissues were significantly higher than those in the controls. There were significant differences both in the positive rates and the expression intensities of NDRG1, VEGF and Ki-67 between the two groups (P <0.05). The Spearman's Rank-Order Correlation analysis indicated that the expressions of NDRG1 protein and VEGF protein were positively correlated by the Spearman's Rank-Order Correlation analysis (r = 0.346, P=0.016). For the CA tissues with high expressions of NDRG1 and VEGF, NDRG1 and VEGF influenced both the occurrence and development of CA.

To the Editor,

Condyloma Acuminatum (CA) is a common sexually transmitted disease infected with human papilloma virus (HPV)(1). CA grows fast and relapses easily after treatment, and has attracted great attention due to its close relationship with the incidence of genital cancer.

In recent years, NDRG1 (N-myc downregulated gene family 1) was found to be associated with cell differentiation, and closely related to tumor occurrence, development and metastasis. NDRG1 can be induced by a variety of differentiation factors (2). VEGF (vascular endothelial growth factor) is a specific vascular regulating factor (3). Ki-67 antigen is a DNA binding protein, with molecular weight of 359kd and 320kd. Ki-67 antigen is one of the most widely used cell proliferation markers, which can accurately reflect the activity of cell proliferation. Very few researches have studied the expressions of NDRG1, VEGF and Ki-67 in CA tissues. Immunohistochemistry was applied in this study to detect the expressions of NDRG1, VEGF and K-67 in CA tissues.

MATERIALS AND METHODS

Study subjects

From August 2009 to June 2010, 48 patients (29 male, 19 female, aged 18-56 years: average 24.15±7.58 years) with CA received treatment in the dermatology department of The First Affiliated Hospital of Zhengzhou University. All the subjects gave signed informed consent

Key words: condyloma acuminatum, NDRG1, VEGF, Ki-67

Mailing address:
Dr GW. Yin,
No.1, Jianshe East Road, The First Affiliated Hospital
Zhengzhou University, Zhengzhou City,
Henan Province, China
Tell:++86 13937160980
e-mail: Tschan2015@163.com

0393-974X (2016)

DISCLOSURE: ALL AUTHORS REPORT NO CONFLICTS OF INTEREST RELEVANT TO THIS ARTICLE.

to participate in the study. The study was approved by the ethics committee of our hospital. All the patients had typical clinical manifestations, and clear diagnosis from the histopathologic examination. The disease course was 16 to 120 days, with average course of (51.29±3.23) days. The 18 male patients (aged from 18 to 28 years; average 22.3 years) with normal circumcision tissues were from the urology department of the same hospital.

Main reagents

Goat anti-human NDRG1 polyclonal antibody was provided by Santa Cruz, USA; mouse anti-human VEGF, Ki-67 ready-to-use immunohistochemistry detection kits and DAB enzyme substrates were purchased from Fujian Agent New Biological Engineering Co., Ltd.

NDRG1, VEGF and Ki - 67 expressions by immunohistochemistry method

Based on the peroxidase marked immunohistochemistry staining kit steps, all the sample slice stainings were conducted under the same conditions. Positive control group and negative control group were used. Positive control group was the known tissue section with positive staining. In the negative control group, the first antibody was replaced with PBS to incubate the tissue section.

Immunohistochemical staining results

The positive staining of NDRG1 was yellow particles, mainly in cytoplasm; VEGF positive staining was tan particles, mainly in protoplasm; Ki-67 positive staining was tan particles in nucleus. The grading standard was

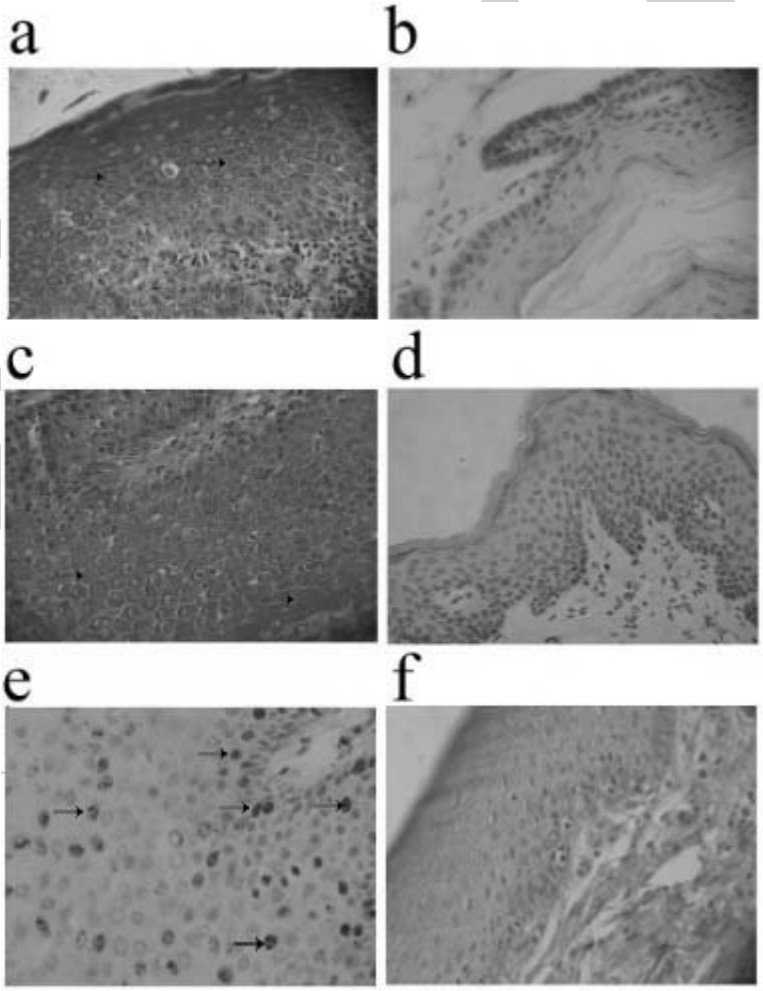

Fig. 1. *Immunohistochemistry assay results of CA tissue and normal tissue.* ***a****) NDRG1 expression in CA tissue.* ***b****) NDRG1 expression in normal foreskin tissue.* ***c****) VEGF expression in CA tissue.* ***d****) VEGF expression in normal foreskin tissue.* ***e****) Ki-67 expression in CA tissue.* ***f****) Ki-67 expression in normal tissue. DAB chromogenic, immunohistochemical SPx400*

taken as reference (4), and the samples were observed under a high magnification microscope, and the cell quantity observed was no less than 200 cells. Semi-quantitative classification scoring was based on the percentage of the positively stained cells in a tissue section and color intensity: 0 points for positively stained cell with percentage of 10% or less, 1 point for 11% ~ 25%, 2 points for 26% ~ 50%, 3 points for 51% ~ 75%, 4 points for 76% or more;

The color intensity: 0 points for no color; 1 point for light yellow; 2 points for yellow; 3 points for tan. The total points were the points of one time.

0 point for negative (-), 1~4 points for weakly positive (+), 6~8 points for positive (++), 9~12 points for strong positive (+++).

Statistical analysis

SPSS17.0 statistical software was applied for statistical analysis, with χ^2 test and Spearman's correlation test.

RESULTS

The expression of NDRG1 in CA tissues and normal foreskin tissues

Among the 48 CA tissues, 40 were with NDRG1 positive expression, and the rate was 83.33% (40/48). The positive staining was yellow and tan particles, and its expression intensity was between ++ and +++, mainly expressed in the cytoplasms or cell membranes, but mainly in cytoplasms with focal or diffuse distribution (Fig. 1A). In the 18 patients of the control group, there were 5 cases with NDRG1 positive expression, and the expression rate was 27.78% (5/18). The expression intensity mainly was between - and ++ (Fig. 1B). The positive expression rate and the positive expression intensity of the two groups had statistical significance.

VEGF expression in CA tissues and normal foreskin tissues

Among the 48 CA tissues, there were 45 cases with VEGF positive expression, mainly expressed in the cytoplasm of CA tissues, and the positive expression rate was 93.75% (45/48). The expression intensity was mainly between ++ and +++, and the positive staining was yellow-mixed tan particles. The positive cells spread in all the layers of epidermis, except for the corneous layer. The expression was more significant in the base layer and the stratum spinosum layer (Fig. 1C). In the control group, VEGF positive expression rate was 94.44% (17/18), and the expressing intensity was between + and ++ (Fig. 1D). The positive expression rate of VEGF in the two groups had no statistical significance, while the intensity of the positive expression between the two groups had statistical significance.

Ki-67 expression in CA tissues and normal epithelium tissues

There were 41 tissues with positive expression in 48 CA tissues. The positive expression rate was 85.42% (41/48), and the expression intensity was mainly between ++ and +++. The nuclei was mainly and positively stained with tan granules, and the positive cells mainly located throughout the base layer and the lower part of the stratum spinosum, and few expression on the upper of stratum spinosum and stratum granulosum (Fig. 1E). The positive rate in the normal control group was 61.11% (11/18), and the expression intensity was between - and +, which mainly located in the basal layer (Fig. 1F). The comparison difference of the positive rate was statistically significant (P <0.05), and the difference of the positive expression intensity between the two groups had statistical significance (P <0.01).

The correlation analysis between NDRG1 and VEGF expressions in CA tissues

In the 40 cases with NDRG1 protein positive expression, there were 39 cases with VEGF protein positive expression. In the 45 cases with VEGF protein positive expression, there were 39 cases with NDRG1 protein positive expression. The Spearman's Rank-Order Correlation analysis was employed to analyze the two groups (r = 0.346, P = 0.016), which indicates that there were positive correlations of the expressions of NDRG1 protein and VEGF protein

DISCUSSION

In this study, we used immunohistochemistry to measure the expressions of NDRG1,VEGF, and

Ki67 in 48 cases of CA and 18 normal skin controls.

Both the positive rates and expression intensity of NDRG1 were significantly higher in CA tissues than those in the control tissues. Although VEGF positive rate did not differ significantly between the cases and the controls, the expression intensity of VEGF was significantly higher than that in the CA group. The positive rate of Ki67, a proliferating marker, was significantly higher in the CA group. The results are consistent with other reports (7-8) that NDRG1,VEGF, and Ki67 might be related to various cancers.

These associated studies provided important clinical evidence to investigate the mechanism and therapy of CA, which is closely related to the incidence of genital cancers.

There are some limitations to this study. Firstly, the number of patients was limited and the conclusion should be further proved. Secondly, Western blotting should be used to further confirm the results.

REFERENCES

1. Partridge JM, Koutsky LA. Genital human papillomavirus infection in men. Lancet Infect Dis 2006; 6:21-23.
2. Kovacevic Z., Richardson DR. The metastasis suppressor, Ndrg-1: a new ally in the fight against cancer. Carcinogenesis 2006; 27:2355-66.
3. Bhushan M, McLaughlin B, Weiss JB. Levels of endothelial cell stimulating angiogenesis factor and vascular endothelial growth factor are elevated in psoriasis. Br J Dermatol 1999; 141:1054-60.
4. Potti A, Moazzam N, Langness E. Immunohistochemical determination of HER-2/neu,c-kit(cd117),and vascular endothelial growth factor(VEGF) overexpression in malignant melanoma. Cancer Res 2004; 130:80-86.
5. Tschan MP, Shan DJ, Laedrach J. NDRG1/2 expression is inhibited in primary acutemyeloid leukemia. Leukemia Res 2010; 24:393-98.
6. Wang WQ, Li YH, Li W. NDRG3 is an androgen regulated and prostate enriched gene that promotes in vitro and in vivo prostate cancer cell growth. Int J Cancer 2009; 124:521-30.
7. Chen B, Nelson DM, Sadovsky Y. N-myc down-regulated gene 1 modulates the response of term human trophoblasts to hypoxic injury. J Bio Chem 2006; 281:2764-72.
8. Stens S, Thomas E K, Herzog B. NDRG1 is necessary for p53-dependent apoptosis. Bio Chemistry 2004; 279:48930-40.
9. Cangul H, Salnikow K, Yee H. Enhanced expression of a novel protein in human cancer cells: a potential aid to cancer diagnosis. Cell Biol Toxicol 2002; 18:87296.
10. Chua MS, Sun H, Cheung ST. Overexpression of NDRG1 is an indicator of poor prognosis in hepatocellular carcinoma. Mod Pathol 2007; 20:76-83.
11. Ferrar N, Henzel W J. Pituitary follicular cell secrete a novel heparin- binding growth factors specific for vascular endothelial cells. Biochem Biophys Res Commun 1989; 161:851-57.
12. Endl E, Gerdes J. The Ki-67 protein: fascinating forms and an unknown function. Exp Cell Res 2000; 257:231-37.

LETTER TO THE EDITOR

EFFECT OF TUMOR NECROSIS FACTOR INDUCED PROTEIN 8 ON T-CELL-MEDIATED IMMUNITY IN MICE AFTER THERMAL INJURY

Y. XIN[1], D-H. WAN[2], X. WANG[2], X-J. GAO[2], X-J. XU[2]. X-L. JU[1] and A-M. LI[2]

[1]Department of Pediatrics, Oilu Hospital, Shandong University, Jinan, P.R. China; [2]Department of Pediatrics, Yantai Yuhuangding Hospital, Yantai, P.R. China

Received December 11, 2015 – Accepted June 10, 2016

The first two authors contributed equally to this study

Tumor necrosis factor-induced protein 8(TNFAIP8), the first identified member of the TNFAIP8 family, shares considerable sequence homology with members of this family. It is expressed in a wide variety of human normal tissues, with relatively higher levels in lymphoid tissues and placenta. The present study was designed to examine the effect of TNFAIP8 on T-cell-mediated immunity secondary to burn injury. Sixty male mice were randomly divided into four groups as follows: sham burn group, burn group, burn with TNFAIP8-siRNA transfection group, and burn with negative control transfection group, and they were sacrificed at designated time points. CD4+ T cells were isolated using MACS microbeads. T-Cell proliferation was analyzed with MTT assay, and IL-2, soluble IL-2R, IL-4, interferon-γ (IFN-γ) were determined with enzyme-linked immunosorbent assay kits. It was found that CD4+ T lymphocyte proliferative activity was significantly down-regulated when TNFAIP8 gene was silenced by siRNA in mice at 24 h post burn. Down-regulation of TNFAIP8 can significantly decrease expression levels of IL-2 and soluble IL-2R at 24 h after thermal injury. These results demonstrated that TNFAIP8 appeared to be involved in the immune regulation of CD4+ T lymphocytes, and the decreased expression of TNFAIP8 could affect T lymphocyte functions after thermal injury.

To the Editor,

Burn wound infection leads to a significant decline in total white blood cell and lymphocyte counts and induces organ injury and sepsis (1). The immune system responds to injury by rapidly producing early and late proinflammatory cytokines, and also suppressing the functions of T lymphocytes, which are effector cells, as well as modulator cells in immune response (2, 3). Severe burn injury also alters T cells by inducing an imbalance in T helper (Th) cell functions caused by a phenotypic imbalance in the regulation of Th1 and Th2 immune response. The immunological reaction mediated by Th2 cells and accompanied by apoptosis of a large number of lymphocytes might lead to a decrease in the resistance to infectious pathogens in host survival.

TNFAIP8, a 21-kDa cytosolic protein, is a member of the FLICE (caspase-8)-inhibitory family of antiapoptotic proteins (4). Expression of exogenous TNFAIP8 in cancer cells is associated with the enhanced survival and inhibition of apoptotic enzymes, caspase-8, and caspase-3 (5). TNFAIP8 protein expression was found to be significantly more decreased in tumor-infiltrating $CD4^+$T cells than in peripheral $CD4^+$T

Key words: tumor necrosis factor-a induced protein 8, T lymphocyte, burn injury, immunity

Mailing address:
Dr Xiu-li Ju,
Department of Pediatrics, Oilu Hospital,
Shandong University, No. 107, Cultural West Road
Jinan, Shandong Province, China
Tel.: +86 531 82169114 - Fax: +86 531 86922707
e-mail: xiuliju01@163.com

0393-974X (2016)

DISCLOSURE: ALL AUTHORS REPORT NO CONFLICTS OF INTEREST RELEVANT TO THIS ARTICLE.

cells (6). Down-regulation of TNFAIP8 in TNF-a-stimulated rheumatoid arthritis synovial fibroblasts causes enhanced apoptosis, and decreased proliferation (7). Here, we tested the mRNA level and protein level of TNFAIP8 in $CD4^+$ T cells in mice. *In vivo* studies were performed to examine the potential role and effect of TNFAIP8 on T-cell-mediated immunity secondary to severe burns in mice.

MATERIALS AND METHODS

All experimental manipulations were performed in accordance with the Shanghai Laboratory Animal Center of Chinese Academy of Science regulations. Male C57BL/6 mice, 8–10 weeks old, were purchased from the Shanghai Laboratory Animal Center of Chinese Academy of Science (Shanghai, China).

Medium and reagents

RPMI 1640, fetal calf serum (FCS), glutamine, penicillin, streptomycin, and HEPES were purchased from Huayasi Biotechnology Co., Beijing, China. Thiazolyl blue (MTT),Triton X-100 and ConA were purchased from Sigma, St. Louis, MO, USA. $CD4^+$T Cell Isolation Kit was purchased from Miltenyi Biotec GmbH, Bergisch Gladbach, Germany. TNFAIP8 was purchased from Sigma-Aldrich, St. Louis, MO, USA. ELISA kits of interleukin (IL)-2, IL-4, and interferon (IFN)-γ were purchased from Biosource, Worcester, MA, USA.

Animal thermal injury model

All male C57BL/6 mice had free access to water but were fasted overnight before the experiment. Mice were anesthetized with aether, and the hair on the animals' backs was removed with 20% sodium sulfide. A 30% total body surface area full-thickness skin scald was then produced by immersing the back of the animal into 94°C water for 10 s (8). Sham Sham-injured mice were subjected to all of the procedures, except the temperature of the bath was of 37°C water. Lactated Ringer solution (40 mL/kg, s.c.) was administered for initial resuscitation 6 h after injury, and, subsequently, 4 mL was administered at 12, 24 and 36 after burn injury.

Experimental design

Sixty mice were randomly divided into four groups as follows: sham injury group (15), burn group (15), burn with siRNA-TNFAIP8 treatment group (15), and burn with negative control treatment group (15). In addition, fifteen mice were taken to serve as normal controls (the main parameters determined in the current study were found to be highly consistent with those in sham-injured animals, so the results are not shown). Recombinant lentiviruses that carry the TNFAIP8 siRNA were injected intraperitoneally to mice 10 days before burn injury in the burn + siRNA-TNFAIP8 group. Animals of all groups were sacrificed at 24 h after burn injury.

Isolation of splenic $CD4^+$ T cells

Spleens were teased in 5 mL RPMI 1640. Cells were dispersed through a 30-2m stainless steel mesh and collected after centrifugation at 300 x g for 10 min, and they were resuspended in 4 mL RPMI 1640. Mononuclear cells were then obtained, and $CD4^+$ T cells were isolated from them with $CD4^+$ T cell Isolation Kit. Total $CD4^+$ T cells with concanavalin A (Con A) stimulation were cultured for 18 h at 37°C.

Determination of mRNA expression

The mRNA expressions of TNFAIP8, IL-2, IL2R were determined by real-time, quantitative reverse transcription-polymerase chain reaction(RT-PCR). Total RNA was extracted from the splenic $CD4^+$ T cells using TRIZOL kits (9, 10). First-strand cDNA was synthesized using oligo-dT primer and AMV reverse transcriptase. The generated cDNA was then added to the reaction mixture with a final concentration of 0.2 2M of specific primers. Primers for TNFAIP8 were forward 5'- CCCAGGGAAGTGGCTACAGA-3' and reverse 5'-GCCTCCTTCTTGTTCTGGGT -3'. Primers for IL-2 were forward 5'- ACATTGACACTTGTGCTCCTTG-3' and reverse 5'- TCCTGTAATTCTCCATCCTGCT -3'. Primers for IL-2R were forward 5'-ATGGAGCCACGCTTGCTGATG-3' and reverse 5'- TAGGATGGTGCCGTTCTTGTAGG -3'. Primers for GAPDH were forward 5'-TGATGACATCAAGAAGGTGGTGAA-3' and reverse 5'- TCCTTGGAGGCCATGTAGGCCAT -3'. The thermal cycling conditions were as follows: 95°C for 15 min, followed by 37 cycles of denaturation, annealing and amplification (94°C for 30 s, 60°C for 50 s, 72°C for 30 s), and a final extension period of 5 min at 72°C. All samples

were run in quadruplicates. The level of glyceraldehyde-3-phosphate dehydrogenase (GAPDH) mRNA was also designed as an internal control for each sample.

Western blot analysis

TNFAIP8 was analyzed by Western blotting. $CD4^+$ T cells were washed with ice-cold PBS, suspended in the lysis buffer containing 1 mM sodium orthovanadate supplemented with protease inhibitor mixture, and then centrifuged at 12,000 × g for 30 min at 4°C. Protein levels were quantified by using bicinchoninic acid protein assay kit. Samples were then concentrated 15-fold with Centricon YM-30 (Millipore) and separated on 10% sodium dodecyl sulfate-polyacrylamide gels. Gel electrophoresis was performed at 80 V for 40 min, followed by 110 V for 2 h. Protein was transferred to immunoblot poly (vinylidene difluoride) membrane. After blocking with 10% skim milk overnight at 4°C, the membrane was incubated for 4 h at room temperature with anti-TNFAIP8 polyclonal antibodies and secondary Ab for 1 h. Finally, the membrane was washed three times, and developed by using the ECL plus chemiluminescence kit.

RNA interference

Small interference RNA to TNFAIP8 (siRNA) was synthesized by Genchem Co., Shanghai, China. The DNA target sequence for siRNA- TNFAIP8 was 5'-GCCTTGTACAATCCCTTTGGA-3', and the scrambled control RNA was 5'-TTCTCCGAACGTGTCACGT-3'. Transfection strictly followed the manufacturer's instructions. Male mice were individually injected with 3×107 TU lentivirous vector via the tail vein, TNFAIP8 expression was determined on day 10 after recombinant lentiviruses were injected intraperitoneally to mice.

T-cell proliferation assay

$CD4^+$ T cells were suspended in RPMI 1640 culture medium supplemented with 10% fetal calf serum (FCS), and then they were plated in 96-well plates at 1×10^5 cells/well. $CD4^+$ T cells were treated with or without 5 μg/mL Con A for 68 h at 37°C in 5% CO2/100% humidified air. Thiazolyl blue (MTT) was added, and incubation was continued for 4 h, and then 100 μg acid isopropanol was added to dissolve the MTT crystals. The suspension of the crystals was repeatedly blown with a pipette, the optical density was measured by the use of a microplate reader at the wavelength of 540 nm.

Cytokine ELISA measurement

IL-2, soluble IL-2R (sIL-2R), IL-4, and IFN-γ levels in serum and culture supernatant were measured by commercially available ELISA kits for mice. ELISA assays were performed strictly following the protocols provided by the manufacturer.

Statistical analysis

Data were expressed as mean ± standard deviation (SD). Statistical evaluation of the continuous data was performed by one-way ANOVA, and individual group means were then compared with Student's paired *t*-test. All statistical tests were two sided and a P value of 0.05 or less was considered to indicate statistical significance.

RESULTS

$TNFAIP8$ expression in $CD4^+$ T cells

Gene expression of TNFAIP8 in $CD4^+$ T cells was assessed by RT-PCR, with GAPDH as the internal standard. A band of the size of 182 bp was noted as expected (Fig. 1B). The expression of TNFAIP8 mRNA in macrophages, which is known to express a high level of TNFAIP8, was determined as a positive control. To further confirm the expression of TNFAIP8, it was measured at the protein level by Western blot analysis using the specific TNFAIP8 antibody, and a clear band with a molecular mass of approximately 21 kDa from either macrophages or $CD4^+$ T cells was found. The latter was used as the positive control (Fig. 1A).

Splenic T-lymphocyte proliferation

In the current study, TNFAIP8 gene silenced by siRNA was used in this experiment (Fig. 1C). By Western blot analysis, TNFAIP8 protein level was markedly decreased in lentivirus-RNAi- TNFAIP8 transfected $CD4^+$ T cells compared with the scramble RNA (negative control) transfection group (Fig. 1C, $P<0.05$). The proliferative activities of $CD4^+$ T cells in reponse to ConA in the burn injury group were significantly decreased at 24, 48 h postburn in comparison to those in the sham injury group ($P<0.05$). To investigate the effect of TNFAIP8 on the decreased cell proliferation after thermal injury, we tested the effect of siRNA silenced TNFAIP8

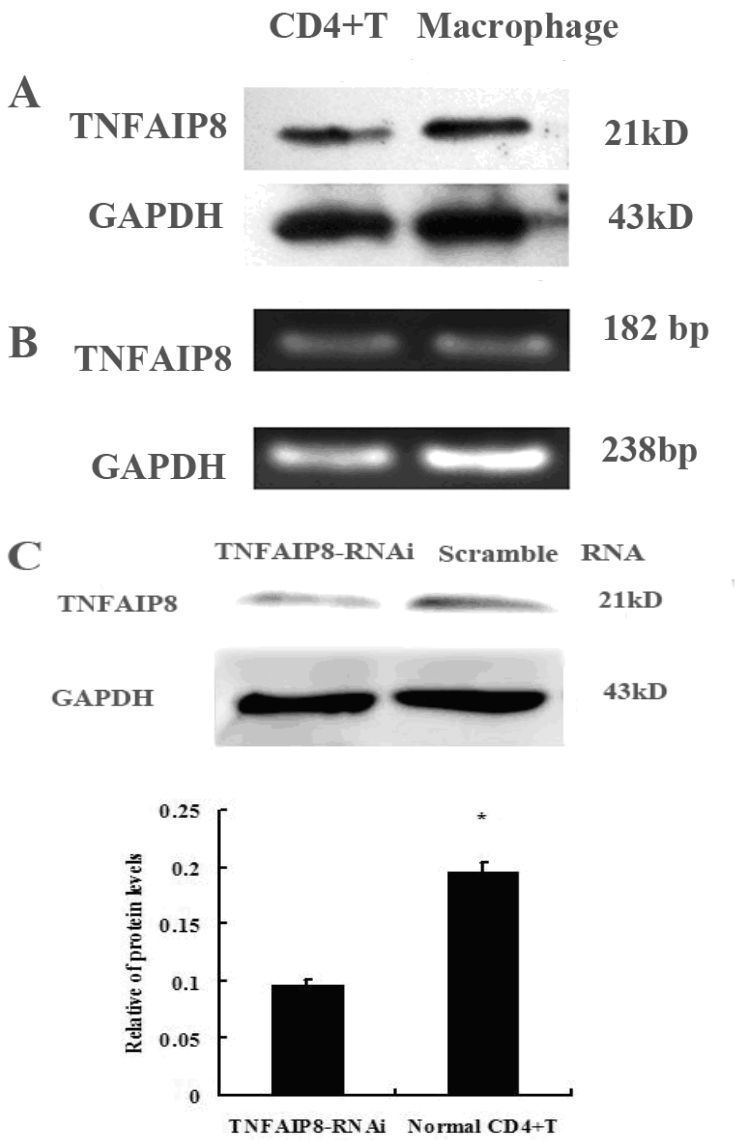

Fig. 1. *TNFAIP8 expression in CD4⁺ T cells and relative abundance of TNFAIP8 protein levels in vivo.* ***A****) Protein levels of TNFAIP8 in CD4⁺ T cells were determined by Western blot (n=5, in each group).* ***B****) TNFAIP8 mRNA expression was measured by RT-PCR analysis in CD4⁺ T cells and macrophages. Expression of GAPDH served as an internal control. (n=5, in each group).* ***C****) Representative Western blot gel showed relative abundance of TNFAIP8 protein levels in DCs (normal), siRNA- TNFAIP8 transfected CD4⁺ T cells (n=5, in each group). Compared with the normal controls, *P<0.05.*

gene *in vivo* at 24 h. As shown in Fig. 2A, the proliferative response was markedly decreased in the burn with TNFAIP8 gene knockdown group ($P < 0.05$), indicating that TNFAIP8 might be closely related to the immune functions of $CD4^+$ T cells.

Production of IL-2

To evaluate the activity of splenic T cells, we assayed the levels of IL-2 in T-cell culture supernatant or serum and also IL-2 mRNA expression of splenic T cells. As shown in Fig. 2B, we found that production and mRNA expression was suppressed to a certain extent at 24 h after burn injury. IL-2 production and mRNA expression were decreased after TNFAIP8 gene was silenced by lentivirus-RNA-TNFAIP8 transfection *in vivo* when compared with the thermal

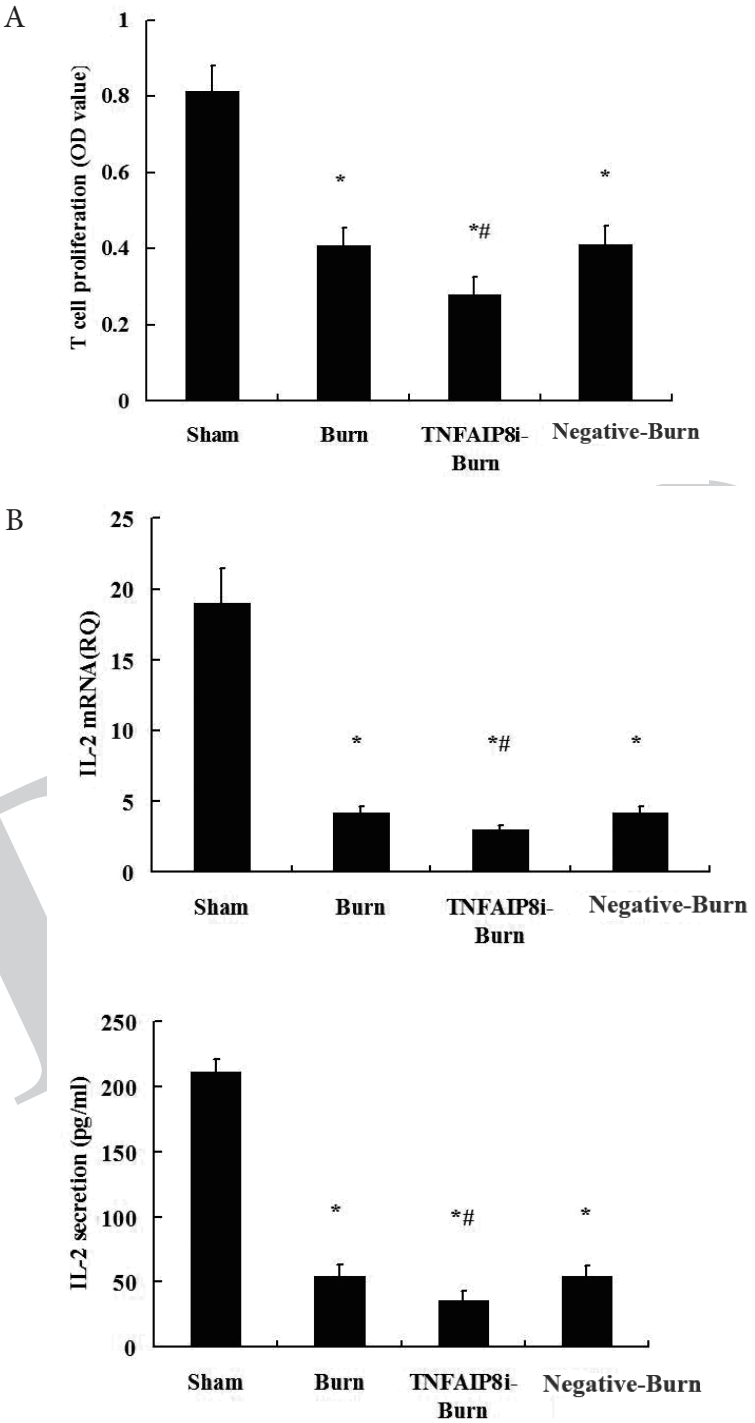

Fig. 2. *Splenic T-lymphocyte proliferation using MTT assay for T-cell proliferation and IL-2 production (n=15, in each group).* ***A****) T-Cell proliferative activity in response to Con A was significantly suppressed at 24 h after thermal injury compared with that in sham-injured group. TNFAIP8 knockdown can markedly suppress T-cell proliferative activity after thermal injury.* ***B****) Enzyme-linked immunosorbent assay analysis for IL-2 was used in the present study. Levels of IL-2 in incubation supernatant of $CD4^+$ T cells were significantly decreased in mice subjected to thermal injury compared with sham injury. TNFAIP8 knockdown can aggravate the lower levels of IL-2 in the supernatant after thermal injury. Statistical significance:*$P<0.05$ as thermal injury group vs sham group. #$P<0.05$ as thermal injury with siRNA- TNFAIP8 transfection group vs thermal injury group.*

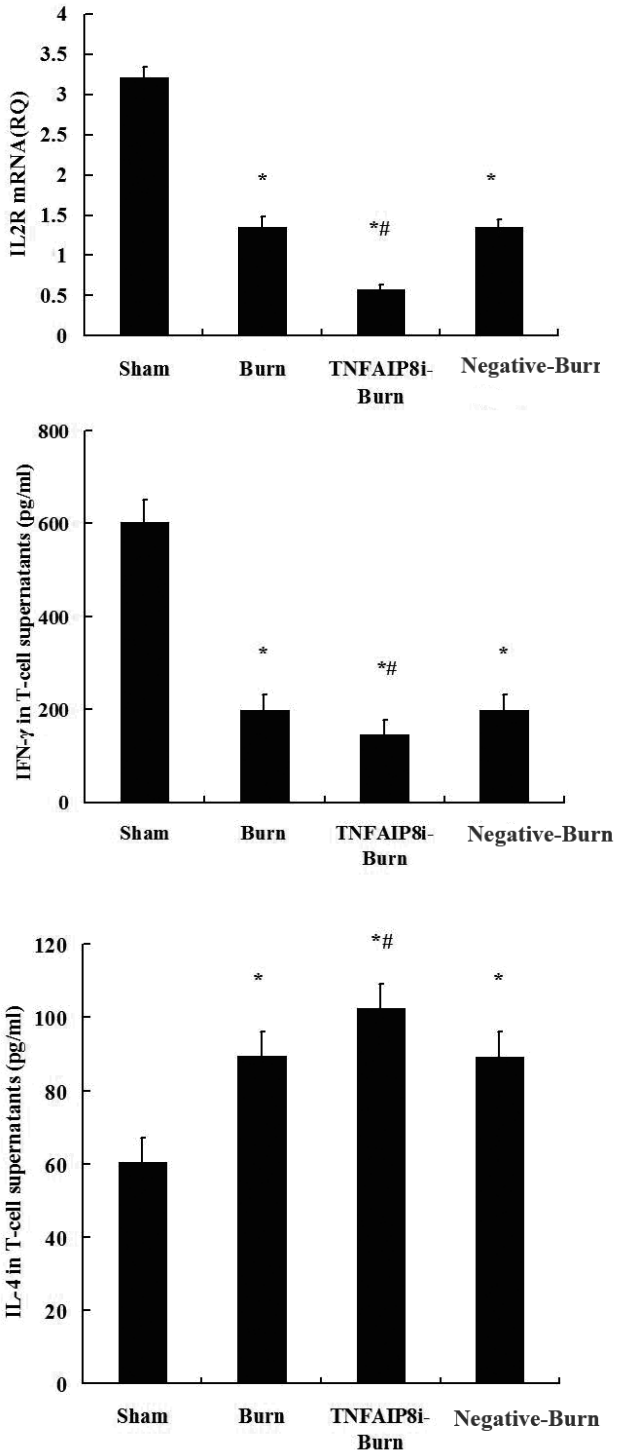

Fig. 3. *IL-2R expression and polarization of T cells (n=15, in each group). **A)** RT-PCR analysis was used for mRNA expression of IL-2R. IL-2R mRNA expression of T cells was significantly lower at 24 h after thermal injury, whereas, silence of TNFAIP8 expression could result in aggravated suppression of IL-2Rα expression in vivo. **B)** Polarization of T cells. Enzyme-linked immunosorbent assay analysis was used to determine IFN-γ and IL-4 levels in culture supernatants of T cells. After thermal injury, IL-4 levels produced by T-cell were markedly elevated, whereas IFN-γ levels were markedly decreased. Silence of TNFAIP8 expression in mice at 24 h after thermal injury significantly decreased the levels of IFN-γ and increased the levels of IL-4 compared with those in the thermal injury group. Statistical significance: *P<0.05 as thermal injury group vs sham group. #P<0.05 as thermal injury with siRNA- TNFAIP8 transfection group vs thermal injury group.*

injury group, whereas no significant difference was found in thermal injury with the negative control transfection group or thermal injury group ($p>0.05$).

IL-2R expression

To test the activation of T cells through self-stimulation, we determined the IL-2R expression on T cells in response to stimulation with Con A. As shown in Fig. 3A, IL-2Rα expression on splenic T cells was significantly lower in the thermal group than in the sham group at 24 h after burn injury ($P < 0.05$). Similarly, the expression of IL-2R mRNA in T cells was significantly decreased in the burn group compared with the sham group at 24 h after thermal injury ($P < 0.05$). The mRNA expressions of IL-2R in $CD4^+$ T cells were markedly down-regulated after TNFAIP8 was silenced with siRNA when compared with the burn injury group and negative control transfection group at 24 h after thermal injury ($P < 0.05$).

Polarization of T-lymphocyte cells

It is well known that TH1 cells produce IFN-γ and TH2 cells produce IL-4; in this study, polarization of naïve T-lymphocyte cells was determined by these two cytokines produced by $CD4^+$ T cells. As shown in Fig. 3B, the levels of IFN-γ in T-cell supernatants were significantly decreased, and the levels of IL-4 were markedly increased at 24 h after thermal injury ($P < 0.05$), indicating that a Th2 cytokine profile with increased production of IL-4 was found in the thermal injury group. However, TNFAIP8 knockdown markedly promoted the decrease in IFN-γ ($P < 0.05$) and increase in IL-4 ($P < 0.05$) in supernatants of culture of T cells after thermal injury.

DISCUSSION

During experimental and clinical sepsis, T cells are critical cellular components of immunity and are essential for an effective immune response to acute insult or septic challenge (11-14). In the present study, it was shown that the proliferative response of splenic T cells was inhibited at 24 h after thermal injury, thus splenic T lymphocyte proliferative activity in the down-regulated expression of TNFAIP8 group at 24 h after thermal injury was significantly lower than that in the thermal injury group. Furthermore, we determined levels of IL-2 secreted by $CD4^+$ T cells. IL-2 production and mRNA expression were markedly decreased in thermal-injured mice compared with those of sham-injured mice. However, the suppression can be aggravated by TNFAIP8 gene knockdown at 24 h after thermal injury. Moreover, IL-2 sensitivity is controlled by IL-2Rα, which is a critical determinant of T-cell proliferation (15-17). In the current study, silence of TNFAIP8 expression could have resulted in aggravated suppression of IL-2Rα expression *in vivo*. In our *in vivo* study, silence of TNFAIP8 expression in mice at 24 h after thermal injury significantly decreased the levels of Th1 cytokine (IFN-γ) and increased the levels of Th2 cytokine (IL-4) compared with those in the thermal injury group.

In summary, our data indicate that silence TNFAIP8 expression can significantly down-regulate IL-2-dependent T-cell proliferation and promote naive T cells to shift to TH2. TNFAIP8 might influence the immune functions of splenic T lymphocytes in mice and have a protective effect after thermal injury. Nevertheless, further studies regarding the precise mechanism of its action are merited.

ACKNOWLEDGEMENTS

This work was supported by grants from Projects of Science and Technology Development program in Yantai (2014WS006).

REFERENCES

1. Patil NK, Luan L, Bohannon JK, Guo Y, Hernandez A, Fensterheim B, Sherwood ER. IL-15 Superagonist expands mCD8+ T, NK and NKT cells after burn injury but fails to improve outcome during burn wound infection. PLoS One 2016; 11:e0148452.
2. Zu H, Li Q, Huang P. Expression of Treg subsets on intestinal T cell immunity and endotoxin translocation in porcine sepsis after severe burns. Cell Biochem Biophys 2014; 70:1699-704.
3. Li X, Rendon JL, Choudhry MA. T cell IFN-γ

suppression following alcohol and burn injury is independent of miRNA155. PLoS One 2014; 9:e105314.
4. 4.You Z, Ouyang H, Lopatin D, Polver PJ, Wang CY. Nuclear factor-kappa B-inducible death effector domain-containing protein suppresses tumor necrosis factor-mediated apoptosis by inhibiting caspase-8 activity. J Biol Chem 2001; 276:26398-404.
5. Zhang HG, Hyde K, Page GP, et al. Novel tumor necrosis factor alpha-regulated genes in rheumatoid arthritis. Arthritis Rheum 2004; 50:420-31.
6. Wang L, Song Y, Men X. Variance of TNFAIP8 expression between tumor tissues and tumor-infiltrating CD4+ and CD8+ T cells in non-small cell lung cancer. Tumour Biol 2014; 35: 2319-25.
7. Kumar D, Gokhale P, Broustas C, Chakravarty D, Ahmad I, Kasid U. Expression of SCC-S2, an antiapoptotic molecule, correlates with enhanced proliferation and tumorigenicity of MDA-MB 435 cells. Oncogene 2004; 23:612-16.
8. Zhang LT, Yao YM, Dong YQ, Dong N, Yu Y, Sheng ZY. Relationship between high-mobility group box 1 protein release and T-cell suppression in rats after thermal injury. Shock 2008; 30:449-55.
9. Huang LF, Yao YM, Zhang LT, Dong N, Yu Y, Sheng ZY. The effect of high-mobility group box 1 protein on activity of regulatory T cells after thermal injury in rats. Shock 2010; 31:322-29.
10. Zhang Y, Yao YM, Huang LF, Dong N, Yu Y, Sheng ZY. The potential effect and mechanism of high-mobility group box 1 protein on regulatory T cell-mediated immunosuppression. J Interferon Cytokine Res 2011; 31:249-57.
11. Zhang C, Chakravarty D, Sakabe I, Mewani RR, Boudreau HE, Kumar D, Ahmad I, Kasid UN. Role of SCC-S2 in experimental metastasis and modulation of VEGFR-2, MMP-1, and MMP-9 expression. Mol Ther 2006; 13:947-55.
12. Hou YC, Wu JM, Wang MY, Wu MH, Chen KY, Yeh SL, Lin MT. Modulatory Effects of astragalus polysaccharides on T-cell polarization in mice with polymicrobial sepsis. Mediators Inflamm 2015; 2015:826319.
13. Zhu M, Liang Z, Wang T, Chen R, Wang G, Ji Y. Th1/Th2/Th17 cells imbalance in patients with asthma with and without psychological symptoms. Allergy Asthma Proc 2016; 37:148-56.
14. Mao M, Qian Y, Sun J. Morphine suppresses T helper lymphocyte differentiation to Th1 type through PI3K/AKT pathway. Inflammation 2016; 39:813-21.
15. Su EW, Moore CJ, Suriano S, et al. IL-2Rα mediates temporal regulation of IL-2 signaling and enhances immunotherapy. Sci Transl Med 2015; 7:311ra170.
16. Ray JP, Staron MM, Shyer JA, et al. The Interleukin-2-mTORc1 kinase axis defines the signaling, differentiation, and metabolism of T helper 1 and follicular B helper T cells. Immunity 2015; 43:690-702.
17. Nakase K, Kita K, Kyo T, Ueda T, Tanaka I, Katayama N. Prognostic relevance of cytokine receptor expression in acute myeloid leukemia: Interleukin-2 receptor α-chain (CD25) expression predicts a poor prognosis. PLoS One 2015; 10:e0128998.

LETTER TO THE EDITOR

PHYTOPHARMACOLOGY OF *TRIBULUS TERRESTRIS*

M. SHAHID[1], M. RIAZ[1], M.M.A. TALPUR[2] and T. PIRZADA[2]

[1]Department of Biochemistry, University of Agriculture, Faisalabad, Pakistan; [2]Institute of Chemistry, Shah Abdul Latif University, Khairpur, Sindh, Pakistan

Received April 13, 2016 – Accepted June 20, 2016

***Tribulus terrestris* is an annual herb which belongs to the *Zygophyllaceae* family. This plant has been used in traditional medicine for the treatment of various diseases for hundreds of decades. The main active phytoconstituents of this plant include flavonoids, alkaloids, saponins, lignin, amides, and glycosides. The plant parts have different pharmacological activities including aphrodisiac, antiinflammatory, antimicrobial and antioxidant potential. *T. terrestris* is most often used for infertility and loss of libido. It has potential application as immunomodulatory, hepatoprotective, hypolipidemic, anthelmintic and anticarcinogenic activities. The aim of the present article is to create a database for further investigation of the phytopharmacological properties of this plant to promote research. This study will definitely help to confirm its traditional use along with its value-added utility, eventually leading to higher revenues from the plant.**

To the Editor,

Tribullus terrestris is a natural herb which belongs to the *zygophyllaceae* plant family. The genus *Tribulus* L. is an annual herb consisting of 25 species worldwide and is characterized by spiny mericarps in the fruit (1, 2). *T. terrestris* is a well-known member of the genus *tribulus* plant found in many warm regions, mostly in many parts of Pakistan, Iran, China, India and Korea (3).

Phytochemical constituents

Biologically active ingredients of *Tribulus terrestris* include saponins, flavonoids, glycosides, phytosterols, alkaloids (4). Gas chromatography-mass spectrometry (GC-MS) analysis revealed the presence of α-amyrin as the major constituent and 3,7,11,15-tetramethyl-2-hexadecen-1-ol, *n*-hexadecadienoic acid, hexadecadienoic acid ethyl ester, phytol, 9,12-octadecadienoic acid, 9,12,15-octadecatrienoic acid, and 1,2-benzenedicarboxylic acid disoctyl ester as minor (5). Wu et al. (4) characterized the active ingredients, such as terrestribisamide, *Tribulus*terine, and 25R-spirost-4-en-3, along with *N*-*p*-coumaroyltyramine, hecogenin, terrestriamide, xanthosine, aurantiamide acetate, fatty acid ester, vanillin, ferulic acid, *p*-hydroxybenzoic acid, and β-sitosterol, from the fruits of the *T. terrestris* plant. Chemical structures of some phyto-constituents of *T. terrestris* are shown in Fig. 1.

Different biological/pharmacological activities profile of *T. terrestris* reported in previous studies along with their findings are shown in Table 1.

Antioxidant activity

The promising natural anti-oxidant agents are medicinal plants containing a variety of bioactive

Key words: Tribulus, phytoconstituents, aphrodisiac, immunomodulatory

Mailing address:
Dr Muhammad Riaz,
Department of Biochemistry,
University of Agriculture,
Faisalabad, Pakistan
e-mail: riazmlt786@gmail.com

0393-974X (2016)

Table I. *Different biological activity profile of Tribulus terrestris.*

Plant parts used	Doses	Animal model	Results	Ref.
Aerial part (leaves, stems and flowers) extracted in methanol	250 mg/kg	Rabbits (1000g) for anti-hyperglycemic activity	Extract showed no toxic symptoms and lowered fasting blood glucose comparable to that of glibenclamide	16
Aqueous Plant extract	5mg/kg daily	Male wistar rats (250-350 g)	*T. terrestris* extract produces significant aphrodisiac effects and increases Testosterone levels in males.	17
Methanolic extract of aerial parts	250mg/kg	Rabbits	Antihyperglycemic activity in glucose loaded normal rabbits.	16
Alcoholic extracts of aerial parts and fruits	12.5 mg /kg	Wistar albino rats (200-250g)	Significant increase in the level of free serum testosterone was observed.	18
Aqueous fruit extract	100 and 200 mg/kg	Swiss white mice (16-19 gm)	Significant increase in diameter of mature follicles, number of growing follicles, endometrial lining cells height and diameter of endometrial glands.	19
Aqueous plant extract	70 mg/kg	Adult albino rats	Extract showed statistically significant increase in mean body and paired testes weight.	20

constituents, principally flavonoids and polyphenols (6-7). Wu et al. (4) reported that the main flavonoids in *T. terrestris* are approximately 1.5 times higher than main saponins content.

Antimicrobial activities

Many microorganisms are known for their resistance against the most commonly used antibiotics. Soleimanpour et al. (8) reported good antibacterial activity of ethanolic extract of *T. terrestris* against *Streptococcus sanguis, Streptococcus mutans, Staphylococcus aureus, Escherichia coli* and *Enterococcus faecalis*.

Aphrodisiac potential

T. terrestris is reported as a natural stimulant of the pituitary gland to secret leutinizing hormone (LH), leading to testosterone production (9). Significant increase in prostate weight and ICP was observed in castrated rats treated with either testosterone or *T. terrestris* extract (10). Singh et al. (11) reported a dose-dependent improvement in sexual behaviour and significant increase in serum testosterone level in males treated with *T. terrestris* extract.

Anti-inflammatory activity

Oh et al. (12) reported that *T. terrestris* ethanolic extract inhibits the mediator's expression accompanying inflammation and inflammatory cytokine expression.

Hepatoprotective effect

A large number of herbal drugs have been found with promising hepatoprotective activities. *T. terrestris* (250 mg/kg) extract displayed a remarkable hepatoprotective potential against acetaminophen-induced hepatotoxicity in *Oreochromis mossambicus* fish (13).

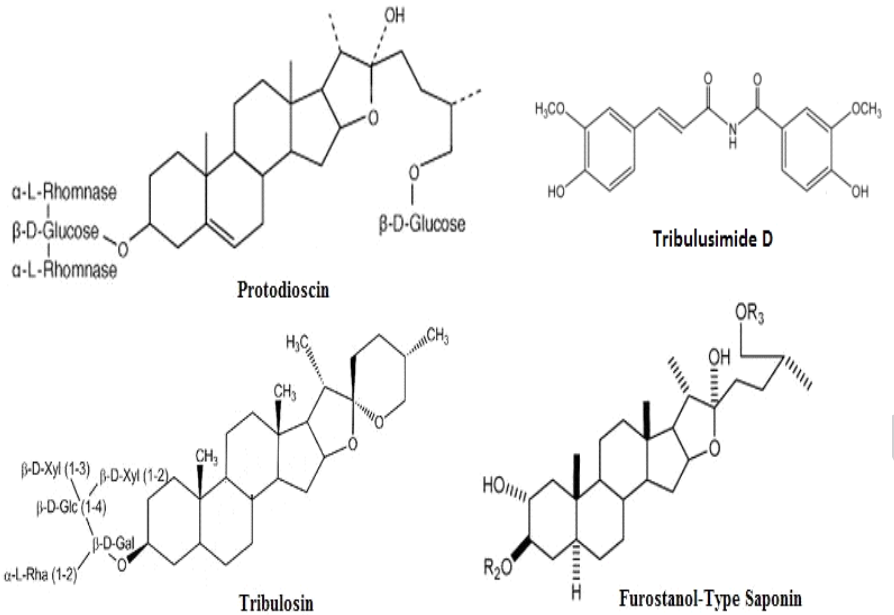

Fig. 1. *Chemical structures of some phyto-constituents of T. terrestris.*

Anti-hypertensive activity

Sharifi et al. (14) found decreased activity of ACE in tissues, especially in kidneys. ACE converts angiotensin I to angiotensin II causing constriction of blood vessels leading to increased blood pressure.

Immunomodulatory activity

Tilwari et al. (15) in their study reported significant dose-dependent immunostimulatory activity of *T. terrestris* extracts.

CONCLUSION

Tribulus terrestris extracts are being extensively used as traditional medicines, in several countries including Pakistan, India and China, for the treatment of sexual dysfunction, libido, nephrotoxicity and inflammatory diseases. The literature reports that the plant has tremendous pharmacological activities including antioxidant, antimicrobial, aphrodisiac and immunomodulatory potential. There is a great need to explore the medicinal properties of novel compounds, and their translational studies should also be documented at molecular level in order to understand the efficacy and mechanism of action against various disorders so that potential herbal formulations can be converted into prescribed drugs.

REFERENCES

1. Mitra N, Mohammad-Mehdi D, Reza ZM. Tribulus terrestris L. (Zygophyllaceae) flavonoid compounds. Int J Mod Botany 2012; 2(3):35-39.
2. Hammoda HM, Ghazy NM, Harraz FM, Radwan MM, ElSohly MA, Abdallah II. Chemical constituents from Tribulus terrestris and screening of their antioxidant activity. Phytochemistry. 2013; 92:153-59.
3. Aslani MR, Movassaghi AR, Mohri M, Ebrahim-Pour V, Mohebi A. Experimental Tribulus terrestris poisoning in goats. Small Ruminant Res 2004; 51(3):261-67.
4. Wu TS, Shi LS, Kuo SC. Alkaloids and other constituents from Tribulus terrestris. Phytochemistry 1999; 50(8):1411-15.
5. Abirami P, Rajendran A. GC-MS Analysis of Tribulus terrestris. Asian J Plant Sci Res 2011; 1(4):13-16.
6. Sebai H, Selmi S, Rtibi K, Souli A, Gharbi N, Sakly M. Lavender (Lavandula stoechas L.) essential

oils attenuate hyperglycemia and protect against oxidative stress in alloxan-induced diabetic rats. Lipid Health Dis 2013; 12(1):1.
7. Shalaby MA, Hammouda AAEK. Assessment of protective and anti-oxidant properties of Tribulus terrestris fruits against testicular toxicity in rats. J Intercult Ethnopharmacol 2014; 3(3):113.
8. Soleimanpour S, Sedighinia FS, Afshar AS, Zarif R, Ghazvini K. Antibacterial activity of Tribulus terrestris and its synergistic effect with Capsella bursa-pastoris and Glycyrrhiza glabra against oral pathogens: an in-vitro study. Avicenna J Phytomed 2015; 5(3):210.
9. Neychev V, Mitev V. Pro-sexual and androgen enhancing effects of Tribulus terrestris L.: fact or fiction. J Ethnopharmac 2016; 179:345-55.
10. Gauthaman K, Adaikan P, Prasad R. Aphrodisiac properties of Tribulus terrestris extract (Protodioscin) in normal and castrated rats. Life Sci 2002; 71(12):1385-96.
11. Singh S, Nair V, Gupta YK. Evaluation of the aphrodisiac activity of Tribulus terrestris Linn. in sexually sluggish male albino rats. J Pharmacol Pharmacotherapeut 2012; 3(1):43.
12. Oh JS, Baik SH, Ahn EK, Jeong W, Hong SS. Anti-inflammatory activity of Tribulus terrestris in RAW264. 7 Cells. J Immunol 2012; 188(Meeting Abstracts 1):54.2.
13. Kavitha P, Ramesh R, Bupesh G, Stalin A, Subramanian P. Hepatoprotective activity of Tribulus terrestris extract against acetaminophen-induced toxicity in a freshwater fish (Oreochromis mossambicus). In Vitro Cell Dev Biol Anim 2011; 47(10):698-706.
14. Sharifi AM, Darabi R, Akbarloo N. Study of antihypertensive mechanism of Tribulus terrestris in 2K1C hypertensive rats: role of tissue ACE activity. Life Sci 2003; 73(23):2963-71.
15. Tilwari A, Shukla N, Devi PU. Effect of five medicinal plants used in Indian system of medicines on immune function in Wistar rats. African J Biotechnol 2013; 10(73):16637-45.
16. El-Shaibany A, Molham AH, Al-Tahami B, Al-Massarani S. Anti-hyperglycaemic activity of Tribulus terrestris L aerial part extract in glucose-loaded normal rabbits. Tropic J Pharmaceut Res 2016; 14(12):2263-68.
17. Elahi RK, Asl S, Shahian F. Study on the effects of various doses of Tribulus terrestris extract on epididymal sperm morphology and count in rat. Glob Veterin 2013; 10:13-17.
18. El-Tantawy WH, Temraz A, El-Gindi OD. Free serum testosterone level in male rats treated with Tribulus alatus extracts. International Braz J Urol 2007; 33(4):554-59.
19. Adaay M, Mosa A. Evaluation of the effect of aqueous extract of Tribulus terrestris on some reproductive parameters in female mice. MHJ Mater Environ Sci 2012; 3(6):1153-62.
20. Bashir A, Tahir M, Samee W, Munir B. Effects of Tribulus terrestris on testicular development of immature albino rats. Biomedica 2009; 25(1):63-68.

LETTER TO THE EDITOR

EFFECTS OF 10-HYDROXYCAMPTOTHECIN ON DIFFERENTIATION OF RAW264.7 CELLS INTO OSTEOCLASTS

M. ZHANG[1], Y. WANG[1], X.L. SUN[2], L.L. REN[1], L.J. ZHANG[1] and H.Q. LU[1]

[1]Department of Rheumatism and Immunology, the Fifth Affiliated Hospital of Zhengzhou University, Zhengzhou, China; [2]Department of Rheumatism and Immunology, Peking University People's Hospital, Beijing, China

Received April 19, 2016 – Accepted June 27, 2016

This study was designed to investigate the effect of 10-hydroxycamptothecin (10-HCPT) on osteoclast formation. RAW264.7 cells were cultured *in vitro* with 100 ng/ml receptor activator for nuclear factor-κ B ligand (RANKL) and 30 ng/ml recombinant macrophage colony stimulating factor (M-CSF), and 10-HCPT with different solubilities were added. After five-day cultivation, tartrate-resistant acid phosphatase (TRAP) staining was used to observe the number of osteoclasts. mRNA expression of osteoclast-specific genes, such as TRAP, cathepsin K (CTSK) and matrix metalloproteinase protease 9 (MMP-9), was detected by real-time Polymerase Chain Reaction (PCR). The effect of 10-HCPT on the proliferation activity of RAW264.7 cells was detected using Cell Counting Kit-8 (CCK-8). CCK-8 detection showed that 10-HCPT with a certain concentration (1 ng/ml to 5 ng/ml) had no effect on cell proliferation (P>0.05); 10-HCPT could inhibit the generation of osteoclasts. With the increase of the concentration of 10-HCPT, the number of osteoclasts generated from cells cultured with 10-HCPT [1 ng/ml (86±11.14), 2 ng/ml (66.67±7.51), 5 ng/ml (27.67±6.51)] was much lower than that of the control group (145±8.19), and the difference was statistically significant (all P=0, P<0.05); mRNA expression of osteoclast-specific gene TRAP [1 ng/ml (24.38±0.68), 2 ng/ml (20.09±1.86), 5 ng/ml (6.23±0.53)], CTSK [1 ng/ml (10.08±0.81), 2 ng/ml (7.30±0.30), 5 ng/ml (3.20±0.56)] and MMP-9 [1 ng/ml (43.54±6.96), 2 ng/ml (28.28±5.83), 5 ng/ml (11.07±2.53)] was much lower than that of the groups added with RANKL and M-CSF only (all P=0, P<0.05), and with the increase of concentration of 10-HCPT, the expression of osteoclast-specific genes showed a decreasing tendency. All the findings suggest that 10-HCPT can inhibit the formation of osteoclasts by reducing the expression of osteoclast-specific genes such as TRAP, CTSK and MMP-9.

To the Editor,

Rheumatiod arthritis (RA) is an autoimmune disease involving surrounding joints; chronic inflammation causes damage to cartilage and bone and then induces joint deformity. Damage of joint is a key factor for joint deformity, and osteoclast is one of the key cells inducing bone damage (1, 2).

10-hydroxycamptothecin (10-HCPT) originated from *Camptotheca acuminata Decne* has been successfully applied for preventing and treating some tumors. Some studies found that the anti-tumor effect of 10-HCPT is associated with topoisomerase I (Topo-I). DNA-Topo which is extensively distributed in the biological world can

Key words: 10-hydroxycamptothecin, RAW 264.7, osteoclast, rheumatoid arthritis

Mailing address:
Dr Yan Wang,
No. 3 Front Kangfu Street,
Department of Rheumatology and Immunology,
the Fifth Affiliated Hospital of Zhengzhou University,
Zhengzhou, Henan, China
e-mail: wangyanwyan@126.com

0393-974X (2016)

change the spatial structure of DNA, regulate the dynamic change of DNA steric configuration, and directly participate in and/or affect the replication and transcription of DNA. A relatively stable ternary complex forms when 10-HCPT combines with the compound of Topo-I and DNA through the hydrophobic interaction between hydrogen bond and molecules, which can thereby inhibit the activity of Topo-I, block the replication of DNA, induce the accumulation of broken DNA within cells, and finally lead to the apoptosis of cells (3). Like local malignant tumor, RA is proliferative and destructive. However, there is no evidence to suggest that 10-HCPT has an inhibitory effect on osteoclasts which can induce joint deformity. In this experiment, RAW264.7 cells were cultured *in vitro* and then they were co-cultured with RANKL and macrophage colony stimulating factor (M-CSF); they were then added with 10-HCPT with different solubilities. This study aims to explore the effects of 10-HCPT at different concentrations on the number of osteoclasts as well as mRNA expression of tartrate-resistant acid phosphatase (TRAP), cathepsin K (CTSK) and matrix metalloproteinase protease 9 (MMP-9), aiming to provide a basis for the treatment of RNA using 10-HCPT.

MATERIALS AND METHODS

Materials and reagents

RAW264.7 cells used were from the Medical Department of Peking University, Beijing, China. The reagents used included Dulbecco's modified eagle medium (DMEM), trypsin, fetal bovine serum (FBS) (Gibco Company, USA), penicillin, streptomycin (North China Pharmaceutical Co., Ltd, China), Cell Counting Kit-8 (CCK-8) (Dojindo Chemical Institute, Japan), TRAP staining kit (Sigma Inc, USA), RANKL (Biolegend, USA), M-CSF (Peprotech, USA), total RNA extraction kit (Beijing Tiangen Science and Technology Co., Ltd, China), complementary deoxyribonucleic acid (cNDA) synthesis transcription kit (Thermo, USA), SYBR Green PCR Master Mix (Applied Biosystems Inc., USA), Polymerase Chain Reaction (PCR) primer (Shanghai Sangon Biotech Co., Ltd, China) and 10-HCPT (Shenzhen Main Luck Pharmaceuicals Inc., China). Before use, 10-HCPT was dissolved in DMEM first and then preserved at -40°C.

Cell cultivation

RAW264.7 cells were cultured with DMEM containing FBS with a final concentration of 10%, 1.6×10^{-2} mol/l penicillin and 2.4×10^{-2} mol/l streptomycin in an incubator (5% CO_2, 37°C). Digestion and passage could be performed after fusion growth of cells had completed for 80%.

Grouping

BA blank group, a control group and three experimental groups were prepared. The blank group included RAW264.7 cells only. The control group included RAW264.7 + RANKL (100 ng/ml) + M-CSF (30 ng/ml). Three experimental groups were RAW264.7 + RANKL (100 ng/ml) + M-CSF (30 ng/ml) + 10-HCPT (1 ng/ml); RAW264.7 + RANKL (100 ng/ml) + M-CSF (30 ng/ml) + 10-HCPT (2 ng/ml); RAW264.7 + RANKL (100 ng/ml) + M-CSF (30 ng/ml) + 10-HCPT (5 ng/ml).

CCK-8 detection method

RAW264.7 cells were inoculated into a 96-well plate (2×10^3 each well) and then cultured in an incubator (37°C, 5% CO_2) for 24 h. DMEM containing 10-HCPT of different concentrations (1, 2, 5, 10 and 20 ng/ml) was added respectively. Supernate obtained was abandoned after 48-h cultivation. After the cells had been washed twice by new DMEM, new DMEM and CCK-8 were added. The absorbance was detected at the wavelength of 450 nm using a microplate reader. Six copies were set for each group, and the average value was taken as the final result. The experiment was repeated for three times.

TRAP staining

RAW264.7 cells were cultured in a 24-well plate, 5×10^3 each well, and then cultured with DMEM. After eight hours, DMEM containing 10-HCPT with different concentrations (1, 2 and 5 ng/ml), 100 ng/ml RANKL and 30 ng/ml M-CSF were added. After five-day cultivation, the cells were fixed and stained as per the instructions on the TRAP staining kit. TRAP positive cells containing three or more cell nucleuses were considered as osteoclasts. Osteoclasts showing positive TRAP staining were counted under a microscope. Each group of slides

was observed in 5 fields. Three copies were set for each group, and the average value was taken as the final result. The experiment was repeated for three times.

Real-time quantitative fluorescence PCR

RAW264.7 cells were inoculated into a 24-well plate, 5×10^3 each well, and cultured with DMEM. After eight hours, DMEM containing 10-HCPT at different concentrations (1, 2 and 5 ng/ml), 100ng/ml RANKL and 30ng/ml M-CSF were added. After five-day cultivation, RNA was extracted from the cells according to the manufacturer's instructions and then RNA concentration and purity were detected (purity of 1.7 ~ 2.0 was considered as qualified). RNA was transcribed into cDNA according to the manufacturer's instructions. The content of cDNA was adjusted into 10 ng. PCR transcription system was 10 μL, containing 3.7 μL of dd H_2O, 0.15 μL of upstream primer, 0.15 μL of downstream primer and 5 μL of SYBR. The amplification conditions were as follows: denaturation at 50°C for 2 min, annealing at 95°C for 15 s, extension at 60°C for 1 min, totally for 40 cycles. Relative quantitative analysis was performed taking expression quantity of reduced glyceraldehyde-phosphate dehydrogenase (GAPDH) as a reference and using the ΔΔCt method. Primer sequence was as follows: GAPDH upstream: ACCACAGTCCATGCCATCAC, downsteam: TCCACCACCCTGTTGCTGTA; TRAP upstream: CAGCAGCCAAGGAGGACTAC, downstream: ACATAGCCCACACCGTTCTC; CTSK upstream: CAGCTTCCCCAAGATGTGAT, downstream: AGCACCAACGAGAGGAGAA; MMP-9 upstream: AAACCAGACCCCAGACTCCTCTCT, downstream: GAGGACACAGTCTGACCTGAACCA.

Every real-time quantitative fluorescence PCR experiment was repeated for three times.

Statistical analysis

SPSS ver. 20.0 and graphPad prism 5 were used for statistical analysis and graph generation, respectively. Data were expressed as mean ± SD. Difference between two groups was compared using two-independent sample *t*-tests. Comparison between multiple groups was performed using single-factor analysis of variance. Difference was considered statistically significant if $P < 0.05$.

RESULTS

Effects of 10-HCPT on cell viability

The viability of cells cultured with 10-HCPT with concentrations of 1 ng/ml, 2 ng/ml and 5 ng/ml and cells cultured without 10-HCPT had no significant difference ($P>0.05$). Cell viability was identified using the following equation: (optical density of experimental group - optical density of blank group) / (optical density of control group - optical density of blank group) (Fig. 1).

Effects of 10-HCPT on the differentiation of RAW264.7 cells to osteoclasts

Among multinuclear cells with positive TRAP staining result, cells with three or more nucleuses

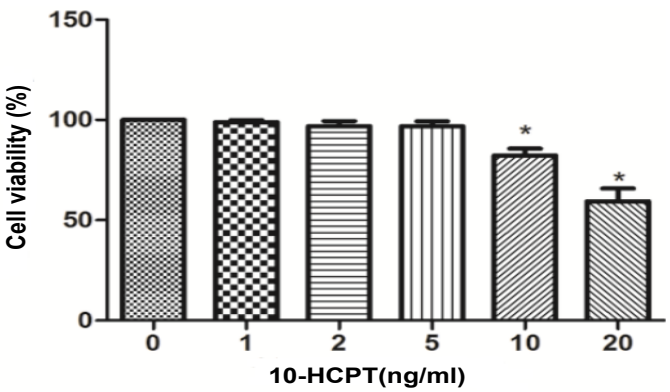

Fig. 1. *Effects of 10-HCPT on cell viability.*

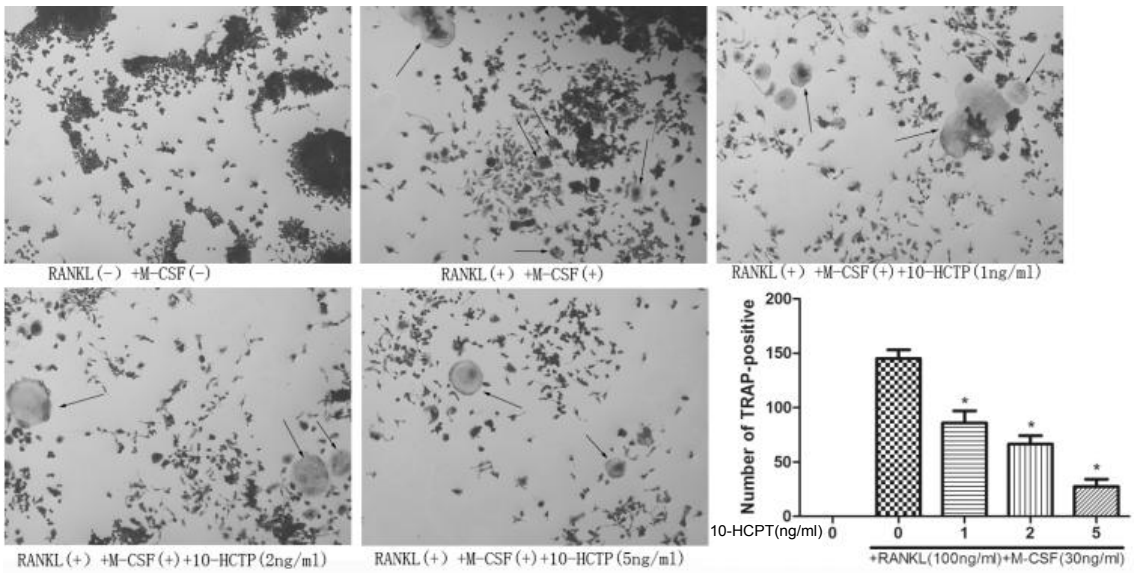

Fig. 2. *Effects of 10-HCPT with different concentrations on the formation of osteoclasts (×100).*

were considered as osteoclasts. Under microscope, osteoclasts were observed with purple nucleus, light red and vesicular cytoplasm, fuzzy cell membrane boundary, pseudopod and fold; and non-induced cells were monocytes. In the blank group, osteoclasts were not observed. In the control group and experimental groups added with RANKL and M-CSF, large multinucleated osteoclasts could be observed. With the increase of concentration of 10-HCPT, the number of osteoclasts showed an obvious decreasing tendency (*, $P<0.05$) (Fig.2).

Real-time quantitative fluorescence PCR results

The inhibitory effect of 10-HCPT on osteoclasts has been proved in the expression of specific genetic markers of osteoclasts. 10-HCPT could significantly lower the expression of TRAP, CTSK and MMP-9, and the difference with the control group had statistical significance (*, $P<0.05$). With the increase of concentration, the inhibitory effect became more obvious (Fig. 3).

DISCUSSION

Bone destruction is a major cause of many clinical problems such as dysfunction in the progress of RA. Some studies concerning RA patients or animal models of arthritis have suggested that osteoblasts play an important role in the pathogenesis of bone injury (4). Recent studies have demonstrated reducing the infiltration of inflammatory cell and the activation of osteoblasts has been a key for the treatment of RA (5-12). Through this study, we found that 10-HCPT could effectively inhibit the activation of osteoblasts, which provides a new choice for clinical treatment of RA.

RAW264.7 cells are usually regarded as a source of osteoclast precursors. RAW264.7 cells can differentiate into osteoclasts while being cultured with RANKL and M-CSF. In this experiment, we found osteoclasts increased significantly when RANKL and M-CSF were added; but with the increase of the concentration of 10-HCPT, the number of osteoclasts remarkably reduced. Hence, we believe that the formation of osteoclasts can be inhibited by 10-HCPT.

A large number of studies (13-16) have indicated that osteoclast precursors can release many osteoclast specific genes, such as TRAP, CTSK and MMP-9, after binding with RANKL and M-CSF, and proteins produced after transcription of those genes are involved in the differentiation, fusion

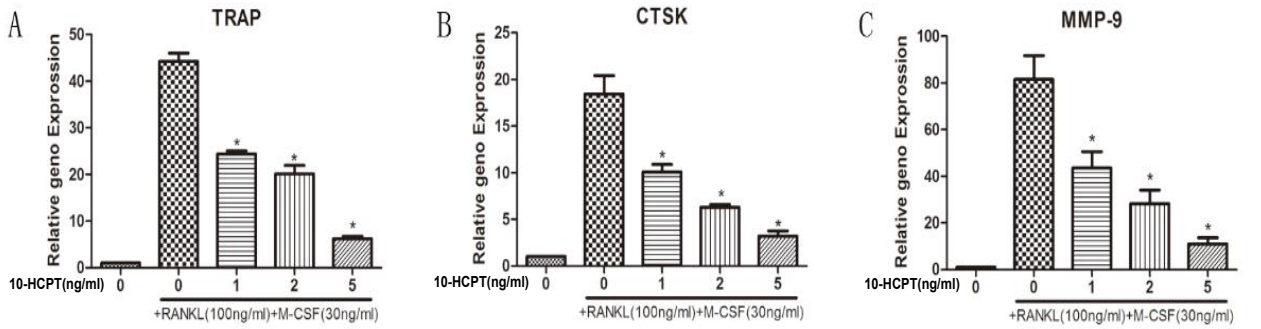

Fig. 3. ***A)*** *Relative expression quantity of TRAP gene mRNA.* ***B)*** *Relative expression. quantity of CTSK gene mRNA.* ***C)*** *Relative expression quantity of MMP-9 gene mRNA.*

and activation of osteoclasts; increased expression quantity of CTSK and MMP-9 has the most significant influence on bone matrix damage and bone resorption. In this experiment, we found that the application of 10-HCPT could significantly lower osteoclast specific genes and, moreover, the relation was dose-independent. Therefore, we assume that, 10-HCPT may treat RA by reducing the expression of osteoclast specific genes.

To sum up, 10-HCPT can remarkably reduce the formation of osteoclasts induced by RANKL and M-CSF and the mechanism may be correlated to the expression of osteoclasts genes TRAP, CTSK and MMP-9.

ACKNOWLEDGEMENTS

The key scientific and technological projects of Henan Province Education Department.

REFERENCES

1. Scott DL, Wolfe F, Huizinga TW. Rheumatoid arthritis. Lancet 2010; 376:1094-108.
2. Scott DL, Pugner K, Kaarela K, Hieke K. The links between joint damage and disability in rheumatoid arthritis. Rheumatology (Oxford) 2000; 39(2):122-32.
3. Dong XL, Gong Y, Chen ZZ, Wang YJ. Delisheng injection, a Chinese medicinal compound, enhanced the effect of cis-platinum on lung carcinoma cell line PGCL3. Chin J Integr Med 2014; 20(4):286-91.
4. Tsuboi H, Matsui Y, Hayashida K, Ochi T. Tartrate resistant acid phosphatase (TRAP) positive cells in rheumatoid synovium may induce the destruction of articular cartilage. Ann Rheum Dis 2003; 62:231-35.
5. Mareki O, Qingshun L, Keiko N, et al. IL-6 signal blockade ameliorates the enhanced osteoclastogenesis and the associated joint destruction in a novel FcγRIIB-deficient rheumatoid arthritis mouse model. Mod Rheumatol 2015; 25(2):270-77.
6. Kim KW, Kim BM, Moon HW, Lee SH, Kim HR. Role of C-reactive protein in osteoclastogenesis in rheumatoid arthritis. Arthritis Res Ther 2015; 17(1):26-30.
7. Kim JY, Kim YK, Yi HJ, et al. Eupatilin ameliorates collagen induced arthritis. J Korean Med Sci 2015; 30(3):233-39.
8. Jhun JY, Lee SH, Byun JK, et al. Coenzyme Q10 suppresses Th17 cells and osteoclast differentiation and ameliorates experimental autoimmune arthritis mice. Immunol Lett 2015; 166(2):92-102.
9. Yang J, Su N, Du XL, Chen L. Gene expression patterns in bone following lipopolysaccharide stimulation. Cell Mol Biol Lett 2014; 19(4):611-22.
10. Sun Y, Yao Y, Ding CZ. A combination of Sinomenine and Methotrexate reduces joint damage of collagen induced arthritis in rats by modulating osteoclast-related cytokines. Int Immunopharm 2014; 18(1):135-41.
11. Park JS, Lee J, Lim MA, et al. JAK2-STAT3 blockade by AG490 suppresses autoimmune arthritis in mice via reciprocal regulation of regulatory T Cells and Th17 cells. J Immunol 2014; 192(9):4417-24.
12. Bostrom EA, Lundberg P. The newly discovered cytokine IL-34 is expressed in gingival fibroblasts,

shows enhanced expression by pro-inflammatory cytokines, and stimulates osteoclast differentiation. Plos One 2013; 8(12):1611-14.

13. Zeng XZ, He LG, Wang S, Wang K, Zhang YY, Tao L, Li XJ, Liu SW. Aconine inhibits RANKL-induced osteoclast differentiation in RAW264.7 cells by suppressing NF-κB and NFATc1 activation and DC-STAMP expression. Acta Pharmacol Sin; 2015.
14. Visagie A, Kasonga A, Deepak V, Moosa S, Marais S, Kruger MC, Coetzee M. Commercial honeybush (Cyclopia spp.) tea extract inhibits osteoclast formation and bone resorption in RAW264.7 Murine Macrophages-An in vitro Study. Int J Environ Res Public Health 2015; 12(11):13779-93.
15. Kim J, Lee HK, Chang TS, Kang KS, Hwang GS. Inhibitory effect of brazilin on osteoclast differentiation and its mechanism of action. Int Immunopharm 2015; 29(2):628-34.
16. Zhai ZJ, Li HW, Liu GW, et al. Andrographolide suppresses RANKL-induced osteoclastogenesis in vitro and prevents inflammatory bone loss in vivo. Br J Pharmacol 2014; 171(3):663-75.

LETTER TO THE EDITOR

RADIOTHERAPY OF THE NECK AND CAROTID STENOSIS

Y. YANG and T. WANG

Department of Radiation Oncology, The Second Hospital of Jilin University, Changchun

Received April 6, 2016 – Accepted June 30, 2016

The first choice of treatment for neck cancer is often radiotherapy. Therefore, we aimed to investigate the microinflammation after radiotherapy of the neck and the incidence of carotid stenosis. This study reports on patients treated with radiotherapy as part of the treatment for laryngeal cancer in the Department of Radiation Oncology, The Second Hospital of Jilin University, Changchun, P.R. China. Sixty-two males and nine females were treated with radiotherapy between 2006 and 3012. The carotid diameter was determined by measuring carotid intima-media thickness (IMT) in the common, external and internal carotid artery. Microinflammatory conditions were assessed by high-sensitivity C-reactive protein (hs-CRP), interleukin-6 (IL-6) and tumor necrosis factor–alpha (TNF-α). Other studied risk factors included age, treatment modalities, radiation dose and energy, the height of the radiation field, and follow-up time. Carotid stenosis was detected in all of the 71 patients. It was mainly clinically unsuspected; 19 patients had sustained a vascular event (14 TIA, 5 CVI) at a median of 3.11 years (range 2.3–5.6 years) following RT. In four of five CVI patients, CVI occurred on the side of the irradiation. Eleven patients who suffered vascular incident had severe stenosis of the carotid artery and 6 had moderate (31-49% of the lumen). Only two patients with mild stenosis on the irradiated side suffered TIAs. Serum hs-CRP levels in carotid stenosis were 9.4 (±SD=5.97) mg/ml, IL-6 = 12.8 (±SD=2.62) pg/ml and TNF-α = 15.4 (±SD=4.49) ng/ml. The clinical detection of asymptomatic carotid stenosis is challenging, and current recommendations regarding the follow-up period should be scrutinized.

To the Editor,

Due to variation between countries that may reflect the different prevalence of risk factors, we cannot be precise, but head and neck squamous cell carcinoma stands for the sixth most common neoplasm worldwide (1). Although they may be treated with surgery, radiotherapy or a combination, radiotherapy is the mainstay of the comprehensive treatments for malignancies of the head and neck. This focuses the research on microvascular and arterial injury after radiation exposure, and underlines its clinical significance as a major sequela of head and neck radiation. On the other hand, the exact mechanism of radiation-induced carotid artery stenosis is not clear, even though it does not consist only of direct and indirect damage, but accelerated atherosclerosis, as well (2).

The risk of radiation-induced carotid stenosis seems to depend on various factors, e.g. site of primary malignancy and the radiation doses. According to the knowledge of athersclerosis to date, inflammatory vascular damage after radiation in humans might increase due the activation of nuclear factor-kappa B (3). Early elevation of inflammatory biomarkers may serve in evaluating the progress of carotid stenosis after RT (4). On the other hand, oxidative stress could

Key words: carotid stenosis, follow-up, inflammatory biomarkers, radiation therapy

Mailing address:
Dr Tiejun Wang,
Department of Radiation Oncology,
The Second Hospital of Jilin University,
Changchun, 130041, P.R. China
e-mail: tiejun@protonmail.ch

0393-974X (2016)

DISCLOSURE: ALL AUTHORS REPORT NO CONFLICTS OF INTEREST RELEVANT TO THIS ARTICLE.

precipitate carotid stenosis as a late complication of RT (5).

Therefore, to study the incidence of carotid stenosis in the micro-inflammatory milieu after the RT, we assessed carotid diameter by measuring carotid intima-media thickness (IMT) as well as high-sensitivity C-reactive protein (hs-CRP), interleukin-6 (IL-6) and tumor necrosis factor–alpha (TNF-α).

MATERIALS AND METHODS

One hundred and forty-six consecutive patients who were treated for neck tumors between 2006 and 2012 were enrolled in the study. All patients had received postoperative unilateral RT on the neck. All patients gave written consent to participate in the study. Patients who had also been treated with chemotherapy were excluded.

Other exclusion criteria were: post-CEA restenosis, hormone replacement therapy, digitalis and corticoid intake, thyroid and gonadal disorders, autoimmune or systemic disease, other known malign process, recent (<1 month) severe infection, recent (<1 month) stroke.

Finally, 71 patient, 62 males, and nine females – all with some degree of carotid stenosis, were included in our study. The control consisted of 65 patients in the similar age and sex group.

All procedures were in accordance with the standards of the ethics committee on human experimentation (institutional and national) and with the Helsinki Declaration of 1975 (in its most recently amended version). Informed consent was obtained from all patients included in the study.

Patient characteristics

All patients completed a standardized questionnaire to assess patient and family history. Hypertension was defined when systolic blood pressure >160 mmHg and/or a diastolic blood pressure >95 mmHg; and/or the patient was taking blood pressure-lowering medication. Diabetes mellitus was considered present if the patient was taking oral antidiabetics or insulin. Smoking history was found positive if the patient was a current smoker or had quit smoking less than three years previously.

Degree of stenosis

Two-dimensional carotid imaging studies were performed with a LOGIC 3600 or EUROSON with linear 7.5 MHz probe. We determined carotid intima-media thickness (IMT, in mm) of the Common Carotid Artery (CCA) and the Internal Carotid Artery (ICA) or both, depending on the anatomical borders of the RT-field, bilaterally using gray-scale analysis. The extent of carotid obstruction was classified as low (0-30%), moderate (31-49%), and severe (≥50%). Intima-media thickness is defined as the distance between the echogenic line representing the blood–intima interface and the echogenic line representing the media–adventitia interface. The IMT was measured on the posterior wall in the longitudinal plane in an anterolateral approach with the transducer head perpendicular to the vessel.

To maximize inter-observer reliability, all the color Doppler assessments were performed by TW.

Radiotherapy

Initially, 102 patients with early or localized laryngeal cancer were scheduled for either surgery or radiation therapy (6, 7).

All patients underwent RT with radical intent, and no patient was treated with preoperative intent. Patients with an early stage vocal cord tumor were treated with small fields.

All patients received prophylactic lymph node irradiation. Therapy was administered using 4-MV linear accelerator X-rays. A conventional fractionation schedule of 2 Gy/day was used. A prophylactic RT of the nodal area (including the retropharyngeal region and supraclavicular nodes) was performed with 40–50 Gy parallel-opposed lateral fields with a matched anterior lower neck field. After that, the primary lesion was boosted with reduced fields. The total RT dose was 70 Gy median (ranging from 60 to 72 Gy).

Prescriptions for irradiation dose varied by the treating physician's preference.

Sample collection and assay for inflammatory markers

Blood samples were taken from fasting participants (each control and case) between 7:30 and 8:30 a.m.. The blood samples for inflammatory markers were collected in tubes containing citric acid and ethylenediaminetetraacetic acid and were stored at −80°C after centrifugation. For determination of hs-CRP values, a high-sensitivity assay (Dade Behring, Marburg, Germany) with a detection level of 0.156 mg/L was used.

Table I. *Overall degree of stenosis of the irradiated carotid artery, and degree of stenosis of the irradiated carotid artery relative to the post-RT interval.*

RT-interval (years)	*Degree of stenosis*		
	Mild (0-30%)	**Moderate (31-49%)**	**Severe (≥50%)**
3.39 (±SD=0.09)	11		
3.39 (±SD=0.09)		16	
3.36 (±SD=0.09)			44

Serum concentrations of IL-6 and TNF-α were determined using the commercially available enzyme-linked immunosorbent assay (ELISA) US (Ultrasensitive) kit (Biosource International CA, USA). The IL-6 ELISA assay has a minimum detectable level at 104 fg/ml. The TNF-α test has a minimum detectable level of 0.09 pg/ml while its performance sensitivity is less than 0.5 pg/ml.

Optical density was read with a microtiter plate reader by dual wavelength at 450 nm. All samples were assayed in duplicate.

Statistical analysis

We used STATISTICA, version 10 (StatSoft, Inc. Tulsa, OK, USA) for statistical analysis. The one-sample Kolmogorov-Smirnov test was used for normality of distributions of continuous variables. Continuous variables with normal distribution were expressed as a mean ± standard deviation and compared with the independent samples *t*-test. The median was used to express continuous variables with a skewed distribution, and they were compared with the Mann-Whitney test. Categorical variables were compared with χ^2 test or Fisher's exact test. Multivariate analysis was performed using a linear stepwise regression model with all clinical and physiologic parameters entered as covariates. Statistical significance was accepted when $P \leq 0.05$.

RESULTS

Sample and RT

Our experimental group consisted of 71 patients (62 males, 9 females), comprised of 45 (63%) patients with a laryngeal carcinoma, 17 (24%) with a pharyngeal carcinoma, five cases (7%) of carcinoma of the tongue and four (5%) with carcinoma of the submandibular gland. The median age at RT was 50.5 years (range 41.2–72.1 years); ultrasonographic and laboratory assessment took place 3.37 (±SD=0.79) years after the RT (median 3.11; min=2.3, max=5.7) years.

The total therapeutic radiation dose ranged from 40 to 66 Gy and was delivered in fractions of 2 Gy. Outline of the overall degree of stenosis of the irradiated carotid artery and degree of stenosis of the irradiated carotid artery regarding the post-RT interval is given in Table I. Patients with an early stage laryngeal tumor were treated with small fields, 6.74 (±SD=2) cm in height and width. Early-stage tumors of hypopharynx were irradiated with the field height less than 7 cm (ranging from 3.55 to 15.4 cm). Median irradiation field in carcinomas of submandibular

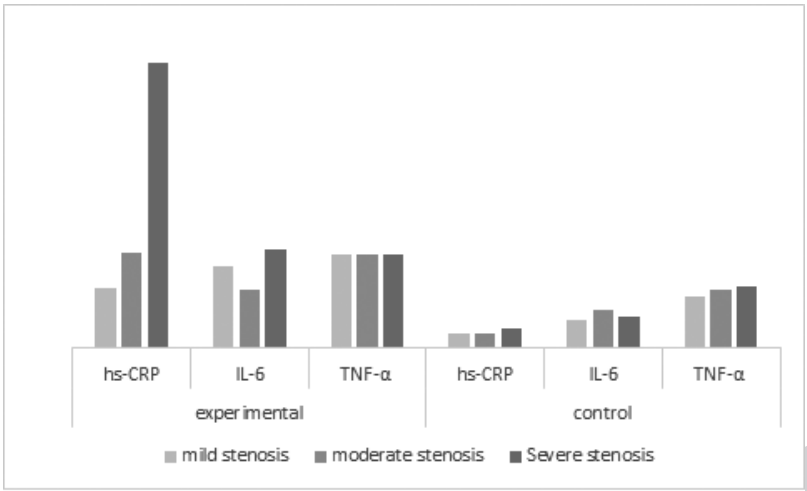

Fig. 1. *Proinflammatory markers of controls and patients after RT. There is a significantly higher hs-CRP, IL-6, and TNF-α in patients following RT compared with normal controls (p<0.05).*

gland was 4.98 (4-12) cm. Even when irradiating tongue cancer, field height was <7 cm (5 cm, range from 4 to 9).

In males, the mean radiation field measured 6.92 (±SD=2.4 cm) and in females it was 6.72 (±SD=2.8 cm).

Occurrence of cerebrovascular incidents

Nineteen patients had sustained a cerebrovascular incident (14 TIA, 5 CVI) at a median of 3.11 years (range 2.3–5.6 years) following RT. In particular, TIAs occurred 3.11 years (range 2.4–5.6 years) following RT and CVIs 2.8 (ranging 2.3-4.9). In four of these five patients, it occurred on the side of the irradiated carotid artery. One patient developed an infarction in the hemisphere contralateral to the side of irradiation. This patient showed >50% of carotid stenosis contralateral of the irradiated side. Eleven patients who suffered vascular incident had severe stenosis of the carotid artery and six had moderate (31-49% of the lumen occluded). Only two patients had mild stenosis on the irradiated side, and both suffered TIAs.

Serum levels of inflammatory markers

Sera of 11 mild-stenosis patients from our experimental group were checked on average 3.1 (±SD=0.23) years after RT for hs-CRP, IL-6, and TNF-α.

Mean serum concentration of hs-CRP was 9.4 (±SD=5.97) mg/ml, IL-6 was 12.8 (±SD=2.62) pg/ml, and TNF-α was 15.4 (±SD=4.49) ng/ml. This differed statistically significantly from the controls, based on the results of the two-sample *t*-test, that gave p-values <0.05 in all cases.

Sixteen moderate-stenosis patients were assessed on average 3.6 (±SD=0.73) years after the RT and their mean serum concentration of hs-CRP was 14.97 (±SD=12.99) mg/ml, IL-6 was 11.24 (±SD=6.13) pg/ml and TNF-α 17.17 (±SD=3.12) ng/ml. This differed statistically significantly from the controls, based on the results of the two-sample *t*-test, that gave p-values <0.05 in all cases.

Forty-four patients were assessed with severe occlusion of the carotid artery on average 3.3 (±SD=0.89) years after the RT. Their mean serum concentration of hs-CRP was 24.90 (±SD=22.86) mg/ml, IL-6 was 7.09 (±SD=5.39) pg/ml and TNF-α 16.08 (±SD=3.29) ng/ml. This differed statistically significantly from the controls, based on the results of the two-sample *t*-test, that gave p-values <0.05 in all cases.

DISCUSSION

To the extent of our knowledge, this is the largest study investigating markers of inflammation in patients with carotid stenosis following RT. The key result of the present study is that our patients have significantly

higher levels of hs-CRP, IL-6, and TNF-α in comparison with normal controls (Fig. 1). The available studies in the literature cited effects of RT without reference to micro-inflammation, or compared the levels of inflammatory biomarkers between patients with symptomatic and asymptomatic carotid stenosis (8), mostly in only a limited number of patients (9). The results of our study could only suggest that irradiation of the carotid area is a significant risk factor for developing carotid stenosis and subsequently cerebrovascular events, i.e. hs-CRP, IL-6 or TNF-α levels in RT treated patients, specifically, might be useful in predicting carotid stenosis.

We found elevated levels of hs-CRP, IL-6 and TNF-α in 71 patients, compared with 63 counter paired controls. Our data suggest that carotid artery atherosclerosis is a disorder characterized by inflammation, but the inflammatory biomarkers should be regarded with caution as tools for identifying symptomatic patients.

These, and previous results, permit us to conclude that radiation oncologists and neurologists should pay more attention to these possible carotid stenosis and cerebrovascular events, which consist of transient ischemic attack (TIA) and stroke. Therefore, surveillance with carotid ultrasound techniques and aggressive modification of the traditional risk factors is cost-effective, and long-term surveillance should begin before 3 years. For RT interval, however, we suggest more prospective investigations to determine the pathogenesis, prevention, and early detection methods.

REFERENCES

1. Chin D, Boyle GM, Porceddu S, Theile DR, Parsons PG, Coman WB. Head and neck cancer: past, present and future. Expert Rev Anticancer Ther 2006; 6:1111-18.
2. Steele SR, Martin MJ, Mullenix PS, Crawford JV, Cuadrado DS, Andersen CA. Focused high-risk population screening for carotid arterial stenosis after radiation therapy for head and neck cancer. Am J Surg 2004; 187:594-98.
3. Halle M, Gabrielsen A, Paulsson-Berne G, Gahm C, Agardh HE, Farnebo F, Tornvall P. Sustained inflammation due to nuclear factor-kappa B activation in irradiated human arteries. J Am Coll Cardiol 2010; 55:1227-36.
4. Gujral DM, Shah BN, Chahal NS, Senior R, Harrington KJ, Nutting CM. Clinical features of radiation-induced carotid atherosclerosis. Clin Oncol (R Coll Radiol) 2014; 26:94-102.
5. Zhao W, Robbins ME. Inflammation and chronic oxidative stress in radiation-induced late normal tissue injury: therapeutic implications. Curr Med Chem 2009; 16:130-43.
6. Fedok FG, Strauss M, Stryker J. The value of preoperative radiotherapy response to maximizing laryngeal conservation in early stage supraglottic carcinoma. Trans Pa Acad Ophthalmol Otolaryngol 1990; 42:1061-67.
7. Nishimura H, Sasaki R, Yoshida K, et al. Radiotherapy for stage I or II hypopharyngeal carcinoma. J Radiat Res 2012; 53:892-99.
8. Rerkasem K, Shearman CP, Williams JA, Morris GE, Phillips MJ, Calder PC, Grimble RF. C-reactive protein is elevated in symptomatic compared with asymptomatic patients with carotid artery disease. Eur J Vasc Endovasc Surg 2002; 23:505-9.
9. Mocco J, Choudhri TF, Mack WJ, Laufer I, Lee J, Kiss S, Poisik A, Quest DO, Solomon RA, et al. Elevation of soluble intercellular adhesion molecule-1 levels in symptomatic and asymptomatic carotid atherosclerosis. Neurosurgery 2001; 48:718-21; discussion 21-2.

LETTER TO THE EDITOR

USE OF THREE-DIMENSIONAL COLOR POWER DOPPLER IN IMAGING OF LIVER CANCER

H. SHI, Y. WANG, H. WANG, H. ZHAO, N. XV, F. LIU and X. PENG

The First Affiliated Hospital of Harbin Medical University, Harbin, China

Received November 28, 2015 – Accepted May 6, 2016

We aimed to assess the role of three-dimensional color power Doppler (3D-CPD) imaging in diagnosis of liver cancer. First of all, we performed 2D- and 3D-CPD imaging on 96 cases of liver tumors with a total of 106 lesions to examine the characteristics of the vascular distribution patterns of the tumors, and in turn, compare the sensitivity and specificity. Also, with the use of three-dimensional volumetric measurement, we calculated the volume of tumors, quantity of intra-tumor blood vessels, and the ratio of the quantity of intra-tumor blood vessels to tumor volumes (vascular index, VI). Finally, we statistically analyzed the vascular index between benign and malignant tumors. We found that the sensitivity/specificity were 21.3%/100% for 2D-CPD, and 81.3%/100% for 3D-CPD, based on the use of type-III of blood vessels for diagnosis of the malignant lesions. In 3D-CPD, the type-III of blood vessels along with VI of > 0.3/cm^3 can be used as the criteria for the diagnosis of liver cancer since we found that average VI was 0.38/cm^3 in 75 malignant tumors, but 0.18/cm^3 in 31 benign tumors ($p<0.05$). The sensitivity and specificity in determining malignancy in the liver based on VI > 0.3/cm^3 were 78.7% and 87.1%, respectively.

To the Editor,

Overall, the five-year survival rate of people with liver cancer is 16%. For 41% of patients who are diagnosed at an early stage, the five-year survival rate increases to 29%. This decrease of survival time depends on whether the liver cancer has spread to the surrounding or distant tissues. In the first case, the five-year survival rate decreases to 10%, and in the latter to 3%. As a result, early diagnosis and treatment are imperative in improving prognosis and survival of patients. Even if the cancer is found at a more advanced stage, treatments are still available, and accurate staging is pivotal for successful treatment (1).

There are no widely recommended screening tests for liver and among the imaging tests, ultrasound is always the first test to examine the liver. Normally, the information acquired from Doppler signals in three dimensions is not analyzed by frequency assessment but by using the amplitude of the signal (2, 3). So, three-dimensional color power Doppler (3D-CPD) ultrasound, as it is capable of detecting very low blood flow signal, is much more sensitive than the conventional color Doppler systems. Mainly for this highly precise ability to evaluate the perfusion, 3D-CPD has become a widely used tool for clinical diagnosis of a variety of malignant or benign diseases (4).

In this study, we sought to investigate vascularity in liver tumors with the use of 3D-CPD, to quantitatively and qualitatively determine the nature of intrahepatic lesions: malignant or benign. Our study is significant because it provides further meaningful information to help clinicians in diagnosis and treatment of liver cancer.

Key words: liver cancer, power Doppler, vascular index

Mailing address:
Dr. Xiangwen Peng,
The First Affiliated Hospital
Harbin Medical University, 23 Youzheng Street,
Nangang District, Harbin,
Hei Longjiang Province, China
e-mail: profpeng@hotmail.com

0393-974X (2016)

DISCLOSURE: ALL AUTHORS REPORT NO CONFLICTS OF INTEREST RELEVANT TO THIS ARTICLE.

MATERIALS AND METHODS

Subjects

Ninety-six patients with liver lesions were enrolled during in the period from May 2004 to January 2006, including 65 males and 31 females with an average age of 46.6 years (a range of 27-75 years). Sixty-six patients were pathologically diagnosed as hepatocellular carcinoma. The remaining patients included 28 cases of hemangioma, 2 cases of inflammatory pseudotumor, and a case of liver abscess. With regard to lesions, 82 patients had only one, while 6 and 8 patients had two and three lesions, respectively. We performed further analysis on 106 lesions with an average diameter of 6.2 cm (ranging from 3.3 to 12 cm), which included 75 malignant ones.

In this study, we used 3D color power Doppler (Medison/Kretz, Voluson 730), which was equipped with the 3D-volume probe (10 MHz), specially designed for application in the scanning of the abdomen or small organs. Also, the 3D ultrasound imaging software (gray and energy) installed in the computer allowed us to perform 2D- or 3D-maging without the need of an additional workstation. The frequencies of convex and line array probes were 3.5 ~ 5.0 and 10 MHz, respectively.

Sonography

In all of the cases, we first performed conventional two-dimensional gray-scale ultrasonography to determine the location, shape, and size of the tumors, which was followed by 3D color power Doppler. As soon as 2D-imgaes of tumors with most abundant vascular blood flow were captured and saved, 3D-CPD was applied with the probe immobilized at the central point to reduce any false signals. The 3D-images of tumors were simulated in the mode of color (for intra-tumor vascular distribution) or gray-scale/color (especially useful for understanding the shape and margin of tumors). The 3D-images were rotated to show the maximal cross-section of tumors and then saved.

In the phase of 3D-image simulation, the measurement of tumor volume was initiated based on an interval degree of 15°. We manually outlined the tumors until the number of volumes automatically appeared on the computer screen

Semi-quantitative analysis of vascularity of liver tumors by 2D- or 3D-CPD imaging

Based on the patterns of vascular distribution and branching in tumors, we classified the signals of intra-tumor Doppler blood flow into four categories: none, rare, relatively abundant, and very abundant. The tumor blood vessels are classified into three types: type-I, no blood flow surrounding the tumor but with spotted signals within the tumor; type-II, the arc or short stripped blood flow signals surrounding the tumor with no or sparse signals within the tumor; type-III, visible blood vessels surrounding the tumor, abundant blood vessel trees or net, branches intertwined or irregularly distributed, always complicated with arteriovenous fistula.

Quantitative analysis of vascularity of liver tumors by 3D-CPD

In this study, we used the criteria for methods of quantifying blood vessels surrounding and within the tumors as described. The total quantity of blood vessels in tumors is dependent on how many terminal branches were identified. The average of three counts was derived by rotating the image. The actual volume of tumor was obtained by subtracting the necrotic one. The vascular index (VI, the ratio of the total count of blood vessels to the tumor volume) was used as an indicator of the abundance of blood flow in the tumor.

Statistical analysis

We used *t*-test for comparison of numeric variables and Pearson correlation analysis of variables, respectively.

All procedures performed in studies involving human participants were in accordance with the ethical standards of the institutional and/or national research committee and with the 1964 Helsinki declaration and its later amendments or comparable ethical standards.

RESULTS

Semi-quantitative analysis by 2D- or 3D-CPD imaging

With use of 3D-CPD imaging, the blood flow signals of four types: none, rare, relatively abundant, and abundant, were observed in cases of 1 (0.9%), 13 (12.3%), 44 (41.5%), and 48 (45.3%), respectively. However, these signals were observed in 1 (0.9%),

54 (50.9%), 49 (46.2%), and 2 (2%), respectively, with use of 2D-CPD (Fig. 1).

Vascular patterns of malignant or benign lesions by 2D- or 3D-CPD imaging

Considering the vascular distribution patterns of 106 lesions (75 malign, 31 benign), using 2D-CPD we were able to identify 20 type-I, 39 type-II and 16 Type-III malignancies. Using this same technique, 21 type-I, 10 Type-II, and none of Type-III benign lesions were discovered. On the other hand, 3D-CPD identified 1 type-I, 13 type-II and 61 type-III malignancies and 14 type-I, 17 type-II and 0 type-III benign tumors. Based on the use of vascular type-III, we found that the sensitivity/specificity for diagnosis of liver cancer with use of 2D-CPD or 3D-CPD were 21.3%/100%, or 81.3%/100%, respectively. If based on the use of vascular type-II, the sensitivity/specificity were 73.3%/67.7% for 2D-US, and 73.3%/45.2% (3D-CPD).

3D-CPD revealed that liver tumors had more enriched blood flow signals than those observed in two-dimensional ultrasound, suggesting that malignant tumors acquire more blood supply than their benign counterparts. In addition, the vascular shape and branching patterns of malignant tumors were more diverse than those of hemangioma (spotted blood flow signals) and liver abscess (no blood signals inside the lesion, but ones surrounding tumors).

Typically, as shown in Fig. 2A, the tumors of the left lobe of the liver showed the vascular type-I, with stripped blood signals surrounding in 2D-CPD (left panel). However, the peri-tumor vascular patterns were classified as type-II, with a basket-shape in 3D-CPD (Fig. 2A, right panel). In the right lobe of liver, tumors typically demonstrated spotted or short-strapped blood signals (type-I) in 2D-CPD, but type-II of blood vessels in 3D-CPD with penetrating blood branches and enlarged arteries (Fig. 2B). In addition, the tumors of right anterior lobe appeared with type-II of blood vessels in 2D-CPD with enriched tripped blood signals in the tumors, but type-III in 3D-CDE. This type-III of blood vessels was characterized with enriched and irregular blood signals existing between right anterior and posterior portal veins and the necrosis having no blood flow (Fig. 2C). Moreover, the tumors of the right posterior lobe had type-I of blood vessels with peri-tumor stripped signals in 2D-CPD, but type-III in 3D-CPD with blood flow signals surrounding the tumors and the arteriovenous fistula (Fig. 2D).

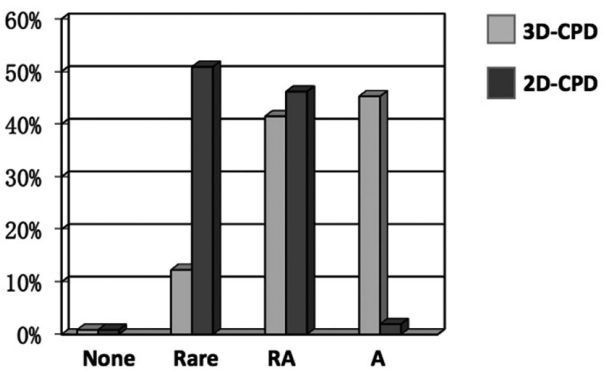

Fig. 1. *Pattern comparison of blood flow signals in liver lesions. RA: relatively abundant; A: abundant.*

In contrast to malignant tumors typically showing type-III of blood vessels with enriched signals surrounding and irregular ones inside the tumors (Fig. 3A), liver abscess usually demonstrated enlarged blood signals surrounding the lesions without penetrating signals, which are pathologically consistent with thickened wall of abscess but no interior blood supply (Fig. 3B).

Quantitative analysis of vascularity of liver tumors by 3D-CPD

We measured the volume of tumors by 3D-CPD on an interval degree of 15°. We then manually outlined the tumors until the number of volume automatically appeared on the computer screen. Finally, we calculated the total quantity of blood vessels in tumors based on how many terminal branches were identified. The vascular index (VI, the ratio of total count of blood vessels to the tumor volume) was used as an indicator for the abundance of blood flow in the tumor.

The average VI for 75 malignant tumors is 0.38/cm3, but 0.18/cm^3 for 31 benign tumors. There was a significant difference in VI between malignant and benign tumors ($u = 11.236$, $p<0.05$). The sensitivity and specificity in determining whether the lesions

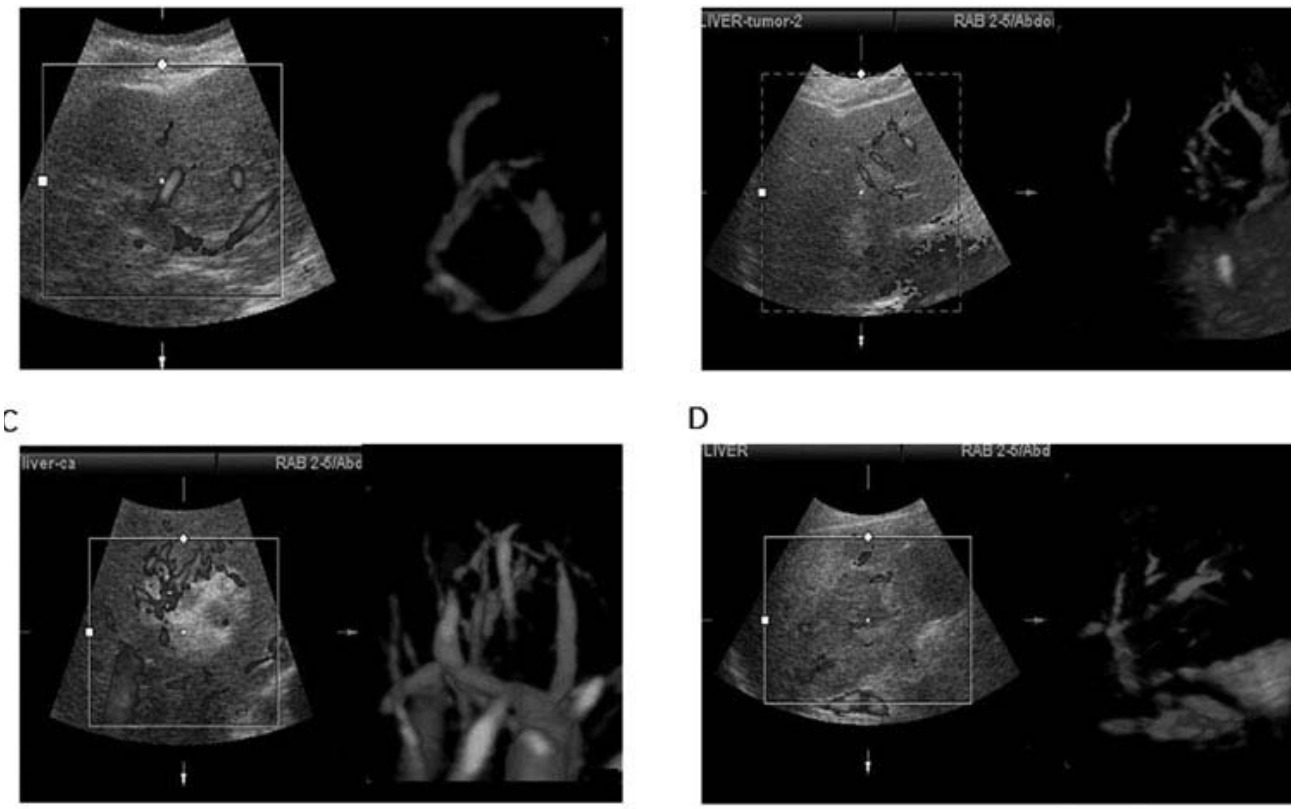

Fig. 2. *Vascular patterns of liver cancer by 2D-CPD or 3D-CPD. Tumors were located in left lobe (**A**), right lobe (**B**), right anterior lobe (**C**) or right posterior lobe (**D**). The vascular pattern of each was demonstrated by 2D- (left panel) or 3D-CPD (right panel).*

were malignant in the liver, based on VI of > 0.3/cm^3, were 78.7% and 87.1%, respectively.

The calculation method of VI is exemplified in Fig. 4. The tumor in the right lobe was the of 8.7 x 7.5 cm in size with strong echo and partial blood flow signal. There was partial loss because of necrosis. As a result, the actual volume of tumor was obtained by subtracting the necrotic part. The measurement was performed three times. The average of tumor volume was 70.32 cm^3 and average quantity of blood vessels was 21.2. Hence, the vascular index (VI, the ratio of total count of blood vessels to the tumor volume) was 0.3/cm^3. In Fig. 5, we further show that the VI of liver tumors ranged from 0.28 (Fig. 5A) to 0.53 (Fig. 5B).

DISCUSSION

This study shows that 61 cases were classified as vascular Type-III, 13 patients were determined as Type-II, showing arc- or short-strip shaped signals in the perimeter of tumors with no or rare blood flow signals, and one patient showed stripped and sparsely distributed blood flow signals within the tumor (type-I).

Quantitative measurement of liver neoplasm with 3D-CPD is VI, and we found that the VI of malignant lesions significantly higher than that of benign ones ($p<0.05$). Based on VI (>0.30/cm^3), the sensitivity and specificity in determining malignancy were 77.8% and 80%, respectively, thus suggesting that VI can accurately reflect the status of tumor angiogenesis and abundance and offer a new approach for differential diagnosis of liver diseases.

Benign and malignant tumors demonstrate remarkable difference in quantity, structure, and distribution of neovascularization (5-7). As the blood flow patterns of tumors are associated with histopathology of the lesions (8) in this study, we

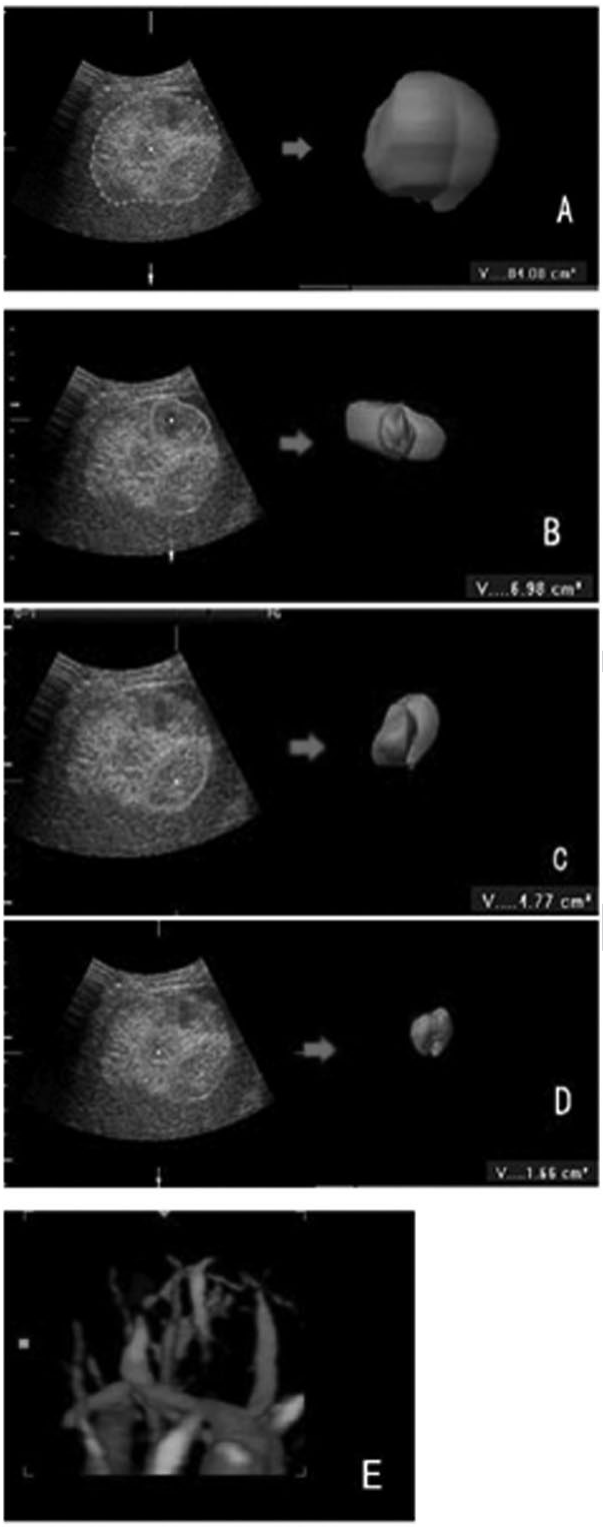

Fig. 3. *Volumetric measurement of liver tumors and VI calculation by 3D-CPD. Each counting was performed three times and the average was obtained.*

found that primary liver cancer usually appeared with an irregular and tortuous shape of arteries. Moreover, 45.3% of liver tumors in this study showed rich blood flow signals in 3D-CPD, in contrast to 2% observed with use of 2D-CPD.

While they have equal specificity (based on the type-III of blood vessels), the sensitivity was much higher in 3D-CPD. Our study supports that 3D-CPD is even more accurate in description of vascular distribution patterns within the tumors, by assisting in classification of the vascularity (9).

In conclusion, 3D-CPD imaging is non-invasive, short time-consuming, reproducible, and has no side effects. It can allow direct visualization of blood flow of the tumor. 3D-CPD is susceptible to interventions by movement of organs or tissues. However, the limitations of 3D-CPD are also obvious, e.g. when patients are unable to control breathing and the lesions are located in the left lobe of the liver, generated signals could easily be false. As in any other ultrasonography, the quality of images can be affected by the individual performer's skills. With regard to the larger tumors, one should acquire images from different angles or locations to more accurately determine the intra- or peri-tumor distribution of blood vessels. In addition, it can only correctly show the blood vessels when the tumors are deeply located.

REFERENCES

1. Chen L, Liu Y, Li GG, Tao SF, Xu Y, Tian H. Quality of life in patients with liver cancer after operation: a 2-year follow-up study. Hepatobiliary Pancreat Dis Int 2004; 3:530-33.
2. Miyagi Y, Masaoka H, Akamatsu N, Sekiba K. Development of a three-dimensional color Doppler system. Med Prog Technol 1992; 18:201-8.
3. Downey DB, Fenster A. Vascular imaging with a three-dimensional power Doppler system. AJR Am J Roentgenol 1995; 165:665-68.
4. Kupesic S, Kurjak A. Clinical application of 3D sonography: CRC Press; 2000.
5. Kamaya A, Maturen KE, Tye GA, Liu YI, Parti NN, Desser TS. Hypervascular liver lesions. Semin Ultrasound CT MR 2009; 30:387-407.
6. Choi BI, Kim TK, Han JK, Chung JW, Park JH,

Han MC. Power versus conventional color Doppler sonography: comparison in the depiction of vasculature in liver tumors. Radiology 1996; 200:55-8.

7. Taylor KJ, Ramos I, Carter D, Morse SS, Snower D, Fortune K. Correlation of Doppler US tumor signals with neovascular morphologic features. Radiology 1988; 166:57-62.
8. Brannigan M, Burns PN, Wilson SR. Blood flow patterns in focal liver lesions at microbubble-enhanced US. Radiographics 2004; 24:921-35.
9. Xu HX, Liu L, Lu MD, Li HP, Liu GJ, Li JP. Three-dimensional power Doppler imaging in depicting vascularity in hepatocellular carcinoma. J Ultrasound Med 2003; 22:1147-54.

LETTER TO THE EDITOR

AN ETHNOBOTANICAL STUDY OF MEDICINAL PLANTS WITH NARCOTIC, SEDATIVE AND ANALGESIC EFFECTS IN WEST OF IRAN

K. SAKI[1], M. BAHMANI[2], M.D RAFIEIANB-KOPAEI[3], K. ASADOLLAHI[4], M. EMANEINI[5] and M. TAHERIKALANI[6]

[1]Shahid Beheshti University of Medical Sciences, Tehran, Iran; [2]Razi Herbal Medicines Research Center, Lorestan University of Medical Sciences, Khorramabad, Iran; [3]Medical Plants Research Center, Shahrekord University of Medical sciences, Shahrekord, Iran; [4]Clinical Microbiology Research Center, Ilam University of Medical Sciences, Ilam, Iran; [5]Department of Microbiology, School of Medicine, Tehran University of Medical Sciences, Tehran, Iran; [6]Razi Herbal Medicines Research Center & Department of Microbiology, School of Medicine, Lorestan University of Medical sciences, Khorramabad, Iran

Received December 17, 2015 – Accepted May 24, 2016

The first step for identification of medicinal plants and their therapeutic effects is to determine their use by local people, traditional medicine books and personal experiences. The aim of this study was to document the medicinal plants used as analgesic, sedative or narcotic agents by local residents of Dehloran, Iran. Interviews conducted with 53 informants (38 male and 15 female) revealed that a total of 32 medicinal plants belonging to 22 families are used in Dehloran as narcotic, sedative and analgesic agents. The most utilized plant families were *Asteraceae*, *Rosaceae* and *Fabaceae*. Approximately 74% of the utilized plants was attributed to herbs, followed by trees (13%) and shrubs (13%). Sixty-six percent of the medicinal plants used in the study area were perennial and the rest were annual or biannual. The most widely used plant parts were flowers (34%) followed by leaves (24%) and fruits (14%). Thirty-nine percent of the medicinal plants were used as sedatives, 39 percent as analgesics, and 24% as narcotics. Recommended plants in this study can be good candidates for further clinical and laboratory trials on diseases that are associated with pain, suffering, stress and depression. They also can be used to develop new sedative, narcotic and analgesic drugs.

To the Editor,

The development of human diseases associated with pain and suffering can lead to a wide variety of types of physical and mental stress, and also the widespread use of psychotropic and addictive substances with a chemical base. Most people use narcotic drugs to relieve pain, depression, fatigue and weakness associated with different diseases (1). Narcotic substances not only do not help patients to reduce their suffering and illness, but also lead to irreparable consequences. There is a need to identify new analgesics with fewer side effects and less potential abuse that can replace addictive and psychotropic drugs. Medicinal plants have been traditionally used to relieve pain and improve mood (2).

The first step to identify medicinal plants and their therapeutic effects is to determine their use by local people, handed down from one generation to the next, traditional medicine books and personal experiences.

Key words: medicinal plants, sedative, narcotic, analgesic, Dehloran, Ilam, Iran

Mailing address:
Dr. Morovat Taherikalani,
Razi Herbal Medicines Research Center
& Department of Microbiology,
School of Medicine, Lorestan University of Medical sciences,
Khorramabad, Iran
e-mail: taherikalani@gmail.com

0393-974X (2016)

Ethno-botanical surveys of medicinal plants and their traditional use by local people provide new area of research to explore new plant-based compounds for drug development (3).

Ilam province is one of the mountainous regions of Iran where approximately 87% of the land is natural resources. The mountains and highlands of Ilam make it an ideal area for the growth of various plants. From thousands of plant species identified in Ilam, more than 300 species possess therapeutic effects (4). Considering the abundance and widespread use of medicinal plants in Ilam, this study aimed to document the medicinal plants used as an analgesic, sedative or narcotic agents by the local people of Dehloran, Ilam.

MATERIALS AND METHODS

Medicinal plants

This ethnobotanical study investigated plants that were used for medical purposes and originally or ethnically were located in Dehloran city, Ilam province, West Iran. The plants or their specimens were identified at the Herbarium unit of the Research Centre of Agriculture and Natural Resources of Ilam.

Experiment

An ethnobotanical survey in the city of Dehloran was carried out from August to October, 2014. The data of native plants were collected from 53 individuals, including herbal practitioners (72% men and 28% women; aged from 24 to 83 years), in 19 villages. The information was collected through a questionnaire, interviews and discussions among the tribal practitioners in their local language (Kurdish). They were asked to name the plants they used for a specific disease. A semi-structured questionnaire was used to extract information on types of ailments treated by medicinal plants and plant parts.

RESULTS

A total of 53 subjects (38 males and 15 females) were interviewed in this study. According to the data obtained, a total of 32 medicinal plants, belonging to 22 families, were used in Dehloran as narcotic, sedative or analgesic agents. Ethno-medicinal information of plants used as analgesic and sedative agents are shown in Table I. The most utilized plant families are *Asteraceae*, *Rosaceae* and *Fabaceae*. Approximately 74% of the plants utilized originated from herbs, followed by trees (13%) and shrubs (13%). Sixty-six percent of the medicinal plants used in the study area were perennial, 28 percent annual and 6 percent were biannual. The most widely used plant parts were flowers (34%), followed by leaves (24%), and fruits (14%). Thirty-nine percent of the medicinal plants were used as sedative, 39 percent as analgesic, and 24% as narcotic agents.

DISCUSSION

This study documented the medicinal plants used as analgesic, sedative or narcotic agents by the local people of Dehloran, Ilam. The results of the present study show that a total of 32 medicinal plants belonging to 22 families are used in Dehloran as narcotics, sedative and analgesic agents. Pain is associated with increase in oxidative stress and medicinal plants with antioxidant activity are able to counteract free radicals, reducing oxidative stress and pain (2, 5). Most of the plants recommended in this study are known to contain considerable amounts of phenolic compounds with antioxidant activity. Therefore, a part of the effects of these plants might be through their antioxidant activities. It should be noted that antioxidants are effective in many diseases (6-10). Hence, these plants might be more beneficial for patients having multiple problems.

Most of the plants were herbaceous perennial species from the *Asteraceae* and *Rosaceae* families. In previous ethnobotanical studies conducted in different areas of Iran including Ilam, Hormozgan, Kohgiluyeh va Boyer Ahmad and Mobarakeh, the most used family was *Asteraceae* which is a large family of flowering plants with more than 25,000 species found in 880 genera. Members of this family are known to possess antioxidant, anti-inflammatory, analgesic and antipyretic effects (24, 25).

In the present study, flowers were shown to be the most frequently used parts of the plants. This may be related to the accumulation of bioactive compounds in the aerial parts of plants especially their flowers.

Therefore researchers can use these parts of the

Table I. *Medicinal plants traditionally used as analgesic and sedative agents: scientific name, common name, family name, plant parts used, life cycle and therapeutic effects.*

Row	Scientific Name	Family name	Persian name	English name	Habit	Life cycle	Parts used	Uses/ Ailments treated
1	*Achillea biebersteinii* Afan.	Asteraceae	Boomadarane-Zard	Yarrow	H	Perennial	Flowers, Leaves	Sedative
2	*Adianthum capillus-veneris* L.	Polypodiaceae	Kamar-Avizeh	Parsiavoushan	H	Perennial	Flowers, Leaves	Analgesic
3	*Allium ampeloprasum* L. subsp. *iranicum* Wendelbo	Aliaceae	Tareh-Koohi	Perennial sweet leek	H	Perennial	Bulbs, Leaves	Analgesic
4	*Amygdalus arabica* Olivier.	Rosaceae	Badame-Koohi	Almond	T	Perennial	Fruits	Analgesic
5	*Astaragalus glaucacanthus* Fisch.	Fabaceae	Asbi-gavan	Astragal	S	Perennial	Fruits	Analgesic
6	*Avena wiestii* Steud.	Poaceae	Youlaf	Wild oat	H	Annual	Seed	Analgesic
7	*Cannabis sativa* L**.**	Canabinaceae	Shahdoneh	Hemp	H	Annual	Fruits	Narcotic
8	*Capparis spinosa* L.	Capparidaceae	Kavar	Caper	H/S	Perennial	Leaves, Roots, Bark and Fruits	Narcotic
9	*Carthamus oxyacantha* M.B.	Asteraceae	Golerange-zard	Safflower	H	Annual	Flowers	sedative
10	*Centaurea iberica* Trev. Ex Spreng.	Asteraceae	Gole-Gandome-chaman-zar	Centaurea	H	Annual	Flowers	Narcotic
11	*Centaurea intricate* Boiss.	Asteraceae	Gole-Gandome Darham-barham	Centaurea	H	Perennial	Flowers	Sedative
12	*Centaurea ovina* Pall. Ex Willd.	Asteraceae	Gole Gandom	Centaurea	H	Annual	Flowers	Analgesic
13	*Cerasus microcarpa* (C.A. Mey) Boiss. subsp. *Microcarpa*	Rosaceae	Albaloye-vahshi	Sour cherry	T	Perennial	Resin	Sedative
15	*Crataegus pontica* C. Koch.	Rosaceae	Zalzalak	Azarole	T	Perennial	Fruits, Leaves	Analgesic
16	*Daphne mucronata* Royle.	Thymelaeaceae	Khoshak	Daphne	S	Perennial	Wood	Analgesic
17	*Dianthus orientalis* Adam.	Caryophylaceae	Mikhak	Pink	H	Perennial	Flowers, Fruits	Narcotic
18	*Echium italicum* L.	Boraginaceae	Gavzaban	Viper's bugloss	H	Biannual	Flower	Sedative
19	*Fritillaria imperialis* L.	Liliaceae	Ashke maryam	Crown imperial	H	Perennial	Bulb	Narcotic
20	*Glycyrrhiza glabra* L. var. *Glabra*	Fabaceae	Shirin-bayan	Licorice	H	Perennial	Roots, Flowers	Analgesic
21	*Hypericum scabrum* L.	Hypericaceae	Gole-raei	St. John's wort	H	Perennial	Inflorescence	Analgesic, Sedative
22	*Lonicera nummulariifolia* Jaub. & Spach.	Caprifoliaceae	Pelakhor	Lonicera	S	Perennial	Leaves, Flowers	sedative
23	*Narcissus tazetta* L.	Amaryllidaceae	Narges	Polyanthus narcissus	H	Perennial	Flowers, Bulb	Sedative, Analgesic
24	*Papaver dubium* L.	Papaveraceae	Khashkashe-tannaz	Great scarlet poppy	H	Annual	Leaves, Flowers	Sedative

25	*Peganum harmala* L.	Zygophyllaceae	Spand	Harmel peganum	H	Perennial	Fruits, Seeds	Analgesic, Narcotic
26	*Periploca aphylla* Decne.	Asclepiadaceae	Gishder	Silk vine	S	Perennial	Leaves, Flowers	Sedative
27	*Rumex ephedroides* Bornm.	Polygonaceae	Torshak-erishbozi	Dock	H	Annual	Leaves	Sedative
28	*Satureja khuzistanica*	Lamiaceae	Marzeh	Summer	H	Annual	Leaves, Flowers	Narcotic
29	*Stachys lavandulifolia* Vahl.	Lamiaceae	Sonbolehei	Stachys	H	Perennial	Leaves, Flowers	Narcotic and Sedative
30	*Stipa capensis* Thunb.	Poaceae	Chaman sozani	Needle grass	H	Annual	Flowers	Sedative
31	*Trifolium repens* L.	Fabaceae	Shabdare-sephid	White clover	H	Biannual	Inflorescence	Analgesic
32	*Viscum album* L.	Loranthaceae	Darvash	White mistle	T	Perennial	Flowers	Analgesic

plants to identify phytochemical compounds with sedative, analgesic and narcotic effects. Recommended plants in this study can be good candidates for further clinical and laboratory trials on diseases that are associated with pain, suffering, stress and depression. They also can be used to develop new sedative, narcotic and analgesic drugs.

REFERENCES

1. Saki K, Bahmani M, Rafieian-Kopaei M. The effect of most important medicinal plants on two important psychiatric disorders (anxiety and depression)- a review. Asian Pac J Trop Med 2014; 7(Suppl 1):34-42.
2. Bahmani M, Shirzad HA, Majlesi M, Shahinfard N, Rafieian-Kopaei M. A review study on analgesic applications of Iranian medicinal plants. Asian Pac J Trop Med 2014; 7(Suppl 1):43-53.
3. Bahmani M, Zargaran A, Rafieian-Kopaei M, Saki K. Ethnobotanical study of medicinal plants used in the management of diabetes mellitus in the Urmia, Northwest Iran. Asian Pac J Trop Med. 2014;7:S348-S54.
4. Bahmani M, Zargaran A, Rafieian-Kopaei M. Identification of medicinal plants of Urmia for treatment of gastrointestinal disorders. Rev Bras Farmacogn. 2014; 24(4):468-80.
5. Delfan B, Bahmani M, Rafieian-Kopaei M, Delfan M, Saki K. A review study on ethnobotanical study of medicinal plants used in relief of toothache in Lorestan Province, Iran. Asian Pac J Trop Dis 2014; 4(Suppl 2):879-84.
6. Bahmani M, Sarrafchi A, Shirzad H, Rafieian-Kopaei M. Autism: pathophysiology and promising herbal remedies. Curr Pharm Des 2016; 22(3):277-85.
7. Sarrafchi A, Bahmani M, Shirzad H, Rafieian-Kopaei M. Oxidative stress and Parkinson's disease: New hopes in treatment with herbal antioxidants. Curr Pharm Des 2016; 22(2):238-46.
8. Shayganni E, Bahmani M, Asgary S, Rafieian-Kopaei M. Inflammaging and cardiovascular disease: Management by medicinal plants. Phytomedicine 2015; http://dx.doi.org/10.1016/j.phymed.2015.11.004
9. Bahmani M, Banihabib E, Rafieian-Kopaei M, Gholami-Ahangaran M. Comparison of disinfection activities of nicotine with copper sulphate in water containing Limnatis nilotica. Kafkas Univ Vet Fak 2015; 21(1):9-11.
10. Bahmani M, Saki K, Rafieian-Kopaei M, Karamati SA, Eftekhari Z, Jelodari M. The most common herbal medicines affecting sarcomastigophora branches: a review study. Asian Pac J Trop Med 2014; 7:S14-S21.
11. Delfan B, Kazemeini H, Bahmani M. Identifying effective medicinal plants for cold in Lorestan province, West of Iran. J Evid Based Complementary Altern Med 2015; 20(3):173-79.
12. Delfan B, Bahmani M, Eftekhari Z, Jelodari M, Saki K, Mohammadi T. Effective herbs on the wound and skin disorders: an ethnobotanical study in Lorestan province, west of Iran. Asian Pac J Trop Dis 2014; 4(Suppl 2):938-42.

LETTER TO THE EDITOR

INVESTIGATION INTO EARLY POSTOPERATIVE INFLAMMATORY SMALL BOWEL OBSTRUCTION BY APPLYING GASTROINTESTINAL DECOMPRESSION

MJ. GUO

Department of General Surgery, Xinxiang Central Hospital, Xinxiang City, Henan Province, P.R.China

Received February 2, 2016 – Accepted July 4, 2016

The objective of this study was to investigate early postoperative inflammatory small bowel obstruction (EPISBO) by applying gastrointestinal decompression to relieve abdominal distension. Thirty-six cases of patients were randomly divided into two groups: a control group (20 cases) and an observation group (16 cases). Routine continuous gastrointestinal decompression was assigned to the control group, while gastrointestinal decompression with dynamic and profound adjustment of the gastric tube and abdomen movement was assigned to the observation group, to induce abundant gastric juice and gas, and significantly relieve abdominal distension. A test was performed for each of the two groups to observe the relief time of the abdominal distension and the difference of abdominal girth of 5 cm before and after gastrointestinal decompression. Compared with the control group, the patients in the observation group with abdominal distension had earlier pain relief. More patients in the observation group had a difference of abdominal girth of 5 cm before and after gastrointestinal decompression. In gastrointestinal decompression, the method of dynamic and profound adjustment of the gastric tube and

To the Editor,

Early postoperative inflammatory small bowel obstruction (EPISBO) usually occurs in children within three weeks after pediatric intestinal surgery. The main symptoms are vomiting, abdominal distension and the cease of farting and defecation. Gastrointestinal decompression was adopted to remove the accumulated gastric contents and gas, which subsequently reduced the gastrointestinal tract distension and digestive tube wall tension, relieved the abdominal distention and reduced the stimulation of gastric content, thereby promoting the recovery of gastrointestinal functions (1). If this method is not adopted, with disease aggravation and increasing abdominal pressure, a lot of gastric juice could return into the trachea and cause aspiration pneumonia, which is life threatening. From February 2012 to April 2014, Xinxiang Central Hospital applied dynamic depth adjustment of the gastric tube and abdomen rocking to relieve pediatric abdominal distension.

MATERIALS AND METHODS

The cases of 36 patients (children) with EPISBO were chosen during hospitalization from February 2012 to April 2014. The subjects comprised 20 male and 16 female patients aged between 2 months and 10 years. All the patients suffered abdominal postoperation EPISBO, and were randomly divided

Key words: children, gastrointestinal decompression, early postoperative inflammatory small bowel obstruction (EPISBO)

Mailing address:
Dr MJ. Guo,
Department of General Surgery,
Xinxiang Central Hospital, Xinxiang City,
453000, Henan Province, P.R.China
e-mail: guomj2016@hotmail.com

0393-974X (2016)

DISCLOSURE: ALL AUTHORS REPORT NO CONFLICTS OF INTEREST RELEVANT TO THIS ARTICLE.

into two groups: 20 cases in the control group and 16 cases in the observation group. Among the 36 patients, there were 13 cases of acute intussusception surgical repairs, 10 cases of enterolysis, 5 cases of enterostomy, 5 cases of necrotizing enterocolitis (NEC), and 3 cases of volvulus reposition surgery. Signed informed consent was given by the family of the children to participate in the study.

The infantile gastric tubes had one hole at the top and three side holes. The gastric tube procedure was nasogastric. The size of the gastric tubes can affect the effect of gastrointestinal decompression, therefore, the strict suitable selection of gastric tubes should be made according to the child's age (5). Generally, the 6th ~ 8th type is suitable for children of 1 year of age, 8th ~10th type for children from 1 to 3 years old, and the 10th type or above for children over 3 years of age (2). Gastric tube insertion depth was the tube depth of the first side hole. This study adopted two methods for gastric tube insertion for the two groups of patients. Firstly, based on basic nursing science, the gastric tube insertion length should be the distance from earlobe to xiphoid via tip of nose. Secondly, according to the application of previous nursing experience data, the gastric tube insertion length should be half the length of the earlobe to belly button distance, via nose tip and xiphoid. Both methods were applied equally in both groups. After the successful insertion of the gastric tube, the gastrointestinal decompression was performed. The gastric tube connected to the negative pressure bottle was drained regularly and the negative pressure condition was maintained. The abdominal girth in both groups before and after surgery was measured accordingly, and the two methods applied for the two groups were compared. In the control group, the conventional pediatric gastrointestinal decompression method was employed. The gastric tube depth was maintained as described above. The negative pressure bottle was drained regularly. The maintained negative pressure bottle could enable the gastric juice and gas to flow into the bottle. In the observation group, when there was no gastric juice drained and the gastric tension became serious, the dynamic depth adjustment on the gastric tube was adopted to loosen the fixed tape

Table I. *Comparison of the first pain relief time after surgery.*

Group name	Case quantity	First pain relief time (min)
Control group	20	84.96±14.64
Observation group	16	37.68±9.84
t-statistic		5.759
P value		<0.01

Table II. *Comparison of 5 cm minimum difference value before and after gastric decompression between two the groups.*

Group name	N	5 cm Minimum difference of the value before and after the gastric decompression
Control group	20	3
Observation group	16	16
P value		<0.01

of the gastric tube and then adjust the tube insertion depth till the draining of gastric juice and gas was accomplished. At the same time, the abdomen was rocked gently. Furthermore, a high volume of gastric juice and gas were drained out under the continuing negative pressure. The gastric tube was fixed by tape till the abdomen girth was reduced by more than 5 cm (3). The first relief time in both groups were recorded, along with the case quantity of difference of abdominal girth of a minimum of 5 cm before and after the surgery.

Statistical analysis

Fisher's exact probability test was used to detect the comparison between the enumeration data of both groups. Two independent samples *t*-test was employed for the comparison of measurement data. $P < 0.05$ implied the difference had statistical significance.

RESULTS

The observation group had first pain relief earlier than the patients in the control group. More patients in the observation group had difference of abdominal girth of a minimum of 5 cm before and after gastrointestinal decompression compared to the control group, and the difference had statistical significance ($P<0.01$) (Tables I and II).

DISCUSSION

Medical treatment is the best treatment for EPISBO to enable children to avoid the pain of reoperation. Among the many treatments available, gastrointestinal decompression is the first and most direct measure employed in the elimination of abdominal distension, and is also an effective method to avoid the flow of gastric juice into the trachea, the formation of aspiration pneumonia and the formation of even a life-threatening condition (3). The combination of effective safe gastrointestinal decompression and comprehensive medical treatment can better improve the gastrointestinal peristalsis function and improve recovery. In conventional gastrointestinal decompression for the gastric tube insertion method, due to the 2~3 side holes, and the 4~6cm distance from the top hole and the last side hole, the last side hole can only reach the esophagus area, when the top hole reaches the cardiac area. It can only drain out the upper gastric juice and gas. Although the conventional gastric insertion depth of the gastric tube can reach the stomach, the pediatric gastric tube is soft and flexible, and can curl, fold and form the valve, while children are turned around or in a semi-reclining position; hence the inability to successfully drain out the gastric juice. Thefore, no matter the depth of the inserted gastric tube, the gastric juice remains very difficult to drain out using a conventional fixed depth of gastric tube. The growing gastric juice could compress the abdomen and the loss of pediatric cardioesophageal sphincter, thereby reducing gastrointestinal functions. All these factors increase the risk of esophageal reflux.

The further pushed gastric tube can drain out the juice and gas in the upper stomach. The gastric tube can stretch the folds and valve. The combination of dynamic depth adjustment of a gastric tube and abdomen rocking can better drain out the gastrointestinal sticky juice. During the flow of gas and gastric tube twisting, the deposit of sticky gastric juice could become diluted, thereby reducing the concentration of gastric juice. The dynamic depth adjustment of a gastric tube and abdomen rocking can induce the draining of gastric juice and gas, relieve the gastric tension and improve postoperative bowel function recovery. The abdomen rocking method did not increase gastric tension, and there was no risk for wound burst. The new method is safe, effective, and significant for clinical popularization and application.

REFERENCES

1. Hong P, Maguire E, Gorodzinsky AY, Curran JA, Ritchie K, Chorney J. Shared decision-making in pediatric otolaryngology: Parent, physician and observational perspectives. Int J Pediatric Otorhinolaryngol 2016; 87:39-43.
2. Malik R, Srivastava A, Yachha SK, Poddar U, Lal R. Childhood abdominal tuberculosis: Disease patterns, diagnosis, and drug resistance. Indian J Gastroenterol 2015; 34(6):418-25.

3. Scarpa M, Martinato M, Bertin E, Da Roit A, Angriman I. Intestinal surgery for Crohn's disease: role of preoperative therapy in postoperative outcome. Dig Surg 2015; 32(4):243-50.
4. Schaufler C, Lerer T, Campbell B, Weiss R, Cohen J, Sayej W, Hyams J. Preoperative immunosuppression is not associated with increased postoperative complications following colectomy in children with colitis. J Pediatric Gastroenterol Nutr 2012; 55(4):421-4.
5. Farrelly PJ, Charlesworth C, Lee S, Southern KW, Baillie CT. Gastrointestinal surgery in cystic fibrosis: a 20-year review. J Pediatric Surg 2014; 49(2):280-3.

LETTER TO THE EDITOR

CLINICAL EFFECT OF MECHANICAL FRAGMENTATION COMBINED WITH RECOMBINANT TISSUE PLASMINOGEN ACTIVATOR ARTERY THROMBOLYSIS ON ACUTE CEREBRAL INFARCTION

XF. JIA[1], Z. HONG[2], JH. FAN[3], and YM. ZHANG[4]

[1]Department of Pharmacy, Cangzhou Central Hospital, Cangzhou, China; [2]Department of Neurology, Cangzhou Central Hospital, Cangzhou, China; [3]Department of outpatient nursing, Cangzhou Central Hospital, Cangzhou, China; [4]Department of Pharmacy, The Second Hospital of Hebei Medical University, Shijiazhuang, China

Received June 16, 2016 – Accepted July 28, 2016

This study aims to explore the clinical effect of mechanical fragmentation combined with recombinant tissue plasminogen activator (rt-PA) artery thrombolysis on acute cerebral infarction (ACI). One hundred and thirty-two cases of ACI patients were randomly divided into an experimental group (66 patients) and a control group (66 patients). The experimental group was treated with mechanical fragmentation combined with rt-PA artery thrombolysis method, while the control group was treated with only the rt-PA artery thrombolysis method. All the patients had their basic information recorded. A computational analysis on National Institutes of Health Stroke Scale (NIHSS) scores, curative effect and bleeding data was carried out. The results showed that in the experimental group the curative effects were better and there were fewer complications. Accordingly, we conclude that mechanical fragmentation combined with rt-PA artery thrombolytic method is a safe and reliable therapy with significant curative effects. It improves the NIHSS scores of the patients markedly and reduces the incidence of subsequent pneumonia.

To the Editor,

Featured by sudden onset, acute cerebral infarction (ACI) can lead to permanent irreversible necrosis in the brain tissue of the ischemia central area within a few minutes (1,2). In this case, restoring blood perfusion with thrombolysis is contributive to saving the dying tissue, reducing infarction range and improving the prognosis (3). Recombinant tissue plasminogen activator (rt-PA) is the second generation of thrombolytic drug that is produced with recombinant DNA technology, mainly existing in the vascular endothelium and tissue (4).

Given the rapidly developing neuron-intervention technology and the significant time window advantages of rt-PA, artery thrombolysis has become a main therapy for ACI (5). Intra-artery thrombolysis is mainly advantageous in maintaining the local blood concentration and the balance of total dose of thrombolytic drugs; moreover, it increases the thrombolysis rate of occlusive vessels and reduces the incidence of complications after thrombolysis (6). However, in the case of single application of artery thrombolysis technology, it is inevitable that the occluded blood vessels cannot be recanalized. To date the combination of drug artery thrombolysis and mechanical means is the main research direction (7-9). Therefore, this paper explores the clinical effect of mechanical fragmentation combined with rt-PA artery thrombolysis on ACI.

Key words: acute cerebral infarction, artery thrombolysis, clinical effect, mechanical fragmentation

Mailing address:
Dr Zhen Hong,
Department of Neurology,
Cangzhou Central Hospital,
No.16, Xinhua Western Road,
Cangzhou, Hebei, 061001, China
e-mail: hzhz1866@163.com

0393-974X (2016)

MATERIALS AND METHODS

Research subjects

One hundred and thirty-two cases of ACI patients were selected who were treated in Cangzhou Central Hospital during May 2014 and October 2015. The patients included 72 males and 60 females, aged from 40 to 81 years. The study was examined and approved by the ethics committee of this hospital. Prior to surgery, all the patients or their families signed informed consent, agreeing on the therapy and willing to take the risks of the operation and possible complications. All the patients had their basic information recorded.

The inclusion criteria of thrombolysis treatment (10) were: patients were diagnosed with acute cerebral ischemic stroke by a neurologist and the diagnostic process was consistent with the diagnostic criteria of stroke specified by the World Health Organization; there were clear and accurate imaging findings; the time interval between morbidity and the treatment was no more than 4.5 hours; the patients signed informed consent.

Exclusion criteria of thrombolysis treatment were: the patients had suspected subarachnoid hemorrhage as well as a history of intracranial hemorrhage; the patients had head injury or the symptoms of cerebral infarction or myocardial infarction in the previous three months, gastrointestinal or urinary system hemorrhage in the previous three weeks, or major surgery in the previous two weeks; the patients had arterial puncture in the hemostasis area that could not be compressed easily in the previous week; the patients had severe renal insufficiency or diabetes mellitus; the physical examination results showed that patients had active bleeding or trauma; the patients had taken anticoagulant drugs orally and the international normalized ratio (INR) was higher than 1.5; the patients had received heparin treatment within the previous 48 hours; the patients had blood coagulation or anti-coagulation diseases; the platelet count was below 100×10^9 /L; blood sugar < 2.7 mmol/L; age was below 18 or above 80 years; there were mild or severe neurologic deficits symptoms, namely, NIHSS ≤ 4 or NIHSS ≥ 25; after antihypertensive treatment, systolic blood pressure was higher than 180 mmHg or diastolic blood pressure was higher than 100 mmHg; pregnancy; non-cooperation and rejection to thrombolysis treatment.

Criteria for the interruption termination of treatment were: the patients had to undergo other therapies due to the deterioration of the disease; the patients could not continue to be involved in the study owing to serious adverse events or deterioration of complications; the patients were unwilling to continue to participate in the study; before the patients were medicated or after the first medication, the primary blood fibrinogen level was below 100 mg/dl.

Research methods

In this study, 132 cases of ACI were divided into an experimental group, treated with mechanical fragmentation combined with rt-PA artery thrombolysis method, and a control group, treated with only the rt-PA artery thrombolysis method.

Therapeutic method for the experimental group

The operation area was disinfected with Anerdian. Lidocaine (2%) was applied to the skin of arteriopuncture site of each patient for local anesthesia, followed by systemic heparinization. The right-side femoral artery was percutaneously punctured with Seldinger technology. Catheter sheath and 8F catheter were implanted for whole cerebral angiography, with ultravist (370 mg/ml) used as the contrast agent. The occlusion site was in the distal artery. The guide wire and catheter were placed in the location of the thrombus; the guide wire was drawn and pulled for a few times to achieve mechanical fragmentation. If vascular recanalization was achieved, 5 mg of rt-PA was injected into the target artery to dissolve the small emboli generating from mechanical fragmentation. If the thrombus in blood vessels was still not removed, 5 mg of rt-PA was injected directly into the thrombus, and the guide wire was drawn and pulled for a few times. When the mechanical fragmentation was completed, if vascular recanalization was achieved, then the thrombolytic therapy could be ended; if the thrombus in blood vessels was still not removed, then the above operation was repeated. In the operation, the upper limit of the total addition amount of rt-PA was 20 mg.

Single artery thrombolysis treatment with recombinant tissue plasminogen activator

The whole cerebral angiography (the procedure was the same as that of the experimental group) was performed. Guide wire and catheter were sent to the

thrombus site. Then, 5 mg of rt-PA was injected into the distal end of the thrombus. While the micro catheter (in the guiding catheter) was drawn back, rt-PA was injected into the proximal end of the thrombus. After each injection, angiography was performed in the site to determine whether the blood vessel was occluded or not. If vascular recanalization was achieved, the thrombolysis treatment could be ended; otherwise, 5 mg of rt-PA was applied again for thrombolytic treatment. During the operation, whether to continue rt-PA injection was determined according to the dissolving conditions of the thrombus. The upper limit of the total addition amount of rt-PA was 20 mg.

Postoperative treatment

During the operation, whole-process electrocardiogram monitoring of the patients was required; it was necessary to closely monitor the patients' consciousness, life signs and pupil changes. If patients had the polarity of tension and dysphoria, it was determined immediately whether to perform sedation treatment. In the case of glossocoma which could affect airway ventilation and lead to the progressive decrease of the patients' blood oxygen saturation, the patients were treated timely with glossopharyngeum breather pipe to help open the airway. In this case, there was no difference in the treatment of the two groups.

One hour after surgery, each patient was treated with 0.4 ml of low molecular heparin calcium through subcutaneous injection for three-day anticoagulation to prevent cerebral thrombogenesis; in addition, the patients were treated with oral administration of bayaspirin (100 mg/day) and clopidogrel (75 mg/day) to resist platelet aggregation and edaravone to protect the nerves. Three days after surgery, each patient underwent computed tomography scan of the head to check whether they had any secondary cerebral hemorrhages.

Observation index

NIHSS scores of all the patients were collected, including the scores before thrombolysis, 24 h after thrombolysis and 7/14/90 days (7/14/90 d) after thrombolysis. The Barthel Index (BI) Scale of daily living ability was used for the patients 0 days after thrombolysis. The modified Rankin score was divided into seven levels from no symptom at all (0 score) to death (6 scores), aiming to evaluate the results of the functional recovery of the patients after having stroke.

Turgor grading of target vascular bed was represented by thrombolysis in cerebral infarction (TICI) classification and its angiography. TICI II-III meant vascular recanalization was successful; TICI 0-I meant vascular recanalization had failed (11).

Statistical analysis

The data in this study were expressed in the form of mean ± standard deviation; SPSS 18.0 software was

Table I. *General data of the patients in experimental group and control group*.

Groups	Cases	Male	Female	Age	Risk factors			
					Hypertension	Diabetes mellitus	Cerebral infarction	Blood sugar
Experimental group	66	38	28	64.88±12	28	12	10	7.54±3.62 (mmol/L)
Control group	66	34	32	67.44±11	32	15	9	8.03±3.56 (mmol/L)

used for statistical analysis; count data were expressed with constituent ratio; *chi*-squared test was applied for the comparison between two samples; *t*-test was used to compare the mean values of two samples; $p < 0.05$ meant the difference was statistically significant.

RESULTS

Analysis of the patients' general data

According to the statistical data in Table I, the differences between the two groups (regarding the age, gender, history of hypertension and diabetes of the patients) were not statistically significant ($p > 0.05$). In addition, it was observed that the onset to thrombolysis time of the experimental group and the control group was respectively (289.71±43.41) min and (290.29±35.80) min.

Analysis of NIHSS score

Table II shows the NIHSS scores of the two groups before treatment and 24 h, 7 days, 14 days and 90 days after treatment. According to the data, it was found that before the treatment, the comparative

Table II. *NIHSS scores of experimental group and control group in different treatment time windows before and after treatment.*

Groups	Before treatment	After treatment			
		24h	7d	14d	90d
Experimental group	15.62±5.11	8.55±6.13	6.83±6.25	6.33±4.25	5.68±3.65
Control group	14.41±5.04	12.54±6.55	10.43±4.66	8.65±4.89	7.98±3.14
p value	0.894	0.011	0.027	0.008	0.03
t	0.038	2.935	2.698	3.056	3.347

Table III. *Comparative analysis on platelet count and coagulation function of the patients in experimental group and control group (after treatment).*

		PT(s)	APTT(s)	FIB(g/l)	PLT(×10^9/l)
7 days after thrombolysis	Experimental group	12.56±0.97	29.33±4.51	3.78±0.25	199.58±50.62
	Control group	12.78±1.23	31.45±4.62	3.91±0.27	197.36±49.87
	p value	0.832	0.178	0.788	0.999
	t	0.254	1.403	0.374	0.109
24 hours after thrombolysis	Experimental group	16.33±0.97	43.55±5.21	2.79±0.54	198.32±52.78
	Control group	17.41±0.92	44.36±5.05	2.84±0.57	204.44±57.89
	p value	0.342	0.567	0.623	0.741
	t	0.997	0.602	0.498	0.405

Note: PT: prothrombin time; APTT: activated partial thromboplastin time; FIB: fibroblast; PLT: platelets.

differences in NIHSS scores between the two groups were not statistically significant ($p > 0.05$). After the treatment, NIHSS scores of the experimental group were evidently lower than those of the control group ($p < 0.05$).

Analysis of curative effect

Barthel index was used to evaluate the living ability of the patients; 90 days after the operation, it was found that the Barthel index of the experimental group (72.56±21.47) was evidently higher than that of the control group (55.41±19.78) ($p < 0.05$).

In the experimental group, the modified Rankin Scale (mRS) scores of 46 cases (69.7%) ranged between 0-1; the mRS scores of 20 cases (30.3%) ranged between 2-6. In the control group, 26 cases (39.4%) scored between 0 and 1, while 40 cases (60.6%) scored between 2 and 6. Ninety days after the operation, the nerve function defect of the experimental group was evidently lower than that of the control group ($\chi^2 = 5.874$, $p = 0.038$).

The recanalization rate was 75.76% in the experimental group, including 50 cases of good recanalization and 16 cases of poor recanalization. The recanalization rate was 51.52% in the control group, including 34 cases of good recanalization and 16 cases of poor recanalization. It can be seen that the vascular recanalization rate in the experimental group was evidently higher than that of the control group ($\chi^2 = 4.567$, $p = 0.041$).

Comparing the curative effect of the experimental group and the control group seven days after treatment, we found that in the experimental group, 14 cases were cured; the treatment was markedly effective on 24 cases, effective on 13 cases and ineffective on 5 cases; the conditions of 3 patients deteriorated and 7 patients died. Accordingly, the effective rate was 77.3% while the cure rate was 21.2%. In the control group, 4 cases were cured; the treatment was markedly effective on 9 cases, effective on 15 cases and ineffective on 18 cases; 10 patients deteriorated; 10 patients died. The effective rate of the control group was 42.4%, while the cure rate was 6.1%. According to the rank sum test, the differences of curative effects 7 days after treatment between the two groups were statistically significant ($p = 0.001$).

Complications after thrombolysis

In the experimental group, there were 16 cases of pneumonia and 5 cases of hemorrhage; in the control group, there were 28 cases of pneumonia and 7 cases of hemorrhage. Accordingly, the occurrence rate of pneumonia in the experimental group was evidently lower than that of the control group ($x^2 = 4.541$, $p = 0.031$), while the occurrence rate of hemorrhage in the experimental group was significantly higher than that of the control group ($\chi^2 = 4.111$, $p = 0.039$).

Comparative analysis of platelet count and coagulation function after treatment

Based on the data in Table III, it can be observed that after treatment, the difference in platelet count and coagulation function between the experimental group and the control group had no statistical significance ($p > 0.05$).

DISCUSSION

As the only drug approved to be used for thrombolysis, rt-PA is featured by its favorable ability to dissolve thrombus, high specificity and satisfactory safeness, which has been proved by many researchers (12-14).

In this study, we found that intravenous thrombolysis had a remarkable curative effect on the neural function defect of ACI patients; compared with the ordinary therapy, its curative effect was more obvious and the effect was enhanced over time. In comparison with the control group, the curative effect was better and there were fewer complications in the experimental group. Mechanical fragmentation combined with rt-PA artery thrombolysis could effectively increase the recanalization rate of occluded blood vessels and promote blood flow perfusion for faster recovery, thus easing ischemia; moreover, through the recovery of blood supply, ischemia and hypoxia of brain tissue were relieved; consequently, more ischemic penumbra cells and moribund brain tissue could be restored. Compared with intravenous thrombolysis, single intra-arterial

thrombolysis is advantageous in concentrating the drug in the local artery, so that the drug concentration in this location is higher and fewer drugs are applied. By combining mechanical fragmentation with rt-PA artery thrombolysis, the advantages are integrated and strengthened; with the combination of the two methods, the contact area of the thrombus and thrombolysis drugs is increased, so that the local drug concentration reaches its maximum, which improves vascular recanalization rate and reduces thrombolysis time greatly.

In summary, mechanical fragmentation combined with rt-PA artery thrombolysis is preferable to not increasing the risks of intra-arterial thrombolysis, such as bleeding rate and pneumonia; moreover, it can improve vascular recanalization rate after treatment and clinical prognosis. Therefore, it is a safe and reliable treatment method for ACI.

REFERENCES

1. Kikuchi K, Miura N, Kawahara KI, Murai Y, Morioka M, Lapchak PA, Tanaka E. Edaravone (Radicut), a free radical scavenger, is a potentially useful addition to thrombolytic therapy in patients with acute ischemic stroke (Review). Biomed Rep 2013; 1(1):7-12.
2. Yamaguchi T, Yamada T, Hirota T. Abstract 195: Reducing frequency of symptomatic intracranial hemorrhage in patients with acute ischemic stroke treated by recombinant tissue-plasminogen activator; interim result of a prospective observational cohort study. Stroke 2013; (2): A195.
3. Zhang S, Zhang LH, Wang YJ, Zhang AL, Zhang X. Effects of synchronous treatment of bilateral scalp acupuncture and rehabilitation training on activities of daily life in patients with cerebral infarction at acute phase. Chin Acupunct Moxibust 2014; 34(9):837-40.
4. Fu ML, He WQ, Dai WZ. Efficacy of Solitaire™ Stent arterial embolectomy in treating acute cardiogenic cerebral embolism in 17 patients. Med Sci Monit 2016; 22:1302-8.
5. Tan G, Liu M, Lei C, Chen Y, Hao Z. Influencing factors analysis of hemorrhagic transformation in non-thrombolysis patients after acute cerebral infarction. Chin J Cerebrovasc Dis 2015; 12(8):409-14.
6. Shen B, Liu Q, Gu Y, Wang Y, Zhnag Z. Efficacy and safety evaluation on arterial thrombolysis in treating acute cerebral infarction. Cell Biochem Biophys 2015; 73(2):297-304.
7. Yan Z, Yu T, Wang Y, Wang M, Liang H. literature review and case report of intravenous thrombolysis in acute cerebral infarction attributed to cervical arterial dissection. J Stroke Cerebrovasc Dis 2015; 24(9):265-9.
8. Won YD, Lee TK, Kim YJ, Chun CW, Yoo DS. Clinical results of intraarterial thrombolysis according to tPA administration and perfusion/diffusion mismatching. Acta Neurochirurg 2015; 157(3):1-10.
9. Jeong HS, Kwon HJ, Song HJ. Impacts of rapid recanalization and collateral circulation on clinical outcome after intraarterial thrombolysis. J Stroke 2015; 17(1):76-83.
10. Wang YX, Chen Y, Zhang CH, et a. Study on the effect of urinary kallidinogenase after thrombolytic treatment for acute cerebral infarction. Eur Rev Med Pharmacolog Sci 2015; 19:1009-12.
11. Suzuki R, Koga M, Yamamoto H. Early recanalization rates following intravenous recombinant tissue plasminogen activator (rt-PA) therapy in acute ischemic stroke. Neurosonology 2015; 28:12-16.
12. Takenaka K, Kato M, Yamauti K, Hayashi K. Simultaneous administration of recombinant tissue plasminogen activator and edaravone in acute cerebral ischemic stroke patients. J Stroke Cerebrovasc Dis 2014; 23:2748-52.
13. Levine SR. Review, historical context, and clarifications of the NINDS rt-PA stroke trials exclusion criteria: part 1: rapidly improving stroke symptoms. Stroke 2013; 44(9):2500-505.
14. You YP. Epigallocatechin gallate extends the therapeutic window of recombinant tissue plasminogen activator treatment in ischemic rats. J Stroke Cerebrovasc Dis 2016; 25(4):990-97.

LETTER TO THE EDITOR

VITAMIN D AND MICRO-INFLAMMATORY STATE IN HEMODIALYSIS PATIENTS A MINI REVIEW AND META-ANALYSIS

L. HUANG, J. ZHOU, Y-J. ZHAO and G-C. HU

Division of Nephrology, Affiliated Hospital of Chengde Medical University, Chengde, Hebei, China

Received February 22, 2016 – Accepted June 20, 2016

There is growing evidence that vitamin D (VitD) plays a role in the pathophysiological mechanism of every patient undergoing hemodialysis, and this role is significantly altered in a microinflammatory state. However, it is unclear whether supplementation dosage or route of administration should be altered due to this state. Thus, the objective of our mini review and meta-analysis was to re-consider supplementation of VitD in HD patients exhibiting micro-inflammatory state. Pubmed, Web of Science and Google Scholar were searched up to January 19, 2016. We included studies that evaluated supplementation in HD patients with micro-inflammatory state. One reviewer extracted data and one reviewer verified the data accuracy. We qualitatively summarized the main results and meta-analyzed data on comparable outcomes across studies. The main outcome measures were serum levels of VitD. Ten eligible studies were published between 2002 and 2016, involving a total 1,239 patients. Average vintage of hemodialysis was 35.36 (±31.08) months. We identified a high degree of clinical diversity (interventions and outcomes) and methodological heterogeneity (sample size and risk of bias) in included trials. The studies we reviewed provide some weak evidence to support VitD supplementation in patients on hemodialysis exhibiting micro-inflammatory state. We recommend that future trials focus on our main outcome measures (that is variable comparable across studies).

To the Editor,

Dialysis patients without obvious clinical signs of infection, but with increased inflammatory factors, are manifested with persistent inflammation. It was recently established that even small increases in the levels of either cytokines or acute-phase proteins predicted vascular disease among populations of otherwise healthy-appearing adults.

Markers of inflammation have the same predictive values for dialysis patients; however, we know that inflammation is not characteristic in all patients but varies with time. The relationship between inflammation and vascular disease in this population is strong enough to obscure other well-known risk factors.

The effectiveness of VitD therapy for HD patients cannot be disputed, at least per reducing PTH levels and treating renal bone disease, however it is less clear from the published literature whether one approach is more efficacious than others, even meta-analysis failed to show superiority of either therapy.

The options of VitD therapy for HD patients are daily oral calcitriol, pulse oral calcitriol, pulse IV calcitriol, and pulse IV VitD analogues. In China, in patients whose kidneys or parathyroid glands are not working normally, VitD is used as calcitriol to treat hypovitaminosis D or secondary hyperparathyroidism, therefore we aimed to evaluate serum levels of VitD in hemodialysis patients with clinically documented micro-inflammatory state.

Key words: calcitriol, hemodialysis, micro-inflammatory state, vitamin D

Mailing address:
Dr. Gui-Cai Hu,
Division of Nephrology, Affiliated Hospital
Chengde Medical University, No. 36 Nanyingzi Road,
Chengde 067000, Hebei, China
Tel.: +86 18571714629
e-mail: hu_guicai@yahoo.com.hk

0393-974X (2016)

DISCLOSURE: ALL AUTHORS REPORT NO CONFLICTS OF INTEREST RELEVANT TO THIS ARTICLE.

MATERIALS AND METHODS

Search strategy, study selection, data extraction and quality assessment

We screened potentially relevant studies via a search of the literature in English language in Pubmed and Web of Science computerized bibliographic databases, and the last search was performed on January 19, 2016.

The subject terms and keywords used in our searches were "vitamin D" (all fields), or "calcitriol "(all fields), and "hemodialysis" (all fields), and "microinflammatory state" (all fields), or "micro-inflammatory state" (all fields) with filters for animal, non-human and non-English publications. We included observational studies of all designs and for duplicate publications including overlapping data sets, only the latest or the most comprehensive study was included. Comments, review articles, case reports, letters, editorials, proceedings and unpublished articles (abstracts only) were excluded. References from the retrieved publications and bibliographies of relevant reviews were checked to identify potential additional articles.

Each title and abstract was reviewed in order to clarify whether the article was relevant or not. We extracted the following information from each study: first author, publication year, country, sample size, sex, disease duration or years of duration of chronic hemodialysis (hemodialysis vintage), vitamin D, interleukin-6 (IL-6) and C-reactive protein (CRP) levels. We considered Meta-analysis Of Observational Studies in Epidemiology (MOOSE) and Preferred Reporting Items for Systematic reviews and Meta-Analyses (PRISMA) guidelines. Newcastle-Ottawa Scale (NOS) for case-control or cohort studies and the Agency for Healthcare Research and Quality (AHRQ) for cross-sectional studies were used to assess methodological quality of the included studies. Credibility of the evidence for each statistically significant association in this manuscript was evaluated by the Venice criteria.

The ethics committee of the Affiliated Hospital of Chengde Medical University approved our study.

Statistical analysis

We used REVMAN software (Version 5.2; the Cochrane Collaboration Oxford, UK) to carry out the meta-analysis, and DerSimonian and Laird random-effects model with a 95% confidence interval to account for measurement variability among the included studies.

In presenting the data on VitD values in patients on hemodialysis with micro-inflammatory state, mean ± standard deviation (SD) was considered. In studies which used mean ± standard errors of means (SEM) we transformed SEM to SD to maintain consistency.

When there was no obvious heterogeneity, data were pooled with a fixed-effects model. Cochran's Q-statistic and inconsistency index (I2) test were used to assess heterogenity. An I2-value >50% or P value <0.05 put forward heterogeneity, and these data were calculated with DerSimonian & Laird random-effects models to accommodate diversity.

RESULTS

Pubmed, Google Scholar and Web of Science searches identified 21 potential articles. The review flow chart is depicted in Fig. l, and we followed the recommendations of the PRISMA statement.

Screening of the 21 titles or abstracts followed exclusion of two non-English papers, one paper describing non-hemodialysis, one book-chapter, and eight review papers or papers describing translational or other basic (non-clinical) studies. Finally, ten reports were studied (1-10) which were published between 2002 and 2016 involving, a total of 1,239 patients. In eight studies, the participants were clearly divided by gender, so 556 males *vs* 412 females were included. Average vintage of HD was 35.36 (±31.08) months.

No studies were excluded based on the quality of study, although some studies did not report sufficient information for a clear bias assessment. All studies reported inclusion and/or exclusion criteria, and stated that the participants met these criteria.

With regard to our main outcome measure, three included papers had stringently defined serum levels of VitD and seven studies had not. In all searched entries, VitD therapy on HD was either in form of oral calcitriol (1, 4, 6) or was not clearly specified (Table I).

Study limitations according to GRADE guidelines

We summarized the study limitations of each included trial following the GRADE guidelines in Table II. In four out of ten studies, allocation to the treatment group was not adequately concealed (1-4). In one case of inadequately concealed allocation, the study was located in China, though without specific location (1) .

It was unclear in eight studies whether both patients and outcome assessors were blinded to the treatment arm to which patients were allocated (1, 3, 5-10). Selective outcome reporting could have occurred, as we did not have access to a protocol developed à priori for any of the ten studies, but the described design of included studies highlights this possibility in two

specific cases (1, 3). Another three studies might have had a problem of selective outcome reporting as they report biased smaller studies (2, 7, 8).

DISCUSSION

Our review and meta-analysis provide weak evidence to support VitD supplementation for hemodialysis patients with micro-inflammatory state. The majority of the studies that we included in our mini-review demonstrated statistically non-consistent results. Among the studies reviewed that found a need for supplementation, they were either limited or inconclusive, which further weakens the fundamental understanding of the pooled estimate of effect reported on the main outcome of our mini-review.

Active VitD is responsible for the reticence of the production and release of PTH and increase of the serum levels of calcium by stimulating calcium absorption from the intestine. Unfortunately, in spite the relatively large amount of literature, it is dominated by poorly designed or insufficiently large studies (2, 3, 9, 11, 12). In parallel, it stimulates phosphate absorption, so its adverse effects include hypercalcemia, hyperphosphatemia, and over-suppression of PTH levels. Two of the studies (13, 14) mainly included patients with only mild hyperparathyroidism, thus the potential role of intermittent oral therapy in severe hyperparathyroidism is not clear. Therefore, we may assert that oral VitD is useful in HD patients, as it lowers PTH levels. Clinical trials with a great number of participants requiring the benefits of intravenous calcitriol may be warranted in those patients resistant to the effects of oral VitD.

Based on the current evidence, this lowering of PTH levels is the cardinal reason to recommend its

Table I. *Studies included in the meta-analysis.*

Study (Number in References)	N/exp	Males	Females	Vintage of dialysis	IL-6	CRP	Serum VITD	supplementation VITD - oral
van Tellingen et al. (5)	74	N/A	N/A	>6 m	2.73±0.75	9.25±5 mg/L	N/A	N/A
Brandenburg et al. (10)	57	36	21	3.1±2.6 years	N/A	10.1±16.1 mg/L	N/A	N = 46
Memoli et al. (7)	12	6	6	>1 year	8.88	CRP= 6.98±0.6 mg/L	N/A	N/A
Wang et al. (3)	66	N/A	N/A	>3 months	N/A	N/A	N/A	N/A
Xiao et al. (2)	64	30	34	6.88±2.94 years	N/A	no statistically significant difference	N/A	N/A
Cai et al. (9)	118	80	38		N/A	higher than in control	N/A	N/A
Gluhovschi et al. (8)	21	6	15	4.92±3.4 years	N/A	higher than in control	N/A	N/A
Zhang et al. (1)	484	247	237	12 m	N/A	HsCRP= 7.8±2.6 9.7±3.3 mg/L	17.6±7.7 nmol/L	0.5 µg/day
Viaene et al. (4)	81	71	10	N/A	3.6	4.4 mg/L	49.4 mg/L	N = 56
Ren et al. (6)	131	80	51	5.94±4.76 years	N/A	hsCRP=2.3 mg/L	26.5±10.7	N/A

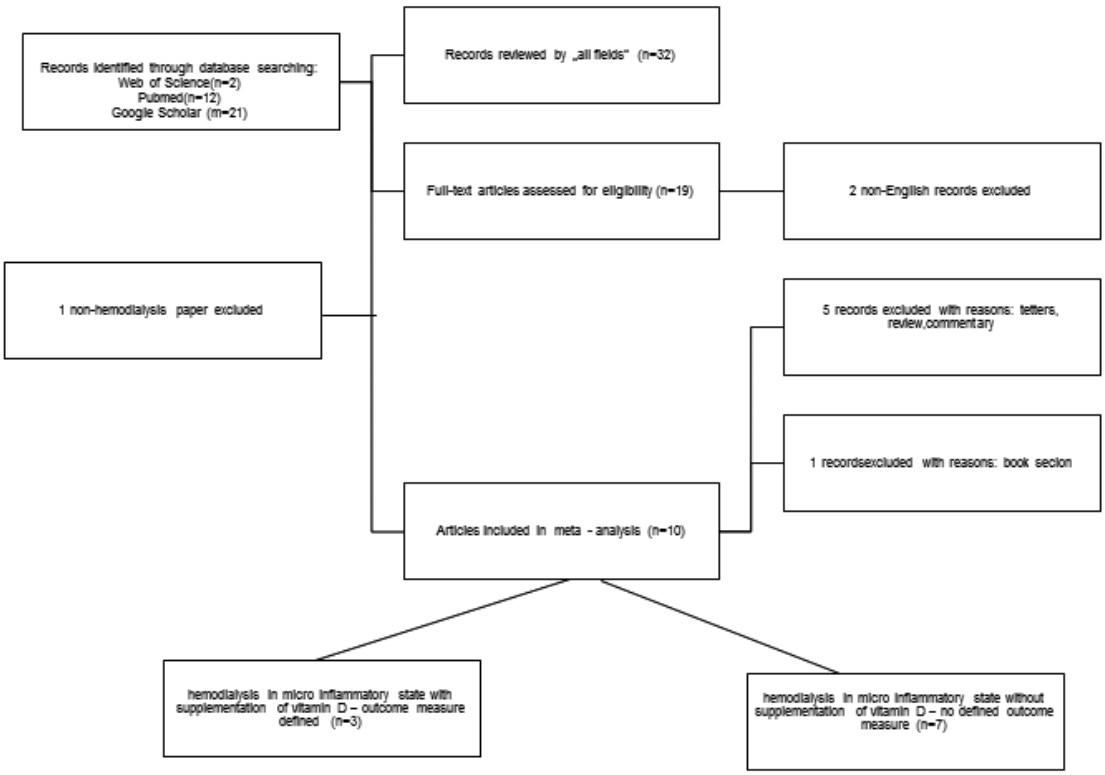

Fig. 1. *Flow chart of meta-analysis wherein we followed the recommendations of the PRISMA statement.*

Table II. *Study limitations and risk of bias.*

Study (Number in References)	Lack of allocation concealment	Lack of blinding	Selective outcome reporting bias
van Tellingen et al. (5)	no major risk of bias	Unclear	no major risk of bias
Brandenburg et al. (10)	no major risk of bias	Unclear	no major risk of bias
Memoli et al. (7)	no major risk of bias	Unclear	major risk of bias
Wang et al. (3)	major risk of bias	Unclear	Unclear
Xiao et al. (2)	major risk of bias	major risk of bias	major risk of bias
Cai et al. (9)	no major risk of bias	Unclear	no major risk of bias
Gluhovschi et al. (8)	no major risk of bias	Unclear	major risk of bias
Zhang et al. (1)	risk of bias	Unclear	Unclear
Viaene et al. (4)	Major risk of bias	no major risk of bias	no major risk of bias
Ren et al. (6)	no major risk of bias	Unclear	no major risk of bias

use. In the studies reviewed we did not noticed that the micro-inflammatory status altered the dosage of prescribed VitD, so we cannot recommend this increase. Use of oral calcitriol and its alternatives (intravenous or VitD analogs) need to be balanced against their significantly higher costs.

REFERENCES

1. Zhang J, Zhang P, Ni X, et al. Vitamin D status in chronic dialysis patients with depression: a prospective study. BMC Psychiatry 2014; 14:125.
2. Xiao DM, Wu Q, Fan WF, Ye XW, Niu JY, Gu Y. Effect of serum FGF-23, MGP and fetuin-A on calcium-phosphate metabolism in maintenance hemodialysis patients. Hemodial Int 2013; 17:483-92.
3. Wang D, Cai S-X, Chen Q-P, Chen J-H, Liao W. Effects of Valsartan on microinflammatory state and pulmonary function in maintenance hemodialysis patients. J Nanchang Uni (Med Science) 2012; 8:007.
4. Viaene L, Behets GJ, Heye S, Claes K, Monbaliu D, Pirenne J, D'Haese PC, Evenepoel P. Inflammation and the bone-vascular axis in end-stage renal disease. Osteoporos Int 2016; 27:489-97.
5. van Tellingen A, Grooteman MP, Schoorl M, et al. Intercurrent clinical events are predictive of plasma C-reactive protein levels in hemodialysis patients. Kidney Int 2002; 62:632-38.
6. Ren H, Gong D, Jia F, Xu B, Liu Z. Sarcopenia in patients undergoing maintenance hemodialysis: incidence rate, risk factors and its effect on survival risk. Ren Fail 2016; 1-8.
7. Memoli B, Salerno S, Procino A, et al. A translational approach to micro-inflammation in end-stage renal disease: molecular effects of low levels of interleukin-6. Clin Sci (Lond) 2010; 119:163-74.
8. Gluhovschi C, Modilca M, Margineanu M, et al. Surprising good antioxidant status in patients with Balkan Endemic Nephropathy on hemodialysis undergoing vitamin C therapy. A pilot study. Rom J Intern Med 2014; 52:158-61.
9. Cai B, Zhang J, Zhang M, Li L, Feng W, An Z, Wang L. Micro-inflammation characterized by disturbed Treg/Teff balance with increasing sIL-2R in patients with type 2 diabetes. Exp Clin Endocrinol Diabetes 2013; 121:214-19.
10. Brandenburg VM, Schlieper G, Heussen N, et al. Serological cardiovascular and mortality risk predictors in dialysis patients receiving sevelamer: a prospective study. Nephrol Dial Transplant 2010; 25:2672-9.
11. Meng L, Fu B. Practical use of sevelamer in chronic kidney disease patients on dialysis in People's Republic of China. Ther Clin Risk Manag 2015; 11:705-12.
12. Davenport A. Effects of hemodiafiltration of inflammation and oxidative stress. Hemodiafiltration: Springer; 2016. p. 153-63.
13. Moe SM, Kraus MA, Gassensmith CM, Fineberg NS, Gannon FH, Peacock M. Safety and efficacy of pulse and daily calcitriol in patients on CAPD: a randomized trial. Nephrol Dial Transplant 1998; 13:1234-41.
14. Herrmann P, Ritz E, Schmidt-Gayk H, et al. Comparison of intermittent and continuous oral administration of calcitriol in dialysis patients: a randomized prospective trial. Nephron 1994; 67:48-53.

LETTER TO THE EDITOR

IN VITRO EFFECT OF IL-17D ON HUMAN OVARIAN CARCINOMA CELL AND INHERENT IMMUNITY

LL. FAN, XZ. XUE AND N. JIAO

Department of Obstetrics and Gynecology, First Affiliated Hospital of Hena University of Science and Technology, Luoyang, Henan, China

Received June 13, 2016 – Accepted August 1, 2016

The first two authors contributed equally to this study

This study explored the expression of interleukin 17D (IL-17D) secreted by human ovariancarcinoma cells and the effect of exogenous IL-17D transfection on MICA, which is the ligand of NKG2D, on the surface of ovary carcinoma cells. Human ovarian papillary serous adenocarcinoma cell line SKOV3, empty vector control cell line SKOV3/vector, exogenous human IL-17D stable-transfected cell line SKOV3/IL-17D, as well as cisplatin (CDDP)-resistant cell SKOV/CDDP were cultured; ovarian adenocarcinoma cell line OVCAR-3, empty vector control cell line OVCAR3/vector and OVCAE3/IL-17D were observed under a microscope. In the study, methyl-thiazolyl-tetrazolium (MTT) method was used to detect the inhibition rate, resistance index and proliferation of SKOV3 and SKOV3/CDDP. It was found that the expression of IL-17 D in SKOV3/CDDP was much higher than that of its parent cell line SKOV3; IL-17D might be correlated to the drug resistance of cells; the proliferation of SKOV3 transfected with IL-17D was significantly accelerated, indicating IL-17D may be effective in promoting the growth of oncocyte.

To the Editor,

Effector T-lymphocyte T help 17 cells (Th-17) play a leading role in inflammatory and autoimmune diseases; moreover, characteristic cytokine interleukin 17 (IL-17) generated by Th-17 has attracted more and more attention (1, 2). The increased expression of IL-17 can be detected in peripheral blood or tumor cell of patients suffering from gastric carcinoma, ovarian cancer and colon cancer (3, 4). The level of IL-17 is considered to be in positive correlation with the malignancy of tumor. IL-17D is generated by CD4+T cells and is capable of inducing neutrophil and endothelial cells to produce IL-6, IL-8 and granulocyte-macrophage colony-stimulating factor (GM-CSF). IL-17 and its products may result in changes of number and types of cell factors in tumor microenvironment; however, the pro-inflammatory cytokine effect of IL-17A, E and F only has been confirmed (6). Fewer studies regard IL-17D, hence its function is not yet clearly known. Currently, a large amount of studies have found that the occurrence and development of tumor is closely related to the autoimmune state of the body.

Moreover, the sensitivity of tumor cells to natural killer (NK) cells is closely correlated with the expression level of MICA. Through detecting the

Key words: ovarian carcinoma cells, IL-17D, resistance index, inherent immunity

Mailing address:
Dr Lili Fan,
Department of Obstetrics and Gynecology,
First Affiliated Hospital, No. 636 GuanLin Street,
Hena University of Science and Technology,
LuoLong District, LuoYang, Henan, 471000, China
e-mail: fanlili2528@163.com

0393-974X (2016)

proliferation of various epithelial ovarian carcinoma cells (7-9), this study explored the *in vitro* effect of IL-17D on human epithelial ovarian carcinoma cells, the role of IL-17D in the occurrence and development of ovarian carcinoma and its correlation with drug resistance, and the effect of IL-17D on the inherent immunity of the body, aiming to provide a basis to find new targets of ovarian carcinoma treatment.

MATERIALS AND METHODS

General materials

Cell lines used in the study included human ovarian papillary serous adenocarcinoma cell line SKOV3, empty vector control cell line SKOV3/vector, stable-transfected cell line SKOV3/IL-17D, cisplatin (CDDP)-resistant cell line SKOV3/CDDP, human ovarian carcinoma OVCAR3, empty vector control cell line and stable transfected cell line OVCAR3/IL-17D.

Reagents used mainly included RPMI-1640, fetal bovine serum (FBS), trypsin, dimethyl sulfoxide, methyl thiazolyl tetrazolium, monopotassium phosphate, CDDP for injection (freeze-dried), Trizols reagent, reverse transcription system, and polymerase chain reaction (PCR) primer.

Experimental method

In vitro cultivation of cells (10): SKOV3, SKOV3/vector, SKOV3/IL-17, SKOV3/CDDP, OVCAR3, OVCAR3/vector and OVCAR3/IL-17D were put into RPMI media containing 20% FBS separately and then cultured in a sterile incubator (37°*C*, 5% CO_2, saturated humidity). Culture solution was changed every one or two days. Then subculture was carried out. Firstly, 2 ml of trypsin (0.25 %) was added. Then the cells were observed under a microscope; 20% FBS and RPMI medium were added when cytoplasm shrank and became round and the space between cells narrowed. Then the mixture was centrifuged. Culture continued after supernate was removed.

Detection of resistance index of CDDP-resistant cells with MTT method: ovarian serous papillary adenocarcinoma parent cells and CDDP-resistant cells were centrifuged after being digested with trypsin. RPMI media were added to adjust the concentration of cells into 8×10^4/ml. The cells were then inoculated into a 96-well plate, 100 μl each well, and cultured in a sterile incubator containing 5% CO_2. CDDP solution in the concentrations of 1 μg/ml, 2 μg/ml, 4 μg/ml, 8 μg/ml, 16 μg/ml and 32 μg/ml was added, respectively. After 24-h culture, 20 μl of MMT solution in a concentration of 5 g/L was added. After 4-h culture, the solution was centrifuged, followed by the removal of supernate and the addition of 150 μl of dimethyl sulfoxide. The absorbancy of the solution was detected after being vibrated.

Detection of proliferative characteristics of 7 kinds of cells: 7 kinds of cells mentioned above were washed by phosphate buffer saline (PBS) twice and then digested with trypsin. After centrifugation, RPMI media containing 20% FBS was added to adjust the concentration of cells into 8×10^4/ml. Afterwards, the cells were inoculated into a 96-well plate, 100 μl each well, and cultured in an incubator containing 5% CO_2. Each well was added with 20 μl of MTT solution (5 g/L) in the dark. After 4-h culture, the solution was centrifuged and supernate was removed. The absorbancy of the solution was measured after the addition of 150 μl of DMSO and vibration.

Detection of IL-17D expression of 7 kinds of cells: after the seven kinds of cells fused for 80% ~ 85%, they were precooled at 4°*C* and then washed with PBS twice. Each kind of cells was added with 1 ml of Trizol reagent and then transferred to eppendorf (EP) tubes for decomposition. Afterwards, 200 μl of chloroform was added into each tube. After vibration and centrifugation, the obtained supernate was transferred to new EP tubes and added with isopropanol with the same quantity to deposit RNA. After centrifugation, the supernate was removed. White transparent sediment was obtained after washing with 75% ethyl alcohol and it was preserved at –80°*C*. RNA obtained was diluted with deionized water and then reversely transcribed to cDNA using reverse transcription kit. 0.2 ml of cDNA was taken and added with total RNA, Oligo (dT), Random Primers and Nuclease-Free water; after 5-min initial denaturation with a PCR amplifier, Nuclease-Free water, Goscript 5× Reaction Buffer, $MgCl_2$, PCR Milleatide Mix, Recombinant RNsin Ribonuclease Inhibitor and Goscipt Reverse Transcriptase were added. Then the whole reaction system was preserved at 25°*C* for 10 min, 40°*C* for 1 h, and 70°*C* for 10 min and finally the reaction proceeded at 4°*C*. cRNA was preserved at -20°*C*. Gene sequence was searched via National Center of Biotechnology Information (NCBI) database and primer sequence was designed

for primer synthesis. As to GAPDH primer sequence (amplified fragment length: 172 bp), forward primer was CGCTGAGTACGTCGTGGAGTC and reverse primer was GCTGATGATCTTGAGGCTGTTGTC; as to IL-17D primer sequence (amplified fragment length: 166 bp), forward primer and reverse primer were TACATAAACAGTCTCAAACTCGCAC and CTGATCCTAAAGCCCTTACAACTAA respectively. GoTaq® qPCR Master Mix real-time quantitative kit (Promega Company, USA) was taken as the reaction system for the amplification of target genes. Real-time (RT) PCR was as follows. A system consisting of upstream primer (10 μM), downstream primer (10 μM), cDNA template, Go Taq® qPCR Master Mix, 2X, CXR 100× and Nuclease-Free Water (20 μl) was processed by initial denaturation at 95°*C* for 10 min, 95°*C* for 15 s and 60°*C* for one min, for 42 cycles. Whether there was non-specific amplification and primer dimer was determined according to solubility curve.

Statistical analysis

SPSS ver. 13.0 statistical software was used for processing data. Data were expressed as mean ± SD. The expression of IL-17D was processed by single factor variance analysis. Difference was considered to be statistically significant if $p < 0.05$.

RESULTS

Resistance index of cells

MTT detection results suggested that the half maximal inhibitory concentration (IC50) of CDDP for SKOV3/CDDP was 36.05 mg/L ($p < 0.05$) and the IC50 of CDDP for SKOV3 was 7.81 mg/L. Thus, the drug resistance of the cells was 4.62, indicating drug resistance test could be carried out.

Detection results of the proliferation of seven kinds of cells with MTT method

The results of detection using MTT method suggested that the cell doubling time of the transfection group significantly shortened and the cells in the transfection group grew faster than those in the non-transfection group and empty vector group ($p < 0.05$), and the difference was remarkably significant; however, there was no significant

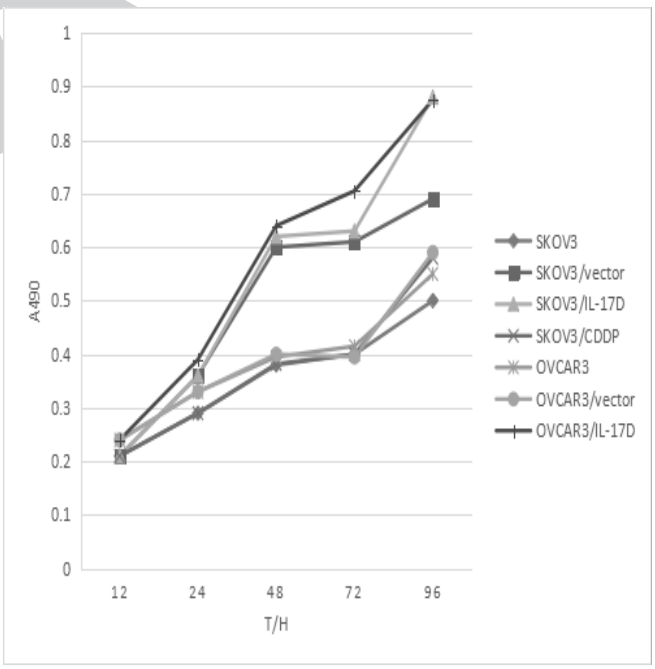

Fig. 1. *Growth curves of seven kinds of cells at different time points.*

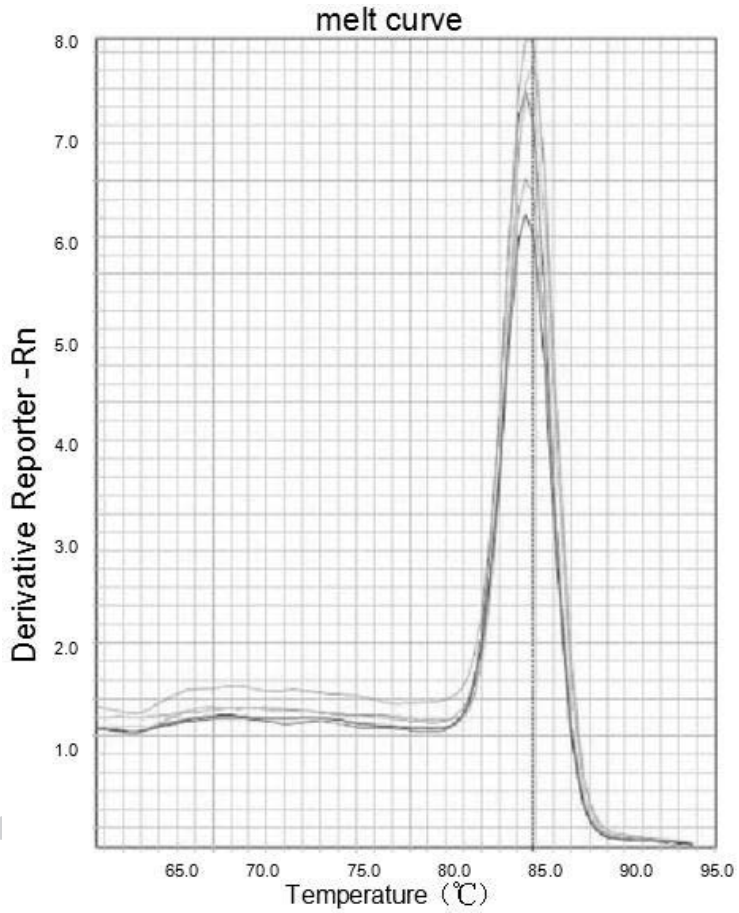

Fig. 2. *The melting curve of IL-17D.*

difference between the non-transfection group and the empty vector group ($p > 0.05$); the growing speed of SKOV3/CDDP cells was much faster than that of SKOV3 cells ($p < 0.05$), and the difference was significant; and the growing speed of SKOV3/CDDP cells was not remarkably different to that of SKOV3/IL-17D cells, as did OVCAR3/CDDP cells and OVCAR3/IL-17D cells ($p > 0.05$). It revealed that cells transfected with IL-17D had significantly shortened cell doubling time and significantly accelerated cell growth, suggesting IL-17D might be effective in promoting the growth of cancer cells. Through detection, it was also found that the growing speed of drug-resistant cell lines was much higher than that of their parent cell lines. Fig. 1 shows the growth curve of the seven kinds of cells.

Expression of IL-17D in seven kinds of epithelial ovarian carcinoma cells

As shown in Fig. 2, melting curves of internal references and target genes both had one single peak, indicating the product was specific and there was no dimer or hybrid product.

Table I demonstrates the expression of IL-17D in different SKOV3 cells and OVCAR3 cells.

C-$2^{\Delta\Delta CT}$ stood for the relative expression quantity of IL-17D in cells. Single factor variance analysis results suggested that the expression of IL-17D in SKOV3/vector cells, SKOV3/IL-17D cells and SKOV3/CDDP cells had no significant differences with that in SKOV3 cells ($F = 45.40$, $p = 0.000 < 0.05$). Results indicated that the expression of IL-17D in the transfection cells was much higher than that

Table I. *The expression level of IL-17D mRNA.*

	Different SKOV3 cells				*Different OVCAR3 cells*		
Group	Parent cells	Empty vector control cells	Stable transfected cells	Cisplatin resistant cells	Ovarian carcinoma cells	Empty vector control cells	Cisplatin resistant cells
ΔC_T	12.34±0.28	12.16±0.17	5.53±0.02	5.91±0.04	14.04±0.01	13.94±0.05	6.48±0.01
$C^{-2\Delta\Delta CT}$	1.00±0.00	1.10±0.21	113.02±24.39	91.95±18.02	1.00±0.00	1.10±0.05	182.61±16.22
F	45.36				368.86		
P	0.000						

(mean ± SD)

of the non-transfection cells and empty vector cells, indicating cell transfection had high efficiency and could be used in experiments. Through comparing the expression of IL-17D in drug resistant and parent cells, it was found that the expression of IL-17D of drug resistant cells was significantly higher than that of the parent cells, indicating there might be a correlation between IL-17D and the drug resistance of the cells.

Moreover, the expression of IL-17D in OVCAR3, OVCAR3/vector and OVCAR3/CDDP had no remarkable differences with that in OVCAR3 ($F = 369.89$, $p = 0.000 < 0.05$). Results indicated that the expression of IL-17D in the transfection cells was much higher than that of the non-transfection cells and empty-vector cells, suggesting cell transfection had high efficiency and thus could be used in experiments.

DISCUSSION

The role that cell factors play in tumors has attracted much attention. Interleukin is a member of the cell factor family and its receptors play important roles in the cellular signaling network. IL-17 is correlated to many autoimmune diseases such as multiple sclerosis, systemic lupus erythematosus, rheumatic arthritis, myocarditis and restrictive cardiomyopathy (11, 12), however, the action mechanism of IL-17D in these diseases it not yet clearly known, hence remains to be further discussed.

In this study, two kinds of epithelial ovarian carcinoma cell lines were established *in vitro*. Using qRT-PCR detection, it was found that the expression of IL-17D in the cells transfected with IL-17D was 113-fold and 182-fold higher than before transfection, suggesting IL-17D showed a specific expression in the ovarian carcinoma cells, which provided a theoretical basis for relevant studies. Through measuring the proliferation of cells with MTT method, it was found that the transfection cells had a significantly shortened doubling time and a higher growth speed than the non-transfection cells and empty-vector cells, and the difference was statistically remarkable. This indicated that IL-17D was capable of stimulating the proliferation of

tumor cells, and the difference of the proliferation of different types of epithelial ovarian carcinoma cells transfected with IL-17D differed slightly.

To sum up, human ovarian papillary serous adenocarcinoma cells and ovarian adenocarcinoma cells proliferate and double faster after being transfected with IL-17D, indicating IL-17D is able to promote tumor cell growth.

REFERENCES

1. Moraes AS, Paula RFO, Pradella F, et al. The suppressive effect of IL-27 on encephalitogenic Th17 cells induced by multiwalled carbon nanotubes reduces the severity of experimental autoimmune encephalomyelitis. CNS Neurosci Ther 2013; 19(9):682-87.
2. Zhou XY, Gao TS, Yang X, Cui P, Qu JQ, Xu J. A comparative study on the effect of iodine-rich herbal decoction and iodine excess on the differentiation of Th17 cells in Iodine-deficiency NOD.H-2h4 Mice. Lishizhen Med Mat Med Res 2014; 25(6):1520-24.
3. Balkwill F, Mantovani A. Inflammation and cancer: back to Virchow? Lancet 2001; 357(9255):539-45.
4. Maeda Y, Ohtsuka H, Tomioka M, Oikawa M. Effect of progesterone on Th1/Th2/Th17 and regulatory T cell-related genes in peripheral blood mononuclear cells during pregnancy in cows. Vet Res Comm 2013; 37(1):43-49.
5. Gaffen S. Structure and signalling in the IL-17 receptor family. Nat Rev Immunol 2009; 9(8):556-67.
6. Camuesco D, Rodríguez-Cabezas ME, Garrido-Mesa N, et al. The intestinal anti-inflammatory effect of dersalazine sodium is related to a down-regulation in IL-17 production in experimental models of rodent colitis. Br J Pharm 2012; 165(3):729-40.
7. Schilling D, Tetzlaff F, Konrad S, Li W, Multhoff G. A hypoxia-induced decrease of either MICA/B or Hsp70 on the membrane of tumor cells mediates immune escape from NK cells. Cell Stress Chap 2014; 20(1):139-47.
8. Gómez-Lomelí P, Bravo-Cuellar A, Hernández-Flores G, et al. Increase of IFN-γ and TNF-α production in CD107a+NK-92 cells co-cultured with cervical cancer cell lines pre-treated with the HO-1 inhibitor. Cancer Cell Int 2014; 14(1):100-100.
9. Mei JZ, Guo KY, Wei HM. Analysis of the expression of MICA on tumor cell lines of different histotypes and their sensitivity to NK cytotoxicity. Chin J Immun 2007; 34-37.
10. Virant-Klun I, Skutella T, Cvjeticanin B, Stimpfel M, Sinkovec J. Serous papillary adenocarcinoma possibly related to the presence of primitive oocyte-like cells in the adult ovarian surface epithelium: a case report. J Ovarian Res 2011; 4(8):1-5.
11. Shirota Y, Yarboro C, Fischer R, Pham TH, Lipsky P, ILLei GG. Impact of anti-interleukin-6 receptor blockade on circulating T and B cell subsets in patients with systemic lupus erythematosus. Ann Rheum Dis 2013; 72(1):118-28.
12. Hu Y, Dong C, Yue Y, Xiong S. In vivo delivery of interleukin-35 relieves coxsackievirus-B3-induced viral myocarditis by inhibiting Th17 cells. Arch Virol 2014; 159(9):2411-19.

LETTER TO THE EDITOR

REAL-TIME SHEAR WAVE ELASTROGRAPHY AND APRI INDEX FOR EVALUATING AUTOIMMUNE HEPATITIS FIBROSIS

LL. SUN[1], G. DONG[1], B. WANG[2], Q. ZHENG[1], S. WANG[1] and RF. ZHANG[1]

[1]Department of Ultrasonography, The First Affiliated Hospital of Zhengzhou University, Henan, China;
[2]Department of Radiology, The First Affiliated Hospital of Zhengzhou University, Henan, China

Received January 28, 2016 – Accepted May 26, 2016

The objective of this study was to investigate the significance of real-time supersonic shear imaging (SSI) and serum biochemical index in evaluating the degree of autoimmune hepatitis fibrosis. Retrospective analysis was carried out to study 291 cases of patients with autoimmune hepatitis, and discuss the value of SSI application, APRI index and bilirubin on autoimmune hepatitis. The area under the receiver operating characteristic curve (AUROC) was taken for statistical analysis to determine its diagnostic accuracy. In the high degree of hepatic fibrosis, the hepatic SSI measured value of autoimmune hepatitis positively correlated to ALT, AST, APRI ratio, AST and AST/ALT. The SSI measured value significantly and positively correlated to the degree of hepatic fibrosis (r=0.598, p=0<0.01). In chronic hepatic fibrosis, the elasticity values of AIH, PBC, AIH-PBC overlap syndrome (OS) were in a rising trend, and the difference in the elasticity value of each fibrosis stage was statistically significant (P<0.01). Hepatic SSI measured value was employed to respectively detect the AUROC of S3 stage and S4 stage for AIH, PBC, and AIR-PBC OS groups, which resulted as being higher than the APRI index detected in S3 stage and S4 stage. SSI measured index had better diagnostic significance than APRI index on hepatic fibrosis for AIH, PBC and AIH-PBC OS groups.

To the Editor,

Autoimmune hepatitis (AIH) is an immune disease which mainly affects the liver, causing primary biliary cirrhosis (PBC) and primary sclerosing cholangitis (PSC) (1). Most patients ultimately develop cirrhosis. In recent years, the incidence of AIH has been on the rise. The reversible intervention method on hepatic fibrosis progress could be a promising measure (2-3).

Supersonic shear imaging (SSI) could measure the elasticity value of the tissue of a specific area, and quickly measure the degree of hepatic fibrosis (4).

This study aims to evaluate the diagnosis of the fibrosis stage in AIH, PBC, and AIH-PBC overlap syndrome (OS) patients.

MATERIALS AND METHODS

Two hundred and ninety-one cases of patients suffering from AIH who underwent hepatic aspiration biopsy in our hospital between May 2011 and September 2015 were included in the study. This total included 125 cases of AIH, 55 of PBC, and 111 of AIH-PBC OS. The study was

Key words: real-time shear wave elastography, hepatic fibrosis, autoimmune hepatitis, primary biliary cirrhosis, overlap syndrome

Mailing address:
Dr Ruifang Zhang,
Department of Ultrasonography,
The First Affiliated Hospital,
Zhengzhou University, No.1, Jianshe East Road,
Zhengzhou City, 450000, PR China
e-mail: Rui_high20151223@hotmail.com

0393-974X (2016)

DISCLOSURE: ALL AUTHORS REPORT NO CONFLICTS OF INTEREST RELEVANT TO THIS ARTICLE.

approved by the ethics committee of our hospital. Informed consent was received from the patients to participate in the study. All cases of patients were confirmed according to the standard diagnosis of Autoimmune Hepatic Guide.

Methods

All patients were subjected to AixPlorer Supersonic shear imaging with 4C convex array probe and a probe frequency of 1.0-6.0 MHz. The hepatic anterior right area was chosen for detection. After the elasticity imaging mode was set, patients were required to hold their breath for 3 ~ 5 seconds. Images were stored when they became stable without shaking; a round detection area of 2 cm diameter in the imaging area was chosen to measure the elasticity value, and Kpa was set as the unit. The measurement detection was repeated 5 times, the average value of the analysis was calculated. The measured elasticity value was calculated using Young's modulus. A higher Young's modulus value indicates tissue hardness (2).

All the patients were subjected to percutaneous liver biopsy using ultrasound within a week after SSI detection. According to the pathology classification stage of chronic hepatitis in Viral Hepatitis Prevention Plan, 2001, the hepatic inflammatory activities were divided into G0, G1, G2, G3 and G4. The degrees of fibrosis were divided into S0, S1, S2, S3 and S4. Fasting venous blood samples were taken for clinical biochemical detection and routine examination.

Statistical analysis

SPASS 17.0 statistical software was applied to analyze the data. The measurement data that met Gaussian distribution were marked as mean±SD. One-way ANOVA was applied for comparison between groups. Kruskal-Wallis detection was employed to analyze the differences between groups. Spearman rank correlation analysis was adopted to study the correlation between two variables. ROC curve was utilized to analyze the accuracy of SSI diagnostic hepatic fibrosis, with a $P<0.05$ marked statistical significant difference. The different AUROCs are to detect fibrosis stage ≥S2, ≥S3 and S4.

RESULTS

From Table I, we can see that with hepatic fibrosis aggravation, Spearman rank correlation analysis detected that hepatic SSI value was positively correlated to ALT, fibrosis degree, APRI index, AST, AST/ALT ratio, and bilirubin level, $P<0.05$.

The correlation of SSI measured value and fibrosis degree in AIH, PBC, and AIH-PBC OS groups is shown in Table II. Table I shows the SSI index has high diagnostic accuracy on moderate and high fibrosis degrees (S≥2). The AUROC, sensitivity and specificity of SSI index and APRI index in the present investigation showed high diagnostic efficiency.

DISCUSSION

This study investigated the significance of applying real-time SSI and serum biochemical index to evaluate the degree of autoimmune hepatitis fibrosis. Using retrospective analysis, we found that the SSI measured index had better diagnostic significance than APRI index on hepatic fibrosis for AIH, PBC and AIH-PBC OS groups.

SWE is the latest clinical elasticity imaging

Table I. *Comparison of results of SSI value of AIH different fIbrosis degrees and APRI index.*

		Fibrosis degree	APRI index	Bilirubin level μmol/L	AST (U/L)	ALT (U/L)	AST/ALT ratio
SSI value (Kpa)	r	0.598	0.348	0.302	0.235	0.18	0.151
	P	0	0	0	0	0.02	0.01

Table II. *SSI values and fibrosis degree in AIH, PBC, AIH-PBC overlap syndrome group.*

cases	Disease classification	SSI measured value					P
		S0	S1	S2	S3	S4	
55 cases	PBC	9.346±2.7 (7 cases)	9.241±2.9 (20 cases)	14.826±5.1 (19 cases)	17.924±11.3 (5 cases)	29.849±3.1 (4 cases)	<0.05
125 cases	AIH	8.724±2.1 (11 cases)	10.770±5.9 (39 cases)	14.303±6.5 (41 cases)	16.623±5.3 (15 cases)	22.774±9.0 (19 cases)	<0.05
111 cases	AIH-PBC overlap syndrome	10.716±4.3(5 cases)	11.037±5.1 4 (27 cases)	11.809±4.3 (46 cases)	19.572±8.02 (41 cases)	28.179±10.8 (12 cases)	<0.05
	P*	>0.05	>0.05	>0.05	>0.05	>0.05	

technology, and can measure the absolute value of the hardness in tissues of certain areas. Many studies showed its significance in the assessment of hepatitic fibrosis (5-6). The study of Feld et al. (7) applied the SSI index for hepatitis hardness to judge the fibrosis stage, and draw the ROC curve. Although all the AUROC were above 0.90, the cases were mainly chronic hepatitis B patients.

At present, there are few reports related to SWE application on evaluating AIH fibrosis, and there are even fewer with regard to SWE on AIH, PBC, AIH-PBC OS classification. Wang et al. (1) applied SWE detection on 71 cases of patients with AIH, and concluded that the AUROC of middle fibrosis stage (S2 and S3), severe hepatic fibrosis and early hepatic cirrhosis (S4) were respectively 0.77 and 0.97. In this study, the SSI measured AUROC of AIH S2 stage, S3 stage and S4 stage of the 291 patients were respectively 0.516, 0.712, and 0.877, the results showing certain differences. SSI index may be related to the differences in specimen quantities. The overall samples in that study were less, just 70 cases.

Compared to the APRI index, the SSI index had higher diagnostic efficiency on each fibrosis stage of AIH, PBC and AIH-PBC OS. SSI index had significance on patients with high risk of liver fibrosis of S3 stage and S4 stage.

REFERENCES

1. Wang YF, Lu LG. The diagnosis and treatment of autoimmune hepatitis and its overlap syndrome. J Clin Hepatol 2012; 28:323-25.
2. Bavu E, Gennisson JL, Couade M. Noninvasive in vivo liver fibrosis evaluation using supersonic shear imaging: a clinical study on 113 hepatitis C virus patients. Ultrasound Med Biol 2011; 37:1361-73.
3. Ferraioli G, Tinelli C, Dal Bello B. Accuracy of real-time shear wave elastography for assessing liver fibrosis in chronic hepatitis C: a pilot study. Hepatology 2012; 56:2125-33.
4. Leung VY, Shen J, Wong VW. Quantitative elastography of liver fibrosis and spleen stiffness in chronic hepatitis B carriers: comparison of shear-wave elastography and transient elastography with liver biopsy correlation. Radiology 2013; 269:910-18.
5. Yang MM, Ma H, Zhou L. Clinical and pathological characteristics analysis of autoimmune hepatitis in 166 cases. J Inter Med 2013; 52:412.
6. Zhou K, Lu LG. Assessment of fibrosis in chronic liver diseases. J Dig Dis 2009; 10:7-14.
7. Feld JJ, Dinh H, Arenovieh T. Autoimmune hepatitis: effect of symptoms and cirrhosis on natural history and outcome. Hepatology 2005; 42:53.

LETTER TO THE EDITOR

COMPARISON OF EFFECTS OF ^{18}F-FDG PET-CT AND MRI IN IDENTIFYING AND GRADING GLIOMAS

PJ. SONG[1], QY. LU[2], MY. LI[3], X. LI[3] and F. SHEN[1]

[1]Department of Radiology, Liaocheng People's Hospital and Liaocheng Clinical School of Taishan Medical University, Liaocheng, China; [2]Department of Pathology, Liaocheng People's Hospital and Liaocheng Clinical School of Taishan Medical University, Liaocheng, China; [3]Department of Neurosurgery, Liaocheng People's Hospital and Liaocheng Clinical School of Taishan Medical University, Liaocheng, China

Received March 31, 2016 – Accepted July 29, 2016

The first two authors contributed equally to this study as co-first authors

Glioma is the most common type of brain tumor. Malignant gliomas tend to have an increasingly higher incidence and are difficult to treat. Therefore, an accurate diagnosis of the grade of glioma before surgery is very important for planning surgery and determining prognosis. To compare the values of ^{18}F-deoxyglucose positron emission tomography/computer tomography (^{18}F-FDG PET-CT) and magnetic resonance imaging (MRI) for identifying and grading gliomas, we selected 70 patients who were diagnosed as having a primary glioma or suspected glioma at the People's Hospital of Liaocheng in Shandong, China, and divided them into an observation group, which was examined by ^{18}F-FDG PET-CT and a control group, which was examined by MRI. Image analysis, visual semi-quantitative analysis and qualitative analysis, follow-up and pathological results of the two groups were compared. Specificity, accuracy and sensitivity of brain MRI and PET-CT in grading the gliomas were calculated, and the results obtained were processed by *Chi*-squared test. Standard uptake value (SUV), $SUV_{correct}$ and L/WM (SUV_{max} ratio of a lesion to normal white matters in the opposite side) of FDG in the different grades of glioma were analyzed by single-factor variance analysis. Postoperative pathological detection confirmed 47 cases of glioma; the sensitivity, specificity and accuracy of PET-CT in grading glioma were all higher than those of MRI (P<0.05); the correlation between SUV and glioma grade, between $SUV_{correct}$ and glioma grade, and between L/WM and glioma had significant difference (P<0.05). Thus, it was concluded that ^{18}F-FDG PET-CT performs better in diagnosing gliomas than MRI and is also more suitable for identifing different grades of glioma.

To the Editor,

Glioma, the most common malignant tumor of the nervous system, accounts for 35.2~61% of intracranial tumors. Diagnosis of gliomas is difficult as they have multiple subtypes and different imaging manifestations; determination of the grade and malignant degree of a glioma is of great importance in planning treatment and evaluating prognosis (1,

Key words: glioma, standard uptake value, image reconstruction, magnetic resonance imaging

Mailing address:
Dr Feng Shen,
Department of Radiology,
Liaocheng People's Hospital, Clinical School,
Taishan Medical University, 67 Dongchang West Road,
Liaocheng, Shandong, 252000, China
e-mail: sfshenfsf@163.com

0393-974X (2016)

DISCLOSURE: ALL AUTHORS REPORT NO CONFLICTS OF INTEREST RELEVANT TO THIS ARTICLE.

2). Previously, magnetic resonance imaging (MRI) was the preferred imaging method for evaluating gliomas, however, MRI plain scan and enhancement scanning have defects in identifying high-grade and low-grade gliomas. For example, a high-grade glioma with MRI performance of no or mild edema, no enhancement in the solid area of the tumor and no necrotic lesion is often misdiagnosed as a low-grade glioma (3, 4). Misdiagnosing a high-grade glioma as a low-grade glioma may result in insufficient treatment, while misdiagnosing a low-grade glioma as a high-grade glioma may lead to excessive treatment; both situations can increase the recurrence and fatality rate (5).

Positron emission tomography (PET), a novel imaging method, can provide functional metabolism imaging information and delicate anatomical morphological images (6-8). ^{18}F-fluorodeoxyglucose (^{18}F-FDG), a substance similar to glucose, is the most commonly used imaging agent (9). This study analyzed MRI and PET-CT images and parameters of 70 patients, who were suspected as having gliomas, before surgery and compared the effectiveness of MRI and ^{18}F-FDG PET-CT in diagnosing and grading gliomas, aiming to provide more comprehensive, accurate and reliable imaging information for the diagnosis of gliomas and for planning the treatment.

MATERIALS AND METHODS

Study subjects

Seventy patients who were diagnosed with primary gliomas or suspected gliomas were selected from the People's Hospital of Liaocheng in Shandong, China from July 2012 to July 2014. Of the 70 patients, 44 were males and 26 were females, with a mean age of 48.00±15.53 years. Major clinical symptoms of those patients included headache, nausea, emesis, paroxysmal limb twitch and loss of consciousness. Sixty patients had supratentorial lesions and 10 patients had subtentorial lesions; 65 patients had a single lesion and 5 patients had multiple lesions. Diameter of the lesions ranged from 1 to 6 cm. All patients signed informed consent before examination. They were divided into an observation group and a control group. Thirty-five patients in the observation group were examined by head PET-CT while the thirty-five patients in the control group were examined by head MRI.

Main instruments

The instruments used included Discovery LS PET-CT scanner composed of Advance PET and Biograph spiral 64-layer CT (GE Healthcare, Milwaukee WI, USA) and installed with PET detection (Bi4Ge3O12, BGO) with 18 rings and thickness of 4.25 mm; Circular accelerator (MINItrace); Activity meter (CRC-15R, CAPINTEC, USA); high-pressure liquid chromatography (HPLC) (Prostar210, Varian, USA); thin layer chromatogram scanner (Mini-Scan, Bioscan, USA); MRI machine (True Form based Verio 3.0T MRI system and matched head birdcage coil, Siemens, Germany).

Imaging method

PET-CT imaging. Patients in the observation group were examined with ^{18}F-FDG PET-CT. Before drug injection, fasting blood-glucose of patients needed to be less than or equal to 7 mmol/L, and they abstained from eating for at least 6 h prior to testing. ^{18}F-FDG was intravenously injected according to the standard of 3.70~5.55 MBq/kg. Collection of images started after patients remained in a static state for 60 min. The bladder was emptied before examination. CT scanning (tube voltage: 120 KV; tube current: 140 mA; layer thickness: 5 mm; layer spacing: 5 mm) was performed first. Then PET scanning (10 min/bed; layer thickness: 5 mm; spacing: 4.25 mm; matrix: 128×128; field of view (FOV): 15.2 cm). Attenuation correction and iteration reconstruction were performed on PET-CT data using low-dose CT. Finally, axial, sagittal and coronal CT, PET and PET/CT fusion images were obtained.

MRI. Patients who received head MRI examination were examined by plain scan, enhanced scan and diffusion weighted imaging (DWI) examination. MRI plain scan items included sagittal T1-weighted Imaging (T1WI), coronal T1WI and axial T1WI, T2WI and DWI. Scanning parameters of fluid attenuated inversion recovery (FLAIR) sequence T1WI were as follows: time of repetition (TR): 2025 ms; time of echo (TE): 8.4 ms; time of inversion (TI): 750 ms; thickness of layer: 6 mm; spacing: 1.5 mm; FOV: 24 cm×18 cm; matrix: 320×224; number of excitation (NEX): 2. Scanning parameters of fast recovery fast spin echo (FRFSE) sequence T2WI were as follows: TR: 4000 ms; TE: 110 ms; layer thickness: 6 mm; spacing: 1.5 mm; FOV: 24cm×24 cm; matrix: 512×512; NEX: 2. Scanning parameters of spin-echo echo-planar imaging (SE-EPI) sequence DWI were as follows: TR: 10000 ms; TE: 80.1 ms; layer thickness: 6 mm;

spacing: 1.5 mm; FOV: 24cm×24cm; matrix: 128×128; NEX: 1.

Head MRI enhanced scan items included axial, sagittal and coronal T1WI. Scanning parameters of Spin echo (SE) sequence T1WI were as follows: TR: 500 ms; TE: 8.4 ms; flip angle: 75°; layer thickness: 6.0 mm; spacing: 1.5 mm; FOV: 24cm×24cm; matrix: 256×150; NEX: 1. The contrast agent used in enhanced scanning was gadolinium-diethylenetriamine pentaacetic acid (Gd-DTPA) (dose: 0.1 mmol/kg).

Image reconstruction and fusion method

PET image was reconstructed using ordered subsets expectation maximum (OS-EM) method. CT scanning data were used in image attenuation correction. CT image was reconstructed into 4.25 mm thick using the standard method. PET image and CT image were transmitted to a workstation for frame-to-frame contrapuntal fusion and display. Sagittal T1WI, coronal T2WI, axial T1WI, axial T2WI and axial DWI data were synthesized and fused by MRI workstation.

Image analysis method

PET-CT images were reviewed by a nuclear medicine technician, an imaging technician and a neurosurgeon. Every PET-CT result was analyzed by visual qualitative analysis and semi-quantitative analysis.

MRI images were reviewed by two imaging physicians and a neurosurgeon. MRI results of every subject were analyzed for enhancement degree.

Postoperative pathological examination

Craniotomy or stereotactic needle biopsy was performed within one week after MRI or PET-CT examination. Effused blood and necrotic tissue were removed from the postoperative tumor and other pathologically changed tissue specimens collected; then the tissue specimens were washed by normal saline, fixed with neutral formaldehyde solution, embedded with paraffin, and cut into 5 μm sections. Finally, pathological examination was performed on the lesion area which was consistent with the analyzed layer of PET transverse image and MRI enhancing center transverse image.

Statistical analysis

Data were statistically analyzed using SPSS 20.0 software. PET/CT image visual qualitative analysis and semi-quantitative analysis results as well as MRI image analysis results were compared to the pathological and follow-up results of patients to calculate the sensitivity, specificity and accuracy of PET-CT and MRI in grading the gliomas. The results were processed by *Chi*-squared test. Standard uptake value (SUV) and corrected SUV of FDG to different-grade gliomas were compared. L/WM (SUVmax ratio of a lesion to normal white matters in the opposite side) of different-grade gliomas was analyzed with single-factor variance analysis. $P < 0.05$ meant there was a statistically significant difference.

RESULTS

General data

The differences in the general data between the two groups had no statistical significance (Table I).

Postoperative pathological detection results

Surgical pathology or stereotactic needle biopsy suggested that 47 out of 70 patients were diagnosed

Table I. *Comparison of general data.*

Group	Gender (n)		Age (year)	Site of location (n)		Duration of symptoms before visiting a doctor (a)
	Male	Female		Supratentorial	Subtentorial	
Observation group	21	14	46.32±13.27	32	3	1.53±1.26
Control group	23	12	47.26±14.52	28	7	1.46±1.17

as having gliomas, 13 patients were diagnosed with other types of highly malignant tumors (mainly lymphoma and metastatic tumors) and 10 patients were diagnosed with non-tumorous lesions (mainly cerebral infarction and arteriovenous malformation). According to WHO central nervous system tumor grading standard (2000), there was 1 case of grade I (pilocytic astrocytoma), 10 cases of grade II (6 cases of diffuse astrocytoma and 4 cases of oligodendroglioma), 14 cases of grade III (9 cases of anaplastic astrocytoma and 5 cases of anaplastic astrocytomas) and 22 cases of grade IV (glioblastoma multiforme).

Comparison of diagnostic results between the two groups

In the observation group, diagnostic results of 26 cases were consistent with postoperative pathological results. In the control group, diagnostic results of 21 cases were consistent with postoperative pathological results. Images of a typical case is shown in Fig. 1. The comparison of sensitivity, specificity and accuracy of PET-CT and MRI in grading gliomas suggested that the diagnostic

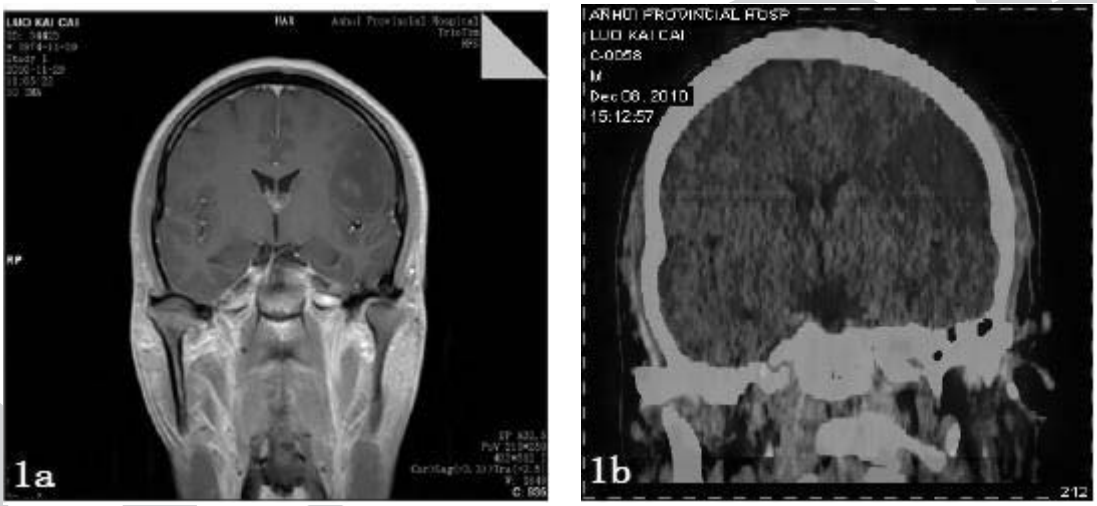

Fig. 1. *A typical case (astrocytoma). a) Head MRI before surgery demonstrated an uneven enhanced region of 4.5 × 3.2 cm in the left insular lobe cortex, left frontal cortex and subcortical region and scattered patchy enhancement inside the lesion; b) PET/CT demonstrated increased diffuse radioiodine uptake in the left fronto-temporal lobe and a slight increase of 11C-MET; SUVmax of the lesion and the opposite side was 1.9 and 1.6 respectively).*

Table II. *Comparison of sensitivity, specificity and accuracy of PET-CT and MRI in grading gliomas (%).*

Parameter	Observation group				Control group			
	Grade I	Grade II	Grade III	Grade IV	Grade I	Grade II	Grade III	Grade IV
Sensitivity	80.60	86.40	87.70	82.10	76.30	82.90	86.30	79.60
Specificity	78.50	87.90	88.40	79.50	72.40	86.30	87.40	76.50
Accuracy	79.80	85.70	86.90	78.60	75.60	84.70	85.10	77.20

efficiency of the observation group was higher than that of the control group and the diagnostic results of grade II and III glioma were better than those of grade I and IV gliomas (Table II).

Correlation between SUV, $SUV_{correct}$ and L/WM of PET-CT and diagnosis of glioma grade

Three groups of data of gliomas with different grades had statistically significant differences (P<0.05). The comparison of corrected SUV of grade II and grade III gliomas and corrected SUV of grade I and IV gliomas showed significant differences (P<0.05), indicating that corrected SUV is suitable for the grading of gliomas. Corrected SUV performed better in identifying grade II and III gliomas than grade I and IV gliomas. Details are shown in Table III.

Semi-quantitative analysis, a commonly used method for diagnosing gliomas, can evaluate PET detection results of brain tumors. The commonly used semi-quantitative analysis index mainly includes SUV, and ratio of tumor uptake to normal tissue uptake. Table II shows that SUV and L/WM of PET-CT had obvious correlation with the grade of glioma (P<0.05). Corrected SUV of PET-CT in diagnosing grade II and III gliomas and in diagnosing grade I and IV gliomas had obvious correlation (P<0.05), suggesting that the corrected parameter is more suitable for diagnosing glioma grades and may perform better in diagnosing grade II or III gliomas rather than grade I and IV gliomas.

There are few current studies on the application of PET-CT corrected SUV in identifying glioma grades. Corrected SUV has been proved to be closer to the actual uptake of tissue than SUV. That is because the maximum correction method aims at partial volume effect (PVE) induced by limited resolution of PET-CT imaging system. In CT scans, CT values of some lesions have a diameter that is smaller than the layer thickness and they are easily confounded with other tissues in PVE calculation, leading to deviation between the results of the CT test and real value; to be specific, measured CT values of micro low-density lesions in high-density tissue may be slightly higher than the actual value, while the values of micro high-density lesions in low-density tissue may be a little lower. PVE can result in degeneration of image quality and distortion of CT values of lesions, thus increasing the misdiagnosis rate.

Resolving the above problems has long been a difficult point in the medical imaging field. An accurate method for correcting PVE of PET-CT images has not yet been identified. This study applied the maximum correction method for correcting PVE of PET-CT images, based on the size and activity of lesions, to increase the accuracy of diagnosis.

DISCUSSION

A glioma is a commonly seen malignant intracranial tumor (10). Previously, MRI was frequently used for the early diagnosis of gliomas; however, pathological vessels in the abnormal structures of patients with gliomas are a high risk to damaging the blood brain barrier, influencing the diagnostic efficacy of MRI (11). ^{18}F-FDG imaging agents penetrate the vascular endothelial cells of a tumor through pinocytosis and, moreover, the enhancement of the glioma is induced by the

Table III. *Correlation between SUV, corrected SUV and L/WM of PET-CT and glioma grade (mean ± SD).*

	Grade of glioma				t	P
	Grade I	Grade II	Grade III	Grade IV		
SUV	7.59±0.28	8.51±0.29	8.91±0.30	7.03±0.37	2.66	<0.05
L/WM	7.91±4.43	8.54±4.66	8.12±4.34	5.28±3.40	3.51	<0.05
Corrected SUV	7.88±5.62	10.83±5.66	10.08±3.43	6.32±3.39	6.53	<0.05

increased permeability of the blood capillary rather than the damaged blood brain barrier (12).

In this study, ^{18}F-FDG-PET-CT demonstrated better diagnostic efficacy compared to MRI, thus it is more suitable for identifying different grades of gliomas. The accuracy of ^{18}F-FDG-PET-CT in diagnosing four grades of gliomas was 79.80%, 85.70%, 86.90% and 78.60% respectively, indicating that ^{18}F-FDG-PET-CT performed better in identifying grades II and III gliomas than grades I and IV gliomas.

Semi-quantitative analysis is a method commonly used in the diagnosis of gliomas using PET-CT because it can objectively evaluate detection results. The commonly used semi-quantitative analysis indexes include SUV, the intake ratio of tumor to normal tissue (13, 14). The corrected critical value of PET-CT parameter corrected SUV was more sensitive to the identification of the grade of gliomas and could be used to arrive at an accurate diagnosis.

To sum up, histopathological grading and prognosis of gliomas can be affected by many factors. Both ^{18}F-FDG-PET-CT and MRI have important clinical values in the diagnosis, grading, curative effect evaluation and prognosis of gliomas; but ^{18}F-FDG-PET-CT is more effective.

REFERENCES

1. Ozsunar Y, Mullins MK, Kwong K, et al. Glioma recurrence versus radiation necrosis? A pilot comparison of aeterial spin-labeled, dynamic susceptibility contrast enhanced MRI, and FDG-PET imaging. Acad Radiol 2010; 17(3):282-90.
2. Goebell E, Fiehler J, Ding XQ, et al. Disarrangement of fiber tracts and decline of neuronal density correlate in glioma patients-a com-bined diffusion tensor imaging and 1H-MR spectroscopy study. AJNR 2006; 27:1426-31.
3. Al-Okaili RN, Krejza J, Woo JH, et al. Intraaxial brain masses: MR imaging-based diagnostic strategy--initial experience. Radiol 2007; 243:539-50.
4. Atkinson M, Juhász C, Shah J, et al. Paradoxical imaging findings in cerebral gliomas. J Neurol Sci 2008; 269:180-83.
5. Bulik M, Jancalek R, Vanicek J, Skoch A, Mechl M. Potential of MR spectroscopy for assessment of glioma grading. Clin Neurol Neurosurg 2013; 115:146-53.
6. van Waarde A, Jager PL, Ishiwata K, Dierckx RA, Elsinga PH. Comparison of sigma-ligands and metabolic PET tracers for differentiaing tumor from inflammation. J Nucl Med 2006; 47(1):150-54.
7. Bochev P, Klisarova A, Kaprelyan A, et al. Brain metastases detectability of routine whole body 18F-FDG PET and low dose CT scanning in 2052 asymptomatic patients with solid extracranial tumors. Hell J Nucl Med 2012; 15(2):125-29.
8. Ryu IS, Roh JL, Kim JS, et al. Impact of 18F-FDG PET/CT staging on management and prognostic stratification in head and neck squamous cell carcinoma: A prospective observational study. Eur J Cancer 2016; 63:88-96.
9. Kassem TW. Do we need 18F-FDG PET/CT scan in staging and management of testicular tumors? Egypt J Radiol Nucl Med 2016; 47(2):445-52.
10. Liu ZL, Zhou Q, Zeng QS, Li CF, Zhang K. Noninvasive evaluation of cerebral glioma grade by using diffusion-weighted imaging-guided single-voxel proton magnetic resonance spectroscopy. J Int Med Res 2012; 40:76-84.
11. Pirotte BJ, Lubansu A, Massager N, et al. Clinical interest of integrating positron emission tomography imaging in the workuop of 55 children with incidentally diagnosed brain lesions. J Neurosurg Pediatr 2010; 5(5):479-85.
12. Pan MH, Huang SC, Liao YP, et al. FLT-PET imaging of radiation responses in murine tumors. Mol Imaging Biol 2008; 10(6):325-34.
13. Spaeth N, Wyss MT, Pahnke J, et al. Uptake of 18F-fluorocholine, 18F-fluoro-ethy1-L:-tyrosine and 18F-fluoro-2-deoxyglucose in F98 gliomas in the rat. Eur J Nucl Med Mol Imaging 2006; 33(6):673-82.
14. Zagzag D, Esencay M, Mendez O, et al. Hypoxia- and vascular endothelial growth factor-induced stromal cell-derived factor-1 alpha/CXCR4 expression in glioblastomas: one plausible explanation of Scherer's structures. Am J Pathol 2008; 173(2):545-60.

LETTER TO THE EDITOR

NDETECTION AND STUDY OF PLASMA D-DIMER CHANGE IN PATIENTS WITH ACUTE EXACERBATION OF CHRONIC OBSTRUCTIVE PULMONARY DISEASE

BH. LIU[1], MX. SUN[1], N. ZHOU[1], YP. LI[1], MZ. WANG[1], J. YU[1] and HS. ZHOU[2]

[1]Respiratory Internal Medicine Department, Dongying People's Hospital of Shandong provincial Hospital Group, Dongying, Shandong, China; [2]Tuberculosis Internal Medicine Department, Shandong Chest Hospital, Shangdong, China

Received June 23, 2016 – Accepted August 5, 2016

The purpose of this study was to observe the change in plasma D-dimer of patients with acute exacerbation of chronic obstructive pulmonary disease (AECOPD). The patients were divided into three groups, i.e., AECOPD group, stable COPD group (COPD kept stable after treatment) and a healthy control group. The content of plasma fibrinogen (FIB) and D-dimer of all research subjects was detected and the difference between groups was analyzed. Moreover, pulmonary functions of patients in the AECOPD group and the stable COPD group, including forced expiratory volume in 1 second (FEV1%) and forced vital capacity rate of 1 second (FEV1/FVC), and blood gas (oxygen partial pressure (PO_2) and partial pressure of carbon dioxide ($PaCO_2$), were detected; and the differences between the two groups and the possible correlation were analyzed. Compared to the COPD stable group and the control group, the AECOPD group had a statistically significant higher content of plasma FIB and D-dimer ($p < 0.05$); the content of plasma FIB and D-dimer of the COPD stable group was much higher than that of the healthy control group, but the difference had no statistical significance ($p > 0.05$); the content of D-dimer of AECOPD patients was in a negative correlation with FEV1 and PO_2 ($p < 0.05$) and in a positive correlation with PCO_2 ($p < 0.05$). It can be concluded that D-dimer is correlated to the severity of AECOPD; hence, it can be used as an evaluation index for the severity of AECOPD.

To the Editor,

Chronic obstructive pulmonary disease (COPD) is frequently seen in the respiratory system and severely threatens the health of humans. Chinese studies (1, 2) have found that the death rate of COPD increases year by year with the aggravation of atmospheric pollution and population aging, as COPD is characterized by airflow limitation. Some studies (3-5) pointed out that COPD has developed from an airway disease to a pulmonary vascular disease and its performance is more obvious in the acute exacerbation stage. In recent years, indexes relating to the changes of coagulation and fibrinolysis system functions of patients with acute exacerbation of COPD (AECOPD) have become research hotspots in the relevant field (6). The level of fibrinogen (FIB), which is a key index for reflecting blood viscosity, plays an important role in coagulation. It is also found that plasma FIB can be used for determining prethrombotic state, airway progressive inflammation and pulmonary tissue injury (7).

In clinical practice, many patients with AECOPD are observed with increased content of D-dimer (8). D-dimer, the product of fibrinolytic enzyme

Key words: acute exacerbation of chronic obstructive pulmonary disease, D-dimer, fibrinogen, pulmonary functions,

Mailing address:
Dr Benhong Liu,
Respiratory Internal Medicine Department,
Dongying People's Hospital Shandong Provincial Hospital Group,
No. 317, South No.1 Road, East District,
Dongying City, Shandong, 257091, China
e-mail: benhongliuliu@163.com

0393-974X (2016)

hydrolysis after the crosslinking of fibrin monomers and activation factors, is one of the markers for thrombosis in the human body and is a specific marker of fibrinolysis process (9).

In physiological status, coagulation and fibrinolysis are in a dynamic balance, which ensures the timely formation and elimination of fibrous proteins. When the balance is damaged, coagulation tends to increase, fibrous proteins gather, and the content of D-dimer increases (10). When patients develop AECOPD, the content of D-dimer in their body undergoes a significant increase, which is correlated to parameters such as PO_2 and PCO_2 (11).

Specific products formed by soluble fibrin monomers under the effect of XIIIa and cellulose can display secondary fibrinolytic characteristics when their plasma concentration increases, which can be used to determine whether there is secondary hyperfibrinolysis in patients with AECOPD. It is also found that patients with AECOPD have abnormal coagulation and fibrinolytic system, and plasma FIB and D-dimer are important molecular markers for reflecting these changes. In view of this, this study investigated the difference of the clinical curative effects between the three groups and the influence on D-dimer, FIB, pulmonary functions and blood gas analysis, which provides a novel clinical treatment for AECOPD.

MATERIALS AND METHODS

General data

Seventy-two patients who were confirmed with COPD by the respiratory internal medicine department in Dongying People's Hospital (Dongying Hospital of Shandong Provincial Hospital Group), Shandong, China, from March 2015 to April 2016, were enrolled in the study. Twenty healthy people who underwent physical examination in the hospital in the same period were selected as controls. Before the study, all subjects and their family members were informed of the research process and possible risks, and all gave signed consent. The medical ethics committee of the Dongying People's Hospital hospital approved the study.

Inclusion criteria

All subjects included in the study conformed to the diagnostic criteria in the Guidance for the Diagnosis and Treatment of COPD (GOLD2007). The disease conditions of the subjects were graded from II to IV, based on

Table I. *Grading of severity degree of COP*

Grade	Criteria
Grade I: Mild	FEV1/FVC<70%; FEV1≥80%
Grade II: Medium	FEV1/FVC<70%; 50%≤FEV1≤80%
Grade II: Severe	FEV1/FVC<70%; 00%≤FEV1<50%
Grade IV: Extremely severe	FEV1/FVC<70%; FEV1<30% or FEV1<50% Accompanied with chronic respiratory failure

pulmonary function related indexes. The specific grading criteria are shown in Table I.

Diagnostic criteria of AECOPD: patients with confirmed COPD who showed symptoms of cough, shortness of breath (or gasp aggravation), expectoration, increased amount of sputum in purulent or sticky state and fever in the previous three days were diagnosed with AECOPD. They were classified as the AECOPD group.

Diagnostic criteria of stable COPD: AECOPD patients who had significantly relieved symptoms, such as cough and shortness of breath, or/and had had improved X-rays for more than 4 weeks were diagnosed with stable COPD; and they were all followed up for a long time by Dongying People's Hospital. They were classified as the stable COPD group.

Inclusion criteria of healthy controls: people who were classified as healthy controls were those who had not developed respiratory infection for at least one month.

All subjects participating in the study signed written informed consent.

Exclusion criteria

Patients who were diagnosed with acute pulmonary embolism, myocardial infarction, cerebral infarction or deep venous thrombosis by physical examination, electrocardiogram, cardiovascular ultrasound and brain computed tomography, allergic to low molecular heparin, had severe hepatic renal dysfunction, who had undergone trauma surgery in the previous three months, or had contraindication to anticoagulants were excluded.

Methods

Fasting blood samples were taken from patients in the AECOPD group in the morning at the beginning of the study and at the end of treatment. For the healthy control group, fasting blood was collected in the morning.

Detection of plasma FIB and D-dimer

Eight ml of venous blood were taken and stored in a tube loaded with anticoagulant solution whose volume was 1/10 that of the tube. Then the blood was centrifuged at 3000 rpm for 10 min. The supernate (plasma) was collected and stored at -20°C. The content of D-dimer was detected using colored substrate method. The content of FIB was detected using an ACL200 coagulometer (Beckman Coulter, Inc., USA).

Blood gas analysis

One ml of venous blood was collected, processed by anticoagulation using heparin and detected by a PL2200 Ruifeng blood gas analyzer (Nanjing Perlong Medical Instrument Co., Ltd., Jiangsu, China).

Pulmonary function detection

Pulmonary function was detected using an S-980A I pulmonary function meter (Sichuan Sikeda Technology Co., Ltd., China).

Statistical analysis

Measurement data normally distributed were expressed as mean ± standard deviation (SD). SPSS ver. 19.0 was used for statistical processing. All statistical tests were bilateral. The significant level was $\alpha = 0.05$. Difference was considered as statistically significant if $p < 0.05$ and as significantly different if $p < 0.01$.

RESULTS

Clinical data

Clinical basic data of all research subjects in the three study groups are shown in Table II.

Measured data of FIB and D-dimer

Table III shows the comparison of measured values of plasma FIB and D-dimer between the two experimental groups and the control group. As shown in Fig. 1, the AECOPD group had a much higher content of plasma FIB and D-dimer compared to the stable COPD group and the control group ($p < 0.05$); compared to the control group, the stable COPD group had much higher levels of FIB and D-dimer, but the differences had no statistical significance ($p > 0.05$).

Analysis of pulmonary functions and blood gas

Paired *t*-test results demonstrated that the FEV1% and PO_2 of patients with stable COPD significantly increased after treatment ($p < 0.01$); rank sum test results demonstrated that the FEV1/FVC of patients with stable COPD increased ($p < 0.01$), but PCO_2 decreased, and the difference had no statistical

Table II. *Statistics of basic data of research subjects.*

Group	No. of cases (N)	Age (year)	Gender (male/ female)	Disease course (year)	Smoking index (per year)
AECOPD group	32	69.56±9.16	20/12	18.87±10.62	655±72
Stable COPD group	40	66.64±8.48	23/17	16.05±10.14	628±110
Control group	20	64.60±7.41	12/8	-	587±101

Note: smoking index = the number of cigarettes every day × the number of years.

Table III. *Comparison of detection values of plasma FIB and plasma D-dimer of the AECOPD group, stable COPD group and control group.*

Group	AECOPD group	Stable COPD group	Control group
No. of cases (N)	32	40	20
FIB (g/L)	4.49±0.95	3.45±0.9	3.15±0.81
D-dimer (μg/L)	1022±91	438±37	326±25

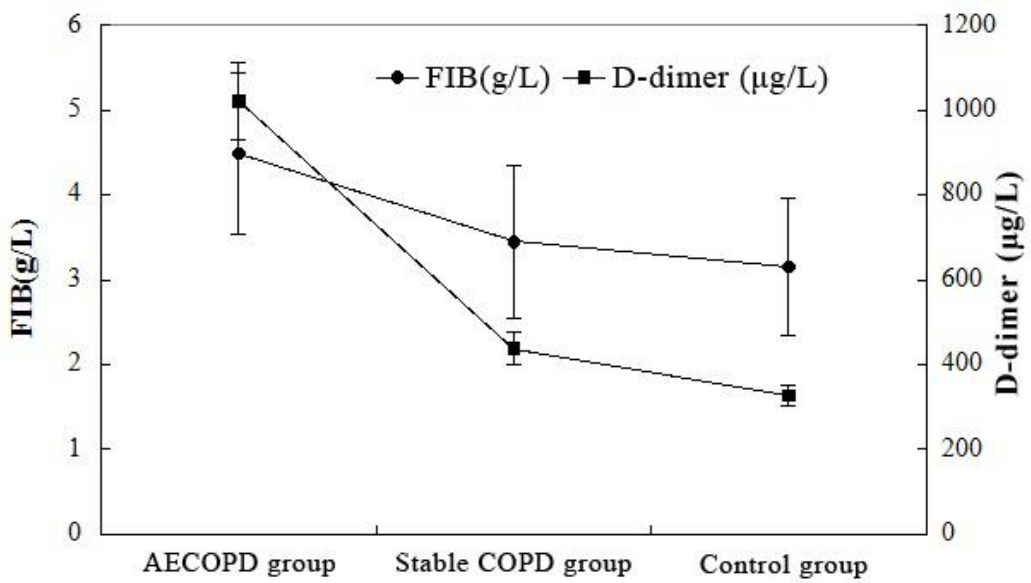

Fig. 1. *Comparison of measured values of plasma FIB and D-dimer between groups.*

significance ($p > 0.05$) (Table IV). The D-dimer of the AECOPD group was in a negative correlation with FEV1% and PO_2 ($p < 0.05$) and in a positive correlation with PCO_2 ($p < 0.05$) Table V).

DISCUSSION

Current studies concerning COPD suggest that blood of patients with AECOPD usually has high viscosity and coagulation (12). Causes for the phenomenon include long-lasting anoxia, carbon dioxide retention, hypercapnia and decreased antithrombin activity. The research results suggested that the content of plasma FIB and D-dimer of the AECOPD group was much higher than that of the stable COPD group and healthy group ($p < 0.05$). Thus, it could be deduced that patients with AECOPD had abnormal airway inflammation and coagulation function and a prethrombotic state and secondary fibrinolysis may be present, which would worsen with the aggravation of disease condition (13).

The fibrinolytic system is the most important human anticoagulant system of which FIB is an important anticoagulant factor: as a blood coagulation factor with the highest content in plasma, it plays a decisive role in thrombosis. FIB synthesized by liver cells is a key factor for determining coagulation function and haemodynamics. Moreover, FIB is also an acute phase reactive protein which can be used for determining prethrombotic state, pulmonary tissue injury and airway progressive inflammation. The level of FIB can increase three-fold in the acute exacerbation stage.

One study (14) suggested that FIB was correlated to the pathogenesis, acute exacerbation incidence, onset frequency, severity and death rate of COPD patients. FIB as an important factor in the anticoagulant system plays an important role in blood coagulation. The results of the present study demonstrate that the level of plasma FIB of the AECOPD group was higher than that of the stable COPD group which shows that FIB, as one of the indexes for AECOPD, can be used for predicting the occurrence and development of COPD and assisting the detection of COPD severity.

For COPD patients with decreased pulmonary function, the increase of FIB will increase the probability of hospitalization; as a result, FIB becomes

Table IV. *Comparison of pulmonary functions between the AECOPD group and the stable COPD group.*

Parameter		AECOPD group	Stable COPD
Pulmonary functions	FEV1%	45.10±11.07	56.03±11.81**
	FEV1/FVC	57.38±6.94	63.30±5.91**
Blood gas	PO_2	62.21±8.47	77.49±8.91**
	PCO_2	47.88±10.79	44.92±7.71

** $p < 0.01$

Table V. *Analysis of linear correlation of D-dimer with PO_2, PCO_2 and pulmonary functions in the AECOPD group.*

	Parameter	Correlation coefficient (Pearson)	*p* value
D-dimer	FEV1%	-0.256	0.047
	PO_2	-0.276	0.035
	PCO_2	0.259	0.043

an independent risk factor for the hospitalization of patients. The research results demonstrate that the D-dimer of patients with AECOPD significantly increased and was in negative correlation with PO_2 and in positive correlation with PCO_2. It was therefore deduced that the increase of D-dimer was closely correlated to hyoxemia and hypercapnia. The reason may be that when patients with AECOPD showed anoxia, infection, oxidative stress, hypercapnia or released inflammatory mediators, the activated endogenous blood coagulation system would make blood highly viscous and concretionary, which could result in the increase of D-dimer and may even induce the formation of micro artery thrombosis.

Plasma D-dimer in the human body is sensitive and accurate in predicting various kinds of vascular embolization diseases; it can lead to the increase of whole blood concentration and plays a certain role in erythrocyte aggregation and coagulation (15). The results of the present study demonstrated that the content of plasma D-dimer of AECOPD patients was much higher than that of patients with stable COPD and healthy subjects, and the differences were statistically significant ($p < 0.05$). For patients with AECOPD, factors such as anoxia, hypercapnia and infection can induce the impairment of blood vessel endothelium and alveolar epithelium, thereby leading to the increased secretion of tissue plasminogen activator, the increased generation of plasmin and the activation of coagulation. Moreover, the disordered energy metabolism of erythrocyte membrane causes the decline of compliance, enhanced aggregation ability of erythrocyte, and improvement of blood viscosity, which results in hypercoagulation and hyperfibrinolysis.

In conclusion, D-dimer is correlated to the severity of AECOPD and can be used as an index for evaluating AECOPD.

REFERENCES

1. Cullinan P. Occupation and chronic obstructive pulmonary disease (COPD). Brit Med Bull 2012; 104(1):1032-34.
2. Herath SC, Poole P. Prophylactic antibiotic therapy for chronic obstructive pulmonary disease (COPD). Cochrane DB Syst Rev 2013; 11(11):CD009764-CD009764.
3. Marco RD, Pesce G, Marcon A, Accordini S, Antonicelli L. The coexistence of asthma and chronic obstructive pulmonary disease (COPD): prevalence and risk factors in young, middle-aged and elderly people from the general population. Plos One 2013; 8(5):1224-30.
4. Hajghanbari B, Holsti L, Road JD, Reid WD. Pain in people with chronic obstructive pulmonary disease (COPD). Respir Med 2012; 106(7):998-1005.
5. Wan Y, Shorr A, Sun S, Corman S, Huang XY, Gao X. Impact of roflumilast on exacerbations among patients with chronic obstructive pulmonary disease (COPD) in the real world. Chest 2013; 144:88-88.
6. Hassett DJ, Borchers MT, Panos RJ. Chronic obstructive pulmonary disease (COPD): evaluation from clinical, immunological and bacterial pathogenesis perspectives. J Microbiol 2014; 52(3):211-26.
7. Burgel PR, Paillasseur JL, Peene B, et al. Two distinct chronic obstructive pulmonary disease (COPD) phenotypes are associated with high risk of mortality. Plos One 2012; 7(12):4193-208.
8. van Gestel A J, Kohler M, Clarenbach CF. Sympathetic overactivity and cardiovascular disease in patients with chronic obstructive pulmonary disease (COPD). Discov Med 2012; 14(79):359-68.
9. Zhang M, Zhang J, Zhang Q, et al. D-dimer as a potential biomarker for the progression of COPD. Clin Chim Acta; Int J Clin Chem 2016; 455:55-59.
10. Silva DR, Coelho AC, Gazzana MB, Menna-Barreto SS, Knorst M. D-dimer levels in stable COPD patients: A case-control study. J Chron Obstruct Pulmon Dis 2012; 9(4):426-31.
11. Song YJ, Zhou ZH, Liu YK, Rao SM, Huang YJ. Prothrombotic state in senile patients with acute exacerbations of chronic obstructive pulmonary disease combined with respiratory failure. Exper Therap Med 2013; 5(4):1184-88.
12. Valvi D, Mannino DM, Müllerova H, Talsinger R. Fibrinogen, chronic obstructive pulmonary disease (COPD) and outcomes in two United States cohorts. Int J Chron Obstr Pulm Dis 2012; 7(2):173-82.
13. Akpinar EE, Hoşgün D, Doğanay B, et al. Should the cut-off value of D-dimer be elevated to exclude

pulmonary embolism in acute exacerbation of COPD. J Thor Dis 2013; 5(4):430-34.
14. Lazovic B. Correlation of CRP and serum level of fibrinogen with severity of disease in chronic obstructive pulmonary disease patients. Med Arch 2012; 66(3):159-60.
15. Torheim H, Kvangarsnes M. How do patients with exacerbated chronic obstructive pulmonary disease experience care in the intensive care unit? Scand J Caring Sci 2014; 28(4):741-8.

LETTER TO THE EDITOR

NON-SURGICAL PERIODONTAL MANAGEMENT IN SCLERODERMA DISEASE PATIENTS

A. LAFORGIA[1], M. CORSALINI[1], G. STEFANACHI[1], S. TAFURI[2], A. BALLINI[3], F. PETTINI[1] and D. DI VENERE[1]

[1]Interdisciplinary Department of Medicine, Dental School, University of Bari Aldo Moro, Bari, Italy; [2]Department of Biomedical Sciences and Human Oncology, University of Bari Aldo Moro, Bari, Italy; [3]Department of Basic Medical Science, Neurosciences and Sense Organs, University of Bari Aldo Moro, Bari, Italy

Received February 10, 2016 - Accepted May 16, 2016

The aim of the present study is to investigate the periodontal status of people with scleroderma and their response to non-surgical treatment protocol aimed at controlling the evolution of the disease. The response to non-surgical periodontal treatment was tested on patients belonging to a scleroderma group and a control group: the data show an improvement of the periodontal conditions of all these patients in response to treatment. When compared on the same diagram, a slight remission of the periodontal disease was obtained in both scleroderma and healthy patients. This highlights the benefit to soft tissues produced by non-surgical periodontal treatment also in patients affected by systemic diseases.

To the Editor,

Scleroderma pathology (SP) is often relatable to changes affecting the whole oral cavity: many of its components are in fact affected by anatomical and functional alterations (1).

Trigeminal neuropathy, a frequent oral sign which often precedes systemic involvement, is associated with collagen lying in the perineural region and/or decrease in vascularisation of the trigeminal nerve, as well as the resorption of the mandibular condyles and coronoid process (2). Mandibular bone resorption is another element commonly found in patients with SP; it occurs as the result of the thinning of facial skin, vasoconstriction and the constant pressure exerted by muscle tension on the jaw bone (3).

A further significant, although not frequent, correlated datum, is the increased risk of oral cancer: in fact the study of Derk et al. (4) highlighted a higher risk of squamous-cell tongue carcinoma. A common oral sign is microstomia caused by excessive collagen accumulation affecting the perioral region (5). Furthermore, because of fibrosis and atrophy of salivary glands, patients with SP show a high incidence of xerostomia, which reduces their quality of life, increases the risk of caries, periodontal disease (PD) and fungal infections, as the masticatory function, eating habits, deglutition and speech can be seriously impaired (1).

With regard to the strictly periodontal aspects, the topic of our work, it must be highlighted that various studies, carried out on SP patients, have reported an increased width of the periodontal space in more elements (32-35%) compared to healthy controls (6).

The aim of the present study was to assess the

Key words: periodontal disease, scleroderma, oral hygiene

Mailing address:
Prof. Francesco Pettini,
Interdisciplinary Department of Medicine,
Dental School University of Bari Aldo Moro,
P.zza Giulio Cesare, 11, 70124, Bari, Italy
Tel./fax: +39 0805478732
e-mail: francesco.pettini@uniba.it

0393-974X (2016)

severity of PD in patients with SP, as compared to a healthy population, and to test the efficacy of a treatment protocol of domestic and professional hygiene aimed at controlling the progression of the disease.

MATERIALS AND METHODS

Patient selection

The patients with SP were referred to the Department of Interdisciplinary Medicine, Dental Clinic, from the Dermatology Clinic, both of the University Hospital of Bari. The study was carried out according to the recommendations of the Declaration of Helsinki, and all patients or parents signed informed consent.

We invited all subjects affected by SP to participate in the study and we selected 44 patients with periodontal disease and SP. A total of 25 patients (17 women and 8 men) agreed to participate in the study; they were age- and sex-matched with 25 systematically healthy subjects (controls), randomly selected among periodontal patients of Bari Dental School. Of them, 13 patients showed a form of localized cutaneous scleroderma (Morphea-like, CREST) and 12 a diffuse cutaneous form. They had all been affected by SP for at least 15 years.

All the test group subjects, at the moment of the study, were under treatment with corticosteroids (prednisone), immunosuppressants (azathioprine) and other antiphlogistic medicaments (colchicines, penicillamine).

The control group was composed of patients who did not show any ongoing diseases and were not assuming any drugs. Subjects of both groups were aged between 40 and 69 years (mean age 54.5 years).

All the cases underwent periodontal assessment to confirm the diagnosis of periodontal disease.

The exclusion criteria of this study were the following: autoimmune disorders of connective (Sjogren Syndrome, Systemic lupus erythematosus, etc), smokers, pregnant women, patients affected by other systemic diseases.

Diagnosis of periodontal disease

Intraoral clinical examination enclosed Plaque Index (PI), Probing Depth (PD), Clinical Attachment Level (CAL), Gingival Recession (GR), Gingival Bleeding Index (GBI) by Ainamo and Bay, 1975 (7), radiographic periodontal space (PDL), and Plaque Record Control (PCR) by O'Leary et al., 1972 (8). PD was determined with a calibrated conventional periodontal probe.

Treatment protocol

After interviewing with regard to smoking habits, clinical and radiographic (orthopantomography) evaluation of periodontal conditions, 18 patients were selected, all with SP, as the test group and 18 periodontally healthy subjects as a control group. Both groups underwent non-surgical periodontal therapy, through the following steps:

i) professional oral hygiene procedures;

ii) use of saliva substitutes for the treatment of xerostomia and deglutition disorders. Pharmacological molecules proposed were: pilocarpine tincture 40 drops/day, pilocarpine 5 mg 3 tablets/day (9);

iii) rinsing with chlorhexidine digluconate-based medicated mouthwashes (0.12%), 5 days per cycle;

iv) fluoride-based toothpaste and gel in order to stimulate the re-mineralization of hard tissues of teeth and, therefore, delay the formation of carious processes (1);

v) exercises for treatment of the issues related to deglutition and vocalization, to improve and increase the elasticity of perioral tissues (9). These exercises were for patients to make an "O" with their mouth, maximal mouth opening followed by a maximal mouth extension, to touch the palatal portion of central upper incisor with the tip of the tongue (for the motility of the tongue).

All data from clinical and radiographic evaluation were collected into a dedicated periodontal folder, with a re-evaluation every 6 months, for 2 years. At the end of the treatment the values of the test group were eventually compared to the control group with the aim to evaluate the response to treatment in both study groups.

Statistical analysis

In order to assess potential change in the mean value of the total of the periodontal indexes after non-surgical periodontal treatment, student's *t*-test was used for matched samples. For all the tests used, a value $p < 0.05$ was considered significant.

RESULTS

Periodontal variables were re-codified attributing a range of values on an ordinal scale for each assessed periodontal parameter according to the criteria shown in Table I.

For PCR values at time 0, no patient in either

Table I. *Numeric value attributed to each analysed periodontal parameter.*

Parameter	Clinical evidence	Attributed value
PCR (O' Leary Index)	0% <10% >10%	0 1 2
GBI	0% <20% >20%	0 1 2
PD	Physiologic if ≤ 3mm Pathologic if > 3mm	Equal to the number of mm Equal to the number of mm
DM	0 1° 2° 3°	0 1 3 6
F	0 1° 2° 3°	0 1 2 3
CAL	0 ≤2mm >2mm	0 1 2
PDL	Normal value in mm if 0.301< PDL<0.324 pathologic value in mm if 0.342<PDL<0.391	

PCR: plaque control record; GBI: gingival index; PD: parodontal depth; DM: dental mobility; F: furcation; CAL: clinical attachment level; PDL: periodontal ligament.

group had a value of 0; in each group two patients had a value of 1 and twenty-three a value of 2 (*chi*-squared=0.00; $p = 1.0$).

Table II shows the total values of periodontal indexes and corresponding means acquired over time at 6, 12, 18 and 24 months, both in scleroderma patients and the healthy ones. We calculated the means of the total values of the periodontal indexes for each patient after 6, 12, 18 and 24 months and, finally, we calculated the mean of the total of the sum of the three totals (for each patient), for each control, to obtain 4 specific values each for the relevant month.

This overall score was on average higher in scleroderma patients (21.29±2.3) than in controls (13.31±5.1; t=7.09; p<0.0001). The *Tcal* value (±7.09), obtained with the statistic comparison of two unknown variance independent samples, was higher than the *Ttab* values (±2.06) seen on dedicated standard tables, according to the number of total

Table II. *Mean values attributed to periodontal indexes, recorded for each single patient.*

	CONTROLS		SCLERODERMA		*t*	*p*
Time	**mean**	**SD**	**mean**	**SD**		
0	14.64	4.05	24.68	0.57	9.05	<0.001
6 months	14.43	3.94	24.62	0.63	9.89	<0.001
12 months	14.40	3.93	24.54	0.63	9.87	<0.001
18 months	14.13	3.98	24.38	0.66	9.84	<0.001
24 months	13.93	3.88	20.54	4.90	4.09	<0.001

subjects of the comparative study and considering a margin of error α/2 of 0.025.

The response to non-surgical periodontal treatment was tested on 15 patients belonging to the scleroderma group and on 15 healthy subjects; significant differences were found at all follow-up times in the mean value of the periodontal indexes after treatment between scleroderma patients and healthy patients.

DISCUSSION

The results obtained in the present study are comparable with pre-existing literature (10, 11) highlighting a strict correlation between systemic diseases and oral and periodontal impairing. The analysis of the data obtained from the two groups allowed us to state that patients with SP had a poorer periodontal status then healthy people. In 2011 Leung et al. found that patients with SP suffer from a more severe clinical presentation of plaque-induced inflammatory periodontal disease (12). In our study, all examined periodontal parameters resulted to be altered. These results can be explained underlining the anatomical and functional alterations in periodontal tissues, typical of subjects with SP.

Similar to previous studies, we found a widening of the periodontal ligament space in SP, probably caused by altered collagen production (6). In our study, the use and application of student's *t*-test enabled us to statistically highlight the significant difference of the overall periodontal status between SP patients and healthy controls, analyzing the mean values obtained by clinical assessments.

Although with the limitation of having a small sample, it can therefore be claimed that SP can be included in the risk factors of PD, both as a negative prognostic factor and as a discriminating element in the aetiology of periodontitis. The second phase of the present study provided an assessment of the response to non-surgical periodontal treatment, administered to scleroderma and control patients.

The use of medicated mouthwashes, medical supplies and the increase in patients' compliance enabled the improvement of periodontal health (9). In conclusion, knowing the correlation between scleroderma and alterations in periodontal tissues is of great importance for dentists and dental hygienists because the outset of this pathology often affects oral tissues.

REFERENCES

1. Tolle SL. Scleroderma: considerations for dental hygienists. Int J Dent Hyg 2008 6:77-83.
2. Fischoff DK, Sirois D. Painful trigeminal neuropathy caused by sever mandibular resorption and nerve compression in a patient with systemic sclerosis: case report and literature review. Oral Surg Oral Med Oral Radiol 2000; 90:456-59.
3. Doucet JC, Morrison AD. Bilateral mandibular condylysis from systemic sclerosis: case

report of surgical correction with bilateral total temporomandibular joint replacement. Craniomaxillofac Trauma Reconstr 2011; 4:11-8.
4. Derk CT, Rasheed M, Spiegel JR, Jimenez SA. Increased incidence of carcinoma of the tongue in patients with systemic sclerosis. J Rheumatol 2005; 32:637-41.
5. Scardina GA, Messina P. Systemic sclerosis: description and diagnostic role of the oral phenomena. Gen Dent 2003; 52:42-47.
6. Mehra A. Periodontal space widening in patients with systemic sclerosis: a probable explanation. Dentomaxillofac Radiol 2008; 37:183.
7. Ainamo J, Bay I. Problems and proposals for recording gingivitis and plaque. Int Dent J 1975; 25:229-35.
8. O'Leary TJ, Drake RB, Naylor JE. The plaque control record. J Periodontol 1972; 43:38
9. Vincent C, Agard C, Barbarot S, et al. Orofacial manifestation of systemic sclerosis: a study of 30 consecutive patients. Rev Stomatol Chir Maxillofac 2010; 111:128-34.
10. Corsalini M, Di Venere D, Pettini F, Lauritano D, Petruzzi M. Temporomandibular disorders in burning mouth syndrome patients: an observational study. Int J Med Sci 2013; 29:1784-89.
11. Ballini A, Scattarella A, Crincoli V, et al. Surgical treatment of gingival overgrowth with 10 years of follow-up. Head Face Med 2010; 6:19.
12. Leung WK, Chu CH, Mok MY, Yeung KW, Ng SK. Periodontal status of adults with systemic sclerosis: case-control study. J Periodontol 2011; 82:1140-45.

LETTER TO THE EDITOR

STANDARDIZATION PROCEDURE FOR THE NASAL NITRIC OXIDE MEASUREMENT METHOD USING NIOX MINO® AND THE TIDAL-BREATHING TECHNIQUE WITH VELUM-CLOSURE

M. GELARDI[1], G. ABBATTISTA[1], V.N. QUARANTA[1], N. QUARANTA[1], V. SECCIA[2], S. BUTTAFAVA[3], F. FRATI[3] and G. CIPRANDI[4]

[1]Section of Otolaryngology, Department of Basic Medical Science, Neuroscience and Sensory Organs, University of Bari, Bari, Italy; [2]Otorhinolaryngology Unit, Department of Neuroscienze, A.O.U. Pisana, Pisa, Italy; [3]Medical and Scientific Department, Stallergenes, Milan, Italy; [4]Department of Internal Medicine, IRCCS A.O.U. San Martino, Genoa, Italy

Received January 7, 2016 – Accepted June 10, 2016

Nitric oxide (NO) is a molecule that performs many functions in the human body. The entire respiratory tract can produce NO, but the highest production occurs in the upper respiratory tract, in the paranasal sinuses in particular. The aim of the present study was to assess a new nasal NO (nNO) measurement method using the Niox MINO Nasal® device (Aerocrine AB, Solna, Sweden) and a special procedure, in order to compare the nNO values obtained in 32 healthy subjects with the values found in the international literature. The measured normal nNO values were equal to 426.76±143.27 ppb, with a 95% confidence interval [160.22-733.30]. Males had an average nNO value equal to 446.76±133.63 [178.64 – 714.02], whereas in females the average value was 403.80±154.90 [94.00 – 713.60]. This study allows us to confirm that we have been able to establish the normal range of nitric oxide quantity produced in the nasal/sinus cavities of healthy individuals using the Niox MINO Nasal® device and tidal-breathing with velum-closure manoeuvre.

To the Editor,

Nitric oxide (NO) is a molecule that performs many functions in the human body. It is produced by 3 different isozymes called nitric oxide synthase (NOS), which synthesize NO from L-arginine and L-citrulline (1). The endothelial (NOS3) and neuronal (NOS1) isoforms are constitutively expressed in endothelial and neuronal epithelia, respectively. They produce NO through a calcium-dependent mechanism, and NO acts as intracellular messenger and neurotransmitter (2). The inducible isoform (NOS2 or iNOS) is not continuously expressed and is produced in response to inflammatory stimuli due to the fact it is calcium-independent. In these conditions NO contributes in a non-specific manner to the defence of the airways against infectious agents, such as bacteria, viruses and fungi (3, 4). The entire respiratory tract can produce NO, but the highest production is in the upper respiratory tract, in the paranasal sinuses in particular (3,5).

Measurement of nasal nitric oxide

The measurement of nasal nitric oxide concentration is a non-invasive technique that is mainly used in paediatrics for the early diagnosis of primary ciliary dyskinesia (PCD) (6-8). Moreover, some studies recommend this diagnostic test for children and adults for the study of certain diseases,

Key words: nitric oxide, nasal assessment, nNO

Mailing address:
Giorgio Ciprandi, M.D.
Largo R. Benzi 10,
16132 Genoa, Italy
Tel.: +39 10 35338120
e-mail: gio.cip@libero.it

0393-974X (2016)

such as allergic and non-allergic rhinitis, nasal polyps, and rhinosinusitis, in order to avoid more invasive tests (9-11).

Recommended methods

Over the last few years, many different nNO measurement methods have been proposed, depending on the subjects considered for the study and on the instruments used, which are increasingly modern and reliable (12, 13). However, because there are so many different methods and available instruments, to date it has not been possible to define a standard for the unambiguous assessment of the effectiveness of each method. There are also no clear and exact reference values that define a range, with values outside this range being an indication of a pathological condition.

The guidelines issued by the American Thoracic Society and the European Respiratory Society (ATS/ERS) in 2005 established that, ideally, nNO should be measured through inspiration via a nostril with soft palate (velum) closure (12). It therefore appears necessary to identify a quick, effective, and reproducible measurement method, suitable for both children and adults, possibly using a small, manoeuvrable, inexpensive, and user-friendly instrument.

Thus, the aim of the present study was to assess a new nNO measurement method using the Niox MINO Nasal® device (Aerocrine AB, Solna, Sweden) and a special procedure, in order to compare the nNO values obtained in healthy subjects with the values found in the international literature.

MATERIALS AND METHODS

The study was carried out between December 2014 and March 2015, in the Rhinology Department of the Otolaryngology Section in the Policlinico Universitario [university hospital] of Bari (Italy). A total of 32 adult subjects were enrolled in the study. They were selected according to these exclusion criteria: age <18 years and >65 years, presence of any respiratory illness, smoking, nasal obstruction because of deviated septum, currently under any medication. Medical history was obtained from all patients, investigating life styles and places of residence/work. The subjects then underwent a rhinologic examination via endoscopy with a flexible fiberscope, nasal cytology, skin prick test and rhinomanometry. All subjects provided informed consent and the study was approved by the local Ethics Committee.

nNO measurement via the "tidal-breathing with velum-closure manoeuvre"

nNO was measured using the Niox MINO Nasal® with the "Nasal Research" option with flow resets. The Niox Mino Nasal device uses an electrochemical sensor suitable for 300 measurements. The measurement range is 5 to 1400 parts per billion (ppb). A cannula with a nasal olive connects the patient to the device. The test procedure is explained to the subject undergoing examination before starting. The most suitable nostril at the time of measurement is selected (according to the natural nasal cycle). After the nasal olive has been introduced into the nostril, the subject is asked to calmly breathe through the mouth, avoiding any kind of breathing through the nose. Breathing in this way allows the soft palate to remain raised, creating two distinct, independent compartments (oropharynx and nasopharynx) that are not connected to each other. nNO is measured using a 5 mL/s flow for 45 seconds. After the measurement is complete, the result is processed and displayed after about 2 minutes directly on the touchscreen display. A single, complete and uninterrupted measurement is required to obtain a result. The device emits an audio signal and an error message if the measurement is incorrect (e.g. "air insufflation inside the cannula").

Statistical analysis

The basic characteristics of the examined subjects were shown as frequency (percentage values) and average ± standard deviation (SD). The normal distribution of measured NO values was checked. The 95% confidence interval of the NO parameter was calculated on the entire sample. The differences between groups for continuous variables were analysed with the independent samples *t*-test. A $p<0.05$ value was considered statistically significant. Analyses were performed using the SPSS 22 test.

RESULTS

Endoscopy, nasal cytology, allergic and rhinomanometry tests did not highlight any

pathological condition in the 32 subjects included in the study. The measurement was successfully completed for all subjects at the first attempt.

The sample was made up of 32 subjects with an average age of 29.94±9.50 years [25th percentile 24 years, 50th percentile 27 years, 75th percentile 30 years], 17 males (53.12%) with average age 27.88±8.28, and 15 females (46.88%) with average age 32.27±10.52. Their ages were not statistically different (p=0.206).

The data distribution of our sample was approximately a Gaussian distribution. The coefficient of skewness was 0.568±2.339 with 0.414 standard error. Because the absolute value of the coefficient of skewness/standard deviation of skewness ratio was below 2.6 (=0.243) the distribution could be considered asymmetrical (Fig. 1). The measured normal nNO values were equal to 426.76±143.27, with a 95% confidence interval [160.22-733.30]. Males had an average nNO value equal to 446.76±133.63 [178.64 – 714.02], whereas in females the average value was 403.80±154.90 [94.00 – 713.60].

DISCUSSION

We believe that nNO measurement using the tidal-breathing technique with velum closure, associated with the use of a new-generation device with an electrochemical sensor and flow reset, is a reliable and reproducible measurement technique. None of the subjects showed discomfort during testing and it is a non-invasive technique. Measurements performed with a hand-held device showed an excellent correlation with measurements performed with stationary devices (14, 15). In addition, an acceptable correlation between a hand-held device and a stationary analyser was demonstrated also for bronchial NO (FeNO), as reported by some studies (16-19). In particular, a correction equation to convert FeNO measured by Niox-MINO into those measured by NIOX has been proposed, allowing to compare data obtainable with the stationary with those measured with the hand-held instrument (19).

Unlike previous models, the present device does not require calibration or maintenance (the sensor is

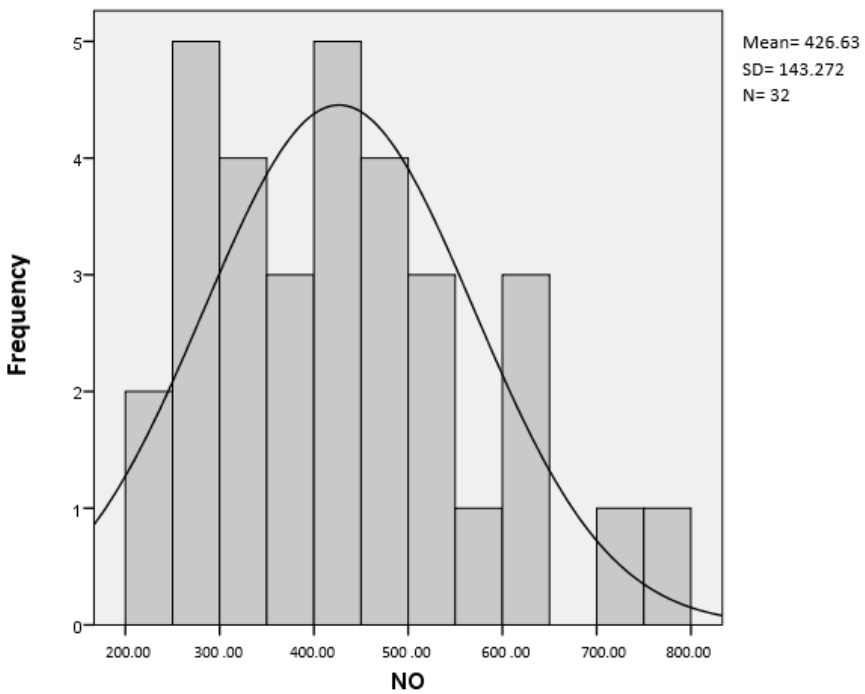

Fig. 1. *Distribution of nNO values in a healthy population.*

Table I. *Definition list of nNO measurement techniques.*

Technique	Description	Velum Closure
Oral exhalation against resistance	Nasal aspiration by a suction pump through a nasal olive placed in one nare at a constant flow rate, while the subject exhales from the mouth against an expiratory resistance after a full inspiration to total lung capacity.	YES
Breath hold	Nasal aspiration by a suction pump though the nasal olive placed in one nare at a constant flow rate, while the subject holds his breath after a full inspiration to total lung capacity	YES/NO [1]
Nasal exhalation	Nasal exhalation through a tightly fitting mask covering the nose connected to the analyzer through a mouthpiece. Subjects start each maneuver by inhaling NO-free air from the nose during a full inspiration to total lung capacity, and then exhaling at a fixed flow rate.	NO
Humming	Nasal aspiration by a suction pump through a nasal olive placed in one nare at a constant flow rate or nasal exhalation through a tightly fitting mask covering the nose connected to the analyzer through a mouthpiece. Subjects start each maneuver by inhaling NO-free air from the analyzer through the nose during a full inspiration to total lung capacity, and then phonating the "m" without opening the lips or forming words as loud as possible for 10 sec at a constant flow rate.	NO
Tidal breath	Nasal aspiration by a suction pump through a nasal olive placed in one nare at a constant flow rate, while the child breathes tidally. Older children are encouraged to breathe through the mouth.	YES/NO [1]

[1]*:Depending on the cooperation of the children*

interchangeable and is suitable for 300 continuous measurements). It is also portable and economical. The cannulas with variable-diameter nasal olives (for adults and children) easily adjust to the nostril morphology of individual patients. All the above makes nNO measurement a painless and non-invasive method. These technical and methodological features make this diagnostic procedure also suitable for general practice surgeries.

The obtained results show that in normal conditions the values are included in a broad range (426.76±143.27 ppb). This implies there is considerable variability of nasal nitric oxide production among individuals. However, even in the case of measurements bordering on the limits of that range, considering the patient's medical history and general conditions, the borderline measurements cannot be considered pathological (and therefore pathognomonic).

Collecting anamnestic data from the patient

followed by the simple measurement of nitric oxide could ultimately allow the exclusion of other rhinologic pathologies without using more invasive tests. If, on the contrary, there are discrepancies between symptoms and measured nNO values, patients should be referred for further tests. In accordance with the international literature, the measured values seem to suggest pathologies of an occlusive nature in the case of values below the normal range and inflammatory conditions in the case of very high values. However, more studies, including patients with upper airways disorders, are needed to validate this hypothesis.

Collecting the air contained exclusively in the nose and paranasal sinuses is very important for precise measurements, which is the reason why it is crucial to use a single, standardised method. There are still a few unresolved issues, such as observing slight differences in nitric oxide values in repeated measurements performed at very short time intervals on the same subject. These differences are probably due to the simple fact that the subject does not ventilate for a few seconds. Alternatively, a more probable hypothesis is that analysing one nasal cavity means that the other is left in direct communication with the outside environment. A few arrangements are necessary to ensure that the nasal nitric oxide values are the most reliable or, better still, the most reproducible. These arrangements include performing measurements on resting subjects, waiting at least 10 minutes before measuring, avoiding nose blowing just before starting the test, suggesting to patients (children especially) who are unable to keep the soft palate closed to breathe with their tongue sticking out.

On the other hand, a limitation of the present study is the absence of the comparison of the data with those obtained with the gold standard chemiluminescence. In fact, an acceptable agreement between electrochemical analysers and chemiluminescence has been reported for FeNO. Thus, further studies should be conducted to address this issue.

The results of this study allow us to confirm that we were able to establish the normal range of nitric oxide quantity produced in the nasal/sinus cavities of healthy individuals using the Niox MINO Nasal® device and tidal-breathing with velum-closure manoeuvre. Nevertheless, more studies on larger populations are required to confirm the present outcomes.

DISCLOSURE: Franco Frati and Serena Buttafava are employees of Stallergenes Italy. Giorgio Ciprandi is a consultant for Stallergenes Italy. The other authors have no conflicts of interest that are directly relevant to the content of the study.

REFERENCES

1. Lefevere L, Willems T, Lindberg S, Jorissen M. Nasal nitric oxide. Acta Otorhinolaryngol Belg 2000; 54:271-80.
2. Moncada S, Higgs A. The L-arginine-nitric oxide pathway. N Engl J Med 1993; 329:2002-12.
3. Maniscalco M, Sofia M, Pelaia G. Nitric oxide in upper airways inflammatory diseases. Inflamm Res 2007; 56:58-69.
4. Wink DA, Hines HB, Cheng RY, Switzer CH, Flores-Santana W, Vitek MP, Ridnour LA, Colton CA. Nitric oxide and redox mechanisms in the immune response. J Leukoc Biol 2011; 89:873-91.
5. Lundberg JO, Farkas-Szallasi T, Weitzberg E, Rinder J, Lidholm J, Anggård A, Hökfelt T, Lundberg JM, Alving K. High nitric oxide production in human paranasal sinuses. Nat Med 1995; 1:370-73.
6. Marthin JK, Petersen N, Skovgaard LT, Nielsen KG. Lung function in patients with primary ciliary dyskinesia. A cross sectional and three-decade longitudinal study. Am J Respir Crit Care Med 2010; 181:1262-68.
7. Barbato A, Frischer T, Kuehni CE, et al. Primary ciliary dyskinesia: a consensus statement on diagnostic and treatment approaches in children. Eur Respir J 2009; 34:1264-76.
8. Hogg C Primary ciliary dyskinesia: when to suspect the diagnosis and how to confirm it. Paediatr Respir Rev 2009; 10:44-50.
9. Sahin G, Klimek L, Mullol J, Hörmann K, Walther LE, Pfaar O. Nitric oxide: a promising methodological approach in airway diseases. Int Arch Allergy Immunol 2011; 156:352-61.
10. Torretta S, Bossi A, Capaccio P, Marchisio P, Esposito S, Brevi A, Pignataro L. Nasal nitric oxide in children with adenoidal hypertrophy: a preliminary study. Int

J Pediatr Otorhinolaryngol 2010; 74:689-93.
11. Keen C, Olin AC, Edentoft A, Gronowitz E, Strandvik B. Airway nitric oxide in patients with cystic fibrosis is associated with pancreatic function, Pseudomonas infection, and polyunsaturated fatty acids. Chest 2007; 131:1857-64.
12. ATS/ERS recommendations for standardized procedures for the online and offline measurement of exhaled lower respiratory nitric oxide and nasal nitric oxide. Am J Respir Crit Care Med 2005; 171:912-30.
13. Manna A, Montella S, Maniscalco M, Maglione M, Santamaria F. Clinical Application of nasal nitric oxide measurement in pediatric airway diseases. Pediatric Pulmonology 2015; 50:85-99.
14. Maniscalco M, de LG, Weitzberg E, Lundberg JO, Sofia M Validation study of nasal nitric oxide measurements using a hand-held electrochemical analyser. Eur J Clin Invest 2008; 38:197-200.
15. Montella S, Alving K, Maniscalco M, Sofia M, De SS, et al. Measurement of nasal nitric oxide by hand-held and stationary devices. Eur J Clin Invest 2011; 41: 1063-70.
16. Alving K, Janson C, Nordvall L. Performance of a new hand-held device for exhaled nitric oxide measurement in adults and children. Resp res 2006; 7:67.
17. Vahlkvist S, Sinding M, Skamstrup K, Bisgaard H. Daily home measurements of exhaled nitric oxide in asthmatic children during natural birch pollen exposure. J Allergy Clin Immunol 2006; 117:127276.
18. Menzies D, Nair A, Lipworth BJ. Portable exhaled nitric oxide measurement. Chest 2007; 131:410-14.
19. Pizzimenti S, Bugiani M, Piccioni P, et al. Exhaled nitric oxide measurements: correction equation to compare hand-hend device to stationary analyser. Resp Med 2008; 102:1272-75.

LETTER TO THE EDITOR

LIGHTS AND SHADOWS OF DENTAL IMPLANTS: FOCUS ON MUCOSITIS AND PERIMPLANTITIS AND THEIR BIOLOGICAL MARKERS

L. BOTTALICO[1], M. TATULLO[2], M. MARRELLI[3,4] and L. SANTACROCE[1]

[1]Jonian Department (DISGEM), University of Bari Aldo Moro, Taranto, Italy; [2]Tecnologica Research Institute, Biomedical Section, Crotone, Italy; [3]Unit of Maxillofacial Surgery, Calabrodental, Crotone, Italy; [4]Marrelli Hospital, Experimental and Clinical Section, Crotone, Italy

Received April 28, 2016 – Accepted May 16, 2016

The increase in oral rehabilitation by means of dental implants has required an evolution of the related managing protocols and correct updating of the skills of dental professionals. Postsurgical management of the clinical case is aimed to stabilize the obtained results and preserve them from adverse conditions: a healthy implant prosthesis is maintained thanks to the huge number of consolidated protocols of oral hygiene. This practice plays a decisive role in the prevention of perimplant pathologies, forming a strong basis to ensure long implant life and avoid unnecessary and painful new surgical procedures. Furthermore, dental companies, in order to satisfy the new needs of professionals in oral hygiene, have produced new instrumentations and targeted drugs, in agreement to the cutting-edge scientific literature, thus creating a new market attracting huge interests in healthcare. The purpose of this topical review is to briefly comment on the state of the art of post-surgical dental implant management. This research is aimed to report the current protocols available to reduce the risk of oral diseases and prevent the progression of perimplant complications. Special focus has been dedicated to the most effective surgical and non-surgical protocols for treating mucositis and perimplantitis.

To the Editor,

Several studies have been carried out on the biological and immunological mechanisms related to osseointegration of dental implants. Premature implant failures can be due to numerous causes and various *noxae*: above all, the most reported and well documented cause of implant failure is related to mechanical factors acting synergically with bacterial infections (1). According to this evidence, high plaque index, progressive bone loss starting from the neck surface of the implant with simultaneous polymorphonucleated cells and plasma-cells prevalence, may be indicative of a bacteria sustained perimplantitis (Table I). The presence of tooth mobility, low plaque index, pain or pressure sensitivity, absence of signs of infection, absence of significant marginal bone loss, granulating tissue surrounding the whole implant, prevalence of macrophages at the level of the new formed fibrous tissue are, instead, indicative of a critical situation near to the implant failure (1-3).

Changes of microbial flora in inflamed perimplant tissues are similar to those characterizing periodontal illness (4). Implant surface and its microscopic geometry are an environment often able to host immunologic processes which have an important role in reaching and maintaining implant-to-bone contact (5).

Key words: perimplantitis, mucositis, oral hygien, oral diseases

Mailing address:
Dr. Marco Tatullo,
Scientific Director, Tecnologica Research Institute,
Biomedical Section, via Enrico Fermi,
Passovecchio, Crotone, Italy
Tel.: +393498742445 - Fax: +390962930414
e-mail: marco.tatullo@tecnologicasrl.com

0393-974X (2016)

Table I. *Clinical-radiological assessments of dental implants.*

Clinical signs		Biological signs	Mobility	Bone loss	Osseointegration
Implant in healthy status	Good Clinical picture	No signs of inflammation or bone resorption.	No implant mobility	No bone loss	Excellent osseointegration
Mucositis	Mucosal inflammation or swelling	Gingival pockets formation	Moderate implant mobility	Minimal bone loss	Good - sufficient osseointegration
Perimplantitis	Suppuration on gentle probing	Presence of deeper dental pockets and gingival fistulas	Severe implant mobility	Severe and circumferential bone loss	Poor - scarce osseointegration

Table II. *Rationale of mucositis therapy.*

Scheduled monitoring	Early recognition of implant suffering
Decontamination of implant surface	Resolution of the inflammatory condition Reduction of bleeding index
Antimicrobial mouthrinses	Reduced bacterial proliferation
Local antibiotics	Reduced acuteness of local infection

Professional removal of bacteria from the dental implant surface is the most effective treatment against implant loss, however, it must be performed paying attention not to alter the titanium implant surface (6). Many studies have been carried out with regard to the best materials to apply safely on the implant surface: the most recent being plastic probes and curettes, or ultrasound tips in carbon composite or coated with Teflon sheath (7).

DISCUSSION

The global dental implants market is expected to grow at a Compound Annual Growth Rate (CAGR) of 10% from US$3.4 billion in 2011 to US$6.6 billion in 2018. Implant dentistry is an evidence-based therapeutic option widely recognized as the gold standard for dental replacement (8).

It is accordingly necessary for dental professionals to know the general rules and the lights and shadows underlying modern therapeutic protocols (Table II). In particular, dental hygienists need to have a good knowledge of microbiological processes able to influence the health of dental implants, to be able to choose the correct preventive protocols to manage, within their competence, perimplant diseases (9).

The increasing requests for dental implant care can be satisfied when the team composed of implant surgeon, dentist and dental hygienist is able to jointly collaborate to ensure a multidisciplinary approach to each patient (10, 11). Targeted therapies are the right approach allowing to prevent possible complications and to ensure a correct follow-up after implant surgery. Therefore, in order to maintain the results achieved by implant surgery, the periodical monitoring of the implant condition plays an important role for early detection of any clinical sign suggestive of inflammation occurring in perimplant tissues. In recent years, a number of studies and protocols aimed to definitely cure perimplantitis have been proposed, however, a continuous search for new and more effective therapies is still needed. Hopefully, a good knowledge of the cutting-edge protocols, as well as a continuous research to find the best treatment, will improve the effectiveness of the overall therapeutic action of dental professionals: this breakthrough will certainly allow a strong reduction of socio-economic costs, improving accordingly the quality of life of all the patients (12).

REFERENCES

1. Watzek G. Oral implants--quo vadis? Int J Oral Maxillofac Implants 2006; 21(6):831-2.
2. Monje A, Galindo-Moreno P, Tözüm TF, Suárez-López Del Amo F, Wang HL. Into the paradigm of local factors as contributors for peri-implant disease: short communication. Int J Oral Maxillofac Implants 2016; 31(2):288-92.
3. Froum SJ, Rosen PS. A proposed classification for peri-implantitis. Int J Periodontics Restorative Dent 2012; 32(5):533- 40.
4. Schierano G, Pejrone G, Roana J, et al. A split-mouth study on microbiological profile in clinical healthy teeth and implants related to key inflammatory mediators. Int J Immunopathol Pharmacol 2010; 23(1):279-88.
5. Eriksson C, Ohlson K, Richter K, Billerdahl N, Johansson M, Nygren H. Callus formation and remodeling at titanium implants. J Biomed Mater Res A 2007; 83(4):1062-69.
6. Hultin M, Gustafsson A, Hallström H, Johansson LA, Ekfeldt A, Klinge B. Microbiological findings and host response in patients with peri-implantitis. Clin Oral Implants Res 2002; 13(4):349-58.
7. Costa MR, Marcantonio RA, Cirelli JA. Comparison of manual versus sonic and ultrasonic toothbrushes: a review. Int J Dent Hyg 2007; 5(2):75-81.
8. Esposito M, Murray-Curtis L, Grusovin MG, Coulthard P, Worthington HV. Interventions for replacing missing teeth: different types of dental implants. Cochrane Database of Systemic Reviews 2007; Issue 4.
9. Persson GR, Salvi GE, Heitz- Mayfield LJ, Lang NP. Antimicrobial therapy using a local drug delivery system (Arestin) in the treatment of peri-implantitis. I: Microbiological outcomes. Clin Oral Implants Res 2006; 17(4):386-93.
10. Marrelli M, Tatullo M, Dipalma G, Inchingolo F. Oral infection by Staphylococcus aureus in patients affected by White Sponge Nevus: a description of two cases occurred in the same family. Int J Med Sci 2012; 9(1):47-50.
11. Inchingolo F, Tatullo M, Abenavoli FM, Marrelli M, Inchingolo AD, Palladino A, Inchingolo AM, Dipalma G. Oral piercing and oral diseases: a short time retrospective study. Int J Med Sci 2011; 8(8):649-52. Epub 2011 Oct 18.
12. Zitzmann NU, Marinello CP, Sendi P. A cost-effectiveness analysis of implant overdentures. J Dent Res 2006; 85(8):717-21.

LETTER TO THE EDITOR

CYTOKINE GENOTYPE DISTRIBUTION IN PATIENTS WITH PERIODONTAL DISEASE AND RHEUMATOID ARTHRITIS OR DIABETES MELLITUS

V. CRINCOLI[1], A. BALLINI[2], L. FATONE[1], M.B. DI BISCEGLIE[1], G.M. NARDI[3], and F.R. GRASSI[2]

[1]Interdisciplinary Department of Medicine, University of Bari Aldo Moro, Bari, Italy; [2]Department of Basic Medical Sciences, Neurosciences and Sense Organs, University of Bari Aldo Moro, Bari, Italy; [3]Department of Oral and Maxillofacial Sciences, Sapienza University of Rome, Rome, Italy

Received March 22, 2016 – Accepted May 16, 2016

The association between oral and systemic health has highlighted the importance of periodontal health and treatment, with the consequence that dental assessment and attention to oral hygiene have assumed an increasingly important part in the clinical management of patients with diabetes mellitus and rheumatoid arthritis. The aim of this work was to assess genotype frequencies in polymorphisms of genes of IL-1α-889 and IL-1β-511 in a case-controlled study population of patients affected by periodontal disease and rheumatoid arthritis or diabetes mellitus.

To the Editor,

The interactions between microorganisms and antigen presenting cells (APC), via pathogen-associated molecular patterns and pathogen recognition receptors leading to induction of host responses in periodontal diseases (PD) are well documented (1, 2). The presence of periodontopathic agents in the gingival sulcus such as *Porphyromonas gingivalis* (*P. gingivalis*), in addition to genetic and environmental aspects, could contribute to the induction of inflammatory responses of periodontal tissues and alveolar bone loss (3). In fact, during the inflammatory response occurring in periodontitis, excessive and/or dysregulated activity of proinflammatory cytokines, such as interleukin (IL)-1 can play an important role in inducing bone resorption by stimulating the proliferation and differentiation of osteoclast progenitors and by activating formed osteoclasts indirectly (2).

IL-1, which includes two different but functionally similar molecules, IL-1α and IL-1β (4), genes which are all located on the long arm of chromosome 2 (region 2q13–14), can also induce the activation of several single nucleotide polymorphisms (SNPs), that present either a pro- and/or anti-inflammatory role in the stimulation of mechanisms of controlling for common inflammatory disorders such as rheumatoid arthritis (RA), diabetes mellitus and PD (5, 6).

The aim of this study was to test whether polymorphisms of genes of IL-1α^{-889} and IL-1β^{-511} were associated with PD, RA and type 2 diabetes (T2D) in a study population. In addition, we evaluated whether or not the resolution of periodontal inflammation in patients with T2D affected the glycemic control.

MATERIALS AND METHODS

This study was conducted at the University Hospital of

Key words: periodontal disease, porphyromonas gingivalis, cytokines, type 2 diabetes, rheumatoid arthritis

Mailing address:
Dr Andrea Ballini,
Department of Basic Medical Sciences,
Neurosciences and Sense Organs ,University of Bari Aldo Moro,
P.zza Giulio Cesare, 11, 70124, Bari, Italy
Tel./fax: +39 0805448583
e-mail: andrea.ballini@uniba.it

0393-974X (2016)

Bari, Italy, on a test group composed of 82 Italian Caucasian patients (50 females and 32 males), with a median age of 47.1 (SD±11) and a history of T2D or current manifestation of RA disease, both correlated with PD.

The study was carried out according to the recommendations of the Declaration of Helsinki, and all patients signed an informed consent to participate in the study.

The test group was divided into two subgroups. Seventy patients were included in the subgroup PD and RA if they met the criteria of American Rheumatism Association (ARA) for rheumatoid arthritis (7). Inclusive criteria for the twelve patients enrolled in the subgroup PD and T2D were T2D not pharmacologically treated but controlled through diet, and fasting plasma glucose data collected before and after therapy (at 6 months after the first sampling), to evaluate the systemic effects of PD non-surgical treatment.

Finally, a group of 82 patients (48 females and 34 males), with a median age of 48.3 (SD±13.8) years, affected by PD and no other systemic diseases, were enrolled as a control group (Table I).

After interviewing for smoking habits, radiographic (orthopantomography) and clinical evaluation of periodontal conditions, together with bleeding on probing (BOP), probing depth (PD) and clinical attachment level (CAL), the patients underwent a non-surgical periodontal therapy, including motivation and oral hygiene instructions, scaling and root planning.

All data from clinical and radiographic evaluations were collected into a dedicated periodontal folder.

Analysis of genetic polymorphisms

Analysis of blood samples was carried out with the blinded method. Five milliliters of venous blood was drawn from the antecubital vein and transferred to a vacutainer containing ethylenediaminetetraacetic acid (EDTA; 3%) to prevent coagulation and stored at −20°C. The following variants were tested by using primer concentrations, optimized thermocycling conditions and gel compositions as already described by Komman et al. in 1997 (8), IL-1α^{-889}

Table I. *Baseline clinical parameters of the subject population (n:82).*

Clinical characteristics	***Patients (n=82)***
Mean age (years±SD)	47.1±11.0
Periodontal disease and Rheumatoid arthritis	70 (76.9%)
Periodontal disease and Diabetes mellitus	12 (23.1%)
Periodontal disease only (controls)	82 (100%)
Smokers	26 (29.9%)

Table II. *The primer sequences for IL-1α and IL-1β polymorphisms.*

LOCUS AND PRIMER SEQUENCES
IL-1α^{-889} F: 5' AAGCTTGTTCTACCACCTGAACTAGGC 3' R: 5' TTACATATGAGCCTTCCATG 3'
IL-1β^{-511} F: 5' TGGCATTGATCTGGTTCATC 3' R: 5' GTTTAGGAATCTTCCCACTT 3'

Table III. *Genotype distribution in the study population.*

Snp	Genotype	Periodontal Disease and Rheumatoid Arthritis	Periodontal Disease and Diabetes Mellitus	Control Subjects
IL-1α $^{-889}$	C/A	(50.2%)	(46%)	(40.8%)
IL-1β^{-511}	A/G	(73.1%)	(58%)	(45.6%)

and IL-1β^{-511} with the primer sequences given in Table II.

RESULTS

A total of 164 subjects were enrolled in this study: 82 patients matched inclusion criteria for the test group and other 82 subjects met acceptation criteria for the control group. The two groups matched for number of individuals, age and gender.

Before therapy, the 12 diabetic patients showed a fasting plasma glucose mean value of 174±9 mg/dL. They declared to have maintained the same diet and, after non-surgical periodontal therapy, showed an improvement in the glycemic control, decreasing the value of fasting plasma glucose to 146±5 mg/dL.

The genotyping ditribution for the test and control groups are shown in Table III. The percentage of the IL-1α SNP (-889; C>A) in the promoter region was similar, but not overlapping, in all the groups: 50.2% in the "PD and RA" subgroup; 46.0% in the "PD and T2D" subgroup and 40.8% in the control group.

IL-1β promoter region SNP (-511; A>G) was detected with a higher frequency in the PD and RA test subgroup (73.1%), followed by PD and T2D subgroup (58.0%), and the control group, where this SNP was observed in 45.6% of the cases.

DISCUSSION

Frequent chronic diseases, such as T2D, RA and PD, generate enormous costs for the public health care system, and their interrelationship is established through a number of pathways supported from literature studies, review articles, and meta-analyses that indicated a mutual influence between periodontitis and other systemic diseases (6).

One plausible biologic mechanism for why diabetics have more severe PD is that glucose-mediated advanced glycation end-product (AGE) accumulation affects the migration and phagocytic activity of mononuclear and polymorphonuclear phagocytic cells, resulting in the establishment of a more pathogenic subgingival flora.

A model was presented by Grossi and Genco in 1998 (9), in which they proposed that an infection-mediated upregulation cycle of cytokine synthesis and secretion by chronic stimulus from LPS and products of periodontopathic organisms may amplify the magnitude of the AGE-mediated cytokine response that is operative in PD.

Taken together, this evidence suggests that a periodontal microbiota dysbiosis could initiate first a regional and then a systemic metabolic inflammation, promoting insulin resistance and T2D.

On the one hand by identifying millions of SNPs, high-throughput genotyping technology has dramatically boosted the yield of genetic association studies, and on the other hand, SNPs could be useful markers only in defined populations, as they are relatively absent in some and excessively present in others, to be considered a useful, unique and diagnostic genetic marker (10).

In the present study, two SNPs were evaluated: IL-1α in the promoter region^{-899} and IL-1β in the promoter region^{-511}.

Our study confirmed the international scientific literature data on the effectiveness of periodontal therapy in improving the control of T2D and the possible identification of periodontal inflammation as a predisposing factor for T2D (5, 6, 11).

Despite the results presented in this and other studies, further research should be conducted using different populations, because polymorphisms at other inflammatory mediator genes should be evaluated in an attempt to clarify the real role of genetic factors in the crosstalk between PD and other systemic diseases.

According to evidence-based dentistry (12), a multidisciplinary collaboration between dental care professionals, endocrinologists, rheumatologists, general medical practitioners, scientific societies and dental associations, is necessary to fully understand the relationship between the host cell invasion by periodontal pathogens in the pathogenesis of the bone, as well as the different lines of evidence supporting the role of genetic periodontal bacteria in systemic diseases.

REFERENCES

1. Wu X, Offenbacher S, López NJ, et al. Association of interleukin-1 gene variations with moderate to severe chronic periodontitis in multiple ethnicities. J Periodontal Res 2015; 50:52-61.
2. Ballini A, Tetè S, Scattarella A, et al. The role of anti-cyclic citrullinated peptide antibody in periodontal disease. Int J Immunopathol Pharmacol 2010; 23:677-81.
3. McGraw WT, Potempa J, Farley D, Travis J. Purification, characterization, and sequence analysis of a potential virulence factor from Porphyromonas gingivalis, Peptidylarginine Deiminase. Infect Immun 1999; 67:3248-56.
4. Dinarello CA. The IL-1 family and inflammatory diseases. Clin Exp Rheumatol 2002; 20:S1–13.
5. Chen HH, Chen DY, Lin SY, et al. Periodontitis exposure within one year before anti-diabetic treatment and the risk of rheumatoid arthritis in diabetes mellitus patients: a population-based cohort study. Rev Bras Reumatol 2014; 54:124-30.
6. Otomo-Corgel J, Pucher JJ, Rethman MP, Reynolds MA. State of the science: chronic periodontitis and systemic health. J Evid Based Dent Pract 2012; 12:20-28.
7. Cornec D, Varache S, Morvan J, et al. Comparison of ACR 1987 and ACR/EULAR 2010 criteria for predicting a 10-year diagnosis of rheumatoid arthritis. Joint Bone Spine 2012; 79:581-85.
8. Komman KS, Crane A, Wang HY, et al. The interleukin-1 genotype as a severity factor in adult periodontal disease. J Clin Periodontol 1997; 24:72-77.
9. Grossi SG, Genco RJ. Periodontal disease and diabetes mellitus: a two-way relationship. Ann Periodontol 1998; 3:51-61.
10. Khoury MJ, Gwinn M, Yoon PW, Dowling N, Moore CA, Bradley L. The continuum of translation research in genomic medicine: how can we accelerate the appropriate integration of human genome discoveries into health care and disease prevention? Genet Med 2007; 9:665-74
11. Taylor GW, Borgnakke WS. Periodontal disease: associations with diabetes, glycemic control and complications. Oral Dis 2008, 14:191-203.
12. Ballini A, Capodiferro S, Toia M, Cantore S, Favia G, De Frenza G, Grassi FR. Evidence-based dentistry: what's new? Int J Med Sci 2007; 4:174-78.

LETTER TO THE EDITOR

THYROID AND SHOULDER DISEASES: THE BASES OF A LINKED CHANNEL

G. VICENTI, L. MORETTI, S. DE GIORGI, I. CARUSO, M. LA MALFA, M. CARROZZO, G. SOLARINO and B. MORETTI

Department of Neuroscience and Organs of Sense, Orthopedics Section, Faculty of Medicine and Surgery, University of Bari, Bari, ltaly

Received March 30, 2016 – Accepted June 6, 2016

The association between thyroid disorders and musculoskeletal diseases has long been suspected, but it is still debated whether they have a role in the pathogenesis of shoulder diseases. In vivo and in vitro studies describe the role of thyroid hormones in bone, cartilage and tendon biology. Retrospective studies and case reports suggest that thyroid diseases should be considered as risk factors and hold prognostic value in some of the most common causes of shoulder pain. Thus, it is advisable to search for underlying thyroid disorders in these patients. The pathophysiologic mechanisms by which thyroid hormone imbalance affects the onset, progression and response to treatment of these diseases are yet to be thoroughly defined and demand further studies.

To the Editor,

A healthy thyroid gland is essential to homeostasis, oxygen consumption, metabolism and functions of most of the human body organs and tissues (1). The association between thyroid dysfunction and joint manifestations has been suspected since the late 19th Century (2), but the debate on the features of this relationship is still ongoing.

Persistent shoulder pain is a very common complaint in patients seeking medical advice from both primary care physicians and orthopedic surgeons (3-5). The differential diagnosis for persistent shoulder pain includes subacromial impingement syndrome (SIS), frozen shoulder, calcific tendinitis and glenohumeral osteoarthritis (3). Collecting patients' history may represent a useful tool in the diagnostic and therapeutic process of the most common shoulder diseases (4). In most of the latest research, thyroid diseases have often been investigated for their role in the pathogenesis as well as risk factors of the main causes of chronic shoulder pain (4).

The aim of this article is to describe the features of the connection between the main shoulder diseases mentioned above and thyroid dysfunction, and to highlight the relevance of the scientific data obtained to date for everyday clinical practice.

MATERIALS AND METHODS

A literature search was carried out on MEDLINE/PubMed, EMBASE/OVID, and Cochrane databases, using the words "shoulder", "thyroid", "periarthritis", "tendinopathy", "hypo/hyper-thyroidism", "tendinitis", "rotator cuff", "calcific tendonitis", "tendon", "frozen shoulder", "adhesive capsulitis", "rotator cuff tears",

Key words: hypothyroidism, hyperthyroidism, thyroid disease, calcific tendinitis, adhesive capsulitis, rotator cuff tear, glenohumeral osteoarthritis, postoperative stiffness, tendinopathy

Mailing address:
Giovanni Vicenti, MD, Department of Neuroscience and Sensory Organs, Orthopedics Section, Faculty of Medicine and Surgery, University of Bari, Policlinico, Piazza Giulio Cesare 11, 70124 Bari, (BA), Italy
Tel.: +39 3480128360
e-mail: dott.gvicenti@gmail.com

0393-974X (2016)

DISCLOSURE: ALL AUTHORS REPORT NO CONFLICTS OF INTEREST RELEVANT TO THIS ARTICLE.

"subacromial syndrome", "osteoarthritis". Any article written in English providing data on both thyroid and shoulder diseases was included in this brief review.

RESULTS

Laboratory findings

Thyroid hormones 3,5,3',5'-L-tetraiodothyronine (T4) and its active form 3,5,3'-L-triiodothyronine (T3) exert both genomic and non-genomic effects. Intracellular enzymes deiodinases 1 (DIO1) and 2 (DIO2) convert T4 to T3, whereas deiodinase 3 (DIO3) inactivates T3 to T2 and T4 to rT3 and is useful to protect the cells from inappropriately high levels of thyroid hormones (1). Thyroid hormones are vital for the development, growth and metabolism of all the tissues composing the human body, including bone, cartilage and tendon (1). Several studies have identified DIO2 and DIO3 as disease susceptibility loci for osteoarthritis (1).

Thyroid hormones are also involved in tendon homeostasis. The tendon extracellular matrix is composed of type I collagen (65-80%) and elastin (1-2%) surrounded by proteoglycans and water and is synthetized by tenoblasts and tenocytes situated among the collagen fibers (6). *In vivo* experiments conducted on rats demonstrated that normal concentration of thyroid hormones should be maintained in order to achieve the right balance between collagen catabolism and anabolism (7). Other *in vitro* studies have shown that thyroid hormones enhance the synthesis of type I collagen and proteoglycans in the presence of ascorbic acid. Notably, treating tenocytes with thyroid hormones has no effect on type III collagen, which is usually involved in tendinopathies and rotator cuff tears (6).

Thyroid hormones are also involved in tenocyte viability. As occurs in other cell types, *in vitro* experiments conducted on human tenocytes have shown that thyroid hormones enhance cell proliferation and prevent apoptosis in a dose- and time-dependent manner (8). Remarkably, Benson and colleagues have demonstrated that tendinopathy is characterized by excessive apoptosis and hypoxia (9). The aetiology of rotator cuff tears is still undefined; however, intrinsic factors are gaining increasing importance and apoptosis might be among the primary causes of tendon degeneration, since it reduces the number of viable tenocytes and therefore impairs the tendon healing process in response to microtrauma (8, 9).

It is also known that low levels of thyroid hormones impair catabolism, leading to GAG accumulation in the extracellular matrix and, as a consequence, making the tendon prone to calcification. In fact, calcific tendinopathy is characterized by metaplastic fibrocartilage tissue interposed between multifocal calcific deposits that stain positive for chondroitin-4-sulphate/dermatan sulphate and chondroitin-6-phosphate surrounding the cells (10).

Clinical findings

In 1997, Knopp at al. reported a case of refractory tendinitis as the only presenting symptom of hypothyroidism, eventually treated with gradual thyroid hormone replacement. Similarly, Pantazis and colleagues described the spontaneous rupture of the long head of the biceps tendon in a woman presenting uncontrolled hypothyroidism. Adequate thyroid hormones levels were restored and shoulder function was almost completely regained one year after the injury (11).

Several retrospective studies showed that the prevalence of idiopathic frozen shoulder was higher in patients suffering from different types of thyroid disorders (10.9%) than in the general population (2-4%) and stated that thyroid diseases should be considered as risk factors for this musculoskeletal disorder (4, 12).

Harvie et al. studied a cohort of 102 patients suffering from calcific tendinopathy and observed that those who were also affected by hypothyroidism experienced earlier onset of symptoms, a longer natural history of the disease and underwent surgery more often because of the higher rate of non-operative treatment failure (13).

In a retrospective study, Oliva et al. hypothesized the role of thyroid disorders as risk factors for rotator cuff tears, highlighting how both of these clinical entities have higher prevalence in females (5). Moreover, Blonna et al. recently suggested that thyroid disease might account for otherwise inexplicable shoulder stiffness following arthroscopic procedures (14).

DISCUSSION

Affecting tendon metabolism and viability, thyroid hormones are likely to be involved in the pathogenesis of calcific tendonitis (10, 13) and rotator cuff disease (8, 9). In fact, thyroid hormones' ability to prevent apoptosis might preserve tendon biology and contribute to its resistance to mechanical overuse and strain, suggesting that low levels of intracellular T3 might induce increased susceptibility to rotator cuff disease (8, 9). Thyroid diseases might also represent a warning sign for adhesive capsulitis in patients complaining of shoulder pain (12), demanding a thorough diagnostic work-up and referral to the orthopedic surgeon. Moreover, a personal history of thyroid disorders might be helpful not only in the differential diagnosis of shoulder diseases but also in predicting the natural development of calcific tendonitis and guiding the choice between the many therapeutic options available (13). In fact, Blonna et al. suggested that subclinical hypothyroidism should be considered a risk factor for severe post-operative stiffness and thus, if present, should discourage a surgical approach to shoulder diseases or demand the adoption of appropriate prophylactic measures (14).

On the other hand, case reports and recent review articles suggest that shoulder pain might be the presenting symptom of an underlying thyroid dysfunction; therefore it may be advisable to screen these patients for hypothyroidism or hyperthyroidism (11, 15). Restoring thyroid function could facilitate response to treatment and full recovery of shoulder function (11).

In light of the laboratory and clinical findings outlined, it would be beneficial to bear in mind that thyroid and shoulder diseases are likely to coexist. Further and detailed studies are needed to better understand how hormonal imbalance is involved in the pathogenesis of each of the most common shoulder diseases and what difference, if any, its presence makes when choosing between treatment options.

Most of the literature on the topic lacks in detailed data regarding one of the two medical branches involved and consists in case reports or retrospective studies and, if prospective, they often have a small sample size. Consequently, it is difficult to make deductions which are easily applicable to the general population.

REFERENCES

1. Bassett JHD, Williams GR. Role of thyroid hormones in skeletal development and bone maintenance. Endocr Rev 2016; 37(2):135-87.
2. Duncan WS. The relationship of hyperthyroidism to joint conditions. JAMA 1928; 91(23):1779-82.
3. Meislin RJ, Sperling JW, Stitik TP. Persistent shoulder pain: epidemiology, pathophysiology, and diagnosis. Am J Orthop (Belle Mead NJ) 2005; 34(12 Suppl):5-9.
4. Raynor MB, Kuhn JE, Kuhn JE. Utility of features of the patient's history in the diagnosis of atraumatic shoulder pain: a systematic review. J Shoulder Elbow Surg 2016; 25(4):688-94.
5. Oliva F, Osti L, Padulo J, Maffulli N. Epidemiology of the rotator cuff tears: a new incidence related to thyroid disease. Muscles Ligaments Tendons J 2014; 4(3):309-14.eCollection 2014.
6. Berardi AC, Oliva F, Berardocco M, la Rovere M, Accorsi P, Maffulli N. Thyroid hormones increase collagen I and cartilage oligomeric matrix protein (COMP) expression in vitro human tenocytes. Muscles Ligaments Tendons J 2014; 4(3):285-91.
7. Kivirikko KI, Laitinen O, Aer J, Halme J. Metabolism of collagen in experimental hyperthyroidism and hypothyroidism in the rat. Endocrinology 1967; 80(6):1051-61.
8. Oliva F, Berardi AC, Misiti S, Verga Falzacappa C, Iacone A, Maffulli N. Thyroid hormones enhance growth and counteract apoptosis in human tenocytes isolated from rotator cuff tendons. Cell Death Dis 2013; 4:e705.
9. Benson RT, McDonnell SM, Knowles HJ, Rees JL, Carr AJ, Hulley PA. Tendinopathy and tears of the rotator cuff are associated with hypoxia and apoptosis. J Bone Joint Surg Br 2010; 92(3):448-53.
10. Speed CA, Hazleman BL. Calcific tendinitis of the shoulder. N Engl J Med 1999; 340(20):1582-84.
11. Pantazis K, Roupas ND, Panagopoulos A, Theodoraki S, Tsintoni, A, Kyriazopoulou V. Spontaneous rupture of the long head of the biceps tendon in a woman with hypothyroidism: a case report. J Med Case Rep 2016;

10(1):2.
12. Wang K, Ho V, Hunter-Smith DJ, Beh PS, Smith KM, Weber AB. Risk factors in idiopathic adhesive capsulitis: a case control study. J Shoulder Elbow Surg 2013; 22(7):e24-9.
13. Harvie P, Pollard TC, Carr AJ. Calcific tendinitis: natural history and association with endocrine disorders. J Shoulder Elbow Surg 2007; 16(2):169-73.
14. Blonna D, Fissore F, Bellato E, La Malfa M, Calò M, Bonasia DE, Rossi R, Castoldi F. Subclinical hypothyroidism and diabetes as risk factors for postoperative stiff shoulder. Knee Surg Sports Traumatol Arthrosc 2015 Dec 12 [Epub ahead of print].
15. Oliva F, Berardi AC, Misiti S, Maffulli N. Thyroid hormones and tendon: current views and future perspectives. Concise review. Muscles Ligaments Tendons J 2013; 3(3):201-3.

LETTER TO THE EDITOR

A SOLITARY UTERINE RELAPSE IN T-CELL ACUTE LYMPHOBLASTIC LEUKAEMIA: CT FEATURES AND PATHOLOGIC CORRELATION

M.A. MAZZEI[1], G. BETTINI[1], C. POZZESSERE[1], S. GUERRINI[1], M. DEFINA[2], M.R. AMBROSIO[3], L. APRILE[2], M. BOCCHIA[2] and L. VOLTERRANI[1]

[1]Department of Medical, Surgical and Neuro Sciences, Diagnostic Imaging, Azienda Ospedaliera Universitaria Senese, University of Siena, Siena, Italy; [2]Division of Hematology and Transplants, Azienda Ospedaliera Universitaria Senese, University of Siena, Italy; [3]Department of Medical Biotechnologies, Section of Pathology, Azienda Ospedaliera, Universitaria Senese, University of Siena, Siena, Italy

Received December 13, 2015 – Accepted June 6, 2016

T-cell Acute Lymphoblastic Leukemia (T-cell ALL) is a rare haematological neoplasia, that affects children and less commonly adults. Female genital tract and particularly uterus involvement in acute ALL is rare. This report presents the CT features of a 64-year-old woman with uterine relapse of T-cell ALL, occurring 11 months after the diagnosis, as a second, unique relapse of disease. The patient was asymptomatic when a CT examination showed a homogenous thickness of the uterine wall in comparison with the previous CT examination. Histology from biopsy specimens, obtained through hysteroscopy, confirmed T-cell ALL localisation (TdT+, CD10+, CD3c+ and CD2+). The uterus could be a site of relapse in patients suffering from ALL. Even though an MRI examination could better demonstrate the disease in cases of suspected female genital tract involvement by ALL, the comparison of differences between a present and a previous CT examination is sufficient to suspect the diagnosis.

To the Editor,

T-cell Acute Lymphoblastic Leukaemia (T-cell ALL) is a rare haematological neoplasia, that affects children and less commonly adults, with a reported incidence rate of 6 per 1,000,000 children from 5 to 14 years of age/year and less than 2 per 1,000,000 adults/year (1). Adult T-cell ALL is usually an aggressive disease, with common extramedullary (EM) infiltration such as mediastinum, spleen and liver (2). EM rarely involves the eye, ear, ovary, uterus, bone, muscle, tonsil, kidney, pleura, or paranasal sinus, thus these lesions are usually overlooked or misdiagnosed by radiologists because of their low incidence rate (3). The first case of uterine recurrence of ALL was reported by Cantwell et al. in a 15-year-old girl, followed by two other cases involving older women, described by Harris et al. (4, 5). The clinical presentation of haematological malignancies of the female genital tract tends to be non-specific (pelvic mass, vaginal bleeding) and can be confused with other malignancies. Therefore, even if the definitive diagnosis has to be proven by histological examination, imaging

Key words: acute lymphoblastic leukaemia, haematological malignancies, uterus, computed tomography, magnetic resonance imaging.

Mailing address:
Susanna Guerrini, MD
University of Siena, Department of Medical,
Surgical and Neuro Sciences, Diagnostic Imaging,
Azienda Ospedaliera Universitaria Senese,
University of Siena, Viale Bracci 10, Siena 53100, Italy
Tel.: +39 0577 585700 - Fax: +39 0577 44496
e-mail: guerrinisus@gmail.com

0393-974X (2016)

DISCLOSURE: ALL AUTHORS REPORT NO CONFLICTS OF INTEREST RELEVANT TO THIS ARTICLE.

can play a pivotal role in the early detection of involvement of genital sites, detecting lesion extension, guiding biopsies, staging disease and allowing an appropriate treatment, resulting in a better prognosis for the patient (6). We report the computed tomography (CT) imaging features of a patient with an isolated uterine relapse of T-cell ALL, with the aim of sharing our knowledge of this rare condition, particularly among radiologists interested in haematological disease.

Case report

A 64-year-old female patient, with a history of breast cancer (diagnosed in 2008) in treatment with hormonal therapy, previously treated with QUART and chemotherapy, was admitted to the hospital in October 2011 because of dyspnea and orthopnea. Complete blood cell count (CBC) showed leukocytosis (WBC 25x103/μL), mild anemia (Hb 10 g/L) and a normal platelet count (PLT 190x103/μL). Serum values revealed an increased level of C reactive protein (PCR), creatinine, lactate dehydrogenase (LDH), uricaemia and erythrocyte sedimentation rate. The diagnosis was obtained by morphological analysis and immunophenotype of bone marrow aspirate showing the presence of T-lymphoblasts. Cytogenetic analysis revealed a normal karyotype. Disease staging was completed with an abdominal and thoracic CT examination (CT 1) that demonstrated multiple enlarged mediastinal lymph nodes (diameter up to 4 cm) pleural and pericardial effusion. In line with these findings, a clinical diagnosis of T-cell ALL/Lymphoblastic Lymphoma was made. The patient was treated with induction therapy, with a sequential combination of prednisone, vincristine, cyclophosphamide and daunorubicin, associated with 5 intratecal injections of methotrexate, dexamethasone and cytarabine, obtaining a morphologic complete remission at the bone marrow evaluation, but showing a severe drug-induced neuropathy. The patient subsequently underwent consolidation treatment with methotrexate and cytarabine, obtaining a negative CT scan evaluation (CT 2); however, still harbouring bone marrow minimal residual disease (MRD), because of a PCR detectable monoclonal TCR rearrangement. Because of disease persistence and considering the unfit status of the patient due to the severe neuropathy, consolidation therapy was not completed, but maintenance treatment with oral 6-Mercaptopurine and i.m. methotrexate was started. In May 2012, during a routine follow-up, a CT (CT 3) scan found retrocaval, retrocrural, para-aortic and intercavo-aortic pathological lymph nodes as well as bilateral renal involvement (Fig. 1). The bone marrow biopsy confirmed a full relapse of T-cell ALL, hence treatment with a re-induction therapy (2 cycles of high dose of cytarabine plus mithoxantrone) was given. Complete marrow remission had already been regained after the first cycle and the follow-up CT (CT 4) scan confirmed the disappearance of all disease localisations. The last follow-up CT examination (CT 5), performed in September 2012, before and after an injection of intravenous contrast media administration, revealed an increased homogenous thickness (30 mm) of the uterine corpus and fundus wall with enhancement features similar to the previous renal ALL lesions. At the time of the uterine recurrence, the patient did not present symptoms or clinical signs of urogenital involvement, such as vaginal bleeding or pelvic mass. Biopsy under hysteroscopy was performed and the analysis of endometrial specimens revealed T-cell-ALL localisation (TdT+, CD10+, CD3c+ and CD2+) (Fig. 2). At the same time, a new bone marrow biopsy was performed, confirming T-cell ALL recurrence and thus proving the diagnosis of uterine relapse of ALL.

DISCUSSION

Haematological malignancies have increasingly grown in the last few years. Moreover, the introduction of new therapies demonstrates a large variety of uncommon sites of relapse and an increase in the susceptibility to the administration of different therapies (7). We report a rare case of uterus involvement in T-cell ALL. Although initially associated with a particularly bad prognosis, the introduction of intensified treatment protocols has improved the outcome of T-cell ALL and current therapies may achieve five

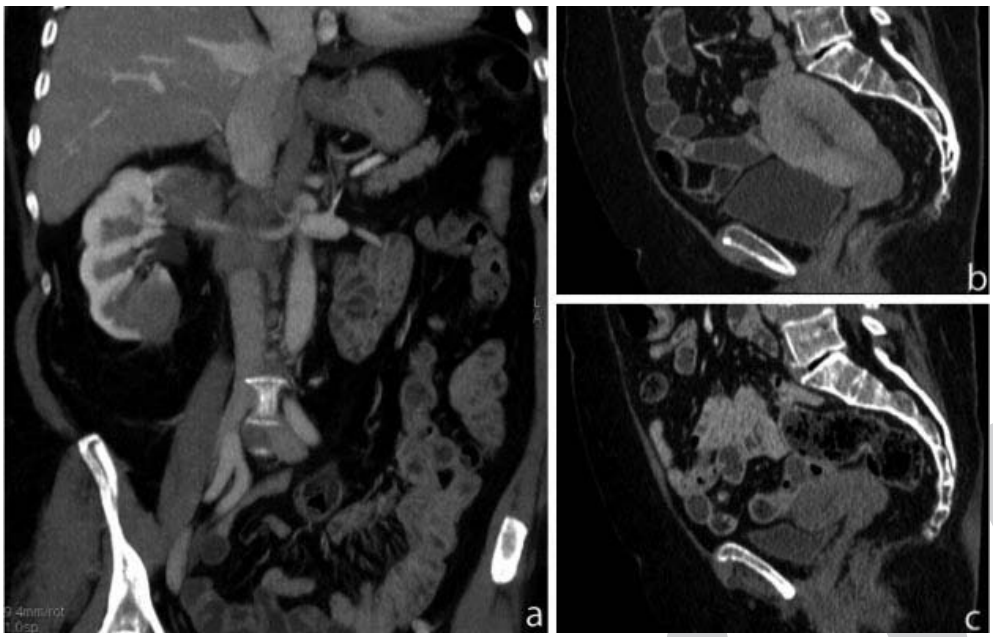

Fig. 1. *2D multiplanar reconstruction on oblique-coronal plane at first relapse (CT 3) showed retrocaval, intercavo-aortic pathological lymph nodes and renal involvement (**a**). 2D multiplanar reconstruction on sagittal plane at second relapse (CT 5) showed an increased homogenous thickness of uterine corpus and fundus wall with enhancement features similar to the previous renal ALL localisations (**b**); the uterus appeared normal at the previous follow-up CT examination (CT4) (**c**).*

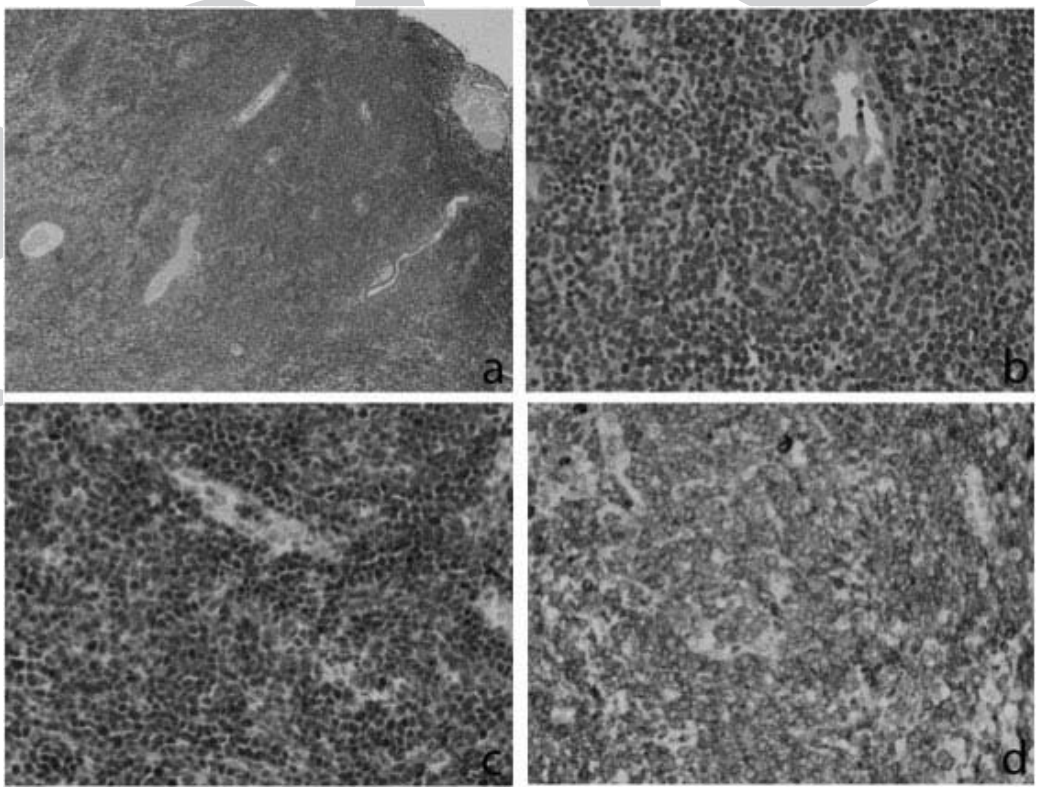

Fig. 2. *At low power, endometrium with massive expansion of the stromal compartment by a uniform population of lymphoid cells is evident, the blasts spared the glands (A, H&E, Å~2.5). At high power, lymphoid cells are small to medium sized, with a fine chromatin pattern and small nucleoli (B, H&E, Å~20). Lymphoid cells show strong nuclear positivity to TdT (C, Å~20) and CD2 (D, Å~20). TdT: Terminal deoxynucleotidyl transferase.*

year relapse-free survival rates of about 75% in children and 50% in adults (8). Female genital tract involvement by haematological neoplasm is rare, even if it is not an uncommon finding at autopsy and it may become a more common clinical problem as increasing numbers of these patients are surviving longer after receiving novel combinations of chemotherapy (6). Moreover, an EM relapse of haematological malignancies is not uncommon in adults and selective involvement of EM sites, preceding marrow relapse, suggesting either a high affinity of blasts to EM sites or specific biological features such as receptors or adhesion molecules or the presence of sites with a predisposition to the involvement, because they are "sanctuary sites", with a biological barrier or immune privileged sites that are not sufficiently accessible (9). In literature, only a few cases of uterine relapse by ALL have been described (4, 10). Magnetic Resonance Imaging (MRI) represents the technique of choice, because it studies the pelvis with a high locoregional spatial resolution and good soft-tissue contrast, with the advantage of the lack of ionizing radiation, particularly important in young females (10). In haematological neoplasms, CT allows an accurate TNM staging by the assessment of chest-abdomen-pelvis using CT protocol that ensures a diagnostic quality and efficacy and a reduction of radiation dose to the patient (e.g. split-bolus CT protocols) in respect to conventional CT (11, 12). Furthermore, in cases of female genital tract involvement, a CT examination performed using a dedicated protocol (thin sections and high resolution multiplanar images) is preferable for the investigation of a possible minimal peritoneal implant due to a peritoneal neoplastic diffusion (13). This case report and review of the literature suggest that radiologists should not overlook unusual sites for EM relapse, which can be the only sign of ALL recurrence in long-time survivors. Comparison of serial CT images is of paramount importance for the early diagnosis of female genital tract involvement, and should prompt an MRI examination in selected cases with the aim of achieving optimal characterisation of the disease and biopsy planning.

ACKNOWLEDGEMENTS

The Authors thank Ms. Julia Hassall for reviewing the English language.

REFERENCES

1. Dores GM, Devesa SS, Curtis RE. Acute leukemia incidence and patient survival among children and adults in the United States, 2001-2007. Blood 2012; 119:34-43.
2. Pui CH, Relling MV, Downing JR. Acute lymphoblastic leukemia. N Engl J Med 2004; 350:1535-48.
3. Lyman MD, Neuhauser TS. Precursor T-cell acute lymphoblastic leukemia/lymphoma involving the uterine cervix, myometrium, endometrium, and appendix. Ann Diagn Pathol 2002; 6:125-28.
4. Cantwell B, Cantwell D, Fennelly JJ. Uterine and ovarian leukaemic relapse during bone marrow remission in acute lymphoblastic leukaemia. Postgraduate Medical Journal 1982; 58:724-25.
5. Harris NL, Scully RE. Malignant lymphoma and granulocytic sarcoma of the uterus and vagina. Cancer 1984; 53; 2530.
6. Salem U, Menias CO, Shaaban A, et al. Hematopoietic tumors of the female genital system: imaging features with pathologic correlation. Abdom Imaging 2014; 39:922-34.
7. Guerrini S, Bucalossi A, Cioffi Squitieri N, et al. Ischemic colitis diagnosed by magnetic resonance imaging during lenalidomide treatment in a patient with relapsed multiple myeloma. Tumori 2015; [Epub ahead of print].
8. Marks DI, Paietta EM, Moorman AV, et al. T-cell acute lymphoblastic leukemia in adults: clinical features, immunophenotype, cytogenetics, and outcome from the large randomized prospective trial (UKALL XII/ECOG 2993). Blood 2009; 114:5136-45.
9. Thanka J, Krishnarathinam K, Rajendiran S. Extramedullary relapse of acute lymphoblastic leukemia in breast: a rare presentation. Indian J Pathol Microbiol 2010; 53:155-6.
10. Novellas S, Fournol M, Deville A, et al. MR features of isolated uterine relapse in an adolescent with acute lymphoblastic leukaemia. Pediatr Radiol 2008;

38:319-21.
11. Scialpi M, Palumbo B, Pierotti L, et al. Detection and characterization of focal liver lesions by split-bolus multidetector-row CT: diagnostic accuracy and radiation dose in oncologic patients. Anticancer Res 2014; 34:4335-44.
12. Scialpi M, Schiavone R, D'Andrea A, et al. Single-phase Whole-body 64-MDCT split-bolus protocol for pediatric oncology: diagnostic efficacy and dose radiation. Anticancer Res 2015; 35:3041-48.
13. Mazzei MA, Khader L, Cirigliano A, et al. Accuracy of MDCT in the preoperative definition of Peritoneal Cancer Index (PCI) in patients with advanced ovarian cancer who underwent peritonectomy and hyperthermic intraperitoneal chemotherapy (HIPEC). Abdom Imaging 2013; 38:1422-30.

LETTER TO THE EDITOR

ENDOMETRIOSIS AND GLANZMANN'S THROMBASTHENIA

L. IMPERIALE[1], L. MANGANARO[2], A. TICINO[1], I. PIACENTI[1], E. ANASTASI[3], S. RESTA[1], P. BENEDETTI PANICI[1] and M.G. PORPORA[1]

[1]Department of Gynecology, Obstetrics and Urology, Sapienza, University of Rome, Policlinico Umberto I, Rome, Italy; [2]Department of Radiological, Oncological, and Pathological Sciences, Sapienza University of Rome, Policlinico Umberto I, Rome, Italy; [3]Department of Molecular Medicine, Sapienza University of Rome, Policlinico Umberto I, Rome, Italy

Received December 28, 2015 – Accepted May 4, 2016

Glanzmann's thrombasthenia (GT) is a rare bleeding syndrome characterized by deficiency or defect of platelet aggregation complex. The pathogenesis of endometriosis is controversial but the strongest evidence leans towards retrograde menstruation. GT probably predisposes to endometriosis. The management of women affected by this disease can be difficult due to the risk of bleeding complications, especially during surgical treatment. We describe the cases of three sisters affected by endometriosis and GT, referred to our Department, who received different therapeutic management.

To the Editor,

Endometriosis is one of the most frequent benign gynecological diseases, characterized by the implant and growth of viable endometrial tissue outside of the uterine cavity, resulting in a general inflammatory response. The reported endometriosis prevalence in women of reproductive age ranges from 10%, and 30%–50% for women with infertility. The pathogenesis of endometriosis is controversial but the strongest evidence suggests its basis to be the retrograde menstruation phenomenon. This pathogenic theory is based on the retrograde flow of endometrial fragments driven through the fallopian tubes into the abdominal cavity(1).

Glanzmann's thrombasthenia (GT) is a rare bleeding syndrome affecting the megakaryocyte lineage. It is an inherited autosomal recessive platelet disorder characterized by deficiency or defect of glycoprotein (GP) IIb/IIIa complex (integrin αIIbβ3) on the platelet surface, which mediates the incorporation of platelets into an aggregate or thrombus at sites of vessel injury. The αIIb and β3 proteins are both localized on the long arm of chromosome 17 (17q21-23) and are encoded by the ITGA2B and ITGB3 genes, respectively. In the majority of patients with GT there is a mutation of these genes, but the defects in the regulatory element affecting the transcription of these 2 genes could be another possible cause. Its incidence is rare, around 1 per million but a relatively high incidence in consanguineous populations is common (2). Although the laboratory parameters show normal platelet morphology and normal platelet count, in the affected patients, there is a prolonged bleeding time and deficient or absent platelet aggregation with physiological agonists. Symptoms include: purpura, bruising, epistaxis, gingival hemorrhage, and menorrhagia. Gastrointestinal bleeding and

Key words: endometriosis, Glanzmann's thrombasthenia, management

Mailing address:
Adele Ticino, MD
Department of Gynaecology, Obstetrics and Urological Sciences,
"Sapienza" University of Rome, Policlinico Umberto I,
Viale del Policlinico 155, 00161 Rome, Italy
Tel.: +39 06 44231967 - Fax: +39 06 4451752
e-mail: adele.ticino@yahoo.com

0393-974X (2016)

DISCLOSURE: ALL AUTHORS REPORT NO CONFLICTS OF INTEREST RELEVANT TO THIS ARTICLE.

hematuria are less common.

GT probably predisposes to endometriosis. The management of women affected by this disease can be difficult due to the risk of bleeding complications, especially during surgical treatment. We report three cases of endometriosis in three sisters, two of them twins, suffering from GT, referred to our Department, who received different therapeutic management.

MATERIALS AND METHODS

The first case regards a 28-year-old Caucasian female (gravida 0, para 0), referred to our Department in June 2010 for dysmenorrhea (VAS 10), deep dyspareunia and severe menometrorrhagia only partially controlled by oral or I.V. tranexamic acid. The patient was affected by GT, diagnosed a few days after birth following a severe episode of epistaxis. She has two sisters, one of whom is her twin, both with GT. Since menarche, cyclic administration of 0.075 mg ethinylestradiol/gestodene 0.030 mg was prescribed to prevent severe menorrhagia.

The second 40-year-old sister (gravida 0, para 0), referred to our Department in January 2011, as, despite the use of oral contraceptives since menarche, she was constantly experiencing severe menorrhagia, mild dysmenorrhea and deep dyspareunia. The patient was affected by GT. Shortly after the menarche the patient had a severe episode of heavy menstruation, therefore she started cyclic administration of 0.075 mg ethinylestradiol/ gestodene 0.030 mg. Her medical history was negative for other diseases.

The last, the 28-year-old twin sister of the first patient described (gravida 0, para0), affected by GT, was referred by her twin to our Department in January 2011, complaining of heavy menstrual bleeding. She had been under oral contraceptive therapy (ethinylestradiol 30μg/ gestodene 75 μg) since the menarche, without significant benefit.

All three patients signed informed consent to the processing of personal data for research purposes.

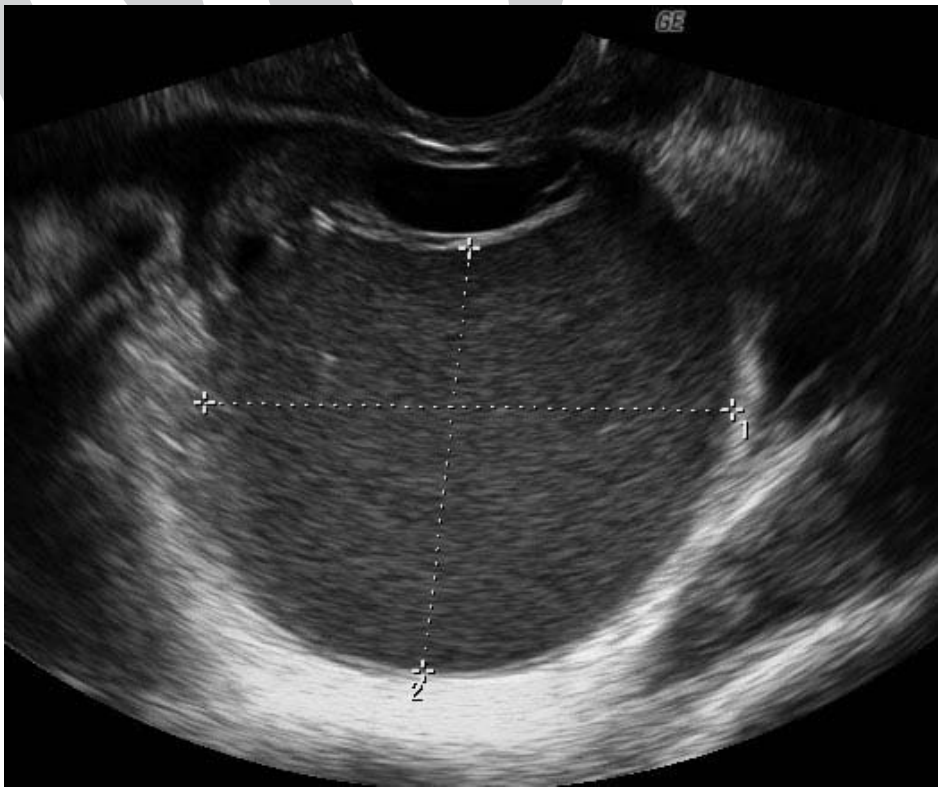

Fig. 1. *Transvaginal pelvic ultrasound scan of ovarian endometriomas.*

RESULTS

Bimanual gynecological/pelvic examination of the first sister revealed a normal anteverted uterus, a normal right adnexa and the presence of a tender left adnexal mass. Speculum examination revealed foci of vaginal endometriosis. Pap smear was negative. Transvaginal pelvic ultrasounds showed the presence of a 70-mm maximum diameter, cystic mass, hypoechoic and corpuscular affecting the left adnexal side, suggestive of endometrioma, and a suspected intrauterine polyp of 20 mm (Fig 1). After consultation with her hematologist, who recommended to avoid or delay surgery as long as possible for the high risk of hemorrhagic complications, the patient started a treatment with medroxyprogesterone acetate (MPA) 150 mg intramuscular, once every three months. Pain-related symptoms improved, however after 11 months of treatment, transvaginal ultrasound (TVUS) documented the persistence of the left endometrioma, the appearance of a new endometriotic cyst of 34x34 mm in size in the same ovary and the persistence of the polyp. The patient was scheduled for surgery after 3 months of treatment with gonadotropin-releasing hormone analogs (GnRH-a) (triptorelin acetate 3.75 mg, intramuscular once a month). Before surgery, TVUS showed a reduction in size of the larger left ovarian endometrioma (50 mm). Laparoscopic excision of the left ovarian endometriomas by stripping was performed along with hysteroscopic polyp removal.

Recombinant activated factor VII (rFVIIa) (~90 mcg/kg) was administered before and after surgery as follows: 5 mg (250 kUI) iv ½ hour before laparoscopy; then every 4 hours from the 3rd to the 72nd hour after surgery and finally, every 6 hours for 7 days. Tranexamic acid 500 mg (4 vials in 500 cc saline slow drip) was administered during the perioperative period. Histological examination confirmed ovarian endometriosis and a benign endometrial polyp. Postoperative laboratory tests were normal but TVUS showed the presence of a hematometra of 11.7 mm (Fig. 2). As suggested by her hematologist, the patient continued therapy with tranexamic acid 500 mg and recombinant factor VIIa 5 mg until resolution. No platelet transfusion was needed. The patient was discharged on the 30th postoperative day in agreement with the hematologist, and tranexamic acid 500 mg (2 tablets/die) was prescribed until hematometra disappearance, occurring four months

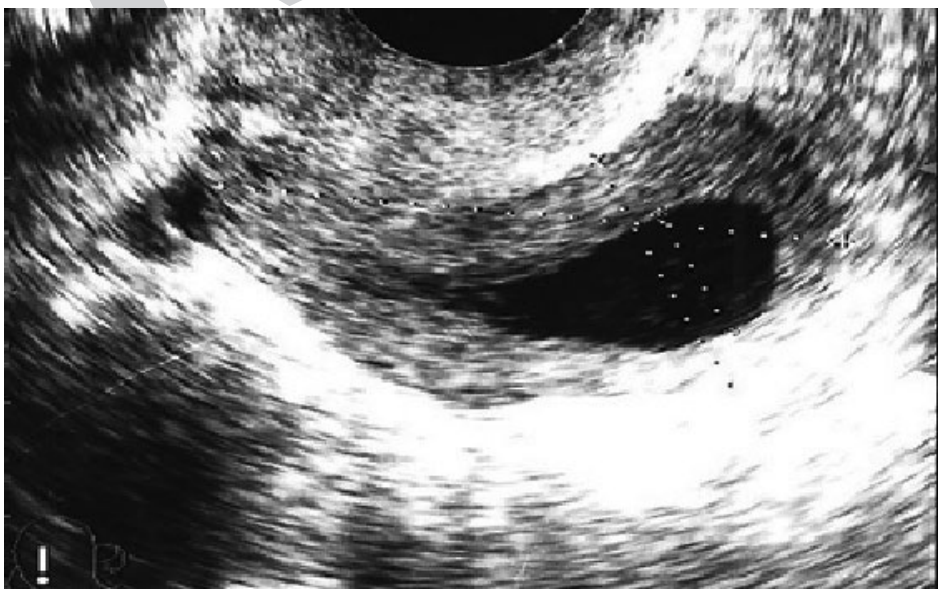

Fig. 2. *Transvaginal pelvic ultrasound scan of hematometra.*

later. GNRh-a depot therapy (triptorelin 3.75 mg) intramuscular once a month for 3 months, was prescribed, followed by MPA 150 mg intramuscular once every three months for 1 year. Afterwards, due to the patient's weight gain, in accordance with her wishes, there was a switch to oral contraceptive with 0.02 mg ethinylestradiol/levonorgestrel 0.1 mg continuously. After 1 year of treatment, the patient complained of irregular vaginal bleeding and oral therapy was changed to cyclic administration of 0.075 mg ethinylestradiol/gestodene 0.030 mg, according to the preference of the patient, with good compliance. Occasional episodes of menorrhagia are well controlled with tranexamic acid 500 mg.

With regard to the second sister, clinical examination using vaginal speculum showed regular cervix and vaginal walls**.** Pap smear was normal. Bimanual pelvic examination showed an endometriotic nodule of about 50 mm in diameter in the rectovaginal septum, very painful on palpation; normal sized anteverted uterus and non-palpable ovaries**.** Abdominal and vaginal ultrasound did not show any other abnormalities. Intramuscular injection of MPA 150 mg once every three months and antifibrinolytic agents **(**tranexamic acid 500 mg) were administered with only partial control of symptoms. Due to the low efficacy of MPA in bleeding control, it was suspended and a levonorgestrel 52 mg releasing intrauterine system (LNG – IUS) was placed. Six months later, the patient complained of heavy menorrhagia resistant to antifibrinolytic agents**.** A pelvic tranvaginal ultrasound scan was performed but no abnormalities were found. The LNG- IUS was still in place. After counseling with the patient and her hematologist on the possible therapeutic options, a cyclic administration of three months therapy with depot GnRH-a **(**triptorelin 3.75 mg) depot intramuscular once a month was administered and the LNG-IUS was removed. After three months she started MPA, intramuscular 150 mg once every three months that is still the current treatment. At the moment she is in good general condition.

Clinical examination of the third sister using vaginal speculum showed regular cervix and vaginal walls. Pap smear was negative. Bimanual gynecological/pelvic examination revealed a normal anteverted uterus, a normal left adnexa and the presence of a tender right adnexal mass. Transvaginal ultrasound revealed the presence of a cystic lesion with mixed echogenicity and a maximum diameter of 35 mm in the right ovary, not vascularized at Doppler valuation. Endometriosis was suspected. According to the patient's preference and the hematological consultation, a levonorgestrel 52 mg releasing intrauterine system was inserted. After two months of therapy she had a significant reduction of the menstrual flow. A transvaginal ultrasound was performed showing a slight reduction in size of the ovarian cyst. At the present she is in good general condition, no other episodes of menorrhagia have occurred, and she has no pain symptoms despite the fact that the ovarian endometrioma, although smaller (30 mm), is still present.

DISCUSSION

Numerous theories have been proposed to explain the pathogenesis of endometriosis: retrograde flow of menstrual and lymphatic spread, immunity, and hormonal, environmental and genetic factors (3). A recent meta-analysis reported that genetic polymorphisms may contribute to individual susceptibility to endometriosis, but further studies with larger sample size and tissue-specific biochemical and biological characterizations are needed (4). An increased prevalence has been observed in first-degree relatives of women affected by endometriosis compared to the general population, particularly in monozygotic twins (5)**.** According to the retrograde menstruation theory of Sampson, eutopic endometrial cells flow back throughout the fallopian tubes into the peritoneal cavity, implant, grow and invade pelvic structures.

It has been universally recognized that menorrhagia is a frequent symptom in women with bleeding disorders. The prevalence of menorrhagia in women affected by von Willebrand disease ranges from 32% to 100% and in women with Glanzmann's thrombasthenia is 98% (6). Kirtava et al. reported in a survey of 102 women with von Willebrand disease a history of endometriosis in 30% of patients, compared to 13% of controls (7). Heavy menstruation might explain a possible correlation between endometriosis and

coagulation disorders as it would increase retrograde flow in the peritoneal cavity.

The diagnosis of GT begins by determining the medical history of the patient. A family history of bleeding and the presence of consanguinity should be investigated. Purpura, petechiae and easy bruising are common features and the disease is mostly, but not always, diagnosed at an early age. The platelet count is relatively normal. Platelet function testing confirms GT because it is the only hematological disorder where platelet aggregation is absent to all agonists (e.g. ADP, collagen, thrombin, arachidonic acid), while the response to ristocetin is maintained.

In the cases described in this article, the patients had several episodes of epistaxis after birth. A hematological disorder was suspected and a prompt diagnosis was made. In literature there is only one paper that describes GT in two sisters with endometriosis. The authors hypothesised that there is a correlation between endometriosis and increased levels of free vitronectin. The GPIIIa subunit can also combine with the a V-integrin subunit to form the aVb 3 ''vitronectin'' receptor. Patients with defects in GPIIIa are also deficient in Vb 3 receptor, so there is an increase of free vitronectin levels. Peritoneal stromal cells in women affected by endometriosis have been shown to be more ''adhesive'' to vitronectin compared with controls (8). ''It seems that vitronectin may represent a substrate that enhances both the attachment and proliferation of ectopic endometrial cells. In patients affected by GT, the platelet disorder causes an increase of menstrual bleeding and retrograde menstruation into the peritoneal cavity; ectopic endometrial cells may have high adhesion and proliferation capability due to the large amount of free vitronectin leading to a higher risk of endometriosis''. It has been reported that patients with GT have had menometrorrhagia since menarche, lasting for more than 10–12 days, leading to severe anemia in 77%. Therefore, in adolescents affected by GT, medical therapy with tranexamic acid and oral contraceptives is frequently necessary to control menstrual bleeding manifestations. Few patients required platelet transfusions to stop the bleeding (9). The management of endometriosis in these patients is therefore a difficult challenge because surgery can sometimes be complicated by hemorrhagic phenomena. This is the reason why a non-surgical approach is preferred. According to international guidelines there are several hormonal therapeutic choices that can be used to treat endometriosis and control abnormal uterine bleeding, such as hormonal LNG-IUS that provides long-term (at least 12 months), norethisterone (15 mg) daily from days 5 to 26 of the menstrual cycle, or injected long-acting progestogens (10). Recombinant factor VII-a may also be an effective tool for treatment of prolonged, intensive menstrual bleeding in GT patients who failed to respond to excessive platelet transfusion (11). When medical therapy fails and the painful symptomatology worsens, surgery becomes necessary. Conservative laparoscopic surgery is the treatment of choice for endometriosis in women of reproductive age who desire to maintain fertility.

Only limited data are available regarding surgical treatment of endometriosis in women with GT. Haemostatic treatment is needed in order to correct the coagulation abnormalities and thus minimize the bleeding risk; the kind of therapy varies according to the type of surgical procedure. When bleeding does not respond to local measures and/or antifibrinolytic drugs, platelet transfusion is currently/becomes the standard treatment. However, repeated platelet transfusions may result in GP IIb-IIIa and/or HLA immunization, and development of platelet refractoriness. An alternative treatment for GT is recombinant factor VIIa (~90 mcg/kg), in order not only to control but also to prevent bleeding during surgical procedures (12). Up to date literature shows that recombinant factor VIIa is a well-known and safe alternative treatment choice that can be successfully used for the prevention of bleeding in gynecological and obstetric procedures (9).

To the best of our knowledge, this is the second article reporting an association between GT and endometriosis. While considering the management of endometriosis in patients with GT, the need of prevention and therapy of specific bleeding episodes and resolution of pelvic pain should be taken into account. The treatment should be individualized. Oral contraceptives, depot medroxyprogesterone acetate, GnRH analogs or local treatments (levonorgestrel-releasing IUS) and non-hormonal therapy (antifibrinolytic drug tranexamic acid) can be administered as successful medical treatment of

endometriosis and menorrhagia. In symptomatic patients with symptoms refractory to medical therapy, laparoscopic surgery can be proposed, but haemostatic treatment is needed to minimize the bleeding risk. In women who no longer wish to preserve their fertility, endometrial ablation or hysterectomy may be options.

REFERENCES

1. Cramer DW, Missmer SA. The epidemiology of endometriosis. Ann N Y Acad Sci 2002; 955:11-22; discussion 34-6, 396-406.
2. Sebastiano C, Bromberg M, Breen K, Hurford MT. Glanzmann's thrombasthenia: report of a case and review of the literature. Int J Clin Exp Pathol 2010; 3(4):443-47.
3. Vichi S, Medda E, Ingelido AM, et al. Glutathione transferase polymorphisms and risk of endometriosis associated with polychlorinated biphenyls exposure in Italian women: a gene-environment interaction. Fertil Steril 2012; 97(5):1143-51.
4. Hu X, Zhou Y, Feng Q, Wang R, Su L, Long J, Wei B. Association of endometriosis risk and genetic polymorphisms involving biosynthesis of sex steroids and their receptors: an updating meta-analysis. Eur J Obstet Gynecol Reprod Biol 2012; 164(1):1-9.
5. Hadfield RM, Mardon HJ, Barlow DH, Kennedy SH. Endometriosis in monozygotic twins. Fertil Steril 1997; 68(5):941-42.
6. James AH. Women and bleeding disorders. Haemophilia 2010, 16 (5):160-67.
7. Kirtava A, Drews C, Lally C, Dilley A, Evatt B. Medical, reproductive and psychosocial expriences of women diagnosed with von Willebrand's disease receiving care in haemophilia treatment centres: a case-control study. Haemophilia 2003; 9:292-97.
8. Alatas E, Oztekin O, Hacioglu SK. Endometriosis in two sisters with Glanzmann's thrombasthenia. Fertil Steril 2009; 92(4):1496.
9. Ray S, Ray A**.** Non-surgical interventions for treating heavy menstrual bleeding (menorrhagia) in women with bleeding disorders. Cochrane Database Syst Rev 2014; 11:CD010338.
10. NICE clinical guideline. Heavy menstrual bleeding. January 2007.
11. Rajpurkar M, Chitlur M, Recht M, Cooper DL. Use of recombinant activated factor VII in patients with Glanzmann's thrombasthenia: a review of the literature. Haemophilia 2014; 20(4):464-71.
12. Demers C, Derzko C, David M, Douglas J. Gynaecological and obstetric management of women with inherited bleeding disorders. Society of Obstetricians and Gynaecologists of Canada. Int J Gynaecol Obstet 2006; 95(1):75-87.

LETTER TO THE EDITOR

CENTRAL APELIN-13 ADMINISTRATION MODULATES HYPOTHALAMIC CONTROL OF FEEDING

C. FERRANTE, G. ORLANDO, L. RECINELLA, S. LEONE, A. CHIAVAROLI, C. DI NISIO, R. SHOHREH, F. MANIPPA, A. RICCIUTI, M. VACCA and L. BRUNETTI

Department of Pharmacy, "G. d'Annunzio" University, Chieti, Italy

Received February 10, 2016 – Accepted May 16, 2016

The 77 amino prepropeptide apelin has been isolated from bovine stomach tissue and several smaller fragments, including apelin-13, showed high affinity for the orphan APJ receptor. The distribution of apelinergic fibers and receptors in the hypothalamus may suggest a role of apelin-13 on energy balance regulation, albeit the studies reporting the acute effects of apelin on feeding control are inconsistent. Considering the possible involvement of apelinergic system on hypothalamic appetite controlling network, in the present study we evaluated in the rat the effects of intrahypothalamic apelin-13 injection on food intake and the involvement of orexigenic and anorexigenic hypothalamic peptides and neurotransmitters. Eighteen rats (6 for each group of treatment) were injected into the ARC with either vehicle or apelin-13 (1-2 µg/rat). Food intake and hypothalamic peptide and neurotransmitter levels were evaluated 2 and 24 h after injection. Compared to vehicle, apelin-13 administration increased food intake both 2 and 24 h following treatment. This effect could be related to inhibited cocaine- and amphetamine-regulated transcript (CART) gene expression and serotonin (5-hydroxytryptamine, 5-HT) synthesis and release, and increased orexin A gene expression in the hypothalamus.

To the Editor,

Hypothalamic feeding control is the result of an articulated interplay of neurotransmitters, neuropeptides, and peripheral signals, which could cross the blood-brain barrier, either by saturable transport systems or by lipophilic diffusion (1). The 77 aminoacid prepropeptide apelin has been isolated from bovine stomach tissue as the endogenous ligand for the orphan APJ receptor, and several smaller peptide fragments, including apelin-13, showed high affinity for this receptor (2). Multiple studies on fish also suggested a stimulatory effect of apelin-13 on food intake, with the possible involvement of hypothalamic neuropeptides (3, 4). This is consistent with the expression of apelin-13 and APJ receptor in the hypothalamus (3). In addition, apelin-13 could also modulate feeding through inhibition of serum leptin levels (5). As regards to food intake control, the hypothalamic arcuate nucleus (ARC) is a key site of interactions between peripheral hormones and neuropeptides. In the ARC, short- and long-term satiety signals arising from gastrointestinal tract and adipose tissue modulate the orexigenic neuropeptide Y (NPY) and agouti-related peptide (AgRP) co-expressing neurons, as well as the anorexigenic proopiomelanocortin (POMC) and cocaine- and amphetamine-regulated transcript (CART) peptide co-expressing neurons. These ARC neurons project to paraventricular nucleus (PVN) and

Key words: Apelin-13, feeding, Orexin A, CART, serotonin

Mailing address:
Professor Luigi Brunetti,
Department of Pharmacy, "G. d'Annunzio" University,
Via dei Vestini 31, 66013 Chieti, Italy
Tel.: +39 0871 3554758 - Fax: +39 0871 3554762
e-mail: luigi.brunetti@unich.it

0393-974X (2016)

DISCLOSURE: ALL AUTHORS REPORT NO CONFLICTS OF INTEREST RELEVANT TO THIS ARTICLE.

lateral hypothalamic area (LHA), where corticotropin releasing hormone (CRH) and orexin-A producing neurons further transduce central feeding signaling (1).

Hypothalamic aminergic neurotransmitters have also been involved in feeding control (1). In this context, we evaluated the effect of apelin-13 on food intake, and the role of NPY, AgRP, CART, POMC, CRH, orexin-A, and dopamine (DA), norepinephrine (NE), and serotonin (5-hydroxytryptamine, 5-HT) in the hypothalamus.

MATERIALS AND METHODS

Animals and drugs

Thirty-six male adult chow-fed Sprague-Dawley rats (290-340 g) were randomized for the experimental paradigms and housed in plexiglas cages (40 cm × 25 cm × 15 cm), one rat per cage, in accordance with the European Community ethical regulations (EU Directive 2010/63/EU) on the care of animals for scientific research. Rat apelin-13 (5 mg/vial, purchased from Vinci-Biochem, Italy) was diluted in saline and dosages selected on the basis of previous experiments (6).

In vivo intrahypothalamic treatment

Eighteen rats were anesthetized by intraperitoneal injection of ketamine-xylazine (50 and 5 mg/kg, respectively), treated with carprofen (4 mg/kg) and subjected to stereotaxic procedure, as previously reported (7). After a midline incision, the skull was scraped clean, washed with sterile saline solution, and disinfected with iodopovidone 10% solution. A drop of lidocaine 2% solution was applied into both the surgical incision and intraperitoneal injection sites. Coordinates for placement of a cannula into the ARC were as follows: anteroposterior (AP), −3 mm (or +3 mm posterior to the bregma); mediolateral (ML), 0.22 mm; dorsoventral (DV), −9 mm (7). After surgery, rats were injected subcutaneously with 1 ml of sterile saline solution and 1 ml of 5% glucose solution (Galenica Senese, Siena, Italy) and then intraperitoneally treated with piperacillin (20 mg/kg/day) (Teva SRL, Italy). During 72 h after surgery and before irisin administration, rats were carefully controlled: they made a rapid recovery and went back to sniff, eat and drink, groom themselves, explore the cage and the sawdust bedding and stand on hind legs as before surgery. There were no signs of hemorrhage. After the recovery period, we did not observe any significant alteration in basal food intake (Table I) in respect to six sham-operated animals, not included in the present experimental paradigm [Food intake (g): 10.66±0.41]. Furthermore, preliminary measurements on spontaneous physical activity, recorded by a video camera (SSC-DC378P, Biosite, Stockholm, Sweden) positioned on the top-center of the cage and connected to a computer, indicated negligible alterations in respect to sham animals. Beginning 72 h after surgery, at 9:00 a.m., rats (6 animals for each group) were injected into the ARC with either vehicle (saline) or apelin-13 (1-2 μg). The cannula was connected with a 10 μl syringe (Hamilton, Switzerland), 1 μl of drug solution or vehicle were injected into the arcuate nucleus. Food was recorded 24 h after apelin-13 administration, as previously reported (7), and finally animals were sacrificed by CO_2 inhalation. In preliminary experiments performed in our laboratories on rats of the same age and weight, we confirmed the location of the cannula tip by injecting dye (Evans blue 0.5% and Zelatin 5%) and histological examinations of frozen hypothalamic sections.

RNA extraction

Immediately after sacrifice, brains (N = 9) were rapidly removed, individual hypothalami were immediately dissected and stored in RNAlater solution (Ambion, Austin, TX) at −20°C until further processing. Total RNA was extracted from the hypothalamus using TRI Reagent (Sigma-Aldrich, St. Louis, MO) according to the manufacturer's protocol. Contaminating DNA was removed using 2 units of RNase-free DNase 1 (DNA-free kit, Ambion, Austin, TX), according to the manufacturer's instructions. The RNA solution was quantified at 260 nm by spectrophotometer reading (BioPhotometer, Eppendorf, Germany) and its purity was assessed by the ratio at 260 and 280 nm readings. The quality of the extracted RNA samples was also determined by electrophoresis through agarose gels and staining with ethidium bromide, under UV light.

Reverse transcription and real-time reverse transcription polymerase chain reaction (real-time RT PCR)

One μg of total RNA extracted from each sample in a 20 μl reaction volume was reverse transcribed using High Capacity cDNA Reverse Transcription Kit (Applied Biosystems, Foster City, CA, USA) according to the manufacturer's manual. Reactions were incubated in a

2720 Thermal Cycler (Applied Biosystems, Foster City, CA, USA) initially at 25°C for 10 min, then at 37°C for 120 min, and finally at 85°C for 5 s. Gene expression was determined by quantitative real-time PCR using TaqMan probe-based chemistry (Applied Biosystems, Foster City, CA, USA). Reactions were performed in MicroAmp Fast Optic 96-well Reaction Plates (Applied Biosystems, Foster City, CA, USA) on an ABI PRISM 7900 HT Fast Real-Time PCR System (Applied Biosystems, Foster City, CA, USA). PCR primers and TaqMan probes were obtained from Applied Biosystems (Assays-on-Demand Gene Expression Products, Rn00567382_m1 for CART gene, Rn01462137_m1 for CRH gene, Rn00595020_m1 for POMC gene, Rn01431703_g1 for AgRP gene, Rn00561681_m1 for NPY gene, Rn00565995_m1 for orexin-A gene). β-actin (Applied Biosystems, Foster City, CA, USA, Part No. 4352340E) was used as the housekeeping gene. In accordance with the manufacturer's instructions, each amplification reaction was performed with 10 µl of TaqMan Fast Universal PCR Master Mix (2X), No AmpErase UNG (Applied Biosystems, Foster City, CA, USA), 1 µl of primer probe mixture, 1 µl of cDNA, 8 µl of nuclease-free water. The thermal cycling conditions (fast operational mode) were: 95°C for 20 s, followed by 40 cycles of amplification at 95°C for 1 s and 60°C for 20 s. The real-time PCR was carried out in triplicate for each cDNA sample in relation to each of the investigated genes. In addition to samples, individual runs included no-template controls (one for each Assay-on-Demand Gene Expression Product) and a reverse transcriptase minus control (for AgRP gene Assay-on-Demand Gene Expression Product). Data were elaborated with the Sequence Detection System (SDS) software version 2.3 (Applied Biosystems, Foster City, CA, USA). The comparative $2^{-\Delta\Delta Ct}$ method was used to quantify the relative abundance of mRNA and then determine the relative changes in individual gene expression (relative quantification) (7). This method uses a calibrator sample to enable a comparison of gene expression levels in different samples. The values obtained indicate the changes in gene expression in the sample of interest by comparison with the calibrator sample, after normalization to the housekeeping gene.

Hypothalamic neurotransmitter extraction and high performance liquid chromatography (HPLC) determination

Immediately after sacrifice, brains (N = 9) were rapidly removed and individual hypothalami dissected and subjected to biogenic amine extractive procedures. Briefly, hypothalamic tissues were homogenized in an ice bath for 2 min with Potter-Elvehjem homogenizer in 1 ml of 0.05 N perchloric acid containing 0.004% sodium EDTA and 0.010% sodium bisulfite. The homogenate was 5-fold diluted in chromatographic mobile phase and centrifuged at 4,500 x g for 10 min. The supernatant was filtered on 0.45 µm PTFE sterile filters (Whatman) and directly injected for HPLC. Neurotransmitter recovery was satisfactory (≥ 90%) and reproducible, with percentage relative standard deviation ≤ 10%. The HPLC apparatus consisting of a Jasco (Tokyo, Japan) PU-2080 chromatographic pump and an ESA (Chelmsford, MA, USA) Coulochem III coulometric detector, equipped with microdialysis cell (ESA-5014b) porous graphite working electrode and solid state palladium reference electrode. The analytical conditions for biogenic amine identification and quantification were selected as previously reported (7).

In vitro hypothalamic perfusion

Hypothalamic synaptosomes were obtained from 18 male adult Sprague-Dawley rats (290-340 g), as previously described (12). Then, the synaptosome suspension was incubated at 37°C, under O_2/CO_2 95%/5%, pH 7.35–7.45, in Krebs-Ringer buffer (mM: NaCl 125, KCl 3, $MgSO_4$ 1.2, $CaCl_2$ 1.2, Tris–HCl 10, glucose 10, ascorbic acid 1). After the incubation period, identical aliquots of synaptosome suspension (1.24 mg protein determined by bicinchoninic acid protein assay) were layered onto 0.8 µm Millipore filters, placed into 37°C water-jacketed superfusion chambers [18 different chambers for each experiment and perfused with Krebs-Ringer buffer (0.6 ml/min)], and perfusate was collected (2 min fractions) to detect released neurotransmitters by HPLC coupled to electrochemical detection, following two experimental protocols. The analytical conditions for amine identification and quantification in the perfusate fractions were selected on the basis of previous experiments performed on hypothalamus homogenate (7). In a first set of experiments, apelin-13 (1–10 nM) was added to the perfusion buffer for 10 min (stimulus period), followed by 8 min with Krebs-Ringer buffer alone (return to basal period). A second set of experiments was run to evaluate the effects of apelin-13 (1–10 nM) on neurotransmitter release induced by a mild depolarizing

stimulus (K^+ 15 mM). After a 15 min equilibration perfusion with buffer alone, a 23 min perfusion with apelin-13 (1–10 nM) was started, where in the final 3 min (depolarization period), K^+ concentration in the perfusion buffer was elevated to 15 mM (after removal of equimolar concentrations of Na^+), followed by 8 min with Krebs-Ringer buffer alone (return to basal period). Perfusate aliquots were stored at −80°C, then lyophilized and finally suspended in 1 ml HPLC grade water for neurotransmitter quantification. Neurotransmitter release was expressed as ng/ml recovered in the perfusate samples.

Statistical analysis

Statistical analysis was performed using GraphPad Prism version 5.01 for Windows (GraphPad Software, San Diego, CA, USA), through analysis of variance (ANOVA) followed by Newman-Keuls post-hoc test. Gene expression measurements were performed according to the relative comparative quantification method ($2^{-\Delta\Delta Ct}$), as previously described. Gaussian distribution of data was assessed by D'Agostino and Pearson omnibus normality test. Statistical significance was set at $P < 0.05$. With regard to the animals randomized for each experimental group, the number was calculated on the basis of the "Resource Equation" $N=(E+T)/T$ ($10 \leq E \leq 20$) elaborated by the "National Centre for the Replacement, Refinement and Reduction of Animals in Research" (NC3RS) and reported on the following web site: https://www.nc3rs.org.uk/experimental-designstatistics.

RESULTS

Intrahypothalamic administration of apelin-13 stimulated food intake 2 h and 24 h after peptide administration, in a dose-independent manner [Table I: (2 h post-injection data: ANOVA, F=5.68, P< 0.05; post-hoc, *P<0.05 *vs* vehicle) (24 h post-injection data: ANOVA, F=28.72, P< 0.0001; post-hoc, ***P<0.001 *vs* vehicle)], without any significant effect on body weight (data not shown).

This is consistent with previous observations of increased food intake following peripheral and central apelin-13 administration, at different times points (3, 4).

In addition, intrahypothalamic apelin-13 administration significantly increased orexin A gene expression (ANOVA, F=11.64, P< 0.01; post-hoc, *P<0.05, **P<0.01 *vs* vehicle) and inhibited CART gene expression (ANOVA, F=10.42, P< 0.01; post-hoc, *P<0.05; **P<0.01 *vs* vehicle), while POMC, CRH, NPY and AgRP mRNA levels were not affected.

Apelin-13 treatment also decreased 5-HT levels (ng/mg wet tissue) in the hypothalamus (Vehicle: 1.32±0.04; Apelin-13 1 µg: 0.96±0.02**; Apelin-13 2 µg: 1.11±0.07**; ANOVA, F=9.58, P< 0.01; post-hoc, **P<0.01 *vs* vehicle), while NE and DA levels (ng/mg wet tissue) were not modified [NE: (Vehicle: 1.61±0.04; Apelin-13 1 µg: 1.70±0.07; Apelin-13 2 µg: 1.68±0.04); DA:(Vehicle: 0.58±0.04; Apelin-13 1 µg: 0.57±0.03**; Apelin-13 2 µg: 0.52±0.03)].

Finally, we tested apelin-13 activity on 5-HT release (ng/ml) from hypothalamic synaptosomes *in vitro*. We found an inhibitory effect on both basal (Vehicle: 1.01±0.06; Apelin-13 1 nM:0.62±0.04***;

Table I. *Food intake (in grams) in rats fed a standard diet and treated with either vehicle or apelin-13 (1-2 µg/rat).*

	Vehicle	Apelin-13 1 µg	Apelin-13 2 µg
2 h post-injection	0.74±0.02	0.86±0.04*	0.86±0.02*
24 h post-injection	10.44±0.41***	16.66±0.40***	16.13±0.19***

*Vehicle or apelin-13 were administered by intrahypothalamic injection, during the light phase, at 9:00 a.m. Food intake was evaluated 2 and 24 h after treatment in each group of rats. Values represent the means ± SEM. Compared to vehicle, apelin-13 significantly stimulated food intake [(2 h post-injection data: ANOVA, F=5.68, P< 0.05; post-hoc, *P<0.05 vs vehicle) (24 h post-injection data: ANOVA, F=28.72, P< 0.0001; post-hoc, ***P<0.001 vs vehicle)].*

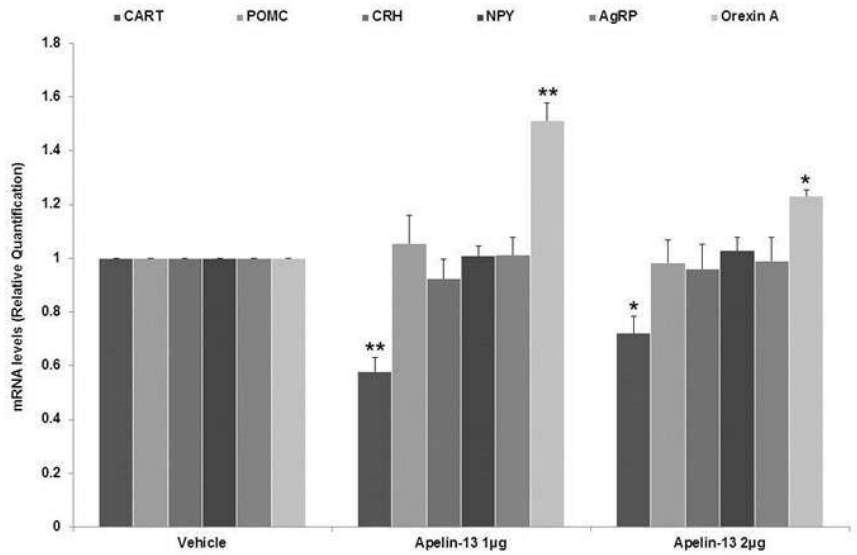

Fig. 1. *Relative gene expression of hypothalamic neuropeptides 24 h after vehicle or apelin-13 (1-2 µg/rat) administration, as determined by real-time RT-PCR. Data were calculated using the* $2^{-\Delta\Delta Ct}$ *method; they were normalized to β-actin mRNA levels and then expressed as relative to vehicle (calibrator sample, defined as 1.00±0.00). Compared to vehicle, apelin-13 significantly decreased CART gene expression (ANOVA, F=10.42, P< 0.01; post-hoc, *P<0.05, **P<0.01 vs vehicle) and increased orexin A gene expression (ANOVA, F=11.64, P< 0.01; post-hoc, *P<0.05, **P<0.01 vs vehicle).*

Apelin-13 10 nM: 0.63±0.03***; ANOVA, F=24.33, P< 0.0001; post-hoc, ***P<0.001 *vs* vehicle) and depolarization (K^+ 15 mM)-induced 5-HT release (Vehicle: 1.41±0.08; Apelin-13 1 nM:0.68±0.05***; Apelin-13 10 nM: 0.71±0.06***; ANOVA, F=33.08, P< 0.0001; post-hoc, ***P<0.001 *vs* vehicle). These inhibitory effects on both basal and depolarization-induced 5-HT release could be related to APJ receptor agonists binding to 5-HT1A autoreceptors (8).

DISCUSSION

Our findings showing stimulated feeding behavior 2 and 24 h after apelin-13 administration (Table I) adds to inconsistent results concerning the role of this peptide on feeding regulation. Previous works found either stimulatory or inhibitory effects, probably arising from differences in experimental conditions, including diet, dosages, time, and route of administration (9). With regard to this latter aspect, we may suggest that the direct administration of apelin-13 into the ARC, as performed in our experiments, provides a better targeting of the hypothalamic nuclei controlling feeding behavior. The observed inhibited gene expression of hypothalamic CART (which mediates anorectic effects) and stimulation of orexin-A (which plays an orexigenic role), as shown in Fig. 1, support a central effect of apelin-13 in the hypothalamic pathways that increases food intake. The present results are also consistent with the stimulation of orexin A and the inhibition of CART gene expression following apelin-13 treatment *in vitro* (10). We also found inhibition of hypothalamic 5-HT synthesis and release induced by apelin-13, which is also consistent with the orexigenic effect shown by apelin-13 *in vivo*. 5-HT release plays an anorectic role in the hypothalamus (1), and 5-HT involvement in mediating central apelin-13 behavioral effects has also been reported in mice (6). A recent study revealed anatomical and functional connections between CART and 5-HT neurons, possibly involved

in energy balance regulation (11). In addition, orexin A was found to inhibit 5-HT release, *in vitro* (12). In this context, we can hypothesize the serotoninergic system as being a key mediator of apelin-13-induced orexigenic effects.

ACKNOWLEDGEMENTS

This work was supported by grants from the Italian Ministry of University.

REFERENCES

1. Brunetti L, Di Nisio C, Orlando G, Ferrante C, Vacca M. The regulation of feeding: a cross talk between peripheral and central signalling. Int J Immunopathol Pharmacol 2005; 18(2):201-12.
2. Tatemoto K, Hosoya M, Habata Y, et al. Isolation and characterization of a novel endogenous peptide ligand for the human APJ receptor. Biochem Biophys Res Commun 1998; 251(2):471-76.
3. Lin F, Wu H, Chen H, et al. Molecular and physiological evidences for the role in appetite regulation of apelin and its receptor APJ in Ya-fish (Schizothorax prenanti). Mol Cell Endocrinol 2014; 396(1-2):46-57.
4. Volkoff H, Wyatt JL. Apelin in goldfish (Carassius auratus): cloning, distribution and role in appetite regulation. Peptides 2009; 30(8):1434-40.
5. Higuchi K, Masaki T, Gotoh K, et al. Apelin, an APJ receptor ligand, regulates body adiposity and favors the messenger ribonucleic acid expression of uncoupling proteins in mice. Endocrinology 2007; 148(6):2690-97.
6. Telegdy G, Adamik A, Jászberényi M. Involvement of neurotransmitters in the action of apelin-13 on passive avoidance learning in mice. Peptides 2013; 39:171-74.
7. Brunetti L, Recinella L, Di Nisio C, et al. Effects of visfatin/PBEF/NAMPT on feeding behaviour and hypothalamic neuromodulators in the rat. J Biol Regul Homeost Agents 2012; 26(2):295-302.
8. Khan AS, Fiorotto ML, Cummings KK, et al. Maternal GHRH plasmid administration changes pituitary cell lineage and improves progeny growth of pigs. Am J Physiol Endocrinol Metab 2003;285:E224-31.
9. Sunter D, Hewson AK, Dickson SL. Intracerebroventricular injection of apelin-13 reduces food intake in the rat. Neurosci Lett 2003; 353(1):1-4.
10. Volkoff H. In vitro assessment of interactions between appetite-regulating peptides in brain of goldfish (Carassius auratus). Peptides 2014; 61:61-68.
11. Lee JS, Lee HS. Reciprocal connections between CART-immunoreactive, hypothalamic paraventricular neurons and serotonergic dorsal raphe cells in the rat: Light microscopic study. Brain Res 2014; 1560:46-59.
12. Orlando G, Brunetti L, Di Nisio C, Michelotto B, Recinella L, Ciabattoni G, Vacca M. Effects of cocaine- and amphetamine-regulated transcript peptide, leptin and orexins on hypothalamic serotonin release. Eur J Pharmacol. 2001; 430(2-3):269-72.

LETTER TO THE EDITOR

USE OF SODIUM HYALURONATE AND SYNTHETIC AMINO ACID PRECURSORS OF COLLAGEN FOR THE SYMPTOMATIC TREATMENT OF MUCOSITIS IN PATIENTS UNDERGOING HAEMATOPOIETIC STEM CELL TRANSPLANTS

T. RUGGIERO[1], R. POL[1], D. CAMISASSA[1], V. ARATA[1], I. MARTINO[1], L. GIACCONE[2] and S. CAROSSA[1]

[1]Department of Surgical Sciences, Dental School, University of Turin, Turin, Italy;
[2]Department of Molecular Biotechnology and Health Science, University of Turin, Turin, Italy

Received February 22, 2016 – Accepted May 31, 2016

Oral mucositis (OM) may occur in up to 100% of patients undergoing condition regimen to hematopoietic stem cell transplant (HSCT). From the patient's perspective, OM is one of the most debilitating side effects of transplantation. It is commonly thought that oral hygiene can modify the incidence and severity of oral mucositis, therefore professional oral health care (POHC) is recommended prior to conditioning regimen for HSCT. A new strategy for the treatment of OM is sodium hyaluronate (SH) combined with amino acid precursors of collagen (Aas) (Mucosamin®). SH is a mucoaderent polymer acting as a mechanical barrier and pain reliever. Furthermore, it allows prolonged contact of the product with the mucous membrane. In this study, a total of 68 adult patients due to undergo HSCT for allogenic and autologous transplant were enrolled at the Stem Cell Transplant Unit. The patients were divided into two groups. One group was treated with POHC before HSCT and applications of Mucosamin® during the recovery after transplantation. The second group served as controls, with the usual treatment of Clorexidine 0.20% adopted by the department. After HSCT the same clinician, an expert in oral medicine trained for the clinical trial, evaluated symptoms of the patients' mucositis of both groups every day. The treated patients developed less severe OM, therefore Mucosamin® seems to have a protective role against the more severe phases of mucositis. The maximum OM pain, measured with the VAS scale, was higher in patients who did not use Mucosamin®. In the treated group OM resolved sooner than in the control group.

To the Editor,

Mucositis is a common sequel of radio- (DXR) and/or chemo-(CXR)-therapy in patients with cancer, with direct and significant impact on the quality of life and cost of care. Mucositis also affects survival, because of the risk of infection. (1) Ulcerations in the oro-esophageal and gastrointestinal mucosae resulting in pain, dysphagia, diarrhea and dysfunction, depending on the tissue affected, are typical symptoms of mucositis. In patients undergoing high-dose conditioning regimen for hematopoietic stem cell transplant (HSCT), the risk of oral and gastrointestinal mucositis is up to 100%. After HSCT, in addition to OM, therapy-induced myelosuppression causes significant risk of bacteremia and sepsis from oral microorganisms resulting in increased days of fever, antibiotic use and hospitalization (1). From the patient's

Key words: oral mucositis, mucosamin, bone marrow, HSCT, sodium hyaluronate, dental care

Mailing address:
Dr Tiziana Ruggiero,
Oral Surgery Unit, Dentistry Section,
Department of Surgical Sciences,
University of Turin, Dental School, Via Nizza 230, 10100 Turin, Italy
Tel.: +39 334 9835933
e-mail: tiziana.ruggiero@alice.it

0393-974X (2016)

perspective, OM is one of transplantation's most debilitating side effects (2).

The pathogenesis of OM associated to chemotherapy or radiation results from nonspecific direct effects of radiation or chemotherapy on rapidly dividing mucosal basal cells; the initial phase involves direct damage to DNA and other cellular components that occurs immediately after exposure to radiation or chemotherapy (3). The ulcerated surface can be colonized by oral bacteria, resulting in production of toxins, additional inflammatory cytokines and angiogenic factors, which may cause bacteremia and sepsis in the presence of granulocytopenia (4).

Most reports concerning dental management during HSCT recommend mouth rinses or use of antibiotic pastilles for oral decontamination (5), however, these have been found ineffective in preventing OM (6). The microorganism in the mouth contains hundreds of species of bacteria as complex, mixed, interdependent colonies in biofilms, and adheres to the teeth (7). The biofilm protects the adhering bacteria against environmental attacks. Antibiotics or oral rinses, without the mechanical removal of plaque (i.e. tooth brushing), are unable to penetrate the plaque to reach the linking film bacteria (8, 9). Almost all patients understand that regular brushing is very important for oral hygiene, but few of them brush properly. This is why professional and repeated instruction on brushing is critical for controlling plaque.

A new strategy for the treatment of OM is the sodium hyaluronate (SH) combined with amino acid precursors of collagen (Aas) (Mucosamin®). SH is a mucoaderent polymer acting as a mechanical barrier and pain reliever. As induce, the production of collagen and glycosaminoglycan by fibroblasts, a key element for the recovery of the tissue during the healing process, as demonstrate in a study by Colella (10).

The aim of the study was to evaluate the clinical efficacy of Mucosamin® in wound healing and pain management in OM after HSCT. We also evaluated the importance of professional oral hygiene by a dental hygienist to reduce the severity of OM in combination with the Mucosamin®.

MATERIALS AND METHODS

Patient characteristics

We designed a case control study. A total of 68 adult patients (average age 51, range 22-70) prepared for HSCT for allogenic and autologous transplant were recruited at the Stem Cell Transplant Unit, Città della Salute e della Scienza of Turin, and in the Oral Surgery Department, Dental School, University of Turin.

Criteria for inclusion were: i) age> 18 years; ii) due for HSCT; iii) informed consent and ability to complete the trial. Exclusion criteria included: i) known allergy to any of the components of the compound; ii) inability to check results; iii) patients with systemic disease, other than hematological malignancies, which impair wound healing (i.e. diabetes); iv) muco-cutaneous diseases; v) not been able/willing to give informed consent.

This study was approved by the Institutional Review Board of our Center and conducted according to the Declaration of Helsinki and all patients provided written informed consent to participate in the study.

Treatment plan

We asked each patient to complete: i) a survey regarding oral hygiene to assess the individual knowledge of the correct oral hygiene procedures and patient compliance; ii) a survey regarding radio/chemotherapy and OM to investigate the level of knowledge of the patient on interactions between drugs, radio and chemotherapy on the oral cavity, and of mucositis.

Group A included patients sent by the Haematology Departments to the Dental School to eliminate infectious foci of the oral cavity, which is mandatory in order to receive the suitability for transplantation. The patients underwent careful intra and extra oral examination, and radiological investigations to assess the need for dental treatment, compatible with the timing of transplantation. All patients in Group A had a periodontal chart analysing: i) O'Leary Index Plaque (Plaque Control Record); ii) Bleeding index; ii) Periodontal Screening and Recording Index (PSR) (11). Each of them received a complete session of professional oral hygiene, with scaling and root planing. At the end of each session, patients were educated on the correlation between oral health and OM and possible complications, and were instructed on correct home oral hygiene procedures and were motivated to maintain such

procedures during the period of hospitalization. Patients who presented periodontal problems underwent a second hygiene session for scaling and root planing of pathological sites. Patients who required further dental treatment, such as conservative treatment, endodontic or extraction, were re-motivated to maintaining a high standard of oral hygiene during the session in which they were given the suitability for transplantation. Furthermore, patients in group A were instructed by a single doctor to recognize symptoms of OM and to apply SH-AAs based spray on these lesions 3-4 times a day after a meal and oral hygiene, keeping the liquid *in situ* for at least 2 minutes and to avoid drinking, eating and rinsing the mouth for at least one hour. The same doctor controlled the patients during hospitalization in order to recognize initial and advanced signs of OM and to remind patients how to apply the compound.

Patients in Group B were recruited directly in the Haematology department, depending on availability of patients, but they were not visited in Dentistry department. They were not involved in dental hygiene sessions and did not receive Mucosamin® but they received the usual treatment of Clorexidine 0.20%. Also, we asked the patients whether they had undergone a session of dental hygiene during the 6 months prior to the transplantation.

Starting the day after HSCT, the same expert trained for the clinical trial, evaluated patients of both group every day, during hospitalization. The evaluation included three scores for OM: i) WHO mucositis scale ranging from 0= no symptoms; 1=soreness, erythema; 2=erythema, ulcers but able to eat solids (12); 3=ulcers but required liquid diet; 4=oral alimentation not possible; ii) Visual analogue scale (VAS) ranging from 0=no pain to 10=worst pain in the world (13); iii) OMAS scale (Oral Mucositis Assessment Scale): Oral cavity for Ulceration 0=No lesion; 1= Lesion <1 cm^2; 2=Lesion 1 to 3 cm^2; 3=Lesion >3 cm^2; Oral cavity for Erythema: 0= None; 1=Not severe; 2=Severe (14).

According to WHO and OMAS scales, we divided the lesions into two groups: light mucositis (WHO grade 1 and 2, OMAS grade 1) and severe mucositis (WHO grade 3 and 4, OMAS grade 2 and 3). Primary indicators of mucositis were the degrees of ulceration and redness measured in specific sites in the mouth. Secondary indicators included oral pain, difficulty swallowing and the ability to eat as assessed by the patient. A single score is not produced from this scale, rather a score for ulceration and redness based on different locations in the mouth are used.

Statistical analysis

The results included continuous and categorical variables. The former are reported as mean and standard deviation. Nonparametric tests were used: the Wilcoxon signed-rank test for comparisons of two correlated samples involving matched pairs and the Mann-Whitney test for comparisons of two independent distributions. Categorical variables, reported as count and percentage, were arranged in cross-correlation tables and compared using the χ^2 test with the Yates correction when all expected values were higher than 5 or Fisher's exact test. Statistical significance corresponded to a probability less than 0.05 that differences could be ascribed to chance.

RESULTS

Patient characteristics

Table I shows the demographic details of the patients and other baseline information. The sample is homogeneous for age and sex. All patients were candidates for HSTC for hematological malignancies. Thirty-two patients were in group A and 28 in group B. Eight patients previously enrolled in the study did not proceed with the transplant because of their poor general health condition, death or lack of available donor. In both groups, the predominant pathology was acute myeloid leukemia. Two patients in group A and 4 patients in group B were treated with Total Body Irradiation (TBI) and chemotherapy while the other patients underwent a conditioning regimen of only high-dose chemotherapy. Three patients in group A and 6 in group B did not develop OM. Patients who did not developed mucositis, were excluded from the results.

Treatment administration

There was no indication of any intolerance to the product. Based on the interview we conducted during the study, all patients except one, liked the consistency of the product in the mouth and they were able to use it during the day based on the instructions of the dentist. There were no differences in OM location among patients receiving Mucosamin® (group A) and in those who did not (group B).

Patients in group A who used Mucosamin® on initial lesions developed less severe OM, while

Table I. *Patients' baseline characteristics.*

		Group A	Group B
	no.	32	28
Sex	M	14 (49%)	14 (50%)
	F	18 (51%)	14 (50%)
Age	< 30 y.	3 (9%)	2 (6%)
	31 - 40 y.	5 (16%)	1 (16%)
	41-50 y.	9 (28%)	6 (23%)
	51 - 60 y.	10 (31%)	9 (32%)
	> 60 y.	5 (16%)	10 (33%)
Transplant	Autologous	5 (16%)	6 (26%)
	Allogenic	27 (84 %)	22 (74%)
Conditioning Regimen	TBI	2 (6 %)	4 (14%)
	Non TBI	30 (94 %)	24 (86%)
Pathology	Acute Myeloid Leukaemia	8 (25 %)	9 (34%)
	Chronic Myeloid leukaemia	4 (13%)	1 (3%)
	Hodgkin's Lymphoma	3 (9%)	1 (3%)
	Non Hodgkin's Lymphoma	8 (25%)	7 (26%)
	Myelofibrosis	1 (3%)	0 (0%)
	Multiple Myeloma	2 (6%)	6 (23%)
	Myelodysplastic Syndrome	6 (19%)	4 (10%)

M: Male; F: Female; TBI: Total Body Irradiation

Table II. *Evaluation of gravity of oral mucositis related to use of Mucosamin and a session of POHC.*

	Light Mucositis	Severe Mucositis	
Group A	20	9	**P=0.02 * RR=0.49 ***
Group B	8	14	
Group A1	19	7	**P=0.006 * RR=0.38 ***
Group CTRL	5	12	

*Group A= Mucosamin group; Group B=No Mucosamin group. Group A1 (Mucosamin and oral hygiene within 6 months from HSTC) Group CTRL (No Mucosamin and oral hygiene more than 6 months from HSTC). P<0.05 *statistically significant.*

patients who did not use the compound developed more severe and painful lesions; this result is statistically significant (P=0.02*). Mucosamin® seems to have a protective role against the more severe phases of mucositis (Table II).

The maximum OM pain, measured with the VAS scale, was higher in patients who did not use Mucosamin®: maximum VAS average in Group A 4.42 (DS ±2.61) and in Group B 4.77 (DS ±3.33). In group A, OM resolved sooner than group B, although the difference was not statistically significant: the average duration in Group A was 9 days (DS ±7), and in Group B 11 days (DS ±16).

Role of professional oral health care (POHC)

To evaluate whether there is a strengthening of the results with the association between Mucosamin® and POHC, patients of group A who had POHC in the 6 months prior to HSTC (Group A1) were compared to patients who neither used Mucosamin® nor had POHC within the 6 month before HSTC (Group CTRL) (Table II).

Patients who had a more recent session of POHC in association with Mucosamin® developed significantly lighter OM. Use of Mucosamin® associated to oral hygiene seems to have a synergy that protects the oral cavity from the highest grades of OM.

DISCUSSION

The present study showed that patients who used Mucosamin® on initial lesions during hospitalization had a lower risk of developing the highest grades of mucositis. Mucosamin® appears to play a role in reducing the severity and the duration of OM, as most of the patients treated had a less severe and less painful type of lesion (grade 1-2) while the control group who has not used the compound, had a predominance of more painful lesions (grade 3-4), statistically confirmed.

Patients educated and motivated on the importance of oral hygiene had reduced mucositis severity and duration, therefore a session of POHC before HSTC, as well as information on the correlation between oral hygiene and mucositis, was effective in maintaining good oral hygiene by patients. These observations are in agreement with several studies that emphasize the importance of effective control of plaque, because oral health conditions are among the most important risk factors for the development of mucositis (15). Our results also corroborate the importance of the role of the dental hygienist and confirm the necessity of creating a team hematologist-dentist-hygienist for management of complications of the oral cavity in patients undergoing bone marrow transplant. Furthermore, when Mucosamin® and POHC are associated, the risk of developing higher grades of mucositis is strongly reduced.

According to our study, the use of Mucosamin® can influence the type and severity of oral mucositis, allowing patients to have a better quality of life. The efficacy of Mucosamin® in decreasing pain and accelerating wound healing relies on its ability in tissue repair, activation and modulation of inflammatory responses, promoting the proliferation and cell migration, angiogenesis, increased re-epithelialization, born of basal keratinocytes and collagen deposition, thus acting on ulcerative mucositis by forming a protective layer.

The analysis of our data showed that the combination of a recent POHC, appropriate oral hygiene during hospitalization and use of Mucosamin® exponentially reduces the severity/duration of mucositis, as well as the discomfort of the patient. Finally, we can say that using Mucosamin® also determines a reduction in the extent of the lesions induced by chemotherapies. This spray based on hyaluronic acid and amino acids can be a valid therapeutic aid in the treatment of mucositis.

REFERENCES

1. Scully C, Sonis S, Diz PD. Oral mucositis. Oral Dis 2006; 12 (3):229-41.
2. Rubenstein EB, Peterson DE, Schubert M, et al. Clinical practice guidelines for the prevention and treatment of cancer therapy-induced oral and gastrointestinal mucositis. Cancer 2004; 100(9 S):2026-46.
3. Sonis ST. Oral mucositis in cancer therapy. J Support Oncol 2004; 6(S 3):3-8.
4. Kashiwazaki H, Matsushita T, Sugita J, et al.

Professional oral health care reduces oral mucositis and febrile neutropenia in patients treated with allogeneic bone marrow transplantation. Support Care Cancer Off J Multinatl Assoc Support Care Cancer 2012; 20(2):367-73.
5. Weisdorf DJ, Bostrom B, Raether D, Mattingly M, Walker P, Pihlstrom B, et al. Oropharyngeal mucositis complicating bone marrow transplantation: prognostic factors and the effect of chlorhexidine mouth rinse. Bone Marrow Transplant 1989; 4(1):89-95.
6. Bondi E, Baroni C, Prete A, et al. Local antimicrobial therapy of oral mucositis in paediatric patients undergoing bone marrow transplantation. Oral Oncol 1997; 33(5):322-26.
7. Pihlstrom BL, Michalowicz BS, Johnson NW. Periodontal diseases. Lancet 2005; 366(9499):1809-20.
8. Landa AS, van der Mei HC, Busscher HJ. Detachment of linking film bacteria from enamel surfaces by oral rinses and penetration of sodium lauryl sulphate through an artificial oral biofilm. Adv Dent Res 1997; 11(4):528-38.
9. Hellström MK, Ramberg P, Krok L, Lindhe J. The effect of supragingival plaque control on the subgingival microflora in human periodontitis. J Clin Periodontol 1996; 23(10):934-40.
10. Colella G, Cannavale R, Vicidomini A, Rinaldi G, Compilato D, Campisi G. Efficacy of a spray compound containing a pool of collagen precursor synthetic aminoacids (l-proline, l-leucine, l-lysine and glycine) combined with sodium hyaluronate to manage chemo/radiotherapy-induced oral mucositis: preliminary data of an open trial. Int J Immunopathol Pharmacol 2010; 23(1):143-51.
11. Landry RG, Jean M. Periodontal Screening and Recording (PSR) Index: precursors, utility and limitations in a clinical setting. Int Dent J 2002; 52(1):35-40.
12. López-Castaño F, Oñate-Sánchez RE, Roldán-Chicano R, Cabrerizo-Merino MC. Measurement of secondary mucositis to oncohematologic treatment by means of different scale. Review. Med Oral Patol Oral Cir Bucal 2005; 10(5):412-21.
13. Price DD, McGrath PA, Rafii A, Buckingham B. The validation of visual analogue scales as ratio scale measures for chronic and experimental pain. Pain 1983; 17(1):45-56.
14. Sonis ST, Oster G, Fuchs H, et al. Oral mucositis and the clinical and economic outcomes of hematopoietic stem-cell transplantation. J Clin Oncol Off J Am Soc Clin Oncol 2001; 19(8):2201-5.

LETTER TO THE EDITOR

PROBIOTIC MIXTURE SUPPLEMENTATION IN THE PREVENTIVE MANAGEMENT OF TRINITROBENZENESULFONIC ACID-INDUCED INFLAMMATION IN A MURINE MODEL

G. TRAINA[1], L. MENCHETTI[2], F. RAPPA[3], P. CASAGRANDE-PROIETTI[2], O. BARBATO[2], L. LEONARDI[2], F. CARINI[4], F. PIRO[2] and G. BRECCHIA[2]

[1]Department of Pharmaceutical Sciences, University of Perugia, Perugia, Italy; [2]Department of Veterinary Medicine, University of Perugia, Perugia, Italy; [3]Department of Legal Sciences of the Society and Sports, University of Palermo, Palermo, Italy; [4]Department of Experimental Biomedicine and Clinical Neurosciences, University of Palermo, Palermo, Italy

Received November 23, 2015 – Accepted June 17, 2016

Inflammatory bowel diseases (IBD) are characterized by inflammatory conditions of the intestine. Probiotic bacteria (PB) can have beneficial effects in several gastrointestinal disorders. The objectives of this study were: (i) to provide an acute experimental IBD model induced by 2,4,6-trinitrobenzenesulfonic acid (TNBS) in CD-1 mice, and (ii) to assess the preventive effects of Citogenex (*Lactobacillus casei* and *Bifidobacterum lactis*) supplementation on intestinal tissues and microbiota. Mice were inoculated intrarectally with saline, ethanol or different TNBS solutions. 1%TNBS induced clinical signs of colitis ($P < 0.01$) and histological damage ($P < 0.01$). Based on these results, mice were pre-treated with Citogenex or saline for 1, 2 or 3 weeks before 1%TNBS treatment. Probiotic pre-treatment determined a reduction of clinical signs ($P < 0.05$), histological alterations of colitis ($P < 0.05$) and increased beneficial bacteria ($P < 0.05$). This study confirms that TNBS-induced colitis in CD-1 mice is useful for studying the mechanisms involved in IBD pathogenesis, and pre-treatment with Citogenex prevents the intestinal damage induced by TNBS.

To the Editor,

Inflammatory bowel diseases (IBD) are a group of chronic idiopathic multifactorial diseases characterized by inflammatory conditions of the colon and small intestine (1).

Several lines of evidence suggest that intestinal microbiota plays a crucial role in the pathogenesis of IBD. Indeed, colitis cannot be induced in germ-free animals (2) and dysbiosis has been observed in patients affected by IBD. It is hypothesized that the disruption of homeostatic mechanisms of tolerance can lead to aberrant immune response of the host to commensal microbiota and then in a chronic inflammation of the gastro-intestinal tract in genetically predisposed subjects (1-3). However, the pathophysiological basis of IBD is still not completely understood.

Current medical approaches for treating IBD are not completely curative, and show many side effects. In recent years, a novel strategy based on the modulation of intestinal microbiota by PB has suscitated great interest. Nevertheless, studies concerning the clinical use of PB in IBD are still limited, and with

Key words: IBD, probiotics; induced-colitis model, disease activity index, microbiota

Mailing address:
Dr Giovanna Traina,
Dipartimento di Scienze Farmaceutiche,
Università degli Studi di Perugia,
Via S. Costanzo, 06126 Perugia, Italy
Tel.: +39 075 5857977 - Fax: +39 075 5857904
e-mail: giovanna.traina@unipg.it

0393-974X (2016)

controversial results (4). Many animal models have been designed to study the pathogenesis of IBD using various chemicals. TNBS induces colitis that resembles human IBD in regard to clinical symptoms and histopathology. TNBS administration still induces considerable levels of mortality, different strains of mice exhibit different susceptibility, therefore a standardization of methods is necessary (4-6). Our interest is focused on the CD-1 strain, an outbred mouse commonly used in pharmacological and toxicological research areas. CD-1 mice mimic the genetic heterogeneity found in humans, eliminating the necessity to study multiple strains.

The objectives of this study were: (i) to establish an experimental model of TNBS-induced colitis in CD-1 mice with the lowest mortality rate for studying IBD pathogenesis; and (ii) to assess the effects of specially selected strains of *Lactobacillus casei* and *Bifidobacterum lactis* able to induce immune modulation, in prevention of intestinal damage induced by TNBS.

MATERIALS AND METHODS

Animals

Six-week-old CD-1 male mice with body weight of 25-34 g (Harlan Laboratories S.r.l., Correzzana D'Adda, Milan, Italy) were housed under controlled conditions: constant temperature of 21±1°C, relative humidity of 55±10% and photoperiods (12:12-hours light/dark cycle). Mice were acclimated to these conditions for 10 days before inclusion in the experiments. Access to food (standard chow) and water were *ad libitum* throughout all the experimental trials. All experimental protocols were approved by the Ethics Committee for Animal Experimentation at the University of Perugia, Italy. Animal care was in compliance with Italian regulations (Ministerial Declaration 116/92), as well as with European Economic Community regulations (O.J. of European Commission L 358/1 12/18/1986). All efforts were made to minimize animal distress and to use only the number of animals necessary to produce reliable results.

Bacterial strains

We used Citogenex (*L. casei* and *B. lactis* mixture) kindly provided by Bromatech, S.p.A, Milan, Italy.

Experiment 1 - TNBS-induced colitis model in CD-1 mice

A preliminary dose–response study was performed to establish the animal model of TNBS-induced colitis. Forty-nine healthy CD-1 male mice weighing 29.6±0.2 g were randomly divided into seven groups (n=7) and were inoculated intrarectally with saline solution (Saline), ethanol 50% solution (Ethanol), or different TNBS solutions: 0.25% (0.25TNBS), 0.50% (0.50TNBS), 1% (1TNBS), 2% (2TNBS) and 3% (3TNBS), respectively. TNBS (Sigma-Aldrich, Milan, Italy) solutions were prepared at the moment of use diluting the different concentrations of the haptinizing agent in ethanol 50%. In particular, mice were fasted for 24 h, lightly anesthetized with isoflurane (Merial, Milan Italy) and then inoculated intrarectally via a catheter (2 biological instruments, Basozzo, Varese, Italy) equipped with a 1-ml syringe. The catheter was lubricated and was advanced through the anus for 3 cm before releasing a total volume of 150 µl of different solutions. In order to ensure distribution of the TNBS within the colon, the mice were held in a vertical position with the head downwards for 1 min after the injection.

Experiment 2 –Effects of Citogenex in TNBS-induced colitis model in CD-1 mice

To evaluate the effect of PB on the previously assessed TNBS-induced colitis model, CD-1 male mice (n = 72) weighing 28.7±0.2 g were randomly divided into six groups (n= 12). Three groups received orally and daily by gavage a PB suspension for 7 (PB1w), 14 (PB2w) or 21 days (PB3w) respectively, before the intrarectal administration of 150 µl 1% TNBS solution (chosen based on the results of Experiment 1. The other 3 groups were administered orally and daily by gavage with saline solution using the previous scheme (S1w, S2w and S3w for 7, 14, and 21 days of saline administration, respectively), before the intrarectal inoculation of TNBS. In particular, the mice received 0.3 mL of a PB suspension (10^9 bacteria/ml, 10 ml/kg BW), reconstituted just before administration, or the same volume of saline solution by a plastic feeding tube for gavage (2 biological instruments, Basozzo, Varese, Italy). The procedures of TNBS treatment were the same as those used in Experiment 1.

Determination of disease activity index (DAI)

DAI determination was made with the method

described by Murano et al. (7) combining score of weight loss, stool consistency and bleeding.

Diarrhoea was estimated with the presence of faecal material adhering to anal fur and was confirmed by the presence or absence of faecal pellet in rectum. A 4-point scale was used where a score of 0 corresponded to a normal faecal pellet and 4 corresponded to frank diarrhoea. Rectal bleeding was evaluated with visible blood in the faecal material and by the presence or absence of gross colonic or rectal bleeding and scored as 0 for negative and 4 for gross bleeding. The animals were monitored daily.

Tissue processing

All surviving mice were euthanized 3 days after the TNBS treatment by cervical dislocation. At autopsy, a gross evaluation of whole digestive tract was made. The gastrointestinal tract was immediately excised intact from anus to oesophagus. The large bowel was subdivided into caecum, colon and rectum. Colon was opened longitudinally. The luminal materials were removed, immediately placed into an anaerobic chamber and dissolved in sterile pre-reduced PBS for the bacteriological assays. Colon tissues were cleaned with saline and several samples were collected for the histological evaluation and fixed in a solution of 10% of buffered formalin.

Histological analyses and scoring

Samples of colon were processed for light microscopy examination. Sections of 4/5 μm were stained with haematoxylin-eosin (H&E) (Merck KGaA, Darmstadt, Germany). All histological evaluations were performed by two expert morphologists on ten random fields at different magnifications. Colon samples were also stained with periodic acid of Schiff (PAS) method (Sigma Aldrich, USA) to point out goblet cells in the colon mucosa, in order to assess changes in the number and epithelial differentiation. Briefly, paraffin sections were incubated in periodic acid for 5 min followed by staining with Schiff reagent for 15 min and finally haematoxylin staining. The goblet cells were quantified in the epithelia of all colon samples and the final value was used to perform the histological score of inflammation.

Histological scoring was based on a semi-quantitative score system modified by McCafferty et al. (8). The following features were graded: extent of destruction of mucosal architecture, presence and degree of cellular infiltration, extent of muscle thickening, and degree of goblet cell depletion. For each feature, a score of 0, 1, 2, or 3 was attributed corresponding to normal, mild, moderate, and extensive damage, respectively. The scores for each feature were summed with a maximum possible score of 12.

Microbiota analysis

The colon content was removed aseptically, immediately placed into an anaerobic chamber and dissolved in sterile pre-reduced PBS. A sterile stick was used to put 1 g of intestinal contents into a sterile test tube together with 2 mL 0.9% sterile saline solution. The stool was pressed and mixed in this solution and the tube was brought to volume (10 mL) with 0.9% sterile saline solution. Each sample (0.1 mL) was serially diluted via 10-fold dilutions. Starting from the lowest concentration, dilutions were plated and cultured on different media in triplicate using the spread plate method. Chromocult agar and Bile Esculin Azide Agar were used for the enumeration of *E. coli,* Coliforms and Enterococci, respectively. All the plates were incubated at 37°C, aerobically, for 24-48 h. Brain heart Infusion agar, Mann Rogosa Sharpe agar (MRS) and modified MRS agar (0.3% w/v) sodium propionate, 0.2% (w/v) lithium chloride, 0.05% (w/v) cysteine hydrochloride and 5% (v/v) defibrinated sheep blood included were used for the enumeration of total anaerobes*, Lactobacillus* spp. and *Bifidobacterium* spp., respectively. Anaerobic incubation was carried out in anaerobic jars (Oxoid) at 37°C for 48-72h. Anaerobic conditions were obtained using Anaerogen (Oxoid) and were checked using methyl blue strips as oxidation-reduction indicator. The number of colonies was counted and all the data are expressed as CFU x log/g.

Statistical analyses

Diagnostic graphics and Levene test were used to test assumptions and outliers. Results are expressed as estimated marginal means ± SE or medians with interquartile range (IQR). Fisher's exact test was used to compare mortality rates. Single factor ANOVA by GLM procedure was used on Experiment 1, where "treatment" was the fixed factor (five levels: saline, ethanol, 0.25TNBS, 0.50TNBS, 1TNBS) and BW change the response variable. Due to high mortality, 2TNBS and 3TNBS groups were not included. In experiment 2, we evaluated

the effect of the PB administration both on BW change during pre- and post-TNBS treatment. We used two factor crossed ANOVAs by GLM procedure with 2 levels of pre-treatment (Saline or PB) and 3 levels of "weeks of pre-treatment" (1, 2 and 3 weeks). These models evaluated the effect of main factors and interaction. Sidak adjustment was used on multiple comparisons. For analysis of DAI and histological scores, Kruskal-Wallis followed by Mann-Whitney test was used.

Bacterial counts were expressed and analyzed as log10 CFU per gram of colon samples. Bacteria were also classified into beneficial (Bifidobacteria and Lactobacilli) and detrimental (*E. coli*) bacteria (9). To describe the relative proportion of each examined bacteria, proportions of each bacterial group are presented where the total of the examined bacteria was set at 100%. *Chi*-square test was used to explore whether the proportion of bacteria differ between groups adjusting pairwise comparisons with Bonferroni correction. Statistical analyses were performed using SPSS Statistics version 20 (IBM, SPSS Inc., Chicago, IL, USA). Exact p value is shown and $P < 0.05$ was the accepted level of statistical significance.

RESULTS

Mortality

Mortality after treatment with 2 and 3% of TNBS was greater than 70% (71.4% and 100.0% on TNBS2 and TNBS3, respectively). Consequently, these groups were excluded from subsequent evaluations. One mouse died on ethanol, 0.5TNBS and 1TNBS groups (14.3%), none in the other groups. However, differences in mortality rate between groups were not statistically significant (Fisher's exact test: $P = 1.000$).

Experiment 1: TNBS-induced colitis model in CD-1 mice

At macroscopic examination, the colon of TNBS-treated mice with a concentration higher than 1% (2TNBS and 3TNBS) was swollen, oedematous and thickened, with strong evidence of mucosal haemorrhage compared to the other groups. These signs were absent in saline, ethanol and 0.25TNBS, mild in 0.5TNBS and moderate in 1TNBS groups. Mice treated with 0.5% ($P = 0.040$) or 1% ($P = 0.000$) of TNBS lost more weight compared to the saline group (-8%, and -13% compared to baseline body weight on 0.5TNBS and 1TNBS, respectively). Signs of inflammation were attenuated on Ethanol and 0.25TNBS groups, where DAI and histological damage did not differ from the Saline group (DAI: median = 0.3, IQR = 0.0-1.0; Histological score: median = 0, IQR = 0-2). Mice treated with 0.5% of TNBS showed higher DAI (median = 1.5, IQR = 1.3-2.0; $P = 0.001$), but no differences on colon inflammation (median = 4, IQR = 1-7; $P = 0.053$) compared to saline. Conversely, 1TNBS produced robust inflammation as measured by increased DAI (median = 3.2, IQR = 1.7-3.7; $P = 0.001$), and histological damage (median = 7, IQR = 6-9; $P = 0.001$). Histological lesions resembling IBD were characterized by distortion of mucosal architecture, infiltration of inflammatory cells at lamina propria and submucosa levels, thickening of muscular layer and goblet cell depletion, particularly marked in samples examined of 1, 2, 3TNBS groups (Fig. 1A).

Experiment 2: Effects of Citogenex in TNBS-induced colitis model

Mortality

One mouse died during the experiment on S1w, S3w, PB2w, and PB3w groups (11.1%; Fisher's exact test: $P = 1.000$). Mortality was 5.5% (2 of 36 mice) both within saline and Citogenex pre-treated mice ($P = 1.000$).

Effect of Citogenex before TNBS treatment

Citogenex was well tolerated by mice and no side effects were observed during the experimental trial. During the pretreatment period, all mice gained weight ($P < 0.001$) but BW of mice receiving PB was 2.5% and 0.8% higher compared to saline pretreated after 2 and 3 weeks of supplementation, respectively ($P < 0.01$). Body weight increased during probiotic administration (1.4 g/week).

During the pre-treatment period, signs of inflammation were absent and median DAI was 0 both on PB and saline pretreated.

Effect of Citogenex in TNBS-treated mice

The positive effect of pre-treatment was

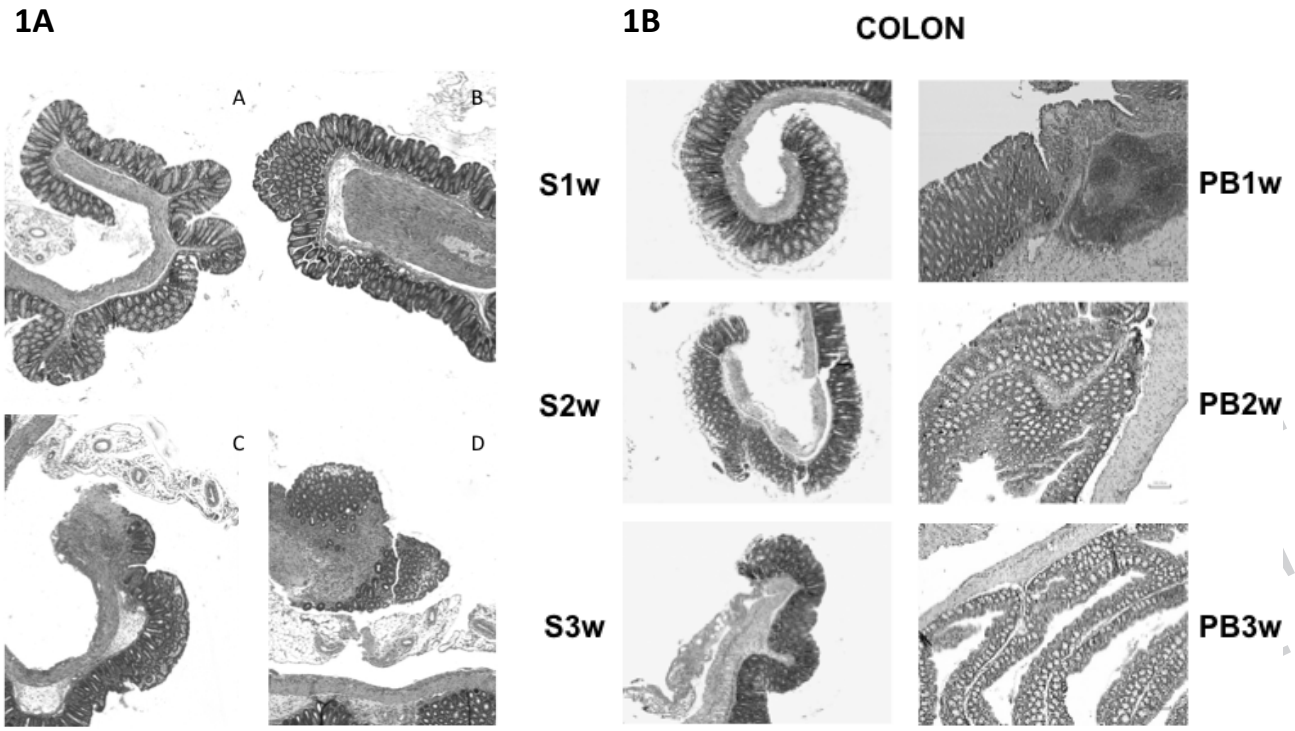

Fig. 1. ***A)*** *Colon histology in TNBS-induced colitis model. Histological analyses of colon sections stained with haematoxylin and eosin and observed at magnification of 20x, from animals treated with:* ***(A)*** *Saline solution (control). Normal architecture of the colonic mucosa and no signs of inflammation may be detected.* ***B)*** *Ethanol. Normal architecture of the colonic mucosa, mild inflammatory infiltration of lymphocytes, and few neutrophils and eosinophils granulocytes in lamina propria and submucosa. Similar histological damages were found in 0.25 and 0.5TNBS groups (figures not shown).* ***C)*** *TNBS solution at 1%. Moderate architectural distortion of the colonic mucosa, erosions of the epithelium, crypt loss accompanied by an inflammatory reaction characterized by massive mixed inflammatory infiltrate with lymphocytes and polymorphonuclear cells (neutrophils and eosinophils granulocytes) in epithelium, lamina propria and submucosal layer. Inflammation also partially involves the muscle layer. In marginal position a moderate area of necrosis is present that involves part of the muscular layer.* ***D)*** *TNBS solution 3%. Severe architectural distortion of the colonic mucosa, erosions of the epithelium, crypt loss, signs of chronic and acute secondary inflammation with massive area of diffuse necrosis. In the same samples some small abscessual areas were identified. Similar histological damage was found in 2TNBS groups (data not shown).* ***B)*** *Colon histology after TNBS and PB treatment. Colon histology after TNBS in mice pretreated with 1, 2, and 3 weeks of Saline (S1w, S2w, and S3w, respectively) and Citogenex (PB1w, PB2w, and PB3w, respectively). Histological analyses of colon sections stained with haematoxylin and eosin and observed at magnification of 100x, from animals treated with: -S1w: Moderate infiltrative pattern of inflammation of colonic mucosa where lymphocytic and granulocitary infiltrations appear to be particularly distributed in submucosa and mucosal layers. -PB1w: Mild inflammatory reaction of the colon tract with mild involvement of submucosa layer by few lymphocytic and granulocitary cells. - S2w: Moderate infiltration of mucosa, submucosa and muscular layers of colon by lymphocytic cell population. -PB2w: Mild to moderate infiltrative pattern of colonic mucosa with mild architectural distortion of the colonic mucosa by inflammatory infiltration. -S3w: Infiltrative pattern of colonic mucosa and submucosa with involvement of crypts and strong inflammatory reaction characterized by the presence of mixed population of cells (lymphocytes and polymorphonuclear cells) infiltrating also lamina propria and strongly the space from submucosa to muscular layers. In this picture the submucosal layer is clearly very thickened. -PB3w: Mild inflammatory reaction of mucosa layer and submucosa of colonic mucosa.*

found even after treatment with TNBS, when BW losses were lower on mice receiving Citogenex supplementation (-12% and -9% on saline and PB pretreated mice, respectively; $P < 0.001$). In particular, differences were found on mice receiving 2 (-12% and -8% on S2w and PB2w, respectively; $P = 0.002$) or 3 weeks (-13% and -6% on S3w and PB3w, respectively; $P = 0.000$) of Citogenex supplementation. Mice pretreated one week with PB showed no differences on DAI or histological damage compared to control (Table I). Two and three weeks of PB pretreatment reduced signs of inflammation after TNBS administration as measured by reduction on DAI (Fig. 1B). On mice receiving 3 weeks of Citogenex (PB3w) also the colon inflammation after TNBS inoculation (destruction of mucosal architecture, cellular infiltration, muscle thickness, goblet cell depletion) was reduced after TNBS inoculation (Table I).

Effect of Citogenex on intestinal microbiota of TNBS-treated mice

Differences between groups were not found on intestinal microbiota composition ($P = 1.000$). Overall, log-count was 7.61±0.31 (19.2%), 7.65±0.19 (20.4%), 9.62±0.06 (26.8%), 8.03±0.16 (21.8%), 4.24±0.06 (11.8%) for *E. coli*, Enterococci, Anaerobes, Lactobacilli, and Bifidobacteria, respectively. However, relative proportions of beneficial and detrimental bacteria after 2 weeks of Citogenex increased if compared to saline pretreatment ($P = 0.046$): the beneficial-detrimental bacteria ratio was 4/1 and 3/2 on PB2w and S2w mice, respectively.

DISCUSSION

In order to characterize critical features of the inflammatory condition and to reduce the levels of mortality of the experimental animals, we reported a model of TNBS-induced colitis in CD-1 mice. The results of experiment 1 show that exposure to TNBS induces dose-dependent local and systemic signs of colitis. TNBS-treated mice with a solution higher than 1% presented a high rate of mortality within 24 h from the treatment while in the other groups statistically significant differences in mortality rate were not found. The data on the mortality are in accordance with Mencarelli et al. (10). Other studies, using different mice strains, age of animals, amount of administered TNBS and percentage of ethanol, found a very high variability in mortality rate (6). One TNBS group showed the typical systemic and local signs of colitis characterized by body weight loss (-13%), increased DAI and strong histological inflammatory damage. The clinical signs of colitis

Table I. *Effects of Citogenex or saline administrated for 1, 2 or 3 weeks before TNBS treatment on clinical indices and histological disease score of mice.*

Score	Weeks of pre-treatment	Pre-treatment		P value
		Saline	*Citogenex*	
Disease activity index	**1**	2.2 (2.0-3.0)	2.3 (2.0-2.8)	1.000
	2	2.5 (1.8-3.2)	1.7 (1.0-2.0)	0.024
	3	2.6 (2.0-3.0)	1.3 (0.7-1.7)	0.002
Histological score	**1**	2 (1-3)	2 (1-2)	0.740
	2	2 (1-3)	1 (1-2)	0.219
	3	2 (2-3)	1 (0-2)	0.014

Values are medians and interquartile range.

were absent or mild in the other groups treated with a solution lower of 1% of TNBS. We previously reported similar inflammatory damage, not only in colon but also in rectum and in liver, even associated to carcinogenetic signs (5). Based on these data, the optimal dose to induce a reproducible adequate inflammatory status of colon without excessively distressing the animal and with a low mortality rate is 1% TNBS solution; thus, this was used in the second experimental trials.

Many studies have shown that PB may have beneficial effects in various gastro-intestinal disorders (3-6). Nevertheless, studies concerning the clinical use of PB in IBD are still limited and with controversial results. In experiment 2 we investigated the effects of *L. casei* and *B. lactis* (Citogenex) supplementation, in TNBS-induced colitis in CD-1 mice. Citogenex reduced weight loss and improved diarrhoea and bleeding score as well as the other macroscopic symptoms of colitis. In addition, it reduced the histological damage in the colonic mucosa in a time-dependent course. Our results are in agreement with the majority of data in the literature that confirm the important role of PB in the treatment of intestinal disease (3-6). It has been suggested that PB can influence the intestinal environment, epithelial barrier and immune system functions (Bifidobacteria and Lactobacilli) and an increase of dangerous bacteria (i.e. *Escherichia coli*) compared to healthy subjects (1-6). In this context, the results of our study evidence that Citogenex administration increased relative proportion of beneficial bacteria while decreasing *E. coli*. In accordance with our results, recent studies have provided evidence that PB administration might balance the indigenous microbiota (2-6, 9, 10).

REFERENCES

1. Manichanh C, Borruel N, Casellas F, Guarner F. The gut microbiota in IBD. Nat Rev Gastroenterol Hepatol 2012; 9(10):599-608.
2. Backhed F, Ley RE, Sonnenburg J.L, Peterson D.A, Gordon JI. Host-bacterial mutualism in the human intestine. Science 2005; 307:1915-20.
3. Cui HH, Chen CL, Wang JD, et al. Effects of probiotic on intestinal mucosa of patients with ulcerative colitis. World J Gastroenterol 2004; 10(10):1521-5.
4. Guo S, Guo Y, Ergun A, Lu L, Walker WA, Ganguli K. Secreted metabolites of Bifidobacterium infantis and Lactobacillus acidophilus protect immature human enterocytes from IL-1β-induced inflammation: a transcription profiling analysis. PLoS One 2015; 10 (4):e0124549.
5. Bellavia M, Rappa F, Lo Bello M, et al. Lactobacillus casei and bifidobacterium lactis supplementation reduces tissue damage of intestinal mucosa and liver after 2,4,6-trinitrobenzenesulfonic acid treatment in mice. J Biol Regul Homeost Agents 2014; 28(2):251-61.
6. Strober W, Fuss IJ, Blumberg RS. The immunology of mucosal models of inflammation. Annu Rev Immunol 2002; 20:495-549.
7. Murano M, Maemura K, Hirata I, et al. Therapeutic effect of intracolonically administered nuclear factor kappa B (p65) antisense oligonucleotide on mouse dextran sulphate sodium (DSS)-induced colitis. Clin Exp Immunol 2000; 120(1):51-58.
8. McCafferty DM, Sihota E, Muscara M, Wallace JL, Sharkey KA, Kubes P. Spontaneously developing chronic colitis in IL-10/iNOS double-deficient mice. Am J Physiol. Gastrointest Liver Physiol 2000; 279(1): G90-99.
9. Fava F, Danese S. Intestinal microbiota in inflammatory bowel disease: friend of foe? World J Gastroenterol 2011; 17(5):557-66.
10. Mencarelli A, Distrutti E, Renga B, et al. Probiotics modulate intestinal expression of nuclear receptor and provide counter-regulatory signals to inflammation-driven adipose tissue activation. PLoS One 2011; 6(7):e22978.

LETTER TO THE EDITOR

AGE-RELATED ULTRASTRUCTURAL AND MONOAMINE OXIDASE CHANGES IN THE RAT OPTIC NERVE

S. TAURONE[1], G. RIPANDELLI[1], A. MINNI[2], R. LATTANZI[3], S. MIGLIETTA[4], N. PEPE[4], L. FUMAGALLI[4], A. MICERA[1], F.S. PASTORE[5] and M. ARTICO[2]

[1]IRCCS G.B. Bietti Foundation, Rome; [2]Department of Sensory Organs, "Sapienza" University of Rome; [3]Department of Physiology and Pharmacology "Vittorio Erspamer", "Sapienza" University of Rome; [4]Anatomical, Histological, Medico-legal and Locomotor System Sciences, "Sapienza" University of Rome; [5]Department of Systems Medicine, "Tor Vergata" University of Rome, Italy

Received April 11, 2016 – Accepted May 17, 2016

The aim of this paper is to study the morphology and the distribution of the monoamine oxidase enzymatic system in the optic nerve of 4 month-old Wistar (young) and 28 month-old Wistar (old) rats. The optic nerve was harvested from 20 young and old rats. The segment of optic nerve was divided longitudinally into two pieces, each 0.1 mm in length. The first piece was used for transmission electron microscopy. The second piece was stained with histochemical reaction for monoamine oxidase. The age-related changes in the optic nerve of rats include micro-anatomical details, ultrastructure and monoamine oxidase histochemical staining. A strong decrease of the thin nerve fibers and a swelling of the thick ones can be observed in optic nerve fibers of old rats. Increased monoamine oxidase histochemical staining of the optic nerve of aged rats is well demonstrated. The increase of meningeal shealth and the decrease of thin nerve fibers of the optic nerve in old rats are well documented. Morphological, ultrastructural and histochemical changes observed in optic nerve fibers of the old rats show a close relation with aging.

To the Editor,

Among the important enzyme regulators of the intracellular microenvironment are monoamine oxidase (MAO) and superoxide dismutase. These enzymes are significant in maintaining a delicate balance of reactive oxidative species. Monoamine oxidases (MAO) play an important role in brain function via the metabolic regulation of monoamine neurotransmitters, such as dopamine (DA), norepinephrine (NE), and serotonin (5-HT) (1). Alterations in MAO activity, which are associated with changes in monoamine neurotransmitter levels as well as with the production of toxic reactive oxygen species, have been implicated in the pathobiology of neuropsychiatric and neurodegenerative disorders. Oxidative stress may cause mitochondrial fragmentation.

MAO is an enzyme attached to the outer membrane of the mitochondria and oxidizes biogenic amines. There are two types of MAO: type A (MAO-A) and type B (MAO-B). With advancing age, the concentration of MAO-A does not change, but MAO-B increases (2). During aging and by increasing amounts of MAO-B attached to the outer mitochondrial membrane, enhanced oxidation of monoamines may cause elevated levels of reactive

Key words: optic nerve, age-related changes, MAO enzymes, light microscopy, histochemistry, transmission electron microscopy

Mailing address:
Prof. Marco Artico,
Department of Sensory Organs,
"Sapienza" University of Rome,
Vle del Policlinico 155, 00161 Rome, Italy
Tel./Fax: +39 0649918054
e-mail: marco.artico@uniroma1.it

0393-974X (2016)

DISCLOSURE: ALL AUTHORS REPORT NO CONFLICTS OF INTEREST RELEVANT TO THIS ARTICLE.

oxygen species that may threaten cellular viability (3). In a normal cell there is an appropriate pro- and antioxidant balance. It is apparent that in long-living cells, such as neurons, accumulation of lesions can be more detrimental. In the past, numerous authors have demonstrated that MAO activity presents age-related changes both in humans and animals (4-6). Nebbioso et al. (7) described age-related changes of the MAO enzymes in rat optic nerve with non-univocal results in a study which did not consider ultrastructural data. These important findings persuaded us to study the modifications which occur during aging due to alterations of MAO-B in the optic nerve of laboratory rats.

MATERIALS AND METHODS

Twenty 4-month-old Wistar rats and twenty 28-month-old Wistar rats, were treated according to the Convention of Helsinki on the utilization of animals in biomedical research. Animals were caged at room temperature (22°C) with a 10-14 dark-light rhythm and free access to water and food. Mean age of the old rats was 28 months. The animals were sacrificed using terminal anesthesia (50 mg/Kg Nembutal). The orbital cavity was opened and the head of the optic nerve was identified, removed and divided longitudinally into two pieces, each 0.1 mm in length. The first piece was treated for transmission electron microscopy. The second piece was fixed in Bouin fluid, cut into serial sections and stained with histochemical reaction for monoamine oxidase.

Transmission Electron Microscopy (TEM)

The tissue was fixed in 2.5% glutaraldehyde for 2–5 days at 4°C. After rinsing in PBS, samples were postfixed with 1% osmium tetroxide (Agar Scientific, Stansted, Essex, United Kingdom) in PBS, and rinsed again in PBS. The samples were then dehydrated through ascending series of ethanol, immersed in propylene oxide overnight for solvent substitution, embedded in Epon 812, and sectioned with a Reichert-Jung Ultracut E ultramicrotome. Semithin sections (1–7 μm thick) were stained with toluidine blue (Sigma, St. Louis, MO), examined by light microscopy (LM) with a Zeiss Axioskop microscope (Zeiss, Munich, Germany), and photographed with a Leica camera (DFC230). Ultrathin sections (60–80 nm) were cut with a diamond knife, mounted on copper grids, and contrasted with saturated uranyl acetate followed by lead citrate. They were examined and photographed with the use of Zeiss EM109 and Zeiss EM 10 electron microscopes at 80 kV.

TEM axon count determinations

Each photograph of a grid square that contained neural tissue was printed and all axons in the sampled area were manually counted, by observers masked to the identity of the tissue. Axons were identified by the presence of myelin sheaths and normal-appearing axoplasm. Axons partially hidden by grid bars or at the edge of the photograph were not counted. The area of the neural tissue in each photograph was measured using a VideoPlan Morphometric Workstation (KrontronBildanalyse, Munich, Germany) and divided into the axon count to calculate axon density for each photograph. The total neural area was then determined by measuring the entire nerve cross-section in a ×530 photograph. Data were calculated based on the axon density and total cross-sectional area of the optic nerve. This method manually counted 60±5% of total axons.

Histochemical analysis

The staining of MAO-B was performed according to the method suggested by Uchida and Koelle (8). This method is based on: i) incubation of the section in 30% Na_2SO_4 solution for 1 h at 37°C; ii) incubation for 1 h at 37°C in 0.05 M phosphate buffer solution (pH 7.6) containing sucrose (8%) with deprenyl as MAO-B specific inhibitor; iii) washing the sections in phosphate buffer solution and staining by solution containing phosphate buffer, nitrobluetetrazolium, sucrose (8%), and tryptamine (1 mmol/Lused as a substrate and starter of the reaction) for 1-2 hours at 37°C. The specificity of histochemical procedure was confirmed by incubating some sections (controls) in a medium either without substrate (tryptamine) or without dye (nitrobluetetrazolium). In both cases the reaction was negative. The reaction was instead recognized as positive when nitro blue tetrazolium precipitates were detected. In the last case, granules appeared blue on slides and black on photographs.

The intensity of the histochemical reaction was assessed microdensitometrically using an IAS 2000 image analyzer (Delta Sistemi, Rome, Italy) connected via a

TV camera to the microscope. Ten 100 μm^2 areas were delineated in each section using a measuring diaphragm. The quantitative data were analyzed statistically using analysis of variance (ANOVA) followed by Duncan's multiple range test as a *post hoc* test. Measurements were performed in triplicate (by different researchers) by means of two instruments and using the double blind method. The samples were identified by a number and recognized only when all experiments were finished. Results were then statistically elaborated to allow the significance index. Statistical analysis was performed by a basic statistical method, i.e. by calculating the arithmetic mean, the extreme values, the variance, the standard deviation, the standard error and the correlation coefficient. The coefficient of correlation was significant if $p<0.05$.

RESULTS

Micro-anatomical details

The optic nerve of rats emerges from the posterior pole of the eyeball and continues towards the apex of the orbita (optic canal) as a cylinder (0.2–0.3 mm). Nerve inner and outer sheaths are fused dorso-medially and ventrally with the dura mater. Both young and old rats have optic nerve sheaths coming from meningeal membrane envelopment whose extensions produce septa within the inner portion of optic nerve. Old rats showed an increase in the thickness and area of the sheaths and septa (Fig. 1A-C and Fig. 2A-C).

Our histochemical results (Fig. 1D and 2D) at high magnification, in comparison to Figs. 1A and 2A, confirm all the above anatomical details. Moreover, in the optic nerve of young rats numerous nerve fibers can be seen (Fig. 1 A and C compared with Fig. 2 A and C). Only the myelin sheath is rich in MAO enzymes, while the axons are clearly not positive. In the optic nerve of old rats we can see a strong decrease in the number of nerve fibers. In addition, myelin sheath was positive at the reaction for MAO-B when compared to young rats. Our ultrastructural results (Figs. 1C and 2C)

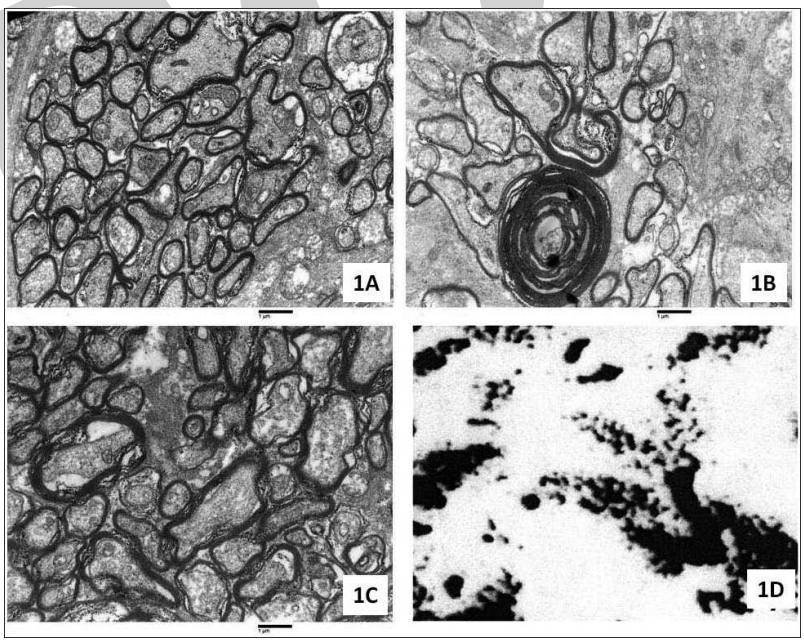

Fig. 1. *Figures obtained from optic nerves of young rats.* ***A)*** *Microphotograph of the optic nerve of a young rat. Transmission electron microscopy (TEM) revealed numerous well preserved nerve fibers with compact myelin sheaths consisting of several layers.* ***B)*** *Electron micrograph of a transverse sections of optic nerve of a young rat. TEM demonstrates that the myelin is well visible and appears very thick around the axons.* ***C)*** *Electron micrograph of a transverse section of the optic nerve in a young rat. Normal nerve fibers are identified by the presence of well preserved myelin sheaths.* ***D)*** *Optic nerve of a young rat (4 months of age) stained with the histochemical reaction for MAO-B. The myelin sheath of the axons is black and it appears weakly positive after the reaction for MAO-B. (magnification 800x).*

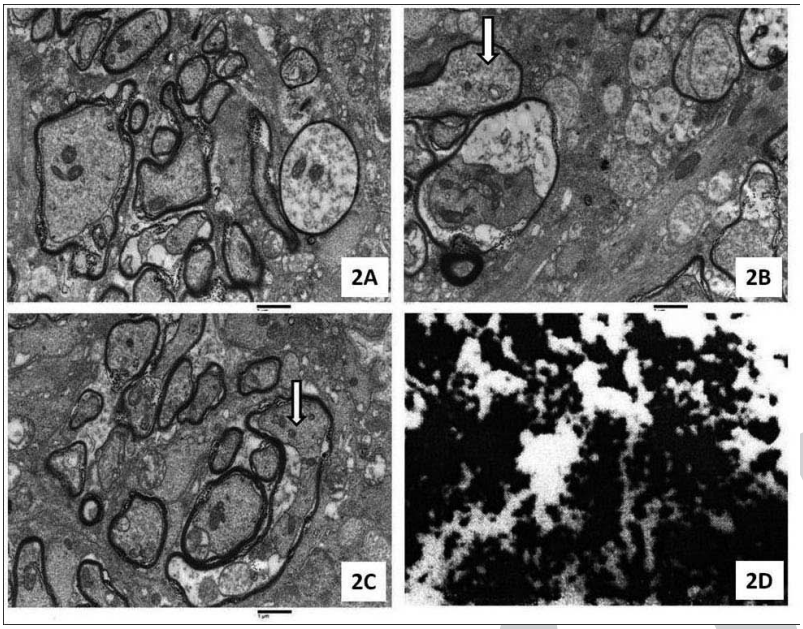

Fig. 2. *Figures obtained from optic nerves of old rats.* ***A)*** *Micrograph of the optic nerve of an old rat. Transmission electron microscopy (TEM) revealed a decrease in the compactness and loss of myelin in the axons, showing a significant variation of the myelin sheath thickness and axon diameter when compared with the optic nerve of young rats.* ***B)*** *Electron micrograph of a transverse section of optic nerve in an old rat. The distribution of the myelin sheath shows irregular thickness. The axons appear not well preserved with an irregular morphology, cellular debris (CD) and lipofuscin granules (LFG) (arrow).* ***C)*** *Electron micrograph of a transverse section of the optic nerve in an old rat. TEM reveals that irregular axonal myelin sheath is thinner than in young rats. Lipofuscin granules and cellular debris are also sometimes visible (arrow).* ***D)*** *Section of the optic nerve in an old rat (28 months of age) stained with the histochemical reaction for MAO-B. The myelin appears strongly positive after the reaction for MAO-B in comparison with that observed in the young rats. (magnification 800x).*

demonstrated that the sheath of the optic nerve is thinner than that of young animals. In young rats we can observe numerous thick nerve fibers while in the old rats the fibers are strongly decreased and show a thinner myelin sheath. Moreover, in the old rats the thick fibers are not well preserved (Fig. 2 B and C).

We studied a great number of sections and photos (at least 5 sections and 10 ocular fields for each rat). The number of rats in each group was 20 (young and old). The diameter of the whole optic nerve was 468±25 mm in young rats and 321±18 mm in old ones. The percentage of ratio nerve fibers was 84.6±5.4 in young ones and 62.2±3.9 in old ones; the total number of nerve fibers was 115.000±698 in young rats and 70000±619 in old ones. The whole area of a cross-section of the optic nerve was 4.89±0.16 mm^2 in old rats and 6.91±0.69 mm^2 in the young ones. The number of black granules indicate the positivity for MAO-B enzymes in the nerve fibers. The percentage of positivity was 76.4±1.3 in young rats and 88.3±1.6 in the old ones.

The thick nerve fibers were numerous in young rats while they were strongly decreased in the old ones. Moreover, in old rats a great number of fibers also presented swellings, dishomogeneous margins, spatial rearrangements and lipofuscin deposits.

DISCUSSION

The rat optic nerve undergoes morphological, histological, ultrastructural and chemical age-related changes and therefore it can be used as an optimum model for studies on aging. A recent study by Singh et al. (9) demonstrated that a deficiency of MAO-A and MAO-B (with a consequent tissue chronic increase of monoamines) leads to changes in

learning and memory of knockout mice. As reported in a previous study (7), MAO_s are located mainly in the mitochondrial membranes and are capable of oxidizing biogenic amines only when they are released by the presynaptic vesicles. In fact, this oxidation induces their catabolism and makes them lose the specific function of neurotransmitters (10). Hyperactivity of MAO_s may lead to a reduction of biogenic amines followed by an excessive production of oxygen free radicals, with subsequent oxidative stress and neurotoxicity (7). The use of MAO inhibitors facilitates neuronal activity, increases cerebral perfusion and prevents neurodegeneration and ischemic axonal damage (7). The morphological, ultrastructural and histochemical age-related changes observed in the optic nerve fibers of the rats we studied showed a close relation with aging and/or all senile pathologic events. We observed that in the elderly rats an increase in the thickness and area of the meningeal sheaths takes place. Moreover, in the elderly rats, the MAO-B activity is strongly increased.

Our study found that increased age was associated with increased levels of MAO-B in the optic nerve. This finding suggests that increased age may be associated with a decrease in the antioxidant capacity of the cell. The combination of increased MAO-B concentration and decreased antioxidant enzymes with advancing age could explain the neurologic, cognitive, affective, and behavioral dysfunction that may occur during aging in the rat tissues. The age-related increase in MAO-B levels and decreased intracellular antioxidants may cause increased production of reactive oxygen species (ROS) and associated cellular dysregulation. This finding suggests that increases in MAO-B levels could play a role in subsequent cell death. MAO-B-catalyzed ROS production has probably been involved in an age-related increase of mitochondrial damage, particularly in the CNS (11). This suggests that MAO-B may be a common initiator for these events and provides a novel model of the mechanisms by which these events may occur in the context of the human condition. Many neuronal cells and their associated neurotransmitters and enzymes show age-related modifications. However, the enzyme MAO-B is an exception because it increases during aging. Indeed, our study suggests that the increase of MAO-B in the old rats determines loss of neuronal cells with the consequent decrease of density of nerve fibers which results in neural damage and development of age-related eye diseases. Further studies are needed to better explain the relationships between an increase in MAO and age-related changes in rat optic nerve fibers.

ACKNOWLEDGEMENTS

The research for this paper was financially supported by the Ministry of Health and Fondazione Roma.

REFERENCES

1. Alzghoul L, Bortolato M, Delis F, et al. Altered cerebellar organization and function in monoamine oxidase A hypomorphic mice. Neuropharmacology 2012; 63(7):1208-17.
2. Kumar P, Taha A, Sharma D, Kale RK, Baquer NZ. Effect of dehydroepiandrosterone (DHEA) on monoamine oxidase activity, lipid peroxidation and lipofuscin accumulation in aging rat brain regions. Biogerontology 2008; 9(4):235-46.
3. Sorato E, Menazza S, Zulian A, et al. Monoamine oxidase inhibition prevents mitochondrial dysfunction and apoptosis in myoblasts from patients with collagen VI myopathies. Free Radic Biol Med 2014; 75:40-7.
4. Lieu CA, Chinta SJ, Rane A, Andersen JK. Age-related behavioral phenotype of an astrocytic monoamine oxidase-B transgenic mouse model of Parkinson's disease. PLoS One 2013; 8(1):e54200.
5. Mazzio E, Deiab S, Park K, Soliman KF. High throughput screening to identify natural human monoamine oxidase B inhibitors. Phytother Res 2013; 27(6):818-28.
6. Zellner M, Baureder M, Rappold E, et al. Comparative platelet proteome analysis reveals an increase of monoamine oxidase-B protein expression in Alzheimer's disease but not in non-demented Parkinson's disease patients. J Proteomics 2012; 75(7):2080-92.
7. Nebbioso M, Pascarella A, Cavallotti C, Pescosolido

N. Monoamine oxidase enzymes and oxidative stress in the rat optic nerve: age-related changes. Int J Exp Pathol 2012; 93:401-5.
8. Uchida E and Koelle GB. Histochemical investigation of criteria for the distinction between monoamine oxidase A and B in various species. J Histochem Cytochem 1984; 32:667-73.
9. Saito M, Yamagata T, Matsumoto A, et al. MAOA/B deletion syndrome in male siblings with severe developmental delay and sudden loss of muscle tonus. Brain Dev 2014; 36:64-69.
10. Singh C, Bortolato M, Bali N, et al. Cognitive abnormalities and hippocampal alterations in monoamine oxidase A and B knockout mice. Proc Natl Acad Sci 2013; 110:12816-21.
11. Carradori S, Silvestri R. New frontiers in selective human MAO-B inhibitors. J Med Chem 2015; 58(17):6717-32.

LETTER TO THE EDITOR

NEWBORN SCREENING OF INHERITED METABOLIC DISORDERS: THE ITALIAN SITUATION

M. FOCARDI[1], V. PINCHI[1], B. DEFRAIA[1], B. GUALCO[1], G. VARVARA[2] and G-A. NORELLI[1]

[1]Department of Health Sciences, Forensic Sciences Section, University of Florence, Florence, Italy;
[2]Department of Medical, Oral and Biotechnological Sciences, Dental School, G. D'Annunzio University of Chieti-Pescara, Chieti , Italy

Received February 2, 2016 – Accepted July 5, 2016

Starting from an international overview of the current status of screening programs, the present paper focuses on the legal situation in Italy and the great differences among Italian regions. Since the introduction of tandem mass spectrometry (MS/MS) in the '90s the paradigm "one spot-one disease" changed. Only recently, some regions issued legislative acts to promote expanded newborn screening with MS/MS. This approach raises medico-legal and ethical issues because a fast neonatal diagnosis of an inborn error of metabolism (IEM) could increase chances of an early treatment and reduce disabilities, therefore citizens ought to have the same access to care countrywide. Enacting a mandatory standard for a disease screening panel using MS/MS and a few centers specialized in diagnosis, treatment and follow-up of patients affected by IEM (inborn errors of metabolism) can reduce legal and ethical

To the Editor,

Inborn errors of metabolism (IEM) represent a vast and heterogeneous collection of approximately 700 genetic diseases, which are included in the rare (orphan) disease group (1). The prevalence of all inborn metabolic diseases in live births is estimated to be 40/100,000 and the rate is increasing, so that one newborn in 200 will be a carrier of a metabolic defect.

IEM usually present in the neonatal period or during childhood, but they can occur at any time, even in adulthood, and sometimes during pregnancy. Patients, especially neonates, may have non-specific symptoms, which can be easily attributed to infection or other common diseases. These non-specific symptoms can cause severe neurological disabilities or evolve into sudden death (2). Hence, it is critical that medical personnel review clinical records and autopsy reports when they are available, thus collecting useful and up-to-date data to provide early diagnosis, treatment and possible prediction of outcome along with genetic counseling for all family members.

The aim of this paper is to report the Italian legal framework concerning IEM and to discuss the connected medico-legal issues.

Diffusion of expanded newborn screenings: international overview

Tandem mass spectrometry (MS/MS) introduced the era of expanded newborn screening for IEM, applying the ten criteria formulated by Wilson and Jungner (3). According to the information retrievable in literature, the number of metabolic disorders

Key words: newborn screening, inborn errors of metabolism, Italian law

Mailing address:
Dr. Martina Focardi,
Department of Health Sciences,
Forensic Sciences Section,
University of Florence, Florence, Italy
Tel.: +39 055 2751770
e-mail: martina.focardi@unifi.it

0393-974X (2016)

DISCLOSURE: ALL AUTHORS REPORT NO CONFLICTS OF INTEREST RELEVANT TO THIS ARTICLE.

screened by MS/MS in newborns actually ranges from 0 to over 40, varying in different countries. Many national laws have not yet implemented MS/MS, while others are still setting panels of diseases that have to be included in the screening assays. This uneven approach is due to several reasons, such as the access to funding for an expensive clinical MS/MS screening infrastructure, but also to the absence of uniformly accepted practice guidelines regarding diseases to be included in a newborn screening program.

In the United States, the Recommended Uniform Screening Panel (RUSP) has recently included 34 core conditions and 26 secondary conditions. Given the introduction of the RUSP, the situation is hypothesized to change, with a noticeable reduction of claims (4). In Australia, Expanded Newborn Screening (ENS) with MS/MS was introduced in 1998; it is now universal and has extended to New Zealand (5). Universal metabolic screening is also carried out in Japan, Taiwan, Singapore, Israel, Chile, and Uruguay (6).

Cornel and Bodamer, who analyzed the situation of expanded newborn screening programs in Europe (7, 8), observed that the disorders chosen to be included in the European newborn screening programs differed considerably, but there was also a progressive diffusion of ENS, especially in western European countries. At that time, 1:3 neonates, born in over 10 countries, were screened using MS/MS.

Despite the low prevalence, rare diseases represent one of the priorities of health care systems in the European Union, which takes actions in order to improve and develop research, diagnosis and treatment of these diseases. The Recommendation of the Council of the European Union, n. 2009/C 151/02 of June 8th 2009, recommends the member states "elaborate and adopt a plan or strategy as soon as possible, preferably by the end of 2013 at the latest", in the field of rare diseases; moreover, member states are requested to "gather national expertise on rare diseases and support the pooling of that expertise with European counterparts in order to support: … the development of European guidelines on diagnostic tests or population screening, while respecting national decisions and competences …". In July 2013, the European Union Committee of Experts on Rare Diseases (EUCERD) published a document on: "Newborn screening in Europe: opinion of the EUCERD on potential areas for European collaboration". One of the topics for potential European collaboration is: "Production of standard operating procedures for the organization and management of newborn screening procedures".

The Italian situation

In February 1992, neonatal screening for congenital hypothyroidism (CH), cystic fibrosis (CF), and phenylketonuria (PKU) became mandatory in Italy. This approach was also validated and confirmed in 2004 by the no. 18 Recommendation of the European Commission Expert Group, which stated that:

a. European Union (EU)-wide network for diagnostic testing of rare genetic diseases be created and financially supported as a matter of urgency;
b. an EU-level incentive system for the systematic development of genetic tests for rare diseases be created and financially supported;
c. for rare but serious diseases for which treatment is available, member states introduce universal neonatal screening as a priority.

Only recently, the 147/2013 law (Disposizione per la formazione del bilancio annuale e pluriennale dello Stato, legge di stabilità 2014, comma 229, art.1) was established, and by allocating five million euros, would have allowed newborn screening to expand nationwide. However, even if the law came into force three months after its promulgation, the expanded newborn screening was not adopted by all the Italian Regions. Only some of them, through specific regional laws, have recently enacted a mandatory Expanded Newborn Screening (ENS), but the number of investigated diseases/disorders varies from region to region and sometimes from one hospital to another. Such a mixed legal approach creates a puzzling mosaic, however, despite this, the Italian situation can be framed into two main categories (Table I).

One category comprises regions where an ENS is mandatory and applied wherever. Tuscany was

Table I. *ENS and Italian regional situation.*

REGION	Expanded newborn screening programme	Territorial coverage	No. of screened diseases
Abruzzo	To be organized with the Marche Region	-	-
Basilicata	Only some samples are sent to Umberto I Hospital of Rome		
Bolzano*	Send samples to one laboratory in Vienna		
Campania	Pilot programme	No information	
Calabria	-	-	-
Emilia-Romagna	Legislative action (2010)	100%	23 IEM + 3 (IPC, PKU,CF) + galactosemia and adrenal hyperplasia
Friuli- Venezia Giulia	Has an Agreement with the Veneto Region	No information	
Lazio	Legislative action	100% of the neonates born in Umberto I hospital area	
Liguria	Pilot programme	100%	30 IEM + 3 (IPC, PKU, CF)
Lombardia	To be organized	Carried out only in private laboratories	
Marche	To be activated in Fano Hospital		
Molise	To be organized with Lazio Region	-	-
Piemonte	Legislative action not activated		
Provincia di Trento*	Has an agreement with Veneto Region	No information	
Puglia	To be organized	-	-
Sardegna	Has an agreement with Liguria	100%	30 IEM + 3 (IPC, PKU, CF)
Sicilia	No legislative action nor pilot study	Extended screening only in some hospitals. About 30% of neonates	
Toscana	Legislative action (2004)	100% (only one centre: Meyer Children's Hospital of Florence)	40 IEM + 3 (IPC, FCH, FC)
Umbria	Legislative action (2010)	100% (Meyer Children's Hospital of Florence)	40 IEM + 3 (IPC, FCH, FC)
Veneto	Legislative action activated only in 2014	100% (Verona and Padua hospitals)	
Valle d'Aosta	-	-	-

the first Italian region introducing mandatory ENS in 2004, and now it encompasses 43 diseases. Laboratory analyses are provided by the Meyer Children's Hospital in Florence for the whole of Tuscany. After legislative action, Umbria came into an agreement with Tuscany and, since 2010, all samples of neonates born in Umbria have been analyzed by the Meyer Hospital.

In Liguria, since 2005, an ENS pilot program has been operating, with 100% coverage of the neonatal population. This pilot program has been now extended to some Sardinian hospitals which, however, do not cover the entire Sardinian territory (9).

In Lazio and Veneto, an extended screening program is in place, but in Veneto it has only been applied by all hospitals since 2014. Since 2010, in Emilia-Romagna, a legislative action officially mandated ENS for 26 diseases.

The second category encompasses regions where ENS is not mandatory or applied by all hospitals or private laboratories (e.g., Puglia, Abruzzo, etc.).

DISCUSSION

The Italian approach to ENS results uneven at a regional level, since the disorders included in regional newborn screening programs differ significantly from European indications. Since all European populations and, largely, the U.S. population have a common genetic background, the reason for these differences cannot be explained by major differences in disease prevalence, but only by different approaches to the estimation of risks and benefits. A survey conducted by Feuchtbaum et al. (10) reported that lack of funds was the main barrier to MS/MS screening implementation. In some countries, such as the USA (http://savebabies.org/screening_info.html), as in some Italian regions, the concept of supplemental newborn screening by MS/MS has been chosen as an addition to routine newborn screening, involving an extra sample and extra cost (11) .

Nevertheless, the right of access to IEM and to its associated care continues to be remarkably different for families and neonates born in different regions, thus an intense debate on the ethical and medico-legal issues persist in the field of neonatal screening.

From the medico-legal point of view, when an Italian hospital cannot provide full IEM screening, the family must receive clear and explicit information, especially concerning the limits of the hospital laboratories, to avoid legal claims. For these reasons, in 2005, the Supreme Court sentenced two physicians to pay damages to a child with PKU, whose family was not informed that the hospital was unable to treat the genetic disease of their son, and failed to refer the parents to a hospital center where the appropriate care would have been provided. Therefore, ENS programs are not just a panel of screening tests, but they aim to integrate qualification, screening follow-up, diagnosis, management and evaluation. Ethical and legal issues invariably emerge when IEM are implemented or expanded.

The lack of a clear and homogeneous legal approach to the diagnosis of rare metabolic diseases and ENS creates disparity in the access to care, and also creates risks of complaints for hospitals and physicians, or worse, legal claims from patients/families who allege a lack of diagnosis.

The national law concerning ENS in Italy should be updated and improved and ENS should be provided for all neonates regardless of the Italian region they are born in. In fact, Italy has an established, and mandatory, screening program (only for PKU, CH and CF) at the national level and regions are entitled to issue legislative acts on pilot programs to expand the ENS. The Italian government (158/2012 Law Decree and 147/2014 law) has recently stated that ENS should be provided by all regions, without costs for families or patients, but the law does not specify how many and what kind of diseases must be investigated. The government statement was issued to address the increasing economic problems of regions and to create a few reference centers of excellence for newborn screening. Nevertheless, at the present time, the situation has not been modified and the new law is not applied.

The costs of ENS, and especially for MS/MS equipment, might be reduced considerably by creating very few specialized centers similar to the Meyer Hospital in Florence, which at the moment serves two entire regions for ENS (Tuscany and

Umbria). Through efficient organization, just three centers may make ENS feasible for all Italian neonates within a very few days of birth, thus maximizing the diagnostic potential of the screenings. Moreover, babies who are suspected to be suffering from rare genetic diseases could have access to a high-level diagnosis offered by these qualified and specialized centers, simply by the sending of biological samples, thus avoiding families having to travel significant distances. Doctors would receive convenient information about the diagnostic potentiality of specialized centers and those ENS covered by regional laws and funds. Thus, doctors could assist families with adequate counseling, provide examinations directly by sending samples to the specialized center and advise whether the family should turn directly to the specialized center to undergo supplementary screenings not offered by the regional health care system. Especially doctors employed by hospitals where ENS is not available must inform the family on the diagnostic potential of specialized centers and about the possibility of carrying out the screening for a higher number of pathologies without any additional costs This will meet the needs of patients and doctors, meanwhile answering the ethical issues raised by the disparity in access to care that emerged from the current legal situation in Italy. Furthermore, the centralization of ENS to a few specialized centers is cost efficient, ensures higher standards of care and eliminates the discrepancies throughout the country, thus reducing the risk of lawsuits because of misdiagnosis and lack of information.

At the present time, to be born in a region where newborn screening is performed (Umbria, Tuscany and Sardinia, for example) compared to another where this is not guaranteed, may mean the difference between life and death, or rather, a normal life or another with disability (if effective therapies for the specific pathology can be carried out) or whether one would know if one is a carrier of an IEM that could present in adulthood.

The mixed legal regulations regarding ENS from one region to another raise specific and meaningful medico-legal issues for the physician, who might face situations in which the investigation of a specific metabolic disorder/disease is not requested by law, but could be included in an appropriate ENS. In these circumstances, the physician might be opposed to a claim of diagnosis omission when the specific legal provisions, and the related difficulties in providing examinations, are not mandatory by law and not covered by the NHS. Nevertheless, the physician continues to be torn between the opportunity for subjects and possibly their parents to undergo the genetic testing and the necessity to request expensive exams that burden the family, especially in those cases in which the utility and validity of ENS is questionable or unsure (12). Even worse risks burden hospitals and physicians who are not aware of care facilities able to provide the most appropriate genetic exams for some specific and are diseases. The unclear and quite heterogeneous legislation ends up putting the highest burden on the shoulders of the physician (13), who is obliged to be regularly updated on rare diseases which have recently become detectable with novel techniques, both in order to provide or suggest the most appropriate ENS and to be able to inform and assist the family when their current care facility is not adapted for the appropriate genetic analysis.

In conclusion, the law requires the physician, in each case, to inform the family and decide when to apply the extended diagnostic screening. In fact, if there are conditions which are presumed to imply a risk, there is no doubt that the failure to use extended screening and/or not inform the family will be regarded as medical negligence. On the basis of Law 147/2014, it is essential to synchronize the different regions' legislation and to adopt national guidelines in order to ensure confidence for users of the NHS and healthcare professionals

REFERENCES

1. Clarke JTR. General principles in Clarke JTR, eds. A clinical guide to inherited metabolic diseases, Cambridge, 3rd ed. Cambridge University Press, 2006
2. Saudubray JM. Clinical approach to inborn errors of metabolism in paediatrics. in: J.M. Saudubray, G. van den Berge, J.H. Walter et al, (Eds.) Inborn metabolic

diseases diagnosis and treatment. 5th edition. lic diseasVerlag Berlin Heidelberg, New York; 2012:3rn
3. Wilson JM, Jungner G. Principles and practice of screening for diseases. Boletin de la Oficina Sanitaria Panamericana 1968; 65:281-393.
4. http://www.hrsa.gov/advisorycommittees/mchbadvisory/heritabledisorders/recommendedpanel/index.html
5. Wilcken B, Wiley V, Hammond J, et al. Screening newborns for inborn errors of metabolism by tandem mass spectrometry. N Engl J Med 2003; 348:2304-12.
6. Marsden D, Larson C, Levy H. Newborn screening for metabolic disorders. J Pediatr 2006; 148(5):577-84.
7. Cornel MC, Rigter T, Weinreich SS, et al. A framework to start the debate on neonatal screening policies in the EU: an Expert Opinion Document. Eur J Hum Genet 2014; 22:12-17.
8. Bodamer OA, Hoffman GF, Lindner M. Expanded newborn screening in Europe 2007. J Inher Metab Dis 2007; 30(4):439-44.
9. 21st National Conference on Neonatal Screening in Italy, 4th December 2012, SIMMESN (Società Italiana Per lo Studio delle Malattie Metaboliche Ereditarie e lo Screening Neonatale).
10. Feuchtbaum L, Faulkner L, Verghese S. Tandem mass spectrometry program implementation challenges for state newborn screening programs: national survey of barriers and issues. J Pediatr 2006; 117(5pt2):S253-60.
11. Stewart F. Ethics of newborn screening . Curr Opin Paediatr 2006; 16(3):216-20.
12. Holtzman NA. Expanding newborn screening: how good is the evidence? JAMA 2003; 290(19):2606-8.
13. Pinchi V, Norelli GA, Bartolini V. Ethical implications of Italian legislation on 'epilepsy and driving. J Med Ethics 2014; 40(8):552-57.

LETTER TO THE EDITOR

IgG4-RELATED CRANIO-SPINAL HYPERTROPHIC PACHYMENINGITIS INVOLVING THE INTERNAL AUDITORY CANAL

Y. YANGUE[1], G. GAMBARACCI[1], P. FLORIDI[2], A. FIACCA[2], A. GUERRIERO[3], M. GIANSANTI[3] and M. SCIALPI[1]

[1]Department of Surgical and Biomedical Sciences, Division of Radiology 2, Perugia University, Santa Maria della Misericordia Hospital, Perugia, Italy; [2]Neuroradiology, Santa Maria della Misericordia Hospital, Perugia, Italy; [3]Department of Experimental Medicine, Surgical Pathology Unit, School of Medicine, Perugia, Italy

Received January 4, 2016 – Accepted May 16, 2016

Immunoglobulin G4 (IgG4)-related hypertrophic pachymeningitis, which is a focally or diffusely thickened dura mater and lymphoplasmacytic infiltration with increased IgG4 bearing plasma cells, is a rare disease, and cases involving the whole cervical spine are even rarer. Here, we describe a case of probable IgG4-related hypertrophic pachymeningitis involving the whole cervical spine and the auditory canals in an 18-year-old male. The patient, who had a history of paresthesia and had previously experienced weakness, presented with generalized tonic seizures. A decompressive laminectomy on cervical vertebrae was performed as a matter of urgency, removing intradural fibrous material. The patient responded well to treatment and was discharged walking independently, with no strength deficit to any of the 4 limbs, and with normal blood tests.

To the Editor,

IgG4-related disease (IgG4-RD) is a largely unknown etiological syndrome, consisting of a group of disorders that share specific pathological, serologic and clinical features (1).

In 1995,Yoshida et al. proposed the concept of autoimmune pancreatitis (AIP), a clinical entity characterized by enlargement of the pancreas, narrowing of the pancreatic duct, increased serum levels of gamma globulin, lymphoplasmacytic infiltration of the organ through fibrosis and an outstanding response to steroid therapy (2, 3). In 2001, Hamano et al. described the occurrence of elevated serum IgG4 as a factor associated with autoimmune pancreatitis (4), yet only in 2003 did Kamisawa et al. (5, 6) find in these manifestations a common systemic condition and propose a new clinical-pathological entity, "IgG4-related disease" (IgG4-RD). This disease was first revealed in the central nervous system in the form of hypophysitis by Chan SK et al. (7).

In the literature there are few reported cases of IgG4-related pachymeningitis (7-9). Our aim is to describe and analyze a case of IgG4-related hypertrophic pachymeningitis in a very young patient with entire cervical spine and bilateral internal auditory canal involvement.

Case report

An 18-year-old patient with a history of paresthesia

Key words: IgG4, pachymeningitis, intracranial, spine, auditory canal

Mailing address:
Dr Michele Scialpi,
Ospedale Santa Maria della Misericordia,
Piazza Menghini 1,
San Sisto 06129, Perugia, Italy
Tel.: 3467471810
e-mail: michele.scialpi@unipg.it

0393-974X (2016)

DISCLOSURE: ALL AUTHORS REPORT NO CONFLICTS OF INTEREST RELEVANT TO THIS ARTICLE.

who had experienced weakness in all 4 limbs during the month of May-June 2014, associated with loss of balance and difficulty walking, presented to the emergency room in October after three incidents of accidental falls, with clearly worsening hyposthenia and an inability to maintain an upright posture.

An unenhanced Computed Tomography (CT) exam of the brain showed hyperdensity at the bulbospinal region, suggesting a herniation of the cerebellar tonsils.

Magnetic Resonance Imaging (MRI) examination of the brain and cervical spine documented altered signal intensity which extended from the medulla oblongata to C7, indicative of spinal cord suffering secondary to an extrinsic compression due to extensive pachymeningeal thickening involving the whole skull base and both internal auditory canals.

After intravenous administration of gadoteric acid (Gd-DTPA), an intense and homogeneous enhancement of the pachimeninge was observed, suggesting hypertrophic pachymeningitis (Figs. 1, 2).

No alterations were revealed during routine laboratory tests. Markers of autoimmunity and neural tumours resulted negative, as did CSF for the presence of bacteria.

The neurological examination showed spastic paraplegia, a positive romberg test, bilateral clonus in the lower limbs, positive babinski signs in both limbs and a positive mingazzini test in all four limbs. Given the clinical and radiological medical case, after neurosurgical evaluation the patient proceeded to decompressive laminectomy surgery, where

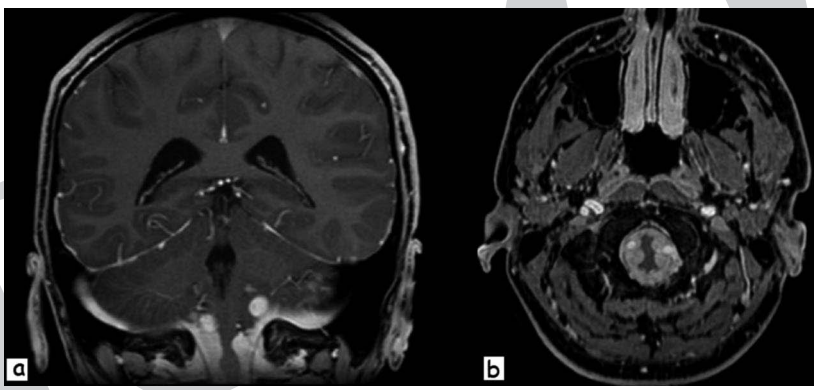

Fig. 1. *Coronal (**a**) and axial (**b**) contrast-enhanced T1-weighted images detect diffuse thickening and enhancement of the dura.*

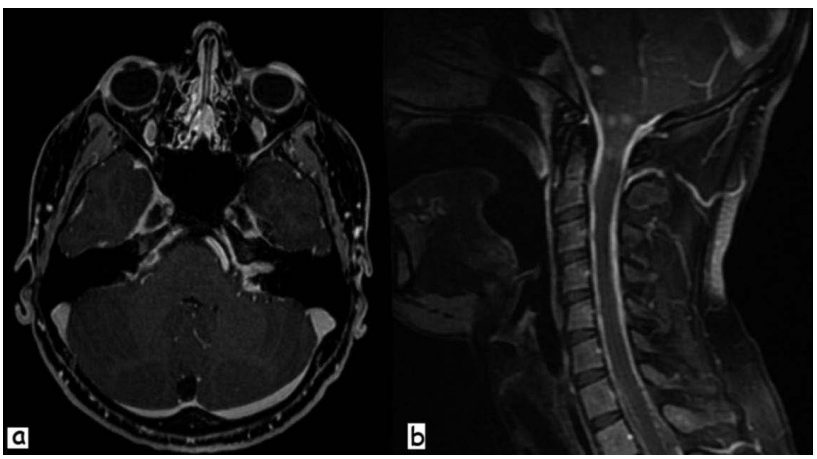

Fig. 2. *Axial contrast-enhanced T1-weighted image reveal pachymeningitis involving the left internal auditory canal (**a**). Sagittal section of a Contrast-enhanced T1-weighted scan detect diffuse dural thickening throughout the cervical spine (**b**).*

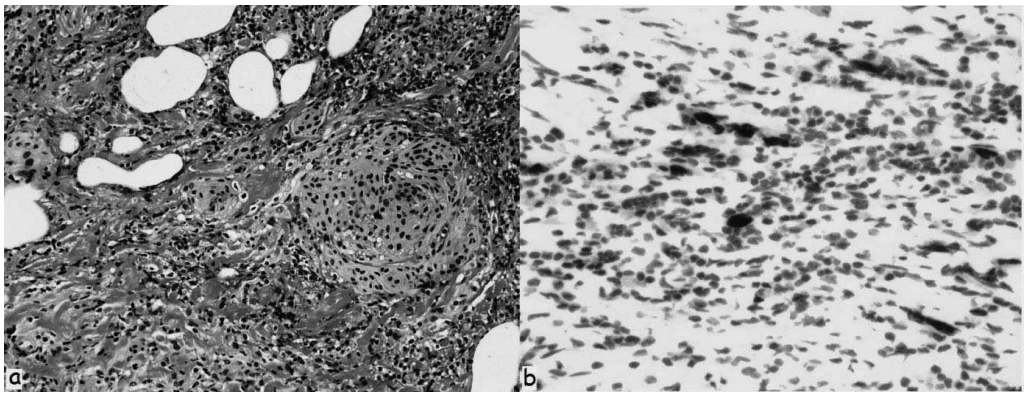

Fig. 3. *Meningothelial nests and intense flogistic infiltrate embedded in a dense fibrous tissue (H-E 20x) (**a**). Plasmacells IgG4 positive are more than 10 X HPF (IgG4 40x) (**b**).*

meningeal fragments were removed and tested. The lumbar puncture revealed low glucose, high protein levels and 28 cells/mmc (mostly lymphocytes).

Given the results of the cerebrospinal fluid exams, antituberculosis therapy was initiated with four different medications and was continued for three weeks, until a culture from the CSF came back negative for Koch's bacillus. After the second day of convalescence, steroid treatment with dexamethasone was introduced. During the patient's time in hospital there was a steady deterioration of strength in the limbs with increased tension and instability of the torso and an ataxic gait.

An MRI scan of the brain and spine showed no changes, therefore a second cervical vertebral decompressive laminectomy was performed, removing intradural fibrous material. In the mean time high-dose steroids (dexamethasone 8 mg x2/ day) were administered.

Surgical specimens, consisting of grayish fragments measuring from 5 to 20 mm, were fixed in 10% formalin, embedded in paraffin wax, sectioned at 4 μm and stained with ematoxylin and eosin. Histologically, all fragments consisted of thick laminae of dense fibrous tissue encompassing a dense plurifocal chronic flogistic infiltrate made of lymphocytes B immunohistochemically positive to CD20 and lymphocytes T immunoistochemically positive to CD3 (Fig. 3a). Numerous polytipic plasma cells immunoreactive to CD38, CD138, light chains Kappa and Lambda. In all examined sections several meningothelial lobules were appreciable, made of uniform arachnoidal cap cells showing oval nuclei with delicate chromatin without atypia and mitosis. Immunohistochemically meningothelial cells were positive to Epitelial Membrane Antigen (EMA), Vimentin and Progestinic Receptor (PR); proliferative index Ki67 was of 1%.

A differential diagnosis between a lymphoplasmacyte-rich meningioma in plaque and an idiopathic hypertrophic pachymeningitis was proposed. Given the inconclusiveness of these results, further analysis of the specimens was carried out and numerous plasma cells showing strong IgG4 immunoreactivity were counted (Fig. 3b), suggesting a diagnosis of IgG4-related pachymeningitis.

Once a diagnosis had been made, a total body PET-CT scan was carried out, looking for multi-system involvement of the disease. With this outcome excluded, the steroids were scaled down to a manageable dosage of 5-10 mg/day. The follow-up was long, even considering the relapse remission characteristic of the disease, and the patient was discharged on the 16th June 2015 walking independently, with no strength deficit to any of the 4 limbs, and with normal blood tests.

The patient gave informed consent to publish this report.

DISCUSSION

Hypertrophic pachymeningitis is characterized

by widespread thickening of the dura mater (10), which can be categorized into diffuse or focal, and linear or nodular thickening (8).

Several clinical pathological entities can cause thickening of the pachimeninge, including idiopathic hypertrophic pachymeningitis (11).

In this particular case, our initial diagnosis was of idiopatic hypertrophic pachymeningitis, then, because of the worsening of the patient's condition and the results of the successive MRI scan, we proceeded to conduct a diagnostic biopsy, which suggested a different interpretation.

In 2011, a group of Japanese researchers proposed comprehensive diagnostic criteria for IgG4-related disease (9). The criteria is as follows: clinical examination highlighting characteristic diffuse/localized thickening or mass in one or multiple organs, hematological examination showing elevated serum IgG4 concentrations (> 135 mg/dL), histopathological examination revealing marked lymphocyte and plasmacyte infiltration, fibrosis, and infiltration of IgG4 + plasma cells (> 10 IgG4 + plasma cells/high power field (HPF)and/or ratio of IgG4 +/IgG+cells> 40%). Thus, a diagnosis of the IgG4-related disease is definitive in patients who meet all of the above conditions, and a diagnosis of the disease is also possible in patients who fulfill the first two criteria but not the last. A diagnosis of IgG4-related disease is probable in patients with organ involvement who also fulfill the histopathological criteria without a high concentration of IgG4 plasma serum.

We did not find a high concentration of IgG4 serum in the patient, but two of the above criteria were present: a thickening of the meninges and the presence of lgG4+ plasma cells (more than 10 lgG4+ plasma cells were found), suggesting a diagnosis of chronic IgG4-related pachymeningitis. The ratio IgG4/IgG plasma cells was not performed, because no established international criteria are present for extra-pancreatic disease (12).

To conclude, lgG4-related pachymeningitis is a very rare entity. Here we have reported a case of probable IgG4-related pachymeningitis in an 18-year-old patient which, according to the literature, is the first case in which we have seen the involvement of the acoustic canals. Although the current literature shows the average age of patients presenting with this disease ranges from 50 to 60 years of age, our case demonstrates the occurrence of probable hypertrophic pachymeningitis in a younger patient.

As a consequence of this, IgG4-related pachymeningitis should also be considered in younger patients and appropriate studies (e.g. immunohistochemical staining) should be carried out.

REFERENCES

1. Stone JH, Zen Y, Deshpande V. IgG4-related disease. N Engl J Med 2012; 366(6):539-51.
2. Yoshida K, Toki F, Takeuchi T, Watanabe S, Shiratori K, Hayashi N. Chronic pancreatitis caused by an autoimmune abnormality. Proposal of the concept of autoimmune pancreatitis. Dig Dis Sci 1995; 40(7):1561-68.
3. Saeki T, Saito A, Hiura T, et al. Lymphoplasmacytic infiltration of multiple organs with immunoreactivity for IgG4: IgG4-related systemic disease. Intern Med 2006; 45(3):163-67.
4. Hamano H, Kawa S, Horiuchi A, et al. High Serum IgG4 concentrations in patients with sclerosing pancreatitis. N Engl J Med 2001; 344:732-38.
5. Kamisawa T, Funata N, Hayashi Y, et al. A new clinicopathological entity of IgG4-related autoimmune disease. J Gastroenterol 2003; 38:982-84.
6. Kamisawa T, Egawa N, Nakajima H. Autoimmune pancreatitis is a systemic autoimmune disease. Am J Gastroenterol 2003; 98:2811-12.
7. Chan SK, Cheuk W, Chan KT, Chan JK. IgG4-related sclerosing pachymeningitis: a previously unrecognized form of central nervous system involvement in IgG4-related sclerosing disease. Am J Surg Pathol 2009; 33:1249-52.
8. Kim EH, Kim SH, Cho JM, Ahn JY, Chang JH. Immunoglobulin G4-related hypertrophic pachymeningitis involving cerebral parenchyma. J Neurosurg 2011; 115(6):1242-47.
9. Umehara H, Okazaki K, Masaki Y, et al. Comprehensive diagnostic criteria for IgG4-related disease (IgG4-RD), 2011. Mod Rheumatol 2012; 22(1):21-30.
10. Rojana-udomsart A, Pulkes T, Viranuwatti K,

Laothamatas J, Phudhichareonrat S, Witoonpanich R. Idiopathic hypertrophic cranial pachymeningitis. J Clin Neurosci 2008; 15(4):465-69.

11. Prabhakar S, Bhatia R, Lal V, Singh P. Hypertrophic pachymeningitis: varied manifestations of a single disease entity. Neurol India. 2002; 50(1):45-52.
12. Lindstrom KM, Cousar JB, Lopes MB. IgG4-related meningeal disease: clinico-pathological features and proposal for diagnostic criteria. Acta Neuropathol 2010; 120(6):765-76.

LETTER TO THE EDITOR

NUTRACEUTICAL APPROACHES TO HOMOCYSTEINE LOWERING IN HYPERTENSIVE SUBJECTS AT LOW CARDIOVASCULAR RISK: A MULTICENTER, RANDOMIZED CLINICAL TRIAL

A. MAZZA[1], A.F. CICERO[2], E. RAMAZZINA[1], S. LENTI[3], L. SCHIAVON[1], E. CASIGLIA[4] and G. GUSSONI[5]

[1]Department of Medicine, S. Maria della Misericordia Hospital, Rovigo, Italy; [2]Department of Medical and Surgical Sciences, University of Bologna, Bologna, Italy; [3]Department of Internal Medicine and Geriatrics, San Donato Hospital, Arezzo, Italy; [4]Department of Medicine, University of Padova, Padua, Italy; [5]Department of Clinical Research, FADOI Foundation, Milan, Italy

Although the role of homocysteine (HCys) in secondary cardiovascular prevention has been scaled down, hyper-homocysteinemia remains a risk factor for cerebrovascular events. The aim of this study was to investigate the efficacy of nutraceuticals in lowering HCys serum levels versus a conventional vitamin supplementation in hypertensive subjects at low cardiovascular risk. One-hundred and four patients (mean age 62.8±14.5 years, 63.5% males), 52 for each treatment group, were enrolled. The study recruited patients with stage 1 essential hypertension and hyper-homocysteinemia (HCys ≥15 µmol/L), without a history of cardiovascular and cerebrovascular disease. They were sequentially randomized to receive a combined nutraceutical containing 400 µg folate-6-5-methyltetrahydrofolate, 3 mg vitamin B6, 5 µg vitamin B12, 2.4 mg vitamin B2, 12.5 mg zinc and 250 mg betaine (Normocis$^{400®}$) once daily for two months, or supplementation with highly dosed folic acid (5 mg/day) (control group). Differences in serum HCys values were compared by ANOVA for repeated measures. A significant HCys reduction in comparison to baseline was found in both groups at the end of the study treatment, from 21.5□8.7 to 10.0±1.7 µmol/L for Normocis$^{400®}$ subjects ($p<0.0001$), and from 22.6±6.2 to 14.3±2.8 µmol/L for controls ($p<0.0001$). HCys reduction was significantly higher among patients treated with Normocis$^{400®}$ ($p<0.035$). The ideal HCys level (i.e. <10 µmol/L) was reached in 55.8% of cases in the Normocis$^{400®}$ group, and it was significantly higher than in controls. No side effects were observed in either treatment group. Randomized clinical trials are ongoing to test the effect of folate, B6, and B12 supplementation in primary prevention of cardiovascular and cerebrovascular events. In the meantime, especially when the ideal HCys level is far from being reached, Normocis$^{400®}$ appears to be safe, well tolerated and effective in reducing HCys levels.

To the Editor,

Homocysteine (HCys) is a non-protein aminoacid involved in methionine and cysteine metabolism (1). Although its role in secondary cardiovascular prevention has been recently scaled down, hyper-homocysteinemia (fasting HCys serum concentration >15 µmol/L) (2) is still considered – like hypertension – a risk factor for cerebrovascular events (3). Among others, Yoo et al. showed that even a modest HCys level increase (average HCys

Key words: cardiovascular risk, folic acid, homocysteine, nutraceutical, prevention

Mailing address:
Alberto Mazza, MD, PhD
Department of Internal Medicine,
Hopital S. Maria della Misericordia ,
Viale Tre Martiri No. 140, 45100 Rovigo, Italy
Tel.: +39 0425 394567 - Fax: +39 0425 394157
e-mail: mazza.alberto@azisanrovigo.it

0393-974X (2016)

DISCLOSURE: ALL AUTHORS REPORT NO CONFLICTS OF INTEREST RELEVANT TO THIS ARTICLE.

in cases: 11.8 μmol) is an independent risk factor for stroke (4). Furthermore, a meta-analysis by a Mayo Clinic research group showed that each increase of 5 μmol/L in HCys plasma level is independently associated with an approximate 20% increased risk of coronary heart disease (5), and a large survey examining US adults reported a two-fold risk of myocardial infarction in patients with HCys concentration >15 μmol/L, independently from ethnicity (6). Hyperhomocysteinemia was found to be significantly associated with cardiovascular and cerebrovascular events also in subsets of hypertensive patients (7).

Despite its well-acknowledged role as a risk factor for cerebrovascular diseases, scientific literature shows many discordant findings with regard to the effects obtained by lowering plasma HCys levels, with many trials claiming no reduction in cardiovascular morbidity and mortality (8). At least a part of these conflicting results could be related to the lack of dietary supplement standardization, the use of underdosed or incomplete dietary supplements and incorrect selection of patients in trials. In this context, the aim of this study was to investigate the efficacy of a combined dietary supplement containing folate-6-5-methyltetrahydrofolate 400 μg, vitamin B6 3 mg, vitamin B12 5 μg, vitamin B2 2.4 mg, zinc 12.5 mg and bethaine 250 mg (Normocis$^{400®}$) versus a conventional single vitamin supplementation (folic acid 5 mg/day) in lowering HCys serum levels in hypertensive subjects at low added cardiovascular risk.

MATERIALS AND METHODS

This is a multicenter, double-blind, randomized clinical trial. One-hundred and four patients (mean age 62.8±14.5 years, 63.5% males), 52 for each treatment group, were consecutively enrolled in our Hypertension Center and gave informed consent for their participation in the study. The study protocol was approved by the local Ethics Committee and institutional review boards and the study was conducted in accordance with ICH Harmonized Tripartite Guidelines for Good Clinical Practice and the Declaration of Helsinki Principles. Subjects were free to withdraw from the study at any time and for any reason, as well as in the occurrence of any adverse event. The study enrolled patients with grade-1 essential hypertension and hyper-homocysteinemia (HCys ≥15 μmol/L), without a history of cardiovascular and cerebrovascular disease, in order to limit the impact of complex and different therapeutic protocols on the observed results. The choice of hypertensive patients was made as it is more likely that HCys is dangerous in patients with at least one cardiovascular risk factor, such as hypertension, but we aimed at excluding patients with more complex therapeutic protocols, which more severe hypertensive patients usually have. Alcohol intake was recorded by means of a questionnaire and considered as ethanol consumption in ml/week, mainly due to wine consumption.

Data collection - at baseline, blood pressure (diastolic Korotkoff phase 5) was evaluated in a lying position with a triple measurement at 10-min intervals, using a mercury sphygmomanometer and taking special care to avoid any terminal digit preference. The average of the last two measurements was considered, in order to minimize a possible white-coat effect; heart rate was also taken at the same time. Fasting total cholesterol (TC), triglycerides (TG), high-density-lipoprotein cholesterol (HDLC) and serum glycemia levels were analyzed by standardized enzymatic methods. Low-density lipoproteins cholesterol (LDLC) was estimated by the Friedewald formula (9). For total HCys assay, whole blood samples were collected in ice-cooled tubes containing K3 EDTA and centrifuged within 30 min at 2000× g for 10 min at 4°C; plasma aliquots were frozen at −80°C until assayed. HCys was assayed according to the HPLC method of Araki and Sako (10) with slight modifications, as reported elsewhere (11). Intra-assay and inter-assay coefficients of variation (CVs) were <3.1% and <4.5% respectively. The limit for detection and quantification were respectively 10 ng/mL and 10 ng/L. Body mass index was calculated as the ratio of weight (in kilograms) to squared height (in meters). According to the number of smoked cigarettes per day, subjects were classified into non-smokers or current smokers (≥1 cigarette daily).

Subjects were sequentially randomized to receive either a combined nutraceutical containing folate-6-5-methyltetrahydrofolate 400 μg, vitamin B6 3 mg, vitamin B12 5 μg, vitamin B2 2.4 mg, zinc 12.5 mg and betaine 250 mg (Normocis$^{400®}$, kindly offered by Inpha Duemila Srl, Lecco, Italy) once daily for two months (56±2 days), or highly dosed folic acid (5 mg/day) (control group).

We estimated that to observe a significant difference of at least 25% reduction between groups with an SD of 2 μmol/L, maintaining a power of 0.80 and a significance level for $p<0.05$, we had to enroll at least 50 patients per group.

Continuous variables were averaged, expressed as mean ± standard deviation and compared with analysis of variance (ANOVA). Comparison between categorical variables was performed using the χ^2 test. Analysis of variance for repeated-measure was used to compare mean changes of HCys levels at baseline and at the follow-up visits. All statistical analyses were performed using the SPSS package version 17.0 for Windows (SPSS, Chicago, IL, USA). The null hypothesis was always rejected for values of $p<0.05$.

RESULTS

All the enrolled patients completed the study. In the entire study group, the mean age was 62.8±14.5 years and it was not significantly different between males and females (61.0±15.0 vs 65.0±12.0, NS). At baseline, SBP and DBP were significantly ($p<0.001$) higher in the active treatment group than in the control group (154.1±12.6 vs 139.0±15.1 and 91.1±6.6 vs 85.4±7.7, respectively). On the contrary, HDL-C levels were significantly lower in the former (56.2±12.1 vs 64.1±15.9, $p<0.001$). The general characteristics of the two groups at baseline are summarized in Table I.

Compared with baseline level, a significant reduction in HCys was found in both groups at the end of the treatment period, with a decrease from 21.5±2.7 (95%CI 17.6, 32.9) to 10.0±1.7 (95%CI 7.2, 13.1) μmol/L for Normocis$^{400®}$ ($p<0.001$), and from 22.6±3.2 (95%CI 16.6, 30.2) to 14.3±2.8 (95%CI 10.6, 18.3) μmol/L for controls ($p<0.001$).

HCys reduction was significantly higher among patients treated with Normocis$^{400®}$ ($p<0.035$, Fig. 1). In fact, the ideal HCys level (i.e. <10 μmol/L) was reached in 55.8% of cases in the Normocis$^{400®}$

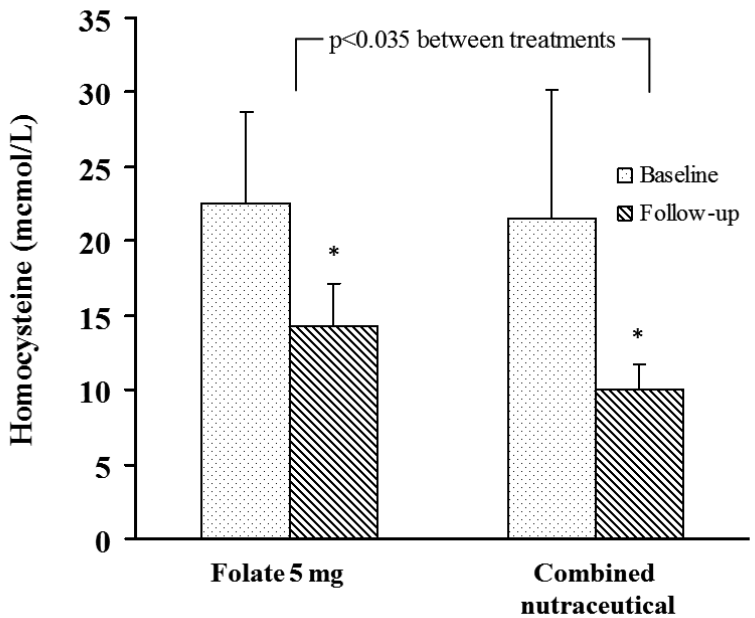

Fig. 1. *Changes of serum homocysteine levels from baseline to follow-up in both active treatment (Normocis$^{400®}$) and control groups. *<0.0001 vs baseline.*

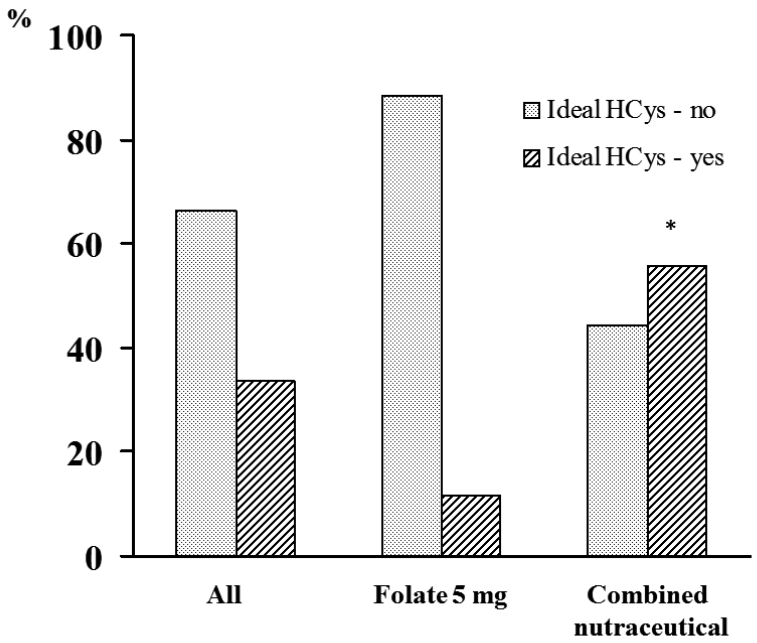

Fig. 2. *Prevalence of subjects reaching the ideal homocysteine (HCys) level (i.e. <10 μmol/L) in both active treatment (Normocis$^{400®}$) and control groups. *<0.0001 vs controls.*

group, and only in 11.5% of cases in controls (Fig. 2). No side effects were observed in either treatment group.

DISCUSSION

At the present time, dietary supplements are acquiring a relevant role in primary cardiovascular and cerebrovascular prevention (12, 13).

Elevated plasma HCys represents a cardiovascular risk factor, due to its active role in provoking endothelial dysfunction, smooth muscle cell proliferation, increased oxidative stress and thus an inflammation state (14). Nonetheless, many trials investigating the effects of folates and other group B vitamins on patients with hyperhomocysteinemia observed that no reduced cardiovascular morbidity or mortality followed an HCys decrease (15). On the other hand, results from the HOPE 2 trial, a broader and longer study examining stroke outcome in subjects with known cardiovascular disease, treated with folate and vitamin B6 and B12 for 5 years, showed a significant decrease in stroke incidence (16). The main reasons behind this inconsistency could lie in the lack of dietary supplement standardization (17), an inaccurate selection of the patients (many of them had borderline HCys levels), an often too short follow-up (generally 1 to 2 years), the bias provoked by confounding factors such as statin or other preventive drug therapies (18) and the existence of pyridoxine insensitive subjects (19).

Of our 104 patients, the sub-group treated for two months with a daily supply of Normocis^{400} showed an average decrease in serum HCys concentration from 21.5±8.7 to 10.0±1.7 μmol/L ($p<0.0001$) and 55.8% of the sub-group patients reached optimal values (HCys<10 μmol/L; $p<0.0001$ vs control group), whereas the control group showed a significantly lower decrease.

Our results are in line with most of the trials published in recent literature examining treatments

Table I. *General characteristics of the study population.*

Items	All subjects (N=104)	Control Group (N=52)	Active treatment (N=52)	ANOVA p Between groups
Age (yrs)	62.8±14.5	61.9±15.3	63.1±14.9	NS
Men gender (%)	63.5	69.2	57.8	NS
Homocysteine (μmol/L)	22.1±2.7	22.6±2.1	21.5±2.7	NS
BMI (kg/m^2)	28.1±4.6	27.9±5.2	28.3±4.0	NS
SBP (mmHg)	146.6±15.7	139.0±15.1	154.1±12.6	<0.001
DBP (mmHg)	88.3±7.6	85.4±7.7	91.1±6.6	<0.001
HR (bpm)	73.6±8.4	72.2±7.8	74.9±8.9	
Creatinine (mg/dl)	0.98±0.2	1.01±0.14	0.95±0.25	NS
Glycemia (mg/dl)	98.4±26.6	93.2±21.0	103.4±30.4	NS
TC (mg/dl)	209.9±24.2	212.9±16.4	206.8±29.8	NS
TG (mg/dl)	108.4±42.3	110.4±41.9	106.3±43.1	NS
HDLC (mg/dl)	60.1±14.2	64.1±15.9	56.2±12.1	<0.001
LDLC (mg/dl)	128.1±25.43	126.7±20.1	129.4±29.9	NS
Ethanol intake (g/day)	29.2±16.7	31.8±19.6	27.3±14.8	NS
Smoking (%)	15.4	9.6	21.2	NS

BMI: body mass index; SBP: systolic blood pressure; DBP: diastolic blood pressure; HR: heart rate; ABPM: ambulatory blood pressure monitoring; TC: total cholesterol; HDLC and LDLC: high-density-lipoprotein and low-density-lipoprotein cholesterol.

with folate and vitamin B6 and B12 (20, 21): we obtained a greater percentage decrease than most of these trials, probably because of the use of the active form of folic acid in spite of standard folate.

Our study has some relevant limitations: a relatively small patient sample and a limited duration; moreover, we did not specifically monitor eventual spontaneous changes in folate content in the patients' diet, and the groups were not balanced as regards baseline blood pressure and HDL-C, but they were as regards HCys levels (the main outcome of the trial).

In conclusion, randomized clinical trials are ongoing to test the effect of folate, B6 and B12 (Normocis$^{400®}$) supplementation in primary prevention of cardiovascular and cerebrovascular events and, even though there are currently no clear recommendations for the treatment of hyper-homocysteinemia, we observed that Normocis$^{400®}$ appears to be safe, well tolerated and effective in significantly reducing HCys levels compared with the standard prescription of folate only.

ACKNOWLEDGEMENTS

The study was supported by Rovigo Public Health Agency institutional funding.

REFERENCES

1. Selhub J. Homocysteine metabolism. Annu Rev Nutr 1999; 19:217-46.
2. Malinow MR, Bostom AG, Krauss RM. Homocyst(e)ine, diet, and cardiovascular diseases: a statement for healthcare professionals from the Nutrition Committee, American Heart Association. Circulation 1999; 99(1):178-82.
3. He Y, Li Y, Chen Y, Feng L, Nie Z. Homocysteine level and risk of different stroke types: a meta-analysis of prospective observational studies. Nutr Metab Cardiovasc Dis 2014; 24:1158-65.
4. Yoo JH, Chung CS, Kang SS. Relation of plasma homocyst(e)ine to cerebral infarction and cerebral atherosclerosis. Stroke 1998; 29:2478-83.
5. Humphrey LL, Fu R, Rogers K, Freeman M, Helfand M. Homocysteine level and coronary heart disease incidence: a systematic review and meta-analysis. Mayo Clin Proc 2008; 83:1203-12.
6. Giles WH, Croft JB, Greenlund KJ, Ford ES, Kittner SJ. Association between total homocyst(e)ine and the likelihood for a history of acute myocardial infarction by race and ethnicity: Results from the Third National Health and Nutrition Examination Survey. Am Heart J 2000; 139:446-53.
7. Catena C, Colussi G, Nait F, Capobianco F, Sechi LA. Elevated Homocysteine Levels Are Associated With the Metabolic Syndrome and Cardiovascular Events in Hypertensive Patients. Am J Hypertens 2015; 28:943-50.
8. Martí-Carvajal AJ, Solà I, Lathyris D, Karakitsiou DE, Simancas-Racines D. Homocysteine-lowering interventions for preventing cardiovascular events. Cochrane Database Syst Rev 2013; 1:CD006612.
9. Friedewald WT, Levy RI, Fredrickson DS. Estimation of the concentration of lowdensity lipoprotein cholesterol in plasma, without use of the preparative ultracentrifuge. Clin Chem 1972; 18:499-502.
10. Araki A., Sako Y. Determination of free and total homocysteine in human plasma by high-performance liquid chromatography with fluorescence detector. J Chromatogr 1987; 422:43-52.
11. De Stefano V, Zappacosta B, Persichilli S, Rossi E, Casorelli I, Paciaroni K, Chiusolo P, Leone AM, Giardina B., Leone G, et al. Prevalence of mild hyperhomocisteinemia and association with thrombophilic genotypes (Factor V Leiden and factor II G20210A) in Italian patients with venous thromboembolic disease. Br J Haematol 1999; 106:564–568.
12. Hohmann CD, Cramer H, Michalsen A, Kessler C, Steckhan N, Choi K, Dobos G. Effects of high phenolic olive oil on cardiovascular risk factors: A systematic review and meta-analysis. Phytomedicine 2015; 22:631-40
13. McCarty MF, O'Keefe JH, DiNicolantonio JJ. Red Yeast Rice Plus Berberine: Practical Strategy for Promoting Vascular and Metabolic Health. Altern Ther Health Med 2015; 21(S2):40-5.
14. Ganguly P, Alam SF. Role of homocysteine in the development of cardiovascular disease. Nutr J 2015; 14:6.
15. Martí-Carvajal AJ, Solà I, Lathyris D, Karakitsiou DE, Simancas-Racines D. Homocysteine-lowering interventions for preventing cardiovascular events. Cochrane Database Syst Rev 2013; 1:CD006612.
16. Saposnik G, Ray JG, Sheridan P, McQueen M, Lonn E. Homocysteine-lowering therapy and stroke risk, severity, and disability: additional findings from the HOPE 2 trial. Stroke 2009; 40:1365-72.
17. Homocysteine lowering trialists' collaboration. Dose-dependent effects of folic acid on blood concentrations of homocysteine: a meta-analysis of the randomized trials. Am J Clin Nutr 2005; 82(4):806-12.
18. Debreceni B, Debreceni L. Why do homocysteine-lowering B vitamin and antioxidant E vitamin supplementations appear to be ineffective in the prevention of cardiovascular diseases? Cardiovasc Ther 2012; 30:227-33.
19. Schiff M, Blom HJ. Treatment of inherited homocystinurias. Neuropediatrics 2012; 43:295-304.

20. Martí-Carvajal AJ, Solà I, Lathyris D, Karakitsiou DE, Simancas-Racines D. Homocysteine-lowering interventions for preventing cardiovascular events. Cochrane Database Syst Rev 2013;1:CD006612.

21. Saposnik G, Ray JG, Sheridan P, McQueen M, Lonn E. Homocysteine-lowering therapy and stroke risk, severity, and disability: additional findings from the HOPE 2 trial. Stroke 2009; 40:1365-72.

LETTER TO THE EDITOR

NEONATAL OXIDATIVE STRESS DEPENDS ON OXYGEN BLOOD PRESSURE IN UMBILICAL ARTERY

F. PROIETTI[1], G. DE BERNARDO[2], M. LONGINI[1], D. SORDINO[2], G. SCARAMUZZINI[3], M.L. TATARANNO[1], E. BELVISI[1], F. BAZZINI[1], S. PERRONE[1] and G. BUONOCORE[1]

[1]Department of Molecular and Developmental Medicine, University of Siena, Italy; [2]Department of Emergency UOC TIN-Neonatology AORN Santobono-Pausilipon Naples, Italy; [3]Neonatology and Obstetrics Nursing C.G. Ruesch, Naples, Italy

Received February 27, 2016 – Accepted June 23, 2016

With advancing gestation, partial pressure of oxygen (pO_2) and pH fall significantly. Hypoxia is a main factor inducing free radical generation and thereby oxidative stress (OS). Placental and fetal tissue response when oxygen becomes restricted is complex and partially known. We tested the hypothesis that changes in umbilical artery and vein blood gas concentrations modulate OS occurrence in the newborn. Seventy umbilical artery and vein plasma samples were collected from healthy term newborns immediately after delivery. F2 Isoprostanes (F2-Isop) were measured in all samples as reliable markers of lipid peroxidation. Significantly lower pCO_2 and higher pO_2 and pH were found in umbilical vein than in artery, as expected. A positive correlation was detected between pH and pO_2 only in umbilical artery (p=0.019). F2-Isop levels were no different between artery and vein in cord blood. Significant correlations were found between F2-Isop and pCO_2 (p=0.025) as well as between F2-Isop and pH in umbilical vein (p=0.027). F2-Isop correlated with pCO_2 (p=0.007) as well as with pO_2 values (p=0.005) in umbilical artery blood. Oxidative stress (OS) in newborns depends on oxygen concentrations in umbilical artery. OS biomarkers significantly correlate with pO_2 and in umbilical artery but not in umbilical vein. In normoxic conditions fetal-maternal gas exchanges occurring in placenta re-establish normal higher oxygen levels in umbilical vein than artery, with a normal production of free radicals without any deleterious effects.

To the Editor,

The placental barrier is gradually breached to maternal blood between 8-12 weeks of gestation, due to invasion of placental-bed uteroplacental spiral arteries by the extravillous trophoblast. Placental oxygen tension thus rises and a phase of branching angiogenesis continues until 24 weeks. Gas-exchanging terminal villi are essential for rapid fetal growth and development of a high-flow, low-resistance fetal-placental circulation (1). Due to these processes umbilical cord blood gases value change with advancing fetal gestational age. Artery and venous partial pressure of oxygen (pO_2) and pH decrease while venous partial pressure of carbon dioxide (pCO_2) increases (2). It has been suggested that the deterioration of placental gas exchanges by placenta aging causes inadequate fetal oxygen supply, anaerobic metabolism, increased lactate production and decreased fetal pO_2 and pH (3). Anaerobiosis induces free radical generation and consequently

Key words: free radicals, oxidative stress, cord blood, oxygen, lipid peroxidation, newborn infants

Mailing address:
Serafina Perrone, MD, PhD,
Department of Molecular and Developmental Medicine,
University of Siena, Policlinico Santa Maria alle Scotte,
Viale Bracci 36, 53100 Siena, Italy
Tel.: +39 0577 586542 - Fax: +39 0577 586182
e-mail: saraspv@yahoo.it

0393-974X (2016)

oxidative stress (OS) occurs. The knowledge of the redox status in normal conditions could be of help to better understand the physiological mechanisms involved in the diseases associated with perinatal oxidative stress and to better indicate therapeutic targets. The knowledge gained on this issue is still very limited. There are few studies aimed at assessing the blood oxidative stress indicators at the time of deliver, in normal condition. Moreover, the majority of the available studies on OS are focused on neonates with pathologies or preterm babies, which limits the global knowledge of the factors involved in healthy childbirth. On the other hand, many studies feature only a partial view of this process as they discuss and feature only data from umbilical cord vein. In addition, these studies (4, 5) have aroused some controversy, partly because they did not consider post hoc oxidation following sampling. Plasma F2-Isoprostanes (F2-Isop), prostaglandin-like compounds produced *in vivo* by non-cyclooxygenase mechanism, are currently considered as the most reliable indicators of OS (6).

The present study was designed to test the hypothesis that changes in umbilical artery and vein blood gas concentrations modulate oxidative stress (OS) occurrence in the newborn.

MATERIALS AND METHODS

Umbilical artery and vein plasma samples were collected from 35 healthy term newborns (15 males, 20 females; gestational age 39±2 weeks: birth weight 3348±414 gr, length 50±1.6 cm, head circumference 35±1.1 cm, Apgar score minimum 8 at 1 min. and minimum 9 at 5 min), from cord blood immediately after delivery. The babies were born at the C.G. Ruesch Hospital in Naples from healthy, non-smoking, mothers with normal gestational course, by elective cesarean section (CS), without labor, due to the mother willing, being worried about spontaneous delivery. All enrolled newborns were healthy, did not require any particular assistance and were discharged on 3rd-4th day of life on breast feeding. Parental consent was obtained. Prior to surgery, all patients were administered 1000 ml Ringer's lactate infusion, standard monitoring was performed with electrocardiography, pulse oximetry, and noninvasive blood pressure. Spinal anesthesia was performed with 2 ml 0.5% levobupivacaine and 20 µg fentanyl injected into the intrathecal space with a 27 gauge pencil point spinal needle (Espocan®, Brown, Germany). No patient recieved supplementary oxygen during the cesarean section, due to the stability of vital parameters. After the baby was delivered, and the umbilical cord clamped, two umbilical artery and vein blood samples were obtained. The first blood sample was assessed for arterial and vein blood gas analyses using IRMA TruPoint Blood Analysis System with CC type cartridges. The Butylated hydroxytoluene solution was added to the serum obtained from the second blood samples which were then stored at -80°C until analysis.

F2-Isop were measured according to the methods previously reported by Casetta B. et al. (7) This method is based on a light deproteinization with acetonitrile followed by an LC-MS/MS analysis.

Statistical analysis

Statistical analysis was performed using IBM SPSS Statistic 20. The Kolmogorov-Smirnov algorithm was used to test the distribution normality of the data. Non-parametric test (Mann-Whitney test) and ANOVA statistic tests were used when needed.

RESULTS

Significant differences were found in pCO_2, pO_2 and pH levels between umbilical artery and vein (Table I). A positive correlation was detected between pH and pO_2 only in the umbilical artery (r^2=0.133; p=0.019; Fig. 1).

F2-Isop levels were no different between artery and vein in cord blood (28±32 pg/mL *vs* 28.5±20.5 pg/mL; median ± interquartile range).

Significant correlations were found, between F2-Isop and pCO_2 (r^2=0.148; p=0.025) as well as between F2-Isop and pH in umbilical vein (r^2=-0.144; p=0.027), (Fig. 2). F2-Isop correlate with pCO_2 (r^2=0.205; p=0.007) as well as with pO_2 values (r^2= -0.264; p=0.005) (Fig. 3) in umbilical artery blood.

DISCUSSION

Our results report, for the first time in literature, significant correlations between pCO_2, pO_2 and OS, detected by F2-Isop concentrations, in umbilical

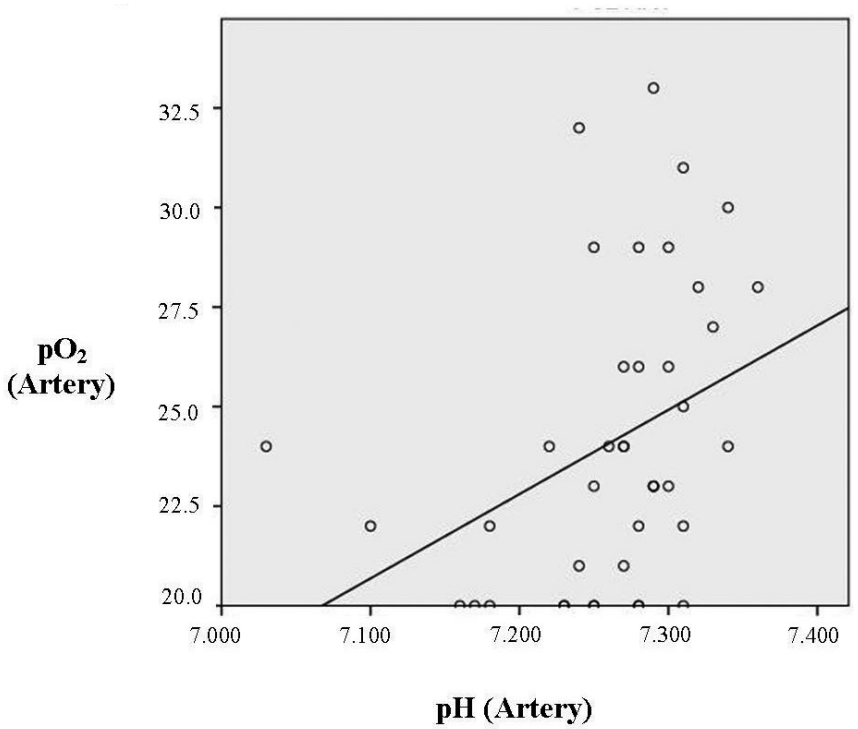

Fig. 1. *Correlation between pH and P O_2 in umbilical artery.*

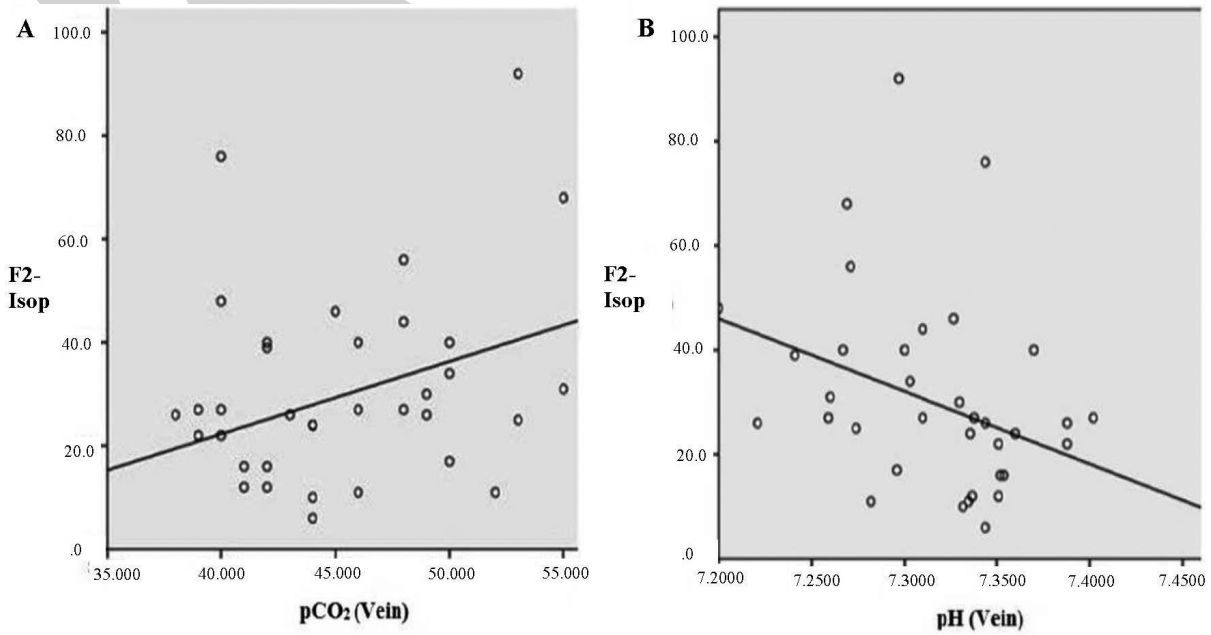

Fig. 2. *Correlation between F2-Isop and pCO_2 (**A**) and between F2-Isop and pH (**B**) in umbilical cord vein.*

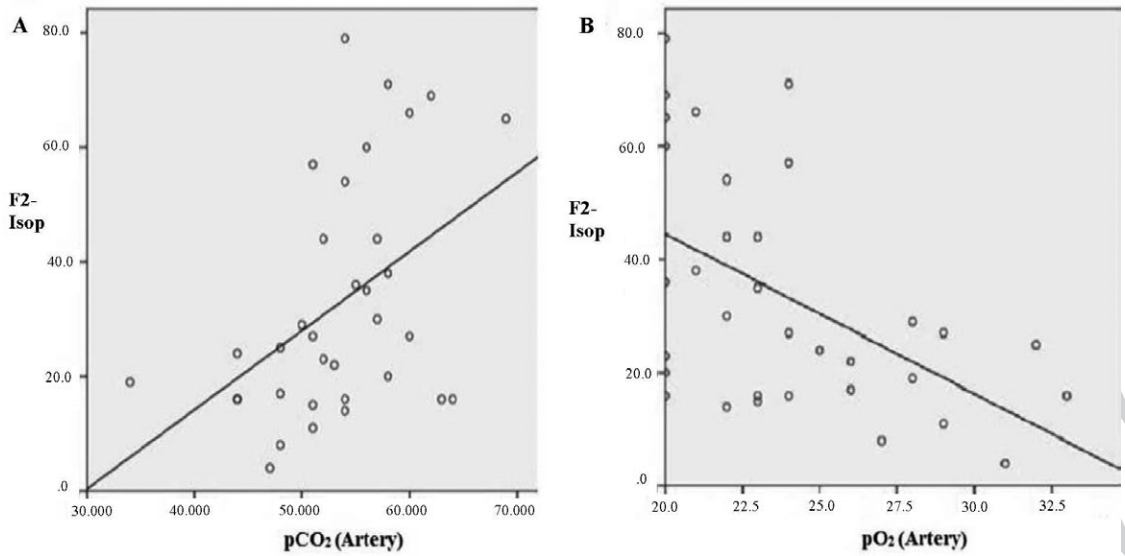

Fig. 3. *Correlation between F2-Isop and pCO_2 (**A**) and between F2-Isop and pO_2 (**B**) in umbilical cord artery.*

artery of normal term fetuses: the lower pO_2 the higher OS; the higher pCO_2, the higher OS. These novel findings are relevant to improve knowledge of multifactorial physiological processes that occur in the fetal-placental unit in response to pO_2. The inaccessibility to the fetus and the complexity of mechanism of OS injury in developing tissues make it extremely difficult to determine the intrauterine processes in fetal life. With the aim of having a complete view of the phenomena, we studied artery and vein cord blood. Taking a sample from each blood type, we can assess which mediators are transferred to the fetus from the mother or produced by the fetus, showing the key role of the placental barrier. If the fetus was the main potential source of free radicals, then the umbilical cord artery F2-Isop would be expected to be higher than the umbilical vein. Another potential source of free radicals is the mother. Parturition increases oxidative damage in the mother, but the indicators of OS were found lower in the umbilical cord artery in respect to the umbilical vein in spontaneous delivery (4). In our study, more physiological levels of pO_2, pCO_2, pH, BE were found in vein than in artery blood and no correlation was found between pO_2 and F2-Isop in umbilical vein. These findings suggest that placenta in normoxic conditions plays a pivotal role in feto-maternal gas exchanges, being able to re-establish higher oxygen levels in umbilical vein than artery and to metabolize free radicals.

The significant correlation between pO_2 and F2-Isop in umbilical artery but not in vein, demonstrates the potential clinical utility of cord blood artery F2-Isop in revealing the redox status of the fetus. F2-Isop are stable products of lipid peroxidation and are universally recognized as reliable markers of OS. Lipid peroxidation by-products may represent a valid tool to caregivers for the early identification of the risk of oxidative injury and of free radical-related diseases of newborns (8-11). It is well known that pO_2 levels in blood modulate mitochondrial activity and mitochondrial-related free radical generation (12, 13). As oxygen concentration increases, the rate of mitochondrial O_2^{-}• production increases linearly. The use of higher FiO_2 in the delivery room has been found to correlate with higher OS in cord blood (14). When supplementary oxygen is given to the mother undergoing cesarean section, the increase in maternal artery pO_2 determines an increase in umbilical venous pO_2 as well as an increase in umbilical vein F2-Isop levels (15). It is worthwhile to note that in our study, in physiologic conditions, OS in cord

Table I. *Blood gas analysis data in umbilical artery and vein.*

	Artery (n° 35)	Vein (n° 35)	p-value
pH	7.27 ±0.05	7.31 ±0.05	p=0.001
pCO_2 (mmHg)	53 ±7	46 ±5	p=0.001
pO_2 (mmHg)	24 ±4	35 ±11	p=0.001
HCO_3^- (mmol/L)	23 ±3	24 ±2	p=0.006
BE (mmol/L)	-2.7 ±1.6	-3.8 ±1.8	p=NS

blood correlated with umbilical artery pO_2 but not with umbilical vein pO_2. This study has the limitation of detecting only lipid peroxidation biomarker, thus we had to face all the different etiologies of OS in cord blood. However, our findings clarify the redox status in normal conditions, advancing the existing gap in the knowledge of the pathophysiological mechanisms in oxidative stress-associated diseases in newborns.

ACKNOWLEDGEMENTS

The Authors are grateful to the Europe Against Infant Brain Injury (EURAIBI) Foundation for its partial unrestricted grant. Grants from the Tuscany Region and Ministry of Health, General Directorate of Scientific and Technological Research for the 2011-2014 Project "Early identification of newborn at high risk of brain injury through a validated biomarkers profile and specific neuro-imaging patterns. A follow-up study of clinical and neurodevelopmental outcome in a large cohort study" RF-2009-1499651.

REFERENCES

1. Kingdom JC, Kaufmann P. Oxygen and placental vascular development. Adv Exp Med Biol 1999; 474:259-75.
2. Kitlinski ML, Källén K, Marsál K, Olofsson P. Gestational age-dependent reference values for pH in umbilical cord arterial blood at term. Obstet Gynecol 2003; 102:338-45.
3. Wiberg N, Kallen K, Olofsson P. Physiological development of a mixed metabolic and respiratory umbilical cord blood acidemia with advancing gestational age. Early Hum Dev 2006; 82:583-9.
4. Díaz-Castro J, Florido J, Kajarabille N, et al. A new approach to oxidative stress and inflammatory signaling during labour in healthy mothers and neonates. Oxid Med Cell Longev 2015; 2015:178536.
5. Fogel I Pinchuk, M. J. Kupferminc, D. Lichtenberg O. Fainaru, I. Oxidative stress in the fetal circulation does not depend on mode of delivery," Am J Obstet Gynecol 2005; 193:241-46.
6. Liu W, Morrow JD, Yin H. Quantification of F2-isoprostanes as a reliable index of oxidative stress in vivo using gas chromatography-mass spectrometry (GC-MS) method. Free Radic Biol Med 2009; 47:1101-7.
7. Casetta B, Longini M, Proietti F, Perrone S, Buonocore G. Development of a fast and simple LC-MS/MS method for measuring the F2-isoprostanes in newborns. J Matern Fetal Neonatal Med 2012; 25:114-18.
8. Perrone S, Tataranno ML, Negro S, et al. Early identification of the risk for free radical-related

diseases in preterm newborns. Early Hum Dev 2010; 86:241-44.
9. Kuligowski J, Aguar M, Rook D, et al. Urinary lipid peroxidation byproducts: are they relevant for predicting neonatal morbidity in preterm infants? Antioxid Redox Signal 2015; 23:178-84.
10. Perrone S, Tataranno ML, Negro S, et al. May oxidative stress biomarkers in cord blood predict the occurrence of necrotizing enterocolitis in preterm infants? J Matern Fetal Neonatal Med 2012; 25:128-31.
11. Perrone S, Tataranno ML, Stazzoni G, Buonocore G. Biomarkers of oxidative stress in fetal and neonatal diseases. J Matern Fetal Neonatal Med 2012; 25:2575-78.
12. Balaban RS, Nemoto S, Finkel T. Mitochondria, oxidants, and aging. Cell 2005; 120:483-95.
13. Barrera G, Gentile F, Pizzimenti S, et al. Mitochondrial dysfunction in cancer and neurodegenerative diseases: spotlight on fatty acid oxidation and lipoperoxidation products. Antioxidants (Basel) 2016; 19:5(1). doi: 10.3390/antiox5010007.
14. Perrone S, Vezzosi P, Longini M, et al. Biomarkers of oxidative stress in babies at high risk for retinopathy of prematurity. Front Biosci (Elite Ed) 2009; 1:547-52.
15. Khaw KS, Wang CC, Ngan Kee WD, Pang CP, Rogers MS. Effects of high inspired oxygen fraction during elective caesarean section under spinal anaesthesia on maternal and fetal oxygenation and lipid peroxidation. Br J Anaesth 2002; 88:18-23.